Supramolecular Resorcin[4]arene-capped Porphyrins: Ligands Towards Homogeneous Catalysis

by

Michael Mc Kay

Supramolecular Resorcin[4]arene-capped Porphyrins: Ligands Towards Homogeneous Catalysis

by

Michael Mc Kay

Submitted in fulfilment of the academic requirements for the degree of Doctor of Philosophy of Science in the School of Chemistry, University of KwaZulu-Natal, Durban

December 2008

ABSTRACT

The synthesis of cavitand-capped porphyrin ligands, with a view towards their potential as ligands in homogeneous catalysis, is described. The ligand apertures, one of which is outlined in the figure below, are focal with the aim of synthesising a ligand which can control access to the active site of the porphyrin *via* these apertures

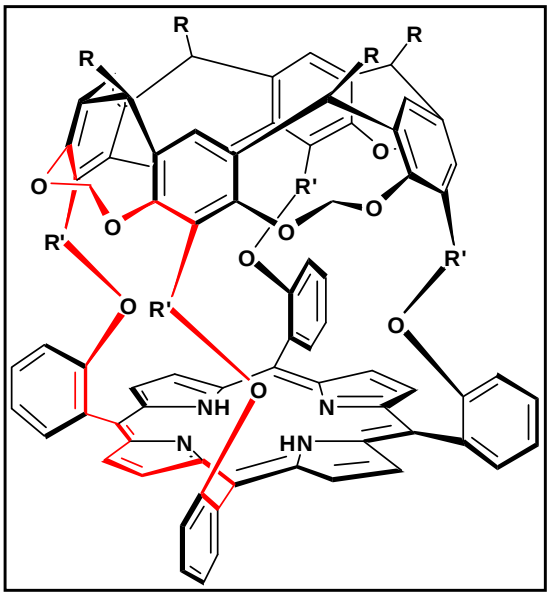

The general structure of the target ligand.

Synthesis of the target ligand (where R' = CH_2 in the figure presented) was attempted *via* two pathways. Synthesis commenced by using an *in situ* protocol, which used successive functionalisation of the cavitand structure towards the required aldehyde precursor for porphyrin formation. It was found that subsequent *in situ* cyclisation and porphyrin formation was hindered by steric factors, arising directly from the short -CH_2O- bridges used to link the cavitand to the porphyrin. Ligand synthesis was thus unsuccessful.

In a second approach, the porphyrin was synthesised in isolation before being coupled with the cavitand in a direct capping protocol, which gave more promising results. In the case of R = $C_{11}H_{23}$ (in the figure above), preliminary UV-Vis analysis indicated a successful synthesis. Subsequent analysis of the reaction product by NMR techniques and mass spectrometry could not conclusively confirm the synthesis of the target ligand. The synthesis could therefore not be deemed a success; conceivably the short bridge length being the decisive factor once more.

Computational chemistry was used to investigate synthetic results, and therefore the viability of using the -CH_2O- bridges to afford limited access to the porphyrin active site. By using molecular mechanics, -CH_2O- bridges were found to be too short, giving an aperture of insufficient size to enable only the terminus of a linear paraffin to gain access to the inner cavity of the ligand. Further investigation using molecular dynamics indicated that a ligand bearing bridges four or five atoms in length would afford an aperture of the desired size to accommodate the terminus of a paraffin exclusively.

Consequently, synthesis was redesigned towards the preparation of two new ligands, bearing -$O(CH_2)_2O$- (four atom, R' = $O(CH_2)_2$ in the figure above) and -$O(CH_2)_3O$- (five atom, R' = $O(CH_2)_3$ in the figure above) bridges. Using 2-phenylethyl feet (R = $CH_2CH_2C_6H_5$ in the figure presented) and adopting the *in situ* synthetic protocol, both ligands were successfully synthesised. Characterisation using UV-Vis and NMR spectroscopic techniques, as well as mass spectrometry confirmed that both ligands had been obtained pure. Additionally, the *in situ* cyclisation (in both ligands) was performed *via* the use of microwave heating, a technique hitherto unreported.

A viable synthetic route was thus established for the preparation of two new cavitand-capped porphyrin ligands towards their use in size-selective catalysis.

In addition, a number of crystal structures of synthetic intermediates are described, five of which are newly reported. These illustrated notable structural features regarding resorcin[4]arene cavitands and their abilities as host molecules. In particular, the structure of the aldehyde precursor to capped porphyrin formation following the (initial) *in situ* synthetic protocol was significant in illustrating the reason as to why *in situ* cyclisation was unsuccessful for the synthesis involving -CH_2O- bridges.

PREFACE

The experimental work described in this dissertation was carried out at the School of Chemistry, University of KwaZulu-Natal, Howard College and Westville campuses, from February 2005 to October 2008, under the supervision of Professor H.B. Friedrich and Doctor G.E.M. Maguire.

These studies represent original work by the author and have not otherwise been submitted in any form for any degree or diploma to any tertiary institution. Where use has been made of the work of others it is duly acknowledged in the text.

ACKNOWLEDGEMENTS

I would like to express my gratitude to the following people for their input to this dissertation:

Professor Holger Friedrich and Doctor Glenn Maguire, my supervisors, for their guidance, patience and support throughout the course of my work. Thank you for encouraging me at all times and assisting me. Dr Kruger for assistance with the computational work.

My parents for always encouraging me in my studies. My gratitude for your support throughout my academic career thus far is immeasurable.

The Department of Science and Technology in conjunction with the National Research Foundation, who, through the c*change Centre of Excellence funded and facilitated this study.

Doctor Melanie Rademeyer, Doctor Manuel Fernandes (WITS) and Doctor Delia Haynes for their assistance in collecting x-ray crystallographic data, and structure refinement. Doctor Andy Dinsmore (WITS) for the FAB mass spectroscopy analysis.

Mr. G. Moodley, Mrs T. Naidoo and Mrs M. Naidoo for technical assistance during the course of my project.

Letitia Pillay and Jason Paraskevopolous for their invaluable input and friendship during the course of study.

My brother, Anthony Mc Kay, and cousin, Neil Versfeld. You guys can never know how your achievements have inspired me; you have shown me what is possible if you set your mind to it, and for that my gratitude is endless.

Finally to the Lord for blessing me with the talent and mind for the sciences.

TABLE OF CONTENTS

ABBREVIATIONS

CD(s)	Cyclodextrin(s)
Å	Angstroms
MM	Molecular Mechanics
MD	Molecular Dynamics
CPK	Corey-Pauling-Koltun
^{1}H NMR	Proton Nuclear Magnetic Resonance spectroscopy
^{13}C NMR	Carbon-13 Nuclear Magnetic Resonance spectroscopy
ppm	Parts per million
IR	Infrared spectroscopy
UV-Vis	Ultraviolet-Visible range spectroscopy
TLC	Thin Layer Chromatography
COSY NMR	(^{1}H-^{1}H) Correlated Spectroscopy Nuclear Magnetic Resonance
HSQC NMR	Heteronuclear Single Quantum Correlation Nuclear Magnetic Resonance
NOESY NMR	Nuclear Overhauser Effect Nuclear Magnetic Resonance
FAB-MS	Fast Atom Bombardment-Mass Spectrometry
ESI-MS	Electrospray Ionisation-Mass Spectrometry
ESI-TOF-MS	Electrospray Ionisation-Time of Flight-Mass Spectrometry
M/z	Mass-to-charge ratio

LIST OF FIGURES AND SCHEMES

LIST OF TABLES

PUBLICATIONS FROM STUDY

1. *7,11,15,28-Tetrakis(bromomethyl)-1,21,23,25-tetrapentylresorcin[4]arene cavitand 0.415 hydrate.*

   Michael G. McKay, Holger B. Friedrich, Glenn E. M. Maguire *Acta Crystallogr. Sect. E: Struct. Rep. Online*, **2007**, E63, o4345.

2. *5,11,17,23-Tetramethyl-2,8,14,20-tetrakis(2-phenylethyl)-4,6,10,12,16,-18,22,24-octahydroxycalix[4]arene methanol pentasolvate 0.10-hydrate.*

   Holger B. Friedrich, R. Alan Howie, Glenn E. M. Maguire, Michael G. McKay *Acta Crystallogr. Sect. E: Struct. Rep. Online*, **2007**, E63, o4346.

3. *7,11,15,28-Tetramethyl-1,21,23,25-tetrakis(2-phenylethyl)resorcin[4]arene cavitand ethyl acetate clathrate.*

   Michael G. McKay, Holger B. Friedrich, Glenn E. M. Maguire *Acta Crystallogr. Sect. E: Struct. Rep. Online*, **2008**, E64, o98.

4. *7,11,15,28-Tetrabromo-1,21,23,25-tetraphenethyl-resorcin[4]arene cavitand-acetone-chloroform (1/1.31/0.69) at 173 K.*

   Michael .G. McKay, Holger B. Friedrich, R. Alan Howie, Glenn E. M. Maguire *Acta Crystallogr. Sect. E: Struct. Rep. Online*, **2009**, E65, o631-632.

5. *7,11,15,28-Tetrakis[(2-formylphenoxy)methyl]-1,21,23,25-tetramethylresorcin[4]arene cavitand ethyl acetate clathrate at 173 K.*

   Michael G. McKay, Holger B. Friedrich, R. Alan Howie, Glenn E. M. Maguire *Acta Crystallogr. Sect. E: Struct. Rep. Online*, **2009**, E65, o692-693.

"*By its very essence, by its ability to create and through the beauty of its objects, chemistry is an art as well as a science. Indeed, it fashions entire new worlds that do not exist before they are shaped by the hand of the chemist, just as matter, shaped by the hand of the sculptor, becomes a work of art.*"

- J-M Lehn.

CHAPTER 1

SUPRAMOLECULAR CHEMISTRY AND HOST-GUEST SYSTEMS

1.1 Introduction

The concept above, put forward by J-M Lehn,[1] that chemistry can be regarded as an art as well as a science is particularly apt in describing the discipline of supramolecular chemistry, and the development thereof. The creativity and diversity which so clearly defines the field has seen the discipline receive the 1987 Nobel Prize in Chemistry [2] (shared by J-M Lehn, D.J. Cram and C. Pedersen), and has led it to be regarded as one of the most dynamic and actively pursued fields of chemistry.[3] Certainly, research involving supramolecular chemistry is having significant implications for a vast number of related scientific fields, ranging from chemical technologies and material sciences, to biological and medical sciences.

In order to define supramolecular chemistry and to grasp its importance, it is vital to understand its place in the science of chemistry, and more importantly, the fundamental concepts on which supramolecular chemistry is based. Synthetic chemistry, or more broadly, molecular chemistry is concerned with the breaking and forming of covalent bonds.[4] Supramolecular chemistry, as shown in Figure 1.1,[5] represents the next step in terms of complexity beyond the molecule: the aggregation of molecules. Supramolecular chemistry is therefore concerned with non-covalent molecular interactions, or intermolecular forces (as opposed to interatomic forces).[1] These interactions are thus largely centered around ion-ion, ion-dipole, dipole-dipole, hydrogen bonding and van der Waal interactions.

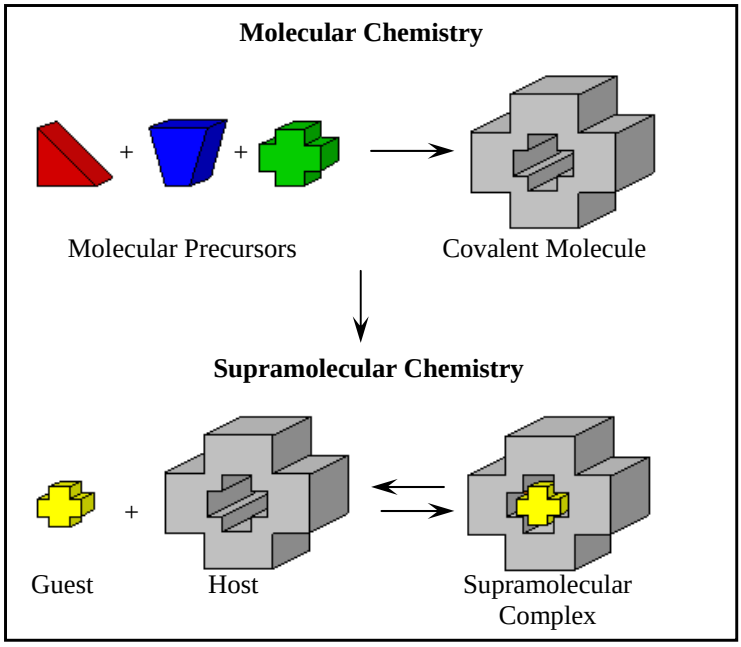

Figure 1.1: Schematic representation of the relationship between molecular and supramolecular chemistry.

1.2 Biological Systems

Biological systems have played a fundamental role in the development of supramolecular chemistry, often serving as both the origin and inspiration of research into supramolecular systems.[5] These systems are considered to be ideal supramolecular arrangements.[6] This is not surprising when taking into account the highly selective, specific and cooperative nature of chemistry taking place in biological systems: nature has an abundance of supramolecular structures, in the form of the proteins which constitute enzymatic receptor sites, genes, antibodies and ionophores.[6] These structures serve to selectively interact with species such as substrates, inhibitors, co-factors, drugs and antigens; interactions which are largely reliant on those abovementioned intermolecular forces.

Therefore, extensive efforts are undertaken to model and/or mimic biological systems with simpler, abiotic synthetic analogues, so hoping not only to gain a better understanding of biological systems and processes, but also to harness and apply their potential to humanity's needs. This is particularly true of processes involving enzymatic catalysis of organic chemical reactions, and the selective transportation of ions or molecular species, such as oxygen.[6]

With the biological basis of this field of chemistry in mind, the fundamental concepts surrounding research into today's supramolecular chemistry can be seen to lie in three fundamental principles described by various scientists a century ago:

1. Molecules cannot interact if they cannot, in some way, coordinate.[7]
2. The coordination of one molecule to another must be selective.[8]
3. The coordination cannot be selective unless the partners involved have a unique affinity for each other, and experience a unique interaction.[9]

Thus, molecular reception, selective coordination and recognition are at the core of supramolecular chemistry.

It is essential that a key and clear distinction be drawn with regards to interactions within biological and biomimetic supramolecular systems: that between host molecule and guest molecule. As will be discussed, the concept of host-guest chemistry embodies the three core principles of supramolecular chemistry outlined above, and is vital to the understanding of the majority of biomimetic supramolecular chemistry.

1.2.1 Host-Guest Systems

Small molecules are extensively involved in isolation, sequestration and selective reactions within biological systems.[1, 10] These processes are largely facilitated by recognition events at a biomolecular level. One of the major themes within bioorganic and –inorganic chemistry is the design of complexes and molecules that are able to mimic the active site responsible for these recognition events.[11] As such, perhaps the most influential force behind the development of host-guest systems has been the challenge of understanding and reproducing the action of biological processes involving enzymes and nucleic oligomers.[12] It was enzymes which served as inspiration to 1987 Nobel laureate,[13] D.J. Cram, to initially enter into the field of supramolecular chemistry and the design and synthesis of simple organic species to imitate naturally occurring complexes.[14, 15]

Enzymes and nucleic oligomers, such as RNA, are well known to bind various substrates and catalyze reactions with remarkable efficiency and selectivity, particularly in the case of enzymes. In an enzymatic system, a reaction initiates and terminates with the respective complexation of a substrate and decomplexation of product. In addition, in many such systems, the initiation and/or termination steps are often the rate determining steps of reaction. A clear distinction can be made with regards to the role of the substrate and enzymatic protein, as shown schematically in Figure 1.2. The enzyme (in grey) is accommodating the substrate (in blue) in its hydrophobic pocket, so acting as a host. Consequently the substrate is a guest molecule to the enzyme.[16]

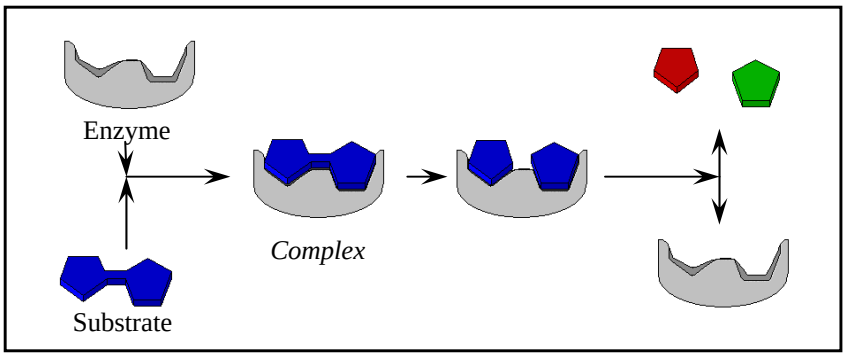

Figure 1.2: Schematic representation of an enzymatic reaction.

The distinction between host and guest molecules thus lies in their respective binding sites as well as the type of atoms which characterise the molecules. Hosts have convergent, usually concave, cavities as binding sites and are characterised by atoms that are Lewis base donors (such as oxygen, nitrogen) or hydrogen bond donors. Conversely, guests have divergent, usually convex, binding sites and are characterised by Lewis acids (such as metal cations) or hydrogen bond acceptors (such as halides).[6, 14, 17] Together, they form a complex (Figure 1.2), where the guest is coordinated to the host *reversibly*, by non-covalent forces (as mentioned above).

It is particularly important to note that the respective shapes and sizes of the host and guest are, in the case of enzymes especially, complementary to each other. This facilitates the unique interaction shared between the substrate and enzyme, and consequently the selective reaction which the substrate experiences. It is these qualities which synthetic, abiotic host-guest systems look to mimic.

Within synthetic host-guest systems, a further distinction is made with regards to complex stability.[6] Complexes, where the host is stable in a solid or crystalline state and where dissociation occurs in solution, are referred to as inclusion complexes, or clathrates. In slight contrast is a second category of host: those hosts which exhibit significant binding in both the solid and/or solution state. It is this second type of host which is the focus of this work.

Biological hosts (such as enzymes and nucleic oligomers) have had millions of years to evolve into the effective hosts that are seen. Synthetic hosts have by contrast only had a little over half a century to develop and, therefore, considerable limitations are found within synthetic recognition systems, particularly in the form of the absence of significant, strong interactions between host and guest molecules.[18] Thus, compared to their natural counterparts, synthetic host molecules are relatively limited. In addition, very few of these synthetic hosts have enforced cavities through which to accommodate guest molecules.[12]

It is generally regarded that the three most common types of host [19] thus far reported by researchers in the field of host-guest chemistry are cyclodextrins (CDs), crown ether-based hosts and arene-based systems.

1.2.2 Cyclodextrins

Due to the lack of obvious synthetic hosts with cavities sufficiently large enough to accommodate guests, much of the pioneering research into host-guest chemistry was undertaken using molecules obtained from natural sources. Cyclodextrins (CDs) represent one of the more common of these naturally synthesised molecules. CDs are regarded as the molecules through which the interest in three-dimensional cavitied hosts originated.[20] Much of the initial research into the use of CDs as hosts was undertaken by Cramer [21, 22] who focused research towards the inclusion complexes resulting from CDs; this as early as the 1950's. CDs are used extensively today as host molecules in wide ranging applications, more recently most notably in the pharmaceutical industry. Exhaustive reviews pertaining to applications are available.[23-25]

CDs are the product of enzyme-catalyzed digestion of starch, the most common of which are α, β and γ CD composed of six, seven or eight glucopyranoside units, respectively, cyclically bound in a head to tail fashion,[22] as seen in Figure 1.3.[26]

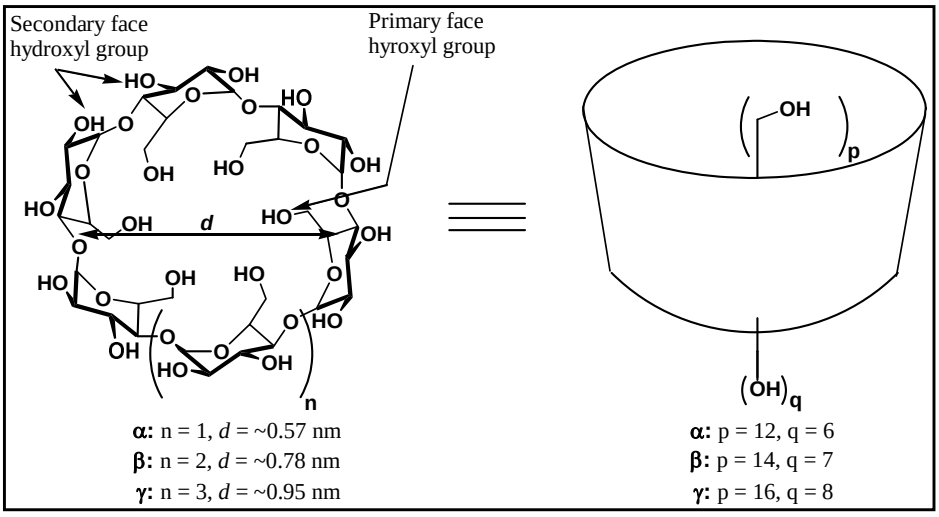

Figure 1.3: Structures and characteristics of α, β and γ cyclodextrins.

As depicted in Figure 1.3, the ether oxygen atoms and their associated hydrogen atoms face inward, with the hydroxyl groups outward. This results in a bowl-shaped hydrophobic cavity in the centre of the macrocycle into which guests can be bound in addition to offering substituent groups (the hydroxyl groups) that can easily be functionalised at the primary and secondary faces of the macrocycle.[17] This arrangement and the properties of the macrocycle form perhaps a blueprint of properties which ideal host molecules should possess:

1. structural preorganisation and rigidity
2. an enforced hydrophobic cavity which guests can occupy
3. substituent groups which can be functionalised

CDs also illustrate the remarkable physico-chemical changes which guest molecules experience on inclusion into the cavity of a host molecule. These changes underline the importance of hosts with enforced cavities as a means of studying and mimicking biological processes. Guests can undergo:[25]

1. enhanced solubility
2. stabilisation (particularly for labile guest molecules)

3. decreased volatility and sublimation
4. physical isolation
5. managed uptake and release

CDs offer particularly attractive characteristics on which to build effective host molecules, and in addition are water soluble. These qualities make them particularly attractive in biomimetic research since biological processes occur in aqueous media. However, CDs generally need extensive functionalisation to ensure a rigid and predictable geometry. Moreover, as evident in Figure 1.3, the cavities of the three most common CDs range from 0.57 nm to 0.95 nm. Given that for an ideal host-guest system, the guest size and shape is complementary to that of the host, CD cavity size proves to be too large for the majority of guests, making CDs unattractive as hosts for many applications.[27]

1.2.3 Crown Ethers

As the second class of supramolecular host molecules, crown ethers represent a milestone; that of the first truly synthetic host molecules. Among the more appealing and simplest macrocyclic structures,[6] their discovery by Pedersen [28] (1987 Nobel Prize laureate) was both fortuitous and important, for it showed that host-guest complexes were a synthetic possibility.

Crown ethers are structurally very simple, consisting of a cyclic arrangement of ether oxygen atoms linked by organic bridges, usually -CH_2-CH_2- carbon (ethyl) spacers.[29] Their ability to act as host molecules is primarily due to the oxygen atoms present in the crown structure; as shown in Figure 1.4.

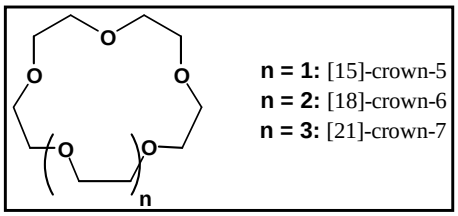

Figure 1.4: Structure of the three most common crown ethers.

Heteroatoms other than oxygen, in particular nitrogen and sulphur, have also been included as part of crown macrocycles. Extensive reviews covering crown ethers and their derivatives are available.[30, 31]

The heteroatoms, as excellent Lewis bases, are able to interact with potential guests and allow for their coordination into the cavity of the macrocycle. Guests are usually metal cations (including lanthanide species), but anions and neutral guests have also been known to be coordinated by crown ethers.[6, 31, 32] Due to their cyclic nature, these molecules are known to have a high degree of selectivity with regards to guest coordination, particularly in cation binding. The cavity for [15]-crown-5 is particularly complementary to the size of a sodium cation, that of [18]-crown-6 for potassium cations, and [21]-crown-7 for cesium cations.[6] Crown ethers therefore show a degree of size selectivity for cationic guests. It should be noted, however, that the apparent "hole-size relationship" alone does not account for the degree of selectivity seen in its entirety: the effective nuclear charge of the cations has a significant influence on complex formation and stability.[33]

The cation coordination abilities of crown ethers are illustrated in Figure 1.5 [14] using [18]-crown-6 as an example.

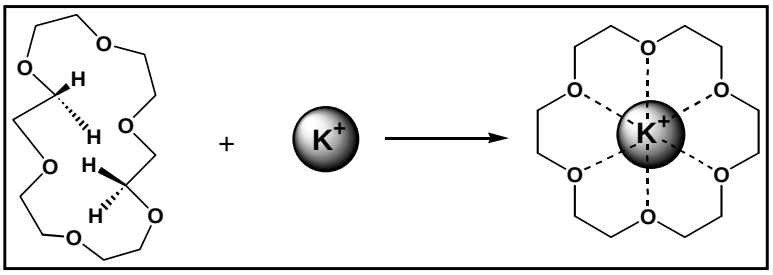

Figure 1.5: The selective potassium coordinating ability of [18]-crown-6.

Crown ethers can undergo a degree of functionalisation at the heteroatoms and at the ethyl bridges to allow for the incorporation of rigidity into the crown ether structure. Functionalisation includes the incorporation of aromatic residues as bridges, as well as the appending of aromatic and crown residues to heteroatoms.[31, 32] Crown ethers have also been elaborated *via* functionalisation with binaphthyl-based substituents into receptors capable of enantiomeric recognition of chiral amine derivatives, amino acids and other biologically important molecules. A review of such crown macrocycles has been published.[34]

In perhaps the first example of three dimensional synthetic hosts, J-M Lehn used Pedersen's crown ether macrocycles as a basis on which to construct cryptands.[1] By using a bicyclic macrocycle, it was anticipated that metal cations in particular could be completely incarcerated

within the crown-like three dimensional cavity. Such an arrangement becomes beneficial in terms of cation selectivity and transport. The structures of the most common members of the cryptand family can be seen in Figure 1.6.[6]

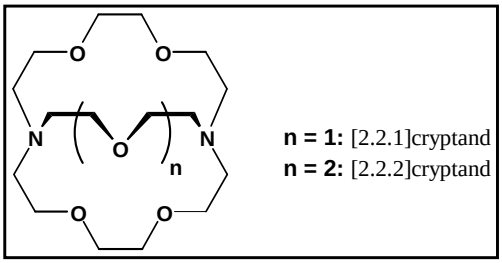

Figure 1.6: Structure of the two most common cryptands.

For [2.2.2]cryptand, relative to its crown ether analogue [18]-crown-6, it too coordinates potassium cations selectively due to the similarity in cavity sizes. However, its ability to bind to potassium cations is four orders of magnitude larger than that of its crown ether analogue.[1] This enhanced binding ability of the cryptand is solely due to the three dimensional cavity of the macrocycle, which allows for a degree of spherical recognition to occur among metal cations.[6] This situation is repeated in the case of [2.2.1]cryptand, where the binding of sodium cations is significantly enhanced relative to the crown ether analogue.

1.2.4 Arene-based Systems

As the third class of host molecules, arene-based hosts are arguably the most extensively researched type of host. The versatility and stability of aromatic structures has undoubtedly led to their popularity, and there exists a multitude of such host systems all bearing unique structures, properties and applications. Among the more common of these hosts are spherands, cyclotriveratrylenes, cryptophanes, cyclophanes and calixarenes. Sample structures of these hosts can be seen in Figure 1.7.[33, 35-37]

It is clear from Figure 1.7 that the different hosts have varying structures, and different cavities in terms of both shape and depth. However, it is calixarenes and their related hosts which are of interest in this study due to their inherent bowl-shaped cavity (evident above in Figure 1.7) of sufficient depth to accommodate guests. Reviews pertaining to the other arene-based variants referred to above are available.[35-37]

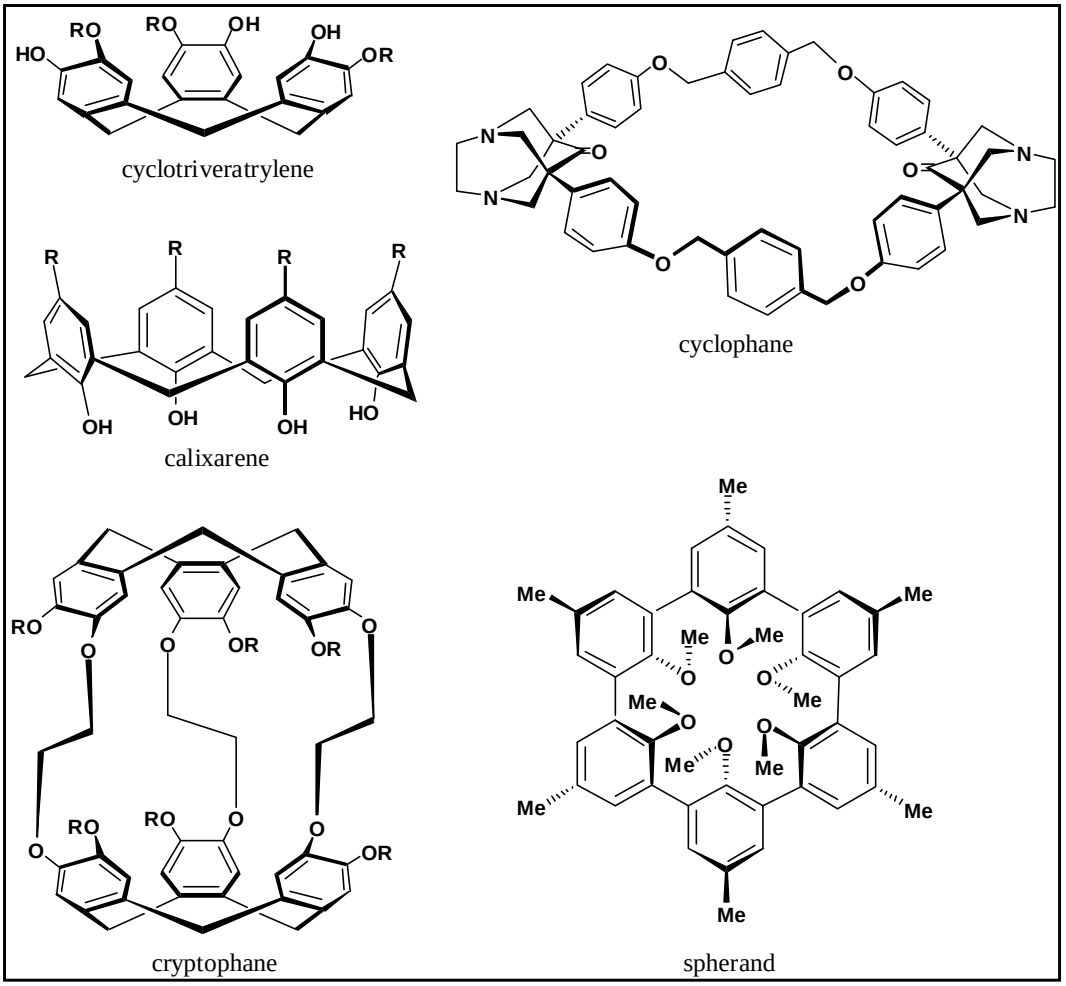

Figure 1.7: Sample structures of arene-based host variants.

1.3 Calixarenes and Related Macrocycles

1.3.1 Calixarenes

Calixarene chemistry is arguably among the earliest synthetic chemistry, with research (on the then largely uncharacterised compounds) dating back to as early as 1872. It was not until C.D. Gutsche's work on the construction of suitable enzyme mimics in 1972, however, that calixarenes were formally characterised.[6, 38] Known more appropriately as calix[*n*]arenes where *n* refers to the number of aromatic residues in the macrocycle,[38, 39] calixarenes are a family of cyclic oligomers which are products of the alkaline condensation of *p*-alkylphenols with formaldehyde.[38] Conditions during synthesis may be varied so that aromatic residues in

the macrocycle can number from a minimum of four (for the most common macrocycle, calix[4]arene) to as many as sixteen.[6, 39, 40] It can be seen in Figure 1.8 [39, 41] that calix[4]arenes possess a bowl shape much like CDs, thus facilitating their use as effective host molecules. However, this class of host molecule has a cavity size smaller to those seen in CDs.

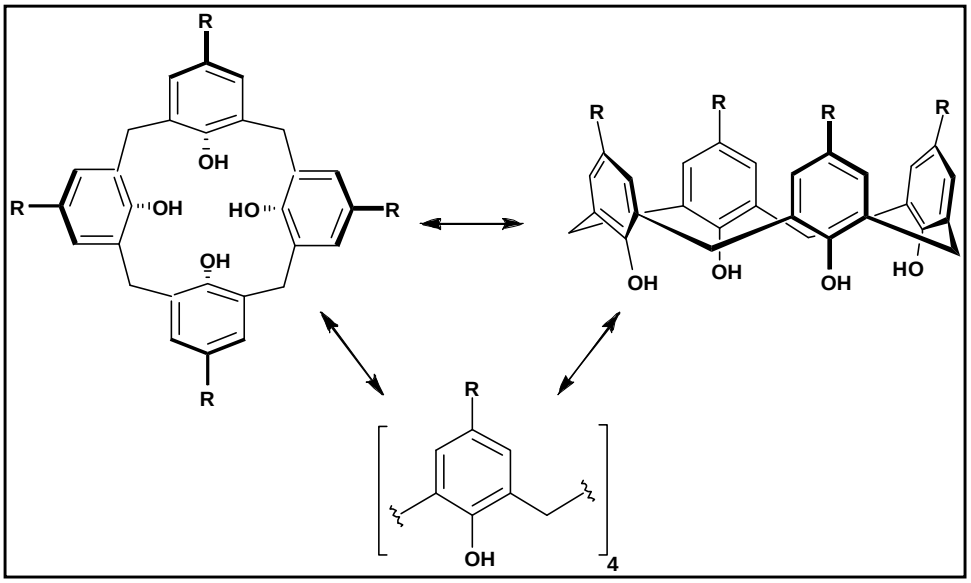

Figure 1.8: The general structure of calix[4]arene.

As with CDs, calix[*n*]arenes can be extensively modified, particularly at the phenolic hydroxyl group, and on the aromatic rings, at the extra-annular (R) position *para* to the hydroxyl group.[36, 41, 42] Therefore, the number of calix[*n*]arene derivatives is vast, allowing the use of calix[*n*]arenes to act as hosts for metal cations, particularly those of the alkali earth metals,[43] as well various lanthanides and actinides,[43a, 44] organic cations,[45] anions [46] and neutral molecules.[47] Reviews dealing with the different types of calixarene derivatives and their applications are available.[48]

However, what makes calix[*n*]arenes more versatile than CDs and crown ethers is that, through facile modification, control over calix[*n*]arene conformation can be achieved. As shown in Figure 1.9,[42] calix[4]arene can exist in four different conformers, due to the free rotation possible about the methylene spacers between the aromatic residues. The conformation that calix[4]arene takes on can be greatly influenced by functionalisation of the phenolic hydroxyl group and at R (Figure 1.8).[41]

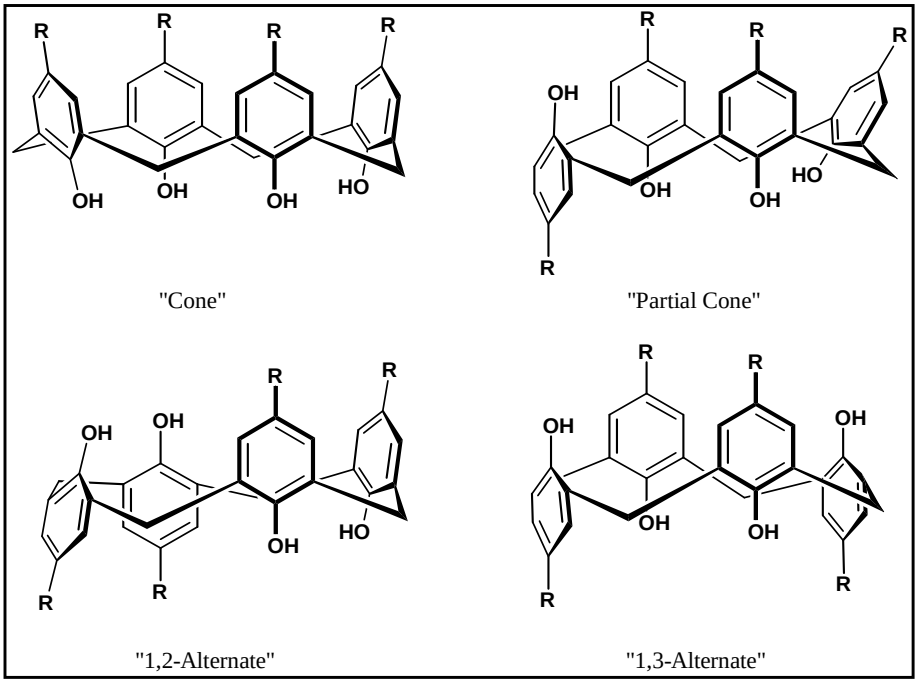

Figure 1.9: The four stable conformers of calix[4]arene.

In solution, however, a *cone* conformation with C_{4v} symmetry is preferred, largely due to the stabilisation offered by the intramolecular hydrogen bonding that occurs between the hydroxyl groups present as seen in Figure 1.10.[37]

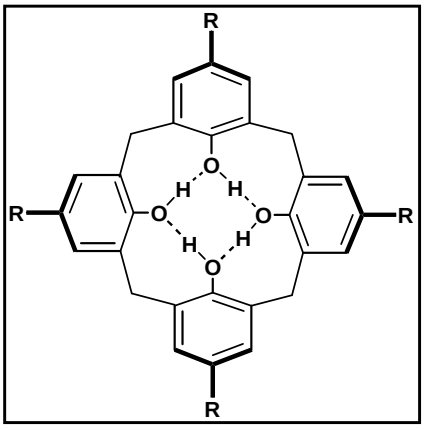

Figure 1.10: The hydrogen bonding present in the *cone* conformer of calix[4]arene.

The high degree of symmetry of the *cone* conformation makes it a particularly attractive and effective host. Ideally, host binding sites should be spaced somewhat apart from one another so as to minimise any repulsive forces which may arise between them, but arranged so as to allow for simultaneous interaction with guests. Such a design allows for more favourable host-guest

interaction and a more stable complex.[6, 49] This highly symmetrical conformation allows for a more effective host molecule.

Calix[4]arenes are clearly versatile hosts, able to accommodate a wide variety of guests. They are also versatile in terms of functionalisation and can be customised to provide cavities of varying shape (as seen by possible conformers). However, although enhancing their versatility, their ability to change conformation, as seen in Figure 1.9, compromises the cone shape, which in turn compromises the favourable C_{4v} symmetry. Bearing in mind that the hydrogen bonding shown above offers some structural rigidity, a potential means of ensuring a more rigid macrocycle (thereby conserving symmetry) lies in a closely related calix[4]arene analogue, resorcin[4]arenes.

1.3.2 Resorcin[4]arenes

Resorcin[4]arenes, like calix[4]arenes, also possess a similar bowl-type shape, so can also be used as effective host molecules. However, synthesis, as established in particular by Högberg,[50] and structural properties of resorcin[4]arenes are remarkably different to those of calix[4]arenes.

Resorcin[4]arenes are the result of the acid-catalyzed condensation of aldehydes (notably, *except* formaldehyde) and resorcinol.[41] The use of resorcinol results in a significantly different structure to that of calix[4]arene, as seen in Figure 1.11.[6, 39, 51] It is immediately noticeable that resorcin[4]arenes have eight hydroxyl groups at the upper rim of the macrocycle, as opposed to four at the bottom of a calix[4]arene macrocycle. In addition, resorcin[4]arenes have two sites at which functionalisation can occur, R_1 and R_2. By changing the length and nature of the organic substituents at R_1, the 'feet' of the macrocycle, a degree of control over the resorcin[4]arene solubility can be attained. Functionalisation at the extra-annular position (R_2) allows a degree of control over the type of guest the cavity may interact with, depending on whether the guest is anionic, cationic or neutral in nature.

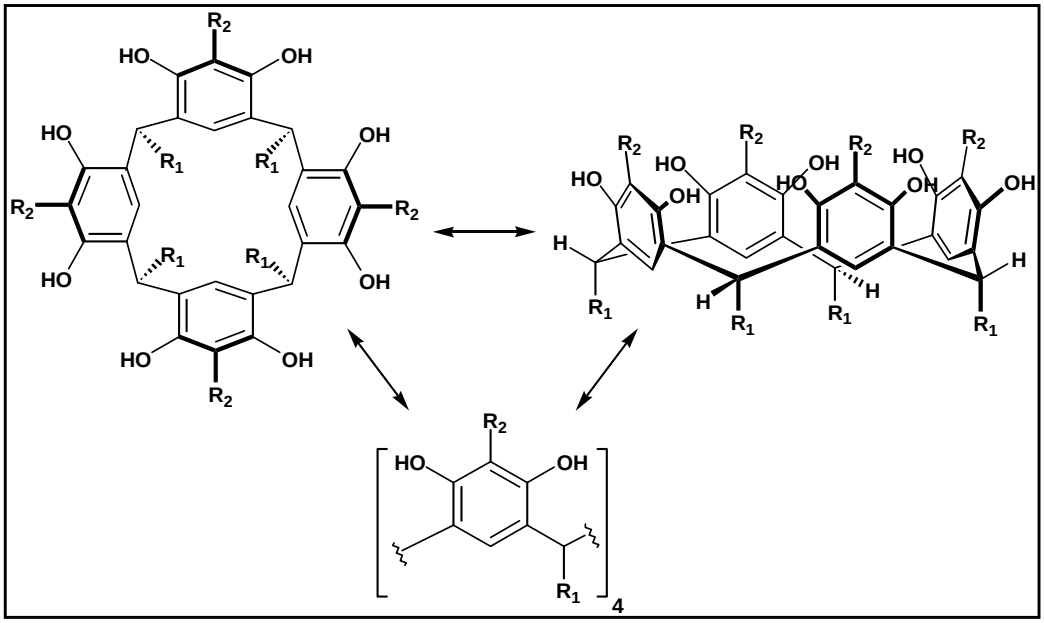

Figure 1.11: The general structure of resorcin[4]arene.

As in the case of calix[4]arenes, the hydroxyl groups are hydrogen bonded to each other as shown in Figure 1.12,[6] which stabilises resorcin[4]arenes such that it preferentially assumes a cone-type structure again possessing C_{4v} symmetry. However, since the hydroxyl groups are on the upper rim, the hydrogen bonding results in a wider and shallower cavity for resorcin[4]arenes relative to calix[4]arenes.[6]

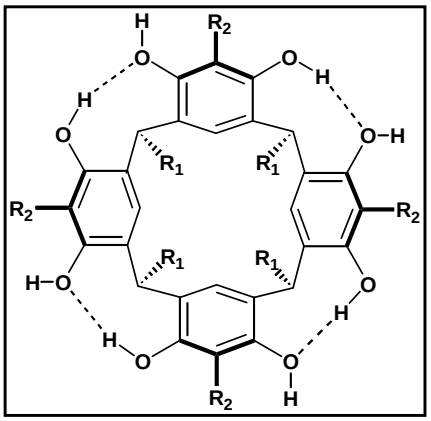

Figure 1.12: The hydrogen bonding present in the cone-type conformation of resorcin[4]arene.

Resorcin[4]arenes have five predominant arrangements in terms of macrocyclic conformers.[51] However, in contrast to calix[4]arenes, the interaction of hydroxyl groups and substituents (R_1 and R_2) in the structure of resorcin[4]arenes makes the macrocycle more rigid. Thus, unlike calix[4]arenes, resorcin[4]arenes are unable to undergo conformational interchange *via* free

rotation about the alkyl bridges connecting the four aromatic residues to “partial cone” or “alternate” structures (see Figure 1.9). What, therefore, results is a host whose basic cone shape is maintained by its structural properties, and whose symmetry is largely conserved.

1.3.3 Resorcinarene Cavitands

Resorcinarene cavitands, or more commonly cavitands, as pioneered by Cram *et al*.[52] represent a class of synthetic organic host macrocycles with an enforced cavity which is of a size suitable to accommodating guest molecules and ions.[51]

The synthesis of cavitands is accomplished relatively simply using resorcin[4]arenes as a basis from which to work. While resorcin[4]arenes are rigidified by relatively weak hydrogen bonding interactions (Figure 1.12), cavitands by contrast are rigidified by *covalent* interactions; that is, by covalently bonding adjacent hydroxyl groups. What results on completing such bridging is a cavitand, a host molecule that has a *fixed* cone shape with fixed C_{4v} symmetry, by virtue of the fact that cavitands have highly limited conformational flexibility. This therefore gives a particularly effective host molecule with perhaps ideal host qualities, in terms of both structural preorganisation and rigidity, and an enforced cavity to accommodate guests. The general structure of cavitands can be seen in Figure 1.13.[6, 51]

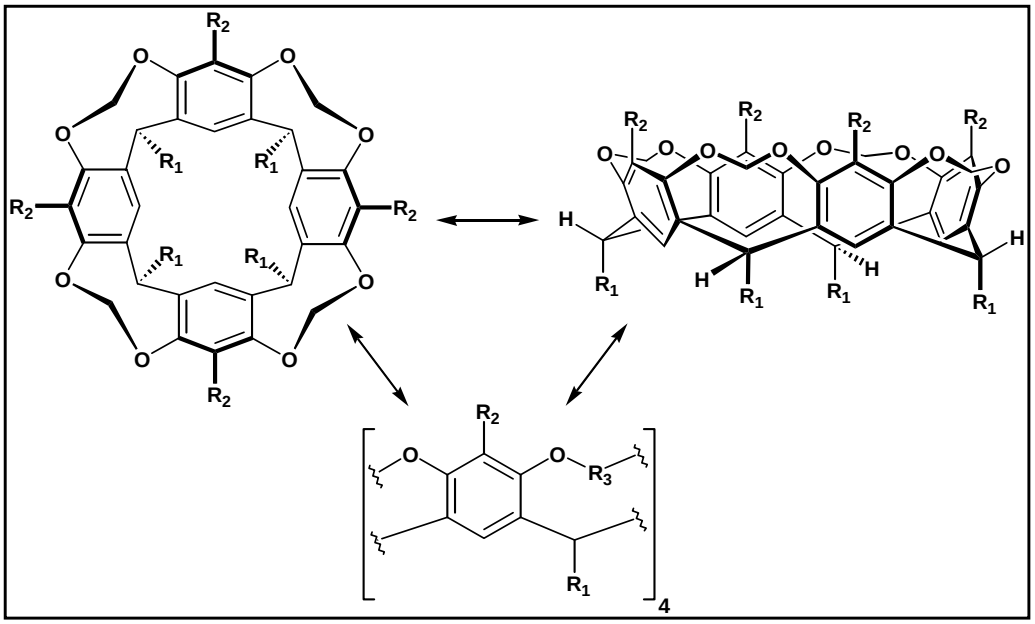

Figure 1.13: The general structure of a cavitand.

It can clearly be seen that by bridging the aromatic residues, they are bound to each other covalently on either side by two bonds. This clearly and completely inhibits any conformative lability, such that the cavitand has an enforced cone-shaped cavity. Methyl bridged cavitands ($R_3 = CH_2$) are most common, as shown in Figure 1.14, but ethyl and propyl bridges,[53] as well as silicon [19] and phosphorus [54] bridges have been reported.

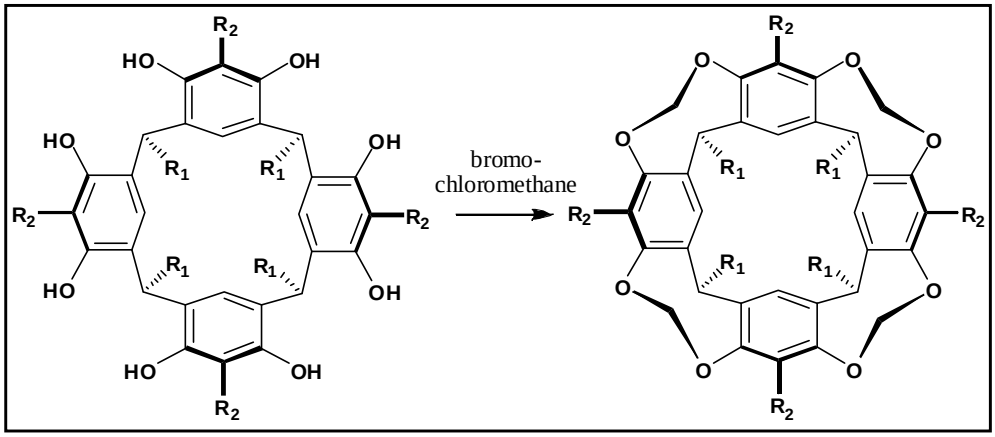

Figure 1.14: General synthesis of a methyl bridged cavitand.

As with resorcin[4]arenes, the feet of the cavitand at R_1 can be synthetically varied in its alkyl or aromatic character in order to control cavitand solubility. Cavitands have been made water soluble *via* the use of hydroxyl, glycolic and phosphate feet.[55, 56]

Extensive modifications can occur at R_2 depending on potential guests, be they anionic, cationic or neutral in nature. Modifications range from the attachment of simple alkyl chains and heteroatoms,[53] to aromatic and pyridinium substituents [57a] (able to complex *p*-cresol and *p*-toluenesulphonate), various hydroxyl and carboxylic groups [57b] (able to complex metal cations in aqueous medium), aromatic amines [57c] (able to complex cyclic adenosine monophosphate, as well as adenosine mono-, di-, and triphosphate), and other macrocyclic and supramolecular structures such as hexamethylenetetraamine [57d] and crown ethers [57e] (able to complex aromatic carboxylates and cations, respectively). All the reported complexes are 1:1 for host:guest.

More interesting modifications include the use of dendritic glycols which were used effectively to enhance the solubility of both cavitand and aromatic guest in aqueous medium,[56] as well as

peptide substituents which were used to complex species such as acetonitrile.[55, 57f] Complexes reported again exhibited 1:1 host:guest ratios.

Guest selectivity and cavity shape and depth can be controlled by varying the structure of the bridge. As mentioned, aromatic bridges may be introduced so adding to the number and nature of guests which can be accommodated into the cavitand cavity. Considered the second generation of cavitands, 'deeper' cavitands, as first synthesised by Cram *et al.*,[52] make use of bridges such as quinoxaline, as shown in Figure 1.15 [14] to produce a cavitand with 'walls'. This results in a cavity shaped like a vase, which is able to accommodate larger guest molecules within the cavity.

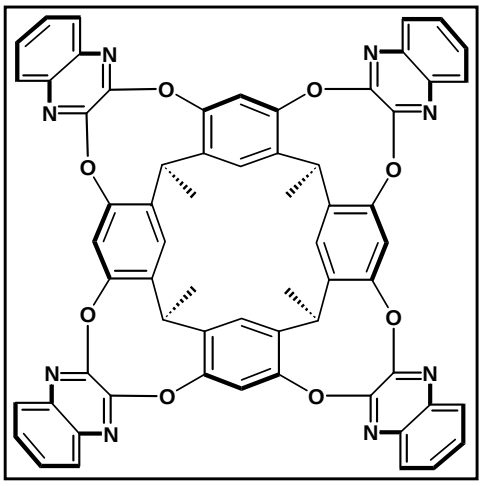

Figure 1.15: The structure of a deepened cavitand as synthesised by Cram *et al*.

Such cavitands are particularly effective in complexing large guests such as substituted benzenes and naphthalenes.[58] Deeper cavitands have also been elaborated such that very large guests such as C_{60} (fullerene) have been complexed within its cavity.[59]

Recently, Rebek *et al.* and Diederich *et al.* have used Cram's deeper cavitands as a basis on which to construct partially and asymmetrically bridged deeper cavitands which have found interesting applications. Rebek *et al.*[59, 60] have synthesised cavitands which have two or three quinoxaline moieties selectively placed resulting in a range of partially bridged cavitands. Rebek *et al.* have also varied bridging moieties. Cavitands with bridges bearing carboxymethylphosphonate substituents have been synthesised and used to selectively bind adamantane derivatives, quinuclidine, ammonium and phosphonium salts, as well as drugs such as ibuprofen.[61]

Very recently, imidazole bridged deeper cavitands have been used to synthesise cavitands of nanoscale proportions; such cavitands were capable of accommodating a series of trimethyl ammonium salts, the largest of which was 10 Å in length.[62] Imidazole bridged, water soluble cavitand derivatives bearing carboxylate groups have also been used as effective phase-transfer catalysts for a number of hydrophobic substrates. The cavitands were able to extract the hydrophobic substrates from the organic layer in a two-phase system, into the aqueous layer where reaction took place, due to their ability to accommodate guests into their hydrophobic cavities.[63] Long alkyl chains have also been appended to the imidazole bridges; such cavitands were observed to contain these alkyl chains inside the cavity, to yield a 'self-containing' host-guest system. Such cavitands stand to have applications as sensors.[64]

Similar deeper cavitands bearing imidazole moieties derivatised with benzoate groups have also been used to create 'revolving doors' on the cavitand through which to regulate binding rates and selectivities of alkanes, again in an aqueous medium.[65] In a slight variation on the imidazole based bridges, Rebek *et al.* have reported a cavitand bearing the amide precursors as bridges, with charged ammonium feet capable of mimicking the inner space of proteins.[66]

Salen and hexaamide diamino bridged cavitands have also been used to produce cavitands able to catalyze the aminolysis of choline derivatives, as well as act as receptors for phosphocholine esters.[67] Sample structures of these cavitands can be seen in Figure 1.16. Analogous cavitands have also been investigated as Diels-Alder catalysts of maleimides.[68] For examples on more elaborate cavitands, a review of the deeper and extended cavitands as synthesised by Rebek *et al.* is available.[69] A critical review of related water soluble cavitands is also available.[70] In more recent work, deepened cavitands have been further elaborated with the inclusion of chiral moieties into the bridge framework.[71] Despite showing only modest results in terms of enantioselectivity for chiral guests, the study represents the next step in terms of application for cavitand host molecules.

Diederich *et al.* have also synthesised partially bridged cavitands making use of quinoxaline walls; such cavitands have been used in the selective recognition of steroids.[72] In an adaption to the above deeper and extended cavitands, Diederich *et al.* have constructed cavitands with varying bridges; that is, cavitands that bear both quinoxaline and diazaphthalimide moieties, and

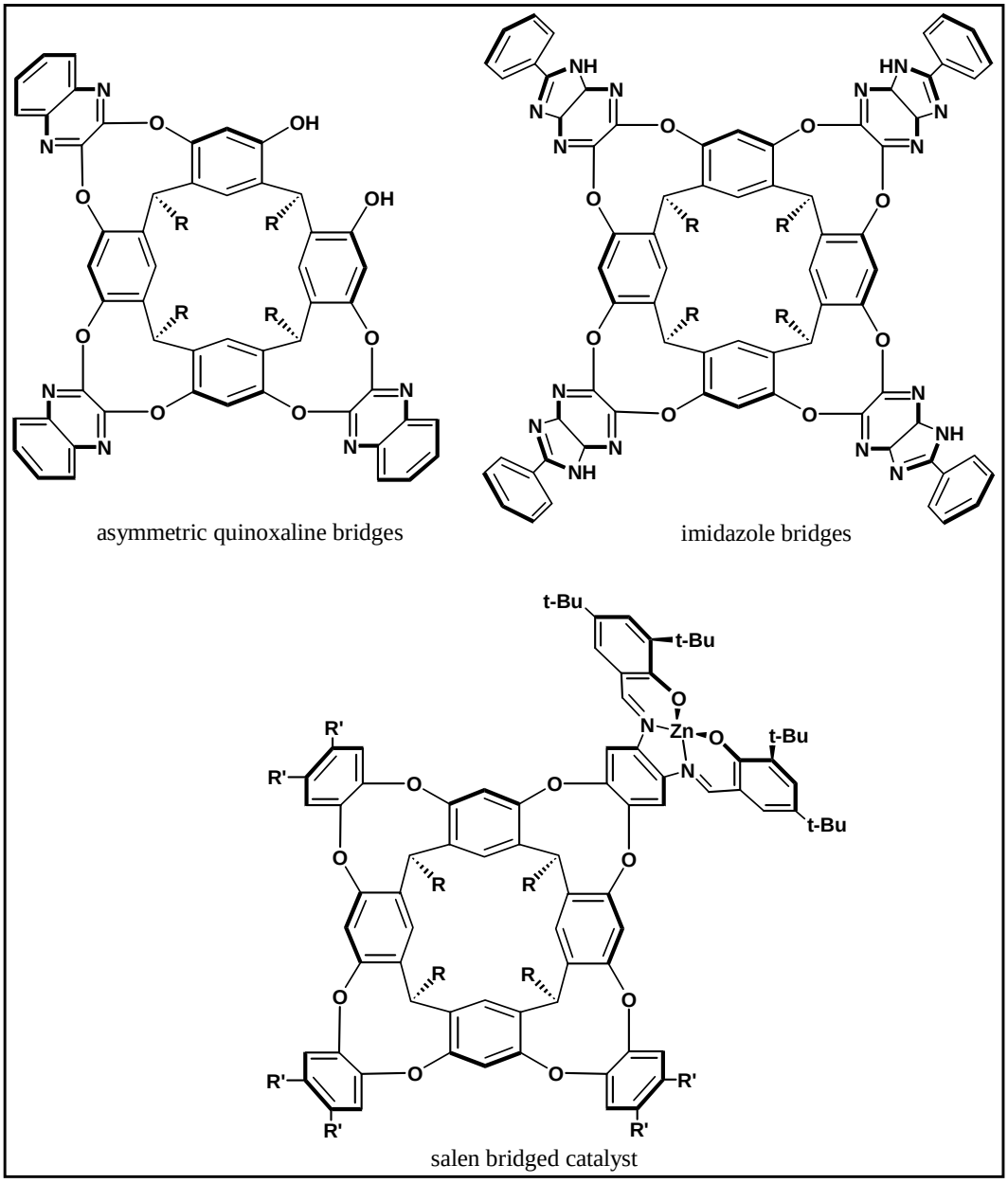

Figure 1.16: Sample structures of deeper cavitands, synthesised by Rebek *et al*.

quinoxaline and tetrathiafulvalene moieties, as walls.[73, 74] The diazaphthalimide moieties were further elaborated such that boron-based substituents were built into the cavitand walls. Sample structures can be seen in Figure 1.17.

In further elaboration of the diazaphthalimide moieties, alkynes have very recently been attached to the bridges to yield molecular containers able to selectively and reversibly complex cyclohexanes.[75] The hosts were able to switch between two different conformations to yield complexation that either showed a ratio of 1:1 for host:guest, or 1:2 depending on conformation.

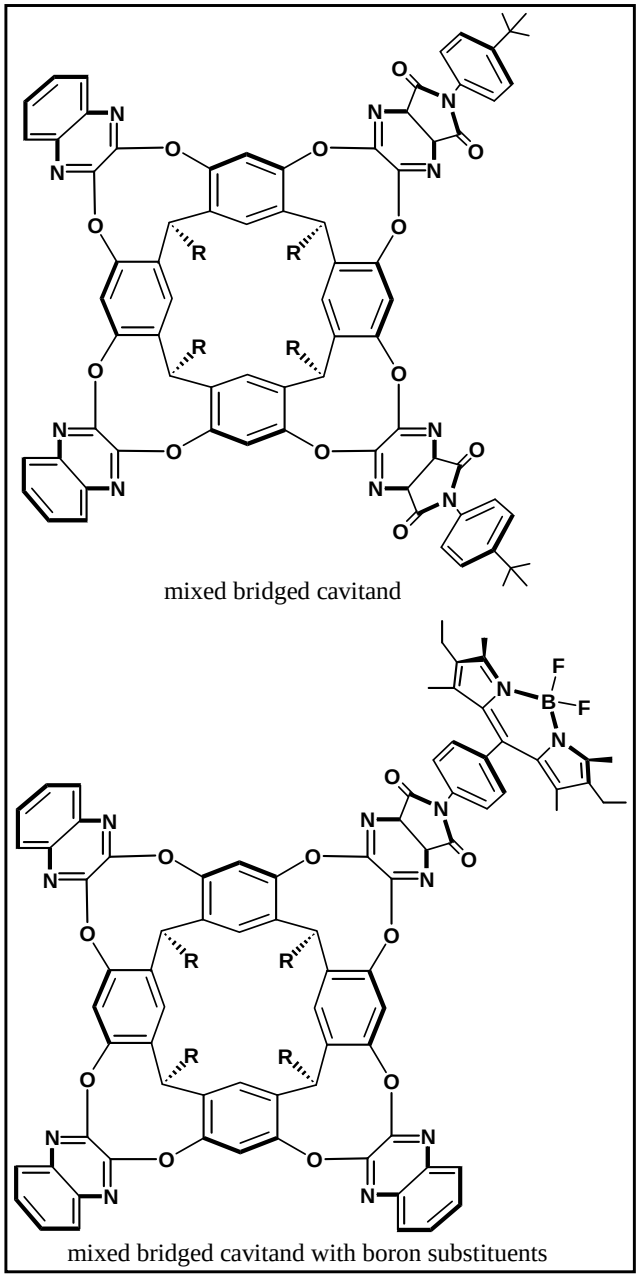

Figure 1.17: Sample structures of deeper cavitands, synthesised by Diederich *et al.*

In a similar study, Diederich *et al.* used cavitands bearing four quinoxaline-based moieties to investigate the controllability and reversibility of guest binding.[76] It was found that conformation had a fundamental influence on these parameters, as well as on the selectivity of binding interactions.

Cavitands, much like calix[*n*]arenes, have moreover been elaborated into [*n*]cavitands, where *n*, the number of aromatic residues, ranges from five to eight.[77] Such species stand to expand the

applications for cavitands, particularly in light of the fact that [6]cavitands and [7]cavitands possess *two* equally sized cavities as opposed to one for all other cavitands.

In conclusion, therefore, cavitands prove to be remarkably suitable structurally preorganised and rigid synthetic host macrocycles with enforced three dimensional cavities. As illustrated, they are exceptionally versatile and easily adapted to complex to a variety of guests. More fundamentally though, they are readily synthesised making them especially accessible and an ideal basis from which to study biomimetic systems.

REFERENCES

1. J-M. Lehn, *Supramolecular Chemistry Concepts and Perspectives*, VCH, Weinheim **1995**.
2. For general information on Chemistry Prize winners, and Nobel lecture manuscripts, see http://nobel.org/
3. H-J. Schneider, A. Yatsimirsky, *Principles and Methods in Supramolecular Chemistry*, Wiley, Chichester **2000**.
4. F. Vogtle, *Supramolecular Chemistry*, Wiley **1991**.
5. W. Kaim, B. Schwederski, *Bioinorganic Chemistry: Inorganic Elements in Chemistry of Life*, Wiley, Chichester **1994**.
6. J.W. Steed, J.L. Atwood, *Supramolecular Chemistry*, Wiley, Chichester **2000**.
7. P. Ehrlich, *Studies in Immunity*, Wiley NY **1906**.
8. E. Fischer, *Ber. Deutsch. Chem. Ges.*, **1894**, *27*, 2985.
9. A. Werner, *Zeitschr. Anorg. Chem.*, **1893**, *3*, 267.
10. ***a)*** D. M. Rudkevich, *Angew. Chem.*, **2004**, *116*, 568-581; ***b)*** D. M. Rudkevich, *Angew. Chem. Int. Ed. Engl.*, **2004**, *43*, 558-571, and references therein.
11. N. Kobayashi, K. Mizuno, T. Osa, *Inorg. Chim. Acta*, **1994**, *224*, 1-3.
12. D.J. Cram, *Science*, **1974**, *183* , 803-809.
13. D.J. Cram, J.M. Cram, *Container Molecules and Their Guests*, Monographs in Supramolecular Chemistry, RSC **1994**.
14. D.J. Cram, *The Design of Molecular Hosts, Guests, and Their Complexes*, Nobel Prize Lecture, *Angew. Chem. Int. Ed. Engl.*, **1988**, *27*, 1009-1020.
15. A.J. Kirby, *Angew. Chem. Int. Ed. Engl.*, **1996**, *35*, 707-724.
16. Picture adapted from http://ghs.gresham.k12.or.us/.../notes/chpt8/chpt8.htm
17. D.J. Cram, R.C. Helgeson, L.R. Sousa, J.M. Tinko, M. Newcomb, P. Moreau, F. de Jong, G.W. Gokel, D.H. Hoffman, L.A. Domeier, S.C. Peacock, K. Madan, L. Kaplan, *Pure Appl. Chem.*, **1975**, *43*, 327-349.
18. J. Nakazawa, J. Hagiwara, M. Mizuki, Y. Shimazaki, F. Tani, Y. Naruta, *Angew. Chem. Int. Ed. Engl.*, **2005**, *44*, 3744-3746.
19. A. Robertson, S. Shinkai, *Coord. Chem. Rev.*, **2000**, *205*, 157-199.
20. J. Rebek Jr, D. Rudkevich, *Eur. J. Org. Chem.*, **1999**, 1991-2005.
21. F. Cramer, *Rev. Pure Appl. Chem.*, **1955**, *5*, 143-164.
22. J. Szejtli, *Chem. Rev.*, **1998**, *98*, 1743-1753.
23. *Chem. Rev.* **1998**, *volume 98*, number 5.

24. E.M.M. Del Valle, *Process Biochem.*, **2004**, *39*, 1033-1046.
25. M. Singh, R. Sharma, U.C. Banerjee, *Biotechnol. Adv.*, **2002**, *20*, 341-359.
26. E. Engeldinger, D. Armspach, D. Matt, *Chem. Rev.*, **2003**, *103*, 4147-4173.
27. R. Breslow, S.D. Dong, *Chem. Rev.*, **1998**, *98*, 1997-2011.
28. C.J. Pedersen, *J. Am. Chem. Soc.*, **1967**, *89*, 7017 & 1967; ***b)*** C.J. Pedersen, *ibid.*, **1967**, *89*, 2495 & 1967.
29. G.W. Gokel, *Crown Ethers*, RSC, Cambridge **1990**.
30. R.M. Izzat, K. Pawlak, J.S. Bradshaw, R.L. Bruening, *Chem. Rev.*, **1995**, *95*, 2529-2586.
31. Y. Habata, S. Akabori, J.S. Bradshaw, R.M. Izzat, *Ind. Eng. Chem. Res.*, **2000**, *39*, 3465-3470.
32. ***a)*** M. Kodama, T Koike, A.B. Mahatma, E. Kimura, *Inorg. Chem.*, **1991**, *30*, 1270-1273; ***b)*** M. Kodama, A.B. Mahatma, T. Koike, E. Kimura, *Bull. Chem. Soc. Jpn.*, **1990**, *63*, 2639-2645.
33. ***a)*** G.W. Gokel, W.M. Leevy, M.E. Weber, *Chem. Rev.*, **2004**, *104*, 2723-2750; ***b)*** G.W. Gokel, D.M. Goli, C. Minganti, L. Echegoyen, *J. Am. Chem. Soc.*, **1983**, *105*, 6786-6788.
34. X.X. Zhang, J.S. Bradshaw, R.M. Izzat, *Chem. Rev.*, **1998**, *98*, 3313-3361.
35. ***a)*** A. Collet, *Tetrahedron*, **1987**, *43*, 5725-5759; ***b)*** M.J. Hardie, *Struct. Bond.*, **2004**, *111*, 139-174; ***c)*** M.J. Hardie, R. Ahmad, C.J. Sumby, *New J. Chem.*, **2005**, *29*, 1231-1240.
36. ***a)*** V.V. Kane, W.H. Dewolf, F. Bickelhaupt, *Tetrahedron*, **1994**, *50*, 4575-4622; ***b)*** F. Diederich, D.R. Carcanague, *Helv. Chim. Acta*, **1994**, *77*, 800-818; ***c)*** D. Heber, P. Rosner, W. Tochtermann, *Eur. J. Org. Chem.*, **2005**, 4231-4247.
37. ***a)*** W. Verboom, D.N. Reinhoudt, *Macrocyclic Synthesis*, Oxford University Press, Oxford **1996**; ***b)*** E. Maverick, D.J. Cram, *Comprehensive Supramolecular Chemistry*, Elsevier, Oxford, **1996**; ***c)*** D.J. Cram, *Angew. Chem. Int. Ed. Engl.*, **1986**, *98*, 1009-1020
38. C.D. Gutsche, *Calixarenes*, RSC Cambridge **1989.**
39. W. Sliwa, M. Deska, *Chem. Heterocycl. Compd.*, **2002**, *38*, 646-667.
40. ***a)*** C.D Gutsche, M. Iqbal, *Org. Synth.*, **1990**, *68*, 234-237; ***b)*** C.D. Gutsche, B. Dharwan, M. Leonis, D. Steward, *ibid.*, **1990**, *68*, 238-242; ***c)*** J.H. Munch, C.D. Gutsche, *ibid.*, **1990**, *68*, 243-246; ***d)*** A. Knop, V. Bohmer, L.A. Pilato, *Comprehensive Polymer Science, Vol. 5*, Pergamon Press, Oxford **1989**; ***e)*** Y. Nakamoto, S. Ishida, *Makromol. Chem. Rapid Commun.*, **1982**, *3*, 705-707.

41. V. Bohmer, *Angew. Chem. Int. Ed. Engl.*, **1995**, *34*, 713-745.
42. A. Ikeda, S. Shinkai, *Chem. Rev.*, **1997**, *97*, 1713-1734.
43. ***a)*** J.M. Harrowfield, M.I. Ogden, W.R. Richmond, A. H. White, *J. Chem. Soc. Dalton Trans.*, **1991**, 2153-2160; ***b)*** H. Otsuka, K. Araki, T. Sakaki, K. Nakashima, S. Shinkai, *Tetrahedron Lett.*, **1993**, *34*, 7275-7278; ***c)*** C.D. Gutsche, L.J. Bauer, *J. Am. Chem. Soc.*, **1985**, *107*, 6052-6059.
44. ***a)*** J.M. Harrowfield, M.I. Ogden, A. H. White, *J. Aust. Chem.*, **1991**, *44*, 1237-1247; ***b)*** J.M. Harrowfield, M.I. Ogden, A. H. White, *ibid.*, **1991**, *44*, 1249-1262; ***c)*** Z. Asfari, J.M. Harrowfield, M.I. Ogden, J. Vincens, A. H. White, *Angew. Chem. Int. Ed. Engl.*, **1991**, *30*, 854-856; ***d)*** J.M. Harrowfield, M.I. Ogden, A. H. White, *J. Chem. Soc. Dalton Trans.*, **1991**, 979-985; ***e)*** J.M. Harrowfield, M.I. Ogden, A. H. White, *ibid.*, **1991**, 2625-2632.
45. J.M. Harrowfield, M.I. Ogden, W.R. Richmond, B.W. Skelton, A. H. White, *J. Chem. Soc. Perkin Trans. 2*, **1993**, 2183-2190.
46. ***a)*** P.D. Beer, Z. Chen, A.J. Goulden, A. Grieve, D. Hesek, F. Szemes, T. Wear, *J. Chem. Soc. Chem. Comm.*, **1994**, 1269-1271; ***b)*** J. Schreerder, M. Fochi, J.F.J. Engbersen, D.N. Reinhoudt, *J. Org. Chem.*, **1994**, *59*, 7815-7820.
47. C.D. Gutsche, K.C. Nam, *J. Am. Chem. Soc.*, **1988**, *110*, 6153-6162; ***b)*** C.D. Gutsche, I. Alam, *Tetrahedron*, **1988**, *44*, 4689-4694.
48. ***a)*** V. Boehmer, *Chemistry Of Phenols 2*, Wiley, Chichester, **2003**; ***b)*** P.D. Beer, E.J. Hayes, *Coord. Chem. Rev.*, **2003**, *240*, 169-189; ***c)*** C. Redshaw, *Coord. Chem. Rev.*, **2003**, *244*, 45-70; ***d)*** S.E. Matthews, P.D. Beer, *Supramolecular Chemistry* **2005**, *17*, 411-435.
49. J.-M Lehn, *Pure Appl. Chem.*, **1994**, *66*, 1961-1966.
50. A.G.S. Högberg, *J. Am. Chem. Soc.*, **1980**, *102*, 6046-6050.
51. P. Timmerman, W. Verboom, D.N. Reinhoudt, *Tetrahedron*, **1996**, *52*, 2663-2704.
52. J.R. Moran, S. Karbach, D.J. Cram, *J. Am. Chem. Soc.*, **1982**, *104*, 5826-5828.
53. D.J. Cram, S. Karbach, H-E Kim, C.B. Knobler, E.F. Maverick, J.L. Ericson, R.C. Helgeson, *J. Am. Chem. Soc.*, **1988**, *110*, 2229-2237.
54. L.M. Tunstadt, J.A. Tucker, E. Dalcanale, J. Weiser, J.A. Bryant, J.C. Sherman, R.C. Helgeson, D.J. Cram, *J. Org. Chem.*, **1989**, *54*, 1305-1312.
55. A.R. Mezo, J.C. Sherman, *J. Org. Chem.*, **1998**, *63*, 6824-6829.
56. O. Middel, W. Verboom, D.N. Reinhoudt, *Eur. J. Org. Chem.*, **2002**, 2587-2597.
57. ***a)*** M.H.B. Grote Gansey, F.K.G. Bakker, M.C. Feiters, H.P.M. Geurts, W. Verboom, D.N. Reinhoudt, *Tetrahedron Lett.*, **1998**, *39*, 5447-5450; ***b)*** S. Pellat-Rostaing, L.

Nicod, F. Chitry, M. Lemaire, *ibid.*, **1999**, *40*, 8793-8796; ***c)*** L. Sebo, F. Diederich, V. Gramlich, *Helv. Chim. Acta*, **2000**, *83*, 93-113; ***d)*** D-R. Ahn, T.W. Kim, J-I. Hong, *Tetrahedron Lett.*, **1999**, *40*, 6045-6048; ***e)*** F. Hamada, S. Ito, M. Narita, N. Nashirozawa, *ibid.*, **1999**, *40*, 1527-1530; ***f)*** C. Berghaus, M. Feigel, *Eur. J. Org. Chem.*, **2003**, 3200-3208.

58. E. Dalcanale, P. Soncini, G. Bacchilega, F. Ugozzoli, *J. Chem. Soc. Chem. Comm.*, **1989**, 500-502.
59. F.C. Tucci, D.M. Rudkevich, J. Rebek Jr, *J. Org. Chem.*, **1999**, *64*, 4555-4559.
60. ***a)*** D.M. Rudkevich, G. Hilmersson, J. Rebek, *J. Am. Chem. Soc.*, **1998**, *120*, 12216-12225; ***b)*** S.D. Starnes, D.M. Rudkevich, J. Rebek, *J. Am. Chem. Soc.*, **2001**, *123*, 4659-4669; ***c)*** S.L. Craig, S. Lin, J. Chen, J. Rebek, *ibid.*, **2002**, *124*, 8780-8781.
61. P. Arnheim, A. Shivanyuk, D.W. Johnson, J. Rebek, *J. Am. Chem. Soc.*, **2002**, *124*, 10349-10358.
62. E. Menozzi, H. Onagi, A.L. Rheingold, J. Rebek, *Eur. J. Org. Chem.*, **2005**, 3633-3636.
63. R.J. Hooley, S.M. Biros, J. Rebek, *Angew. Chem. Int. Ed. Engl.*, **2006**, *45*, 3517-3519.
64. R.J. Hooley, J. Rebek, *Org. Lett.*, **2007**, *9*, 1179-1182.
65. R.J. Hooley, H.J. Van Anda, J. Rebek, *J. Am. Chem. Soc.*, **2006**, *128*, 3894-3895.
66. S.M. Butterfield, J. Rebek, *J. Am. Chem. Soc.*, **2006**, *128*, 15366-15367.
67. ***a)*** A. Gissot, J. Rebek, *J. Am. Chem. Soc.*, **2004**, *126*, 7424-7425; ***b)*** S. Richeter, J. Rebek, *ibid.*, **2004**, *126*, 16820-16821; ***c)*** F.H. Zelder, R. Salvio, J. Rebek, *J. Chem. Soc. Chem. Comm.*, **2006**, 1280-1282.
68. R.J. Hooley, J. Rebek, *Org. Biomol. Chem.*, **2007**, *5*, 3631-3636.
69. ***a)*** B.W. Purse, J. Rebek, *Proc. Natl. Acad. Sci U.S.A.*, **2005**, *102*, 10777-10782; ***b)*** M.P. Schramm, J. Rebek, *Chem. Eur. J.*, **2006**, *12*, 5924-5933.
70. S.M. Biros, J. Rebek, *Chem. Soc. Rev.*, **2007**, *36*, 93-104.
71. E. Mann, J. Rebek, *Tetrahedron*, **2008**, *64*, 8484-8487.
72. M. Cacciarini, V.A. Azov, P. Seiler, H. Kunzer, F. Diederich, *J. Chem. Soc. Chem. Comm.*, **2005**, 5269-5271.
73. ***a)*** V.A. Azov, P.J. Skinner, Y. Yamakoshi, P. Seiler, V. Gramlich, F. Diederich, *Helv. Chim. Acta*, **2003**, *86*, 3648-3670; ***b)*** V.A. Azov, A. Beeby, M. Cacciarini, A.G. Cheetham, F. Diederich, M. Frei, J.K. Gimzewski, V. Gramlich, B. Hecht, B. Jaun, T. Latychevskaia, A. Lieb, Y. Lill, F. Marotti, A. Schlegel, R.R. Schlittler, P.J. Skinner, P. Seiler, Y. Yamakoshi, *Adv. Funct. Mater.*, **2006**, *16*, 147-156.
74. M. Frei, F. Diederich, *Helv. Chim. Acta*, **2006**, *89*, 2040-2057.
75. T. Gottschalk, B. Jaun, F. Diederich, *Angew. Chem. Int. Ed. Engl.*, **2007**, *46*, 260-264.

76. T. Gottschalk, P.D. Jarowski, F. Diederich, *Tetrahedron*, **2008**, *64*, 8307-8317.

77. C. Naumann, E. Roman, C. Peinador, T. Ren, B.O. Patrick, A.E. Kaifer, J.C. Sherman, *Chem. Eur. J.*, **2001**, *7*, 1637-1645.

CHAPTER 2

ENZYME BIOMIMESIS AND METALLOPORPHYRINS

2.1 Introduction

Living organisms successfully maintain numerous internal metabolic processes when in a healthy state.[1] Such processes and their equilibria are largely dependant on the action of a range of enzymes which, often in conjunction with cofactors and coenzymes, facilitate the biosynthesis and transport of biologically important compounds (such as vitamins), as well as the biodegradation of many other compounds (such as steroids, lipids, fatty acids and prostaglandins).[2] In the case of humans, enzymes are also vital in the metabolism of drugs and numerous toxins.[3] The ability of enzymes to play these roles in biological systems stems from their capability to catalyze a vast array of reactions, involving a multitude of substrates, in a highly efficient and selective manner. It is therefore of interest to scientists to gain a better understanding of enzyme function, and how their potential may be harnessed, through the study and use of simpler, synthetic abiotic analogues.

2.2 Biochemical Ligands

In looking at enzymes and their functions from a physico-chemical perspective, it is particularly important to note that in many cases the active centre of an enzyme is a metal, which is buried within the pocket of the protein constituting the enzyme.[1] More noteworthy, however, is that in the case of such metal centered enzymes, the ligand to which the metal is complexed is commonly macrocyclic in nature, and able to chelate to the metal *via* a number of Lewis bases (such as oxygen and nitrogen atoms).[4] Indeed, such macrocyclic arrangements are not limited exclusively to metal-centered enzymes, but are found to be key in a number of biological processes such as electron and energy transfer,[4-6] redox processes,[6] and the transport and storage of molecular oxygen.[4, 6, 7]

Bearing in mind that the metal complexes involved in such enzymes are often substitutionally labile, the preference for macrocyclic ligands lies in two important effects:[4, 8]

1. *The chelate effect:*
   Since the ligand complexes to the metal through more than one (multidentate) interaction, the resulting complex experiences enhanced stability (both thermodynamically and kinetically), particularly in solution.

2. *The macrocyclic effect:*
   Closely related to the chelate effect, the macrocyclic effect further enhances stability of the ligand-metal complex *via* the preorganisation of the chelating Lewis bases; binding energy is thus not exhausted on rearrangement of ligand binding sites.

Ligand-metal interactions and metal-centered enzymes in biochemistry, and in host-guest interactions as discussed in Chapter 1, are therefore synonymous with each other.

Biochemistry's preference for macrocyclic ligands is clearly illustrated in the complexes which constitute arguably among the most important biological processes: energy transfer and oxygen transport and storage. As the prime example of energy transfer,[5] photosynthesis is vital in the propagation of life on earth; as such, the chlorophylls as macrocyclic ligands are fundamental to biochemistry. Equally as important to life is hemoglobin and myoglobin, both of which are instrumental in the function of the mammalian respiratory systems, serving to complex and transport oxygen.[9] The structure of the active sites of these macrocyclic ligands can be seen in Figure 2.1.[4]

Based on the Fe(II) protoporphyrin XI, heme not only finds use in hemoglobin and oxygen uptake and transport, but also serves as the prosthetic ligand which constitutes the class of heme-based enzymes, the monooxygenases.[10] Such enzymes are readily used in the biosynthesis and biodegradation of lipids and steroids, and are also involved in the metabolism of drugs and toxins.[11] They facilitate an extensive array of important oxidation reactions, such as the epoxidation of alkenes and aromatic rings, hydroxylations of alkanes, and the transfer of

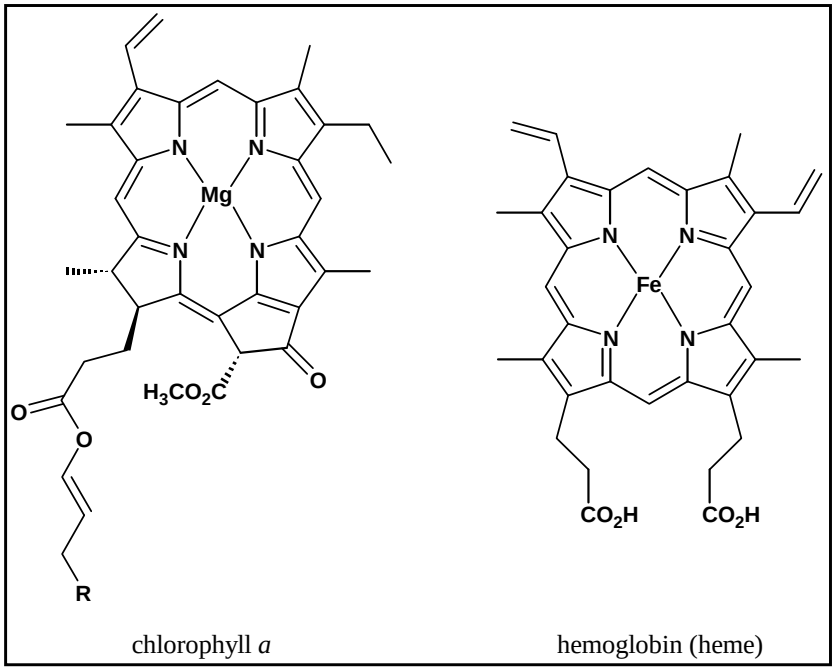

chlorophyll *a* hemoglobin (heme)

Figure 2.1: The structures of macrocyclic ligands important in biochemistry.

oxygen to amine nitrogen atoms and thioether sulphur atoms.[3, 11, 12] It is these heme based enzymes which are of interest in this study.

2.2.1 Tetrapyrrole Ligands

In looking at the structures in Figure 2.1, it is evident that the basic skeleton on which the macrocycles are based is very similar. These ligands form part of the broader class of tetrapyrrole ligands. It is this basic skeleton in particular which has seen these macrocycles used in a wide variety of conditions, where relatively strong and size-selective binding of main group and transition metals is necessary.[4]

Their significance can be attributed to their structural features which facilitate their excellent complexation abilities:[2, 4]

1. Tetrapyrroles are planar or near planar in structure, enhancing stability.
2. Bearing four nitrogen atoms, they are able to chelate to a metal cation, and are able to carry both a single and double negative charge, so allowing labile

cations to coordinate. Dissociation can only occur on the simultaneous severing of the four cation-nitrogen interactions.

3. Since the four nitrogen atoms are in a fixed position and the macrocycle rigid, the coordination of metal cations has a degree of size selectivity.
4. The coordination sites are in the plane of the macrocycle, allowing coordination of species from above and below the cation.
5. There is extensive conjugation that obeys Hückel's rule for aromaticity; so not only allowing tetrapyrroles good stability, but also extensive redox chemistry (the framework itself may be readily reduced).

The general structure of a tetrapyrrole ligand illustrating these structural properties can be seen in Figure 2.2,[4] which shows a basic porphyrin ligand forming a metalloporphyrin.

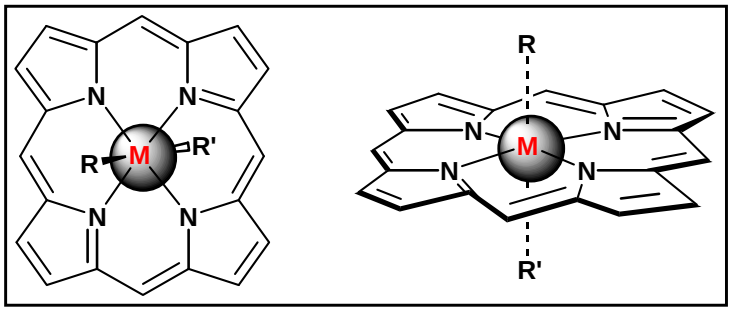

Figure 2.2: The general structure of tetrapyrrole-based ligands.

2.3 Heme-based enzymes

Heme-based enzymes represent a class of oxygenases which have outstanding oxidative catalytic abilities.[12] Extensive research has been undertaken on metalloporphyrins in order to mimic their catalytic abilities and harness their potential. However, in order to understand research into synthetic heme mimics, it becomes important to grasp the nature of biological heme enzymes in terms of their structure and function.

As mentioned, heme-based enzymes use as a structural basis a Fe(II) protoporphyrin XI ligand, which serves as the enzyme's active site. This moiety is situated within a protein pocket which governs substrate access to the site. Accessibility is regulated by the protein based on the shape and size of substrates; thus the protein pocket plays an important role in the selectivity of the enzyme.[1,12] In addition the iron metal centre is not only coordinated to the four nitrogen

Lewis bases of the protoporphyrin, but also has coordinated to it a proximal, fifth thiolate ligand from a cysteine residue (R' in Figure 2.2).[11]

This leaves a remaining sixth coordination site (R in Figure 2.2) where initially water, then dioxygen (which serves as the oxidant), is coordinated reversibly. It is from this coordination that the enzyme catalyzes the transfer of a single oxygen atom to substrates, which are present in close proximity. This catalysis thus occurs exclusively from one "face" of the ligand. The generally accepted mechanism of substrate oxidation can be seen below in Figure 2.3.[13] The structure of R can vary widely, ranging from simple aliphatic and aromatic structures to more complex, heteroatom-containing substrates, and is always found in close proximity to the active site of the enzyme.[6] In addition, while Figure 2.3 shows the hydroxylation of a substrate, the formation of aldehydes and carboxylic acids are also possible.

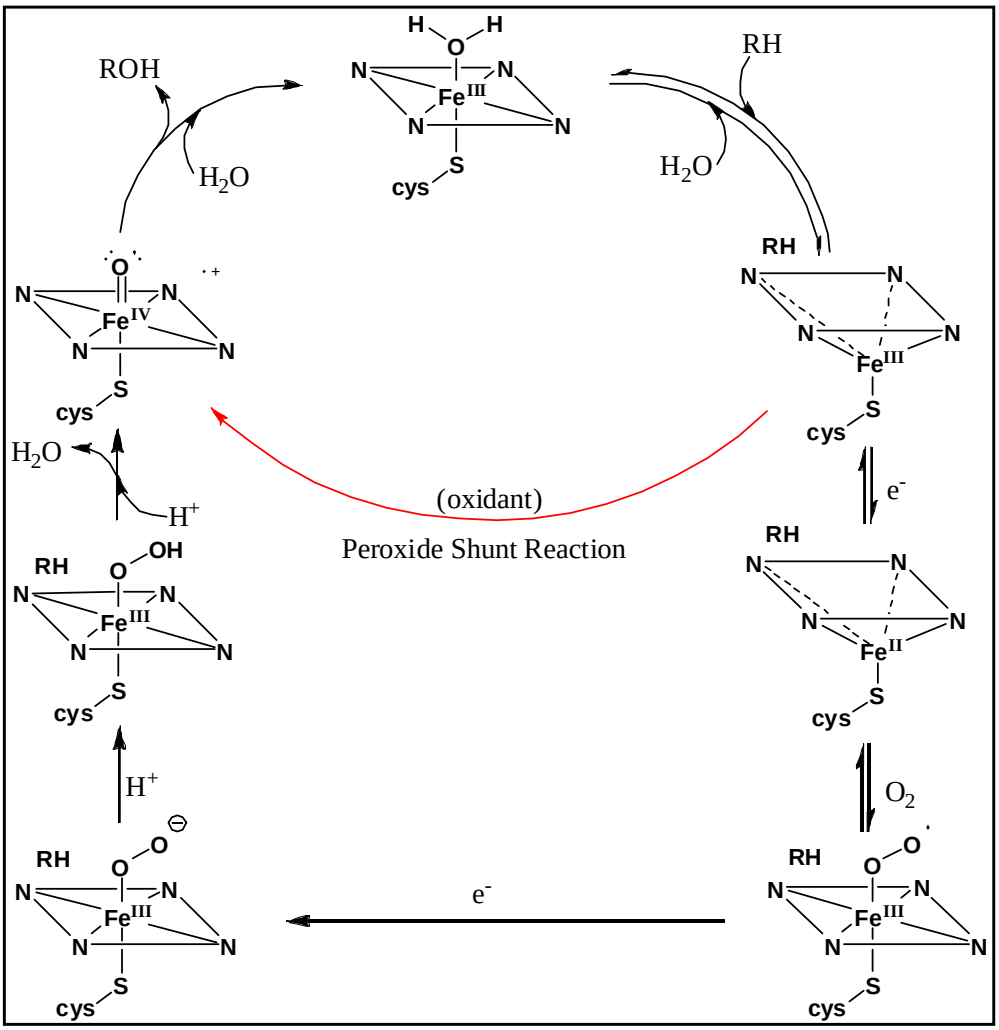

Figure 2.3: General (schematic) mechanism for substrate oxidation by heme-based enzymes.

The peroxide shunt reaction noted above is limited to synthetic models only, where the use of peroxide oxidants circumvents the reaction following the pathway shown when oxygen is used as oxidant. In-depth discussion of mechanistic aspects of heme-catalysed oxidation can be found in a recent review article, and the references cited therein.[14]

It is thought that the nature of oxidative chemistry (hydroxylation, epoxidation, etc., known as chemoselectivity) performed on the substrate as catalyzed by heme-based enzymes is dependant on the activity of the iron centre and the proximal cysteine ligand attached to it. Substrate selectivity, in contrast, is dependant on the nature and shape of the protein which constitutes the hydrophobic pocket in which the active protoporphyrin is found.[3] It is these two areas in particular which have been focal in much of the research into synthetic metalloporphyrin heme mimics.

2.4 Synthetic Heme Analogues: Sterically Hindered Porphyrins

Porphyrins and metalloporphyrins have become particularly useful synthetic macrocycles through which to study heme-based enzymes.[12] They are the product of the condensation of pyrrole with an aldehyde (usually benzaldehyde), and were first synthesised in low yield by Rothemund 70 years ago.[15] Since then, synthetic conditions have been largely revised by Adler *et al.*,[16] and more recently by Lindsey *et al*.[17] to give better yields

Their popularity as ligands in the study of heme analogues stems from their structural properties as evident in Figure 2.4 below,[4] which shows an abbreviated repeat unit structure for simplicity. It is immediately evident that synthetic porphyrin ligands have a basic skeleton identical to that of the heme protoporphyrin XI ligand; this is particularly useful given the excellent characteristics of tetrapyrrole macrocycles discussed above. Synthetic porphyrins can be readily functionalised at the *meso* and β-pyrrole positions (shown in Figure 2.4) thus allowing a degree of control over the steric environment in which the catalytically active site of the porphyrin may be established.[12] The substituents at the *meso* position (R, in Figure 2.4) are classically aromatic phenyl substituents, which themselves may bear further functional groups.

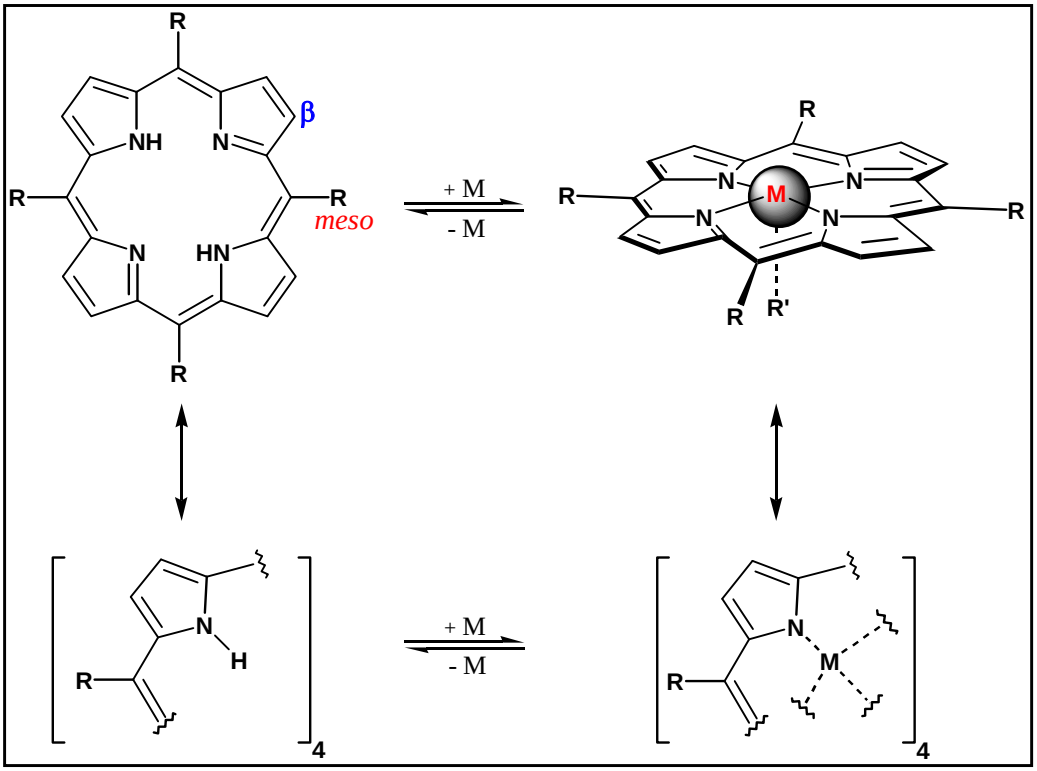

Figure 2.4: General structure of a porphyrin ligand.

In terms of modeling heme enzymes using porphyrins, it has been established [9b] that the following requirements must be satisfied in order to produce an effective model system:

1. The formation of a five-coordinate heme precursor having a proximal base (cysteine, pyridine, imidazole, etc), must be possible;
2. Structural properties of the porphyrin ligand must be such that irreversible oxidation is prevented.

With regards to the first requirement, by using a porphyrin ligand this condition is readily met, as can be seen by the presence of R' in Figure 2.4. It is the second requirement which has proven to be more difficult to meet.

Synthetic metalloporphyrins, particularly Fe(II) centered species in combination with a proximal base are extremely sensitive to air and light.[11] In the presence of molecular oxygen, the metalloporphyrins tend to undergo rapid and irreversible auto-oxidation to form the μ-oxo Fe(III) dimer, which is catalytically inactive.[18] This process is shown in Figure 2.5.[4]

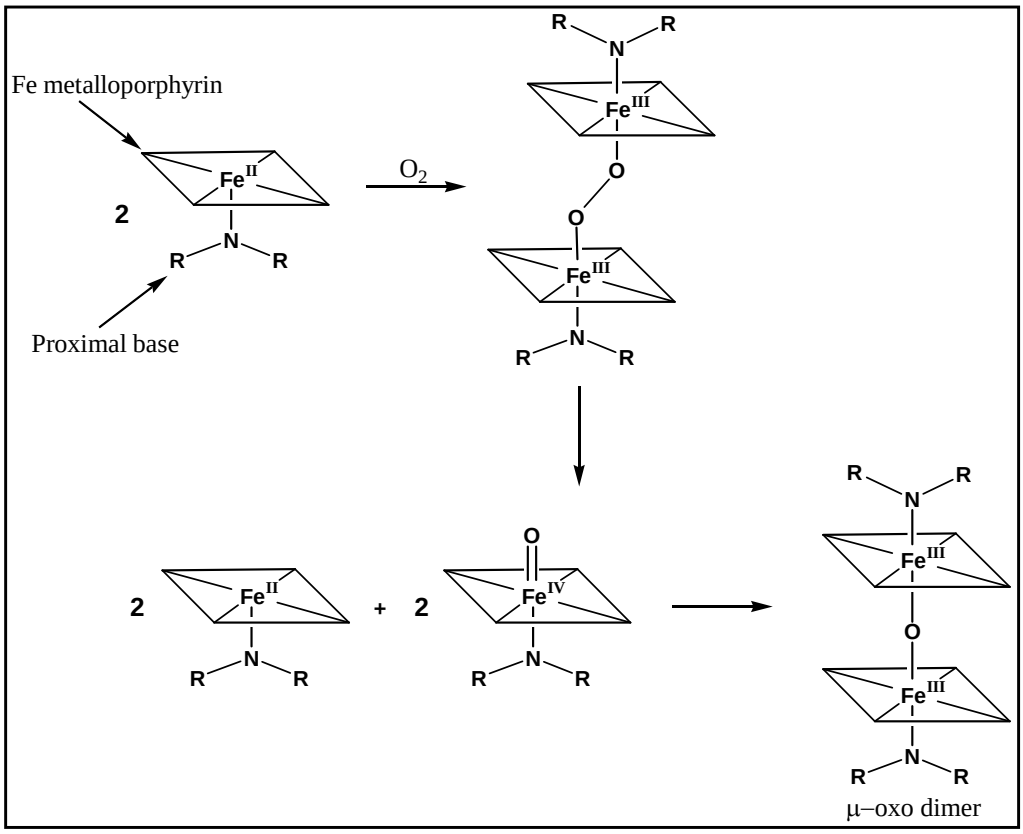

Figure 2.5: Reaction pathway towards μ-oxo dimer formation.

In order to avoid this, it is necessary to sterically hinder either the axial ligand (the proximal base), or one or both faces of the porphyrin moiety. In creating such steric hindrance, not only is the μ-oxo dimer reaction pathway blocked, but oxidation of the porphyrin ligand is also prevented.[11] This greatly improves the stability and activity of the synthetic heme analogue.

In one of the earliest examples of successful catalytic oxidation of an organic substrate by a synthetic metalloporphyrin, Groves *et al.*[19] reported the use of a simple iron centered tetraphenylporphyrin, TPP (where R is C_6H_5, and R' is Cl in Figure 2.4) to catalyze oxygen transfer to cyclohexane and cyclohexene, *via* the shunt reaction pathway (Figure 2.3) with a peroxide oxidant. Yields were low to moderate, while the catalysts proved to be unstable, and readily lost activity. While results clearly showed that metalloporphyrins can function as oxidative catalysts, Groves' work also serves as an illustration of the necessity to sterically hinder porphyrin-based catalysts: examining the TPP catalyst employed, it can be seen that there is a lack of significant steric hindrance, which has a marked effect on both the catalytic activity and stability.

It was through the subsequent research by Collman *et al.* that the most significant contributions to the use of sterically hindered porphyrins as a means of catalyzing oxidative reactions were made.[12] This was achieved *via* the use of functionalisation to construct steric hindrance at one face of the porphyrin moiety, in what came to be known as 'picnic-basket' or 'basket handle' porphyrins.[20-22] The use of a proximal base (as mentioned above) meant that oxidation was limited only to the sterically hindered face of the porphyrin moiety.

This initiated a succession of sterically hindered porphyrin variations, including 'capped',[23] 'strapped',[24] 'bridged',[25] 'co-facial' [26] and 'twin coronet' [27] metalloporphyrin species, of which the former was largely pioneered by the research of Baldwin *et al.* Sample structures of these species can be seen in Figure 2.6, where the bridges used in the strapped, bridged and twin coronet species represent alkyl and aryl chains of varying length and character.[9b] The proximal base in each structure has been omitted for purposes of clarity.

The above variations have been used effectively in a variety of oxidative reactions. With regards to the simpler TPP derivatives, the most common application has been the epoxidation of alkenes, based on a manganese centered porphyrin moiety.[28] Yields and catalyst activity with regards to substrate oxidation, and product selectivity, have improved vastly from Groves' initial work.

Collman's picnic-basket active site analogues have been shown to be shape-selective with regards to olefin epoxidation.[22, 29] Strapped metalloporphyrins have been used in mimicking cytochrome monooxygenases,[30a, b] as well as in enantioselective oxidative catalysis of olefins. In the case of the latter catalysts, remarkable enantiomeric excesses and, more recently, catalytic turnover numbers have been detailed.[30c, d]

Co-facial metalloporphyrins have largely been used as surface-adsorbed species,[31a, b] and have been reported to catalyze multi-electron reductions and oxidations of various molecules.[31c] More recently, these porphyrins have been used as photo-oxidation catalysts in the oxidation of sulphides and olefins, with high turnover numbers.[31d] Twin-coronet analogues have been shown to be selective with regards to oxidation products; again mostly in epoxidation reactions with olefin substrates.[27b, c, 32]

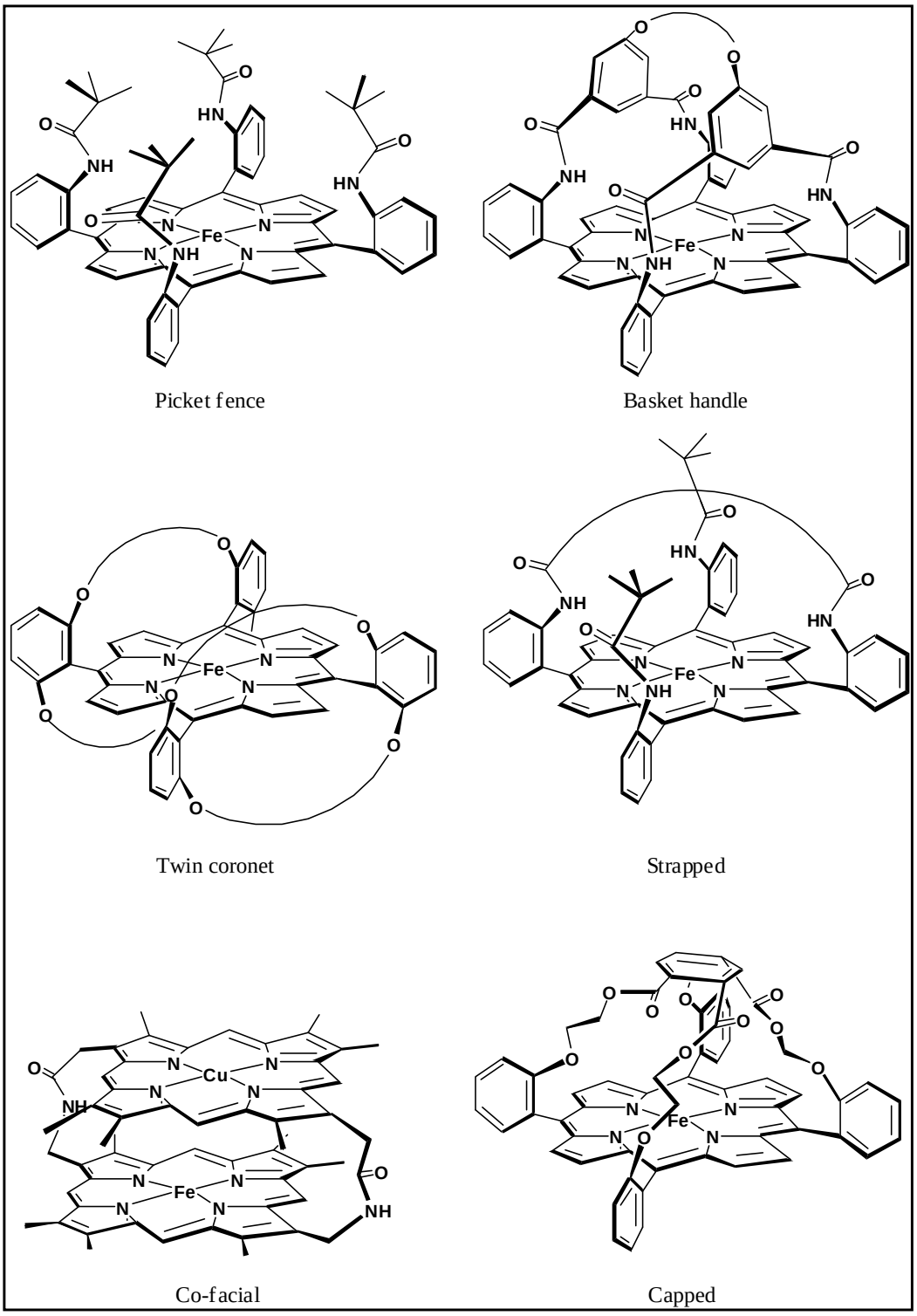

Figure 2.6: General structures of common sterically hindered metalloporphyrins. The proximal base in each case has been omitted for clarity.

Capped metalloporphyrins have found limited use, having been employed in studies into cytochrome monooxygenases,[33a] as well as having been shown to be effective epoxidation catalysts.[33b, c]

These single face hindered species have moreover been elaborated into particularly effective regio- and enantioselective catalysts, as well as efficient asymmetric catalysts. By building chiral moieties into the straps and bridges of the above catalysts, remarkable selectivities with respect to enantiomeric distribution and regioselective oxidation have been achieved, most notably in epoxidation reactions of alkenes. Thus steric bulk has not only become a means by which to improve heme analogue stability and activity, but it has also become a way in which to control where and how a substrate may undergo oxidation. Reviews pertaining to chiral and asymmetric catalysis by metalloporphyrin species are available.[12, 13, 34]

In light of the necessity to sterically hinder metalloporphyrins, the use of supramolecular structures to form superstructured metalloporphyrins has become progressively more common. It should be remembered that biological enzymatic active centers are largely found within the confines of a protein pocket.[1] Therefore, by using supramolecular structures and macrocyclic assemblies (many of which contain hydrophobic cavities capable of accommodating molecules as guests as outlined in Chapter 1), not only will such superstructured metalloporphyrin-based analogues have enhanced stability and activity, but the function of the protein pocket in the biological enzymes may also be mimicked. Bearing in mind that substrate selectivity (and thereby oxidative selectivity) is dependant on the shape of the protein in biological enzymes, it is conceivable that by sterically hindering synthetic porphyrin moieties in such a manner, a degree of control over substrate and oxidative selectivity may be achieved.

2.5 Supramolecular Porphyrins

In an effort to improve on the single face, sterically hindered porphyrins and their catalytic properties as outlined above, supramolecular porphyrins have become increasingly popular. The ability of supramolecular structures to act as host molecules by providing hydrophobic cavities into which guest molecules may be accommodated is undoubtedly one of their most decisive features which has seen their common use as a means of sterically hindering metalloporphyrins. The enhanced stability and solubility imparted on guests that are complexed

within supramolecular cavities can become particularly useful when it comes to binding a range of substrates, especially in the case of biomimetic applications, where the binding and orientation of substrates is important.

Thus, given these qualities of supramolecular macrocycles, there have been a range of reported supramolecular porphyrins; that is, porphyrins appended with macrocyclic species, as well as porphyrins bearing macrocyclic 'caps' much like Baldwin's 'capped' porphyrins noted above. Porphyrins appended and/or capped with crown ether macrocycles,[35] cyclophane derivatives [36] as well as resorcinarene moieties [37] have been described. More common, however, are those porphyrins bearing cyclodextrin (CD) and calixarene moieties.

2.5.1 CD-Porphyrins

CD's are arguably the most popular means by which to construct artificial enzymes and other biomimetic processes and materials; hence their widespread use to construct supramolecular porphyrins.[38] This is largely attributed to their availability and importantly, their ease of functionalisation. Certainly, porphyrin-CD supramolecular catalysts constitute some of the most effective enzyme mimics and biomimetic catalysts to date.[38, 39]

Coenzyme B_{12} mimics based on β-CD-appended porphyrins have been shown to be successful in mimicking steps in enzymatic rearrangements accomplished by biological coenzyme B_{12}.[40, 41] In such studies, it was most notably the ability of the β-CD to accommodate the substrate as a guest which facilitated the biomimetic reaction by the supramolecular porphyrin.

Metalloporphyrin species carrying two or four β-CD rings appended as substituents to TPP phenyl moieties, as shown in Figure 2.7, have been synthesised by Breslow *et al.*[42] Using a Mn(III) centre, such catalysts not only performed effectively, but exhibited a degree of selectivity in the oxidation of olefin substrates. It was again the abilities of the CD as a host which facilitated catalytic activity, by suspending the substrate across the metalloporphyrin's metal centre. Utilizing the same CD-porphyrin species, Breslow *et al.* were also able to mimic the heme-based Cytochrome P_{450} enzymes *via* hydroxylating a dihydrostilbene substrate, with selectivity for the benzylic carbon atoms.[43]

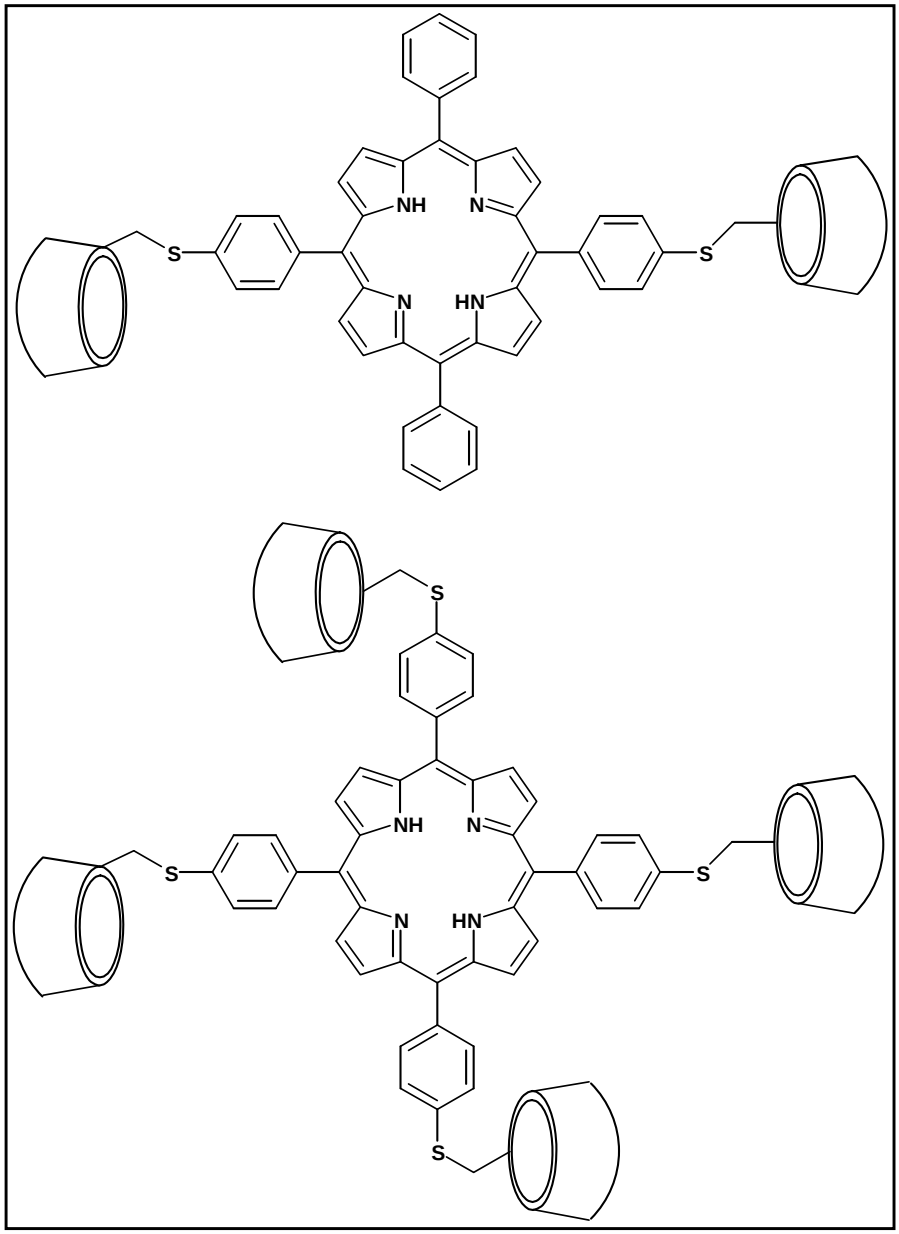

Figure 2.7: Structures of the CD-appended porphyrin ligands of Breslow *et al.*

Moreover, with a protected androstanediol steroid substrate, and the same catalyst, it was shown that hydroxylation could be achieved with complete regio- and stereoselectivity at carbon-6,[43a, 44, 45] a result based explicitly on the ability of the CD macrocycles to bind both ends of the substrate into their cavities.

CD's have also been used to form capped porphyrin catalysts. The bis-capped species of Ogoshi *et al.* [46] seen in Figure 2.8 below was synthesised such that a β-CD cap was held at each face of the metalloporphyrin moiety. The CD rings were able to bind cyclohexene and

catalyze oxidation far more effectively than the equivalent metalloporphyrin without any binding CD groups.

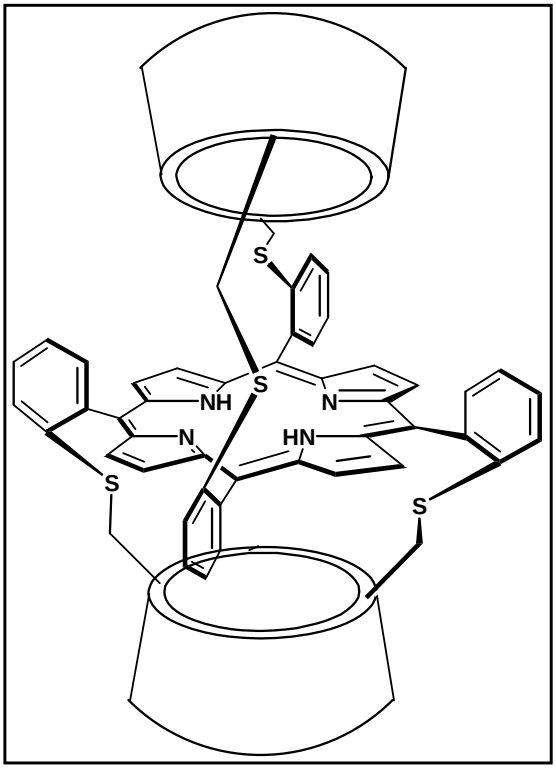

Figure 2.8: Structures of the *bis*-CD-capped porphryin of Ogoshi *et al.*

2.5.2 Calixarene-Porphyrins

Calixarenes have also become popular macrocycles from which to construct supramolecular porphyrins through which to study molecular recognition and biomimetic oxidative processes. **[47]** Due to their inherent versatility as host molecules, the reported number of calixarene-porphyrin derivatives is vast; reviews and literature on these species are available.**[48, 49]** However, it is the family of calixarene-capped porphyrins (most notably the calix[4]arene derivatives) which are of particular interest, especially since calixarenes can mediate the binding of small molecules within their cavities, as in the case of CD's.**[47]** This ability has important effects on the capability of porphyrins to recognise and coordinate molecules, as illustrated in the work noted above with CD-porphyrin species.

The first reported example of a calix[4]arene-capped porphryin was by Shinkai *et al.* **[47]** who used chiral amide-based spacers to link the calix[4]arene to a Zn(II) metalloporphyrin. It was

shown that the resulting supramolecular porphyrin was able to bind a range of hard-soft ditopic metal compounds, some with remarkably strong interactions. The structure of the ligand can be seen in Figure 2.9, where metal cations and amine protons have been omitted for clarity.

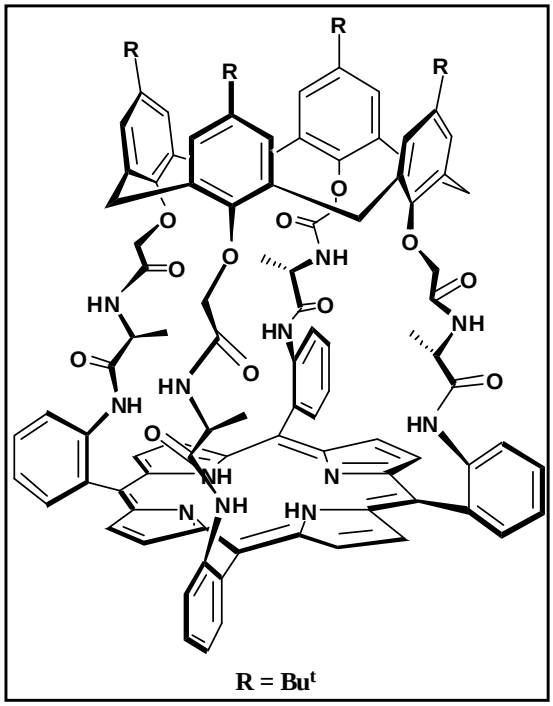

Figure 2.9: Structure of the calix[4]arene capped porphyrin of Shinkai *et al.*

As in the case of CD-porphyrin species, calix[4]arenes have also been used to hinder both faces of a porphyrin moiety to form a *bis*-capped ligand, as reported by Reinhoudt *et al.*[50] Again using amide spacers, as evident in Figure 2.10, it was shown that the Zn(II) metalloporphyrin was able to complex a range of pyridine derivatives, piperidine and most notably, *N*-methylimidazole, regarded as analogous to the binding interaction of molecular O_2.[51] Importantly, the binding observed was up to 1000 times stronger than for the unhindered Zn TPP analogue; an effect attributed to the abilities of calix[4]arenes as host molecules.

Porphyrins have also been capped by larger calix[5]- and calix[6]arenes. Fukazawa *et al.* [52] have successfully synthesised a calix[5]arene-capped porphyrin with amide spacers (Figure 2.10), and used the Zn(II) metalloporphyrin to complex a range of pyridine derivatives. Again it was illustrated that, in general, guests were bound with a stronger interaction in the case of the calixarene-capped species than in the case of the unhindered TPP analogue. However, significantly, it was found using UV-Vis techniques, that the bulkier guests were excluded from binding in the calixarene cavity since they could not pass through the apertures between the

porphyrin and calixarene moieties. Such guests were instead bound on the *unhindered* face in a weaker interaction than those seen for the interaction between the same guest and the TPP analogue.

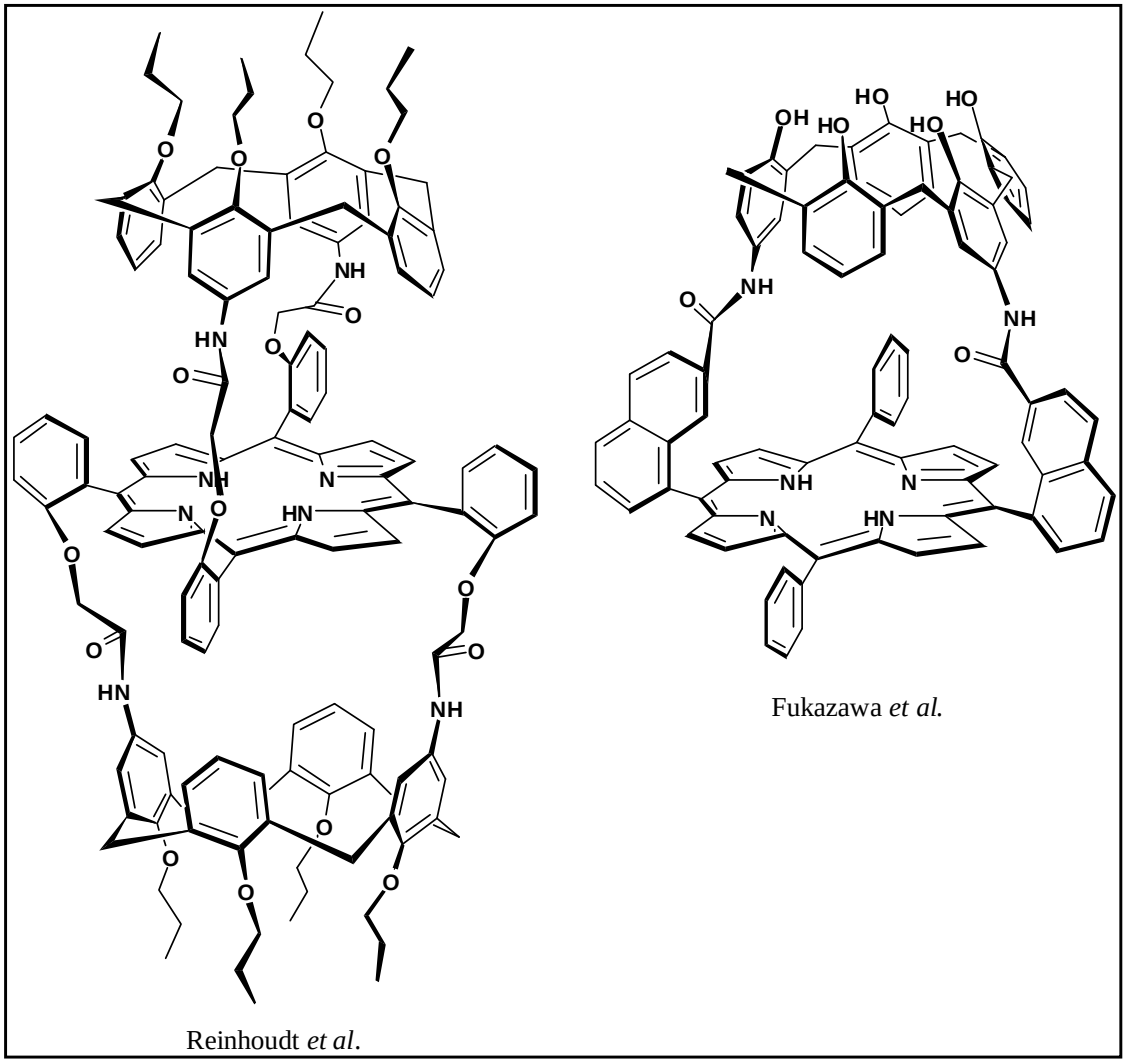

Figure 2.10: Structures of the calix[4]arene capped porphyrins of Reinhoudt *et al.* and Fukazawa *et al.*

Calix[6]arene-capped porphyrins have also been reported, and are the only example of a catalytically active calixarene-capped superstructured porphyrin. In a variation to the *bis*-capped calix[4]arene-porphyrin described by Reinhoudt *et al.*, Zhao *et al.* **[53]** attached two porphyrin moieties to a calix[6]arene and investigated the ligand's ability as an epoxidation catalyst. Results showed that, in comparison to the simple TPP analogue, the calix[6]arene-porphyrin species had a greater catalytic activity due to the calixarene's host capabilities.

2.5.3 Cavitand-Porphyrins

Few examples of cavitand-porphyrin ligands are found in the literature as a means to sterically hinder porphyrins. As in the case of calixarene-porphyrins, there have been many reported examples of cavitand *appended* porphyrins and derivatives, which have been used to complex various guests.[54] However, of interest in this study is the cavitand-*capped* species of porphyrin, of which there are only two known examples in the literature.

In the first example of a cavitand-capped porphyrin, Reinhoudt *et al.* [51] synthesised a range of these species with either two or four amide-based spacers, of varying length, linking the cavitand to the porphyrin as shown in Figure 2.11. Using the Zn(II) metalloporphyrin, and pyridine and imidazole derivatives as guests, among them *N*-methylimidazole, enhanced binding interactions of molecules were observed as a result of the cavitand's rigidity and abilities as a host molecule.

Importantly it was also observed that spacer length had a marked effect on the binding ability of the capped porphyrin. The longer, more flexible spacers, although allowing the bigger guests to be accommodated by the cavitand, resulted in a less defined environment through which to complex guests. Binding interaction between guest and capped porphyrin was thus found to be diminished.

In contrast, the shorter, rigid spacers had a more profound effect on binding interactions; the cavitand-porphyrin encapsulating guests *via* a stronger interaction due to a better defined and rigid binding environment. Additionally, it was also observed that the use of four spacers further enhanced binding ability, showing up to a 700-fold improvement with respect to various guests. Spacer distance was also shown to have a clear effect on the symmetry of the ligands.

More recently, Naruta *et al.* [55] used a cavitand-capped porphyrin to encapsulate small hydrocarbons. A degree of flexibility in the system was introduced by having two adjacent spacers linking the cavitand to the porphyrin, as evident in Figure 2.12. Notably the spacers were simple ether bridges, resulting in a cavitand-capped porphyrin with the smallest cavity hitherto reported and importantly, one with a high degree of size selectivity.

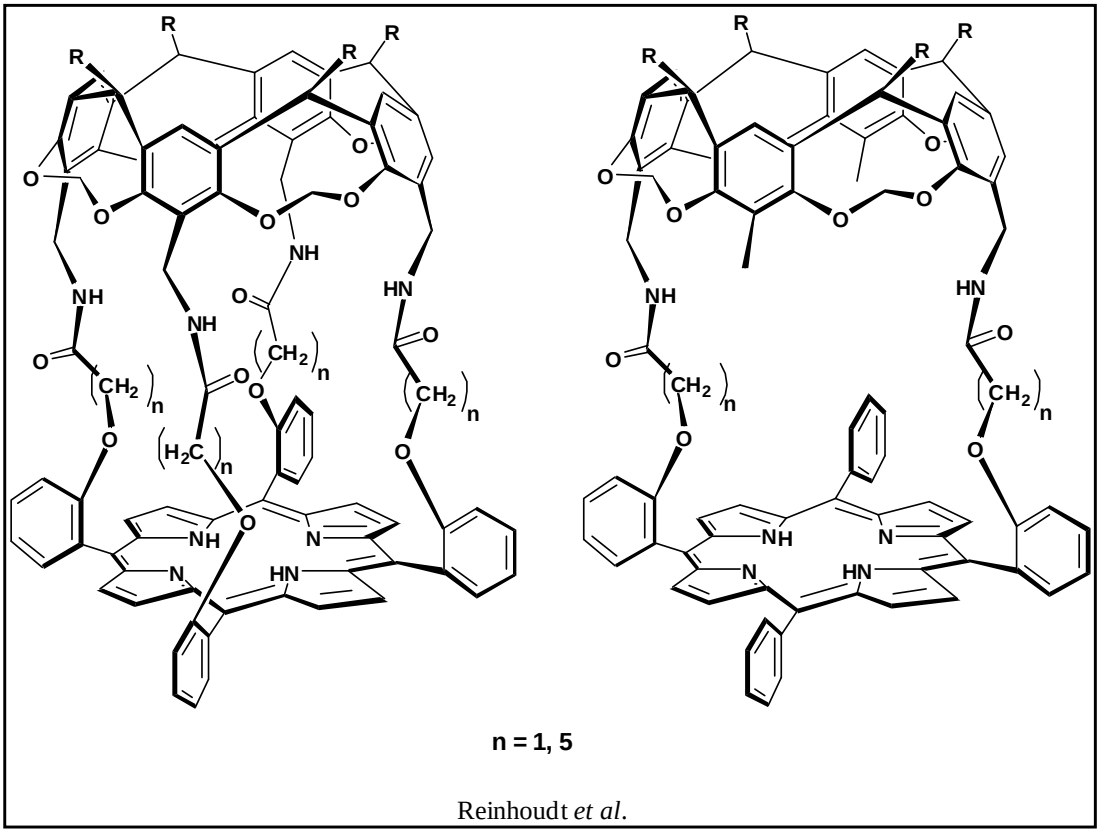

Figure 2.11: Structures of reported cavitand-capped porphyrin ligands of Reinhoudt *et al*.

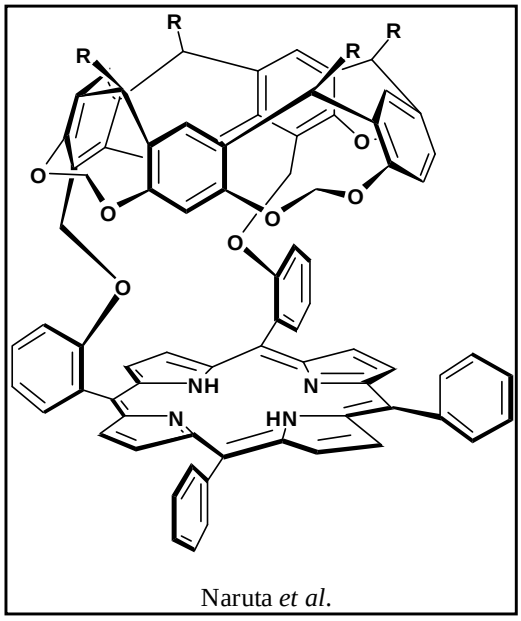

Figure 2.12: Structures of reported cavitand-capped porphyrin ligands of Naruta *et al*.

2.6 Aims and Objectives of Study

Given the ability of sterically hindered porphyrins to perform catalysis, and the enhanced and selective encapsulation of guests by supramolecularly hindered porphyrins, the interest in this study lies in the synthesis of cavitand-capped metalloporphyrins towards a homogeneous (solution phase) catalyst. In light of the importance of spacer length on binding ability and selectivity of capped porphyrins, as illustrated by Fukazawa (in the case of calixarenes) and Reinhoudt (in the case of cavitands), it is envisaged that spacer properties may be used to induce a degree of regioselectivity into the oxidative catalysis reaction.

The ligands synthesised by Reinhoudt *et al.* show that the use of four spacers linking the cavitand to the porphyrin results in four apertures between the cavitand and porphyrin. It was also observed that for those guests that proved to be too bulky to fit through the apertures, they were prevented access to the cavity within the ligand. Therefore, by varying these aperture sizes, a degree of size-selectivity with regards to guest complexation may be achieved. Thus, should the apertures be made sufficiently small, such that only the terminus of a linear hydrocarbon can gain access to the cavity, the exclusive oxygen transfer from the metalloporphyrin to this terminus can occur; thereby regioselectively oxidizing hydrocarbons at the terminal positions. Oxidation from outside of the cavity (from the metalloporphyrin's sixth coordination site) would be prevented by the use of a cysteine residue, in keeping with biological heme enzymes.

In terms of the other structural properties of the envisaged ligand, simple ether spacers would be used to link the cavitand and the porphyrin moieties as shown in Figure 2.13 (the abovementioned aperture outlined in red; the sixth ligand on metal centre M has been omitted). Spacer length (R'), and therefore aperture size, would be investigated *via* computational methods in order to see if the chosen aperture size matches that of the terminal end of a linear hydrocarbon. The solubility of the cavitand may be controlled by varying the length and hydrophobicity of the cavitand 'feet' (R, in Figure 2.13) as discussed in Chapter 1, depending on the nature of the solvent used in catalysis.

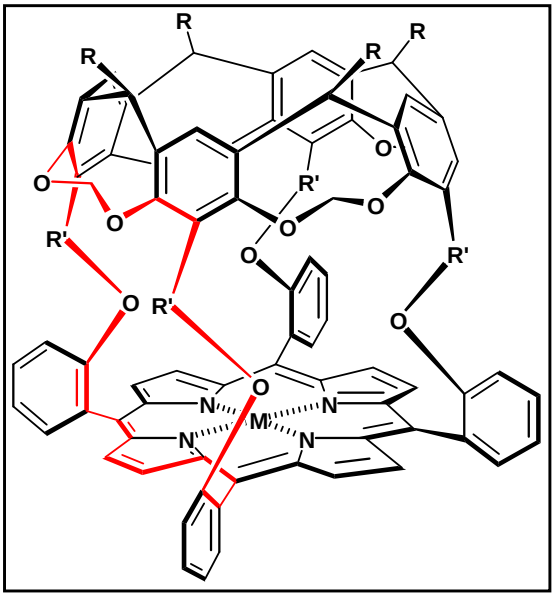

Figure 2.13: Structure of proposed cavitand-capped porphyrin catalyst.

In summary, therefore, the primary aims of this work are as follows:

1. To establish a procedure for the synthesis of the cavitand-capped porphyrin ligand with the appropriate bridges, varying cavitand ‘feet’ to vary ligand solubility.
2. Identify what bridge length affords a successful synthesis in addition to the desired size selectivity.
3. *Via* computational methods, investigate if cavitand-porphyrin bridges are suitable in giving aperture sizes appropriate for the intended regioselective oxidative catalysis.

REFERENCES

1. Y. Murakami, T. Kikuchi, Y. Hisaeda, O. Hayashida, *Chem. Rev.*, **1996**, *96*, 721-758.
2. P. Ortiz de Montellano, *Cytochrome P450: Structure, Mechanism and Biochemistry*, 2nd Edition, Plenum Press NY, **1995**.
3. D. Mansuy, P. Battioni, J-P Battioni, *Eur. J. Biochem.*, **1989**, *184*, 267-285.
4. J.W. Steed, J.L. Atwood, *Supramolecular Chemistry*, Wiley, Chichester **2000**.
5. For reviews on energy transfer and photosynthesis, and synthetic analogues, see ***a)*** M.R. Wasielewski, *Chem. Rev.*, **1992**, *92*, 435-461; ***b)*** S. Fukuzumi, *Bull. Chem. Soc. Jpn.*, **2006**, *79*, 177-195.
6. W. Kaim, B. Schwederski, *Bioinorganic Chemistry: Inorganic Elements in the Chemistry of Life*, Wiley **1999**.
7. For reviews on synthetic oxygen binding analogues, see ***a)*** J.P. Collman, L. Fu, *Acc. Chem. Res.*, **1999**, *32*, 455-463; ***b)*** E. Tsuchida, T. Komatsu, *Methods Enzymol.*, **1994**, *231*, 167-193; ***c)*** R. Fiammengo, M. Crego-Calama, D.N. Reinhoudt, *Curr. Opin. Chem. Biol.*, **2001**, *5*, 660-673.

For examples of progress from the first porphyrin-based oxygen binding analogues, see ***d)*** J.P. Collman, R.R. Gagne, T.R. Halbert, J.C. Marchon, C.A. Reed, *J. Am. Chem. Soc.*, **1973**, *95*, 7868-7870; ***e)*** J.P. Collman, R.R. Gagne, C.A. Reed, W.T. Robinson, G.A. Rodley, *Proc. Natl. Acad. Sci U.S.A.*, **1974**, *71*, 1326-1329; ***f)*** J.P. Collman, R.R. Gagne, C.A. Reed, T.R. Halbert, G. Lang, W.T. Robinson, *J. Am. Chem. Soc.*, **1975**, *97*, 1427-1439; ***g)*** H. Imai, S. Sekizawa, E. Kyuno, *Inorg. Chim. Acta*, **1986**, *125*, 151-158; ***h)*** G.E. Wuenshell, C. Tetreau, D. Lavalette, C.A. Reed, *J. Am. Chem. Soc.*, **1992**, *114*, 3346-3355; ***i)*** N. Kobayashi, K. Mizuno, T. Osa, *Inorg. Chim. Acta*, **1994**, *224*, 1-3.

8. R.D. Hancock, *J. Chem. Ed.*, **1992**, *69*, 615-621.
9. ***a)*** R.D. Jones, D.A. Summerville, F. Basolo, *Chem. Rev.*, **1979**, *79*, 139-179; ***b)*** M. Momenteau, C.A. Reed, *Chem. Rev.*, **1994**, *94*, 659-698.
10. M. Sono, M.P. Roach, E.D. Coulter, J.H. Dawson, *Chem. Rev.*, **1996**, *96*, 2841-2887.
11. M.C. Feiters, A.E. Rowan, R.J.M. Nolte, *Chem. Soc. Rev.*, **2000**, *29*, 375-384.
12. J.P. Collman, X. Zhang, V.J. Lee, E.S. Uffelman, J.I. Barauman, *Science*, **1993**, *261*, 1404-1411.
13. E. Rose, B. Adrioletti, S. Zrig, M. Quelquejeu-Etheve, *Chem. Soc. Rev.*, **2005**, *34*, 573-583.
14. B. Meunier, S.P. de Visser, S. Shaik, *Chem. Rev.*, **2004**, *104*, 3947-3980.

15. ***a)*** P. Rothemund, *J. Am. Chem. Soc.*, **1936**, *58*, 625-627; ***b)*** P. Rothemund, *J. Am. Chem. Soc.*, **1939**, *61*, 2912-2915.
16. A.D. Adler, F.R. Longo, J.D. Finarelli, J. Goldmacher, J. Assour, L. Korsakoff, *J. Org. Chem.*, **1967**, *32*, 476-477.
17. J.S. Lindsey, I.C. Schreiman, H.C. Hsu, P.C. Kearney, A.M. Marguerettaz, *J. Org. Chem.*, **1987**, *52*, 827-836.
18. Q.H. Xia, H.Q. Ge, C.P. Ye, Z.M. Liu, K.X. Su, *Chem. Rev.*, **2005**, *105*, 1603-1662.
19. J.T. Groves, T.E. Nemo, R.S. Myers, *J. Am. Chem. Soc.*, **1979**, *101*, 1032-1033.
20. J.P. Collman, J.I. Brauman, J.P. Fitzgerald, P.D. Hampton, Y. Naruta, J.W. Sparapany, J.A. Ibers, *J. Am. Chem. Soc.*, **1988**, *110*, 3477-3486.
21. ***a)*** A. Lecas, Z. Renko, E. Rose, *Tetrahedron Lett.*, **1985**, *26*, 1019; ***b)*** E. Rose, M. Quelquejeu, R.P. Randian, A. Lecas, A. Nawrocka, A. Vilar, G. Picart, J.P. Collman, Z. Wang, A. Straumanis, *Polyhedron*, **2000**, *19*, 581-586.
22. ***a)*** J.P. Collman, X. Zhang, R.H. Hembre, J.I. Brauman, *J. Am. Chem. Soc.*, **1990**, *112*, 5356-5357; ***b)*** J.P. Collman, X. Zhang, V.J. Lee, R.H. Hembre, J.I. Brauman, *ACS Adv. Chem. Ser.*, **1992**, *230*, 153-162.
23. ***a)*** J. Almog, J.E. Baldwin, J. Huff, *J. Am. Chem. Soc.*, **1975**, *97*, 227-228; ***b)*** J. Almog, J.E. Baldwin, M.J. Crossley, J.F. Debernardis, R.L. Dyer, J.R. Huff, M.K. Peters, *Tetrahedron*, **1981**, *37*, 3589-3601; ***c)*** J.E. Baldwin, P. Perlmutter, *Top. Curr. Chem.*, **1984**, *121*, 181-220.
24. ***a)*** H. Ogoshi, M. Sugimoto, Z. Yoshida, *Tetrahedron Lett.*, **1976**, *49*, 4481-4484; ***b)*** T.P. Wijesekers, J.B. Paine, D. Dolphin, *J. Org. Chem.*, **1988**, *53*, 1345-1352; ***c)*** D. El Kasmi, C. Tetreau, D. Lavalette, M. Momenteau, *J. Chem. Soc. Perkin Trans. 2*, **1993**, 1799-1803.
25. A.R. Battersby, D.G. Buckley, S.G. Hartly, M.D. Turnbull, *J. Chem. Soc. Chem. Comm.*, **1976**, 879-881.
26. ***a)*** J.P. Collman, G.M. Elliot, T.R. Halbert, B.S. Tovrog, *Proc. Natl. Acad. Sci U.S.A.*, **1977**, *74*, 18-22; ***b)*** B. Ward, C. Wang, C.K. Chang, *J. Am. Chem. Soc.*, **1981**, *103*, 5236-5238; ***c)*** J.P. Collman, D.A. Tyvoll, L.L. Chng, H.T. Fish, *J. Org. Chem.*, **1995**, *60*, 1926-1931.
27. ***a)*** Y. Naruta, F. Tan, K. Maruyama, *Chem. Lett.*, **1989**, 1269-1272; ***b)*** Y. Naruta, F. Tan, K. Maruyama, *Tetrahedron Lett.*, **1992**, *33*, 6323-6326; ***c)*** Y. Naruta, N. Ishihara, F. Tani, K. Maruyama, *Bull. Chem. Soc. Jpn.*, **1993**, *66*, 158-166.
28. ***a)*** D. Mohajer, S. Tangestaninejad, *J. Chem. Soc. Chem. Comm.*, **1993**, *3*, 240-241; ***b)*** W. Lu, J.F. Bartoli, P. Battioni, D. Mansuy, *New J. Chem.*, **1992**, *16*, 621-628; ***c)*** P.

Leduc, P. Battioni, J.F. Bartoli, D. Mansuy, *Tetrahedron Lett.*, **1988**, *29*, 205-208; ***d)*** D. Mansuy, M. Fontecave, J.F. Bartoli, *J. Chem. Soc. Chem. Comm.*, **1983**, *6*, 253-254.

29. J.P. Collman, J.I. Brauman, J.P. Fitzgerald, P.D. Hampton, Y. Naruta, T. Michida, *Bull. Chem. Soc. Jpn.*, **1988**, *61*, 47-57.
30. ***a)*** D. Ricard, M. L'Her, R. Philippe, B. Boitrel, *Chem. Eur. J.*, **2001**, *7*, 3291-3297; ***b)*** K. Konishi, K. Oda, K. Nishida, T. Aida, S. Inoue, *J. Am. Chem. Soc.*, **1992**, *114*, 1313-1317; ***c)*** E. Rose, Q-Z. Ren, B. Andrioletti, *Chem. Eur. J.*, **2004**, *10*, 224-230; ***d)*** J.P. Collman, V.J. Lee, C.J. Kellen-Yuen, X. Zhang, J.A. Ibers, J.I. Brauman, *J. Am. Chem. Soc.*, **1995**, *117*, 692-703.
31. ***a)*** R.R. Durand, C.S. Benscome, J.P. Collman, F.C. Anson, *J. Am. Chem. Soc.*, **1983**, *105*, 2710-2718; ***b)*** K. Oyaizu, A. Haryono, J. Natori, H. Shinoda, E. Tsuchida, *Bull. Chem. Soc. Jpn.*, **2000**, *73*, 1153-1163; ***c)*** J.P. Collman, P.S. Wagenknecht, J.E. Hutchinson, *Angew. Chem. Int. Ed. Engl.*, **1994**, *33*, 1537-1620; ***d)*** J. Rosenthal, B. Pistorio, L.L. Chng, G. Daniel, *J. Org. Chem.*, **2005**, *70*, 1885-1888.
32. ***a)*** E. Matsui, Y. Naruta, F. Tani, Y. Shimazaki, *Angew. Chem. Int. Ed. Engl.*, **2003**, *42*, 2744-2747; ***b)*** Y. Naruta, N. Ishihara, F. Tani, K. Maruyama, *Chem. Lett.*, **1991**, *11*, 1933-1936.
33. ***a)*** A. Didier, M. L'Her, B. Boitrel, *Org. Biomol. Chem.*, **2003**, *1*, 1274-1276; ***b)*** J.A.A.W. Elemans, E.J. Bijsterveld, A.E. Rowan, R.J.M. Nolte, *J. Chem. Soc. Chem. Comm.*, **2000**, *24*, 2443-2444; ***c)*** J.P. Collman, X. Zhang, V.J. Lee, J.I. Brauman, *J. Chem. Soc. Chem. Comm.*, **1992**, *22*, 1647-1649.
34. ***a)*** E. Rose, A. Lecas, M. Quelquejeu, A. Kossanyi, B. Boitrel, *Coord. Chem. Rev.*, **1998**, *178-180*, 1407-1431; ***b)*** B. Meunier, *Chem. Rev.*, **1992**, *92*, 1411-1456; ***c)*** B.S. Lane, K. Burgess, *Chem. Rev.*, **2003**, *103*, 2457-2473.
35. ***a)*** P. Even, B. Boitrel, *Coord. Chem. Rev.*, **2006**, *250*, 519-541; ***b)*** M. Lochner, L. Mu, W.D. Woggon, *Adv. Synth. Catal.*, **2003**, *345*, 743-765; ***c)*** M. Jahan, N. Safari, H. Khosravi, A. Moghimi, B. Notash, *Polyhedron*, **2005**, *24*, 1682-1688.
36. ***a)*** H. Ogoshi, H. Sugimoto, M. Masao, Z. Yoshida, *Tetrahedron*, **1984**, *40*, 579-592; ***b)*** D.R. Benson, R. Valentekovich, F. Diederich, *Angew. Chem. Int. Ed. Engl.*, **1990**, *29*, 191-193; ***c)*** D.R. Benson, R. Valentekovich, S-W. Tam, F. Diederich, *Helv. Chim. Acta*, **1993**, *76*, 2034-2060; ***d)*** R. Breslow, Z. Fang, *Tetrahedron Lett.*, **2003**, *43*, 5197-5200.
37. B. Botta, P. Ricciardi, C. Galeffi, M. Botta, A. Tafi, R. Pogni, R. Iacovino, I. Garella, B. Di Blasio, G. Delle Monache, *Org. Biomol. Chem.*, **2003**, *1*, 3131-3137.
38. R. Breslow, S.D. Dong, *Chem. Rev.*, **1998**, *98*, 1997-2011.
39. E. Engeldinger, D. Armspach, D. Matt, *Chem. Rev.*, **2003**, *103*, 4147-4173.

40. R. Breslow, P.J. Duggan, J.P. Light, *J. Am. Chem. Soc.*, **1992**, *114*, 3982-3983.
41. M. Rezae, R. Breslow, *Tetrahedron Lett.*, **1997**, *38*, 5763-5766.
42. R. Breslow, X.X. Zhang, R. Xu, M. Maletic, *J. Am. Chem. Soc.*, **1996**, *118*, 11678-11679.
43. ***a)*** R. Breslow, X.X. Zhang, Y. Huang, *J. Am. Chem. Soc.*, **1997**, *119*, 4535-4536; ***b)*** R. Breslow, Y. Huang, X.X. Zhang, J. Yang, *Proc. Natl. Acad. Sci U.S.A.*, **1997**, *94*, 11156-11158.
44. J. Yang, B. Gabriele, S. Belvedere, Y. Huang, R. Breslow, *J. Org. Chem.*, **2002**, 5057-5067.
45. Z. Fang, R. Breslow, *Bioorg. Med. Chem. Lett.*, **2005**, *15*, 5463-5466.
46. ***a)*** Y. Kuroda, T. Hiroshige, H. Ogoshi, *J. Chem. Soc. Chem. Comm.*, **2000**, *24*, 2443-2444; ***b)*** Y. Kuroda, T. Hiroshige, T. Sera, Y. Shiroiwa, H. Tanaka, H. Ogoshi, *J. Am. Chem. Soc.*, **1989**, *111*, 1912; ***c)*** Y. Kuroda, Y. Egawa, H. Seshimo, H. Ogoshi, *Chem. Lett.*, **1994**, 2361.
47. T. Nagasaki, H. Fujishima, M. Takeuchi, S. Shinkai, *J. Chem. Soc. Perkin Trans 1*, **1995**, 1883-1888.
48. N. Zh. Mamardashvili, O.I. Koifman, *Russ. J. Org. Chem.*, **2005**, *41*, 787-806.
49. R.G. Khoury, L. Jaquinod, K. Aoyagi, M.M. Olmstead, A.J. Fisher, K.M. Smith, *Angew. Chem. Int. Ed. Engl.*, **1997**, *36*, 2497-2500.
50. D.M. Rudkevich, W. Verboom, D.N. Reinhoudt, *J. Org. Chem.*, **1995**, *60*, 6585-6587.
51. O. Middel, W. Verboom, D.N. Reinhoudt, *J. Org. Chem.*, **2001**, *66*, 3998-4005.
52. H. Iwamoto, Y. Yukimasa, Y. Fukazawa, *Tetrahedron Lett.*, **2002**, *43*, 8191-8194.
53. D-H. Li, S-H. Chen, H-M. Zhao, *Chin. J. Chem.*, **2003**, *21*, 683-686.
54. S.D. Starnes, D.M. Rudkevich, J. Rebek, *J. Am. Chem. Soc.*, **2001**, *123*, 4659-4669.
55. ***a)*** J. Nakazawa, J. Hagiwara, M. Mizuki, Y. Shimazaki, F. Tani, Y. Naruta, *Angew. Chem. Int. Ed. Engl.*, **2005**, *44*, 3744-3746; ***b)*** J. Nakazawa, J. Hagiwara, M. Mizuki, Y. Shimazaki, F. Tani, Y. Naruta, *Bull. Chem. Soc. Jpn.*, **2006**, *79*, 1431-1443; ***c)*** J. Nakazawa, Y. Sakae, M. Aida, Y. Naruta, *J. Org. Chem.*, **2007**, *72*, 9448-9455.

CHAPTER 3

SYNTHESIS OF CAVITAND-CAPPED PORPHYRIN TARGET LIGAND

The length of bridge to couple the cavitand to the porphyrin, as shown in Chapter 2, was based on an initial Corey-Pauling-Koltun (CPK) modeling of the target ligand. It was observed that the use of -CH_2O- ether bridges to link the cavitand and porphyrin moieties resulted in apertures of a sufficient size to accommodate the terminus of an alkane substrate. Therefore, it was vital that the synthetic design of the ligand take into account these requirements. In terms of porphyrin formation and synthesis of the target ligand, a review of the literature reveals that supramolecularly-capped porphyrins were synthesised *via* two different approaches: an *in situ* approach, and a direct capping approach. Since the proposed ligand is novel, both approaches were attempted to see if either afforded the desired ligand.

3.1 In situ Approach

The synthetic methods by which cavitands and their derivatives are obtained have been well established, particularly by Cram *et al.*,[1-5] over the last fifteen years. The *in situ* approach seeks to make use of these methods to successively functionalise the cavitand to facilitate the cyclisation reaction that forms a porphyrin moiety above the cavitand structure. It should be remembered that synthetic porphyrins are generally synthesised by the condensation of pyrrole with an aromatic aldehyde. The success of an *in situ* approach in the formation of a cavitand-capped porphyrin therefore requires that the aromatic aldehyde be incorporated into the framework of a functionalised cavitand structure. Thereafter, the aromatic aldehydes are reacted with pyrrole towards the *in situ* formation of the porphyrin.

This approach of porphyrin formation was first reported in the case of calix[*n*]arene- and cyclophane-capped porphyrins, and was used to make a range of supramolecules with a variety of applications.[6] It was also used by Reinhoudt *et al.* in the synthesis of the first cavitand-capped porphyrin molecules as discussed in Chapter 2.[7] The functionalisation of their cavitands can be seen in Scheme 3.1, which shows the incorporation of the required aromatic aldehyde.

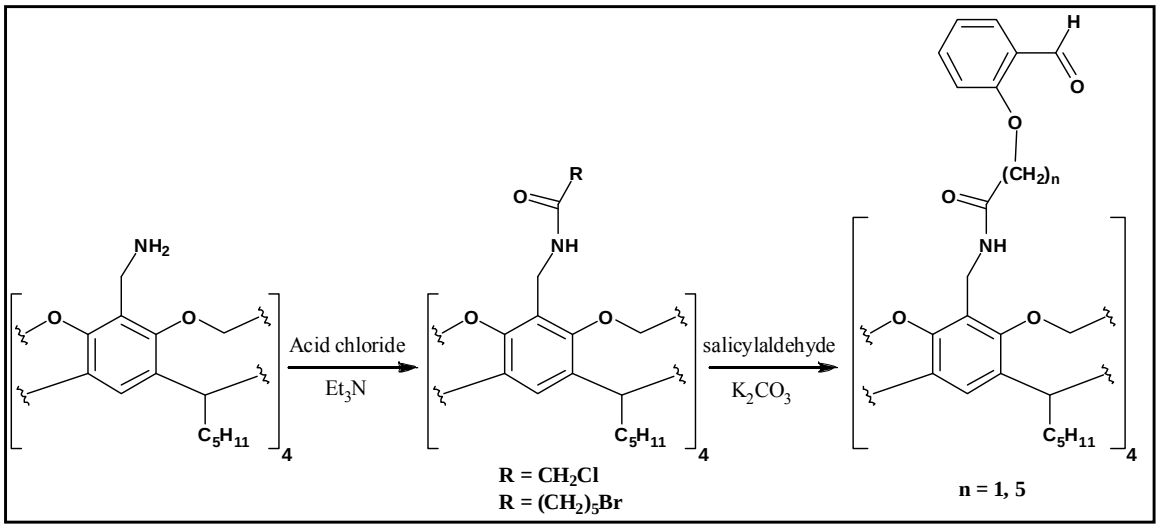

Scheme 3.1: Functionalisation of cavitands by Reinhoudt *et al.* towards aldehyde incorporation.

The final porphyrin formation step from the tetraaldehyde precursor was accomplished in low yields (<10 %) and was seen to be strongly dependant on the synthetic conditions applied as well as bridge length. The low yields achieved may be rationalised by the large entropic effect of arranging the eight interactions required, between the four aldehyde residues and four pyrrole units, for porphyrin formation. In the synthetic protocol, two sets of conditions were employed: the Adler conditions,[8] and the Lindsey conditions.[9] Importantly, Reinhoudt *et al.* observed that for the different bridge lengths, *in situ* formation proceeded by only one set of conditions, *never both*. Thus, for n = 1, ligand synthesis was successful only by the Adler conditions, whereas for n = 5, synthesis proceeded only by the Lindsey conditions.

Scheme 3.2 is a proposed retrosynthetic pathway towards the synthesis of the ligand of interest in this study. As is evident, this pathway uses procedures largely established and which provide good reported yields. The subsequent, complete synthetic scheme towards the target ligand is shown in Scheme 3.3.

Formation of resorcin[4]arene **3** is the result of the acid-catalyzed condensation of 2-methylresorcinol, **1**, and acetaldehyde, **2**. The synthesis of cavitand **4** can proceed by two possible pathways. Firstly, cavitands are prepared by heating a solution of the resorcin[4]arene starting material and the alkylating reagent (bromochloromethane in this case) in the presence of potassium carbonate at atmospheric pressure.[1b] The reaction proceeds over a number of days, and is often accompanied by addition of further equivalents of the alkylating reagent.

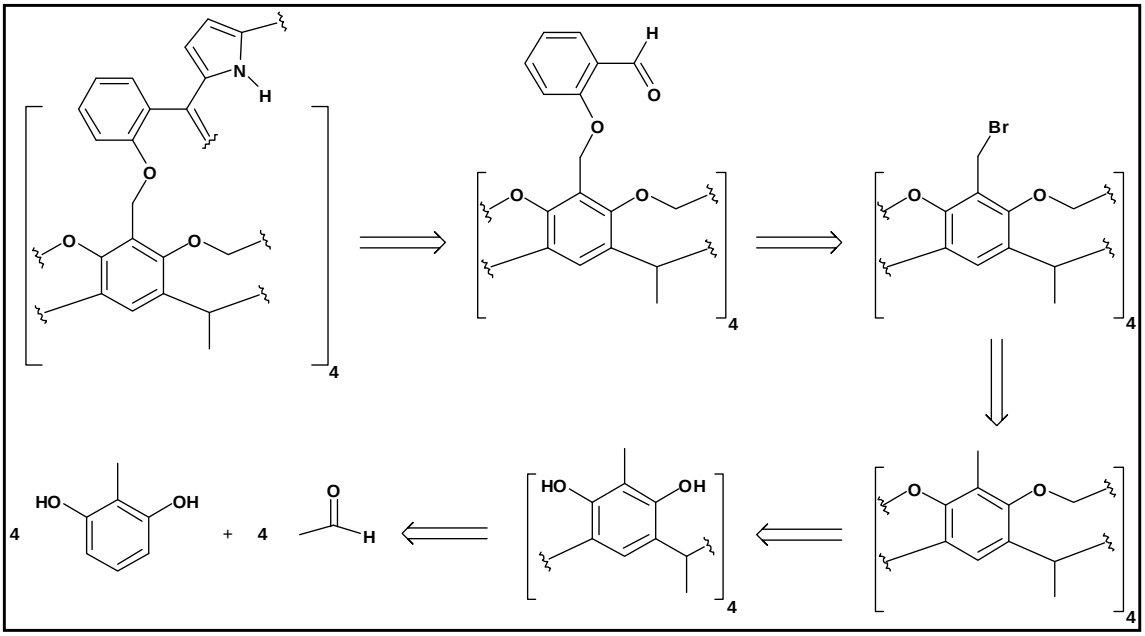

Scheme 3.2: Retrosynthetic pathway of the *in situ* porphyrin formation for the proposed ligand in this study.

Since bromochloromethane is volatile and boils at 68 °C, reaction temperature is limited to a range between 60 and 70 °C. This in turn affects yields of cavitand, which by using such a reaction protocol are typically in the order of 40 – 60 %. More recently, Kaifer *et al.*[4] reported a procedure which solved the problem of bromochloromethane volatility, *via* the use of a sealed tube as a reaction vessel, heated to 88 °C. The reagents were heated in the presence of cesium carbonate, which is used instead of potassium carbonate due to the templating ability of the cesium cation, which aids in the formation of macrocyclic assemblies such as cavitands.[10] Under these conditions, yields are in excess of 80 %. However, the pressures involved and the size of the reaction vessel used limits the protocol by Kaifer *et al.* to a scale of 1 g of starting material *per* reaction.

The bromination of the extra-annular methyl position of methyl cavitand **4** to give **5** is accomplished by free radical bromination using *N*-bromosuccinimide, under conditions set out by Sorrell *et al*.[2] Reported yields for such brominations are in the order of 70 %. In a Williamson-type ether synthesis, this bromomethyl cavitand precursor can be reacted with salicylaldehyde in the presence of NaH to give the novel tetrasalicylaldehyde cavitand **6** which serve as the precursors to the *in situ* porphyrin formation.

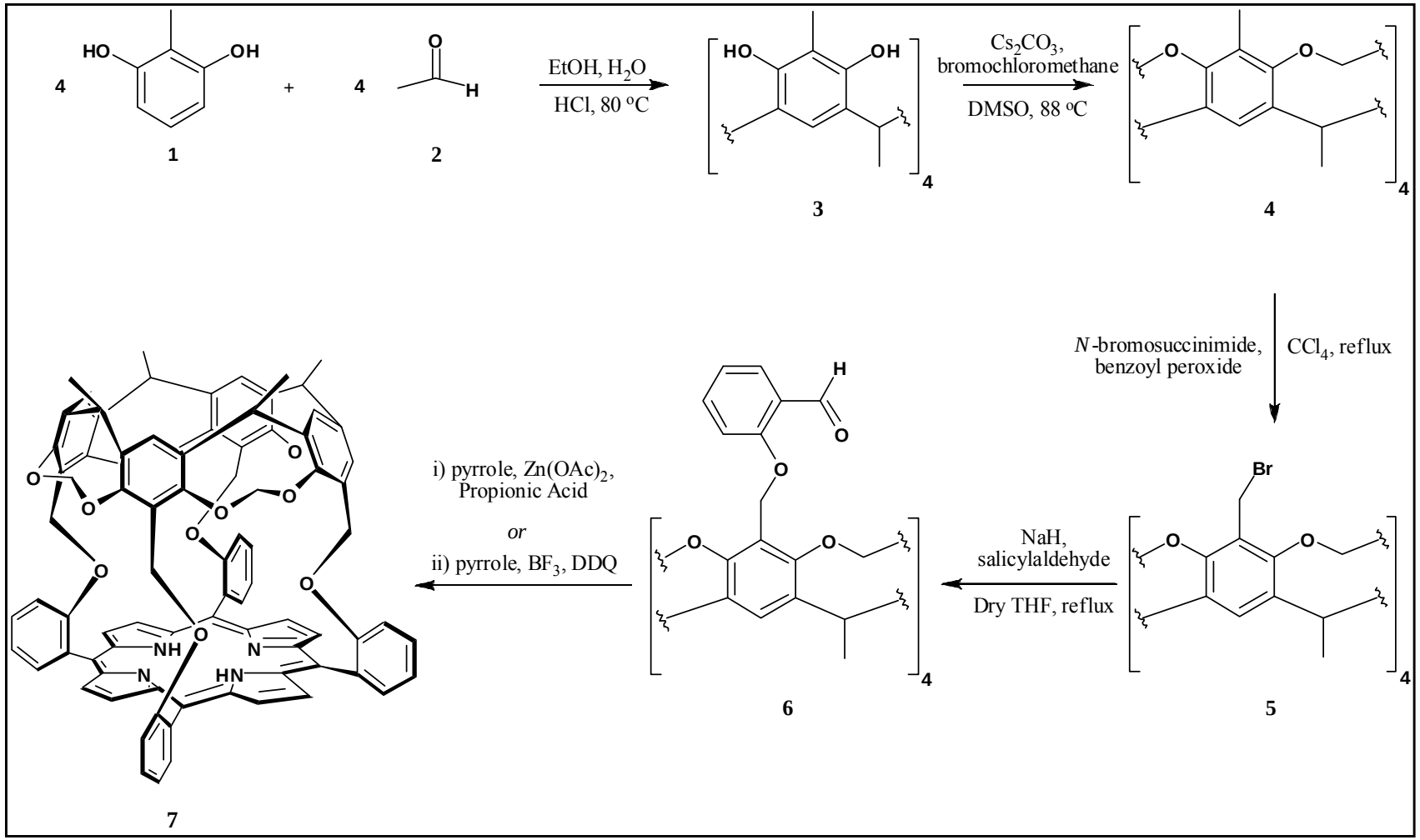

Scheme 3.3: The synthetic pathway towards the target ligand. The *in situ* step can be seen in the conversion of **6** to **7**.

With regards to the synthetic conditions to form porphyrin **7**, both the Adler and Lindsey conditions need to be used in order to determine which set of conditions favour porphyrin formation. Adler conditions are the more severe of the two sets of conditions, requiring the dried tetrasalicylaldehyde starting material and freshly distilled pyrrole to be added (in high dilution) simultaneously to refluxing propionic acid at 100 °C. Variations on these conditions, including the use of $Zn(OAc)_2 \cdot 2H_2O$ as a templating agent,[11] as well as the use of microwave irradiation as a source of energy,[12] have been reported as a means by which to improve yields.

The Lindsey conditions are more rigorous, requiring freshly distilled, dry chloroform (as a reaction solvent) and pyrrole under an inert atmosphere. The reaction makes use of a Lewis acid catalyst (BF_3) and an auxiliary oxidizing agent (2,3-dichloro-5,6-dicyano-*p*-benzoquinone, DDQ) to form the porphyrin, which generally forms in higher yields in comparison to the Adler conditions. However, in addition to the requirement of dry glassware and reagents, reagent concentrations are particularly influential in determining porphyrin formation and yields. Optimum conditions require the concentrations of starting material and pyrrole to be 0.01 M.

3.1.1 Results: In situ Protocol

Resorcin[4]arene **3** was synthesised in good yields according to procedures set out and results in the literature.[1c] Subsequent synthesis of cavitand **4** was completed according to the method by Kaifer *et al*. in yields approaching 90 %. Characterisation of both **3** and **4** was completed using proton (^1H) and carbon (^{13}C) NMR, spectra of which can be seen in Appendix 1 (Spectrum 1.1 and 1.4, respectively for the ^1H NMR, and Spectrum 1.2 and 1.5 for the ^{13}C NMR). Proton signals can be assigned with reference to Figure 3.1, showing the expanded structures of **3** and **4**.

Figure 3.1 clearly illustrates the symmetrical nature of resorcin[4]arene-based molecules, which results in relatively uncomplicated ^1H NMR spectra. With regards to **3**, the most prominent protons are those belonging to the eight hydroxyl groups (H_1), which in d_6-DMSO appear as a singlet downfield at 8.68 ppm, due to the deshielding nature of the oxygen atoms to which these protons are attached. This signal integrates to eight protons. The aromatic protons (H_3) also appear as a singlet in the aromatic region at 7.40 ppm, integrating to four protons. The protons associated with the feet appear in the alkyl region at 1.69 ppm, integrating to twelve protons, yielding a doublet *via* coupling with the four H_2 protons.

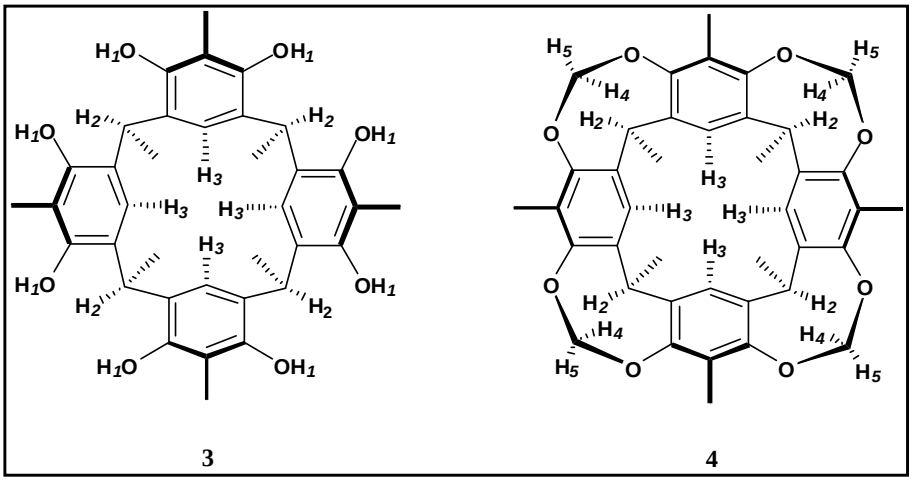

Figure 3.1: Expanded structures of **3** and **4**, showing distinctive protons.

The H_2 protons, which are able to couple to the methyl protons of the feet, give a distinct quartet downfield at 4.44 ppm, integrating to four protons. Finally, the benzylic protons, associated with the methyl groups at the extra-annular position of the aromatic rings, appear at 1.94 ppm as a singlet integrating to twelve protons. These are of particular interest since any functionalisation at this position will result in a change in this signal.

Alkylation of **3** to give **4** resulted in the appearance of two distinct signals characteristic of cavitands. The methylene protons are orientated such that one is facing into the cavity of the cavitand (H_4) and the other facing outwards (H_5). This results in these two sets of protons being anisotropic, and therefore able to couple with each other. This yields two doublets in the ^1H NMR spectrum in $CDCl_3$, one at 4.26 ppm (for H_4), and another at 5.91 ppm (for H_5). Both signals integrate to four protons. The signals for H_2 and H_3 remain unchanged, appearing at 4.97 ppm and 7.10 ppm, respectively, while also maintaining their multiplicity. The same applies to the methyl feet and the extra-annular methyl groups, which appear at 1.73 ppm and 2.00 ppm, respectively.

The bromination of **4** to give **5** proceeded according to literature in yields between 60 and 70 %. The synthesis of the novel tetrasalicaldehyde cavitand **6** initially required that salicylaldehyde and NaH be added to DMF under nitrogen, to form the corresponding phenolate salt, before the addition of the bromomethyl cavitand precursor as a powder to the resulting solution. Thereafter, the solution was heated to approximately 40 $^{\circ}$C. It was found by TLC that reaction proceeded to give the tri- and tetrasalicylaldehyde products. However, on workup of the reaction solution by pouring it into water followed by extraction of the organic material using

chloroform, it was found that significant amounts of product was lost as an emulsion. This could not be avoided even by using a brine solution.

It was decided to change the reaction solvent from DMF to THF. On employing THF, TLC showed four distinct products formed corresponding to the mono-, di-, tri- and tetra salicylaldehyde products with the tetra-substituted product being the dominant product. The desired product was isolated and purified, and vacuum dried. Crystals of **5** and **6** were obtained, both of which recrystallised from 1:1 ethyl acetate:hexane. The X-ray structures of **5** and **6** have hitherto not been reported, and as such samples were analysed by single X-ray crystallography, and their structures solved. The single crystal data will be discussed in more detail in Chapter 6.

With reference to Figure 3.2, the various signals present in the ^{1}H NMR spectra of **5** and **6** (Spectrum 1.7 and 1.10, respectively in Appendix 1) can be assigned. It is notable again that **5** and **6** retain the high degree of symmetry seen in the case of **3** and **4**, which yields simplified ^{1}H NMR spectra. Bromination of the extra-annular aromatic methyl groups in the case of **5** results in a significant downfield shift in the signal of the associated protons. The signal for these methyl protons previously appeared as a singlet at 2.00 ppm in $CDCl_3$, which after bromination appears at 4.43 ppm, due to the deshielding nature of the bromine atoms which have displaced four of the twelve benzylic protons. Since the remaining protons (H_6, Figure 3.2) are isotropic, the signal remains a singlet, integrating to eight protons. The remaining signals, as discussed above (H_2, H_3, H_4 and H_5, Figure 3.1), essentially remain unchanged in terms of both chemical shift and multiplicity.

Conversion of **5** to **6** yields a number of aromatic signals in the ^{1}H NMR spectrum, as well as a distinct singlet for aldehyde protons, as shown in Figure 3.2 (H_7 - H_{10}, and H_{Ald} respectively). The aromatic region shows new signals at 7.04, 7.14, 7.53 and 7.73 ppm (all integrating to four protons), corresponding to the four different protons present on the aromatic salicylaldehyde residues. The multiplicity of the signals, two doublets (at 7.14 ppm and 7.73 ppm) and two triplets (at 7.04 ppm and 7.53 ppm) supports the presence of an *ortho*-substituted aromatic ring. The doublets arise from the coupling of H_7 with H_8, and H_{10} with H_9, while the triplets arise from the coupling of H_8 and H_9 with the neighbouring protons on either side of both these protons. Most prominent in the spectrum is the presence of the signal for the aldehyde proton, H_{Ald}, which appears at 10.18 ppm integrating to four protons. The downfield position of this

signal is characteristic of the deshielded nature of aldehyde protons due to the presence of the carbonyl functional group.

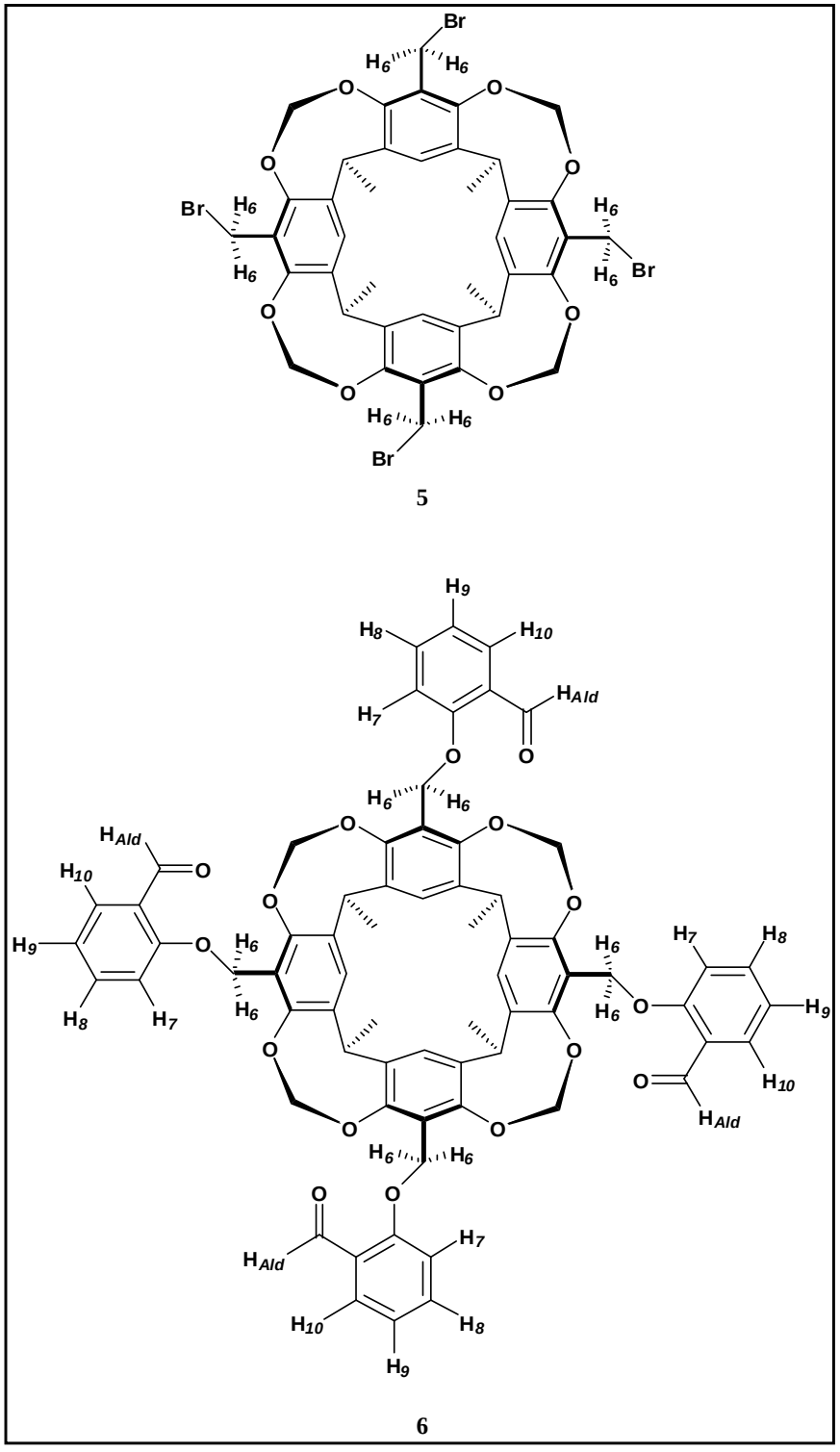

Figure 3.2: Expanded structures of 5 and 6, showing distinctive protons.

The signal due to the methylene H_6 protons again appears downfield, at 4.96 ppm, due to the deshielding nature of the neighbouring oxygen atoms. This signal, along with the signals relating to the feet (including H_2, Figure 3.1) and those relating to cavitand (H_3, H_4 and H_5, Figure 3.1) remain unchanged in terms of multiplicity and integration. However, all these protons have experienced very small changes in terms of chemical shift.

3.1.2 In situ Cyclisation and Crystallographic Analysis

With the -CH_2O- bridges and the required aromatic aldehyde successfully incorporated into the cavitand structure for *in situ* porphyrin formation, a number of approaches were taken towards obtaining the target ligand. With regards to the conditions set out by Adler, several attempts were undertaken varying the synthetic conditions. Initial protocols made use of the classical Adler conditions, where the starting materials were added simultaneously to refluxing propionic acid. Tracking of the reaction by TLC using a benzene mobile phase indicated that no product formed. Thereafter, the protocol was changed to include the use of $Zn(OAc)_2 \cdot 2H_2O$ as a templating agent; however, again no product was detected by TLC. As a final modification, the classical Adler conditions were attempted with the use of microwave irradiation as an energy source. In addition, this method made use of high concentrations of reagents, as opposed to high dilution. Nonetheless, again, no product was detected by TLC.

Synthetic conditions were therefore changed in favour of the more stringent Lindsey conditions. However, analysis of the material by ^1H and ^{13}C NMR did not confirm the presence of the target ligand. The ^1H NMR spectrum (Spectrum 1.13) did not show the presence of the required aromatic signals from either the cavitand or the porphyrin, while the signals from the inner and outer cavitand protons were also absent. The ^{13}C and attached proton test (APT) spectra (Spectrum 1.14 and 1.15, respectively) showed more conclusively that the desired ligand had not been formed. Subsequent UV-Visible spectroscopy (Spectrum 1.16) in $CHCl_3$ showed the distinct absence of a strong Soret band, associated with porphyrins, at ~ 420 nm. It was concluded that both the Adler and Lindsey conditions proved inadequate in affording the target ligand.

Initial modeling of the target ligand using CPK models indicated that the use of short -CH_2O- bridges used to bridge the cavitand to the porphyrin, in conjunction with the rigidity of the resorcinarene itself, may introduce inherent inflexibility preventing the *in situ* cyclisation

required to form the porphyrin according to Scheme 3.3. However, single crystal X-ray crystallographic analysis (see Chapter 6) of cavitand **6** provides structural information offering an explanation as to why *in situ* preparation of the target ligand was not a possibility. Figure 3.3 shows the molecular structure of cavitand **6**.

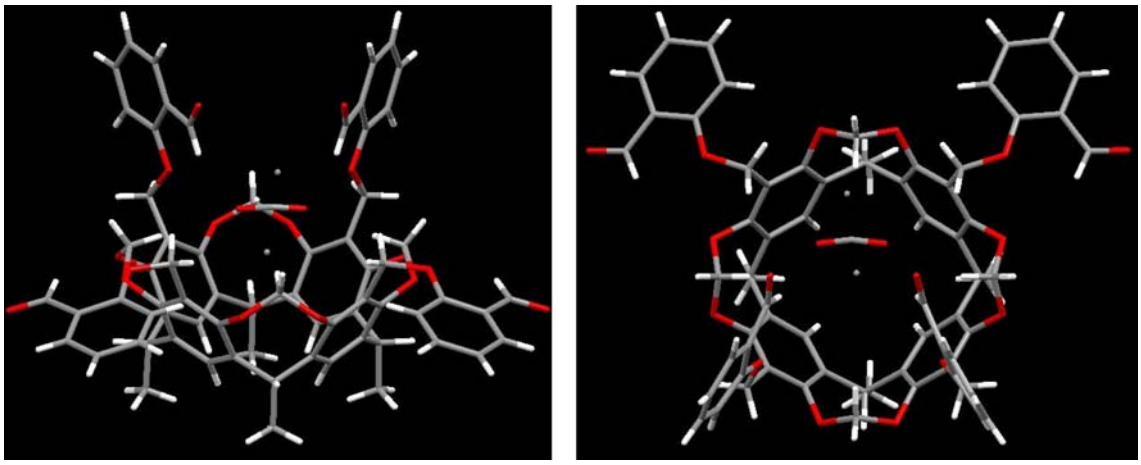

Figure 3.3: Molecular structure of **6** from side on (left), and from above (right).

It is evident that the aldehyde residues above the molecular cavity of **6** are accommodated in a non-symmetric fashion. This indicates that perhaps it is not the flexibility of the -CH_2O- bridges that is most influential in the *in situ* formation of porphyrin, but rather spatial issues above the cavitand, coming about as a direct result of the short -CH_2O- bridges. The relative positioning of the salicylaldehyde residues seems to indicate a significant degree of steric crowding above the cavitand. This steric hinderance creates insufficient space to accommodate the salicylaldehyde residues in a symmetric manner. It should be remembered that *in situ* cyclisation requires the interaction of these four salicylaldehyde residues with an additional four pyrrole units in order to complete cyclisation. Potentially, therefore, while a number of the salicylaldehyde residues may indeed react with a corresponding pyrrole unit, the accommodation of the remaining pyrrole units may be difficult, leading to incomplete cyclisation and resulting in polymer formation.

Considering the bridges of supramolecularly-capped porphyrins synthesised by the *in situ* approach, as reported in the literature,[6, 7] bridge length varies widely. In terms of cavitand-capped porphyrins, the shortest reported bridge consists of five atoms (Scheme 3.1), which allows for enough space for the salicylaldehyde residues to orientate in order to complete porphyrin formation. Shorter bridges consisting of three atoms have been reported in the case of calix[4]arene-capped porphyrins,[6c] however, it should be remembered that unlike cavitands,

calix[*n*]arenes themselves have a degree of flexibility which aids in the *in situ* porphyrin formation process.

To summarise, the *in situ* synthetic protocol did not afford the target ligand as required, primarily due to the short nature of the two-atom -CH_2O- bridges required to bridge the cavitand to the porphyrin. This is evident by the X-ray structure of the tetraaldehyde precursor **6**, as discussed above. Therefore, in order to synthesise the desired ligand, an alternative approach of direct capping of the porphyrin was investigated.

3.2 Direct Capping Approach

As with *in situ* formation, the direct capping approach of forming supramolecularly-capped porphyrins was first reported in the case of calix[*n*]arenes [13] and thereafter recently in the case of resorcin[4]arenes.[14] This approach essentially involves porphyrin, synthesised in isolation, being directly coupled with a suitable cavitand by a Williamson-type ether synthesis, reminiscent of the reaction required to form the tetrasalicylaldehyde **6** above, and therefore represents a somewhat different approach to that of the *in situ* protocol above.

In terms of cavitand-capped porphyrins, this approach has been recently used by Naruta *et al.* [15] to synthesise a host with the smallest reported cavity, able to reversibly encapsulate small hydrocarbons. Importantly with respect to the bridges used, Naruta *et al.* made use of the same -CH_2O- bridges used in this study to couple the cavitand to the porphyrin, as shown in Scheme 3.4. As is evident, the ligand reported by Naruta *et al.* made use of a cavitand-capped porphyrin where the cavitand was attached to the porphyrin by two ether bridges. This allowed retention of some flexibility in the system, and enabled the reversible encapsulation of guests. The proposed retrosynthetic pathway pertaining to the synthetic target in this study can hence be seen in Scheme 3.5 clearly showing the separate synthetic development of cavitand and porphyrin.

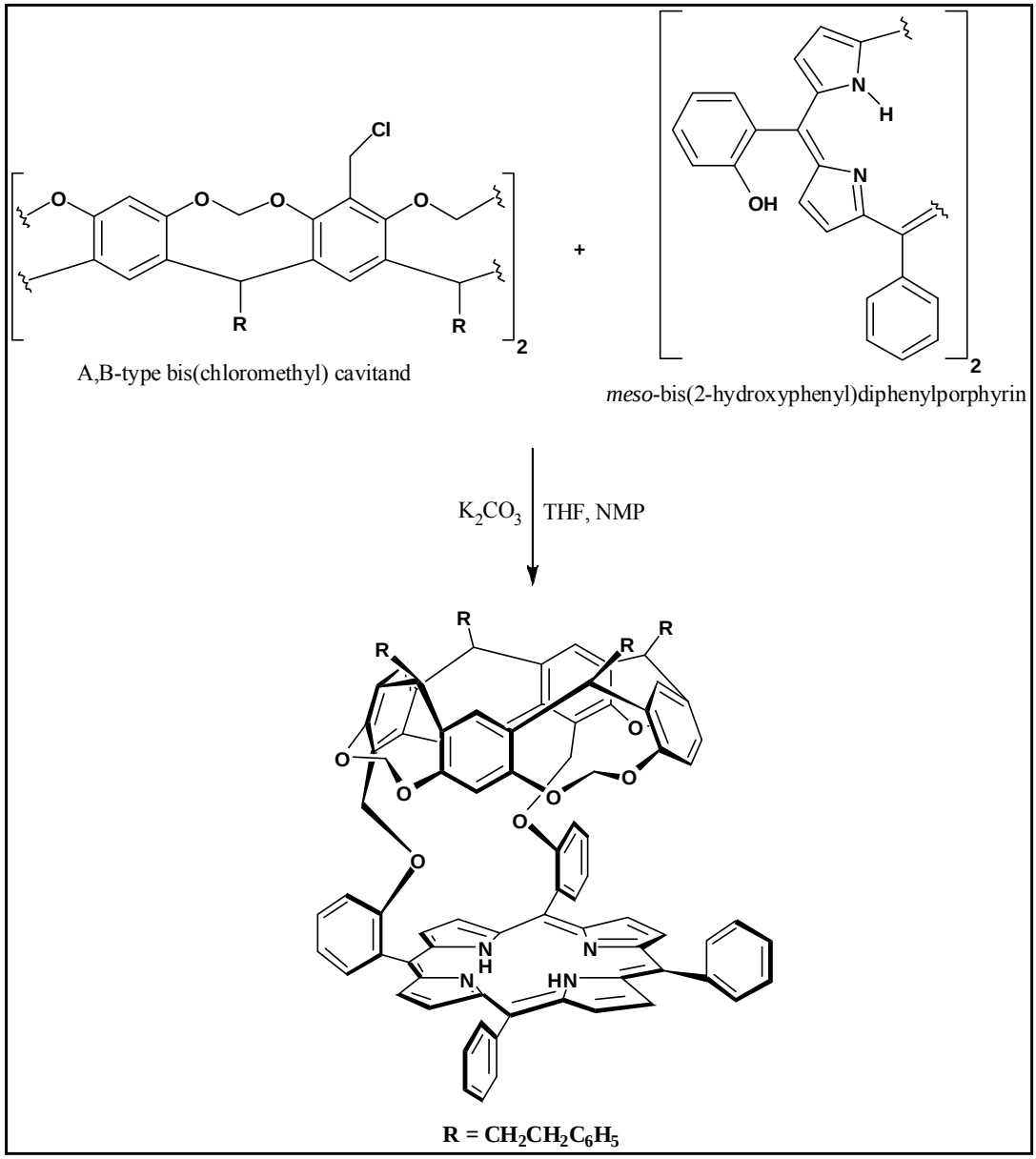

Scheme 3.4: Synthesis of Naruta *et al.* towards the reported cavitand-capped porphyrin.

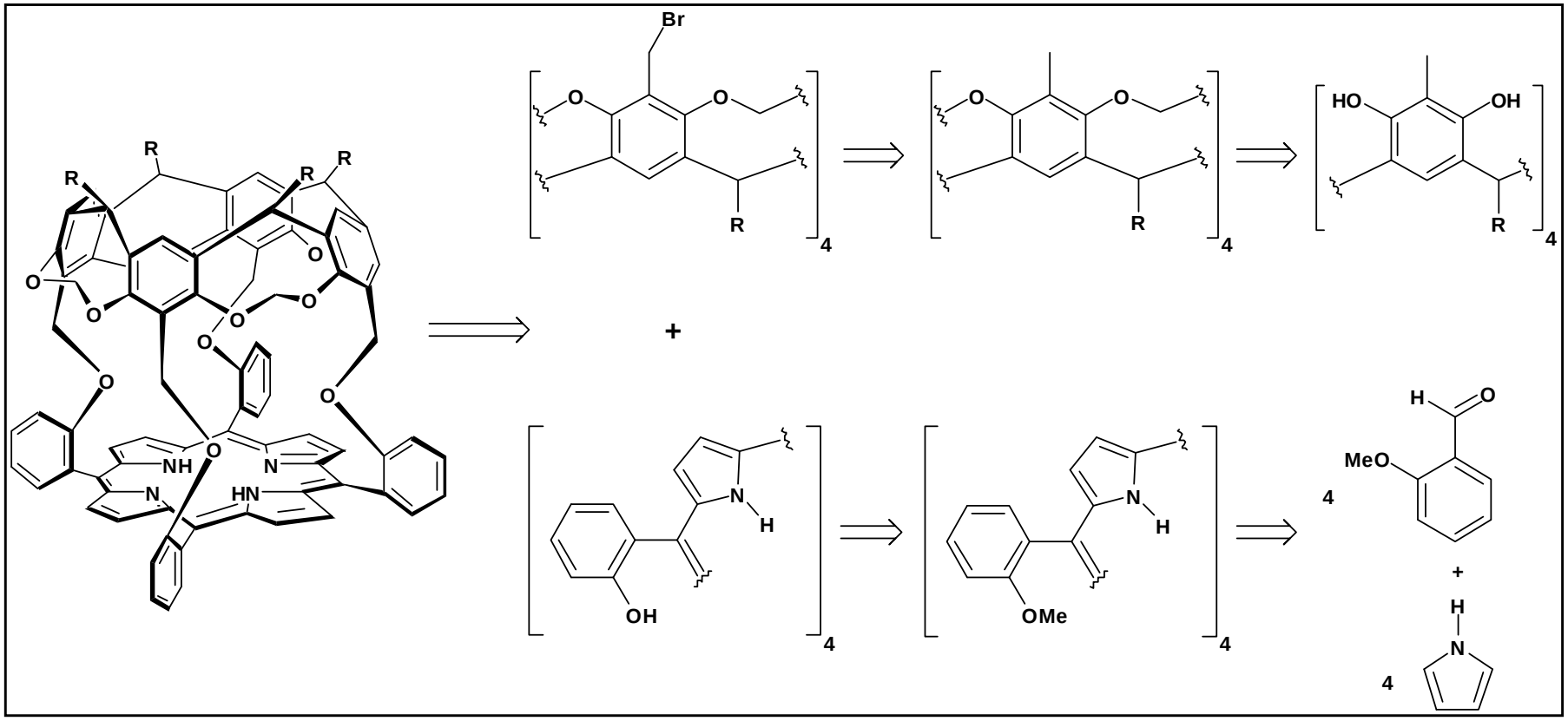

Scheme 3.5: Retrosynthetic pathway towards direct capping of porphyrin by cavitand to form the proposed ligand.

In terms of porphyrin synthesis, the two conditions (Adler conditions, and Lindsey conditions) available for porphyrin formation have been discussed. Scheme 3.6 illustrates and compares these two conditions. With regards to porphyrin **12**, both conditions give best yields when the synthesis is performed *via* the tetramethoxyphenylporphyrin **11** pathway. It has been shown that use of the 2-hydroxybenzaldehyde starting material results in an especially low yield of product, regardless of what set of reaction conditions are used.[8, 16] For this study, however, the chosen set of synthetic conditions was in favour of the Lindsey conditions, since it provided fewer synthetic steps towards the desired porphyrin in higher yields, as evident in Scheme 3.6. Adler conditions give increased yields when synthesis is performed using zinc around which to template the porphyrin formation to give metalloporphyrin **10**.[17] In addition to representing an extra synthetic step towards the desired porphryin **12**, demetallation of porphyrin **10** is not quantitative. As such, overall yield towards porphyrin **12** using the Adler conditions is in the order of 10 – 20 %, in contrast to the Lindsey conditions, which yields 35 % of porphyrin **12** in fewer synthetic steps.

Porphyrin synthesis therefore commenced with the use of *o*-anisaldehyde as the starting material. This gives rise to a product which is a mixture of four possible atropisomers, with the methoxy substituents (or hydroxy substituents, after subsequent removal of methoxy groups, Scheme 3.6) on the phenyl rings facing in different directions in various combinations, namely αααα, αααβ, αβαβ, and ααββ, where α refers to 'down' and β to 'up'. In order to facilitate the coupling of cavitand to porphyrin by four ether bridges, it is preferable to isolate the αααα isomer. The required chromatography has been reported [17] and requires careful and meticulous control of chromatographic conditions. In addition, the literature also shows that the desired αααα isomer forms in least abundance along with the ααββ isomer, with the αααβ isomer forming in preference. The complete synthesis of the target ligand *via* the direct capping approach can be seen in Scheme 3.7.

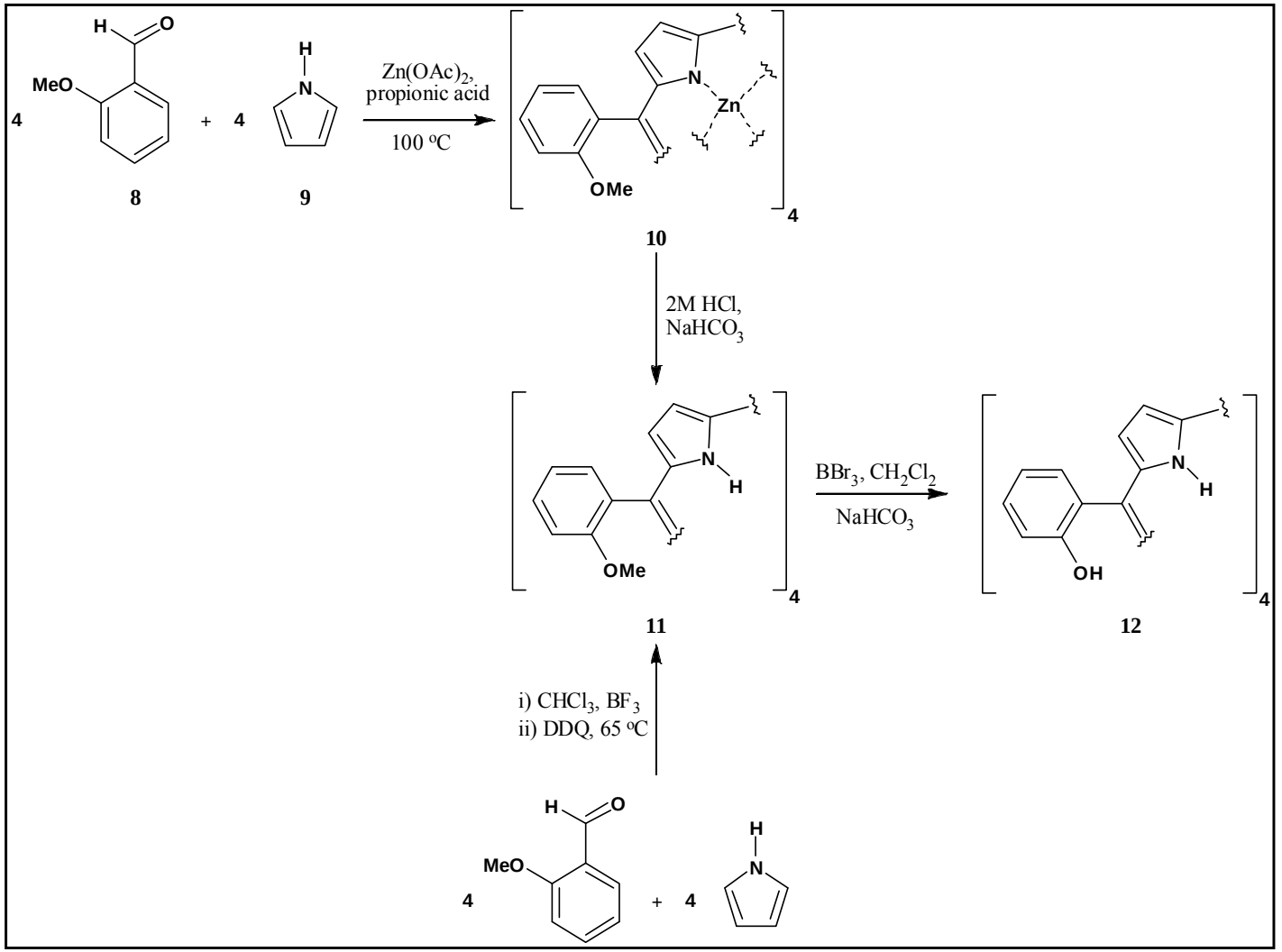

Scheme 3.6: Formation of porphyrin *via* the Adler conditions (above) and the Lindsey conditions (below).

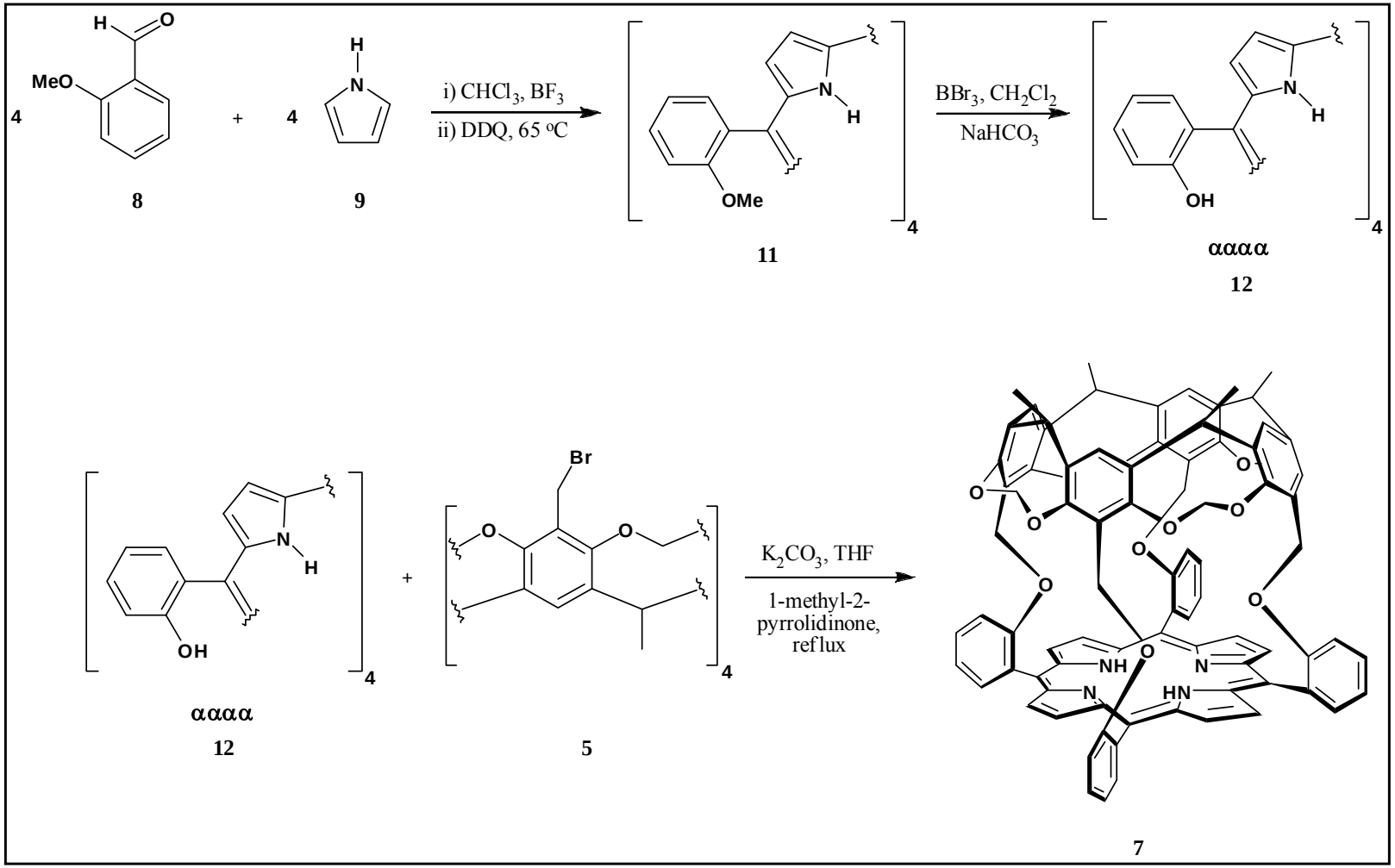

Scheme 3.7: The proposed direct capping synthetic pathway towards the target ligand.

3.2.1 Results: Porphyrin Synthesis

The synthesis of the required porphyrins **11** and **12** was completed successfully in yields comparable to those reported in literature. Analysis using ^{1}H NMR as well as UV-Vis spectroscopy was carried out in order to confirm porphyrin formation. In order to discuss the ^{1}H NMR spectra of **11** and **12**, reference will be made to Figure 3.4, the complete structure of porphyrins **11** and **12** showing distinctive protons.

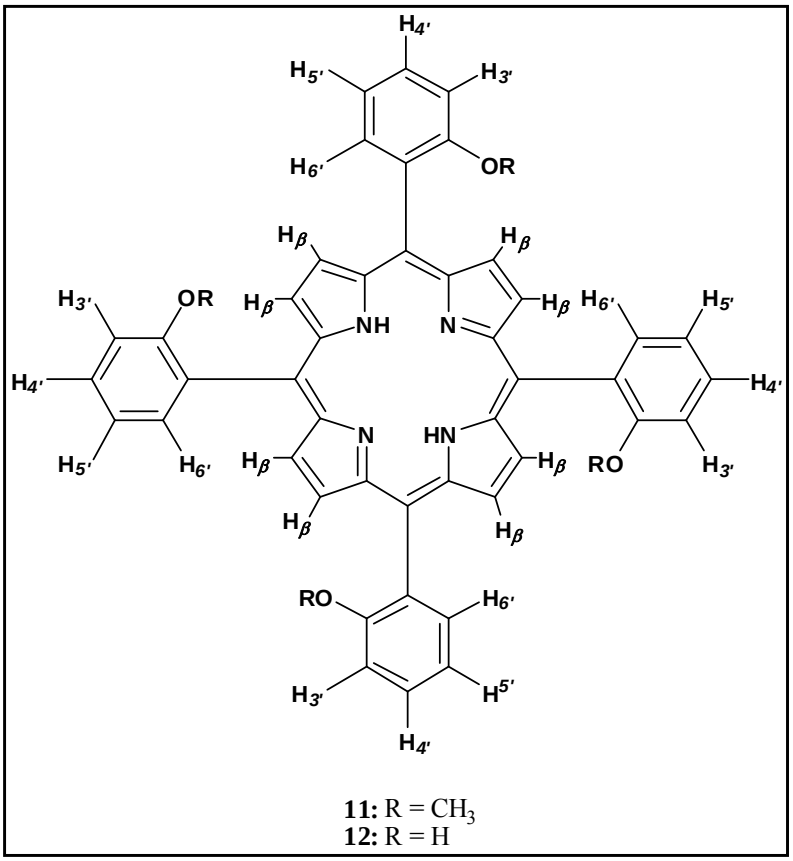

Figure 3.4: Expanded structures of **11** and **12**, showing distinctive protons.

Figure 3.4, as with Figures 3.1 and 3.2, again illustrates the symmetry of the molecules being dealt with. The equivalence of the protons present as evident in Figure 3.4 again leads to simplified ^{1}H NMR spectra. The most notable feature of the porphyrin free ligand is the presence of the protons associated with the nitrogen atoms. The signals due to these protons appear at chemical shifts of between -2 ppm to -3 ppm, largely due to the electronic delocalisation of the porphyrin ring and the well-documented ring current associated with it.[18] In the case of **11** and **12**, in addition to the signals from the amine protons, characteristic signals

appear as a result of the R groups on the *meso*-aromatic rings, as well as from the eight *β*-pyrrole protons (H_β).

Looking at Spectrum 1.17, the ^{1}H NMR spectrum of **11**, the amine protons could not be seen below 0 ppm and are hence not shown on the spectrum. The methoxy groups (R = CH_3, Figure 3.4) give rise to signals in the methoxy region, at a chemical shift of 3.55 ppm to 3.60 ppm. This signal integrates to twelve protons as expected, but appears not as a singlet but as a multiplet, due to the presence of the four different isomers of **11**, as discussed. The *meso*-aromatic protons $H_{3'}$ to $H_{6'}$ yield signals in the aromatic region, from 7.28 ppm to 8.03 ppm. Protons $H_{3'}$ and $H_{5'}$ give rise to a multiplet signal ranging from 7.28 ppm to 7.36 ppm. The multiplicity is due to coupling of these protons with protons on either side: $H_{3'}$ couples with $H_{4'}$ while $H_{5'}$ couples with $H_{4'}$ and with $H_{6'}$. The signal integrates to eight protons. The signal from $H_{4'}$ yields a triplet integrating to four protons at 7.76 ppm; multiplicity as a result of coupling with protons $H_{3'}$ and $H_{5'}$. Finally, proton $H_{6'}$ results in a set of doublets at 7.93, 7.99 and 8.03 ppm, with the set integrating to a total of four protons. The signals are a result of the superposition of six doublet of doublets, which appear due to the coupling of these protons with the neighbouring $H_{5'}$ protons. Interestingly, the intensity for these signals appears in a ratio of 1:1:2:2:1:1, which arises as a result of the presence of the four isomers. This ratio corresponds to the product distribution of the isomers, which is in the ratio of 1:4:2:1 for αααα:αααβ:ααββ:αβαβ.[17] Lastly, the signal for the *β*-pyrrole protons appears as two singlets at 8.69 ppm and 8.80 ppm having relative intensities of 3:1, collectively integrating to eight protons.

Cleaving of the methoxy groups in **11** to the corresponding tetrahydroxyporphyrin **12** leads to a notable change in the ^{1}H NMR spectrum of **12** (Spectrum 1.22, Appendix 1) from that of **11**, in the region of 3 ppm to 5 ppm. The disappearance of the methoxy groups results in the disappearance of the corresponding signals at 3.55-3.60 ppm, and the appearance of a signal at 4.93 ppm integrating to four protons. This indicates the presence of the hydroxyl group and confirming the removal of the methoxy groups. The signal has also become broad compared to that of the methoxy signals, which is indicative and characteristic of hydroxyl protons. With regards to the signals related to the *meso*-aromatic protons, signal position and multiplicity has remained largely unchanged, with some simplification of some of the signals occurring. The signals for protons $H_{3'}$ and $H_{5'}$ again appear as a multiplet in the region of 7.32 ppm to 7.38 ppm, integrating to eight protons. The signal from $H_{4'}$ remains as a triplet integrating to four protons, as it did for porphyrin **11**. However, the signal for $H_{6'}$ no longer appears as a set of

doublets, but instead has simplified down to a broad multiplet at 7.95 ppm integrating to four protons. In addition, the signals for the *β*-pyrrole protons have also simplified from two singlets, down to one singlet at 8.91 ppm integrating to eight protons.

While porphyrin synthesis was a success, the isolation of the αααα isomer proved to be problematic. Replication of the column chromatographic conditions cited in literature could not be achieved. However, on examination of the procedure of Naruta *et al.* it was found that in the case of the reported cavitand-capped porphyrin, the synthesis was completed *via* the use of a mixture of porphyrin isomers, since isomerisation was observed to occur at room temperature. Once reaction was complete, separation of the different products was possible by careful column chromatography.

Since the αααα isomer could not be exclusively obtained in this study, the mixture of porphyrin isomers was used to couple cavitand to porphyrin under the same conditions as those used by Naruta *et al*.

3.2.2 Results: Direct Capping of Porphyrin

The procedure by Naruta *et al.*[15] to cap the porphyrin makes use of the starting materials shown in Scheme 3.4, accompanied by long reaction times (four days) at temperatures of 120 °C in a sealed stainless steel reaction tube. It was decided to repeat the procedure, using a lower temperature (100 °C) under reflux for a longer period of time (five days) using **5** and **12**, as evident in Scheme 3.7.

After five days it was found by TLC that, in addition to polymeric material, only one additional compound was observed. A possible explanation of this observation lies in the reaction conditions that were used: the high temperature used over the period of five days is sufficient to facilitate the isomerisation of the porphyrin phenyl rings, about the *meso* bonds. This would allow the *meso*-OH substituents to be orientated accordingly to facilitate the coupling of the cavitand to the porphyrin. Indeed, the energy required for this interconversion between the atropisomers of porphyrin **12** has been reported, and is in the order of 100.42 $kJ.mol^{-1}$ (24 $kcal.mol^{-1}$).[19] It should be remembered that molecules have sufficient kinetic and thermal energy to allow processes ranging from 62.8 to 83.7 $kJ.mol^{-1}$ (15 to 20 $kcal.mol^{-1}$) at room

temperature.[20] Therefore, the reaction conditions are more than sufficient to facilitate isomerisation.

Since the target ligand is a non-polar compound, analogous to tetraphenylporphyrin in terms of polarity, the compound with the highest R_f value was identified as potentially being the target ligand. The chromatographic protocol followed by Naruta *et al.* (a benzene mobile phase on a silica gel column) was used to isolate this material. It was, however, found that separation using benzene was greatly affected by the amount of polymeric material present in the crude product. In this regard, a preliminary column using a mobile phase of chloroform was very effective in removing the majority of the unwanted material from the crude product, and improving separation on the subsequent benzene eluted column.

The potential product was successfully isolated according to the above protocol. However, on removing of the eluant to obtain a violet solid, it was found that the product became insoluble in most organic solvents, including chloroform as well as DMF and DMSO. As a result, ^{1}H and ^{13}C NMR spectroscopy could not be completed on the material. However, while solubility rendered the characterisation of the synthesised material difficult, it had further implications for synthesis of a catalyst based on this ligand. In order to place a metal within the porphyrin macrocycle, the ligand needed to be soluble in DMF, the solvent most commonly used for metallation of porphyrins.[15-17] The insolubility of the material meant that, even if the ligand was indeed successfully synthesised, metallation would prove to be impossible. Such insolubility issues related to methyl feet have been encountered before, in the case of the first closed molecular container, a carcerand, as reported by Cram *et al*.[1b] Since the target ligand is analogous to such molecules, as discussed in Chapter 4 to follow, cavitands with enhanced solubility in organic solvents need to be considered in order to improve solubility of the target ligand.

3.2.3 Synthesis of Cavitands Having Improved Solubility

As discussed in Chapter 1, cavitand solubility can be controlled by varying the hydrophobicity or hydrophilicity of the cavitand feet. In the interests of improving solubility of the target porphyrin therefore, longer cavitand feet were required. As such, the synthesis towards obtaining bromomethyl cavitands similar in structure to **5** was undertaken, according to Scheme 3.8 below.

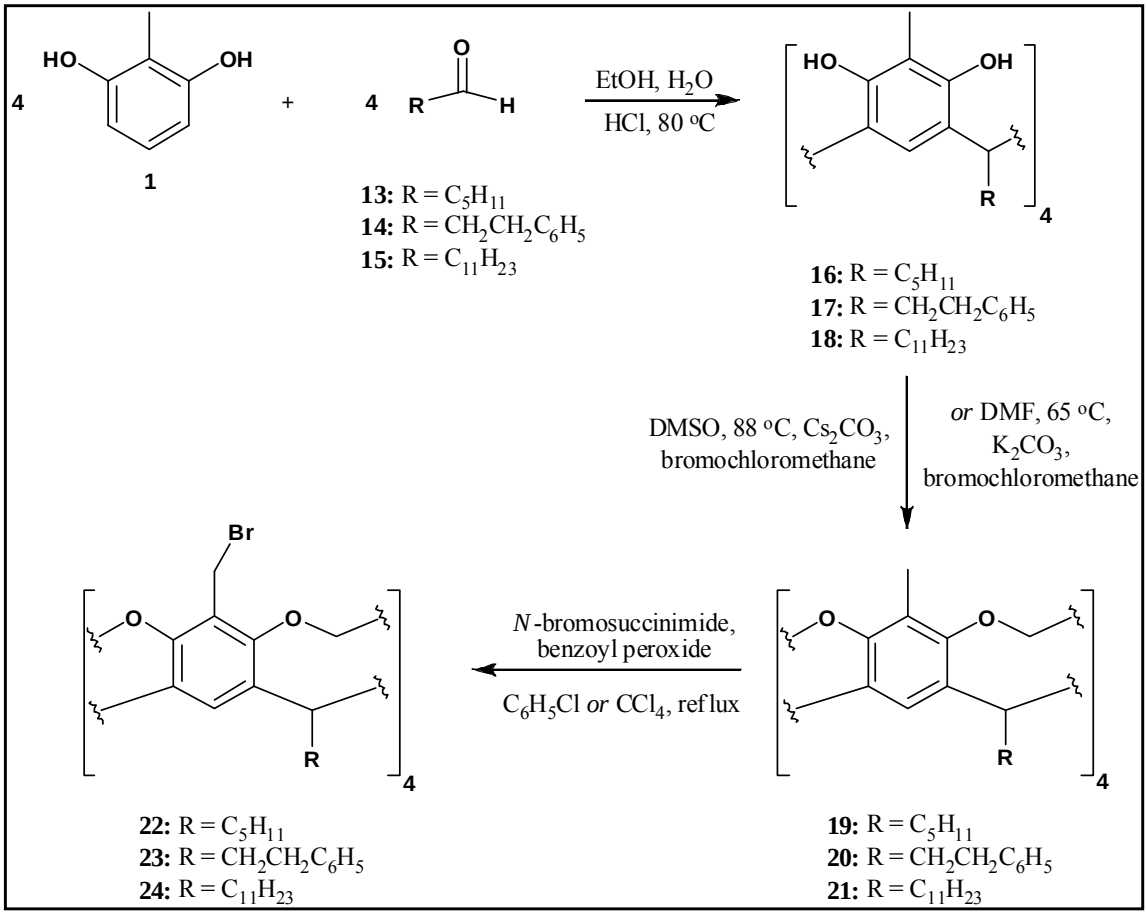

Scheme 3.8: Proposed synthetic protocol towards bromomethyl cavitands bearing longer feet.

The synthesis of resorcin[4]arenes **16** - **18** from **1** and aldehydes **13** - **15** was accomplished according to the protocol as set out in section 3.1 above. Resorcin[4]arenes **16** [1c] and **18** [21] have already been reported in the literature; however **17** is a novel resorcin[4]arene, synthesised according to the protocol as for **16**. These resorcin[4]arenes were again characterised using ^{1}H NMR; spectra for **16**, **17** and **18** appear in Appendix 1 as Spectrum 1.27, 1.30 and 1.33, respectively. Since the ^{1}H NMR spectrum of **3** has been fully discussed above, the ^{1}H NMR data for **16** - **18** is tabulated in Table 3.1 below. Reference is made to Figure 3.1 above, regarding the labeling of the different protons. As a novel compound, crystals of **17** were grown from methanol; samples were sent for crystallography and the X-ray structure solved. Data obtained will be discussed in more detail in Chapter 6.

Table 3.1: ^{1}H NMR data for compounds **16 - 18**.

	Chemical shift/ppm (multiplicity‡, integration/protons)		
Proton	**16***	**17***	**18†**
H_1	8.67 (*s*, 8)	8.73 (*s*, 8)	7.98 (*s*, 8)
H_2	4.18 (*t*, 4)	4.26 (*t*, *J* = 7.0 Hz, 4)	4.34 (*t*, 4)
H_3	7.25 (*s*, 4)	7.39 (*s*, 4)	7.43 (*s*, 4)
Feet	0.86 (*t*, 12)	2.49 (*m*, 28)≠	0.91 (*t*, 12)
	1.33 (*m*, 24)	7.13 (*m*, 20)	1.32 (*m*, 72)
	2.20 (*m*, 8)		2.29 (*m*, 8)

‡ *s* refers to a singlet, *t* to a triplet, and *m* to a multiplet.

***** Spectrum recorded in d_6-DMSO; **17** is a novel compound.

† Spectrum recorded in d_6-acetone.

≠ Includes residual solvent signals from DMSO in integration.

With regards to the synthesis of the corresponding cavitands from the resorcin[4]arene starting materials, cavitand **19** could not be synthesised from **16** using the method as set out by Kaifer *et al.*, and the original protocol as set out by Bryant *et al.*[1d] was attempted. This procedure was successful in yielding the desired cavitand. In contrast, cavitands **20** and **21** were successfully synthesised from corresponding resorcin[4]arenes **17** and **18** *via* the method of Kaifer *et al*. These cavitands were again characterised using ^{1}H NMR, the data for which appears in Table 3.2. Full spectra again appear in Appendix 1, Spectrum 1.36, 1.39 and 1.42 applicable to **19**, **20** and **21**, respectively. Reference is made to Figure 3.2 regarding the labeling of the protons present in **19 - 21**. In addition, crystals of the novel cavitand **20** were grown from liquid diffusion of methanol, into a solution of **20** in 1:1 ethyl acetate:hexane. Samples were sent for single crystal X-ray crystallography, and the structure was solved. A more detailed discussion of crystal data will be presented in Chapter 6.

Table 3.2: ^{1}H NMR data for compounds **19 - 21** in $CDCl_3$.

	Chemical shift/ppm (multiplicity‡, integration/protons)		
Proton	**19**	**20***	**21**
H_2	4.73 (*t*, 4)	4.83 (*t*, *J* = 8.0 Hz, 4)	4.73 (*t*, 4)
H_3	6.95 (*s*, 4)	7.00 (*s*, 4)	6.95 (*s*, 4)
H_4	4.25 (*d*, 4)	4.26 (*d*, *J* = 7.0 Hz, 4)	4.25 (*d*, 4)
H_5	5.85 (*d*, 4)	5.88 (*d*, *J* = 7.0 Hz, 4)	5.85 (*d*, 4)
Aromatic methyl	1.95 (*s*, 12)	2.00 (*s*, 12)	1.93 (*s*, 12)
Feet	2.15 (*m*, 8)	2.44 (*m*, 8)	2.16 (*m*, 8)
	1.33 (*m*, 24)	2.62 (*m*, 8)	1.24 (*m*, 72)
	0.89 (*m*, 12)	7.11 (*m*, 20)	0.86 (*t*, 12)

‡ *d* refers to doublet.

***20** is a novel compound.

Bromination of the benzylic methyl groups of cavitands **19 - 21** proved to give mixed results. The bromination of **20** to synthesise **23** using the method set out by Sorrel *et al.*[2] did not afford the desired brominated cavitand; instead, ^{1}H NMR analysis indicated the presence of a mixture of partially brominated compounds, accompanied by loss of signal resolution and broadening of signals. Reaction conditions were changed in favour of the conditions of Gardner *et al.*[21] where chlorobenzene instead of CCl_4 is used as reaction solvent in order to facilitate higher reflux temperatures. However, ^{1}H NMR analysis of reaction product again gave the same results as above. In order to ascertain whether or not loss of symmetry was resulting in the broadened and unresolved ^{1}H NMR signals, variable temperature ^{1}H NMR was performed on products from both bromination protocols. Spectra were recorded at -20 $^\circ$C, 0 $^\circ$C, room temperature, and 50 $^\circ$C, however, no improvement in signal quality was observed. Subsequent synthesis involving the $CH_2CH_2C_6H_5$-footed cavitand was thus abandoned.

In contrast, the bromination of **19** and **21** to give **22** and **24**, respectively, proceeded as *per* conditions set out in the literature.[2, 21] The resulting bromomethyl cavitands were again characterised by ^{1}H NMR, results of which are tabulated in Table 3.3. Complete spectra appear in Appendix 1, Spectrum 1.45 and 1.48 pertaining to **22** and **24**, respectively. Again, reference is made to Figure 3.2 regarding the manner in which protons present in **22** and **24** are labeled. Additionally, crystals of **22** were grown by slow liquid diffusion of methanol into a solution of **22** in 1:1 ethyl acetate:hexane. Samples were again sent for single X-ray crystallography, and its X-ray structure solved. A more detailed discussion of crystal data follows in Chapter 6.

Table 3.3: ^{1}H NMR data for compound **22** and **24** in $CDCl_3$.

	Chemical shift/ppm (multiplicity, integration/protons)	
Proton	**22**	**24**
H_2	4.76 (*t*, 4)	4.72 (*t*, 4)
H_3	7.11 (*s*, 4)	7.14 (*s*, 4)
H_4	4.55 (*d*, 4)	4.53 (*d*, 4)
H_5	6.02 (*d*, 4)	6.05 (*d*, 4)
H_6	4.40 (*s*, 8)	4.38 (*s*, 8)
Feet	0.89 (*t*, 12)	0.85 (*t*, 12)
	1.33 (*m*, 24)	1.31 (*m*, 72)
	2.19 (*m*, 8)	2.16 (*m*, 8)

3.2.4 Results: Capping of Porphyrin Using Cavitands With Improved Solubility

With the successful synthesis of **22** and **24**, the reaction to couple cavitand to porphyrin was repeated using the same reaction protocol as in the case of **5** and **12**, and as shown in Scheme 3.9. In both cases, the crude material was isolated and purified as *per* the protocol which was used towards the synthesis of **7**.

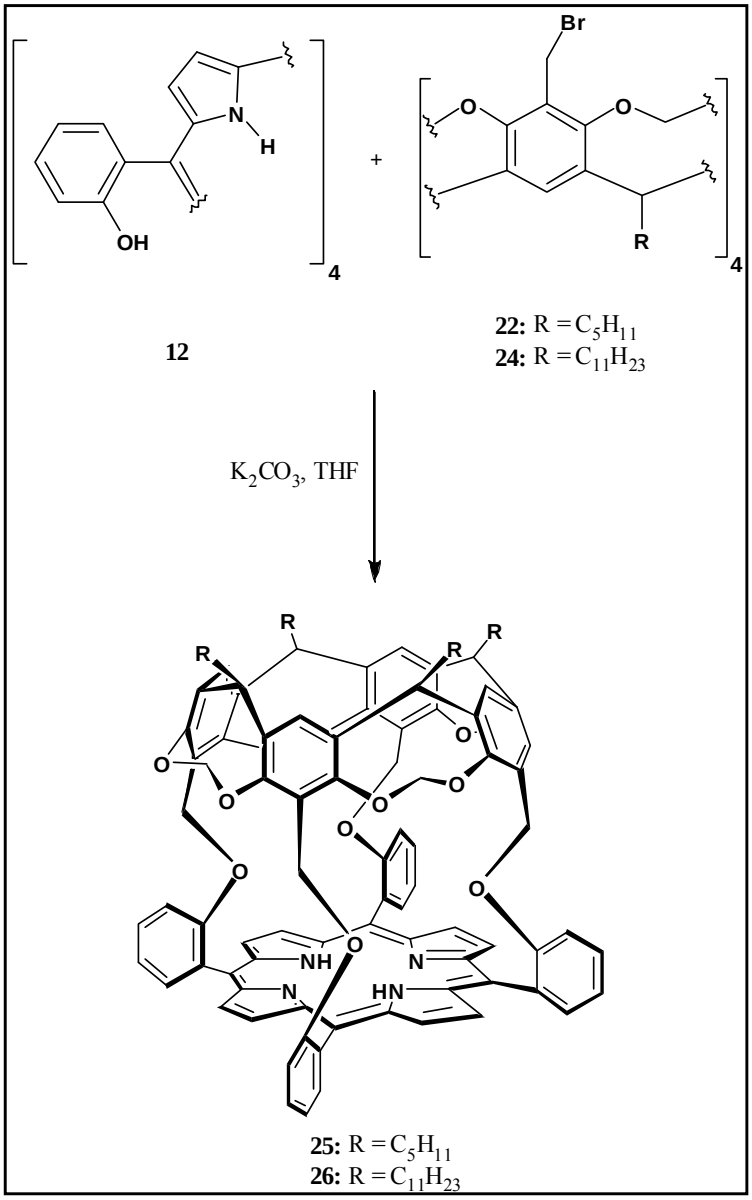

Scheme 3.9: Synthetic protocol towards target ligand bearing longer feet.

The use of **22** as ligand precursor in reaction towards **25** gave very low yields of material once isolation was complete. Preliminary analysis using UV-Vis spectroscopy in $CHCl_3$ showed the distinct absence of a strong Soret band, associated with porphyrins, at ~ 420 nm. In addition, ^1H

NMR analysis indicated a lack of aromatic signals, with signals belonging to the *β*-pyrrole absent in the spectrum. It was consequently concluded that the reaction was unsuccessful in affording **25**.

Reaction involving **24** as ligand precursor proved to be different in terms of yield and result. Upon isolation, the yield of material was found to be 22 %. Preliminary analysis using UV-Vis spectroscopy indicated the presence of the Soret band, at 418 nm (Spectrum 1.58). In addition, Spectrum 1.58 exhibits additional signals associated with porphyrins at wavelengths between 480 and 700 nm (seen more clearly in Spectrum 1.59), which are also seen in the UV-Vis spectrum of porphyrin **12**. The spectrum also shows two signals between 200 and 350 nm (Spectrum 1.60), which are a result of the presence of the cavitand structure as seen in the UV-Vis spectrum of **24** (Spectrum 1.51). The UV-Vis spectrum thus appears as a combination of the spectra of **12** and **24**, indicating the formation of cavitand-capped porphyrin **26**. This is shown more clearly in Spectra 1.61 and 1.62, comparisons of the UV-Vis spectra of the respective starting materials (in blue) with **26** (in red) over corresponding wavelengths. A summary of the UV-Vis signals present in **26**, compared with those of the two starting materials, **12** and **24**, appears in Table 3.4.

The analysis of **26** using NMR techniques (at 400 MHz) was anticipated to give the same results as *per* the UV-Vis analysis, with both the ^{1}H and ^{13}C NMR spectra expected to appear as combinations of the respective spectra for the two starting materials. Regarding the ^{1}H NMR spectrum (Spectrum 1.52) of **26**, the presence of the aromatic *β*-pyrrole protons as well as the protons belonging to the *meso* tetraphenyl rings, is suggested by the range of signals from 7.75 ppm to 9.03 ppm. Protons belonging to the feet of **26** give signals at 0.88, 1.26 and 2.18 ppm, which are consistent with the chemical shifts and multiplicity of the corresponding signals of the bromomethyl cavitand starting material (Table 3.3). The two signals associated with the methylene bridges of the cavitand structure (at approximately 4.5 and 6.0 ppm), along with the signal arising from the uncoupled methylene protons of the -CH_2O- cavitand-porphyrin bridges (at approximately 4.4 ppm) lack resolution but appear to be present. In order to improve the quality and resolution of these signals, low temperature ^{1}H NMR experiments were attempted. However, as shown in Spectrum 1.53, the ^{1}H NMR spectrum of **26** at -40 $^{\circ}$C, no significant improvement in resolution is evident, despite acquisitions performed at 600 MHz.

Table 3.4: Comparison of UV-Visible data between starting materials **12** and **24**, and **26** in $CHCl_3$.

	λ_{max} **of UV-Vis signal/nm**	
Starting Material		**26**
12	642.55	640.00
	586.99	586.33
	547.05	544.50
	512.95	513.83
	418.46 (Soret)	419.33 (Soret)
	398.53	402.16
	350*sh*‡	365.83*sh*
	310*sh*	348.33*sh*
24	290.00	280.16
	250.50	239.66

‡ *sh* refers to the presence of a shoulder.

Given the poor resolution and the number of additional signals in the ^{1}H NMR spectra, ^{13}C NMR spectroscopy stood as a valuable tool in the characterisation of **26**. However, signals, particularly in the aromatic regions of the ^{13}C NMR spectrum of **26** (Spectrum 1.54), proved to be very broad and weak. Subsequent two dimensional NMR experiments, such as HSQC therefore proved to be difficult, and correlations, especially in the aromatic region, were absent. NOESY experiments were also attempted. The initial CPK modeling of the ligand showed that protons from the cavitand -OCH_2O- ether bridges were in close proximity to the *β*-pyrrole protons of the porphyrin. Such proton-proton interactions through space were identified as a possible means of confirming complete capping. Thus, NOESY was anticipated to give a correlation between the cavitand protons (at approximately 4.5 and 6.0 ppm) with the *β*-pyrrole

protons (at between 8.0 and 9.0 ppm). NOESY spectra of **26** were recorded at both room temperature, and at -20 °C (Spectrum 1.55 and 1.56, respectively) at 600 MHz. However, in both cases, only correlations between the cavitand protons were seen, and none between the *β*-pyrrole protons and the cavitand protons.

Therefore, NMR techniques offered no absolute proof of the successful synthesis of **26**, and that the capping protocol afforded the desired ligand. Therefore, as a means to conclusively show a successful synthesis, mass spectrometry was employed. Both fast atom bombardment (FAB) and electrospray ionization (ESI) mass spectrometry (MS) were attempted. The FAB mass spectrum of **26** (Spectrum 1.63) was unable to show a parent *M/z* signal at 1880 as expected; indeed, no signal higher than approximately 700 *M/z* in value was observed.

As an alternative method, ESI-MS techniques were employed. ESI is commonly used for macromolecules since it prevents the tendency of the molecule to fragment on ionization.[22] As such, this technique stood to give more promising results. However, while larger fragments were observed at high *M/z* values (Spectrum 1.64), the parent signal was again absent. Therefore, both MS techniques failed to confirm that **26** had been successfully synthesised.

3.2.5 Crystallographic Analysis of Precursors to Direct Capping

Crystallography again proved useful in offering an explanation as to why the direct capping protocol failed to give the desired capped porphyrin. As mentioned in section 3.1.1, crystals of bromomethyl cavitand **5** were obtained and the X-ray structure (hitherto unknown) solved. As a representative precursor of the cavitands used in the direct capping procedure, the structural characteristics obtained from the X-ray analysis provided invaluable information regarding synthesis.

Figure 3.5 shows the molecular structure of cavitand **5**. Although one bromine atom appears to be disordered, the symmetry typical of such functionalised cavitands is evident. The bromine atoms are orientated such that two (opposite) bromines face into the cavity, and two out. The methylene carbons which have inward-facing bromine atoms are 9.83 Å apart, while the same distance for those carbons having outward-facing bromine atoms is found to be 9.36 Å. Significantly, the average distance between the carbon atoms is approximately 9.6 Å.

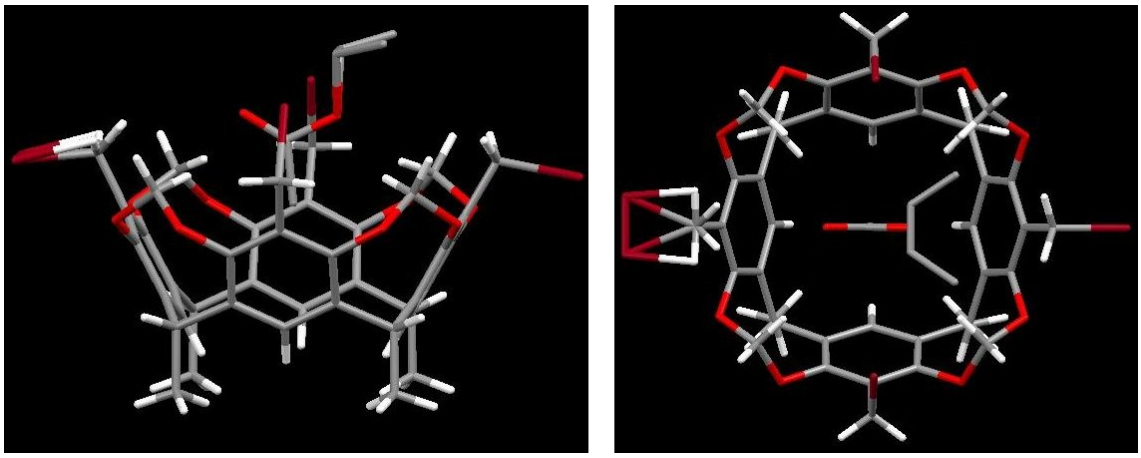

Figure 3.5: Molecular structure of **5** from side on (left), and from above (right).

In contrast, the distance between two opposing hydroxyl oxygen atoms of porphyrin **12** is (by crystallographic analysis) approximately 10.1 Å.[23] The porphyrin therefore appears to be too large to fit comfortably with the cavitand and complete capping. Since the methylene carbons are unable to move significantly due to the rigidity of the cavitand scaffold, and given the rigid, planar character of the porphyrin macrocycle, the nucleophilic porphyrin oxygen atoms remain too far apart to completely interact with the cavitand carbon atoms to cap the resorcinarene.

Observations in hemicarcerand chemistry additionally support the notion that the porphyrin was unable to suitably fit over the resorcinarene to complete capping. Hemicarcerands[24] are the result of an analogous synthetic procedure. However, it has been noted that shell closure of a container molecule such as a hemicarcerand, or indeed, a capped porphyrin, does not proceed when the enclosure process occurs around empty space. It is conceivable that container molecules require solvent within the confines of the host molecules in order to solvate and stabilise the transition state through which the guest molecules pass during synthesis.[25] Should the cavitand have solvent molecules within the confines of the molecular cavity stabilising the required transition state, it is possible that the porphyrin may experience difficulty in reacting across the open bonds at all four points to complete capping.

In summary, while UV-Vis suggested that the synthesis of **26** was successful, it could not be conclusively proved by NMR and MS methods. Therefore, the direct capping approach, in essence, failed to afford the target ligand. As seen in the *in situ* approach, crystallography played an important role in illustrating that the chosen bridge length was in fact too short to allow a successful synthesis. The porphyrin appears to be too large to comfortably fit over the

cavitand during synthesis to complete capping. This is a direct result of the short -CH_2Br- functional groups required to ultimately yield the desired -CH_2O- capped porphyrin bridges.

3.3 In situ Approach Revisited

In order to verify the results seen in the *in situ* approach which made use of the methyl footed cavitand derivatives, the same protocol was applied to cavitands bearing longer feet. Therefore, using **22** as a precursor, *in situ* formation of target ligand **25** bearing C_5H_{11} feet was attempted *via* the tetrasalicylaldehyde pathway as shown in Scheme 3.10.

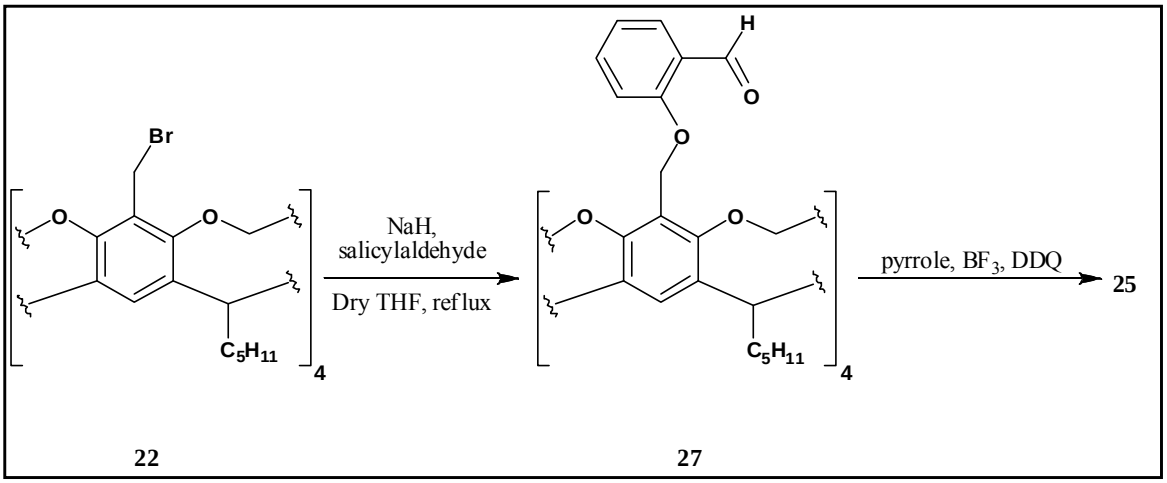

Scheme 3.10: *In situ* synthetic pathway towards **25**.

Although identical synthetic conditions were applied to the synthesis of **27** as in the synthesis of **6**, tracking the reaction by TLC showed only tri- and tetrasubstituted products. This is in contrast to the synthesis of **6**, which showed the formation of mono-, di-, tri- and tetrasubstituted products. In addition, the yield of **27** was vastly improved; 80 % in the case of **27** as opposed to 28 % in the case of **6**. Since the precursor to tetrasalicylaldehyde formation in each case differs only in feet length (CH_3, in the case of precursor **5**, *versus* C_5H_{11}, in the case of precursor **22**) it is conceivable that this increased yield is due to improved solubility of **22** relative to **5**.

Characterisation of **27** was completed, again using ^{1}H NMR at 400 MHz. Since the ^{1}H NMR spectrum of **6** has been discussed in detail already, the results for **27** (Spectrum 1.65) are tabulated in Table 3.4, with reference to Figures 3.1 and 3.2 regarding the labeling of the various protons.

Table 3.4: ^{1}H NMR data for compound **27** in $CDCl_3$.

	Chemical shift/ppm (multiplicity, coupling constant, integration/protons)
Proton	**27**
H_2	4.83 (*t*, *J* = 8.1 Hz, 4)
H_3	7.27 (*s*, 4)
H_4	4.54 (*d*, *J* = 7.1 Hz, 4)
H_5	5.77 (*d*, *J* = 7.0 Hz, 4)
H_6	4.95 (*s*, 8)
H_7	7.03 (*t*, *J* = 7.5 Hz, 4)
H_8	7.14 (*d*, *J* = 8.4 Hz, 4)
H_9	7.53 (*t*, *J* = 8.9 Hz, 4)
H_{10}	7.75 (*d*, *J* = 7.5 Hz, 4)
H_{Ald}	10.17 (*s*, 4)
	0.91 (*t*, *J* = 7.1 Hz, 12)
Feet	1.36 (*m*, 24)
	2.26 (*m*, 8)

The use of a 400 MHz instrument to record the spectrum of **27** yielded particularly noteworthy information in terms of the salicylaldehyde aromatic signals. As seen in Spectrum 1.66, the COSY spectrum for **27**, and more clearly in Spectrum 1.67, the triplet at 7.53 ppm and the doublet at 7.75 ppm exhibit secondary coupling, and appear as a triplet of doublets, and a doublet of doublets, respectively. The coupling constants for the secondary coupling are in the

order of 1 - 2 Hz, which is indicative of long range coupling present between salicylaldehyde protons.

The cyclisation reaction protocol towards **25** made use of the Lindsey conditions, as described in section 3.1.2. Again, however, no porphyrinic material was detected. It can therefore be concluded that solubility and the length of the feet used in capped porphyrin formation has no bearing on the ability to form the porphyrin *in situ* and thereby form the cavitand-capped porphyrin.

3.4 Conclusion

The synthesis of the target ligand was attempted *via* the two approaches reported in the literature. The *in situ* protocol as reported by Reinhoudt *et al.*[7] in the synthesis of the first cavitand-capped porphyrin, was unable to afford the ligand. The use of longer feet had no effect on the success of the synthesis, thereby showing that improved solubility did not significantly influence synthesis. Indeed, from the crystallographic evidence obtained during the course of synthesis, it is suggested that in fact the -CH_2O- bridge length was most influential in determining the success of the *in situ* protocol.

The direct capping approach as used by Naruta *et al.*[15] gave more promising results. The use of methyl feet in synthesis led to insoluble material as a final product. As such, longer feet were used to improve synthesis. However, the synthesis of the target ligand using $C_{11}H_{23}$ feet could not be conclusively confirmed by a number of NMR techniques, or by MS techniques. Instead, UV-Vis analysis suggested only qualitatively that the synthesis of **25** yielded a cavitand-capped porphyrin. Therefore, the direct capping protocol cannot be deemed successful. Crystallographic analysis was again used to illustrate that the inability to form **25** *via* the direct approach was, once more, a result of the short bridge length used in synthesis.

Thus, both the *in situ* protocol and the direct capping protocol failed to produce the target ligand. Bearing in mind the ligands synthesised by Reinhoudt *et al.* and Naruta *et al.*, however, noteworthy conclusions can be drawn with regards to the synthetic results.

The ligand reported by Naruta *et al.*, bearing short -CH_2O-bridges identical to those in this study, was a ligand without *complete* capping. That is, only *two* bridges linked the cavitand to

the porphyrin, as opposed to four. In contrast, the shortest bridge seen for a completely capped cavitand-capped porphyrin is five atoms in length, as reported by Reinhoudt *et al.* In addition, this ligand was synthesised using the *in situ* protocol, and was shown to be highly dependant on bridge length.

In this study, however, the following was observed:

1. The success of the *in situ* synthetic procedure is dependant on bridge length, as observed by Reinhoudt *et al.*
2. The use of bridges as short as -CH_2O- proves to be too short to successfully complete cyclisation following the *in situ* protocol.
3. The use of bridges as short as -CH_2O- appears to be too short even when employing a direct capping approach.

Therefore, in conclusion, the synthetic results of this study suggest that there appears to be a *minimum* requirement for bridge length in order to synthesise a completely capped cavitand-capped porphyrin. This also seems to apply to *both* synthetic protocols, not just the *in situ* approach as observed in this study, as well as by Reinhoudt *et al.* Moreover, the failure to completely cap the porphyrin in this study using an identical bridge length *and* (direct capping) synthetic procedure, as reported by Naruta *et al.*, may be an additional indication that direct capping using very short bridges is not a possibility. Thus, it is necessary to use bridges (at least) longer than the -CH_2O- bridges employed in this study in order to afford a successful synthesis.

REFERENCES

1. ***a)*** D.J. Cram, S. Karbach, H-E Kim, C.B. Knobler, E.F. Maverick, J.L. Ericson, R.C. Helgeson, *J. Am. Chem. Soc.*, **1988**, *110*, 2229-2237; ***b)*** D.J. Cram, S. Karbach, H-E Kim, C.B. Knobler, L. Baczynskyj, K. Marti, R.M. Sampson, G.W. Kalleymeyn, *J. Am. Chem. Soc.*, **1988**, *110*, 2554-2560; ***c)*** L. M. Tunstad, J.A. Tucker, E. Dalcanale, J. Weiser, J.A. Bryant, J.C. Sherman, R.C. Helgeson, C.B. Knobler, D.J. Cram, *J. Org. Chem.*, **1989**, *54*, 1305-1312; ***d)*** J.A. Bryant, M.T. Blanda, M. Vincenti, D.J. Cram, *J. Am. Chem. Soc.*, **1991**, *113*, 2167-2172.
2. T.N. Sorrell, F.C. Pigge, *J. Org. Chem.*, **1993**, *58*, 784-785.
3. B.C. Gibb, R.G. Chapman, J.C. Sherman, *J. Org. Chem.*, **1996**, *61*, 1505-1509. Harrowfield, M.I. Ogden, A. H. White, *J. Chem. Soc. Dalton Trans.*, **1991**, 979-985;
4. E. Roman, C. Peinador, S. Mendoza, A.E. Kaifer, *J. Org. Chem.*, **1999**, *64*, 2577-2578.
5. A.R. Mezo, J.C. Sherman, *J. Org. Chem.*, **1998**, *63*, 6824-6829.
6. ***a)*** Z. Asfari, J. Vincens, J. Weiss, *Tetrahedron Lett.*, **1993**, *34*, 627-628; ***b)*** N. Kobayashi, K. Mizuno, T. Osa, *Inorg. Chim. Acta*, **1994**, *224*, 1-3; ***c)*** D.M. Rudkevich, W. Verboom, D.N. Reinhoudt, *J. Org. Chem.*, **1995**, *60*, 6585-6587; ***d)*** D.R. Benson, R. Valentekovich, S-W. Tam, F. Diederich, *Helv. Chim. Acta*, **1993**, *76*, 2034-2060.
7. O. Middel, W. Verboom, D.N. Reinhoudt, *J. Org. Chem.*, **2001**, *66*, 3998-4005.
8. A.D. Adler, F.R. Longo, J.D. Finarelli, J. Goldmacher, J. Assour, L. Korsakoff, *J. Org. Chem.*, **1967**, *32*, 476.
9. J.S. Lindsey, I.C. Schreiman, H.C. Hsu, P.C. Kearney, A.M. Marguerettaz, *J. Org. Chem.*, **1987**, *52*, 827-836.
10. O. Piepers, R.M. Kellog, *J. Chem. Soc. Chem. Comm.*, **1978**, 383-384; ***b)*** B.J. van Keulen, R.M. Kellog, O. Piepers, *J. Chem. Soc. Chem. Comm.*, **1979**, 285-286.
11. B. Staubli, H. Fretz, U. Piantini, W-D Woggon, *Helv. Chim. Acta*, **1987**, *70*, 1173-1193
12. S.M.S. Chauhan, B.B. Sahoo, K.A. Srinivas, *Synth. Commun.*, **2001**, *31*, 33-37.
13. T. Nagasaki, H. Fujishima, M. Takeuchi, S. Shinkai, *J. Chem. Soc. Perkin Trans. 1*, **1995**, 1883-1888.
14. B. Botta, P. Ricciardi, C. Galeffi, M. Botta, A. Tafi, R. Pogni, R. Iacovino, I. Garella, B. Di Blasio, G. Delle Monache, *Org. Biomol. Chem.*, **2003**, *1*, 3131-3137.
15. ***a)*** J. Nakazawa, J. Hagiwara, M. Mizuki, Y. Shimazaki, F. Tani, Y. Naruta, *Angew. Chem. Int. Ed. Engl.*, **2005**, *44*, 3744-3746; ***b)*** J. Nakazawa, J. Hagiwara, M. Mizuki, Y. Shimazaki, F. Tani, Y. Naruta, *Bull. Chem. Soc. Jpn.*, **2006**, *79*, 1431-1443.

16. M. Momenteau, J. Mispelter, B. Loock, E. Bisagni, *J. Chem. Soc. Perkin Trans. 1*, **1983**, 189-196.
17. B. Staubli, H. Fretz, U. Piantini, W-D Woggon, *Helv. Chim. Acta*, **1987**, *70*, 1173-1193.
18. For representative papers which document the nature of porphyrin ring currents and the associated effects on porphyrin NMR, see ***a)*** E.D. Becker, R.B. Bradley, *J. Chem. Phys.*, **1959**, *31*, 1413-1414; ***b)*** R.J. Abraham, *Mol. Phys.*, **1961**, *4*, 145-152; ***c)*** R.J. Abraham, F. Eivazi, H. Pearson, K.M. Smith, *Tetrahedron*, **1977**, *33*, 2277-2285; ***d)*** K.J. Cross, M.J. Crossley, *Aust. J. Chem.*, **1992**, *45*, 991-1004; ***e)*** R.J. Abraham, I. Marsden, *Tetrahedron*, **1992**, *48*, 7489-7504; ***f)*** E. Steiner, P.W. Fowler, *ChemPhysChem.*, **2002**, 114-116; ***g)*** E. Steiner, P.W. Fowler, *Org. Biomol. Chem.*, **2004**, *2*, 34-37; ***h)*** H. Iwamoto, K. Hori, Y. Fukazawa, *Tetrahedron Lett.*, **2005**, *46*, 731-734.
19. ***a)*** L.K. Gottwald, E.F. Ullman, *Tetrahedron Lett.*, **1969**, *36*, 3071-3074; ***b)*** R.A. Freitag, J.A. Mercer-Smith, D.G. Whitten, *J. Am. Chem. Soc.*, **1981**, *103*, 1226-1228.
20. J.B. Hendrickson, D.J. Cram, G.S. Hammond, *Organic Chemistry*, McGraw-Hill, New York, **1970**.
21. J.S. Gardner, Q.P. Peterson, J.O. Walker, B.D. Jensen, B. Adhikary, R.G. Harrison, J.D. Lamb, *J. Membr. Sci.*, **2006**, 165-176.
22. J.B. Fenn, M. Mann, C.K. Meng, S.F. Wong, C.M. Whitehouse, *Mass. Spectrom. Rev.*, **1990**, *9*, 37-70.
23. P. Bhyrappa, S.R. Wilson, K.S. Suslick, *J. Am. Chem. Soc.*, **1997**, *119*, 8492-8502. The related crystallographic data can be found on the CD accompanying this work.
24. Hemicarcerands are analogous to the capped porphyrins under investigation in this study. They are the result of the coupling of two cavitands *via* four bridges of varying alkyl or aryl character. More detail will be discussed in subsequent chapters.
25. J.C. Sherman, C.B. Knobler, D.J. Cram, *J. Am. Chem. Soc.*, **1991**, *113*, 2194-2204.

CHAPTER 4

COMPUTATIONAL CHEMISTRY AND MOLECULAR MODELLING

The inability to synthesise the desired target ligand, and the suggestion of the existence of a minimum requirement of bridge length in order to successfully couple the cavitand to the porphyrin, prompted a computational investigation of cavitand-capped porphyrin ligands. This was in order to gain insight into the ability of the proposed ligand to selectively accommodate the terminus of a paraffin, in addition to identifying a bridge length which would afford a successful synthesis. Before describing the computational study, a short overview of computational chemistry, pertinent to this study, will be presented. Additional detail on the material discussed can be obtained elsewhere.[1]

4.1 Introduction

Computational chemistry is a branch of chemistry which makes use of mathematical tools and principles, and the laws of physics (both those of classical and quantum physics) to simulate and analyze chemical properties and processes. The majority of mathematical theory and algorithms required for computational chemistry have been available for many years. However, the great advances made over the past twenty years in computer hardware and software have resulted in the discipline becoming more accessible and significant as a chemical tool.[1b, e]

The discipline allows chemists a more comprehensive understanding of chemical reactions and processes, ranging from prediction of stability of chemical reactions and explanation of reaction mechanisms, to estimation of energy differences between different chemical states.[2] It also aids in the design of experiments, interpretation of experimental results, as well as the design of new compounds and materials with desirable properties.[1e] The information gained by computational chemistry is thus indispensable and invaluable in research, especially where laboratory-based experiments can be financially restrictive and time consuming.

The basis by which computational chemistry simulates chemical structures and reactions numerically is firmly grounded in the fundamental laws of physics.[3] There are accordingly two major categories within computational chemistry, electronic structure theory and molecular mechanics.

4.2 Electronic Structure Theory

Electronic structure theory is a category of computational chemistry which uses the laws of quantum physics as its governing basis, in conjunction with the values of a number of physical constants. These include the speed of light, the mass and charge of both electrons and atomic nuclei, and Planck's constant.[3] Electronic structure theory consists largely of three methods: *ab initio*, density functional theory, and semi-empirical methods.

4.2.1 Ab initio Methods

Ab initio methods are based explicitly on theoretical principles governing quantum physics (as listed above) and therefore do not include any experimental data as input into the algorithm. The method is therefore the most expensive in terms of time and computer resources.

Ab initio computations find solutions to the empirically derived Schrödinger equation (**Eq. 4.1**) *via* the use of a series of mathematical approximations, so providing high quality quantitative predictions for a wide range of atomic and molecular systems.[3] The equation is as follows:

$$\hat{H}\,\Psi = E\,\Psi \qquad \textbf{(4.1)}$$

where Ψ represents the wave function, and $\hat{H}$ the Hamiltonian operator (**Eq. 4.2**), expressed as:

$$\hat{H} = -\frac{h^2}{8\pi^2}\sum_{A}^{nu}\frac{1}{M_A}\nabla_A^2 - \frac{h^2}{8\pi^2 m}\sum_{a}^{elec}\nabla_a^2 - e^2\sum_{A}^{nu}\sum_{a}^{elec}\frac{Z_a}{r_{Aa}} + e^2\sum_{A}^{nu}\sum_{>B}^{nu}\frac{Z_A Z_B}{R_{AB}} + e^2\sum_{a}^{elec}\sum_{>b}^{elec}\frac{1}{r_{ab}} \qquad \textbf{(4.2)}$$

Here, M represents nuclear masses, a electrons, and A nuclei. R_{AB} represents the distance between nuclei, r_{ab} that between electrons, and r_{Aa} that between nuclei and electrons. The first two terms describe the kinetic energy of nuclei and electrons, with the remaining three terms describing Coulombic interactions between particles.[4]

The Schrödinger equation is a combination equation derived from the differential equations defining the profile of a simple harmonic oscillator, and dé Broglie's premise that matter (particles) have wave-like properties.[5, 6] On manipulating the equation, a description of molecules (in terms of nuclei-electron interactions) and molecular geometry (in terms of energy minima or maxima in nuclei arrangement) can be obtained.[7]

However, as an equation describing many electrons, the Schrödinger equation cannot be solved exactly when systems involving three or more interacting particles are considered. Thus, in order to solve for such systems, a number of approximations need to be introduced.[8] It should be noted that the accuracy of the solution decreases as the approximations become more drastic.

Born-Oppenheimer Approximation

The Born-Oppenheimer approximation assumes that all nuclei within a system are stationary, and only electrons move.[7] Atomic nuclei have a mass which is a number of orders of magnitude larger than that of electrons. Thus, nuclei move slowly relative to electrons, while electrons essentially move instantaneously in relation to nuclear movements.[9] The energy of a molecule in its ground state can thus be exclusively treated as a function of nuclear coordinates, since the movement of nuclei are independent of the movement of electrons. Since these are essentially fixed according to the Born-Oppenheimer approximation, electron wavefunctions can be considered to be dependant only on the position of the nuclei, and not the momenta of nuclei.[1e, 9]

Such an approximation greatly simplifies the Schrödinger equation to give the electronic Schrödinger equation. The equation is free of the term describing nuclear kinetic energy, while the term describing the inter-nucleic Coulombic interactions is a constant. The Hamiltonian operator consequently simplifies to:

$$\hat{H} = -\frac{h^2}{8\pi^2 m}\sum_{a}^{elec}\nabla_a^2 - e^2\sum_{A}^{nu}\sum_{a}^{elec}\frac{Z_a}{r_{Aa}} + e^2\sum_{a}^{elec}\sum_{>b}^{elec}\frac{1}{r_{ab}} \qquad (4.3)$$

to give the electronic Schrödinger equation in the form:

$$\hat{H}^{elec}\,\Psi^{elec} = E^{elec}\,\Psi^{elec} \qquad \textbf{(4.4)}$$

The total energy of the system under consideration in the computation therefore becomes:

$$E_{Total} = \quad E^{elec} + e^2 \sum_{A}^{nu} \sum_{>B}^{nu} \frac{Z_A Z_B}{R_{AB}} \qquad \textbf{(4.5)}$$

Hartree-Fock Approximation **[7]**

Even though the Born-Oppenheimer approximation simplifies the Schrödinger equation to give the electronic Schrödinger equation, the latter still proves to be intractable. As another approximation in an attempt to simplify matters further, the Hartree-Fock approximation assumes that electrons move independently of each other.**[8, 9]** What thus results is substitution of the many electron wavefunction, Ψ, with a total wavefunction. The total wavefunction is represented by a single determinant (a Slater determinant, **Eq. 4.6**) which results from the product of many one-electron wavefunctions, termed spin orbitals.**[8]** This determinant is as follows:

$$\Psi = \quad \frac{1}{\sqrt{N!}} \begin{vmatrix} \chi_{1(1)} & \chi_{2(1)} \cdots\cdots \chi_{n(1)} \\ \chi_{1(2)} & \chi_{2(2)} \cdots\cdots \chi_{n(2)} \\ \chi_{1(N)} & \chi_{2(N)} \cdots\cdots \chi_{n(N)} \end{vmatrix} \qquad \textbf{(4.6)}$$

χ_i represents individual spin orbitals, themselves the product of a spatial function (or molecular orbital), ψ_i, and a spin function, α or β. The fact that there are only two types of spin functions stems from the fact that only a maximum of two electrons may occupy any molecular orbital at any one time, provided they possess opposite spin. Hartree-Fock level of theory represents the minimum level of theory required for *ab initio* computations. However, the Hartree-Fock approximation is particularly drastic and results in a curtailed description of the manner in which the motion of one electron affects that of all the other electrons. As such, Hartree-Fock (HF) models are in many cases ineffective in modeling transition states, and bond breaking and formation.**[8]** The description of interactions and correlations between electrons may be improved with the use of Electron Correlation (EC) methods, which will be discussed in section 4.2.2 below.

LCAO Approximation

Through the application of the Hartree-Fock approximation, a set of differential equations (known as the Hartree-Fock equations) result. While these have numerical solutions, it is useful to introduce a further approximation that allows the Hartree-Fock equations to become algebraic in nature.[8] The LCAO approximation uses molecular orbitals expressed as linear combinations of a finite set (basis set) of prescribed functions, known as basis functions, ϕ. Since basis functions are usually centered at nuclear positions, they are referred to as atomic orbitals. The equation used to describe the approximation (**Eq. 4.7**)

$$\psi_i = \sum_{\mu}^{basis\ functions} c_{\mu i}\phi_{\mu} \qquad (\mathbf{4.7})$$

is termed the linear combination of atomic orbitals, or LCAO approximation. Here, *c* represent the molecular orbital coefficients (often incorrectly referred to as molecular orbitals). It is important to note that Hartree-Fock theory makes use of the variation principle to solve for the set of molecular orbital coefficients. This solution is such that the set of coefficients, where the resultant wavefunction energy is at a minimum, is found. This principle is also involved for the determination of saddle points (the lowest maxima on any energy profile) in transition state modeling.

Roothaan-Hall Equations [7]

If both the Hartree-Fock and LCAO approximations are simultaneously applied to the electronic Schrödinger equation, the Roothaan-Hall equations result,[7, 8] expressed as:

$$\sum_{v}^{basis\ functions}\left(F_{\mu v} - \varepsilon_i S_{\mu v}\right)c_{vi} = 0 \qquad (\mathbf{4.8})$$

where ε_i are orbital energies, *F* the Fock matrix and *S* the overlap matrix (extent to which the basis functions correlate with one another). The Fock matrix is analogous to the Hamiltonian operator in the Schrödinger equation [8] and can be represented in atomic units as:[4]

$$F_{\mu v} = \left\langle \phi_{\mu} \middle| -\frac{1}{2}\nabla^2 - \sum_{A}^{nu}\frac{Z_A}{r_A} \middle| \phi_v \right\rangle + \sum_{\lambda}^{bf}\sum_{\sigma}^{bf} P_{\lambda\sigma}\left[\left(\phi_{\mu}\,\phi_{\lambda}|\phi_{\lambda}\,\phi_{\sigma}\right) - \frac{1}{2}\left(\phi_{\mu}\,\phi_{\lambda}|\phi_{\lambda}\,\phi_{\sigma}\right) \right] \qquad (\mathbf{4.9})$$

The first term represents the kinetic and potential energy of individual electrons, and the second term represents the interactions between electrons. P is the density matrix, the energy of a single electron in the field of the bare nuclei; $P_{\lambda\sigma}$ is expressed as:

$$P_{\lambda\sigma} = \quad 2 \sum_{i}^{occupied\ MOs} c_{\lambda i}\, c_{\sigma i} \qquad \textbf{(4.10)}$$

Solutions to Roothaan-Hall equations for a considered system, are referred to as *ab initio* (or Hartree-Fock) models, and provide good accounts of equilibria in terms of geometries and conformations.[8]

4.2.2 Electron Correlation (EC) Methods

As mentioned, HF models are in many cases ineffective in modeling transition states, and bond breaking and formation; a phenomenon that stems directly from the HF approximation. As such, EC methods represent a means of obtaining more accurate modeling *via* an improved description of electronic interactions.[8] EC methods largely consist of two different models: Møller-Plesset and DFT models. It should be noted, however, that these methods involve higher cost in terms of computational resources and time.

Møller-Plesset Models

A common means by which to represent electron correlation is in the use of perturbation theory;[10] specifically second-order Møller-Plesset (MP2) models. Considered superior to DFT in describing electron correlation, MP2 models make use of more accommodating descriptions of electronic motion. This involves using a combination of HF models, where HF models are used to describe systems in ground states, as well as in excited states.[8, 10] What results through application of MP2 theory is a specific calculation of the effect of electron correlation. This affords exceptional descriptions of equilibrium geometry and conformations, as well as the breaking and forming of bonds. For detail on this method and application thereof, literature is available.[11]

Density Functional Theory

Density functional theory (DFT) methods are similar to *ab initio* methods in terms of requirements on computer resources, but are not as costly in terms of time.[12] DFT is based on the theories as set out by Kohn and Hohenberg [13] and is based on the premise that any molecule in a ground energy state can be described in terms of total electron density. Therefore, each molecule has a unique functional determining its geometry and ground state energy.[8] DFT approximates the effect of electron correlation in its calculation of total electron density of a system. In contrast, HF models do not calculate electron density but instead consider an average electron density in the algorithm by considering the average interaction of electrons with both nuclei and all other electrons.[7] HF models thus overestimate system energy, relative to DFT models which give more accurate modeling *via* the calculation of total electron density through the modeling of electron correlation. DFT in general gives more reliable results, particularly in the modeling of equilibrium geometries and conformations, and transition states.[8] However, results are largely dependant on the choice of basis set and density functional.[4] In addition, in the case of the density functional, there appears to be no means of systematically improving algorithms such that experimental results are approached asymptotically, as they are in *ab initio* methods. DFT is also unable to describe van der Waals interactions.[8b]

4.2.3 Semi-empirical Methods

Semi-empirical methods follow directly from Hartree-Fock models. The fundamental difference to Hartree-Fock models again lies in the manner in which electrons are treated. Semi-empirical methods consider only valence electrons, since these valence orbital electrons are involved in bonding.[2, 3, 8] In addition, semi-empirical methods may also take into account parameters obtained from experimental data, or high level *ab initio* calculations. These factors greatly simplify calculations and reduce demand on computer resources.

Apart from the valence orbital electron approximation, a second significant approximation is implemented in restricting basis sets to a minimal representation. Thus, main group elements

comprise a single *s*-type function, and a set of *p*-type functions; for example, 2*s*, $2p_x$, $2p_y$ and $2p_z$. Transition metals have an additional set of *d*-type functions.[12]

Fundamental to semi-empirical methods is maintaining that atomic orbitals belonging to different atomic centers do not overlap significantly. Such an approximation, known as the Neglect of Diatomic Differential Overlap (NDDO) approximation, further simplifies the Roothaan-Hall equations. It is, however, important to include some overlap in even the simplest semi-empirical models.[12]

Semi-empirical methods are able to produce a range of experimental data, such as heats of formation, dipole moments and ionisation potentials. Accuracy can vary widely, and results are greatly influenced by the parameters used in the calculation.[2] Thus, for any given system considered by semi-empirical methods, it is important to choose an appropriate method if reasonable results are to be obtained. This is particularly important for systems which involve transitions states and bond breaking and formation; indeed, semi-empirical methods are not suitable for such modeling.[8, 10b, 12]

4.3 Molecular Mechanics

While electronic structure theory provides important information about chemical properties and processes, many systems prove to be too large (for current resources and software) for consideration and modeling *via* quantum mechanical methods. Electronic structure theory, as its name suggests, deals largely with electrons; however, even if electronic characteristics are simplified (semi-empirical methods), there still remains a large number of particles for consideration.

Molecular mechanics (or force field methods) allow for the consideration of larger systems, as electronic motions are ignored, and only the positions of nuclei are considered.[3] Molecular mechanics (MM) assumes that electrons are stationary, in contrast to electronic structure theory, which assumes that nuclei are stationary (Born-Oppenheimer approximation).

MM is characterised by the use of force fields, analogous to basis sets for electronic structure theory. Force fields are a set of equations describing variations in the potential energy of a

molecule, as a function of the position of its component atoms. These are used to obtain good estimates of molecular energy and geometry, taking into account all the forces between atoms calculated *via* a mechanical approach. The energy of any system is thus calculated based on classical physics, again in contrast to electronic structure theory which makes use of quantum physics.

The energy in a system considered by MM is described as the sum of contributions arising from distortions from idealised bond distances, bond angles and torsion angles. These contributions are taken into account in conjunction with contributions due to "non-bonded" interactions (van der Waals and Coulombic interactions).[8, 10b] Given the inclusion of the contribution from non-bonded interactions, the van der Waals radii of the atoms under consideration thus play a major role in MM modeling. These interactions are described by **Eq. 4.11**, as well as in Figure 4.1 below.

$$E_{Total} = \sum_{i}^{bonds} E_i^{stretch} + \sum_{i}^{bondangles} E_i^{bend} + \sum_{i}^{torsionangles} E_i^{torsion} + \sum_{i}^{non-bonded} \sum_{j}^{non-bonded} E_{ij}^{nonbonded} \qquad \textbf{(4.11)}$$

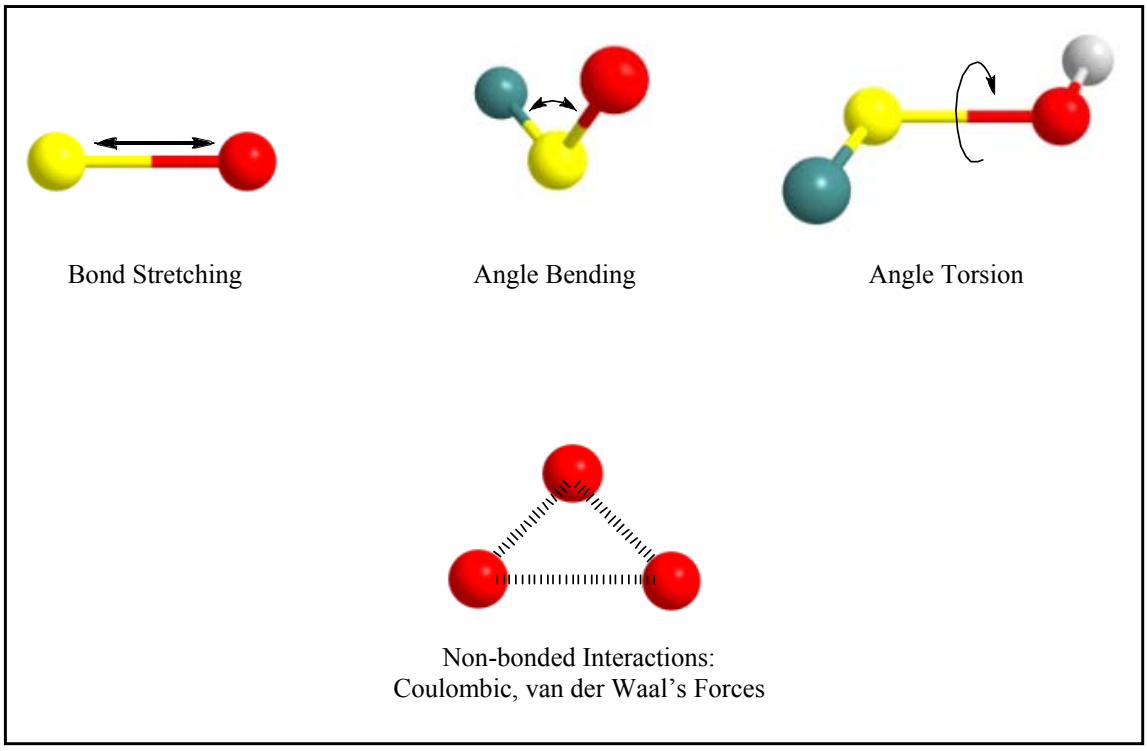

Figure 4.1: Schematic representations of energy contributions in a molecular mechanics system.

The first three terms in **Eq. 4.11** are the energies arising from all bonds, bond angles and torsion angles. In contrast to electronic structure theory, bond information serves as an input into MM calculations, whereas in the former, such information is as a result of calculation.[8] The remaining term in **Eq. 4.11** serves to describe energies over all non-bonded atom pairs.

Bond lengths, bond angles and torsion angles can be changed using potential energy functions during optimisation processes. Such dynamic methods can in fact yield particularly accurate results for large systems in terms of molecular energies and geometries. Importantly, these results can be achieved in a fraction of the time and cost of *ab initio* methods.[12] However, MM is prone to significant error if a force field not specific to the system under consideration is used. In addition, because MM ignores electronic motions and assumes electrons to be stationary, MM calculations cannot be used to investigate bond breaking or formation, such as in transition states.

4.4 Molecular Dynamics

In many applications of both electronic structure theory, and MM, it is important to first obtain the arrangement of atoms in a system which represents the global energy minimum. This is particularly important where the molecule under consideration has a number of conformers, resulting in the possibility that multiple minima may exist.[14] The starting geometry of the system under consideration is particularly important in obtaining the global minimum. Should the starting geometry be far from the geometry of the global minimum, it becomes necessary to perturb the system by providing atoms with enough energy to overcome vibrational, rotational and conformational energy barriers.

The classical means of providing energy to atoms is *via* molecular dynamics (MD) simulations. MD simulations follow the time dependant movements of each atom in a molecule, on application and solution of Newton's equations of motion to molecules.[1e, 6, 15] During MD simulations, kinetic energy is provided to the system under consideration (*via* a mathematical algorithm) such that any vibrational, rotational and conformational energy barrier can be overcome. Importantly, the time scale used must be sufficiently long to allow the system to attain equilibrium. At the equilibrium temperature, all conformations should be observed over

time; should this not be the case, the temperature at which MD was performed should be increased and the system allowed to reach a new equilibrium.[1e, 6]

The amount of time spent at a particular conformation during a MD calculation is directly proportional to the stability of the conformation. Therefore, the system will spend more time assuming the global minimum conformation than any other conformation. For very flexible systems, the identification of the global minimum is often completed with the aid of statistical analysis.[9, 12]

MD calculations make use of a mathematical scale of temperature, such that simulations can be completed at a range of theoretical temperatures so as to control the amount of energy provided to atoms in order to overcome the respective energy barriers.[15] It is, however, particularly important to note that the mathematical temperature scale may not be reflective of real temperature and as such the simulation system should ideally be calibrated to gauge simulation temperature relative to real temperature.[16] An effective means of demonstrating this is through the use of cyclohexane:[16] it is well known that cyclohexane can interconvert between its energetically favourable chair conformations, and its less favourable boat conformations, at room temperature. Therefore, by performing MD on cyclohexane at various temperatures, and observing at which temperature the molecule is able to interconvert between conformers, an estimation of room temperature can be made with respect to the simulation system.

4.5 Computational Investigation of the Target Ligand

4.5.1 Introduction

The target ligand, with the ether bridges can be regarded as being analogous to the hemicarcerands which were studied by Cram *et al*. As mentioned previously, hemicarcerands are a class of host molecules which are the result of the coupling of two cavitands joined at the extra-annular position by up to four short bridges of varying alkyl or aryl character, as evident in Figure 4.2,[17a] showing the more common bridges. This results in a host which has four apertures representing access points into the host cavity, much like the proposed ligand in this study.

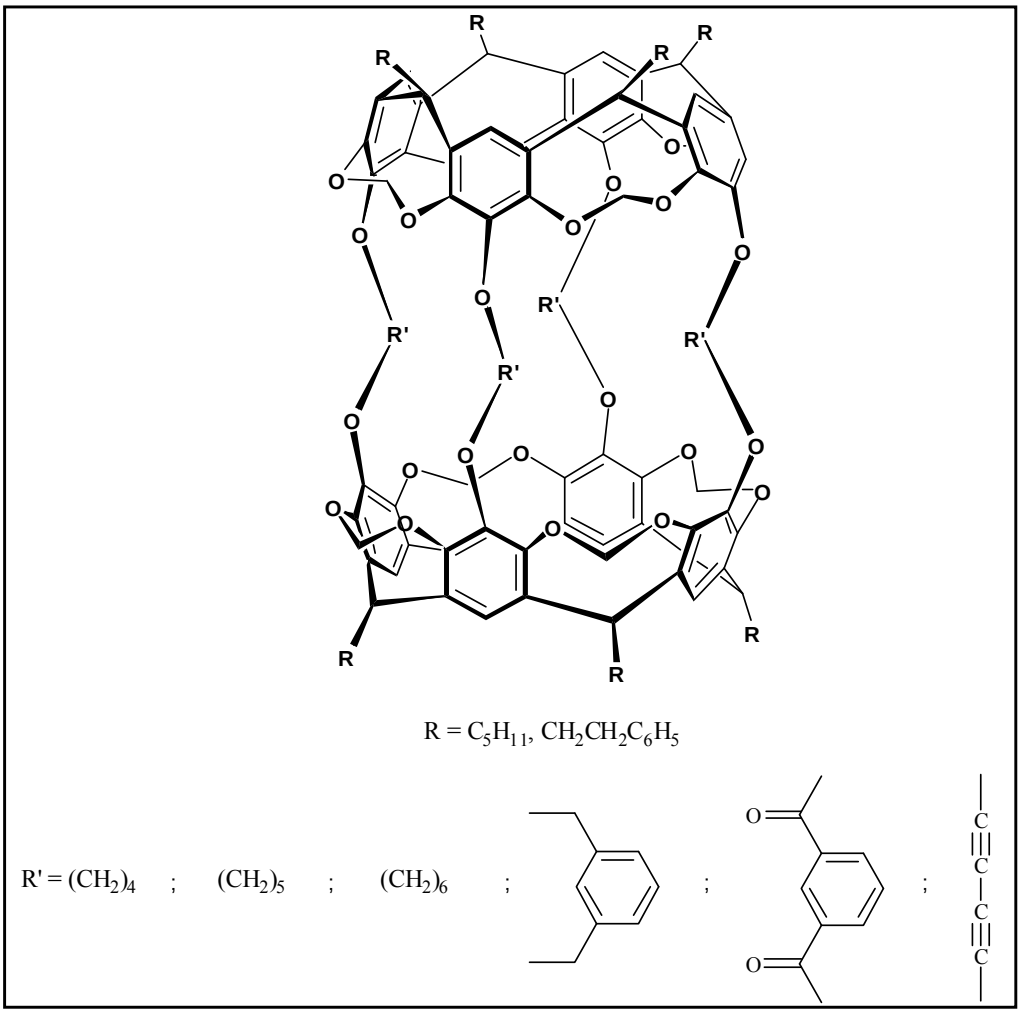

Figure 4.2: General structure of a hemicarcerand showing more common bridges used to create apertures.

Hemicarcerands are able to accommodate guests within the molecular cavity in a size selective manner; therefore, hemicarcerands serve as the basis for the concept of size selectivity in this study. Reviews pertaining to hemicarcerand chemistry, their host-guest capacity and their applications are available.[17] Both computational [18-20] and experimental [20, 21] investigations of hemicarcerands and their complexes (hemicarceplexes) indicate that aperture size can be appreciably increased such that guests can be accommodated through the apertures of a hemicarcerand and into its cavity by heating the host sufficiently. This physical process is usually performed in the presence of excess guest. The process can be reversed upon reheating the complex to the same degree that was needed to initially incarcerate the guest.

The inherent size selectivity exhibited by hemicarcerands stems from the ability of the bridges of the host to expand and contract upon heating and cooling, thereby widening and narrowing the apertures that afford access to the molecular cavity. Therefore, by using bridges of a

particular length, a specific aperture size can be attained at increased temperatures. Should this aperture size correspond to that of the guest molecule, the guest is able to be complexed within the confines of the hemicarcerand.[18e, 21] Guests which have shapes that complement the aperture also aid in ease of hemicarceplex formation.[19]

This study seeks to use the same principles as seen in hemicarcerand chemistry; that is, to create a ligand which possesses bridges linking cavitand to porphyrin such that, upon heating, an aperture size is afforded which matches that of the terminus of a paraffin. Such an aperture size would effectively govern access to the active site of the porphyrin, such that oxidation only of the paraffin terminus occurs, as discussed in more detail in section 2.6 of Chapter 2.

According to the studies by Cram *et al.*, among the most versatile hemicarcerands prepared was that bearing four tetramethylene bridges,[22] as seen in Figure 4.2 above. Guests incarcerated included *p*-xylene, nitrobenzene, DMA and *p*- and *o*-hydroquinone. Interestingly, Cram and coworkers observed that for hemicarcerands bearing such alkane-based bridges, the use of penta- or hexamethylene bridges did not necessarily afford better selectivity towards larger guests compared with the tetramethylene bridged hemicarcerand.[18d] Thus, the computational investigation of the proposed ligands, which follows, will make use of a range of bridge lengths.

4.5.2 Preliminary Investigation: CPK Study

Before any computational modeling was undertaken on the target ligand, a preliminary modeling study was done using Corey-Pauling-Koltun (CPK) models. With reference to Figure 4.3, the basic structure of the target ligand, a series of variations were built where bridge length *n* varied, ranging from one to four. For simplicity, R, the feet of the model, were kept as methyl groups.

It was found that the CPK models of the molecules were rigid and did not have significant flexibility; an observation which was expected given the inherent rigidity of both the porphyrin and cavitand moieties. It was further observed that by using either one or three methylene spacers (n = 1 or 3), the cavitand cap fitted comfortably over the top of the porphyrin moiety, while the use of two or four methylene spacers (n = 2 or 4) resulted in significant strain in the bridges in order to complete the coupling of the cavitand to the porphyrin.

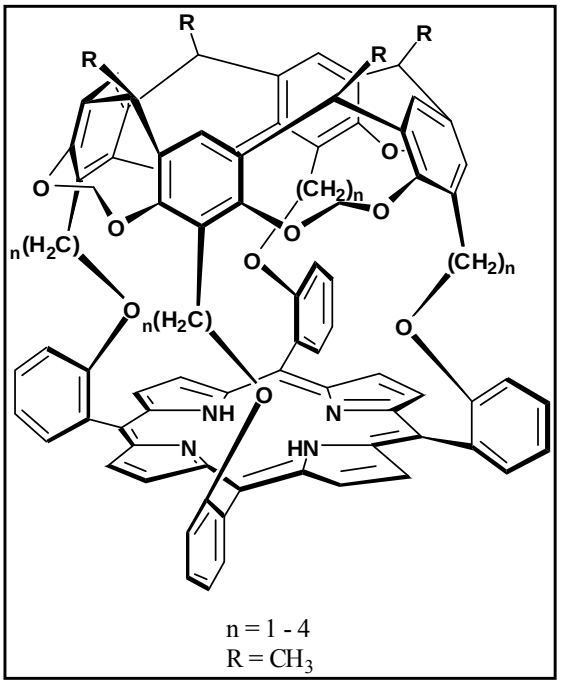

Figure 4.3: Target ligand structures used as basis for CPK modeling.

4.6 Choice of Computational Method

A review of the literature reveals that computationally, hemicarcerands and hemicarceplexes have been studied *via* both MM [18] as well as semi-empirical methods.[19] In a MM study by Sheu and Houk,[18f] a number of observations were made regarding hemicarcerands, hemicarceplexes and their properties. The minimised structure of the host obtained by MM was found to be highly dependant on the orientation of the atoms found at the extra-annular position of the cavitand scaffold. In addition, the -OCH_2O- bridges of the cavitand structures were found to interconvert between a chair and boat formation during MD studies, which allowed passage of guest molecules in and out of the host cavity, even though in some cases the guest was *larger* than the minimised aperture size.

The semi-empirical study by Liddell *et al.* [19] differed slightly in that focus was placed on the thermodynamic and kinetic properties of hemicarcerands and hemicarceplexes, in an effort to investigate whether hemicarceplex formation could be predicted using computational tools. It was found that the semi-empirical (AM1) investigation was precise in replicating data with respect to experimental results of complexation-decomplexation of guests, as well as the crystal data of hemicarceplexes. The study also represented the first investigation of the electronic

structure of hemicarcerands and hemicarceplexes. While the study showed good precision regarding complexation behaviour, it exhibited difficulty in predicting orientations of guests within the host molecule, relative to crystal data of corresponding hemicarceplexes.

In terms of computational investigation of cavitand-capped porphyrins, there has been only one study by Naruta *et al.* into the complexation of the reported ligand with various small hydrocarbons.[23] The computations were performed at an *ab initio* level, and were able to accurately reproduce experimental binding constants. However, given the rigidity, and importantly, the larger number of atoms present in the target ligand as well as resources available in this study, MM becomes an attractive and efficient means of investigating the target ligand computationally.

There is in addition no need to compute transition states, making MM more attractive. Indeed, MM has been shown to be particularly suited to investigating a variety of host-guest systems involving calixarenes and related hosts as discussed in Chapter 1. The conformational aspects of calixarene chemistry have been extensively studied computationally with wide use of MM methods. Typical force fields used included the CHARMM and MM3 force fields.[24] Similar studies have been performed investigating resorcin[4]arene conformation using MM3 and AMBER force fields.[25] Cavitands and hemicarcerands (molecules consisting of two cavitands bridged at the extra-annular position) have also been investigated through the use of MM calculations, implementing the CVFF, AMBER* and MM3* force fields.[18f, 26]

Porphyrins and metalloporphyrins have also been the subject of computational investigation using MM. Investigations into the effect of porphyrin flexibility, orientation of phenyl groups in the case of tetraphenylporphyrins, axial ligation, and size of metal cation (in the case of metalloporphyrins) have all been undertaken using MM2 force fields.[27] Heme model compounds and the influence of steric hinderance on the competitive binding of carbon monoxide and oxygen has also been investigated using AMBER and MM2 force fields.[28] In addition, methods have also made use of hybrid quantum mechanical-molecular mechanical techniques.[29] For systems involving supramolecularly-capped porphyrins, a very limited number of computational studies have been reported in the literature; however, in these systems and investigations, MM has also found application.[30] Exhaustive reviews on the various force fields, and comparative studies of these force fields, are available.[6, 31]

In order to decide on a method of calculation and a force field, the structure of a simple cavitand bearing methyl feet, and a proton at the extra-annular position was minimised and examined using MM. Since the crystal structure of this cavitand has been reported,[32] the interatomic distances between atoms are known. Therefore, the precision of the computational investigation and the applicability of the chosen force field can be gauged. The distances considered in the comparison are presented in Figure 4.4.

In terms of the choice of force field, previous investigation, as noted above, indicates that MM2 and MM3 are particularly effective in simulation of molecules such as cavitands and porphyrins. Indeed, it has been shown in the literature that in terms of predicting various parameters in organic molecules, MM2 and MM3 (and force fields based on these) performed best in a number of investigations.[6, 33] Therefore, the MM3* force field was the chosen force field in this study. Based on the original MM3 force field, the MM3* force field differs only slightly in the manner in which electrostatic and hydrogen bonding interactions are treated.[6]

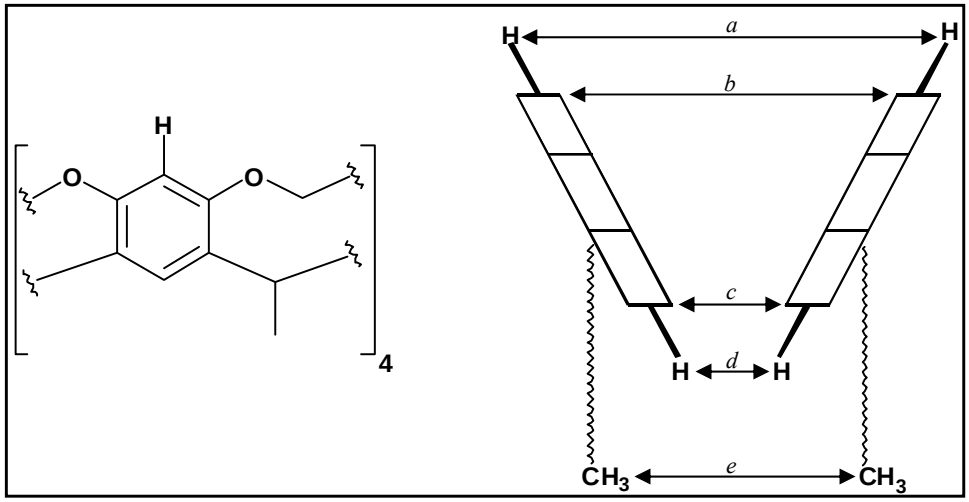

Figure 4.4: Structure and criteria used for comparison between computation and crystal structure.

As such, the computational minimisation of the simple cavitand made use of the following parameters:

Software: Maestro 7.0.113.
Force field: MACROMODEL's MM3* force field.
Minimisation method: Polak-Ribiere Conjugate Gradient (PRCG) method.
Maximum iterations: 1000
Convergence threshold: (energy) less than 0.01 kJ.mol-$Å^{-1}$

Minimisation commenced by a conformational search, using Monte Carlo (MC) low-mode sampling. The search made use of 1000 steps, taking 50 of the lowest energy structures. The global minimum identified after a complete search was then submitted for a further 1000 steps to ensure the global minimum was obtained. The minimisation process was also accompanied by MD in order to obtain respectable starting geometries in addition to aiding in identifying the global minimum of the cavitand structure. MD simulation was performed as vacuum simulations, where fifty low energy structures were sampled during the course of simulation. Thereafter, each structure was minimised, such that the structure having the lowest potential energy was used for a subsequent round of minimisation. The MD parameters were as follows:

Force field: MACROMODEL's MM3* force field.
Method of dynamics: Stochastic.
Time step: 1.5 fs.
Equilibrium time: 5.0 ps.
Simulation time: 100.0 ps.
Temperature: 800 K

As is evident from the results of the minimisation procedure in Table 4.1 after application of the above method, the percentage deviation of the computationally obtained measurements from those obtained experimentally from the crystal structure indicates a close agreement.

Table 4.1: Comparison of selected (MM3*) calculated interatomic distances[‡], with X-ray data reported in the literature for a simple cavitand structure bearing a proton at the extra-annular position.

Parameter	Reported measurement (X-ray structure)/nm	Calculated measurement/nm	% deviation
a	**0.904**	**0.929**	**2.8**
b	**0.796**	**0.814**	**2.2**
c	**0.526**	**0.522**	**0.8**
d	**0.419**	**0.401**	**4.3**
e	**0.721**	**0.727**	**0.8**

[‡] Cartesian coordinates of the computed structure are available on the CD accompanying this thesis.

Interestingly, Liddell *et al.* made use of a similar method of calculation in order to choose an algorithm for use in the semi-empirical study of hemicarcerands.[19] The cavitand used has also been reported,[31] accompanied by a crystal structure, and differs from the cavitand in Figure 4.4 only by the presence of a bromine atom at the extra-annular position, as shown in Figure 4.5.

The minimisation performed by Liddell *et al.* was repeated using Hyperchem [34] and the AM1 algorithm. The results obtained for each parameter, as shown in Figure 4.5, were in exact agreement with the data obtained by Liddell *et al.* In order to gauge the precision and accuracy of the chosen MM3* force field, the same cavitand was minimised according to the above minimisation and MD methods outlined above, and the results compared to both the crystal data as well as the semi-empirical data. The collective data is presented in Table 4.2 below.

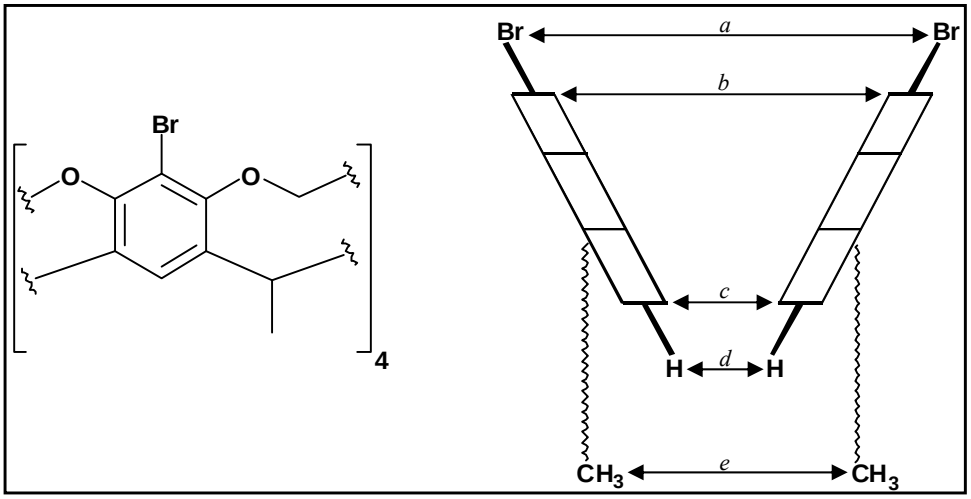

Figure 4.5: Structure and criteria used for comparison between computation and crystal structure in investigation by Liddell *et al.*

The results in Table 4.2 indicate that the semi-empirical calculation give values which are closer to the reported X-ray data, than does the MM3* calculation. Semi-empirical methods of computation therefore seem to give superior results over the molecular mechanics methods (for this system, at least). Interestingly, the study by Liddell *et al.* made use of two other semi-empirical algorithms (MNDO, PM3) in addition to the chosen AM1. While these algorithms were not as accurate as AM1, they were all more accurate than MM3* in modeling the cavitand crystal structure.

Table 4.2: Comparison of selected (MM3*) calculated interatomic distances[‡], with those reported in literature and calculated by AM1 for a simple cavitand structure bearing a bromine atom at the extra-annular position.

Parameter	Reported measurement (X-ray structure)/nm	Calculated measurement/nm		% deviation[†]
		AM1[≠]	MM3*	
a	**0.958**	**0.960**	**1.022**	**6.7 (6.5)**
b	**0.792**	**0.787**	**0.820**	**3.5 (4.2)**
c	**0.524**	**0.524**	**0.520**	**0.7 (0.8)**
d	**0.428**	**0.421**	**0.397**	**7.2 (5.7)**
e	**0.718**	**0.716**	**0.720**	**0.3 (0.4)**

[‡] Cartesian coordinates of the computed structure are available on the CD accompanying this thesis.

[†] Deviation of MM3* calculation relative to X-ray data. Values in brackets represent deviation from AM1 results

[≠] AM1 results calculated by Liddell *et al.*; values obtained in this study agreed exactly with those presented.

4.6.1 Additional Investigations of Resorcin[4]arene-based Molecules

The synthetic work described in Chapter 3 of this work resulted in a number of novel crystal structures of synthetic intermediates, all of which are resorcin[4]arene-based molecules. Discussion of these X-ray structures appears in Chapters 3 and 6, and the complete data sets are in Appendix 3. These intermediates were investigated computationally in an identical manner to those cavitands appearing in Figures 4.4 and 4.5, making use of both MM and semi-empirical methods. While the synthetic intermediates bear different feet, methyl feet were used in the computations in keeping with the two cavitand structures already investigated. The results of the MM3* and AM1 optimisations of three of these intermediates are presented below.

Computational studies of the intermediates commenced with an investigation of a cavitand bearing a methyl group at the extra-annular position, as shown in Figure 4.6.

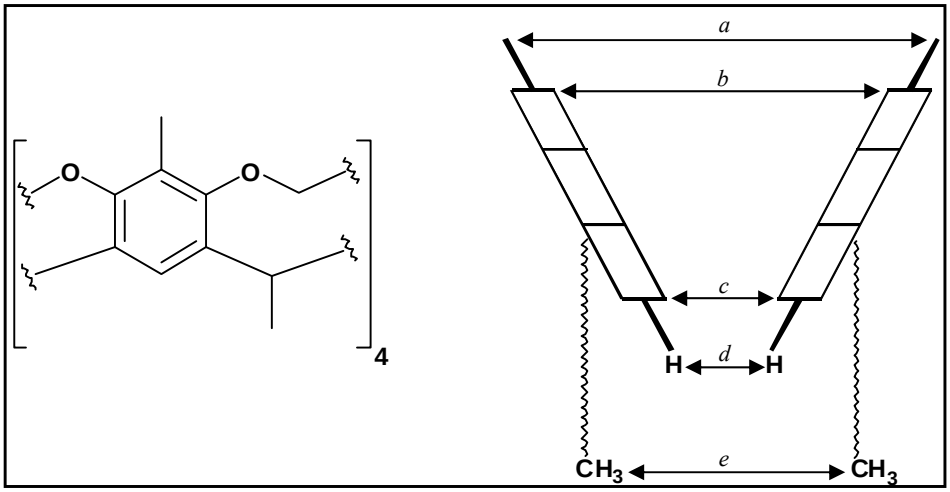

Figure 4.6: Structure and criteria used for comparison between computation and crystal structure of a methyl cavitand, as synthesised in this study (see Appendix 3 for the complete data).

Table 4.3 shows the results of the two minimisation calculations, compared with the corresponding measurement taken from the crystal structure of the cavitand. In general, good agreement exists between the X-ray measurements in comparison with both computationally derived measurements. With regards to accuracy, the computationally derived parameters are very similar to the corresponding X-ray measurements, with neither computational method showing superior accuracy over the other.

Precision of the MM3* calculation relative to the AM1 calculation also shows close agreement between the two methods of computation. This is evident particularly in the RMS error reported between the two computationally optimized structures, which is an error resulting from the superimposition of the MM3* minimised structure *versus* the corresponding AM1 minimised structure. In this particular case, the error is 0.022 nm, which reflects a small difference between the two minimised structures.

In addition, the deviations from the X-ray data as well as the disagreement between the two methods of calculation, in this case, are comparable with those seen in the study of the cavitand bearing a bromine atom at the extra-annular position. The largest deviation also occurs for parameters *a* and *d*, as it does in the case of the bromo-cavitand (Figure 4.5).

Table 4.3: Comparison of selected calculated interatomic distances[‡], with those obtained from the X-ray structure of the methyl cavitand.

Parameter	X-ray structure measurement/nm	Calculated measurement/nm		% deviation[†]
		AM1[≠]	MM3*[≠]	
a	**0.947**	**0.933**	**0.966**	**2.0 (3.4)**
b	**0.799**	**0.788**	**0.799**	**0.0 (1.4)**
c	**0.528**	**0.526**	**0.513**	**2.8 (2.5)**
d	**0.433**	**0.423**	**0.393**	**9.5 (7.6)**
e	**0.719**	**0.724**	**0.728**	**1.3 (0.5)**

[‡] Cartesian coordinates of the computed structure are available on the CD accompanying this thesis.

[†] Deviation of MM3* calculation relative to X-ray data. Values in brackets represent deviation from AM1 results.

[≠] Both the AM1 and MM3* sets of data were generated from calculations performed in this study.

The second intermediate investigated had slightly more elaborate functionalisation at the extra-annular position of the cavitand, in the form of a bromomethyl group. The structure of this cavitand appears in Figure 4.7, and the comparative data in Table 4.4.

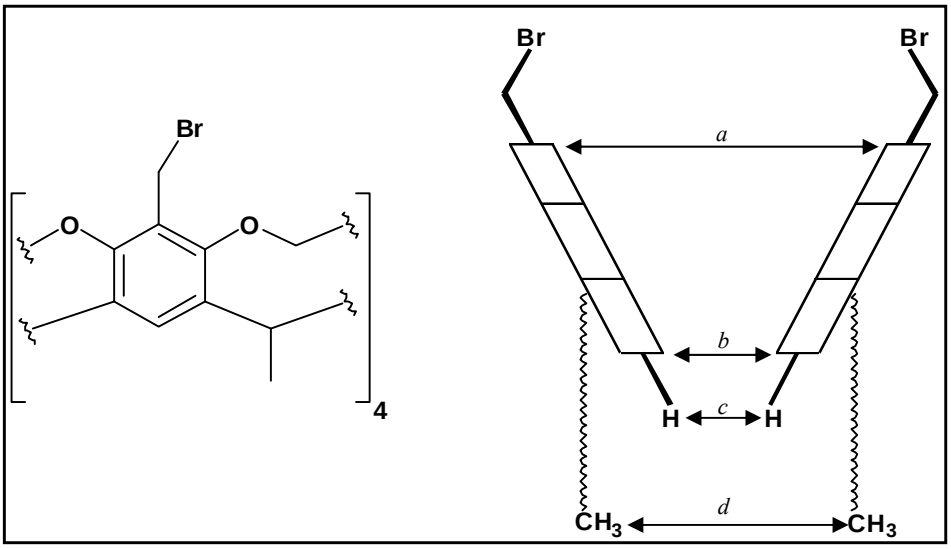

Figure 4.7: Structure and criteria used for comparison between computation and crystal structure of a bromomethyl cavitand, as synthesised in this study (see Appendix 3 for complete data).

Table 4.4: Comparison of selected calculated interatomic distances[‡], with those obtained from the X-ray structure of the bromomethyl cavitand.

Parameter	X-ray structure measurement/nm	Calculated measurement/nm		% deviation[†]
		AM1[≠]	MM3*[≠]	
a	**0.795**	**0.794**	**0.826**	**3.9 (4.0)**
b	**0.524**	**0.524**	**0.520**	**0.8 (0.8)**
c	**0.430**	**0.420**	**0.395**	**8.1 (5.9)**
d	**0.730**	**0.718**	**0.724**	**0.8 (0.8)**

[‡] Cartesian coordinates of the computed structure are available on the CD accompanying this thesis.

[†] Deviation of MM3* calculation relative to X-ray data. Values in brackets represent deviation from AM1 results.

[≠] Both the AM1 and MM3* sets of data were generated from calculations performed in this study.

The four parameters compared indicate that the computationally minimised structures are divergent from that of the X-ray structure. Indeed, the accuracy of the computationally derived parameters relative to the X-ray measurement is poorer here than in the case of the methyl cavitand. However, the AM1 results are more accurate than those from the MM3* calculation. The difference between the two methods of calculation shows far poorer precision than for the methyl cavitand above, with an RMS error of 0.423 nm between the two computationally derived structures.

The largest deviations observed, however, highlights the fundamental difference between the structure forming part of a crystal structure, and that calculated using theoretical models. It should be remembered for all such comparisons in this study, the data obtained from the crystal structure relates to a structure that is static, while that obtained from the minimization process is derived from only one structural conformation. Thus, for more complex structures bearing flexible side chains such as that in Figure 4.7, poorer precision should be anticipated.

The final intermediate investigated was a resorcin[4]arene, the structure of which is shown in Figure 4.8. The structure differs significantly from the four previous cavitand structures, in that the aromatic moieties are no longer bound by -OCH_2O- bridges. Therefore, the rigidity of the cavitand structure is absent from the resorcin[4]arene structure.

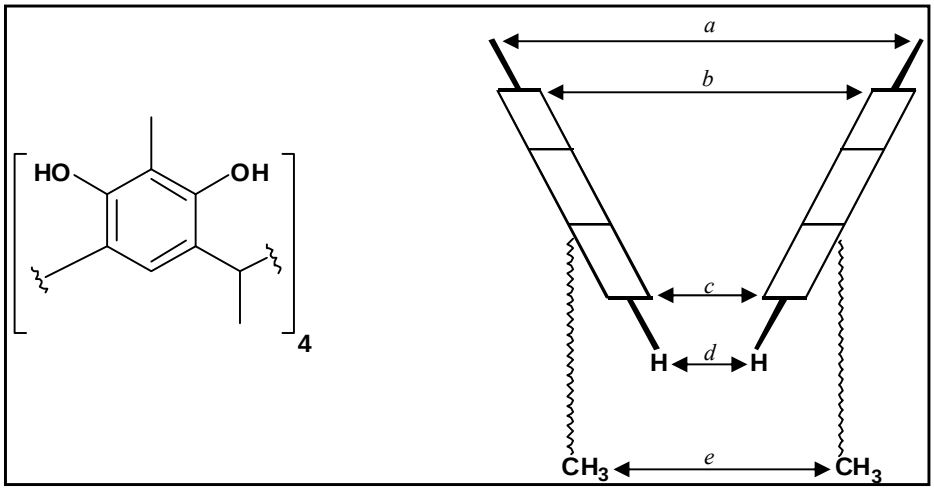

Figure 4.8: Structure and criteria used for comparison between computation and crystal structure of a resorcin[4]arene, as synthesised in this study (see Appendix 3 for complete data).

The comparative data appears in Table 4.5. Results indicate significant differences between parameters obtained from the X-ray data, and those obtained by calculation. Accuracy of both models seems to be significantly affected by the lack of rigidity of the structure under consideration.

Table 4.5: Comparison of selected calculated interatomic distances[‡], with those obtained from the X-ray structure of the resorcin[4]arene.

Parameter	X-ray structure measurement/nm	Calculated measurement/nm		% deviation[†]
		AM1[≠]	MM3*[≠]	
a	**1.015**	**1.275**	**1.131**	**11.4 (12.7)**
b	**0.941**	**1.010**	**0.908**	**3.5 (11.2)**
c	**0.518**	**0.512**	**0.511**	**1.4 (0.2)**
d	**0.404**	**0.315**	**0.354**	**12.4 (11.0)**
e	**0.682**	**0.716**	**0.712**	**4.4 (0.6)**

[‡] Cartesian coordinates of the computed structure are available on the CD accompanying this thesis.

[†] Deviation of MM3* calculation relative to X-ray data. Values in brackets represent deviation from AM1 results.

[≠] Both the AM1 and MM3* sets of data were generated from calculations performed in this study.

Interestingly, the AM1 results in this case are *less* accurate than the MM3* results.

This is as a result of the resorcin[4]arene cavity narrowing and pinching closed during the minimisation process. This phenomenon is consistent with the experimental observations, where the absence of a guest from the cavity of molecules such as resorcin[4]arenes results in the puckering of the cavity.[35] Such puckering was not observed in the case of the MM3* minimisation, potentially due to the force field used, which makes use of laws of classical physics, as opposed to the quantum nature of the physics used in the AM1 minimisation.

Indeed, in terms of precision between the two minimisation processes, the deviations reported in Table 4.5 indicates relatively poor precision. This is further illustrated by an RMS error of 0.471 nm. Again, the largest deviations are seen for parameters *a* and *d*, which is expected since these two parameters would be most affected by any puckering of the molecular cavity. In addition, the data again suggests that structure complexity influences the accuracy of the computational model.

4.6.2 Summary and Aims

The above comparisons indicate that both MM3* and AM1 models of molecules that have been observed and investigated experimentally *via* X-ray crystallography, deviate from reality; in some cases quite considerably. However, the deviation of the MM3* models from the cavitand and resorcin[4]arene crystal structures as seen above is within an acceptable margin in order to obtain useful insight into the behaviour of the proposed ligands in this study. In addition, although the semi-empirical methods above give more accurate results in general, their quantum mechanical nature, as discussed in section 4.2, means that the demand on computer time and resources during calculation is greater. This is particularly true relative to MM methods, and is a situation further compounded by the large molecules dealt with in this study.

Therefore, although the above comparisons are based only on (relatively) simple resorcin[4]arene-based molecules, it should be remembered that cavitands, porphyrins and indeed, hemicarcerands have all been investigated effectively using MM2 and MM3 force fields. Thus, the treatment of a cavitand-capped porphyrin system using MM3* and the same parameters as for the simple cavitand stands to give reliable results.

It should be noted (from Chapter 2) that in terms of the proposed ligand, aperture size must be such that guests must enter into the host ligand exclusively *via* the apertures highlighted, based on size. Therefore, the apertures must have a degree of size selectivity. With this in mind, the aims of the computational investigation were as follows:

1. Since the ligands are novel, examine the ligand structures obtained by simulation in order to gauge model precision.
2. Minimise the structures of a series of cavitand-capped porphyrin ligands, investigating the size of the apertures obtained.
3. Based on minimisation and MD, examine which bridge length will afford the most appropriate aperture size so as to ensure the desired size selectivity.

4.7 Computational Minimisation of Target Ligand Variations [36]

Computational investigations commenced by calculating the minimised structures of the series of ligands shown in Figure 4.9 using the minimisation parameters as set out in section 4.5.2 above. Once the minimised structures were obtained, the aperture width for the respective structures was measured.

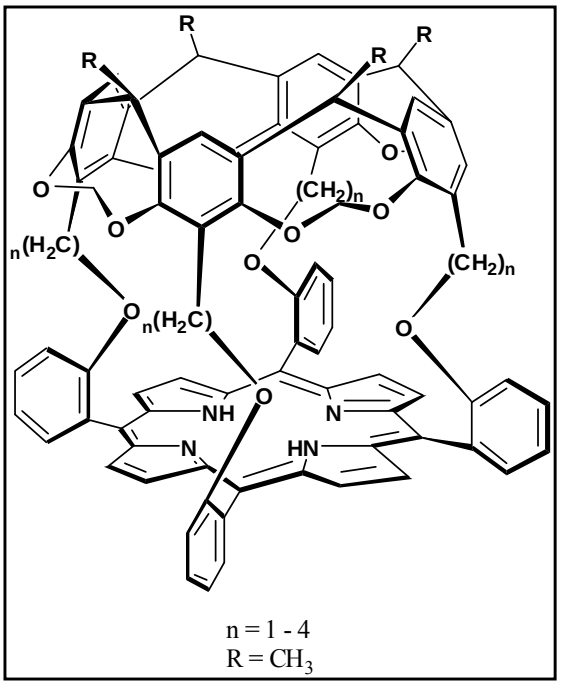

Figure 4.9: Target ligand structures used as basis for computational modeling.

Aperture size was measured between the points of the cavitand and porphyrin that were closest to each other. This is represented by the outer protons of the -OCH_2O- bridges of the cavitand structure, and the β-pyrrole protons of the porphyrin structure. This distance can be seen in Figure 4.10, the minimised structure of the target ligand bearing -$(CH_2)_2O$- bridges.

Results of the minimisation procedure and approximate aperture sizes can be seen in Table 4.6. It should be noted that the distance as measured by MACROMODEL is taken from nucleus to nucleus. Therefore, in order to obtain an effective aperture size, twice the van der Waal's radius of a proton, that is, 0.240 nm,[37] was subtracted from the measured value. In addition, since this measurement is not along a straight line between the cavitand and the porphyrin, the aperture size is reported as an approximation.

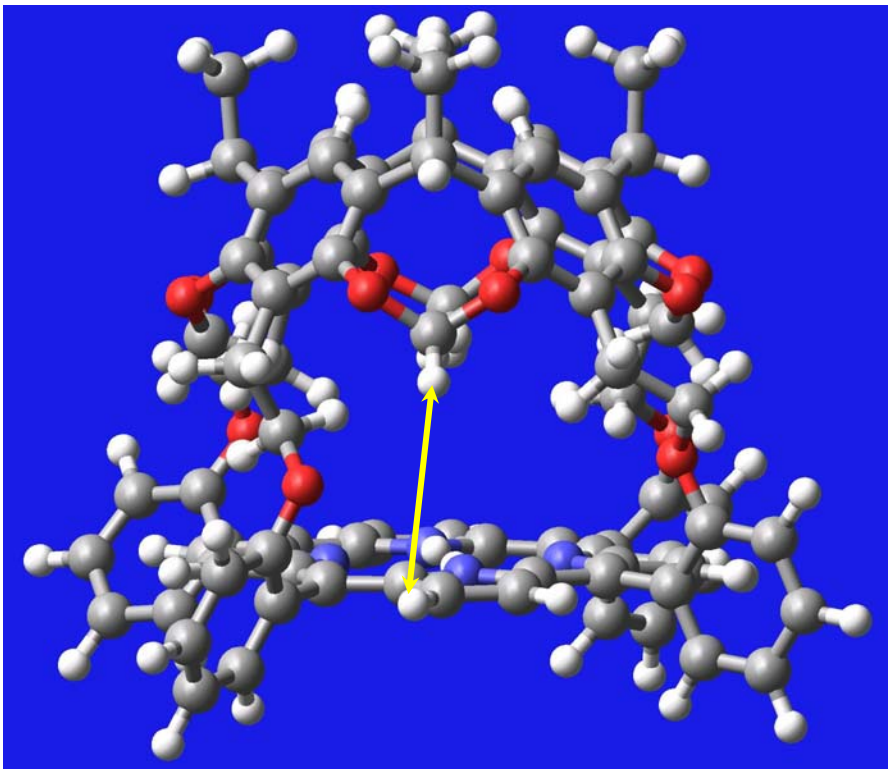

Figure 4.10: Ball and stick representation of a minimised ligand structure showing aperture measurement.

It should be remembered that aperture size must be such that it is able to selectively allow the terminus of a paraffin into the ligand cavity. In essence therefore, to afford the terminus-selective oxidation, the aperture needs to be large enough to allow a methyl group entry into the cavity but small enough to simultaneously prevent the paraffin passing through the cavity in its entirety.

Table 4.6: Potential energies and approximate aperture sizes of varied target ligand structures using MM3*.[‡]

Bridge length (*n*)	Potential energy/kJ.mol^{-1}	Approximate aperture width/nm[†]
1	**799.16**	**0.098**
2	**909.43**	**0.127**
3	**788.52**	**0.221**
4	**893.88**	**0.341**

[‡] Cartesian coordinates of the computed structure are available on the CD accompanying this thesis.

[†] Values based on van der Waal's radii.

The van der Waal's radius of a methyl group is 0.20 nm, to give a diameter of 0.40 nm;[38] therefore, an aperture size of this order is required to accommodate the terminal methyl group of a paraffin into the cavity. From Table 4.6, it can be seen that the minimised aperture size for all the ligands investigated fall short of the desired 0.40 nm.

The same minimization study was carried out on the same set of ligands, with Hyperchem software, using the semi-empirical AM1 algorithm. Aperture size was measured and treated as above for the MM3* study and results are shown in Table 4.7. Again, it is evident that all of the ligands investigated possess a minimum aperture size smaller than the desired 0.40 nm. In comparison to the MM3* study however, aperture sizes in the AM1 study are, in general, smaller. In the case of the shortest bridge (n = 1), the difference from the MM3* study is particularly significant, reflected by the large percentage deviation (33%).

The difference between corresponding structures minimised by the two methods, as indicated by the RMS error, suggests that the difference between the two is not significant when considering the minimisation of the proposed ligands. This indicates a high degree of precision between the two models. Importantly, since the semi-empirical calculation is arguably a more accurate means of calculating the minimised structures, the high degree of precision indicates that the chosen MM3* method is capable of giving accurate results in this study. There is the additional suggestion from trends within the data that as bridge length increases, the relative error decreases and the agreement between the two means of modeling improves.

Table 4.7: Approximate aperture sizes of varied target ligand structures using AM1.[‡]

Bridge length (*n*)	Approximate aperture width/nm[†]	% deviation*	RMS error[≠]/nm
1	**0.066**	**32.7**	**0.025**
2	**0.135**	**6.3**	**0.023**
3	**0.201**	**9.1**	**0.015**
4	**0.327**	**4.1**	**0.018**

[‡] Cartesian coordinates of the computed structure are available on the CD accompanying this thesis.

[†] Values based on van der Waal's radii.

* Deviation of AM1 results relative to MM3* results.

[≠] Error in fit between ligand structure minimised using MM3*, *versus* the corresponding AM1 minimisation.

The results of the optimisation in the MM3* study (Table 4.6) agree with the observations seen for the CPK model study. The structures that fitted particularly well in the CPK study (where n = 1 or 3, for bridge length in Figure 4.3) correspond to the structures with the lowest potential energy in the computational optimisation. Similarly, those which exhibited particular strain in the bridge (where n = 2 or 4, for bridge length in Figure 4.3) in the CPK study show the highest potential energy in the optimisation process.

In summary, therefore, the minimisation of the series of ligands using MM3* and AM1 produced the following results:

1. Both MM3* and AM1 minimisations indicate that the target ligand in Chapter 3 possesses apertures too small to accommodate the terminus of a paraffin.
2. The MM minimisation in conjunction with the CPK results support the observations and conclusions regarding the synthetic results in Chapter 3: the bridge length chosen proved to be too short to afford the target ligand.
3. In comparing the MM3* minimisation to the AM1 minimisation, superimposition of corresponding ligand structures indicates (*via* RMS error) that modelling using MM3* does not deviate significantly from AM1. The MM3* model thus has a high degree of precision. In addition, *both* show that the target ligand bears apertures which are too small.

It should be remembered that, as discussed in section 4.5.1, aperture sizes can be altered by changing the temperature and the thermodynamic environment in which the ligand is found. As such, MD calculations are especially attractive as a means by which to vary aperture size, and thereby identify a suitable bridge length able to afford apertures capable of accommodating the terminus of a paraffin.

4.8 Molecular Dynamics Investigation of Ligand Apertures

4.8.1 MD Study of a Reported System: Reinhoudt's Ligand

MD investigations of the ligands considered in the minimisation process commenced by first considering a similar ligand system which has been reported and observed experimentally to bind to a number of guests. As mentioned in Chapter 2, the first examples of cavitand-capped porphyrins were reported by Reinhoudt *et al.*,[39] which were subsequently used to encapsulate *N*-methylimidazole and a number of pyridine guests. Among the ligands synthesised was a capped porphyrin bearing four amide-based bridges five atoms in length, as seen in Figure 4.11.

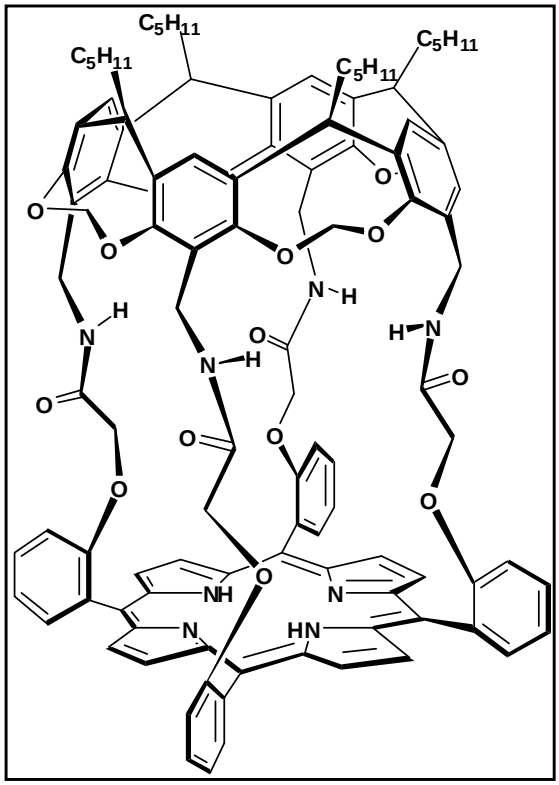

Figure 4.11: Ligand reported by Reinhoudt *et al.*, bearing four bridges five atoms in length.

The similar bridge length incorporated in this ligand in comparison to the ligands investigated in the minimisation study made Reinhoudt's ligand an attractive subject for dynamics simulations. In addition, the reported ligand (as a zinc metalloporphyrin) was observed, by UV-binding experiments, to form 1:1 complexes with the guests seen in Figure 4.12, with the guests binding to the zinc in an axial manner within the ligand cavity. In contrast, larger guests such as those seen in Figure 4.13 were observed not to enter into the ligand cavity and thus could not form a complex with Reinhoudt's ligand.

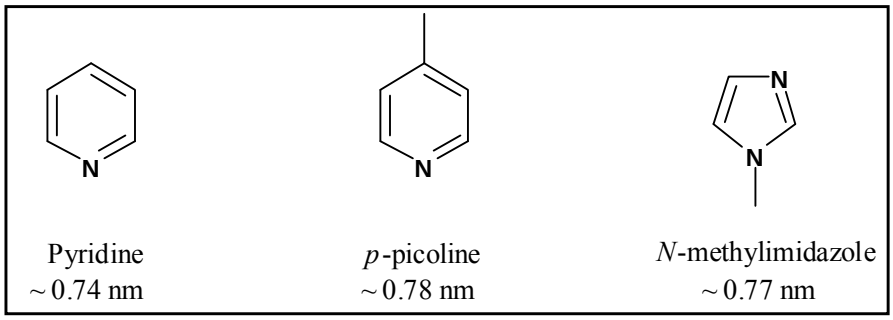

Figure 4.12: Guests encapsulated by Reinhoudt's ligand. The approximate size of these guests is shown.

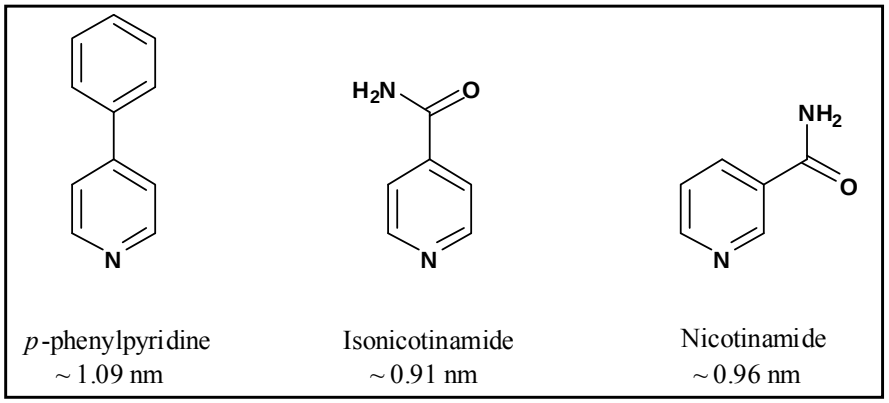

Figure 4.13: Guests unable to enter Reinhoudt's ligand. The approximate size of these guests is shown.

By considering the apertures of Reinhoudt's ligand computationally bearing in mind the nature and size of the guests which were complexed, the reliability and validity of the MD procedure and results can be assessed. Investigation commenced with the minimisation of Reinhoudt's ligand, according to the procedure as set out in section 4.6. The aperture size for the ligand in minimised configuration was measured at 0.463 nm, clearly too small to accommodate the guests shown in Figure 4.12.

Subsequently, MD simulations were performed on the molecule. A calibration was completed using cyclohexane, and the MM3* force field and parameters as set out in section 4.5.2 above. It was found that at approximately 730 K, cyclohexane was observed to undergo conformer

interconversion. Therefore, room temperature (25 °C) can be approximated as being 730 K in the simulation, with this specific force field. With this in mind, dynamics were completed on Reinhoudt's ligand at this temperature, since the reported binding experiments were performed at ambient temperature.

The simulations were done over 100 ps while monitoring the same interatomic distance used to calculate the width of ligand aperture size in the minimisation process above (Figure 4.9). In addition, snapshots of ligand aperture size were taken every 0.50 ps to give 200 sample structures over 100 ps; in effect illustrating the variation of aperture size during the course of simulation. The respective van der Waal's radii were again subtracted from all measurements, and aperture size plotted as a function of time for each ligand at each temperature. As seen in Figure 4.14, the graph indicates that at this particular temperature (approximated as room temperature), aperture size is of sufficient size to comfortably accommodate the guests as seen in Figure 4.12. Maximum aperture size approaches 0.80 nm which matches the approximate size of the guests accommodated within the ligand cavity. Additionally, the guests excluded from the cavity can be seen to have an approximate size greater than that of the aperture, explaining why exclusion occurred.

It is, however, important to note the behaviour of the cavitand in affording the observed aperture size. In minimised form, the -OCH_2O- ether bridges between the aromatic scaffolding of the cavitand arrange such that one methylene hydrogen is found within the ligand cavity, with the other outside of the cavity, as shown in Figure 4.15 (left). During MD, the additional energy from the simulation allows the methylene group to rotate such that both protons face outwards (Figure 4.15, right).

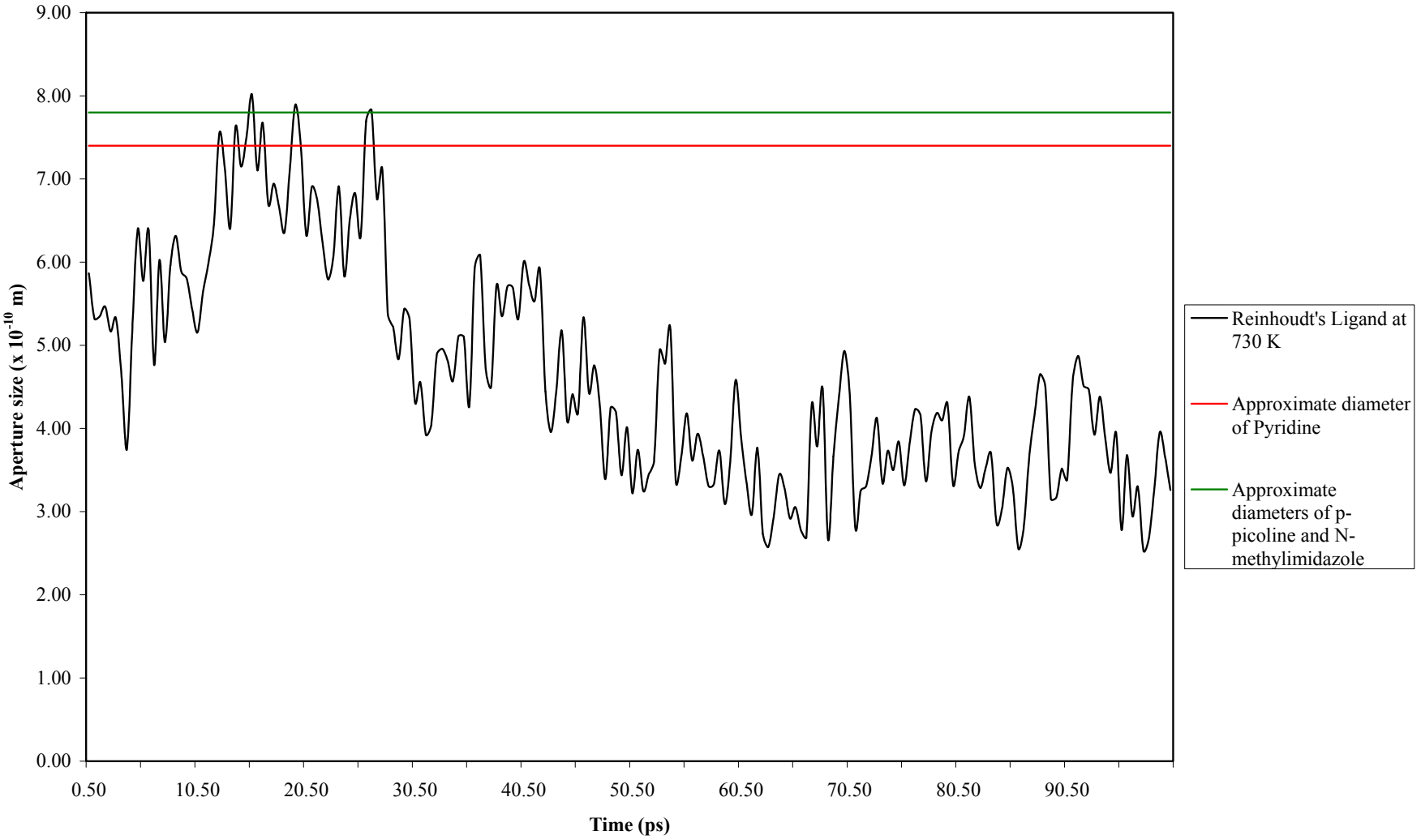

Figure 4.14: Graph of variation of aperture size at a temperature of 730 K for Reinhoudt's ligand.

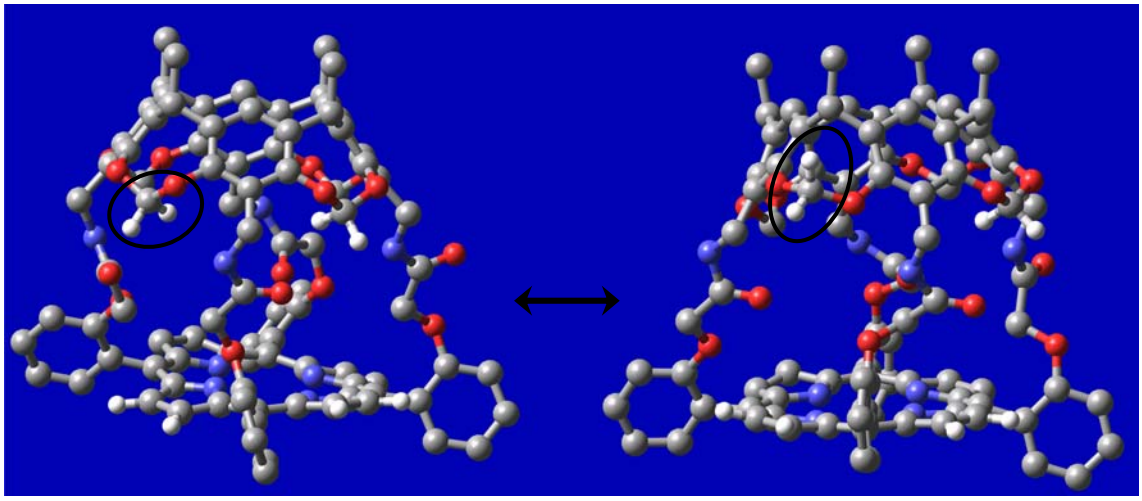

Figure 4.15: The rotation of the cavitand ether bridges during MD simulation. Protons not of interest have been omitted for purposes of clarity.

It should be remembered, from Figure 4.10, that the aperture size is measured between these hydrogen atoms and the β-pyrrole hydrogen atoms of the porphyrin. This measurement changes significantly upon rotation of the methylene hydrogen atoms due to the enlarged aperture. Interestingly, this phenomenon was also observed by Sheu and Houk in the MD study of hemicarcerands *via* MM3*[18f] and used to explain why guests seemingly larger in dimension than aperture size were found to enter the hemicarcerand cavity. Additionally, the conversion, essentially a conformational change from a chair to a boat conformation, was calculated (using MM3* methods) as having an activation barrier of 12 kcal.mol^{-1} by Sheu and Houk. Bearing in mind that processes in the order of 15 to 20 kcal.mol^{-1}[40] occur at room temperature, such a conformational change is possible at room temperature.

Therefore, given the results of the MD simulation performed on cyclohexane and the associated chair-boat conformational interconversion, as well as the conformational change noted above in Figure 4.15, the use of 730 K as a room temperature approximation is justifiable. The phenomenon in Figure 4.15 and the kinetic and thermodynamic data presented by Sheu and Houk further offers an explanation as to why the guests in Figure 4.12 were able to enter into the ligand cavity. As a retrospective investigation, MD simulations were performed on the ligand at 300, 500 and 700 K in order to confirm 730 K as a valid approximation of room temperature. It was found that rotation of the cavitand methylene hydrogen atoms was not observed at any of these temperatures, even when performing duplicate simulations over 200 ps. As shown in Figure 4.16, aperture size does not approach 0.80 nm as above, peaking at approximately 0.72 nm.

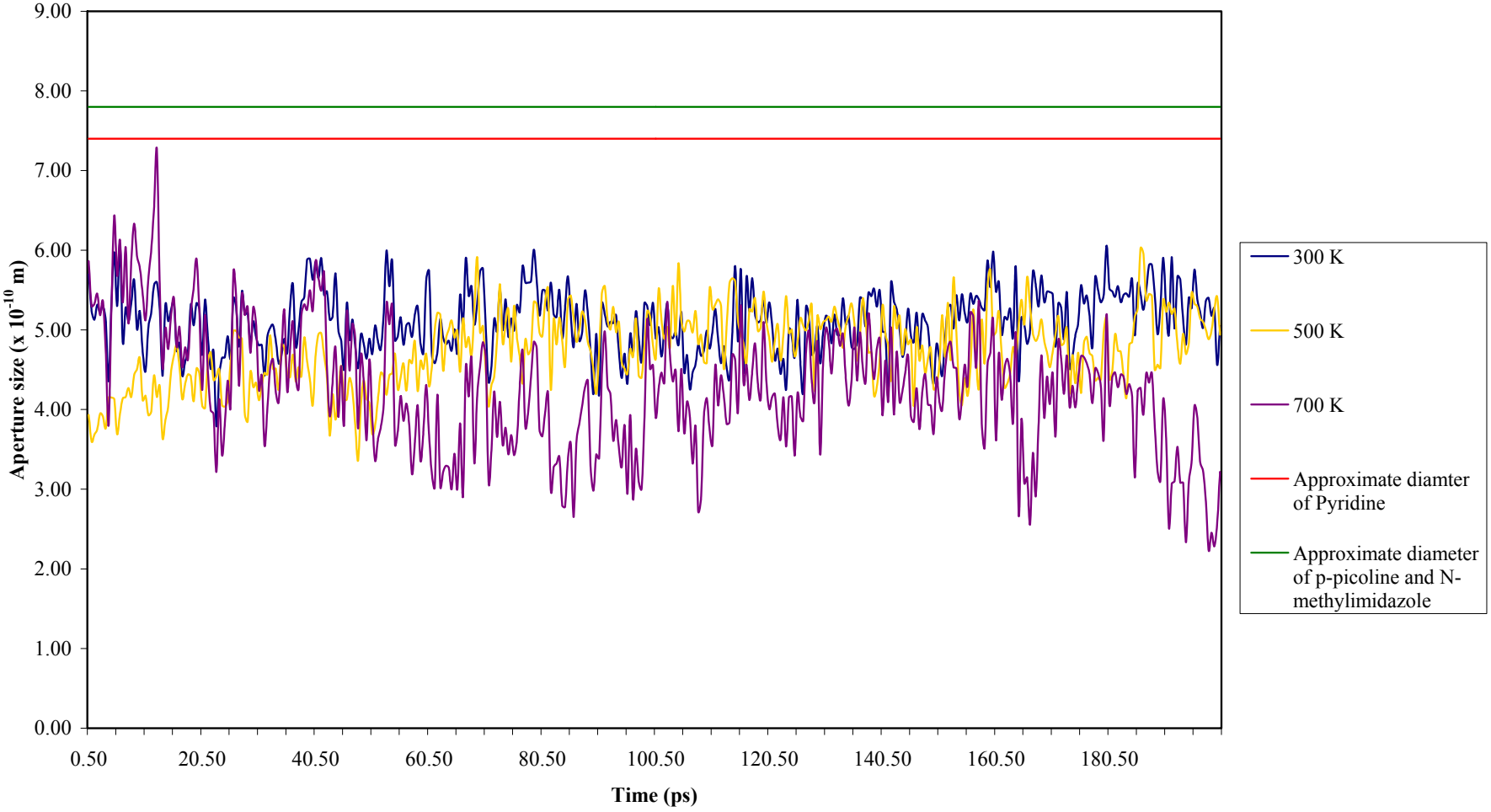

Figure 4.16: Graph of variation of aperture size at temperatures lower than approximated room temperature for Reinhoudt's ligand.

Indeed, this aperture size arose as the system possessed sufficient energy at 700 K to rotate the cavitand methylene groups to the point of conformation change; however, insufficient energy was present to overcome the activation barrier.

It can hence be seen that the computational model and methods applied are able to replicate the experimental observations seen by Reinhoudt *et al.* In particular, the investigation illustrated why the smaller guests exhibited enhanced binding, while the larger guests could not be accommodated within the ligand cavity. The study also shows that the MD simulation can be reliably used to predict whether or not bridge length can afford ligand apertures able to selectively allow guests into the molecular cavity.

It should however be noted that there are inherent differences between the above modeled system and Reinhoudt's experimental system; most notably the absence of the Zn(II) metal centre used to complex any guests, and the use of amide-based bridges. The inclusion of a metal in the ligand stands to rigidify the ligand framework to a degree, but modeling of a system incorporating metals is not suited to MM calculations using MM3*. Nonetheless, although the ligands optimised thus far are ether-based, MD simulations can be used to investigate which of these affords an aperture size capable of selectively accommodate the terminus of a paraffin.

4.8.2 MD Simulations of Ligands Forming Part of this Study

It is evident from the minimisation process and Table 4.6, that all of the proposed molecules give aperture sizes that fall short of the desired size of approximately 0.40 nm. As such, MD studies were carried out on the ligands bearing bridges as shown in Figure 4.17 in order to see how aperture size varies as a function of temperature.

The MD simulations were performed in the same manner as *per* Reinhoudt's molecule in section 4.8.2. In addition to monitoring the same aperture dimension as in the above MD study, the distance perpendicular to this measurement (horizontally, between two neighbouring bridges linking the porphyrin to the cavitand) was also monitored to see if this distance would also become a factor in limiting access to the ligand cavity at elevated temperatures. Additionally, the distance between the single aromatic protons of opposite aromatic residues in the cavitand structure (parameter *d*, Figure 4.4 - 4.8) was also monitored for each molecule for the same reasons. The results of the MD simulations were treated in the same manner as for Reinhoudt's

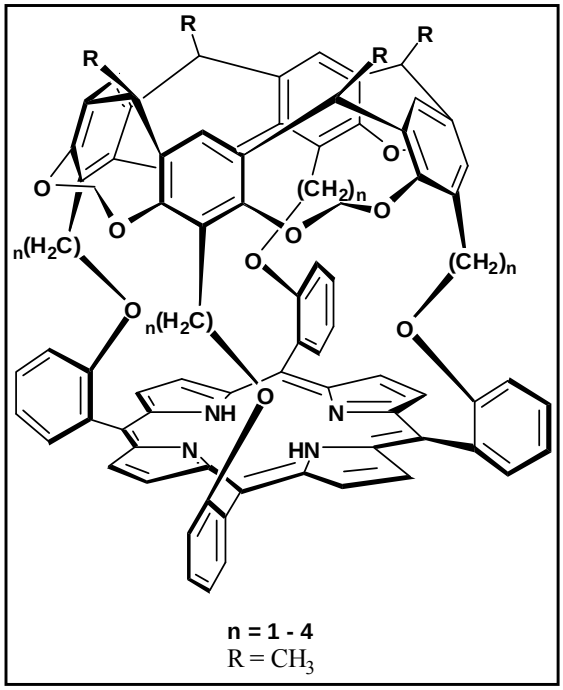

Figure 4.17: Ligand structure variations used in MD studies.

ligand, are summarised as graphs in the figures below. In each graph, 0.40 nm is included as a reference aperture size.

The MD simulation for the synthetic target (n = 1, Figure 4.17) in Chapter 3, as illustrated by Figure 4.18, indicated that despite the elevated temperatures, aperture size does not approach the desired 0.40 nm. A maximum of approximately 0.30 nm is reached. Interestingly, the graph shows that the temperature variation has no significant effect on how the aperture varies, and essentially shows a trace of results over the four simulations. This indicates that there is a significant degree of rigidity associated with this particular ligand, brought about by the short bridges used to link the cavitand and porphyrin moieties. It was also found that the maximum horizontal distance between two neighbouring bridges ranged between 0.44 and 0.47 nm over the temperature range. The distance between opposite cavitand aromatic protons (parameter d) remained in the order of 0.16 nm, and did not vary appreciable as a function of temperature. Both of these results indicate that these distances would not influence access to the ligand cavity at elevated temperatures.

The ligand bearing -$(CH_2)_2$O- (n = 2, Figure 4.17), having an extra methylene group present in the bridge, also has an average aperture size that falls short of 0.40 nm. Figure 4.19, however, does indicate a lot more variation of aperture size as a function of temperature in comparison to

the ligand seen in Figure 4.18. This is indicative of the increased flexibility in the ligand system as a result of the introduction of the additional methylene group into the bridges.

Interestingly, the ligand does reach an aperture size which exceeds 0.40 nm on one isolated occasion. This can be explained by the rotation of the -OCH_2O- ether bridges forming part of the cavitand scaffold as discussed above (illustrated by Figure 4.14). This rotation only occurs at elevated temperatures, in contrast to Reinhoudt's ligand, which exhibits the rotation at room temperature. This is indicative of the increased rigidity of this particular ligand relative to that of Reinhoudt's, brought on by the shorter bridge length, in this case. Analysis of the horizontal distance between two bridges as well as the distance between opposite cavitand aromatic protons (parameter *d*) again showed these parameters would not influence access to the ligand cavity at elevated temperatures.

The use of a ligand having bridges four atoms in length proved to give more promising results. As seen in Figure 4.20, the use of -$(CH_2)_3O$- bridges (n = 3, Figure 4.17), the calculation results in an aperture size which exceeds 0.40 nm on a number of occasions during simulation, even at lower temperatures. In addition, the general aperture size does not become excessively large. The ligand does exhibit rotation of the cavitand -OCH_2O- ether bridges, at 900 and 1000 K, to give enlarged apertures. However, this may (in theory) be prevented by avoiding the use of such temperatures during laboratory experimentation. This becomes particularly important considering that, while the terminus of a paraffin is 0.40 nm in diameter, the remainder of the paraffin ranges from 0.46 to 0.49 nm.[38] Thus, to achieve selective entry of only the paraffin terminus into the ligand cavity, the aperture should ideally not exceed 0.49 nm.

Additionally, the horizontal distance between adjacent bridges and the distance between opposite cavitand aromatic protons again proved not to be a factor able to influence access to the ligand cavity at elevated temperatures.

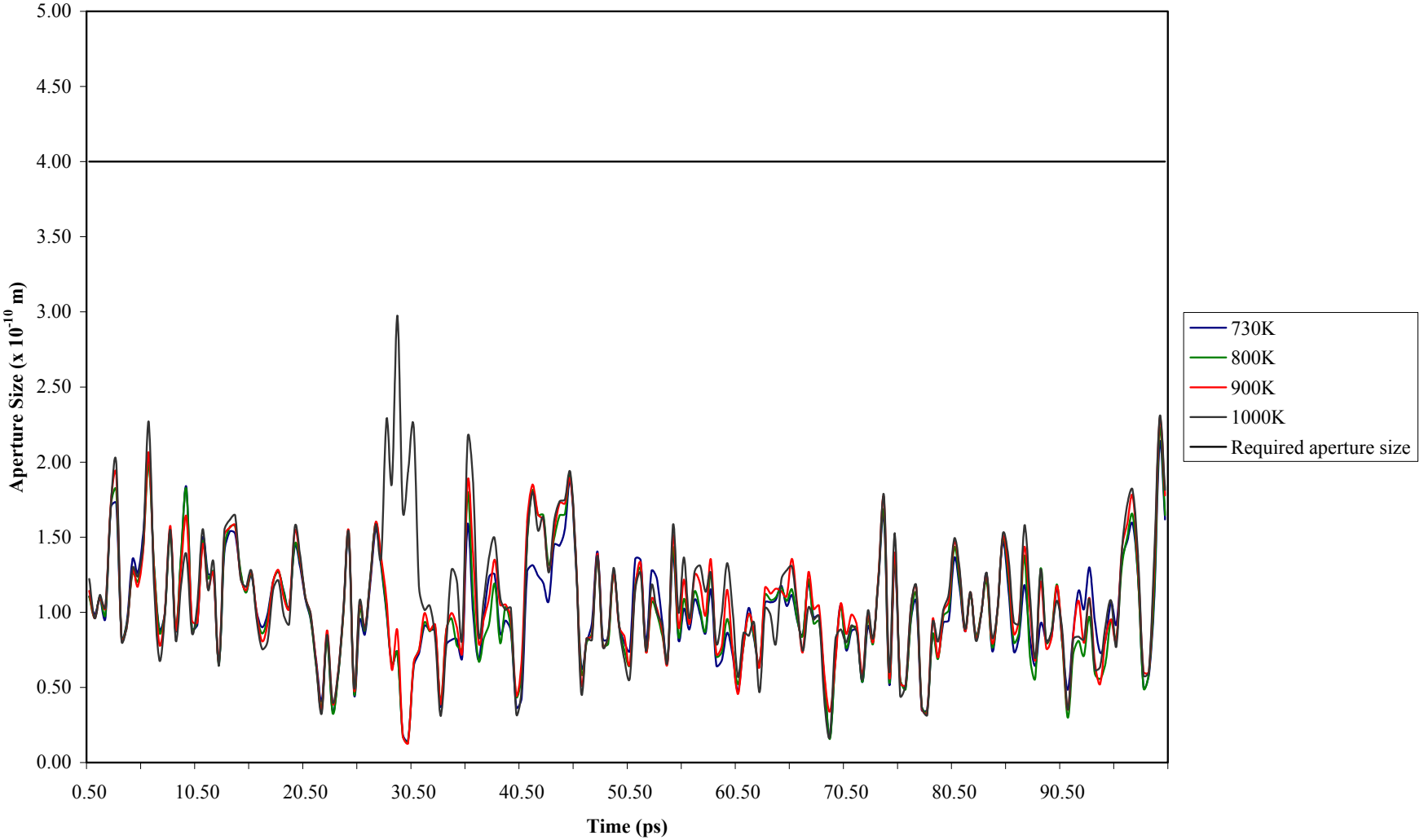

Figure 4.18: Graph of variation of aperture size as a function of temperature for ligand bearing -CH_2O- bridges.

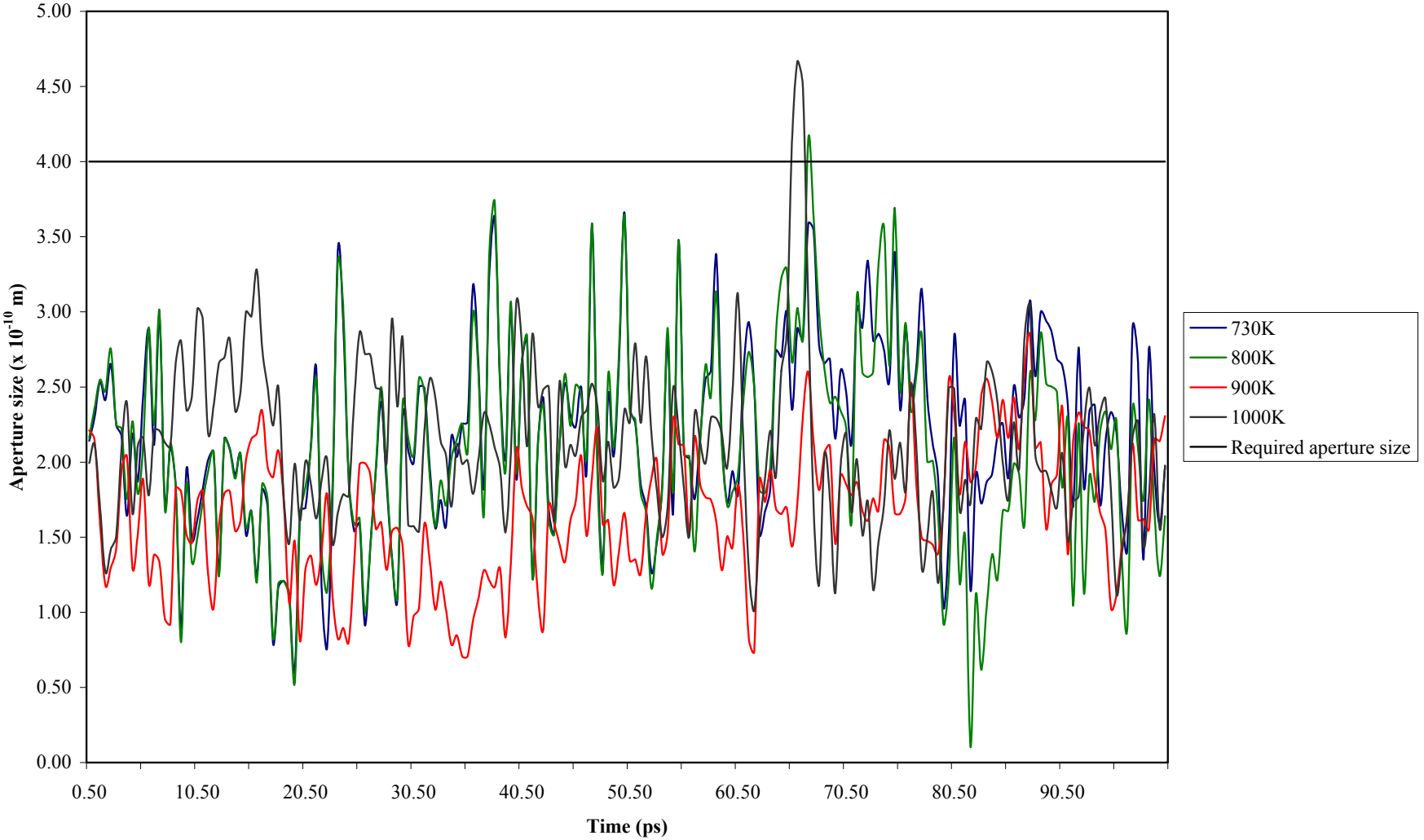

Figure 4.19: Graph of variation of aperture size as a function of temperature for ligand bearing -CH_2CH_2O- bridges.

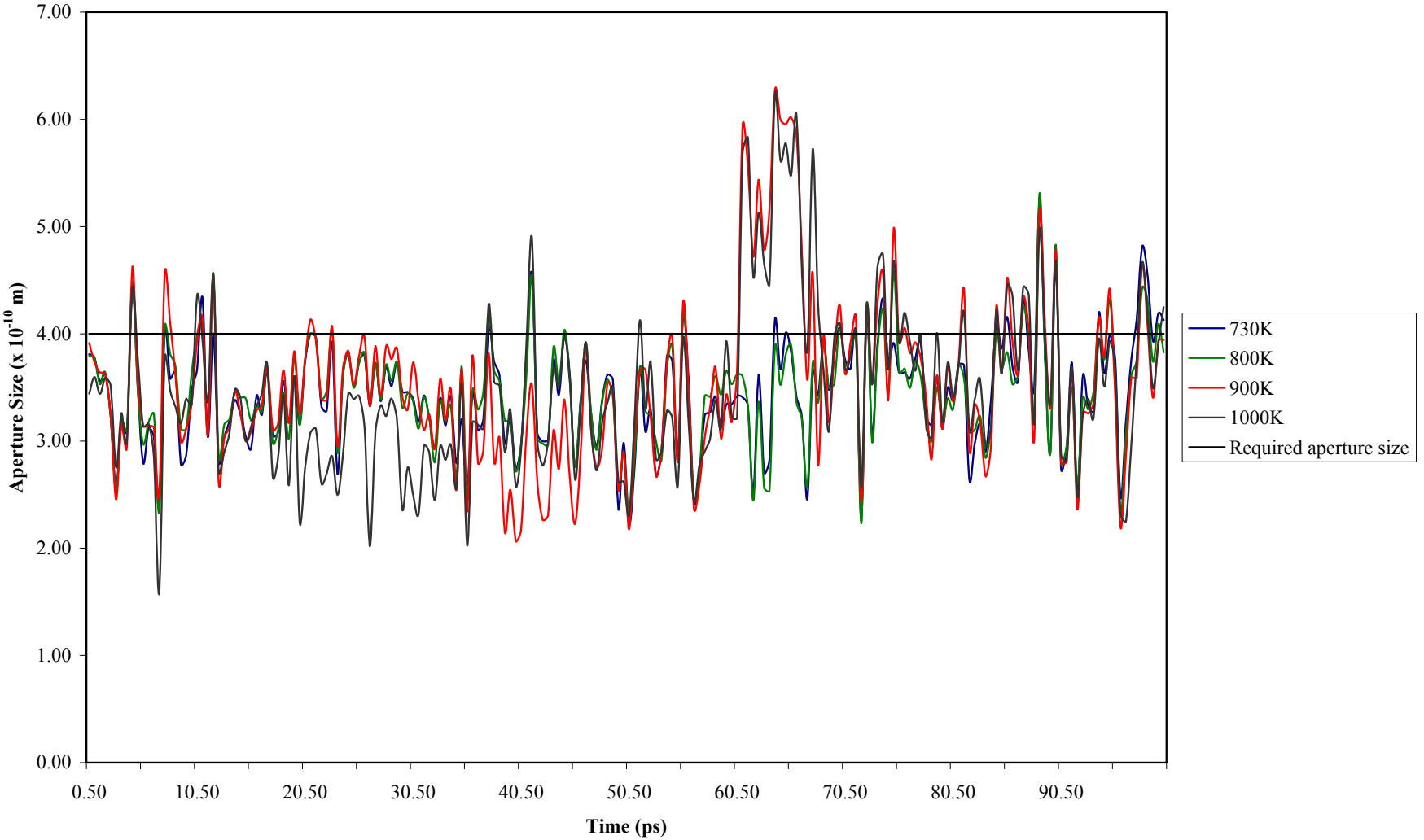

Figure 4.20: Graph of variation of aperture size as a function of temperature for ligand bearing -$CH_2CH_2CH_2O$- bridges.

The final ligand considered in the MD studies possessed a five atom bridge (n = 4, Figure 4.17). As evident in Figure 4.21, the relatively long -$(CH_2)_4O$- bridges meant that the ligand apertures easily exceeded 0.40 nm, even at room temperature. This was expected given the results presented for Reinhoudt's ligand, which had a similar bridge length. However, the apertures in this case approach and exceed 0.50 nm on a regular basis. This potentially indicates that in terms of size selectivity for the terminus of a paraffin, this ligand may prove to have apertures which are too large. In addition, the cavitand ether bridges can again be seen to undergo rotation, also at room temperature, to give excessively large aperture sizes. Moreover, as with the previous three ligand variations, the horizontal distance between adjacent bridges and that between opposite cavitand aromatic protons proved not to be a factor influencing access to the ligand cavity at elevated temperatures.

In summary, therefore, a number of noteworthy conclusions may be drawn from the above MD study:

1. Access to the ligand cavity is feasible only through the molecular apertures investigated, and not through any other aperture forming part of the ligand structure (such as the base of the cavitand). Therefore, size selectivity can be achieved *via* the apertures formed by a suitable length of cavitand-porphyrin bridge.
2. The use of -CH_2O- moieties as part of the target ligand in Chapter 3 results in bridges that are insufficiently long to accommodate an alkane terminus. The MD studies further show that the ligand is especially rigid in nature, and unable to accommodate the terminus of a paraffin through its small apertures, even at elevated temperatures. Thus even if ligand synthesis were a success, the ligand would be unable to function selectively as intended.
3. In order to achieve a suitable aperture size for the desired selectivity, a bridge length of four or five atoms seems most viable, giving significant direction to any subsequent synthesis. In addition, control over rotation of the cavitand -OCH_2O- ether bridges is possible by avoiding high temperatures, thereby maintaining a suitable aperture size for selectivity towards a paraffin terminus.

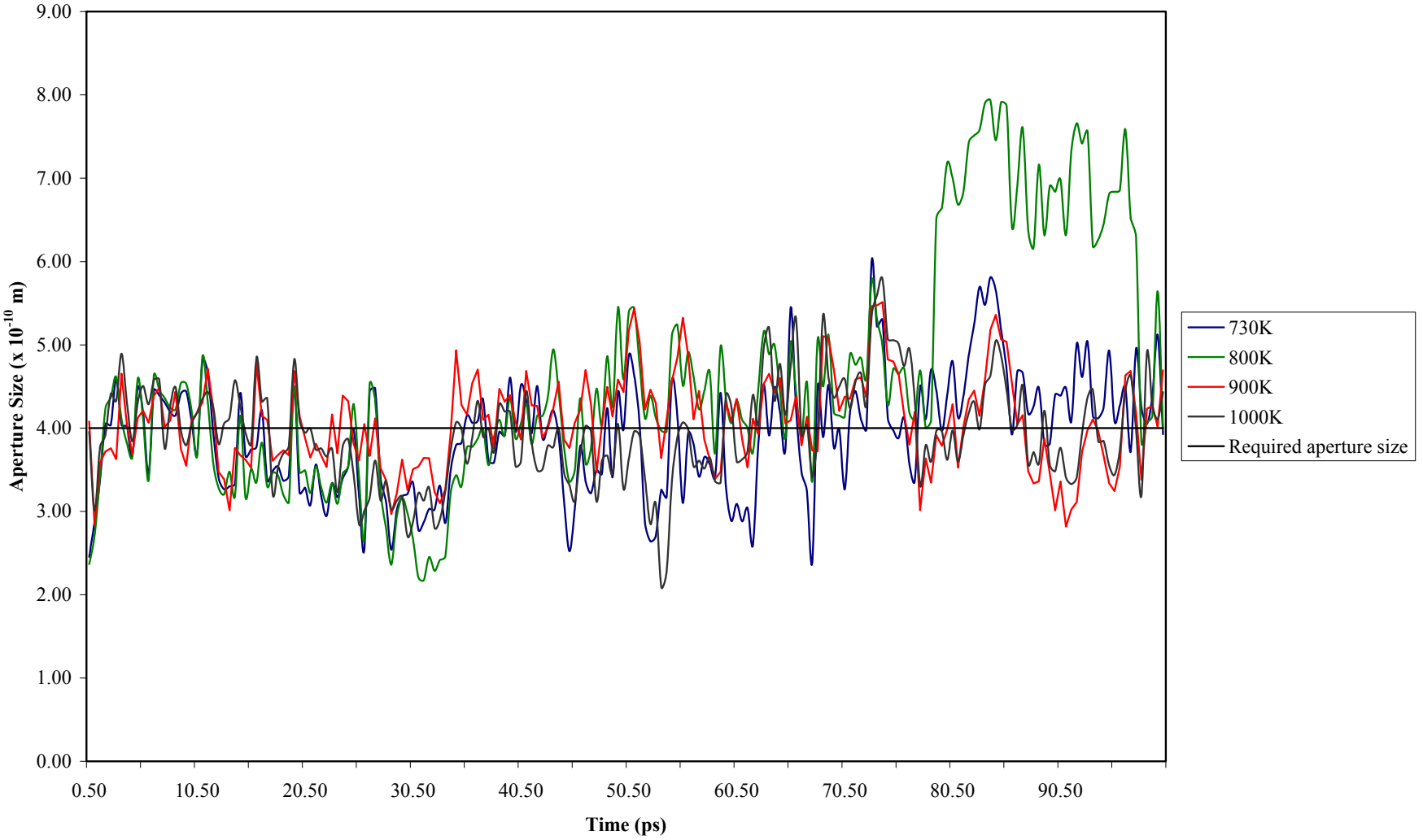

Figure 4.21: Graph of variation of aperture size as a function of temperature for ligand bearing -$CH_2CH_2CH_2CH_2O$- bridges.

4.8.3 Subsequent MD Studies: Ligands Bearing Bridges of Four or Five Atoms

Two ligands were identified as offering a way forward to achieving both synthesis and selectivity: one bearing -O(CH$_2$)$_2$O- bridges and another the -O(CH$_2$)$_3$O- bridges, to give bridges four and five atoms in length, respectively. The introduction of the additional oxygen atom compared with the equivalent length of bridge as seen in the ligands studied in section 4.8.2 will be discussed in Chapter 5, along with the subsequent synthesis. However, in order to confirm whether the chosen ligands are capable of affording a desirable aperture size of approximately 0.40 nm, an identical set of MD studies were undertaken as *per* the method set out.

Computation again commenced with minimisation of the ligands under investigation according to the method set out in section 4.5.2. The aperture sizes were measured, and compared with those seen for the four- and five-atom bridged ligands considered in section 4.8.2. The minimisation and comparative results can be seen in Table 4.8. It is evident that there is a minimal difference in minimised aperture size between corresponding ligands.

Table 4.8: Approximate aperture sizes of four- and five-atom bridged ligand structures using MM3*.[‡]

Bridge	Effective bridge length/atoms	Approximate aperture width/nm[†]
-(CH$_2$)$_3$O-	**4**	**0.221**
-O(CH$_2$)$_2$O-	**4**	**0.219**
-(CH$_2$)$_4$O-	**5**	**0.341**
-O(CH$_2$)$_3$O-	**5**	**0.360**

[‡] Cartesian coordinates of the computed structure are available on the CD accompanying this thesis.

[†] Values based on van der Waal's radii.

As expected, the minimised aperture sizes for the identified ligands fall short of the desired 0.40 nm thereby justifying performing MD on the two ligands in question.

MD results for the ligand bearing -O(CH$_2$)$_2$O- bridges can be seen in Figure 4.22. It is evident that aperture size exceeds 0.40 nm on a number of occasions. Indeed, the frequency is very

much comparable to that of the ligand bearing an equivalent bridge length as seen in Figure 4.20. Once again the rotation of the cavitand -OCH_2O- ether bridges (Figure 4.15) is observed, occurring during the course of dynamics performed at 900 and 1000 K. This is also observed in Figure 4.20. However, dynamics performed at lower temperatures, and indeed, at room temperature (730 K), show an aperture size able to accommodate the terminus of a paraffin.

Regarding the ligand bearing -$O(CH_2)_3O$-, a similar result (Figure 4.23) was again obtained when compared to the equivalent molecule (Figure 4.21): the apertures easily exceed 0.40 nm and, on a regular basis, 0.50 nm. Noticeably, Figure 4.23 does not exhibit the rotation of the cavitand ether bridges; however, on extending the MD simulation to 200 ps, rotation is observed. It is also evident that at room temperature (approximated at 730 K in this study), the aperture size does not become excessively large despite the increased flexibility in this ligand in comparison to the ligand bearing -$O(CH_2)_2O$- bridges. Indeed, an aperture size between 0.40 to 0.46 nm is maintained during the MD simulation at room temperature.

In essence, therefore, there is not a significant difference between the two newly proposed ligands and the two equivalent ligands examined in section 4.8.2. Indeed, both are capable, by the computational results, of the selective accommodation of a paraffin terminus. The two new ligand variations are thus promising toward obtaining selective oxidation.

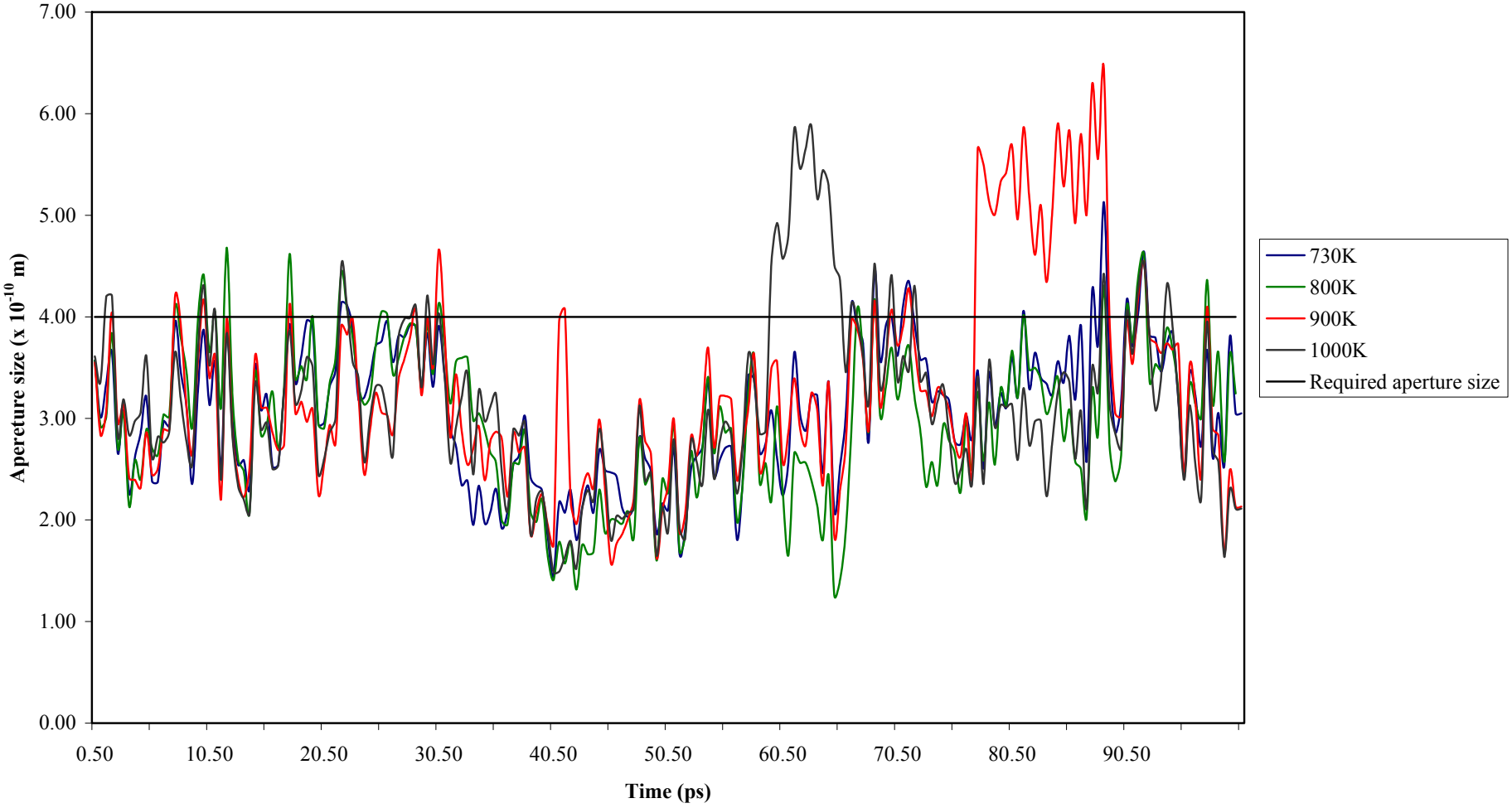

Figure 4.22: Graph of variation of aperture size as a function of temperature for ligand bearing -OCH_2CH_2O- bridges.

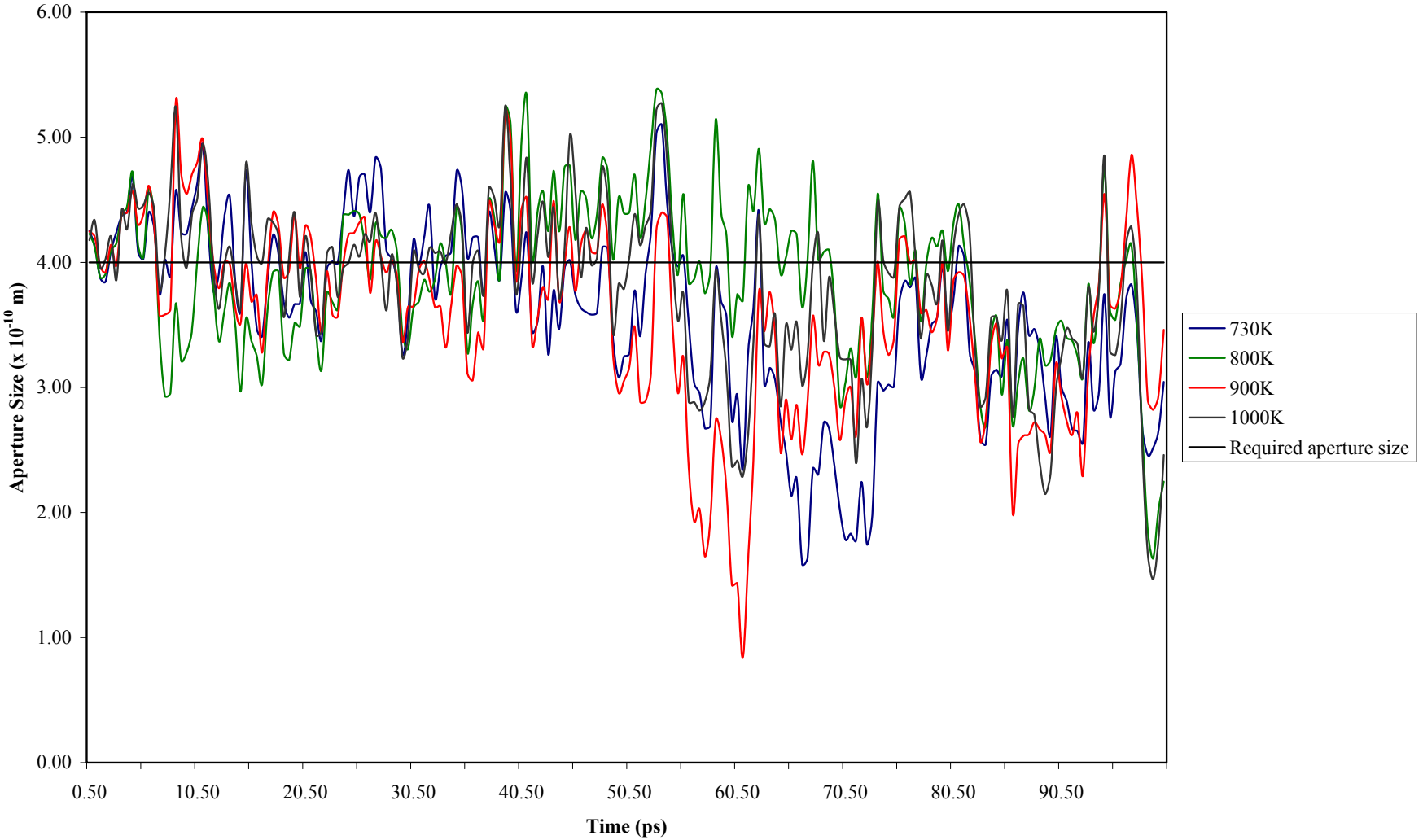

Figure 4.23: Graph of variation of aperture size as a function of temperature for ligand bearing -O $CH_2CH_2CH_2O$- bridges.

4.9 Conclusion

As evident in Chapter 3, the chosen bridge length for the target ligand makes it difficult to synthesise, by an *in situ* protocol or by a direct capping protocol. Indeed, the synthetic observations suggested a minimum requirement of bridge length exists for a successful synthesis (regardless of protocol used), and that the -CH_2O- bridge used is *below* this minimum. The results of the computational investigation further substantiate this conclusion; the minimisation results in particular supporting the conclusion that the short bridge length was a primary reason for the inability to synthesise the target ligand in Chapter 3. Additionally, the MD study indicates that the -CH_2O- bridges afford apertures that are too small to accommodate the terminus of a paraffin, both in a minimised configuration, and at elevated temperatures. Thus, even if a successful synthesis was achieved, the ligand appears to be unable to selectively allow only the terminus of a paraffin access to the ligand cavity.

With this minimum requirement in mind, it is also important to note the observations by Cram *et al.*,[22a] and Sheu and Houk[18f] regarding the formation of complexes. Both reported that longer bridge lengths and larger aperture sizes in the case of hemicarcerands did not necessarily afford size selectivity towards larger guests. Therefore, while *this* study suggests a minimum requirement, the reported observations additionally suggests that a maximum bridge length requirement exists in order to maintain selectivity. Beyond this maximum, hosts are *no longer* able to effectively be selective in terms of discriminating between guests based on size.

Therefore, there is experimental evidence to support the notion that there exists both a minimum and a maximum requirement of bridge length with regards to cavitand-capped porphyrins. Since this study shows that -CH_2O- bridges are of insufficient length to fulfill either requirement regarding synthesis and selectivity, longer bridges are an obvious way forward. Subsequent computational investigation demonstrated that ligands having four- or five-atomed bridges are capable of affording an aperture size suitable for the desired selectivity towards a paraffin terminus. The ligand bearing bridges consisting of five, however, may give apertures too large to yield the desired size selectivity. Nonetheless, these two ligands represent viable synthetic targets, and will be the focus of subsequent synthetic work to follow in Chapter 5.

In terms of viable computational and theoretical models, due to the novelty of the ligands under consideration, no absolute conclusions may be drawn regarding model accuracy and precision in

this study. However, semi-empirical methods appear to be more promising, given the accuracy of the results obtained above in section 4.6, relative to the corresponding MM results. Indeed, it has been shown that MM has problems describing the unusual environment inside hosts such as hemicarcerands (thus, cavitand-capped porphyrins),[18f, 19] since, as mentioned in section 4.3, MM models do not explicitly consider electronic interactions. The description of the interior of such host molecules as a new phase of matter [41] thus warrants quantum mechanical approaches, such as semi-empirical or *ab initio* methods. In this regard, the work reported by Naruta *et al.* illustrates the ability of *ab initio* methods to replicate experimentally observed results with analogous host molecules.[23] Such methods, however, require greater computing resources, which were not available at the time of this study.

REFERENCES

1. ***a)*** T. Clark, *A Handbook of Computational Chemistry*, Wiley, **1985**; ***b)*** D.M. Hirst, *A Computational Approach to Chemistry*, Blackwell, **1990**; ***c)*** A. Hinchcliffe, *Modeling Molecular Structure*, Wiley, **1996**; ***d)*** T. Schlick, *Molecular Modeling and Simulation*, Springer, **2002**; ***e)*** P. Comba, T.W. Hambley, *Molecular Modeling of Inorganic Compounds*, Wiley, Verlag, **2001**.
2. Hyperchem Inc., *Hyperchem, Computational Chemistry*, **1996**.
3. J.B. Foresman, A.E Frisch, *Exploring Chemistry with Electronic Structure Methods*, Gaussian Inc., **1996**.
4. I.N. Levine, *Quantum Chemistry*, Prentice Hall, **2000**.
5. P. Atkins, J. de Paula, *Atkin's Physical Chemistry*, Oxford University Press, **2002**.
6. C.J. Cramer, *Essentials of Computational Chemistry*, Wiley, Chichester, **2004**.
7. W.J. Hehre, J.Yu, P.E. Klunzinger, L. Lou, *A Brief Guide to Molecular Mechanics and Quantum Chemical Calculation*, Wavefunction, Inc., **1998**.
8. ***a)*** A.R. Leach, *Molecular Modeling, Principles and Applications*, Addison Wesley Longman, England, **1996**; ***b)*** F. Jensen, *Introduction to Computational Chemistry*, Wiley, Chichester, **2007**.
9. K. Bissety, PhD Thesis, and references therein, *University of Natal Durban*, **2002**.
10. ***a)*** A. Hinchliffe, *Chemical Modeling From Atoms to Liquids*, Wiley, Chichester, **1999**; ***b)*** A. Hinchcliffe, *Molecular Modeling for Beginners*, Wiley, Chichester, **2003**.
11. ***a)*** J.L. Banks, H.S. Beard, Y.X. Cao, A.E. Cho, W. Damm, R. Farid, A.K. Felts, T.A Halgren, D.T. Mainz, J.R. Maple, R. Murphy, D.M. Philipp, M.P. Repasky, L.Y. Zhang, B.J. Berne, R.A. Friesner, E. Gallicchio, R.M. Levy, *J. Comput. Chem.*, **2005**, *26*, 1752-1780; ***b)*** W. Klopper, K.L. Bak, P. Jorgensen, J. Olsen, T. Helgaker, *J. Phys. B.: At., Mol. Opt Phys.*, **1999**, *32*, 103-130; ***c)*** P.R. Rablen, J.W. Lockman, W.L. Jorgensen, *J. Phys. Chem. A*, **1998**, *102*, 3782-3797; ***d)*** J. Simons, *J. Phys. Chem.*, **1991**, *95*, 1017-1029.
12. T. Raasch, M.Sc Thesis, and references therein, *University of Natal Durban*, **2002**.
13. ***a)*** P. Hohenberg, W. Kohn, *Phys. Rev. B*, **1964**, *136*, 864; ***b)*** W. Kohn, L.J. Sham, *Phys. Rev. A*, **1965**, *140*, 1133.
14. P. Comba, *Coord. Chem. Rev.*, **1993**, *123*, 1-48.
15. J.M. Haile, *Molecular Dynamics Simulation: Elemental Methods*, Wiley, New York, **1992**.

16. ***a)*** H.D. Holtje, G. Folkers, *Methods and Principles in Medicinal Chemistry*, VCH, New York, **1996**; ***b)*** K. Bisetty, F.J. Corcho, J. Canto, H.G. Kruger, J.J. Perez, *THEOCHEM*, **2006**, *770*, 221-228.

17. ***a)*** J.C. Sherman, *Tetrahedron*, **1995**, *51*, 3395-3422; ***b)*** E. Maverick, D.J. Cram, *Comprehensive Supramolecular Chemistry* **1996**, *2*, 367-418; ***c)*** J. Rebek, *Chem. Soc. Rev.*, **1996**, *4*, 255-264; ***(d)*** R. Warmuth, J. Yoon, *Acc. Chem. Res.*, **2001**, *34*, 95-105.

18. ***a)*** D.J. Cram, M.E. Tanner, C.B. Knobler, *J. Am. Chem. Soc.*, **1991**, *113*, 7717-7727; ***b)*** D.J. Cram, M.T. Blanda, K. Paek, C.B. Knobler, *J. Am. Chem. Soc.*, **1992**, *114*, 7765-7773; ***c)*** D.J. Cram, R. Jaeger, K. Deshayes, *J. Am. Chem. Soc.*, **1993**, *115*, 10111-10116; ***d)*** T.A. Robbins, C.B. Knobler, D.R. Bellew, D.J. Cram, M.E. Tanner, *J. Am. Chem. Soc.*, **1994**, *116*, 111-122; ***e)*** J. Yoong, C. Sheu, K.N. Houk, C.B. Knobler, D.J. Cram, *J. Org. Chem.*, **1996**, *61*, 9323-9339; ***f)*** C. Sheu, K.N. Houk, *J. Am. Chem. Soc.*, **1996**, *118*, 8056-8070.

19. M.J. Liddell, D. Margetic, A.S. Mitchell, R.N. Warrener, *J. Comput. Chem.*, **2003**, *25*, 542-557.

20. ***a)*** C. von dem Bussche-Hunnefeld, D. Buhring, C.B. Knobler, D.J. Cram, *J. Chem. Soc. Chem. Comm.*, **1995**, 1085-1087; ***b)*** K. Nakamura, K.N. Houk, *J. Am. Chem. Soc.*, **1995**, *117*, 1853-1854.

21. ***a)*** D.J. Cram, M.T. Blanda, K. Paek, C.B. Knobler, *J. Am. Chem. Soc.*, **1992**, *114*, 7765-7773.

22. T.A. Robbins, D.J. Cram, *J. Am. Chem. Soc.*, **1993**, *115*, 12199.

23. J. Nakazawa, Y. Sakae, M. Aida, Y. Naruta, *J. Org. Chem.*, **2007**, *72*, 9448-9455.

24. ***a)*** S. Fischer, P.D.J. Grootenhuis, L.C. Groenen, W.P. van Hoorn, F.C.J.M. van Veggel, D.N. Reinhoudt, M. Karplus, *J. Am. Chem. Soc.*, **1995**, *117*, 1611-1620; ***b)*** I. Thondrof, J. Brenn, W. Brandt, V. Bohmer, *Tetrahedron Lett.*, **1995**, *36*, 6665-6668; ***c)*** B.P. Hay, L. Yang, J-H Lii, N.L. Allinger, *THEOCHEM*, **1998**, *428*, 203-219; ***d)*** H. Otsuka, K. Araki, H. Matsumoto, T. Harada, S. Shinkai, *J. Org. Chem.*, **1995**, *60*, 4862-4867; ***e)*** I. Thandorf, J. Brenn, *J. Chem. Soc. Perkin Trans. 2*, **1997**, 2293-2297.

25. ***a)*** F. Weinelt, H-J Schneider, *J. Org. Chem.*, **1991**, *56*, 5527-5535; ***b)*** I. Thondrof, J. Brenn, V. Bohmer, *Tetrahedron*, **1998**, *54*, 12823-12828; ***c)*** A. Tafi, B. Botta, M. Botta, G. Delle Monach, A. Filippi, M. Speranza, *Chem. Eur. J.*, **2004**, *10*, 4126-4135.

26. ***a)*** P.D. Beer, E.L. Tite, M.G.B. Drew, A. Ibbotson, *J. Chem. Soc. Dalton Trans.*, **1990**, 2543-2550; ***b)*** G.J. Chen, R. Cruz, G.M. Martinez, F. Lara-Ochoa, *THEOCHEM*, **2000**, *496*, 73-81; ***c)*** K.N. Houk, K. Nakamura, C. Sheu, A.E. Keating, *Science*, **1996**, *273*, 627-629.

27. O.Q. Munro, J.C. Bradley, R.D. Hancock, H.M. Marques, F.W. Marsicano, *J. Am. Chem. Soc.*, **1992**, *114*, 7218-7230.
28. ***a)*** M.A. Lopez, P.A. Kollman, *J. Am. Chem. Soc.*, **1989**, *111*, 6212-6222; ***b)*** R.D. Hancock, J.S. Weaving, H.M. Marques, *J. Chem. Soc. Chem. Comm.*, **1989**, 1176-1178.
29. ***a)*** F. Maseras, *New J. Chem.*, **1998**, 327-332; ***b)*** J-D Marechal, G. Barea, F. Maseras, A. Lledos, L. Mouawad, D. Perahia, *J. Comput. Chem.*, **2000**, *21*, 282-294.
30. ***a)*** B. Botta, P. Ricciardi, C. Galeffi, M. Botta, A. Tafi, R. Pogni, R. Iacovino, I. Garella, B. Di Blasio, G. Delle Monache, *Org. Biomol. Chem.*, **2003**, *1*, 3131-3137.
31. ***a)*** M. Jalaie, K.B. Lipkowitz, *Rev. Comput. Chem.*, **2000**, *14*, 441-486; ***b)*** T. Liljefors, K. Gundertofte, P-O. Norrby, I. Pettersson, *Computational Medicinal Chemistry for Drug Discovery*, Marcel Dekker, New York, **2004**.
32. D.J. Cram, S. Karbach, H-E Kim, C.B. Knobler, E.F. Maverick, J.L. Ericson, R.C. Helgeson, *J. Am. Chem. Soc.*, **1988**, *110*, 2229-2237.
33. ***a)*** K. Gundertofte, J. Palm, I. Pettersson, A. Stamvick, *J. Comput. Chem.*, **1991**, *12*, 200-208; ***b)*** K. Gundertofte, T. Liljefors, P-O. Norrby, I. Pettersson, *J. Comput. Chem.*, **1996**, *17*, 429-449.
34. Hyperchem, Release 7.51 for Windows, Hypercube Inc., **2002**.
35. J.W. Steed, J.L. Atwood, *Supramolecular Chemistry*, Wiley, Chichester **2000**.
36. All data from the complete computational investigation is included on the CD accompanying this thesis, as Appendix 2.
37. R.S. Rowland, R. Taylor, *J. Phys. Chem.*, **1996**, *100*, 7384 - 7391.
38. M.S. Whittingham, A.J. Jacobson, *Intercalation Chemistry*, Academic Press, **1982**.
39. O. Middel, W. Verboom, D.N. Reinhoudt, *J. Org. Chem.*, **2001**, *66*, 3998-4005.
40. J.B. Hendrickson, D.J. Cram, G.S. Hammond, *Organic Chemistry*, McGraw-Hill, New York, **1970**.
41. ***a)*** D.J. Cram, M.E. Tanner, R. Thomas, *Angew. Chem. Int. Ed. Engl.*, **1991**, *30*, 1024-1027; ***b)*** J.C. Sherman, D.J. Cram, *J. Am. Chem. Soc.*, **1989**, *111*, 4527-4528.

CHAPTER 5

SYNTHESIS OF CAVITAND-CAPPED PORPHYRIN TARGET LIGANDS BEARING LONGER BRIDGES

The results from MD simulations in Chapter 4 indicated that in order to obtain apertures of a size selective towards the terminus of a paraffin, bridges consisting of four or five atoms need to be incorporated into the target ligand. This requirement therefore needed to be taken into consideration when synthesising the ligands.

Computational investigation in Chapter 4 showed that -$(CH_2)_3O$- and -$(CH_2)_4O$- bridges gave a suitable aperture size to accommodate a paraffin terminus. However, attaching such alkyl bridges directly to the cavitand structure *via* functionalisation of the extra-annular position is synthetically more challenging than for the original synthetic target (Chapter 3). Therefore, to allow for a more facile synthesis, an additional oxygen atom, directly attached to the extra-annular carbon atom, is incorporated into the bridges. This gives apertures formed *via* -$O(CH_2)_2O$- or -$O(CH_2)_3O$- bridges, as shown in Figure 5.1. As discussed in Chapter 4, such apertures are analogous in size and behaviour to those formed using -$(CH_2)_3O$- and -$(CH_2)_4O$- bridges, respectively.

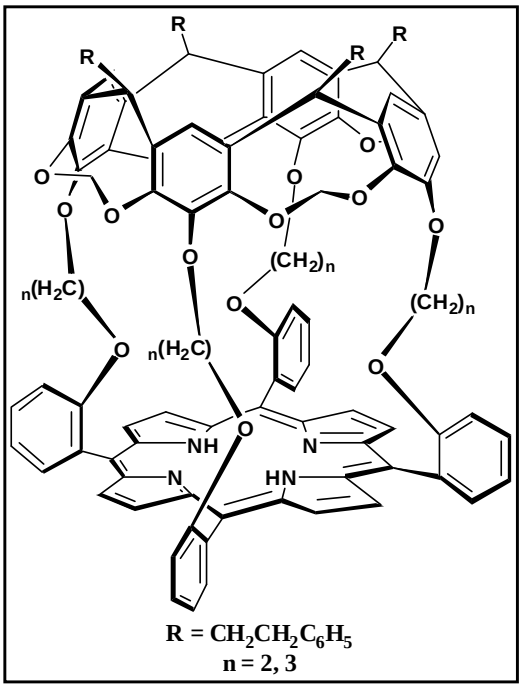

Figure 5.1: General structure of the proposed cavitand-capped porphyrin ligands bearing longer bridges.

The novel nature of these ligands again required that both the *in situ* and direct capping synthetic protocols be attempted to determine if either yield a successful synthesis, as in Chapter 3. Both protocols and their respective origins have thus been discussed in detail and will not be dealt with further.

5.1 In situ Approach

Bearing in mind the new requirements in terms of bridge length, Scheme 5.1 illustrates a retrosynthetic pathway towards the synthesis of the target ligands. Scheme 5.2 subsequently shows the complete synthetic scheme yielding the desired cavitand-capped porphyrins. Both schemes show that the chosen synthesis uses procedures and functionalisation which are largely established and provide adequate yields.

Synthesis commences with the preparation of resorcin[4]arene **29**.[1] The choice of **14** as aldehyde starting material stems from the solubility issues which were encountered in Chapter 3. The use of **14** results in the synthesised resorcin[4]arene having 2-phenylethyl feet that renders **29**, and any subsequent cavitands, soluble in most organic solvents. Noticeably, **29** merely has a proton at the extra-annular position. This position is readily brominated to give **30** in good yield using *N*-bromosuccinimide at 0 $^{\circ}$C, conditions which allow for control of the exothermic nature of reaction.[2] Thereafter, synthesis of cavitand **31** can be completed by using either the procedure as set out by Bryant *et al.*[2] or the pressurised-vessel method of Kaifer *et al.*[3] The two methods of cavitand formation have been discussed in detail in Chapter 3. Interestingly, however, synthesis of **31** is accomplished only *after* the bromination of **29**, and is not attempted using **29** as the reaction precursor.

Conversion of **31** to tetrol **32** proceeds *via* a two step, one pot synthesis.[4] Vacuum dried precursor **31** is dissolved in THF, itself dry and freshly distilled from sodium benzophenone ketal prior to use, before being cooled to -78 $^{\circ}$C The extra-annular positions are metallated by the addition of *n*-butyllitium. The bromine atoms are thus displaced by lithium to yield an organometallic complex, which subsequently undergoes quenching by the addition of trimethyl borate, $B(OCH_3)_3$. The resultant arylboronic esters are then treated with a solution of 1:1 15 % H_2O_2: 1.5 M NaOH, oxidizing the esters to alcohols.

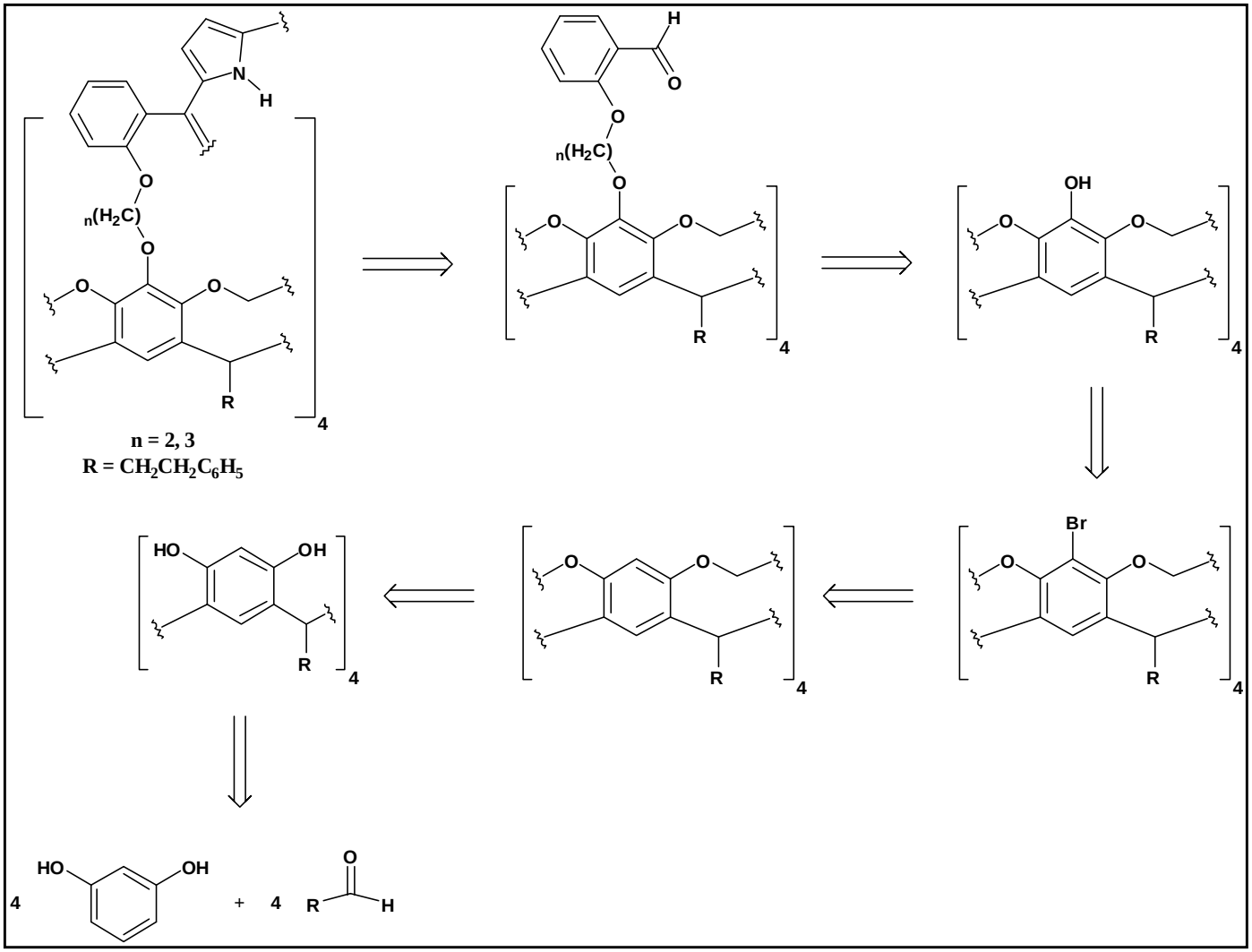

Scheme 5.1: Retrosynthetic pathway of the *in situ* formation of porphyrin to form the proposed ligands.

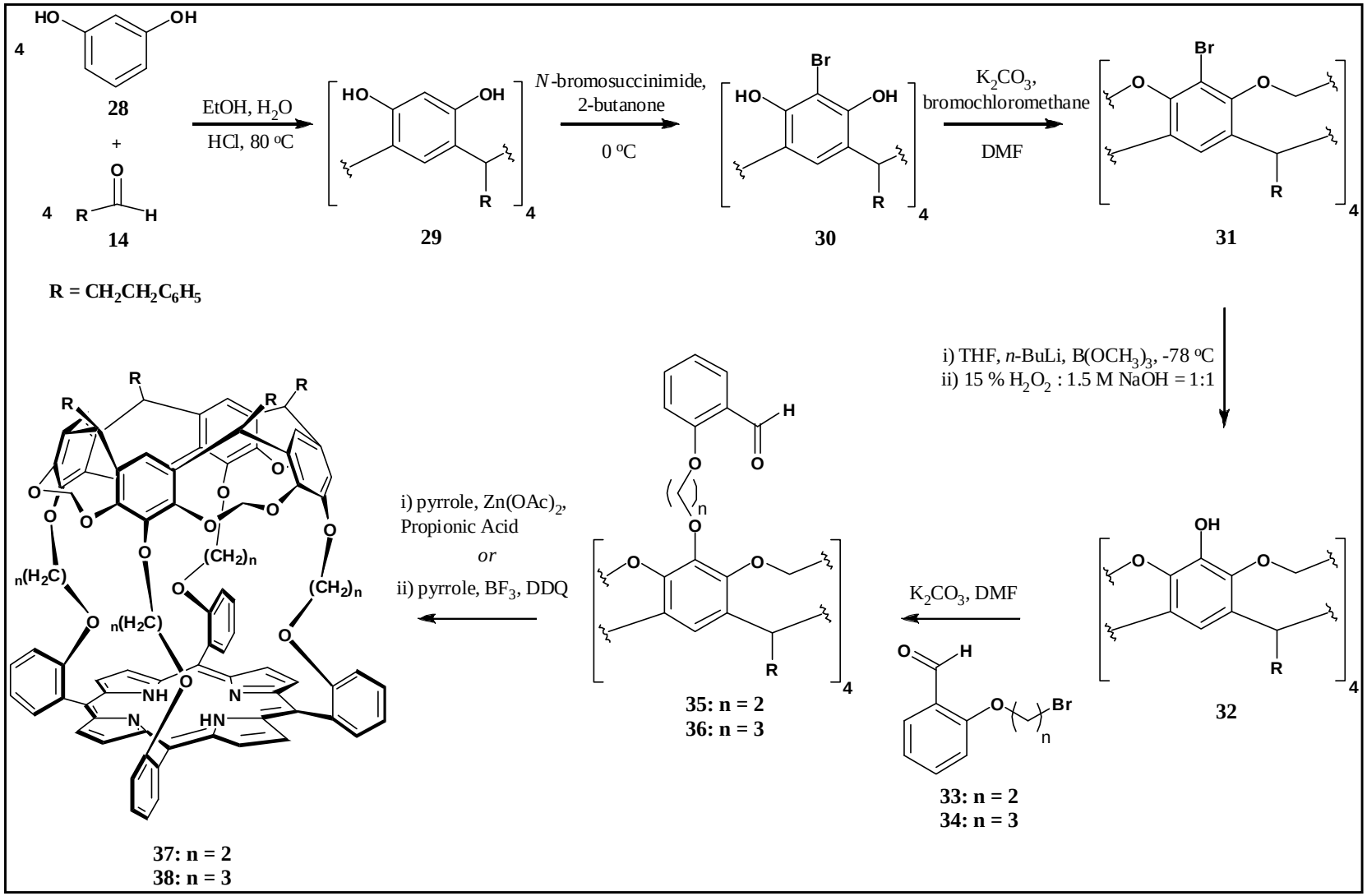

Scheme 5.2: *In situ* synthetic pathway towards the new target ligands.

The nature of this reaction and indeed, the reagents involved, require that all glassware be thoroughly dried and that synthesis be done under an inert atmosphere. The exclusion of water in particular is important, since both *n*-butyllitium and trimethyl borate are especially moisture sensitive. The presence of moisture during the lithiation step is likely to result in incomplete lithiation of all four extra-annular positions of **31**. Additionally, the lithiation of **31** does not result in the exclusive formation of **32**, where all four bromine functionalities are converted to alcohols. Instead, byproducts result, in the form of a mixture of the tri-, di- and monosubstituted alcohols. The product profile seen is likely as a result of the oxidation step, which has been studied in depth elsewhere.[5] Nonetheless, **32** forms as the majority product (in a yield of approximately 50 %) and can be isolated from the various byproducts using column chromatography. Despite the stringent and involved nature of the reaction, and the relatively poor yield, **32** represents a particularly versatile cavitand, used not only as a vital precursor to both the *in situ* and direct synthetic protocols in this study, but also in carcerand and hemicarcerand synthesis.[3, 6]

Reaction of **33** and **34** with **32**, in the presence of a base, results in the synthesis of novel aldehydes **35** and **36**, respectively. The aldehyde reagents **33** and **34** have been synthesised in very good yields and characterised previously, by coupling salicylaldehyde with 1,2-dibromoethane, or 1,3-dibromopropane, respectively, in the presence of K_2CO_3 and DMF.[7]

Once **35** and **36** have been synthesised, the final *in situ* porphyrin formation is attempted by following the Adler (i, Scheme 5.2) or Lindsey (ii, Scheme 5.2) conditions, so as to afford **37** and **38**, respectively. In this regard, it should be remembered that the capped porphyrin ligand bearing bridges consisting of five atoms as reported by Reinhoudt *et al.* was synthesised exclusively *via* the use of the Adler conditions. Therefore, these conditions may be most suitable in affording **37** and **38**, given the analogous bridge length.

5.1.1 Results: In situ Protocol

Resorin[4]arene **29** was synthesised in yields comparable to that reported in the literature.[1] The bromination of **29** using the cited method of addition of *N*-bromosuccinimide (NBS) to a solution of **29** in 2-butanone at 0 $^{\circ}$C, in contrast, gave **30** in poor yields (23 %) relative to that reported.[2] Reaction protocol was changed slightly, resorting to the addition of the NBS over

approximately an hour, whilst maintaining the reaction solution at -5 °C. While both these factors allowed for an improved control over the reaction isotherm, yields remained in the order of 25 %. An alternative means of bromination was subsequently attempted, whereby **29** was suspended in glacial acetic acid, and the suspension treated with elemental bromine at room temperature.[8] The method yielded a suspension of **30**, which was filtered and washed with water to give an 87 % yield. Proton (^{1}H) NMR continued to be used as means of characterisation, as it was in Chapter 3.

The NMR spectra of **29** and **30** will be discussed with reference to Figure 5.2, which shows the protons present in the respective resorcin[4]arenes.

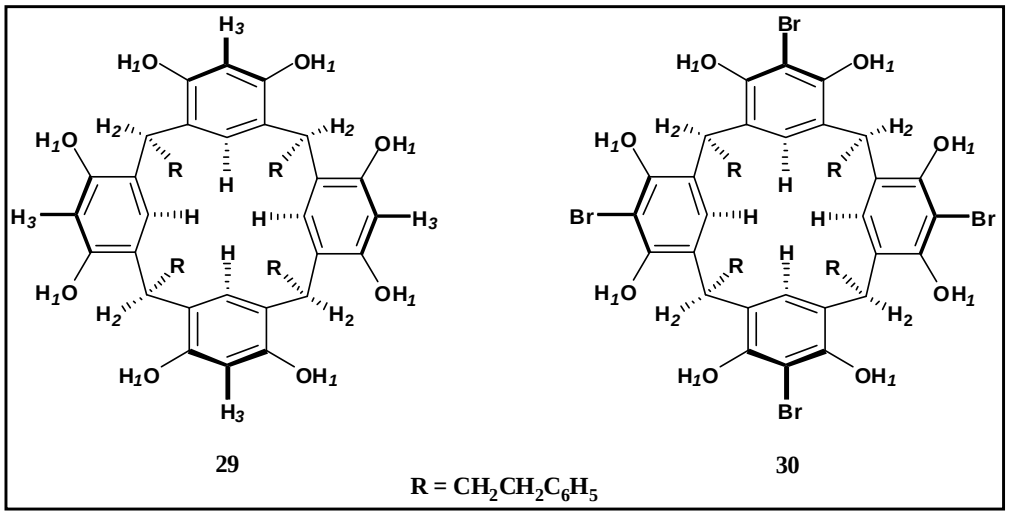

Figure 5.2: Expanded structures of **29** and **30**, showing distinctive protons.

The hydroxyl groups of **29** allow for easy identification using ^{1}H NMR, with the eight associated protons (H_1) appearing collectively as a singlet at 8.53 ppm in d_6-acetone integrating to eight protons, as evident in Spectrum 1.70. The protons associated with the 2-phenylethyl feet (R) give rise to multiplets at 2.52-2.61 (integrating to 16 protons) and 7.14-7.25 ppm (integrating to 20 protons), due to the presence of the -CH_2CH_2- and aromatic moieties, respectively. Due to coupling with the CH_2CH_2- moieties of the feet, H_2 appears as a multiplet at 4.38 ppm, integrating to four protons. Finally, the two aromatic protons belonging to the resorcin[4]arene scaffold appear as singlets at 6.25 and 7.74 ppm; H_3 appears further upfield. Since **30** differs from **29** only by the substitution H_3 with bromine atoms at the extra-annular position, the ^{1}H NMR spectrum of **30** (Spectrum 1.73) appears very similar to that of **29**, except for the disappearance of the singlet at 6.25 ppm. The loss of this signal thus serves to confirm the successful bromination of **29**. H_2 appears, again as a multiplet, at 4.52 ppm, integrating to four protons, while the signal arising from the remaining aromatic proton appears at 7.76 ppm.

Those signals belonging to the feet are unchanged both in terms of chemical shift and multiplicity.

The alkylation of the eight hydroxyl groups of **30** to form cavitand **31** was first attempted using the method of Kaifer *et al.*[3] in the interests of improved yields. However, this method was unable to afford **31**. Given this results in addition to the mixed results seen in using this synthetic method in Chapter 3, the method does appear to have some limitations. Nonetheless, **31** was successfully synthesised *via* the protocol of Bryant *et al.*[2] in yields approaching 70 %. Conversion of **31** to **32** proceeded readily using the conditions cited, in a 45 % yield.[4] Separation of the mono-, di- and tri-substituted alcohols from the desired tetrol, however, proved difficult using the reported silica gel chromatographic conditions. The use of 3:1 ethyl acetate:hexane as the eluant did not afford the exclusive isolation of tetrol **32**, and traces of triol were found to be present by TLC after completion of the column. In order to improve the separation of tetrol from triol, column conditions were altered, whereby a chloroform-methanol eluant was employed. Gradient elution (by the slow introduction of methanol into chloroform) was used towards a final chloroform:methanol ratio of 85:15, which was found to be successful in isolating tetrol **32**.

With reference to Figure 5.3, the ^{1}H NMR signals of **31** and **32** (Spectrum 1.76 and 1.79, respectively) were assigned.

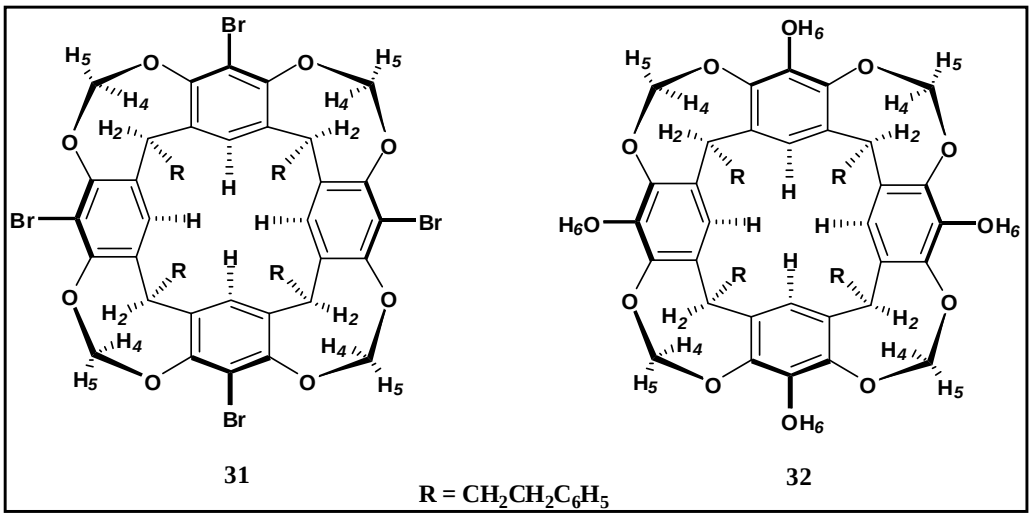

Figure 5.3: Expanded structures of **31** and **32**, showing distinctive protons.

As discussed in Chapter 3, the introduction of the methylene groups as part of **31** gives rise to distinct signals characteristic of cavitands. The anisotropic nature of the associated protons (H_4

and H_5) results in the appearance of two doublets, both integrating to four protons: one at 4.41 ppm (for the 'inner' proton, H_4) and another at 5.94 ppm (for the 'outer' proton, H_5). The signal for H_2 has resolved into a triplet, which has shifted slightly downfield to 4.94 ppm, integrating to four protons. The signals due to the ethyl protons associated with the 2-phenylethyl feet have also resolved into two multiplets at 2.47 - 2.49 ppm and 2.62 - 2.64 ppm, both integrating to eight protons. The remaining aromatic protons associated with the feet, as well as those associated with the cavitand scaffold appear as a multiplet at 7.08 - 7.24 ppm. Conversion of **31** to **32**, as seen in Spectrum 1.77, results most notably in the appearance of a singlet at 7.96 ppm due to H_6, integrating to four protons. The successful synthesis and isolation of **32** can be determined by the nature of this signal, as well as from those related to protons H_4 and H_5. The presence of triol gives rise to multiple singlets at approximately 8.0 ppm as well as an additional pair of doublets at approximately 4.5 and 6.0 ppm. The absence of these signals from Spectrum 1.77 further serves to confirm the synthesis of tetrol **32**. Indeed, the remainder of the signals associated with the feet, H_2, H_4 and H_5 are largely unchanged from **31**, and maintain the associated multiplicity and chemical shift. Additionally, crystals of **31** were grown by the slow solvent evaporation of a solution of **31** in chloroform/acetone, and samples analysed using single crystal X-ray crystallography. Discussion of the data follows in Chapter 6.

Before *in situ* formation of porphyrin could take place, the required aldehyde residues needed to be incorporated into the cavitand scaffold. In order to facilitate this, salicylaldehyde derivatives **33** and **34** were synthesised from salicylaldehyde and the appropriate dibromoalkane. Synthesis took place in DMF in the presence of K_2CO_3, using an excess (8 equivalents) of dibromoalkane reagent. Yield in the case of **33** was 70 %, while that in the case of **34** was 97 %. Interestingly, reaction was unsuccessful in yielding either **33** or **34** when using NaH in THF. Additionally, while the reaction towards **34** proceeded readily to completion, the reaction towards **33** was unable to go to completion and unreacted salicylaldehyde remained, despite gentle heating during the course of reaction. It was thus particularly important to thoroughly wash the reaction mixture during workup with 10 % NaOH in order to remove excess salicylaldehyde. Excess dibromoalkane was removed *in vacuo* to yield **33** as a yellow, crystalline solid, and **34** as a yellow oil. Crystals of **33** were sampled and analysed *via* X-ray crystallography. The data is discussed in Chapter 6 to follow. Synthesis of novel aldehydes **35** and **36** took place under conditions very similar to those applied to the synthesis of **33** and **34**. Tetrol **32** was dissolved in a small amount of dry DMF and reacted, in the presence of K_2CO_3, with **33** and **34** at 55 $^{\circ}$C. This afforded **35** (93 % yield) and **36** (81 % yield), respectively. Interestingly, pure **35** and **36** were obtained without further chromatography *via* working up the reaction by filtering off the

excess K_2CO_3, removing the DMF under reduced pressure, and stirring the resultant oily residue in methanol overnight. In addition, scaling up of the reaction beyond 0.5 g of tetrol starting material resulted in diminished yields and mixtures of products. With reference to Figure 5.4, the ^{1}H NMR signals of compounds **33 - 35** will be discussed.

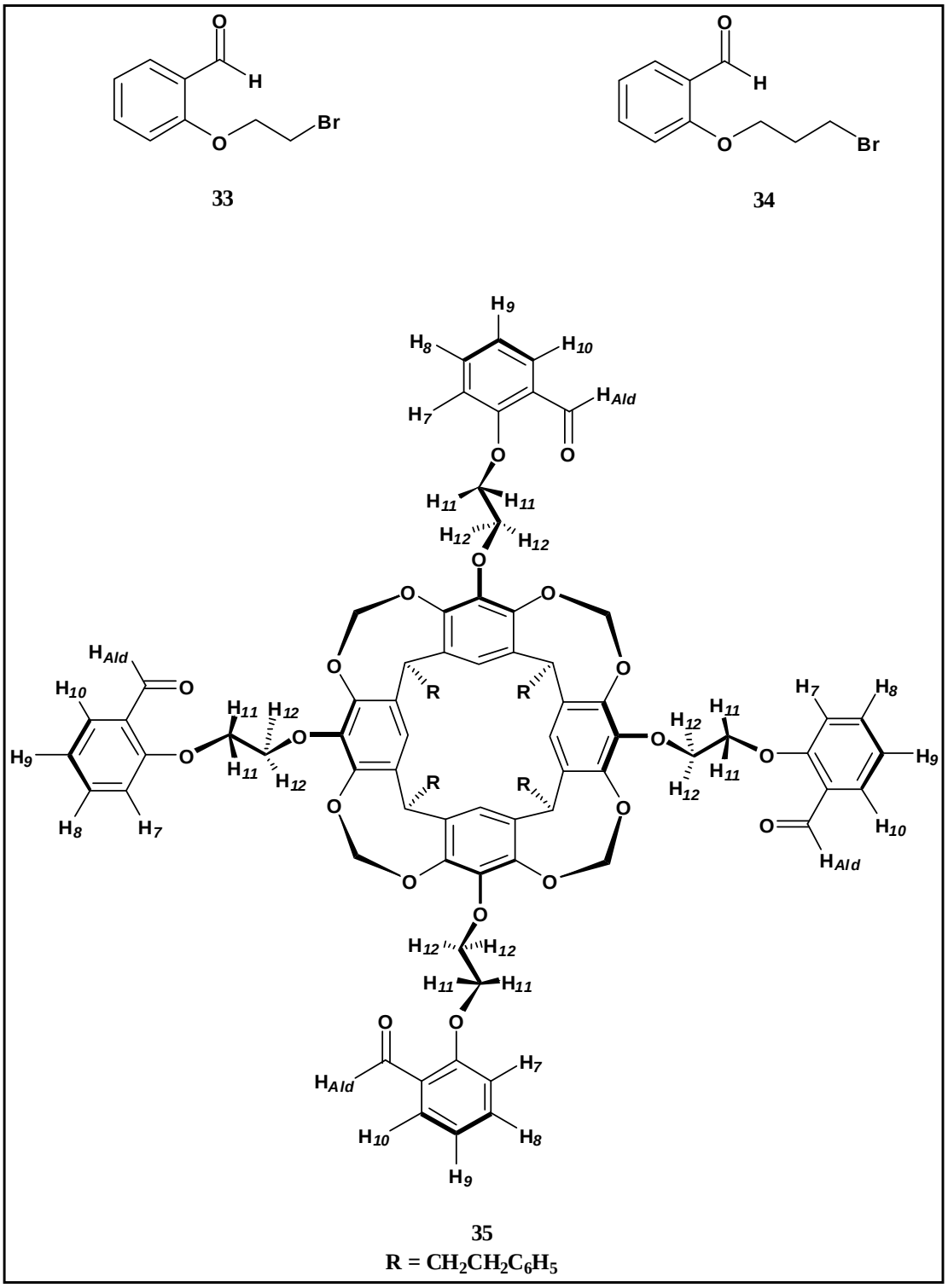

Figure 5.4: Expanded structures of **33**, **34** and **35**, showing distinctive protons.

In the case of **33** and **34**, most prominent in the spectra (Spectrum 1.82 and 1.85, respectively) is the presence of the aldehyde proton, appearing as a singlet at approximately 10.40 ppm integrating to one proton. The downfield nature of this signal is characteristic of aldehyde protons. In the case of **33**, the presence of an *ortho*-substituted aromatic ring can be confirmed by the multiplicity of the aromatic signals, all of which integrate to one proton. Spectrum 1.80 exhibits two doublets (at approximately 7.80 ppm and 6.90 ppm) and two triplets (at approximately 7.50 ppm and 7.10 ppm), indicative of the respective protons coupling with neighbouring protons, as discussed in Chapter 3. The signals at 7.80 and 7.50 ppm additionally show secondary coupling, and appear as a doublet of doublets, and a triplet of doublets, respectively. In the case of **34**, the analogous signals at these chemical shifts maintain this multiplicity and secondary splitting. However, the signals at approximately 7.0 ppm appear unresolved, as a multiplet integrating to two protons.

Compound **33** differs from **34** with respect to the number of methylene groups present in the alkyl chain attached to the salicylaldehyde residue. Thus, the spectrum of **33** exhibits two triplets at 4.40 ppm and 3.69 ppm due to the coupling of the protons of one methylene group with the remaining protons associated with the other methylene group, and *vice versa*. The spectrum of **34** has an added signal associated with it, as a result of the additional methylene group. Appearing along with two triplets at 4.21 ppm and 3.60 ppm, is a multiplet appearing at 2.36 ppm arising from the presence of the centre methylene group in the propyl chain. All of the methylene signals in **33** and **34** integrate to two protons each, as expected. The downfield position of the two triplets in **33** and **34** arise due to the deshielding nature of the neighbouring atoms, with the triplets appearing at 4.40 and 4.21 ppm (for **33** and **34**, respectively), shifted downfield as a result of the close proximity to the ether oxygen atom, while the triplets at approximately 3.60 ppm are due to proton proximity to the bromine atom.

Conversion of **32** to **35** yields a number of additional aromatic signals in the ^{1}H NMR spectrum (Spectrum 1.88), as well as a distinct singlet for aldehyde protons, as shown in Figure 5.4 (H_7 - H_{10}, and H_{Ald} respectively). The aromatic region shows new signals at 6.99, 7.16, 7.52 and 7.78 ppm (all integrating to four protons), corresponding to the four protons present on the salicylaldehyde residues. Signal multiplicity at 7.78 and 7.52 ppm appear as exhibited in both **33** and **34**; a doublet of doublets, and a triplet of doublets, respectively. The COSY spectrum (Spectrum 1.90) of **35** confirms the secondary coupling present as discussed in Chapter 3. The remaining two aromatic signals associated with the salicylaldehydes (at 7.16 and 6.99 ppm), however, appear as multiplets as opposed to a triplet and a doublet (respectively). The presence

of the four signals supports the presence of an *ortho*-substituted aromatic ring, as discussed above for **33** and **34**. The aldehyde proton, H_{Ald}, is seen to be present by the signal at 10.31 ppm, integrating to four protons. The signals due to methylene protons H_{11} and H_{12} appear downfield (4.32 ppm) due to the deshielding nature of the two neighbouring oxygen atoms. The isotropic nature of the two methylene groups results in the respective signals for protons H_{11} and H_{12} coinciding at the same chemical shift. This signal also coincides with that of H_4 (Figure 5.3); thus, this signal integrates to 20 protons. The signals relating to the feet and the cavitand remain unchanged in terms of multiplicity and integration. However, all these protons have experienced very small changes in terms of chemical shift. The ^{1}H NMR signals for **35** are summarised in Table 5.1, with reference to Figure 5.5, which shows the ^{1}H NMR spectrum of **35** from 2.0 to 11.0 ppm.

Table 5.1: ^{1}H NMR data for compound **35** in $CDCl_3$.

	Chemical shift/ppm (multiplicity, coupling constant, integration/protons)
Proton	**35**
H_4, H_{11}, H_{12}	4.33 (*m*, 20)
H_2	4.72 (*t*, *J* = 7.8 Hz, 4)
H_5	5.64 (*d*, *J* = 7.1 Hz, 4)
H_7	6.99 (*m*, 4)
H_8	7.16 (*m*, 4)
H_9	7.52 (*td*, *J* = 7.8, *J* = 1.8 Hz, 4)
H_{10}	7.80 (*dd*, *J* = 7.9 Hz, *J* = 1.7 Hz, 4)
H_{Ald}	10.31 (*s*, 4)
Feet	2.39 - 2.46, 2.59 - 2.63 (each *m*, 8); 7.18 - 7.24 (*m*, 20)

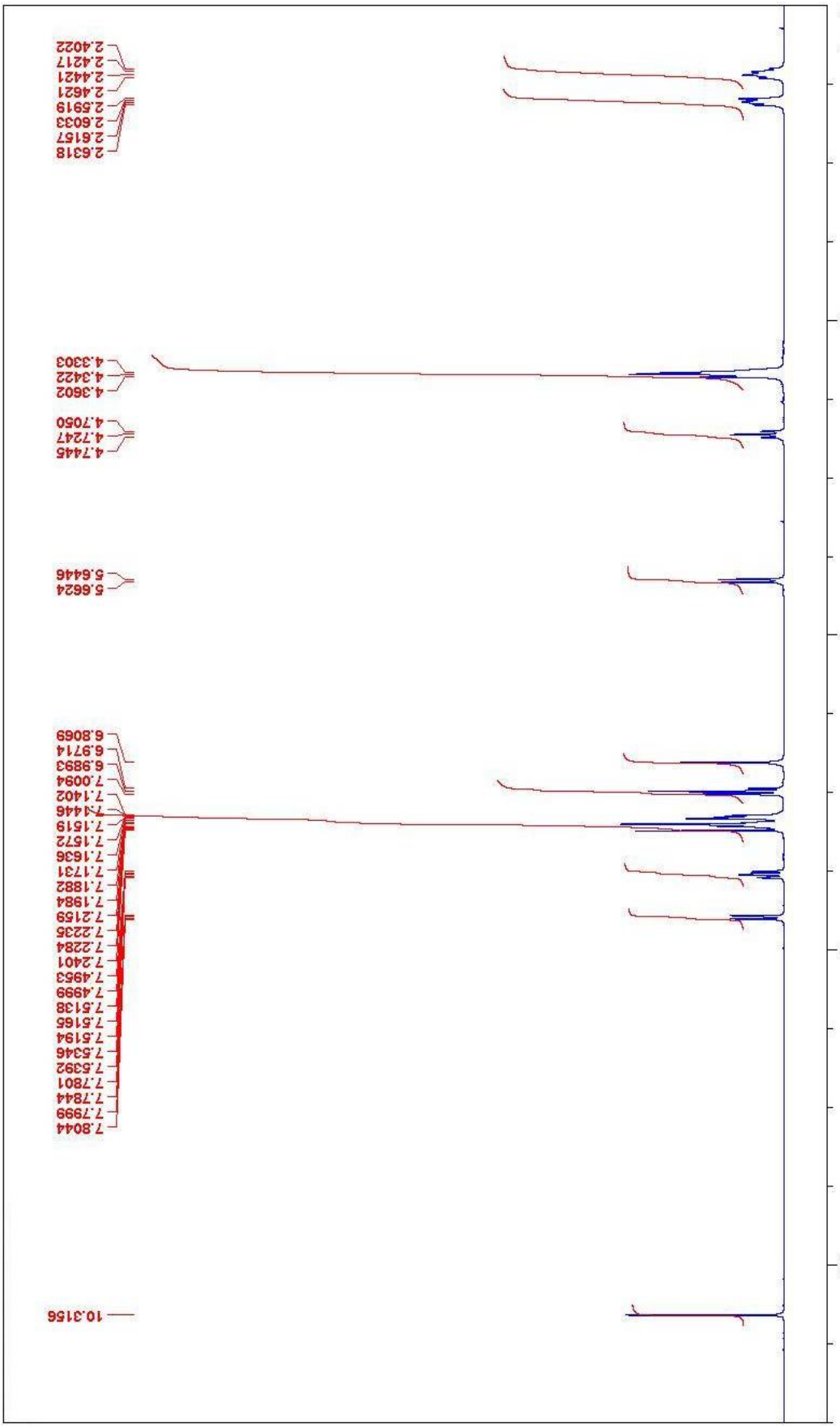

Figure 5.5: ^{1}H NMR spectrum of **35** in $CDCl_3$, from 2.0 to 11.0 ppm.

As seen in Figure 5.6, **36** differs from **35** only by the introduction of an additional methylene group in the alkyl chains linking the cavitand moiety to the salicylaldehyde residues.

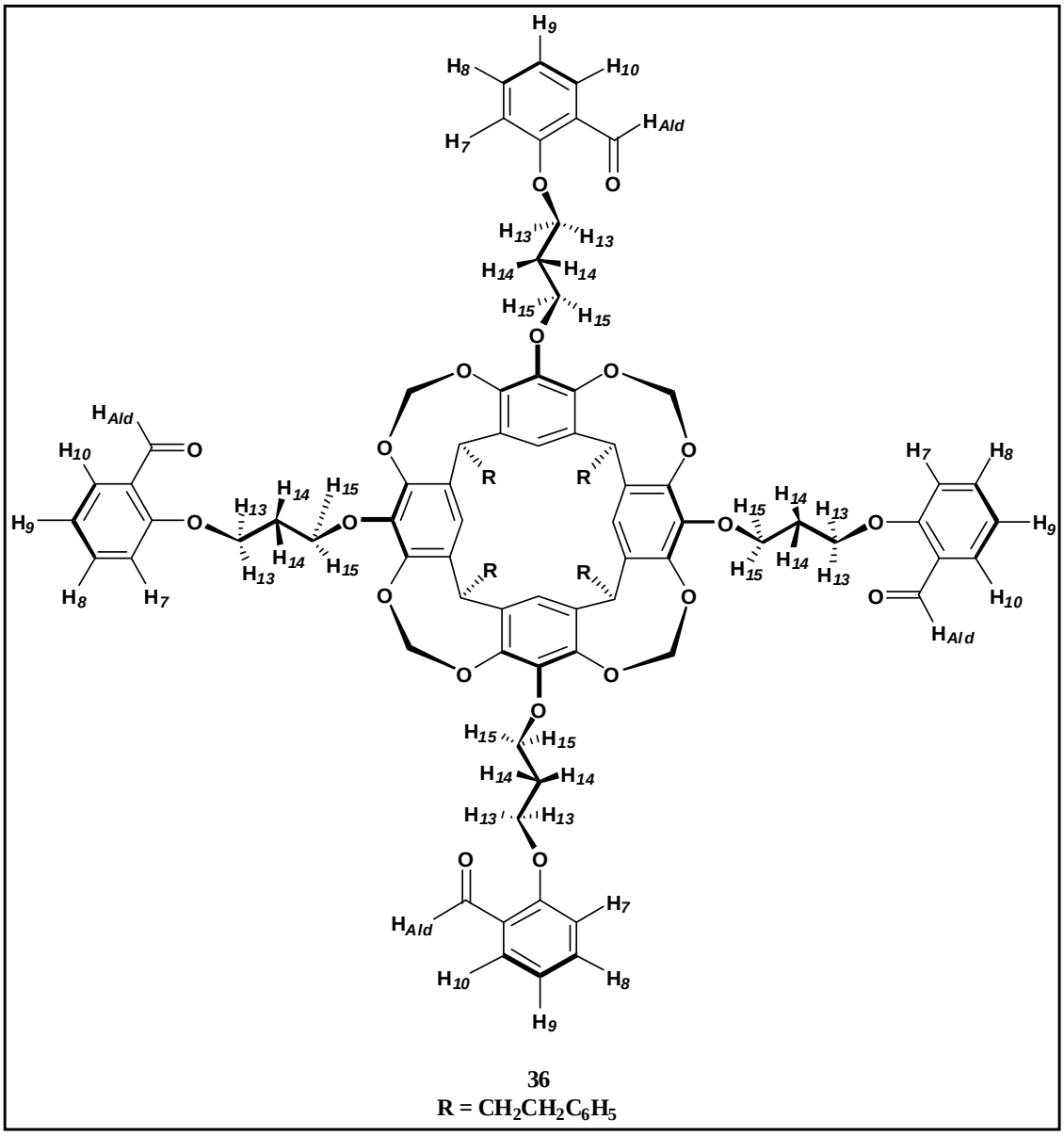

Figure 5.6: Expanded structures of **36**, showing distinctive protons.

As is evident in Spectrum 1.92 and 1.94, **36** exhibits very similar signals in terms of chemical shift and multiplicity in the aromatic region, arising from the presence of protons H_7-H_{10}. Also evident is the signal due to H_{Ald} at 10.48 ppm. All of these signals integrate to four protons. Signals relating to protons present in the feet and the cavitand moiety again remain largely unchanged in terms of multiplicity and integration, while experiencing slight changes in chemical shifts. However, the presence of the extra methylene group, as noted, has led to some resolution of the signals at approximately 4.30 ppm, as well as an additional multiplet at 2.14

ppm. The signal due to H_4 (Figure 5.3) has resolved into a doublet integrating to four protons appearing at 4.33 ppm, and the signals due to H_{13} and H_{15} appear as two triplets at 4.13 and 4.25 ppm integrating to eight protons each. The signal multiplicity, in this case, is a result of the respective coupling of H_{13} and H_{15} with H_{14}. The multiplet at 2.14 ppm arises due to the coupling of H_{14} with H_{13} and H_{15}, and integrates to eight protons. Table 5.2 summarises the ^{1}H NMR signals of **36**, while Figure 5.7 shows the spectrum of **36** from 2.0 to 11.0 ppm.

Table 5.2: ^{1}H NMR data for compound **36** in $CDCl_3$.

	Chemical shift/ppm (multiplicity, coupling constant, integration/protons)
Proton	**36**
H_{14}	2.15 (*m*, *J* = 6.0 Hz, 8)
H_{13}, H_{15}	4.14, 4.25 (each *t*, *J* = 5.9 Hz, 8)
H_4	4.33 (*d*, *J* = 7.1 Hz, 4)
H_2	4.74 (*t*, *J* = 7.9 Hz, 4)
H_5	5.63 (*d*, *J* = 7.1 Hz, 4)
H_{10}	6.98 (*m*, 4)
H_9	7.13 (*m*, 4)
H_8	7.50 (*td*, *J* = 7.8 Hz, *J* = 1.8 Hz, 4)
H_7	7.81 (*dd*, *J* = 7.9 Hz, *J* = 1.9 Hz, 4)
H_{Ald}	10.48 (*s*, 4)
Feet	2.41 - 2.45, 2.60 - 2.64 (each *m*, 8); 7.18 - 7.24 (*m*, 20)

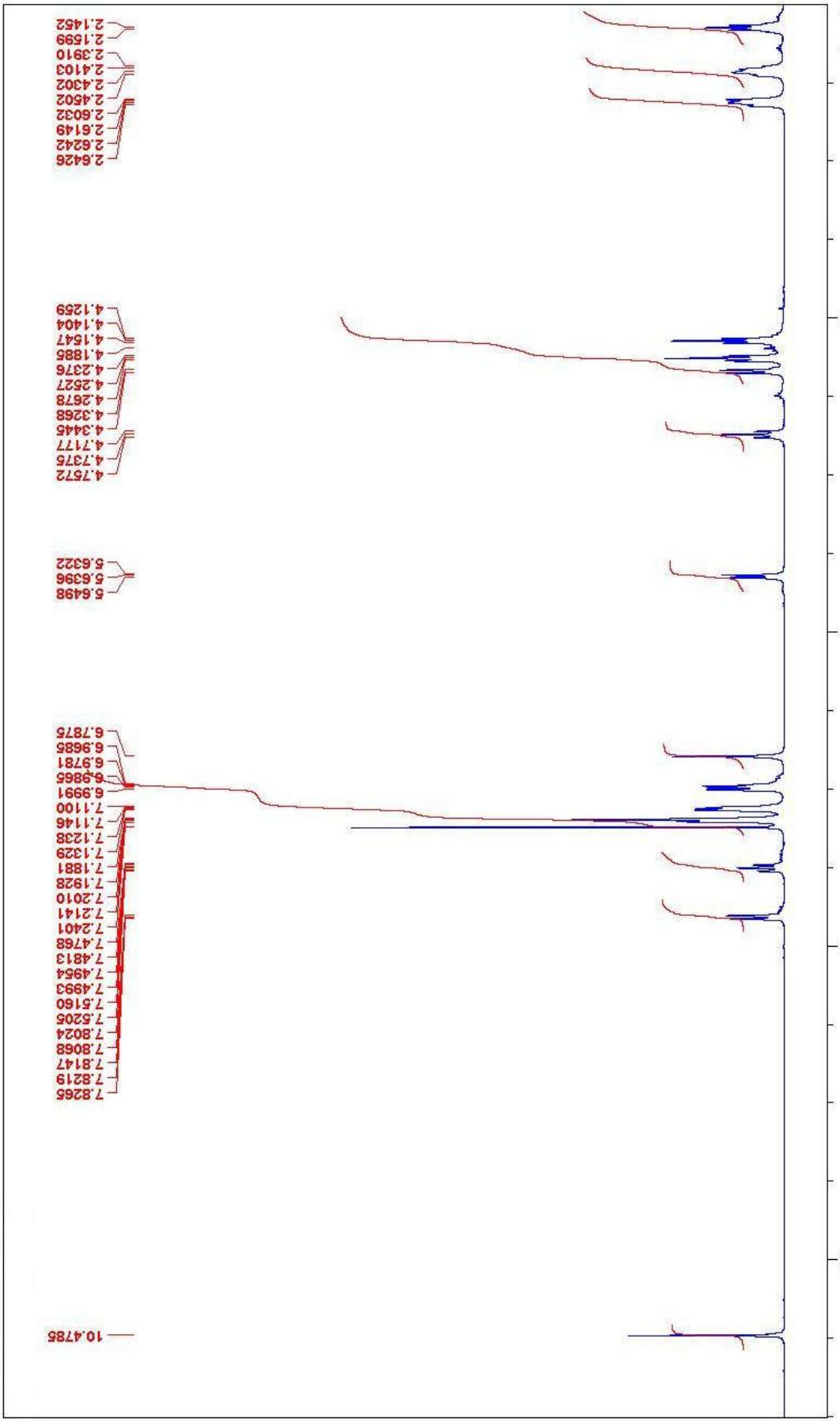

Figure 5.7: ^{1}H NMR spectrum of **36** in $CDCl_3$, from 2.0 to 11.0 ppm.

5.1.2 In situ Cyclisation and Ligand Synthesis

The *in situ* cyclisation towards the synthesis of **37** and **38** commenced with the use of the Adler conditions. The decision to use these conditions was based primarily on the observations by Reinhoudt *et al*. as discussed in Chapter 3.

Synthesis initially adopted the conditions set out by Reinhoudt *et al*. (as per Chapter 3) towards the synthesis of **37**, whereby aldehyde precursor **36** was added to refluxing propionic acid in high dilution (approximately 0.1 mM, based on **36**). Once dissolved, freshly distilled pyrrole was added and the reflux continued overnight. At this time, a small aliquot was removed and subjected to TLC using a benzene mobile phase. However, no porphyrin material was observed.

A review of the literature regarding mechanistic aspects of the Adler conditions [9] revealed that, in general, porphyrin formation reached a maximum after 8 - 10 hours of reflux. Moreover, the general procedure of porphyrin synthesis following the Adler conditions [9b, 10] involved a reflux ranging from 25 - 30 minutes to 5 hours, at which time the solution was allowed to stir at room temperature overnight. As such, the reaction was repeated using **36** and freshly distilled pyrrole. After a 30 minute reflux, the mixture was left to cool at room temperature, and after 5 hours of reaction time, an aliquot was sampled and subjected to TLC using benzene as the eluant. A purple porphyrinic material was observed at an R_f of approximately 0.5, in addition to a bright blue compound at an R_f of approximately 0.4. The latter compound was identified as the chlorin product; a compound analogous in structure to a porphyrin, but without complete structural conjugation *via* the absence of a double bond between a pair of β-pyrrole carbon atoms. Since the chlorin oxidises to the porphyrin in air, the reaction was left to stir at room temperature overnight, at which time the TLC was repeated. Only a porphyrin product was observed as a purple compound at an R_f of approximately 0.6; the chlorin was now absent from the reaction mixture. The presence of the porphyrin product was further confirmed by preliminary analysis using UV-Vis spectroscopy, which exhibited the distinctive Soret band at 419 nm indicative of porphyrinic compounds.

Isolation of **37** was achieved with relative ease using silica gel chromatography, where elution with benzene was able to free the target ligand readily from the polymeric matrix arising from the cyclisation reaction. However, in order to obtain **37** as analytically pure, residual polymeric

material was removed by further column chromatography. Thereafter, the purple material was recrystallised by liquid diffusion of methanol into a solution of **37** in chloroform, to yield the ligand as a dark purple, microcrystalline material. This material was characterised by NMR spectroscopy, with reference to Figure 5.8, which shows the repeat unit of **37** indicating the associated distinctive protons. Figure 5.9 shows the ^{1}H NMR spectrum of **37** from 2.0 to 9.0 ppm for discussion purposes; the full spectrum can be seen in Appendix 1, Spectrum 1.96.

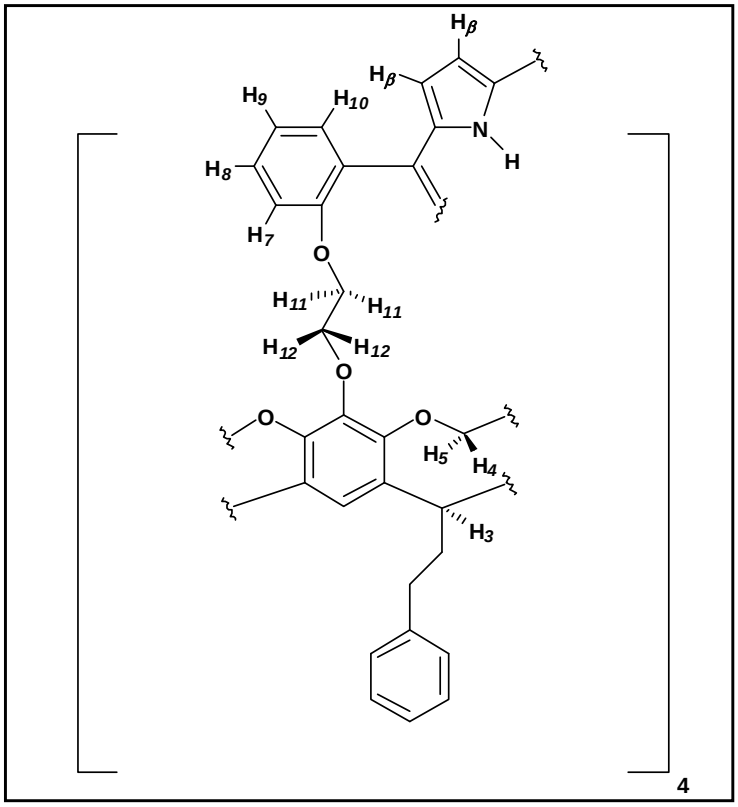

Figure 5.8: Repeat unit of **37**, showing distinctive protons.

As evident in Figure 5.9, the ^{1}H NMR spectrum of **37** exhibits signals characteristic of both a porphyrin and a cavitand. With regards to the porphyrin, the most distinctive signal appears upfield at -2.90 ppm (not shown in Figure 5.9), integrating to two protons due to the presence of the two amine protons of the porphyrin free base. The position of these signals is due to the large ring current of the porphyrin, which was discussed in Chapter 3. The presence of the β-pyrrole protons (H_{β}, Figure 5.8) can be seen by the appearance of the two singlets at 8.80 and 8.70 ppm, collectively integrating to eight protons. The signals appear in a ratio of 1:2, reminiscent of the nature of the β-pyrrole proton signals of porphyrin **12**.

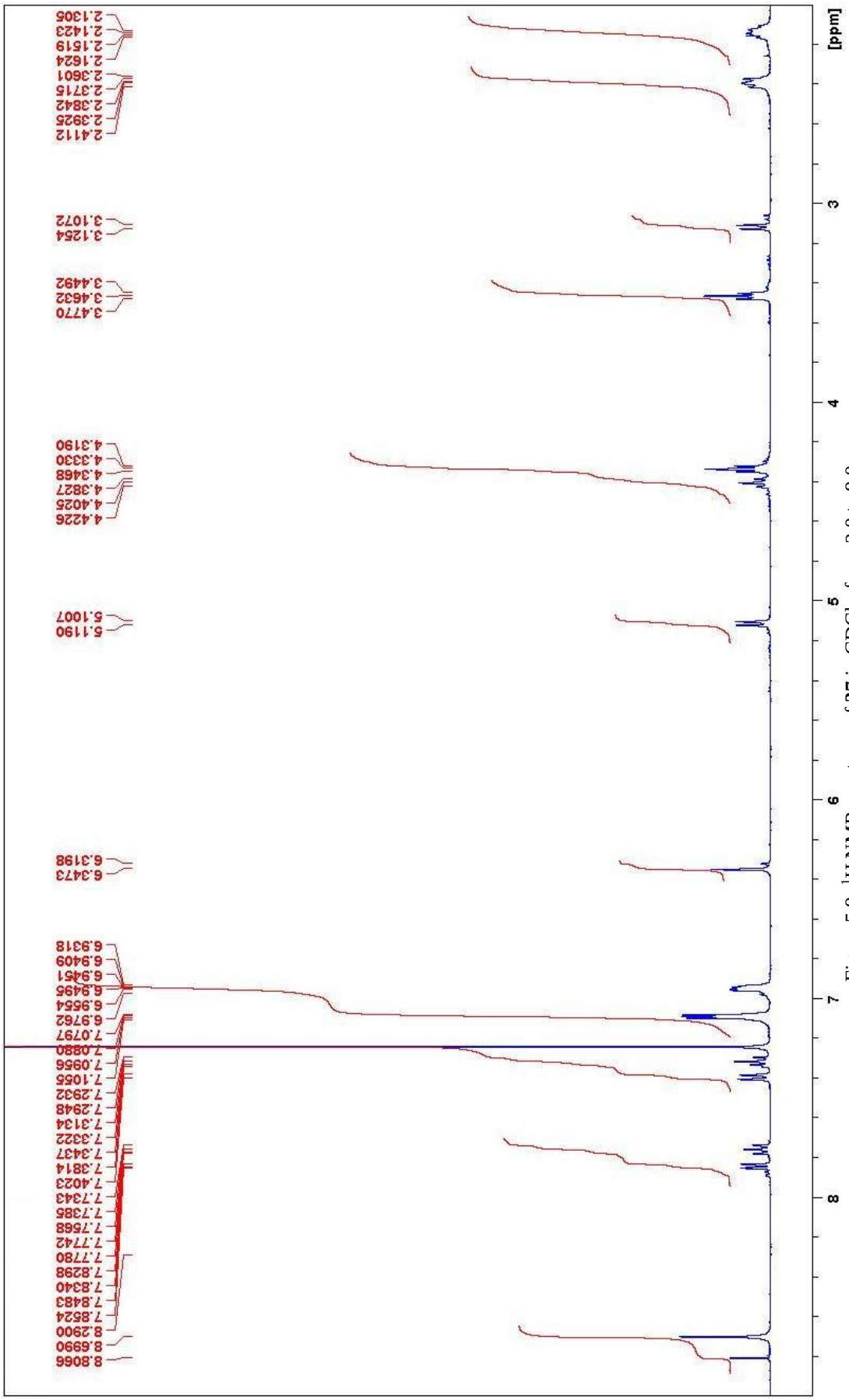

Figure 5.9: ^{1}H NMR spectrum of **37** in $CDCl_3$, from 2.0 to 9.0 ppm.

Signals related to the *meso*-phenyl rings (H_7 - H_{10}) appear as a series of multiplets at 7.84, 7.75, 7.40 and 7.31 ppm, all integrating to four protons. The multiplicity observed is similar to that seen in the **35** and **36**; the multiplets at 7.84 and 7.75 appearing as a doublet of doublets, and a triplet of doublets, respectively. The presence of the ring current has seen these signals experience a slight downfield shift, relative to the analogous signals in precursor **35**.

The signals from H_{11} and H_{12} appear as a pair of triplets integrating to eight protons each. The chemical shifts and multiplicity of these protons, however, have changed markedly in comparison to aldehyde precursor **35**, as a result of the presence of the porphyrin ring current. While the signals from these protons appear concurrently at 4.33 ppm in the case of **35**, the ring current in the case of **37** results in the protons becoming anisotropic in nature. As such, the signal from H_{11} appears as a triplet at 3.48 ppm, while the signal from H_{12} appears as a triplet at 4.35 ppm. Since H_{11} is located alongside an ether oxygen atom, which electronically couples to the porphyrin macrocycle by virtue of its electron lone pairs, the related proton signal appears further upfield than for H_{12}. Indeed, H_{12} resonates at essentially an identical chemical shift compared with the analogous signal present in **35**.

The signals related to H_4 and H_5 have also undergone changes in terms of chemical shift. While both still appear as doublets integrating to four protons, H_5 has shifted to 5.10 ppm, while H_4 now appears at 3.13 ppm. This represents an upfield shift of approximately 0.5 ppm and 1 ppm, respectively, relative to cavitand precursor **35**. The marked shift is due to the capsule-like nature of the ligand, which, particularly in the case of H_4 which lies within the ligand cavity, has a shielding effect on both protons. The signal due to H_2 appears as a triplet, integrating to four protons, at 4.40 ppm, which represents a small upfield movement in chemical shift compared with the cavitand precursor discussed above. Additionally, the remaining protons related to the 2-phenylethyl feet, as well as the single cavitand aromatic proton, maintain the respective signal multiplicity and chemical shift seen in **35**. Table 5.3 summarises the ^{1}H NMR signals of **37**, which includes the signals of analogous protons for precursor **35** for comparative purposes.

Subsequent COSY and HSQC NMR (Spectra 1.98 and 1.99, Appendix 1) analysis of **37** confirmed the presence of the target ligand, showing the expected contact of H_4 with H_5, H_{11} with H_{12}, and the various contacts seen between the *meso*-aromatic protons H_7 - H_{10}. With regards to these latter protons, the COSY spectrum again illustrates the long range coupling present between the various protons. There were additionally no contacts observed for the two amine protons, and the β-pyrrole protons.

Table 5.3: ^{1}H NMR data for compound **37**, compared with precursor **35**, in $CDCl_3$.

	Chemical shift/ppm (multiplicity, integration/protons)	
Proton	**35**	**37**
H_2	4.72 (*t*, 4)	4.40 (*t*, 4)
H_4	4.33 (*m*, 20)‡	3.13 (*d*, 4)
H_5	5.64 (*d*, 4)	5.10 4(*d*, 4)
H_7	7.80 (*dd*, 4)	7.84 (*dd*, 4)
H_8	7.52 (*td*, 4)	7.75 (*td*, 4)
H_9	7.16 (*m*, 4)	7.40 (*m*, 4)
H_{10}	6.99 (*m*, 4)	7.31 (*m*, 4)
H_β	-	8.80, 8.70 (*s*, 8)
H_{11}	4.33 (*m*, 20)‡	3.48 (*t*, 8)
H_{12}	4.33 (*m*, 20)‡	4.35 (*t*, 8)
Feet	2.39 - 2.46, 2.59 - 2.63 (each *m*, 8); 7.18 - 7.24 (*m*, 20)	2.10 - 2.16, 2.36 - 2.41 (each *m*, 8); 6.93 - 7.11 (*m*, 20)

‡ The signal for these protons in the case of **35** appears concurrently as a multiplet with other protons, collectively integrating to twenty protons.

Importantly, the ^{1}H NMR spectrum of **37** exhibits sharp signals, indicating that **37** does not exist as a mixture of rotamers,[11] but assumes only one conformation. The COSY spectrum serves further to confirm this. Indeed, the spectra suggest that **37** is symmetrical in nature (presumably C_4), which is in keeping with the structural characteristics of the minimised structure of this ligand investigated in Chapter 4.[12] Mass spectrometry (MS) (using ESI-TOF methods) additionally gave a molecular ion *M/z* signal of 1800.5112, which matches the expected mass

for **37** of 1800.6771. This served as confirmation of the successful synthesis and isolation of the target ligand.

In order to further confirm the Adler conditions as the exclusive synthetic conditions by which to obtain **37** (as observed by Reinhoudt *et al*.), the Lindsey conditions were implemented as a means of performing the *in situ* cyclisation. Preliminary UV-Vis analysis of the reaction indicated the absence of the Soret band at approximately 420 nm, and as such the conditions were deemed unable to afford **37**.

*5.1.3 In situ Synthesis of **37** Using Microwave Techniques*

The use of classical Adler reflux conditions for the *in situ* cyclisation gave **37** in a yield of 11 %. In order to improve on this yield, a microwave heating source for the cyclisation reaction was investigated; a method which has become increasingly popular as a means by which to synthesise *meso*-tetraphenylporphyrin derivatives and corresponding metalloporphyrins.[13] Since the production of a porphyrin from pyrrole and an aromatic aldehyde is determined largely by kinetic factors,[9, 10] the use of microwave irradiation as a heating source was proposed as a means by which to increase the kinetic energy of the reactants. Microwave energy has been shown to increase reaction rates of organic reactions by rapidly heating at a molecular level, which is unlike conventional heating methods.[14] Thus, the yield of porphyrin stood to be improved by increasing the rate of condensation of pyrrole molecules with aldehyde molecules. Certainly, microwave synthesis is hitherto unreported as a means by which to synthesise cavitand-capped porphyrin ligands.

Microwave synthesis commenced by dissolving up 75 mg of **35** in 2 mL of acid, and microwaving in a closed tube at 160 $^{\circ}$C. This temperature was chosen primarily since it is in excess of the boiling point of propionic acid (141 $^{\circ}$C), which ensured that the reaction conditions were (at least) similar to those in the classical reflux conditions. After maintaining the reaction vessel at 160 $^{\circ}$C for 20 minutes, it was allowed to cool to room temperature, at which time the tube was opened and the reaction mixture stirred overnight in air. Investigation of the mixture by TLC the next day, using benzene as mobile phase, confirmed the presence of porphyrin. After chromatographic isolation and purification of the reaction material using identical conditions as discussed above for the classical Adler reaction, the microwave reaction yielded **37** in a 23 % yield.

The reported microwave synthesis of porphyrins showed that yields were maximised when reaction times were in the order of three to five minutes.[13a, f] As such, the reaction was repeated on the same scale using the same volume of propionic acid and temperature as per the first reaction, changing reaction time to five minutes. After purification, the yield of **37** increased to 27 %, which is approaching the yield of simple (uncapped) porphyrins synthesised by the Adler, and indeed, the Lindsey conditions.

In order to optimise synthetic conditions for the microwave synthesis of cavitand-capped porphyrins, a number of further reactions were attempted on an identical scale (75 mg), varying reaction temperature, volume of propionic acid used, and reaction time. Table 5.4 summarises the varied conditions and the resultant yield of **37** after purification.

Table 5.4: Summary of variable conditions and yields of **37**, synthesised *via* microwave techniques.

Volume acid/mL	**Temperature/°C**	**Time/minutes**	**Yield/%**
2	160	20	23
2	160	5	27
2	160	3	21
4	160	5	24
2	145	5	12
4	145	5	10
2	120	5	-
4	120	5	-

As is evident in Table 5.4, the reactions performed at 160 °C all produced **37** in yields above 20 %. Additionally, the reactions that proceeded for five minutes gave the best yields, while those at slightly shorter, or longer reaction times giving somewhat diminished yields. The volume of

propionic acid, and therefore the concentration of reagents in cyclisation appears not to significantly influence yields. The yields regarding reactions performed at temperatures approximately at the boiling point of propionic acid (145 °C) are essentially half of those performed at 160 °C. These reactions gave yields comparable to those seen for the refluxed reactions which initially afforded **37**. Again, the concentration of reagents has not seen any significant differences in terms of yield. Finally, the reactions performed at temperatures below boiling point (120 °C) gave no product.

It can therefore be concluded that microwave reactions performed at 160 °C for five minutes give the best conditions for the formation of cavitand-capped porphyrin **37**. These conditions compare favourably with the synthetic optimisation reported elsewhere in the literature for the microwave synthesis of porphyrins. Indeed, Cavaleiro *et al.*[13f] found yields to be optimal in the synthesis of tetraphenylporphyrin using similar reaction times and temperatures.

5.2 In situ Synthesis of 38

In light of the results obtained for synthesis of **37** from **35**, an identical reaction protocol was adopted for the synthesis of **38** from precursor **36**.

As such, synthesis of **38** commenced *via* the use of the classical Adler conditions, whereby **36** was dissolved in refluxing propionic acid, freshly distilled pyrrole added to the reaction and reflux continued for 30 minutes. Once the solution was cooled to room temperature and allowed to stir overnight in air, TLC was used to track the reaction as in the case of **37**. Reaction again yielded a porphyrinic material, which was further confirmed by the presence of the Soret band in preliminary UV-Vis analysis.

However, attempts to isolate and purify **38** from the reaction matrix using silica gel chromatography was more difficult than in the case of **37**. It was found that benzene was able to free the purple product from the polymeric matrix of reaction, but thereafter the material became immobile on the column. The product was found to be immobile on the silica gel and could not be eluted with benzene. Further elution with chloroform was unable to displace the purple material from the silica gel. However, upon changing the mobile phase to 50 % ethyl acetate in chloroform, the product eluted from the silica gel. Despite co-elution of some polymeric material with the product, the majority of the polymeric material from reaction was removed. A secondary column was attempted, using a benzene mobile phase, but the product

again struggled to elute from the column. Although various changes to the mobile phase were made, including the use of ethyl acetate and dichloromethane, **38** could not be obtained in a purified form free of polymeric material, *via* chromatography. Additionally, recrystallisation was also ineffective in affording pure **38**.

*5.2.1 In situ Synthesis of **38** Using Microwave Techniques*

Results from the computational study offered a possible explanation as to why the chromatographic behaviour of **38** was so different to that of **37**. As mentioned, the four-atom bridge of **37** results in a highly symmetrical molecule. However, the additional atom in the bridges of **38** breaks this symmetry, and results in more conformational flexibility.[12, 15] The differences in symmetry is illustrated in Figure 5.10, showing the minimised structures of **37** (left) and **38** (right), and offers a possible explanation as to why the interaction of **37** with silica gel is significantly different than in the case of **38**.

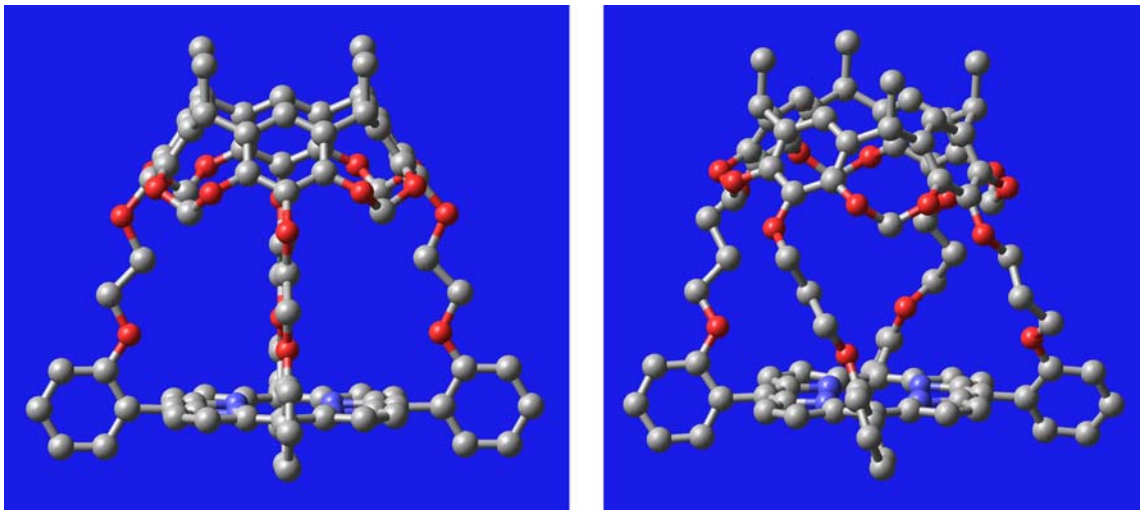

Figure 5.10: The minimised structures of the target ligands; **37** (left), and **38** (right). Hydrogen atoms are omitted for clarity.

With this in mind, microwave synthesis offered a potential means by which to obtain **38**. Microwave techniques have been shown to help overcome inter- and intramolecular aggregation as well as steric hindrance.[16] Thus, the issues posed by the additional conformational flexibility of **38** in synthesis may be overcome. As such, the microwave protocol used in the synthesis of **37** was adopted for the synthesis of **38**.

The presence of **38** as product from microwave reaction was confirmed by UV-Vis analysis. Column chromatography was again employed as a means by which to purify the reaction material. A preliminary column using a mobile phase 95:5 chloroform:ethyl acetate was able to free the reaction product from the majority of the polymeric material which arose from reaction. Subsequently, a column using a benzene eluant was effective in isolating **38** from the residual polymeric material, this time without the purple product becoming immobilized on the silica gel. Analytically pure material was obtained by successive liquid diffusion recrystallisations (as per **37**) to yield **38** as a purple, microcrystalline material. This material was again characterised by NMR spectroscopy. Figure 5.11 shows the repeat unit of **38** indicating distinctive protons, whilst Figure 5.12 shows the ^{1}H NMR spectrum of **38** from 2.0 to 9.0 ppm, for discussion purposes. The complete spectrum can be seen in Appendix 1, Spectrum 1.103.

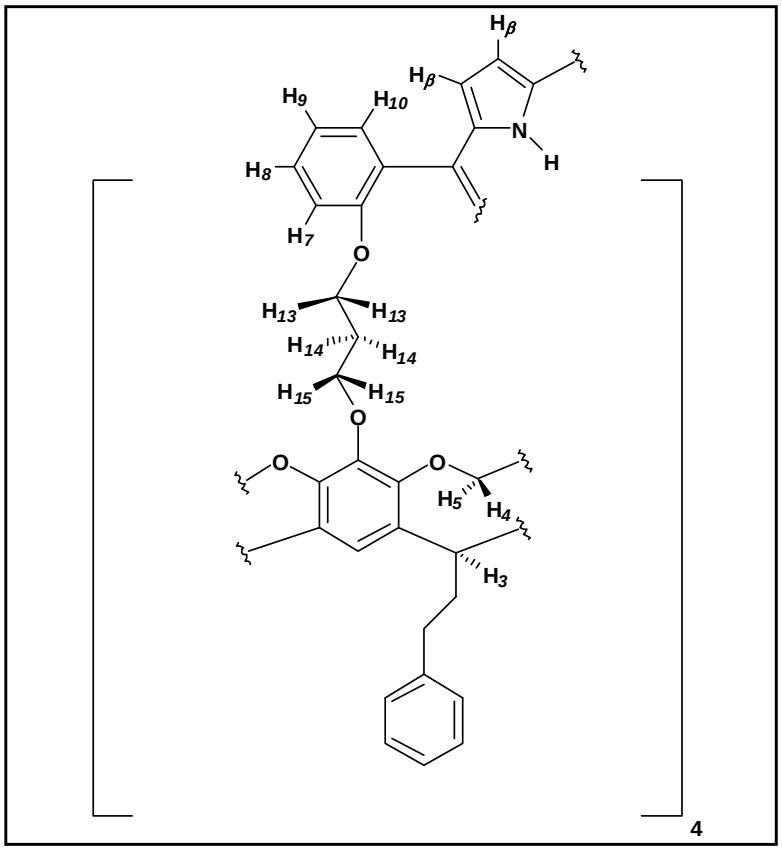

Figure 5.11: Repeat unit of **38**, showing distinctive protons.

Figure 5.12 exhibits a ^{1}H NMR spectrum which is a combination spectrum of cavitand and porphyrin, as in the case of **37**. Although not shown in Figure 5.12, the distinctive signals from the two amine protons associated with the porphyrin structure are again present upfield, at -2.82 ppm, integrating to two protons. This is indicative of the successful *in situ* formation of **38**. Additionally indicating the presence of a porphyrin is the signal at 8.72 ppm (integrating to

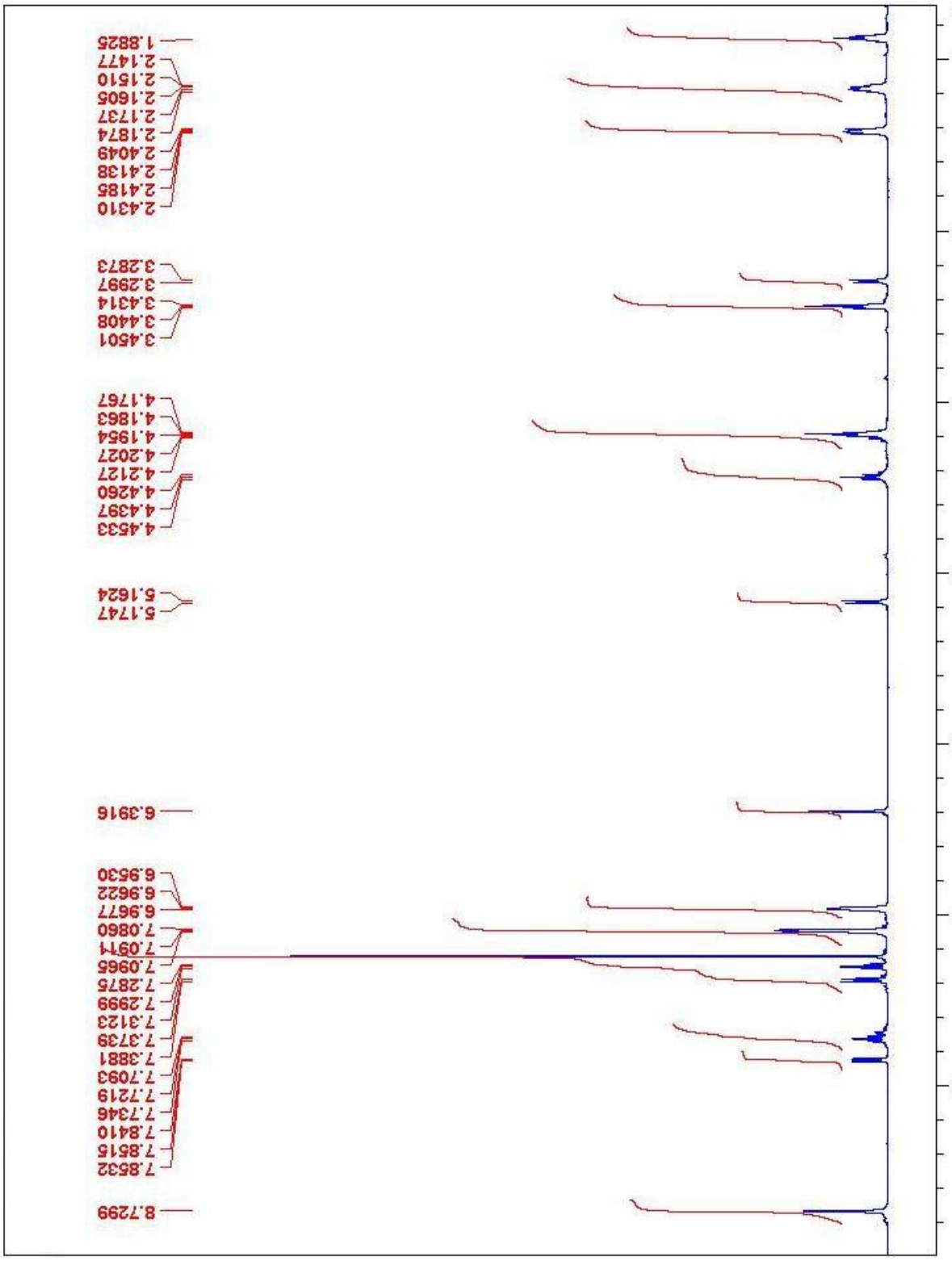

Figure 5.12 ^{1}H NMR spectrum of **38** in $CDCl_3$, from 2.0 to 9.0 ppm.

eight protons) associated with the β-pyrrole protons, H_β (Figure 5.11). The signal resonates as a singlet, which is in contrast to the equivalent signal in the case of **37**.

Signals arising from protons H_7 - H_{10} again appear as a series of multiplets, at 7.85, 7.72, 7.38 and 7.30 ppm, all of which integrate to four protons. These signals exhibit the same multiplicity as observed and discussed in the case of **35**, **36**, and indeed, **37** previously. Relative to precursor **36**, the signals due to protons H_7 - H_{10} have again experienced a shift downfield.

As the distinctive difference between **37** and **38**, the additional methylene group present in the bridges of **38** accounts for an additional signal in the ^{1}H NMR spectrum in comparison to the spectrum of **37**. As such, a multiplet due to the presence of H_{14} is observed in the alkyl region at 1.87 ppm, integrating to eight protons. In terms of precursor **36**, this represents a slight upfield shift relative to the analogous protons. The signals from H_{13} and H_{15} appear as a pair of triplets integrating to eight protons each. The signal arising from H_{13} again appears further upfield (relative to H_{15}) due to proximity of this methylene group to the ether oxygen atom, which is electronically coupled to the porphyrin macrocycle. The associated chemical shift for H_{13} of 3.44 ppm is very similar to the chemical shift of H_{11}, the analogous protons in ligand **37**. The signal due to H_{15} yields a similar situation, giving a chemical shift (4.19 ppm) very similar to that of H_{12} present in **37**.

The signals due to H_4 and H_5 have undergone dramatic upfield shifts as observed in the case of **37**. In the case of **38**, the signal due to H_5 appears at 5.16 ppm, while H_4 appears at 3.29 ppm. Both signals maintain their multiplicity, appearing in each case as doublets integrating to four protons. Interestingly, the noted upfield shift is less dramatic in **38** than in **37**. This is likely due to the presence of the extra methylene group built into the ligand bridges, which yields a larger capsule-like ligand in comparison to **37**. As such, the degree of shielding that the capsule affords to these protons is diminished, thus resulting in a less dramatic upfield shift.

The signal due to H_2 appears at 4.44 ppm as a triplet, integrating to four protons. The remaining signals relating to the 2-phenylethyl feet, as well as the single cavitand aromatic proton, maintain the respective signal multiplicity and chemical shift seen in **36**. Table 5.4 summarises the ^{1}H NMR signals of **38**, which includes the signals of analogous protons for precursor **36** and ligand **37** for comparative purposes.

Table 5.3: ^{1}H NMR data for compound **38**, compared with precursor **36** and ligand **37**, in $CDCl_3$.

	Chemical shift/ppm (multiplicity, integration/protons)		
Proton	**36**	**37**	**38**
H_2	4.74 (*t*, 4)	4.40 (*t*, 4)	4.44 (*t*, 4)
H_4	4.33 (*d*, 4)	3.13 (*d*, 4)	3.29 (*d*, 4)
H_5	5.63 (*d*, 4)	5.10 (*d*, 4)	5.16 (*d*, 4)
H_7	7.81 (*dd*, 4)	7.84 (*dd*, 4)	7.85 (*dd*, 4)
H_8	7.50 (*td*, 4)	7.75 (*td*, 4)	7.72 (*td*, 4)
H_9	7.13 (*m*, 4)	7.40 (*m*, 4)	7.39 (*d*, 4)
H_{10}	6.98 (*m*, 4)	7.31 (*m*, 4)	7.30 (*t*, 4)
H_β	-	8.80, 8.70 (*s*, 8)	8.73 (*s*, 8)
H_{11} (H_{13})‡	(4.14 (*t*, 8))‡	3.48 (*t*, 8)	(3.44 (*t*, 8))‡
H_{12} (H_{15})‡	(4.25 (*t*, 8))‡	4.35 (*t*, 8)	(4.19 (*t*, 8))‡
H_{14}	-	-	1.87 (*m*, 8)
Feet	2.41 - 2.45, 2.60 - 2.64 (each *m*, 8); 7.18 - 7.24 (*m*, 20)	2.10 - 2.16, 2.36 - 2.41 (each *m*, 8); 6.93 - 7.11 (*m*, 20)	2.14 - 2.19, 2.40 - 2.43 (each *m*, 8); 6.95 - 7.09 (*m*, 20)

‡ The protons appearing in parenthesis are only present in **36** and **38**, while the protons appearing outside are related to **37** exclusively. Comparison is made due to the analogous nature of the related chemical shifts.

COSY and HSQC NMR (Spectra 1.105 and 1.106) analysis of **38** served to further confirm the successful synthesis and isolation of the target ligand, showing the expected contacts as discussed above regarding **37**. MS analysis further served to confirm the synthesis of 38, yielding a *M/z* signal of 1856.5912, in close agreement with the calculated mass of 1856.7397.

The use of microwave heating thus not only provided improved yields (as in the case of **37**), but additionally aided in simplifying the isolation of **38**. The results also highlight the significance of the bridge length and its effect on ligand symmetry. As shown in Chapter 4, bridges comprising an even number of atoms resulted in ligands of lower potential energy and increased symmetry; those comprising an odd number of atoms conversely gave ligands having higher potential energy and decreased symmetry. The above synthetic observations indicate that this 'odd-even' effect extends to the synthesis and physical behaviour of these ligands.[17]

Again to confirm the Adler conditions as the exclusive synthetic conditions by which to obtain **38**, the Lindsey conditions were investigated as the synthetic protocol for the *in situ* cyclisation. As in the case of **37**, preliminary UV-Vis analysis of the reaction product showed that the Soret band at approximately 420 nm was absent, indicating that the protocol was unable to afford **37**.

5.3 Identification of Minimum Bridge Length for Successful Capped-porphyrin Synthesis

The results from Chapter 3 indicated that a minimum bridge length exists which affords a successful synthesis of cavitand-capped porphyrins. Given the successful synthesis of ligands bearing four- and five-atom bridges, as well as the results from Chapter 3, it is of interest to identify the minimum bridge length required for a successful capping. Since a two-atom bridge was shown to be too short for a successful synthesis using the *in situ* synthetic protocol, while bridges four atoms in length were capable of affording a cavitand-capped porphyrin, a bridge consisting of three atoms was investigated in order to see if capping could be completed.

Cavitand **32** was used as the precursor towards the synthesis of the corresponding aldehyde as shown in Scheme 5.3. Aldehyde reagent **39** was synthesised as *per* the method used in the formation of **33** and **34**; by coupling salicylaldehyde to bromochloromethane in the presence of K_2CO_3. Coupling of **39** to **32** thus ensured that the required three-atom (OCH_2O) bridges would be incorporated into **40**, which served as the precursor to *in situ* cyclisation.

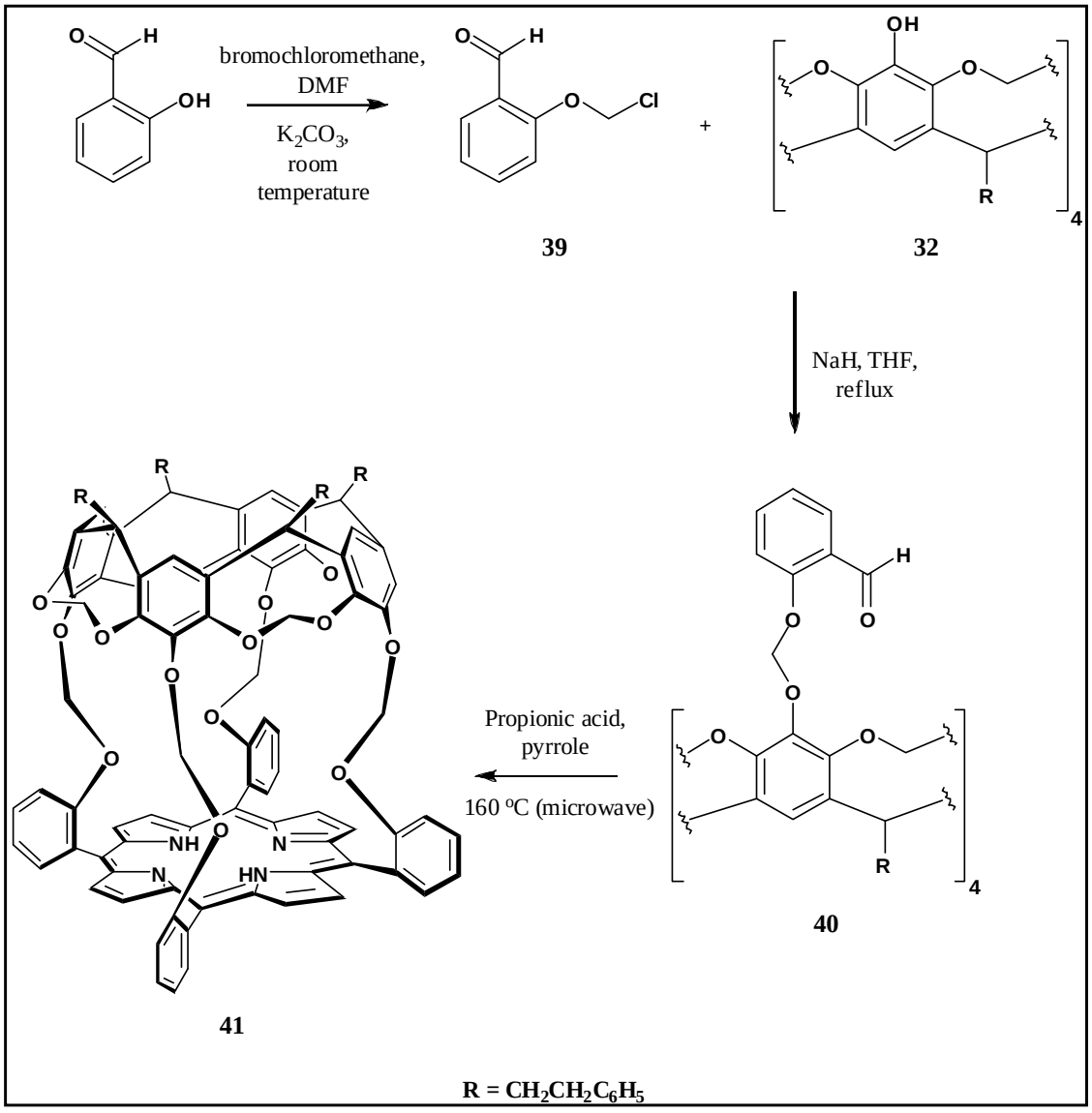

Scheme 5.3: Synthesis towards a cavitand-capped porphyrin bearing bridges three atoms in length.

The synthesis of **39** was achieved in a 67 % yield. Coupling of **39** with **32** proved to proceed differently than in the case of analogues **35** and **36**. Attempts to follow the related synthetic conditions, whereby **32** (in DMF) was coupled to the aldehyde reagent in the presence of K_2CO_3, were unsuccessful in yielding aldehyde **40**, whether reaction was performed at room temperature or at 55 °C. As such, reaction conditions were altered in favour of those conditions which successfully yielded aldehydes **6** and **27** (Chapter 3); **32** was dissolved in dry THF and treated with NaH before addition of **39** and reflux. Under these conditions, **40** was successfully obtained, albeit in diminished yields (34 %) relative to analogues **35** and **36**. The ^{1}H NMR spectra of **39** and **40** are very similar to the analogues bearing longer alkyl bridges discussed above; the full spectra can be seen in Appendix 1.

The conversion of **40** to cavitand-capped porphyrin **41** was attempted following the microwave conditions which yielded **37** and **38**. However, on work up of the reaction material and subsequent preliminary analysis using UV-Vis spectroscopy, the Soret band at approximately 420 nm was absent (Spectrum 1.116). It was thus concluded that the reaction was unsuccessful. The negative result therefore implies that, with respect to this system, the minimum requirement of bridge length to successfully obtain a cavitand-capped porphyrin is four atoms; with regards to the *in situ* protocol at least.

5.4 Direct Capping Approach Revisited

Results from Chapter 3 indicated that, in terms of the direct capping protocol, ligands bearing two atom bridges could not be synthesised. The reason for this was based on crystallographic evidence which suggested that the porphyrin and the cavitand were mismatched in terms of size; the porphyrin being too large to comfortably interact with the cavitand and complete capping. However, given the results of the attempted *in situ* synthesis of **41**, it is of interest to investigate the synthesis of **41** by adopting the direct capping procedure. The use of three atoms as bridge length (as opposed to two) may be sufficient to allow for an interaction between cavitand and porphyrin conducive to porphyrin capping.

In order to find conditions which would afford the desired capping, synthesis began with an investigation into the formation of **38** *via* the direct capping protocol. Since **38** has been successfully synthesised and fully characterised, identification of reaction product, and hence evaluation of the direct capping procedure used, stood to be significantly simplified. Additionally, the longer bridges (five atoms) and their increased flexibility negates any possible problems regarding mismatching of cavitand size relative to the porphyrin. The synthetic approach can be seen in Scheme 5.4.

Synthesis again commenced with the use of **32** as precursor, which was coupled to 1,3-dibromopropane (under conditions identical to those which afforded **35** and **36**) to give **42** in a 63 % yield.

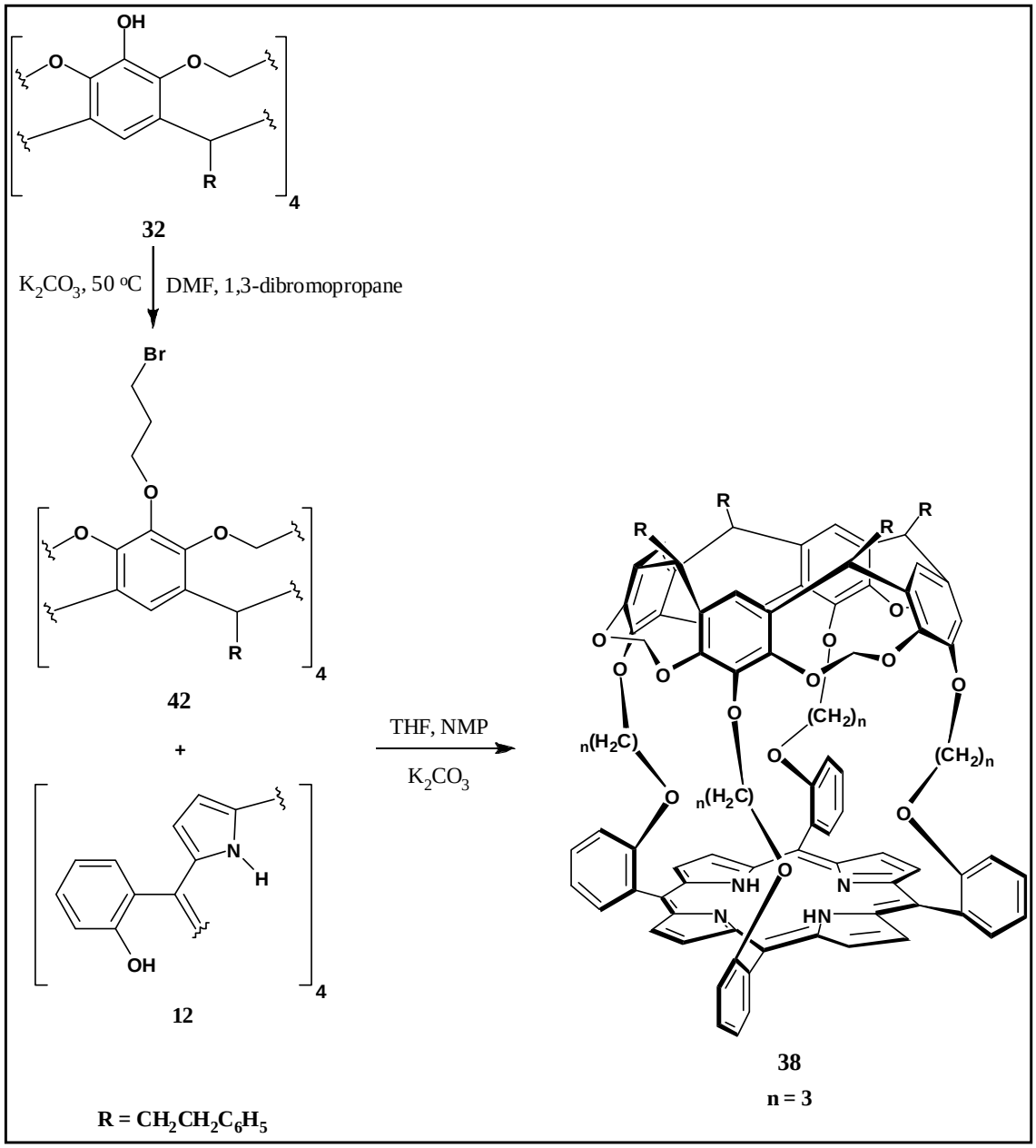

Scheme 5.4: Synthesis towards **38** following a direct capping protocol.

The subsequent coupling of **42** with porphyrin **12** was attempted by adopting the conditions of Naruta *et al.*[18] whereby **42**, **12** and K_2CO_3 in THF and NMP (all reagents dried) were heated in a sealed pressure tube for four days at 120 °C. Thereafter, the reaction was stopped and worked up *via* evaporation of the THF, neutralisation of excess K_2CO_3 with dilute HCl, and extraction of the NMP. However, TLC of the organic phase using a benzene mobile phase did not show any product when spotted against **38**. Further TLC of the crude product in 1:1 ethyl acetate:hexane indicated that **42** had completely reacted; presumably consumed in polymerisation side reactions. As such, the reaction was attempted again, this time making use

of high dilution conditions and refluxing the reaction solution for five days at 100 °C under a nitrogen atmosphere. Again, TLC of the crude product did not indicate the presence of **38**, despite the complete reaction of **42**.

Since the conditions of Naruta *et al.* were unable to afford **38**, synthetic conditions were changed once again towards gentler reaction conditions. THF was replaced by DMF, and the reaction mixture stirred at room temperature under a nitrogen atmosphere. After five days, a small aliquot was removed and added to water saturated with $NaHCO_3$, which was subsequently extracted with chloroform. TLC of the dried organic layer using a benzene mobile phase again failed to show the presence of **38**. However, unreacted starting materials **42** and **12** could be seen by TLC, and consequently, the reaction was heated to 55 °C. After a further four days of reaction, TLC nevertheless indicated that **38** had not formed, despite the complete reaction of **42**.

It was therefore concluded that the direct capping procedure was incapable of affording **38**, despite numerous changes to reaction conditions. Importantly, it is evident given the results above as well as those in Chapter 3 that the direct capping protocol is inadequate in affording cavitand capping of a porphyrin involving *four* bridges. Indeed, given that **41** possesses bridges that are two atoms shorter in length than **38**, and hence, more rigid than **38**, the use of the direct capping protocol in the synthesis of **41** is likely to be ineffective.

5.5 Conclusion

A successful synthetic pathway towards the preparation of two cavitand-capped porphyrins has been identified. Ligands bearing four and five atom bridges have been fully characterised by UV-Vis and NMR spectroscopy, as well as mass spectrometry. All three methods indicated that **37** and **38** have indeed been synthesised, isolated and purified.

Additionally, the *in situ* protocol was shown to be the exclusive method by which to prepare the synthetic targets. This was, however, the case only on implementing the Adler conditions during the final cyclisation step. The use of the Lindsey conditions failed to yield the intended ligands, an observation which is consistent with those made by Reinhoudt *et al.* when reporting similar ligands with analogous bridge lengths. The use of microwave heating in the final *in situ* cyclisation step presented a novel means by which to prepare cavitand-capped porphyrins. It

was, moreover, observed to increase yields relative to reactions performed using conventional heating, as well as aid in simplifying the isolation of **38**.

Further synthetic investigation has also revealed that in terms of the *in situ* method of synthesis, a bridge length of four atoms is the minimum requirement to afford a successful cyclisation and porphyrin formation. As such, **37** bears the shortest bridges hitherto reported for cavitand-capped porphyrins bearing four interconnecting bridges. It therefore also possesses the smallest molecular cavity hitherto reported for such capped porphyrins host molecules.

Additionally, the direct capping synthetic protocol failed to afford a cavitand-capped porphyrin bearing four bridges, despite the success of the *in situ* approach in the synthesis of an identical molecule. Bearing in mind this result, together with results from Chapter 3 regarding the same synthetic methodology, it is clear that this protocol is ineffective in preparing cavitand-capped porphyrins bearing four bridges.

REFERENCES

1. L. M. Tunstad, J.A. Tucker, E. Dalcanale, J. Weiser, J.A. Bryant, J.C. Sherman, R.C. Helgeson, C.B. Knobler, D.J. Cram, *J. Org. Chem.*, **1989**, *54*, 1305-1312.
2. J.A. Bryant, M.T. Blanda, M. Vincenti, D.J. Cram, *J. Am. Chem. Soc.*, **1991**, *113*, 2167-2172.
3. E. Roman, C. Peinador, S. Mendoza, A.E. Kaifer, *J. Org. Chem.*, **1999**, *64*, 2577-2578.
4. J.C. Sherman, C.B. Knobler, D.J. Cram, *J. Am. Chem. Soc.*, **1991**, *113*, 2194-2204.
5. ***a)*** E.S Barret, J.L. Irwin, P. Turner, M.S. Sherburn, *J. Org. Chem.*, **2001**, *66*, 8227-8229; ***b)*** J.I. Irwin, M.S. Sherburn,. *J. Org. Chem.*, **2000**, *65*, 602-605.
6. Cavitand precursor 32 has found use most notably in hemicarcerand chemistry, acting as the synthetic foundation for the first soluble carceplexes as reported by Sherman *et al.* (see reference 3). For representative reports citing the use of 32 as a synthetic precursor, see ***a)*** N. Edwards, R. Helgeson, Y-L. Zhao, K.N. Houk, *Mol. Cryst. Liq. Cryst*, **2006**, *456*, 175-192; ***b)*** D.A. Makeiff, J.C. Sherman, *J. Am. Chem. Soc.*, **2005**, *127*, 12363-12367; ***c)*** R. Warmuth, E.F. Maverick, C.B. Knobler, D.J. Cram, *J. Org. Chem.*, **2003**, *68*, 2077-2088; ***d)*** K. Paek, H. Ihm, S. Yun, H.C. Lee, K.T. No, *J. Org. Chem.*, **2001**, *66*, 5736-5743; ***e)*** K. Paek, H. Ihm, S. Yun, H.C. Lee, *Tetrahedron Lett.*, **1999**, *40*, 8905-8909; ***f)*** N. Chopra, J.C. Sherman, *Angew. Chem. Int. Ed. Engl.*, **1997**, *36*, 1727-1729; ***g)*** Y-S. Byun, T. A. Robbins, C.B. Knobler, D.J. Cram, *J. Chem. Soc. Chem. Comm.*, **1995**, 1947-1948; ***h)*** J.R. Fraser, B. Borecka, J. Trotter, J.C. Sherman, *J. Org. Chem.*, **1995**, *60*, 1207-1213; ***i)*** T.A Robbins, C.B. Knobler, D.R. Bellew, D.J. Cram, *J. Am. Chem. Soc.*, **1994**, *116*, 111-122.
7. H. Nate, K. Matsuki, A. Tsunashima, H. Ohtsuka, Y. Sekine, K. Oda, Y. Honma, A. Ishida, H. Nakai, H. Wada, M. Takeda, H. Yabana, Y. Hino, T. Nagao, *Chem. Pharm. Bull.*, **1987**, *35*, 2394-2411.
8. B. Noll, F. Weinhelt, H. Weinhelt, S. Hauptmann, G. Mann, D. Herhardt, W. Mertens, VEB Chemiekombinat Bitterfield, Germany, Ger (East), **1991**, Patent no. DD 287481.
9. ***a)*** A.D. Adler, F.R. Longo, W. Shergalis, *J. Am. Chem. Soc.*, **1964**, *86*, 3145-3149; ***b)*** J.B. Kim, J.J. Leonard, F.R. Longo, *J. Am. Chem. Soc.*, **1972**, *94*, 3986-3992.
10. A.D. Adler, F.R. Longo, J.D. Finarelli, J. Goldmacher, J. Assour, L. Korsakoff, *J. Org. Chem.*, **1967**, *32*, 476.
11. The ligand as reported by Reinhoudt *et al.* was observed to consist of at least two rotamers/isomers which were observed to broaden the NMR signals.

12. The Cartesian coordinates for the minimised structure of **37** can be found in Appendix 2 on the CD accompanying this thesis.
13. ***a)*** S.M.S. Chauhan, B.B. Sahoo, K.A. Srinivas, *Synth. Commun.*, **2001**, *31*, 33-37; ***b)*** M.O. Liu, C-H. Tai, A.T. Hu, *Mater. Chem. Phys.*, **2005**, *92*, 322-326; ***c)*** D. Samaroo, C.E. Clifford, L.J. Todaro, C.M. Drain, *Org. Lett.*, **2006**, *8*, 4985-4988; ***d)*** B.F.O. Nascimento, M. Pineiro, A.M. Gonsalves, M.R. Silva, A.M. Beja, J.A. Paixao, *J. Porphyrins Phthalocyanines*, **2007**, *11*, 77-84; ***e)*** M.L. Dean, J.R. Schmink, N.E. Leadbeater, C. Brueckner, *J. Chem. Soc. Dalton Trans.*, **2008**, 1341-1345; ***f)*** R. De Paula, M.A.F. Faustino, D.C.G.A. Pinto, M.G.P.M.S. Neves, J.A.S. Cavaleiro, *J. Heterocycl. Chem.*, **2008**, *45*, 453-459; ***g)*** I. Elghamry, L.F. Lutz, *Tetrahedron Lett.*, **2008**, *49*, 3972-3975.
14. ***a)*** B.L. Hayes, *Microwave Synthesis: Chemistry at the Speed of Light*, CEM Publishing, Matthews **2002**; ***b)*** A. Loupy, *Microwaves in Organic Synthesis*, Wiley **2002**.
15. The Cartesian coordinates for the minimised structure of **38** can be found in Appendix 2 on the CD accompanying this thesis.
16. J.M. Collins, M.J. Collins, R.C. Steorts, *Novel Method for Solid Phase Peptide Synthesis Using Microwave Energy*, paper presented at the American Peptide Symposium, **2003**.
17. The ligand bearing -$O(CH_2)_4O$- (six atom) bridges has been successfully synthesised in our laboratory, as an extension to this current investigation. Although not reported or investigated computationally in this study, the synthesis and physical behaviour of this ligand is identical to that of the corresponding ligand bearing -$O(CH_2)_2O$- (four atom) bridges.
18. ***a)*** J. Nakazawa, J. Hagiwara, M. Mizuki, Y. Shimazaki, F. Tani, Y. Naruta, *Angew. Chem. Int. Ed. Engl*., **2005**, *44*, 3744-3746; ***b)*** J. Nakazawa, J. Hagiwara, M. Mizuki, Y. Shimazaki, F. Tani, Y. Naruta, *Bull. Chem. Soc. Jpn.*, **2006**, *79*, 1431-1443.

CHAPTER 6

CRYSTALLOGRAPHIC INVESTIGATION OF SYNTHETIC INTERMEDIATES

6.1 Synthetic Intermediates From Initial -CH_2O- Bridged Ligand

The resorcin[4]arene-based hosts which were recrystallised as described in Chapter 3, represent both the synthetic intermediates towards the target ligand, as well as examples of clathrate complexes as mentioned in Chapter 1. Resorcin[4]arene **17** is the starting compound in the synthesis of cavitand **20**, *via* a synthetic pathway identical to that used in the synthesis of the methyl-footed resorcin[4]arene-based hosts seen in the *in situ* approach. In this regard, **5**, **22** and **6** represent more complex resorcin[4]arene-based hosts that result from the successive functionalisation of simpler hosts very similar to compounds **17** and **20**. Although previously known compounds, the crystal structures of **5** and **22** have not been reported, while **6**, **17** and **20** represent entirely new compounds. As such, all the crystallography performed on these compounds is novel, and therefore an overview of the respective crystal structures will be presented.[1]

Samples were sent for analysis to the University of Kwazulu-Natal (UKZN), Pietermaritzburg (in the case of **17**), as well as to the University of the Witwatersrand (WITS) (**5**, **6**, **20** and **22**). Intensity data for **17** was collected on an Oxford Xcalibur 2 area detector diffractometer with Mo K_α radiation (50 kV, 40 mA). The collection method involved ω-2θ scans. Data reduction was carried out using the program *CrysAlis RED 1.171.29.9*,[2a] absorption corrections were performed using the multi-scan method.[2b]

For the samples analysed at WITS, intensity data were collected on a Bruker APEX II CCD area detector diffractometer with graphite monochromated Mo K_α radiation (50 kV, 30 mA) using the *APEX 2* [3a] data collection software. The collection method involved ω-scans of width 0.5° and 512 x 512 bit data frames. Data reduction was carried out using the program *SAINT-NT*.[3b] All of the crystal structures were solved by direct methods using *SHELXTL*.[2c] Non-hydrogen atoms were first refined isotropically, followed by anisotropic refinement by full matrix least-

squares calculations based on F^2 using *SHELXTL*. Hydrogen atoms were first located in the difference map then positioned geometrically and allowed to ride on their respective parent atoms. Diagrams were generated using Mercury.[4]

Table 6.1 shows selected crystal data for compounds **5**, **6**, **17**, **20** and **22**.[5]

*6.1.1 2-phenylethyl resorcin[4]arene, **17***

As a representative starting point to cavitand formation and subsequent functionalisation, novel resorcin[4]arene **17** is a particularly illustrative structure through which to commence this crystallographic analysis. As set out in Chapter 3, **17** is the result of the acid catalysed condensation of 2-methyl resorcinol and 3-phenylpropionaldehyde. Although bearing eight hydroxyl groups, the hydrophobicity of the 2-phenylethyl feet renders **17** only partially soluble in methanol. As a means of purification therefore, **17** was recrystallised from hot methanol to yield a microcrystalline solid which was pure enough to use in subsequent reactions. In order to obtain crystals suitable for single crystal X-ray crystallography, **17** was slowly recrystallised at room temperature to yield orange needle-like crystals. Interestingly, the crystals obtained disintegrated upon their removal from the supernatant liquid. Nonetheless, samples were obtained and sent for analysis. The molecular structure of **17** can be seen in Figure 6.1 below, in a stick representation.

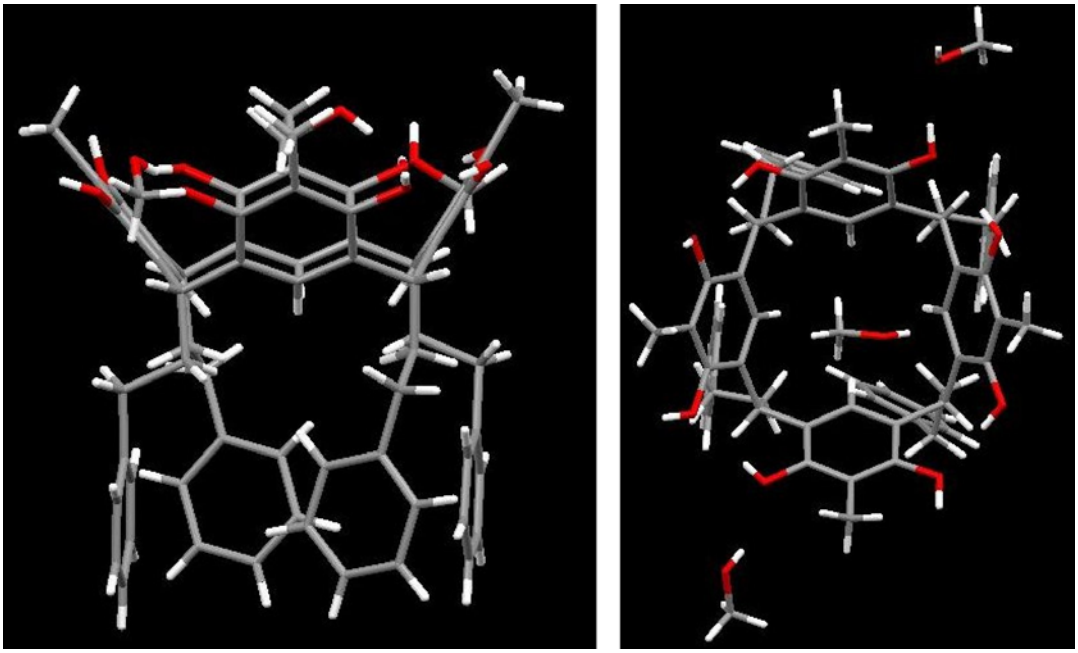

Figure 6.1: Molecular structure of **17** from side on (left), and from above (right).

Table 6.1: Selected refinement data for compounds **5**, **6**, **17**, **20** and **22**.

	5	**6**	**17**	**20**	**22**
Acquisition temperature (K)	173	173	105	173	173
Crystal system	orthorhombic	monoclinic	monoclinic	orthorhombic	triclinic
Space group	*Pnma*	$P2_{1/m}$	$P2_{1/n}$	*Pna2*	*P-1*
a (Å)	16.684	11.923	12.311	24.329	11.515
b (Å)	19.006	23.281	30.615	20.628	11.932
c (Å)	13.470	12.232	16.502	11.783	22.799
α (º)	90.000	90.000	90.000	90.000	93.655
β (º)	90.000	117.005	92.8385	90.000	92.921
γ (º)	90.000	90.000	90.000	90.000	118.676
V (Å^3)	4271.4	3025.0	6212.7	5913.2	2730.8
Z	4	1	4	8	2
D_c (g cm^{-3})	1.624	1.257	1.199	1.233	1.455
R_{int}	0.1045	0.0822	0.0284	0.0619	0.0653
$R1$ [$F^2 > 2\sigma(F^2)$]	0.1122	0.0965	0.0594	0.0634	0.0574

Figure 6.1 illustrates several interesting features regarding **17**. The orientation of the 2-phenylethyl feet is particularly noteworthy. These are arranged perpendicular to one another, in an edge-to-face manner to form a 'box'. Such C-H…π interactions are well known, and have been seen in a number of systems.[6] Indeed, such interactions have been seen in related X-ray structures.[7] The presence of a residual methanol molecule in the cavity illustrates the ability of these compounds to act as host systems. Figure 6.2 (in a space-filled representation) clearly illustrates both the orientation of the feet to form a box, and the guest methanol molecule, which can also be seen occupying the cavity from the bottom, through the box. Peripheral methanol solvent molecules have been omitted for clarity.

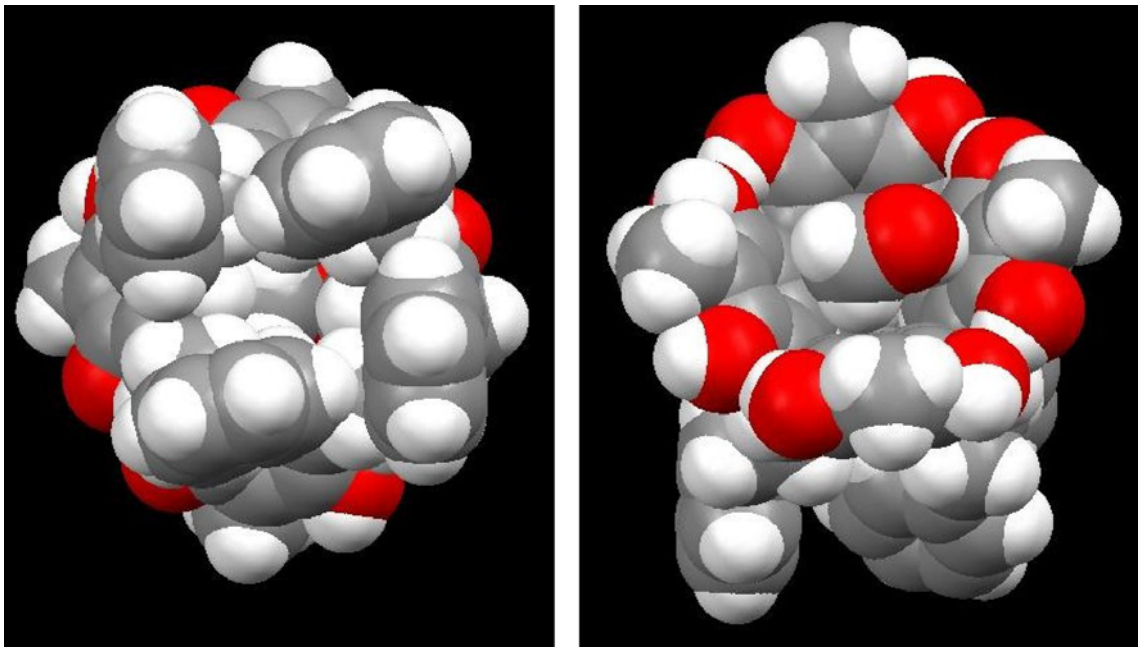

Figure 6.2: Space filled representation of **17** showing the orientation of the feet (left), and the presence of residual methanol in the cavity (right).

Although hydrophilic in nature, the cavity is able to accommodate methanol, orientated with the hydroxyl group of the methanol away from the cavity. This is conceivably due to the hydrophilic nature of the methanolic hydroxyl group conflicting with the hydrophobic nature of the cavity.

A number of intra- and intermolecular hydrogen bonding interactions are observed in the structure of **17**, as alluded to in Chapter 1. Both inter- and intramolecular interactions are formed between the numerous hydroxyl groups which constitute the rim of the resorcin[4]arene cavity. The intramolecular hydrogen bonds between the hydroxyl groups constituting the cavity rim of **17** range between 1.86 and 2.06 Å. As shown in Figure 6.3, the hydrogen bonding

appears to occur in pairs with two opposite interactions approximately equal in length: a pair of the order 1.866 and 1.873 Å, and another pair 2.003 and 2.060 Å. In addition to these intramolecular interactions, there are four intermolecular interactions between individual resorcin[4]arene molecules, and the residual methanol. The van der Waals O…O range from 2.04 to 2.63 Å. In the case of the methanol inside the cavity, the intermolecular hydrogen bonding distance is 2.639 Å, although does not appear in Figure 6.3 for purposes of clarity.

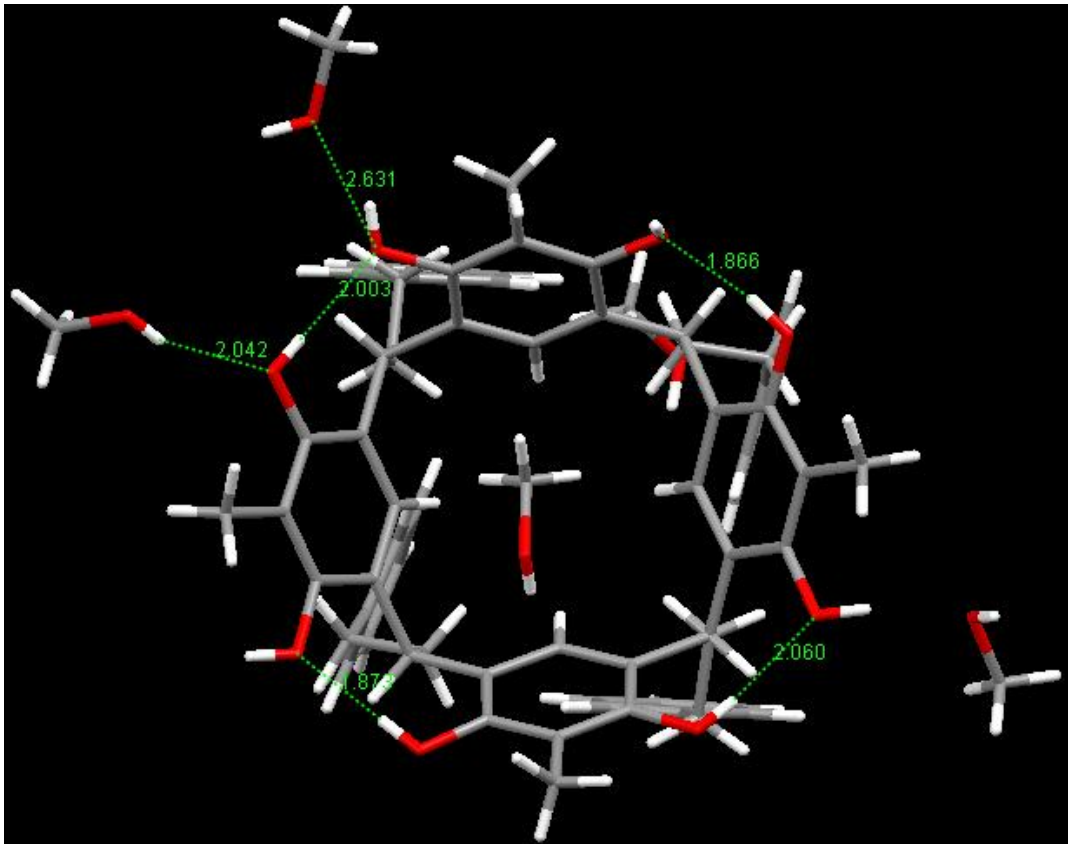

Figure 6.3: Hydrogen bonding interactions of **17**.

In addition, there are a number of interactions between the residual methanol solvent (particularly within the resorcin[4]arene cavities) and the resorcin[4]arene hydroxyl groups. As mentioned, the crystals of **17** disintegrated on removal from the methanol from which they were crystallised. This is an indication that these intermolecular hydrogen bonds are significant in the crystal structure. Figure 6.4 shows more clearly the influence of the methanol within the molecule cavities, and the associated hydrogen bonding. The methanol is coloured in yellow, and appears in ball and stick representation for purposes of clarity.

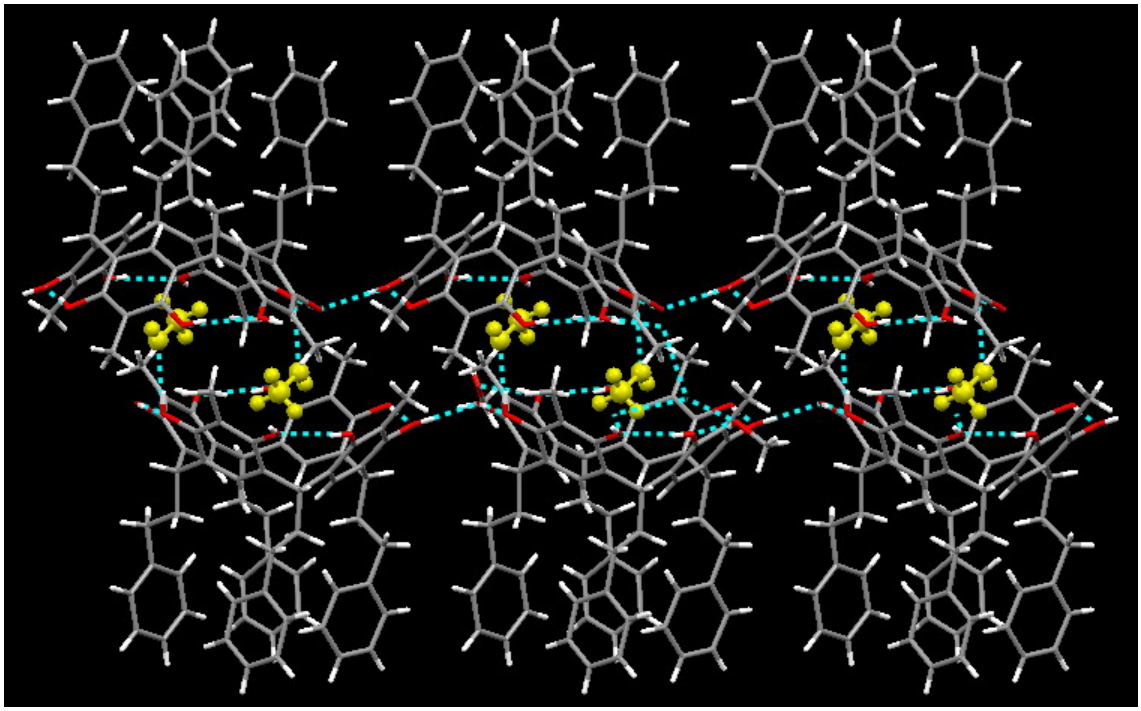

Figure 6.4: Hydrogen bonding interactions of **17**.

In order to illustrate more clearly the role of the residual methanol in maintaining the packing and integrity of the crystals themselves, Figure 6.5 shows one layer of resorcin[4]arene molecules (viewed down the *a* axis). Clearly evident is the presence of a vein of methanol (again in yellow, in ball and stick representation) in between each column of interdigitated resorcin[4]arene molecules.

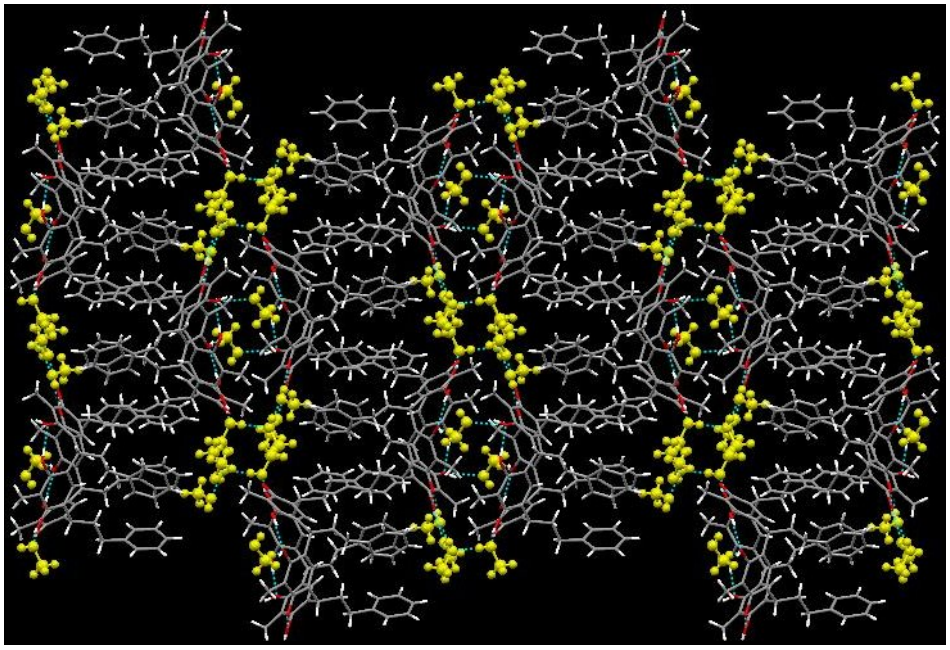

Figure 6.5: The packing of one layer of **17**, illustrating the cohesive role of the residual methanol.

*6.1.2 2-phenylethyl cavitand, **20***

Novel cavitand **20** results from the alkylation of the hydroxyl groups of **17**, to give a more rigid cavitand, as discussed in Chapter 1. Therefore, **20** is representative of the second synthetic intermediate of the target ligand. The 2-phenylethyl feet again give the cavitand a high degree of hydrophobicity; as such crystals of **20** were grown by slow diffusion of methanol into a solution of **20** in 1:1 ethyl acetate: hexane. The crystals obtained were white, needle-like species which were sampled and sent for single X-ray crystallography at WITS. The molecular structure of **20** appears in Figure 6.6.

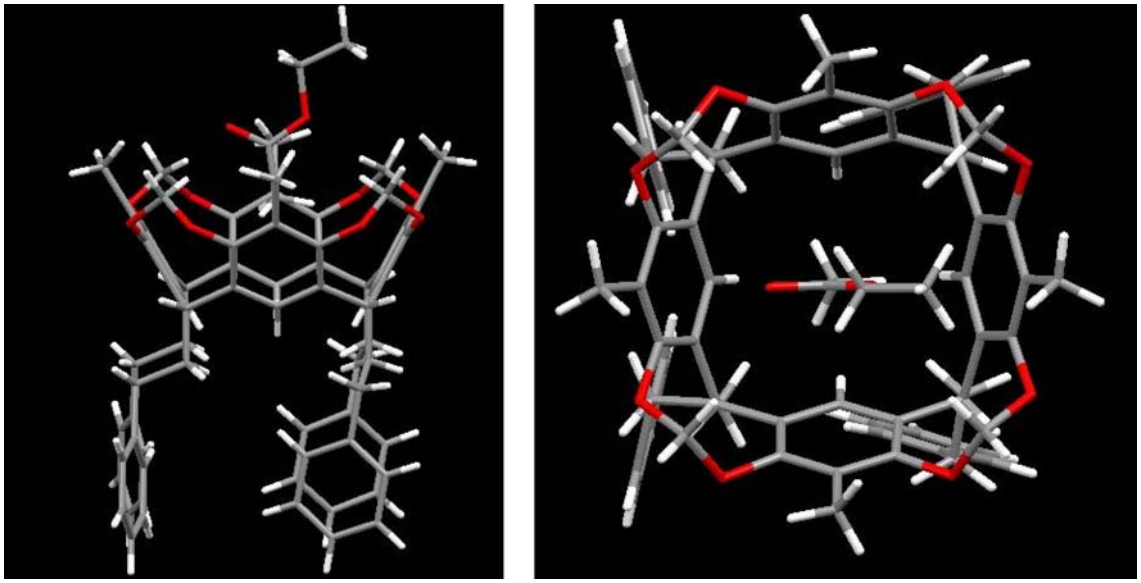

Figure 6.6: Molecular structure of **20** from side on (left), and from above (right).

The newly-introduced methyl bridges, replacing the eight hydroxyl groups in **17**, and linking the four aromatic moieties, are clearly apparent. In this regard, the origin of the anisotropy related to the 'inner' and 'outer' protons is particularly evident, as discussed in Chapter 3. The inner protons are visibly pointing into the cavity, with the outer protons facing the opposite direction. The feet of **20**, although identical to those in **17**, differ in orientation from what was seen in **17**. Although the π-CH interaction mentioned previously is still present, it only occurs between two of the four phenyl rings constituting the feet, and consequently the 'box' seen in **17** does not form.

In terms of the cavity, **20**, like **17**, also has residual solvent from recrystallisation. In this case, the ethyl acetate molecule occupying the cavity is clearly evident. Interestingly, it is the presence of this residual solvent in the cavity which is responsible for the disruption in the

organization of the feet noted above. This kind of disruption by solvent has been reported in similar structures bearing identical feet, where the presence of solvent has given a very similar orientation of the aromatic rings.[8] The orientation of the feet, as well as the guest ethyl acetate molecule found in the cavity of **20**, is shown in Figure 6.7.

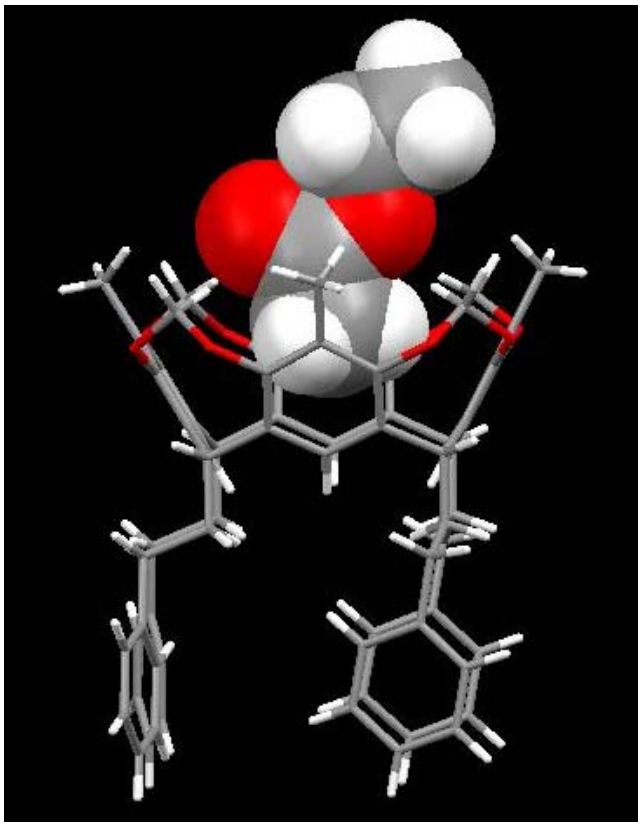

Figure 6.7: The presence of ethyl acetate in the cavity of **20**.

The disruption in feet organization by the ethyl acetate can be seen more clearly in Figures 6.8. The angled representation on the right clearly shows the occurrence of the ethyl acetate in between the phenyl rings of the feet. Solvent appears in a spacefilled representation and is coloured yellow.

The relative orientation of the molecules of **20** also differs to that seen in **17**. The individual cavitand molecules are orientated such that their cavities face in the same direction relative to their neighbours, tilted at an angle (approximately 20°) with respect to the *b* axis. The row above or below has molecular cavities facing in the same direction, however, this now appears slanted (again with respect to the *b* axis) in the opposite direction to the first row. The degree of tilt appears to be the same, and gives a 'zigzag' appearance to a layer of molecules.

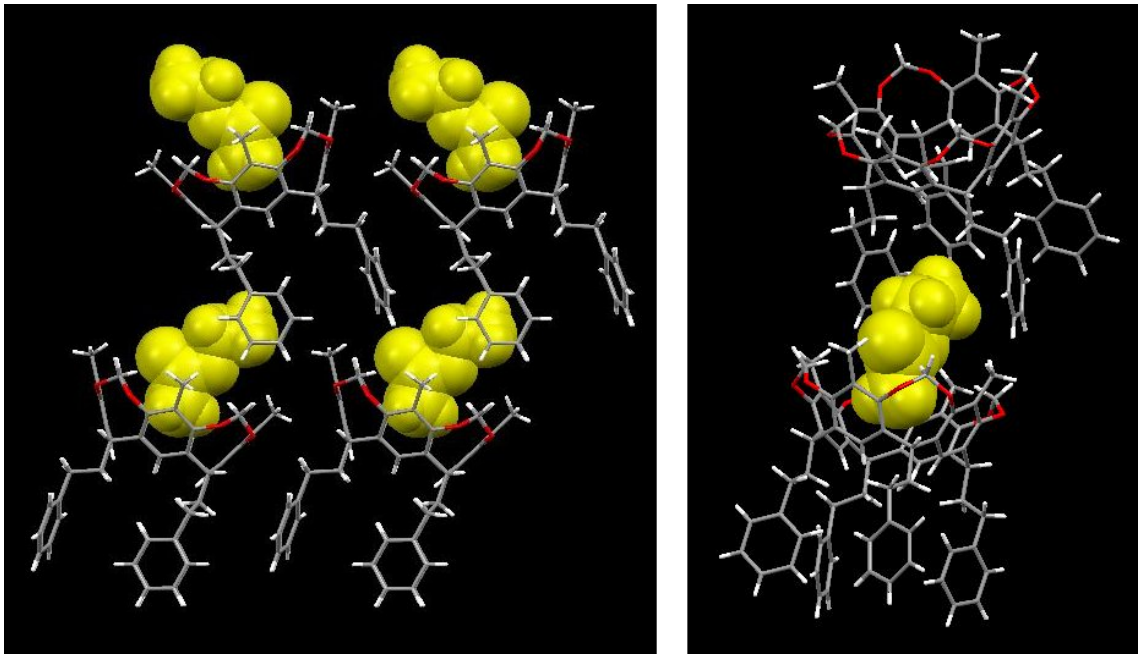

Figure 6.8: The orientation of the ethyl acetate in **20**, disrupting the phenyl rings of the feet.

The next layer possesses the same arrangement of individual molecules, but is rotated by 180°. There is thus no interdigitation, which is in contrast to the packing seen in **17**. In addition, the absence of any significant hydrogen bond donors and acceptors in **20**, as a result of the alkylation of the hydroxyl groups of **17**, results in a lack of any hydrogen bonding interactions in the packing of **20**.

A representative layer of cavitand molecules showing the 'zigzag' columns present in the packing is shown in Figure 6.9. The orientation of the next layer, relative to the first (Figure 6.9) can be seen in Figure 6.10, where the cavitand molecules have been coloured accordingly to clarify illustration. Red illustrates the layer in front, as it appears in Figure 6.9, with the second layer appearing behind in yellow.

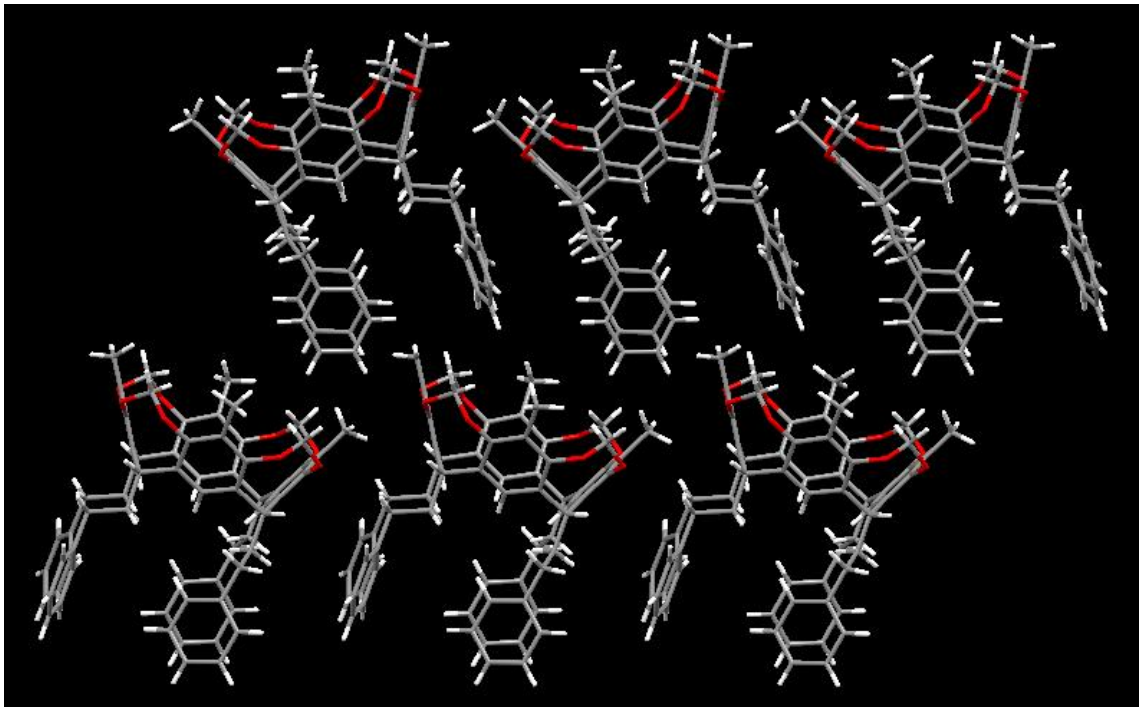

Figure 6.9: Representative layer showing nature of the packing in the crystal structure of **20**.

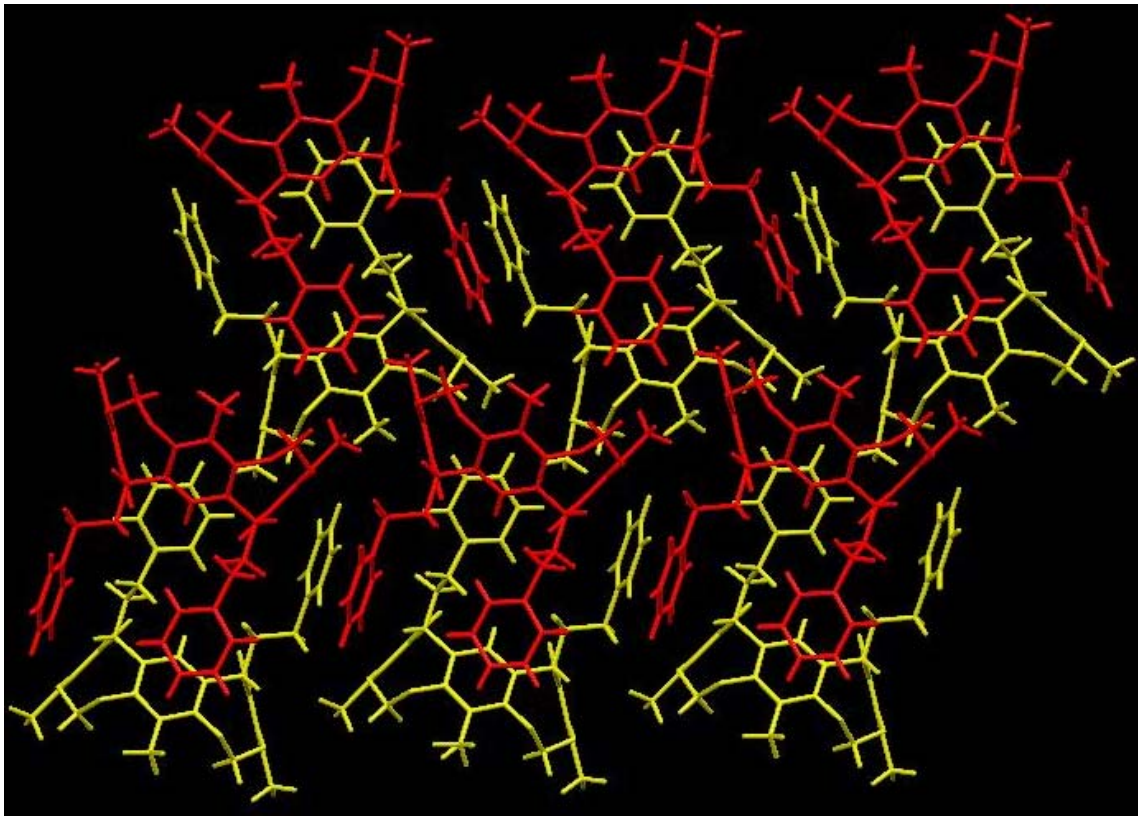

Figure 6.10: Orientation of the layering present in the crystal structure of **20**.

*6.1.3 Bromomethyl cavitand, **5** (methyl feet)*

Representing the brominated cavitands which served as the basis for the coupling reaction between cavitand and porphyrin, cavitand **5** is the result of the first functionalisation of the benzylic methyl groups of a simple cavitand precursor. In this particular case, **5** bears simple methyl feet as opposed to the more complex feet which were seen in **17** and **20**. However, the feet still allowed for slow recrystallisation from a solution of **5** in 1:1 ethyl acetate: hexane to yield white block-like crystals. Crystals were selected and data collected at WITS, which was subsequently solved. The molecular structure can be seen in Figure 6.11 below.

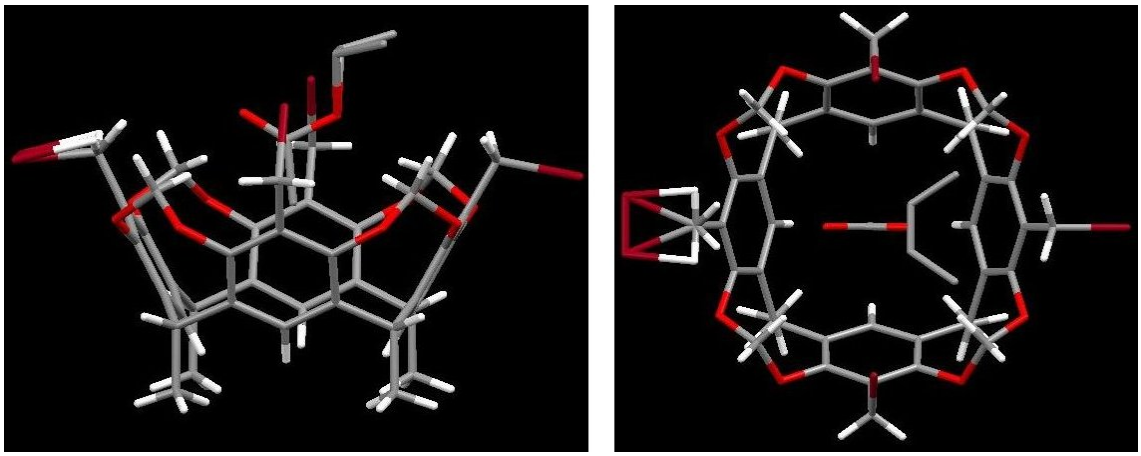

Figure 6.11: Molecular structure of **5** from side on (left), and from above (right).

As can be seen, the newly introduced bromine atoms are orientated such that two (opposite) bromines face into the cavity and two out. One outward-facing bromine atom appears to be disordered. The 'inner' and 'outer' protons are again evident as they were in **20**. However, the short length of the feet is particularly noteworthy, in comparison to the 2-phenylethyl feet seen in **17** and **20**. As discussed in Chapter 3, the target ligand synthesised using this particular precursor gave especially insoluble material. The origin of this insolubility is clearly evident in Figure 6.11, as the feet, which essentially render the bottom of the cavitand a rounded surface, are unable to interact significantly with any solvent.

The host capabilities of cavitands are again illustrated in Figure 6.12 by the presence of residual ethyl acetate within the cavity. The solvent molecule is also disordered across the mirror plane. The individual molecules of **5** are packed and layered in very much the same way as in the case of **20**, appearing in the same tilted configuration as discussed previously with layers rotated 180° with respect to each other. The angle of the tilt is again approximately 20°. Again, no hydrogen bonding occurs, as in the case of **20**.

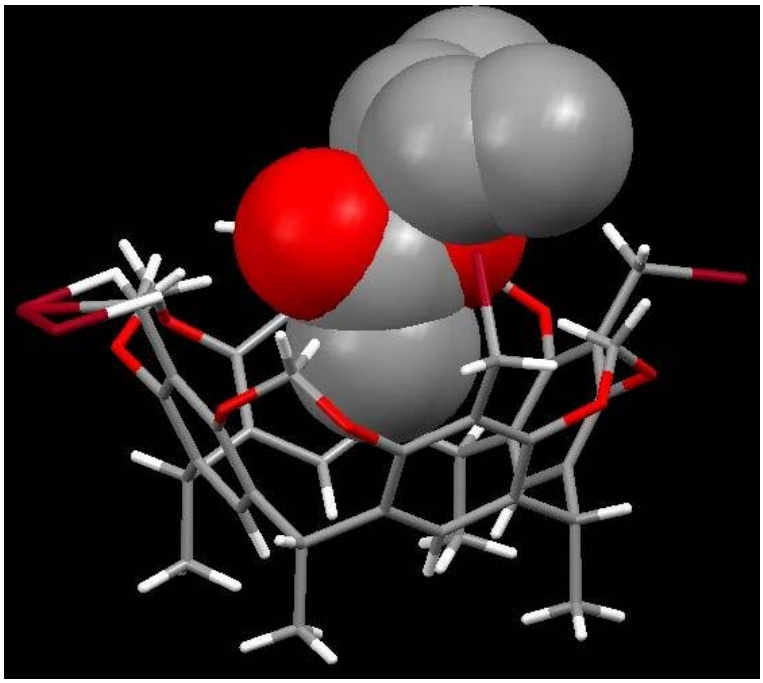

Figure 6.12: The presence of ethyl acetate in the cavity of **5**.

The packing and the layering within the crystal structure can be seen in Figure 6.13 and 6.14 respectively. Again, the different layers in Figure 6.14 have been coloured in order to differentiate and illustrate the arrangement of layers relative to each other. The layer as seen in Figure 6.13 appears in front in red, with the second layer behind, in yellow.

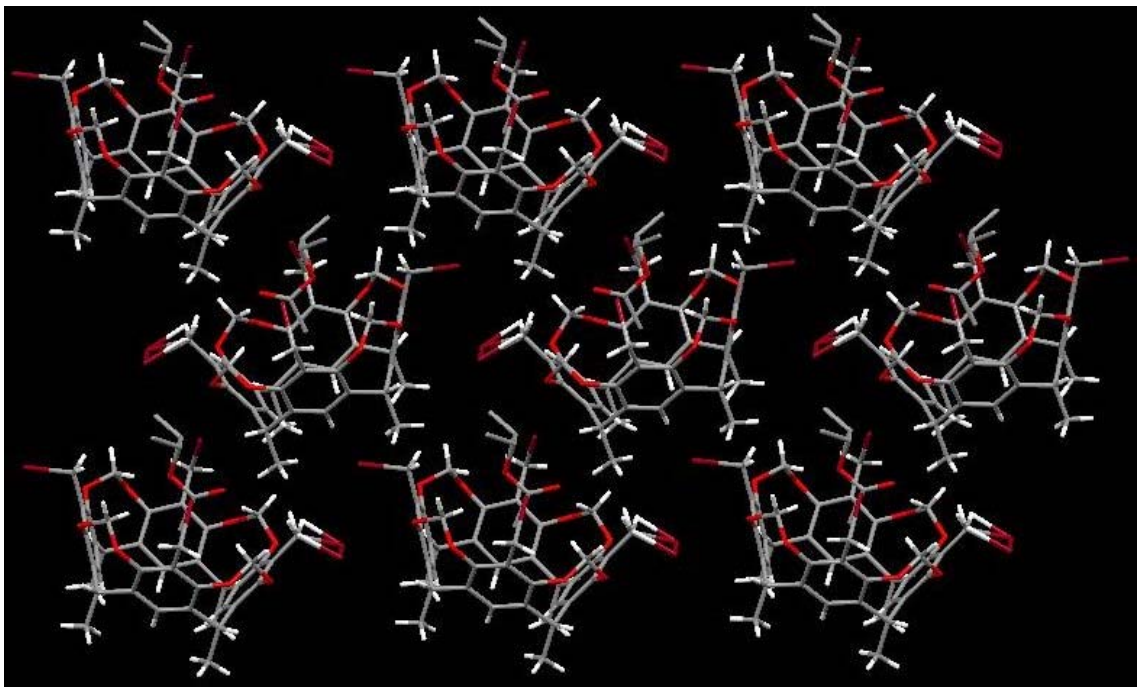

Figure 6.13: Representative layer showing nature of the packing in the crystal structure of **5**.

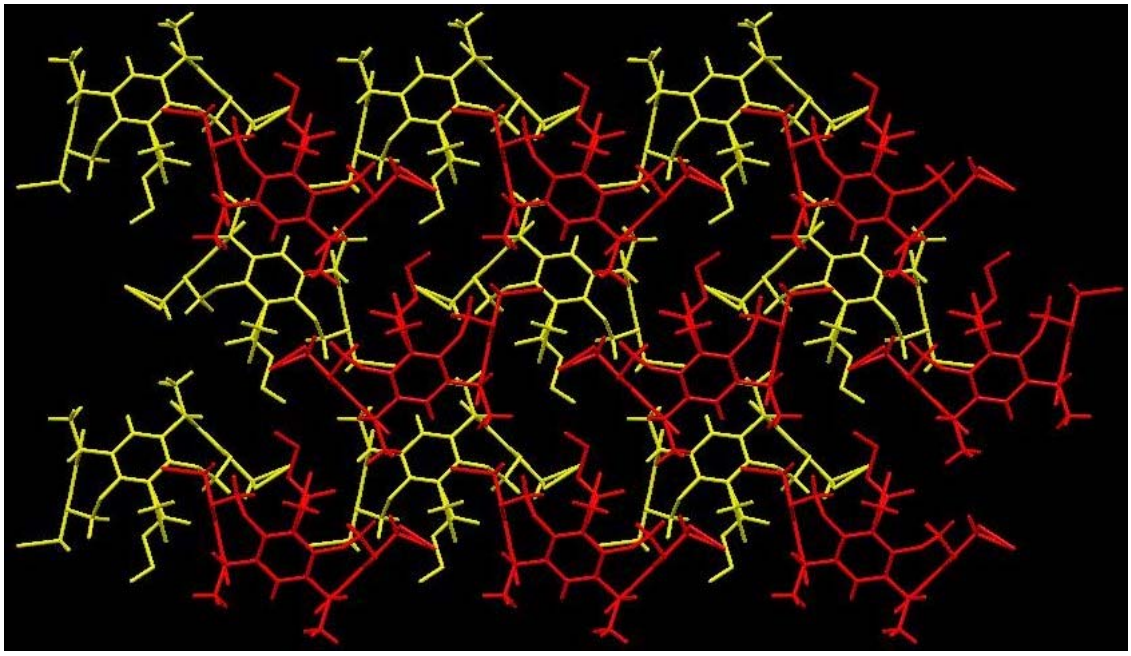

Figure 6.14: Orientation of the layering present in the crystal structure of **5**.

*6.1.4 Bromomethyl cavitand, **22** (pentyl feet)*

The pentyl-footed bromomethyl cavitand **22**, although bearing the same functionalisation as **5** and differing merely in the length of the feet, is remarkably different in terms of both molecular and crystal structure. As seen in Figure 6.15, the C_5H_{11} feet of **22** are arranged such that two adjacent feet appear structured and linear, whereas the remaining two are kinked and appear less regular. In addition, the arrangement of bromine atoms exhibited by **22** is in contrast to that seen in **5**: all four bromine atoms face inwards towards each other and the molecular cavity, as opposed to two inwards, two outwards as seen in the case of **5**. This is indicated more clearly in Figure 6.16, a space filled representation of **22**.

Figure 6.15 also shows the distinct lack of any solvent molecule present within the cavity of **22**. This is in contrast not only to **5**, but also the other resorcin[4]arene-based hosts discussed. The reason for this potentially lies in the orientation of the bromine atoms, as seen in Figure 6.16. The large bromine atoms are arranged such that they prevent any residual solvent from occupying the molecular cavity.

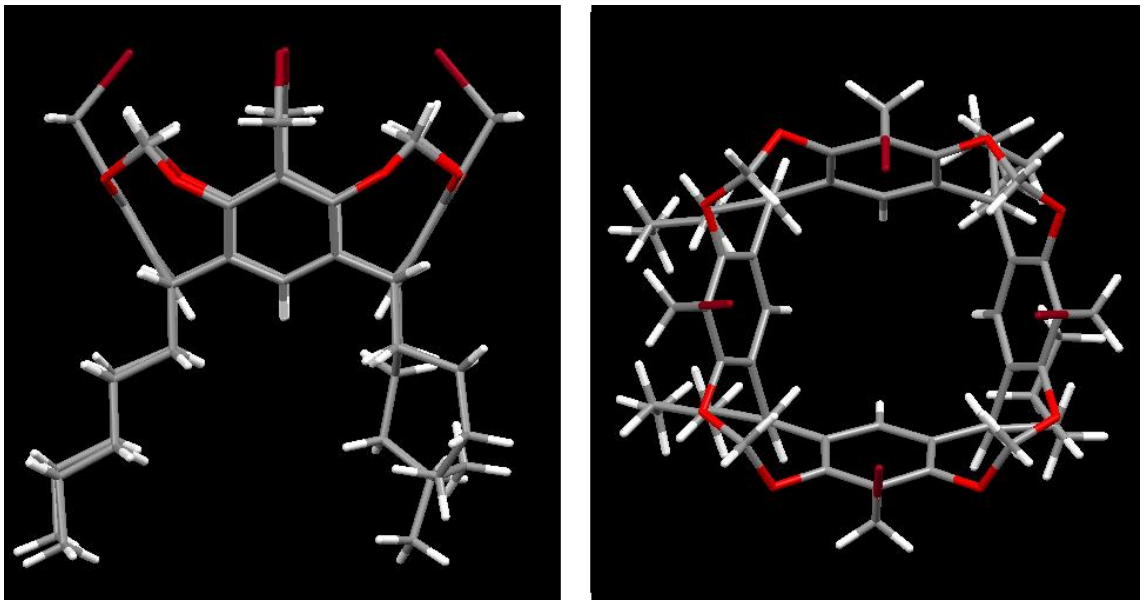

Figure 6.15: Molecular of **22** from side on (left), and from above (right).

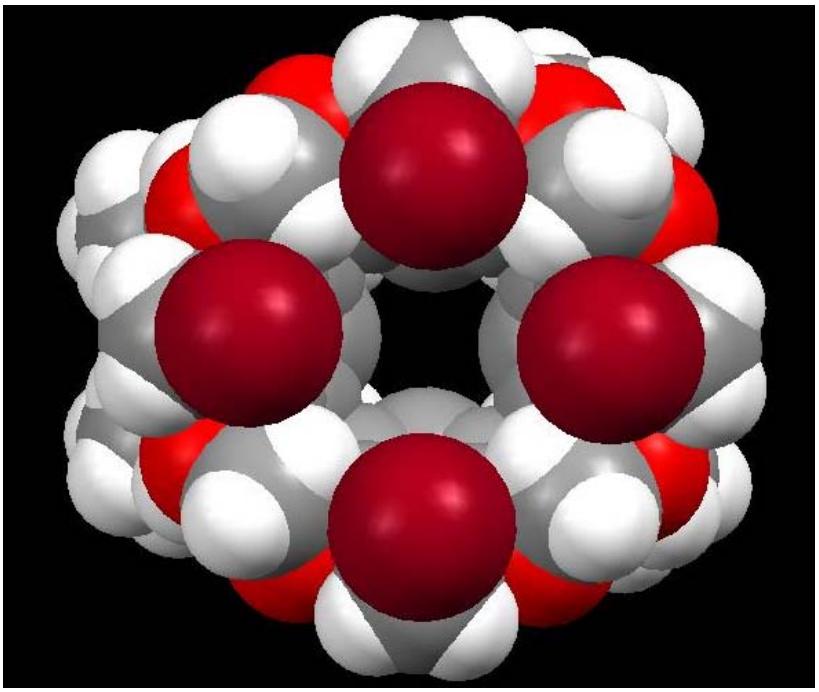

Figure 6.16: Space filled representation of **22** showing the orientation of the bromine atoms.

The bromine atoms are also involved in a particularly interesting intermolecular arrangement of the individual cavitand molecules. The individual molecules are arranged in opposite orientations such that the bromine atoms face each other in close contact, as seen in Figure 6.17, again in space filled representation.

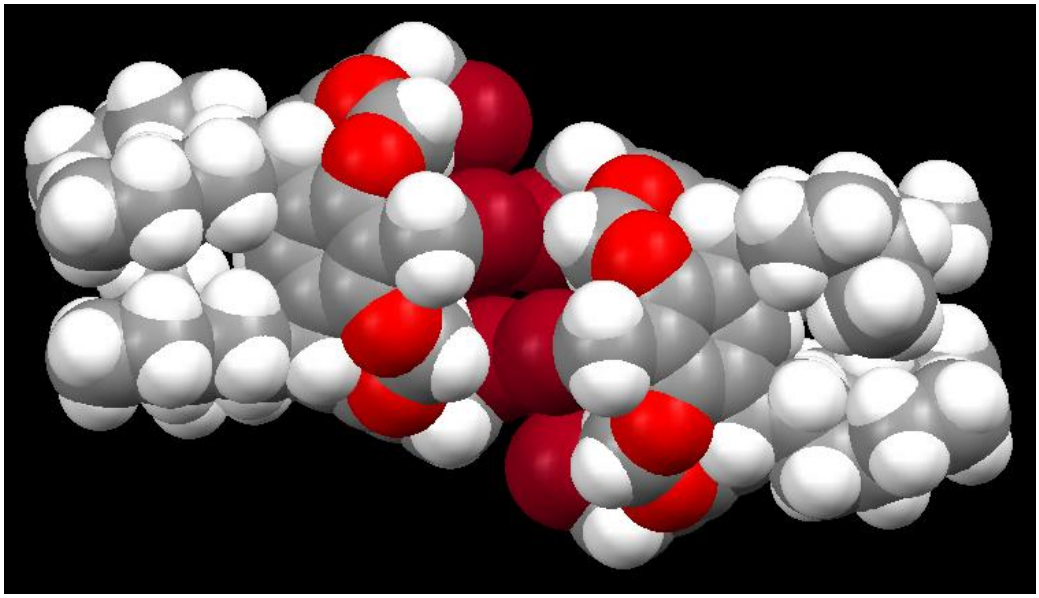

Figure 6.17: Interaction of the bromine atoms present due to the orientation of individual molecules of **22**.

What therefore results is a packing arrangement with alternate layers of bromine atoms, in between the cavities and feet representing the remainder of the cavitand structures, as evident in Figure 6.18.

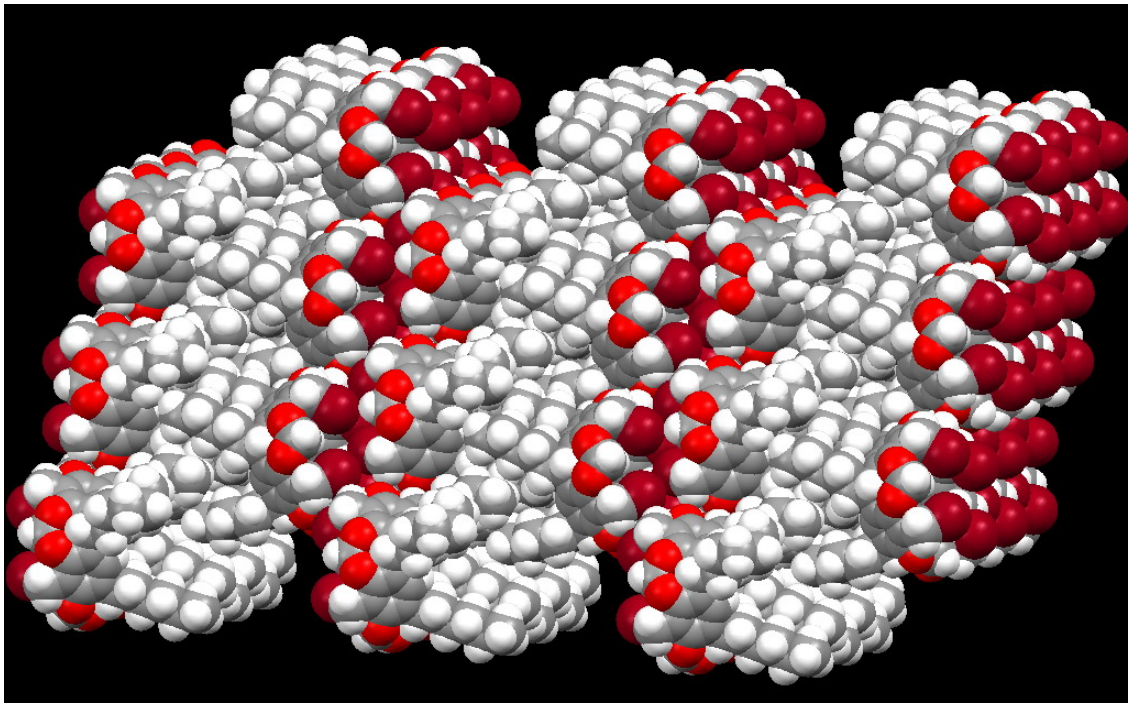

Figure 6.18: Packing present in **22**, with the alternating layers of bromine atoms.

The packing observed can also be seen to be responsible for the way in which two of the pentyl feet of **22** appear linear and structured, while the other two appear bent and kinked. Figure 6.19

shows that the pair of linear feet from one cavitand molecule interdigitates with the corresponding pair from a neighbouring cavitand molecule. This results in insufficient space

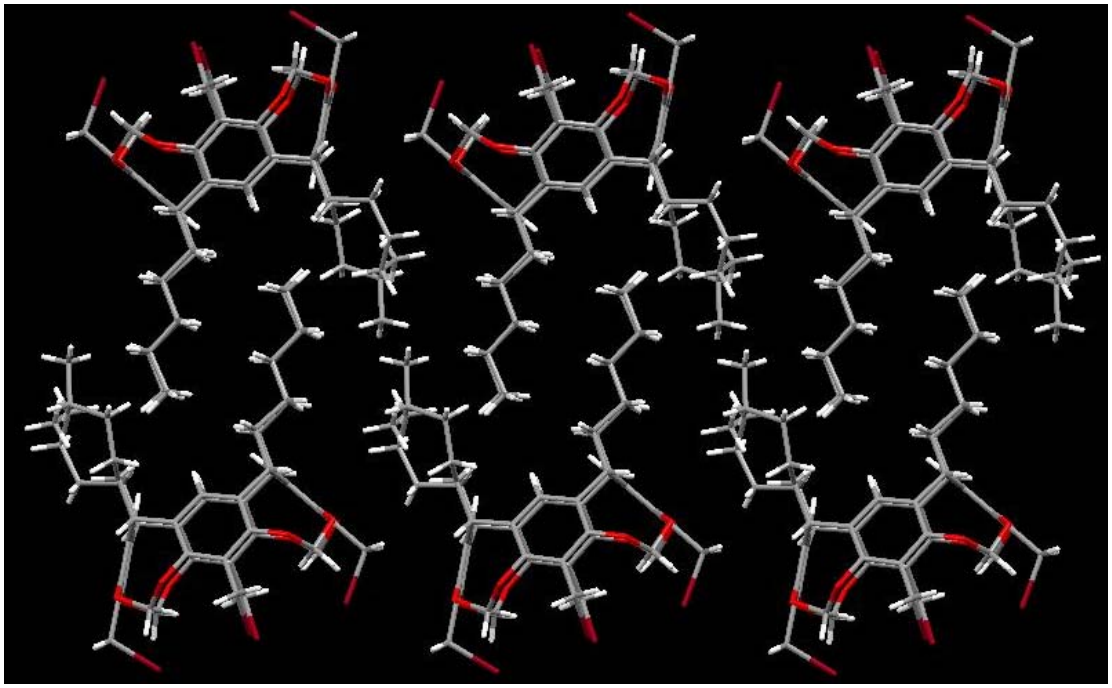

Figure 6.19: Representative layer showing the orientation of the feet in the packing of **22**.

for the remaining pair of feet in each case to extend in a linear fashion. As a result, these appear bent and kinked.

Figure 6.19 also shows layering in the crystal structure of **22** which is similar to that seen in the case of **17**, and in contrast to **19** and **5**. In the case of **22**, the individual molecules are orientated such that cavities face in opposite directions relative to each other, as opposed to in the same direction in the case of **19** and **5**. In addition, as seen in Figure 6.20, the next layer (in yellow) is orientated in the same direction as the first layer (in red), again in contrast to **19** and **5**.

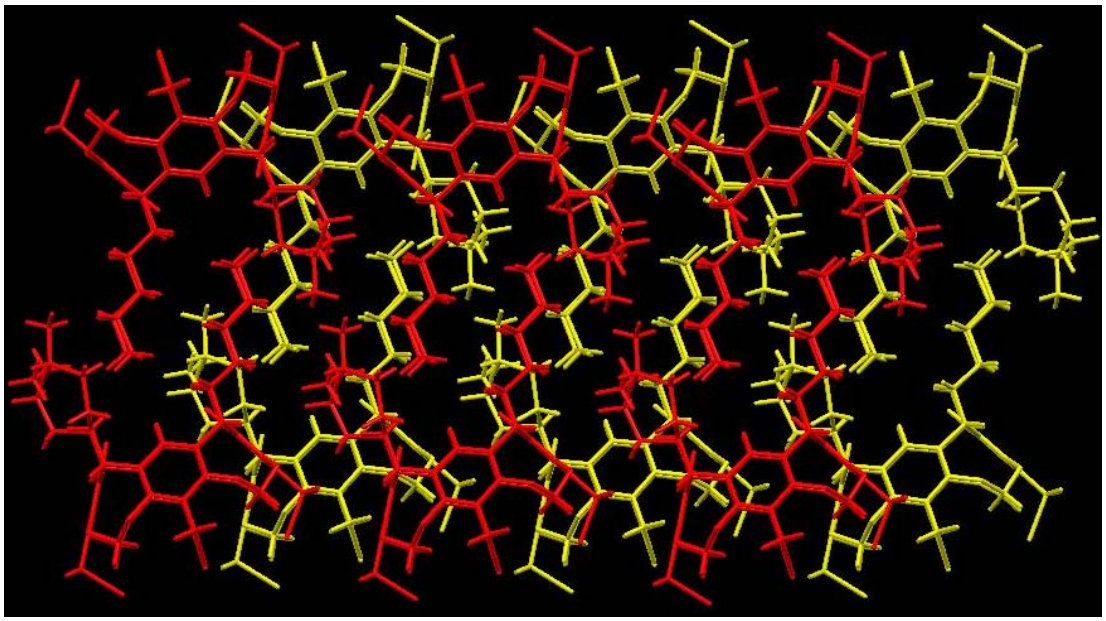

Figure 6.20: Orientation of the layering present in the crystal structure of **22**.

*6.1.5 Tetrasalicylaldehyde, **6***

Novel tetrasalicylaldehyde **6** serves as the precursor to the attempted formation of the target ligand following the *in situ* synthetic protocol outlined in Chapter 3. As with **5**, recrystallisation of **6** took place from a solution in 1:1 ethyl acetate:hexane. The molecular structure of **6**, and its implication for synthesis, has been discussed in Chapter 3 and will not be dealt with here. However, the packing of **6** proves to be remarkably different to the other three structures discussed.

As shown in Figure 6.21, the unit cell of **6** consists of two molecules as opposed to four in all the other structures. The individual molecules are orientated such that one is inverted relative to the other, with the two splayed salicylaldehyde residues of each molecule facing in opposite directions.

In terms of packing, the 'one up, one down' orientation as seen in Figure 6.22 results in layers of molecules which can be broken down into columns of molecules, running in opposite directions to each other. This orientation allows for the π electrons of the salicylaldehyde phenyl rings to interact resulting in stacking of the salicylaldehyde residues. This is illustrated in Figure 6.22, which shows a representative layer of molecules.

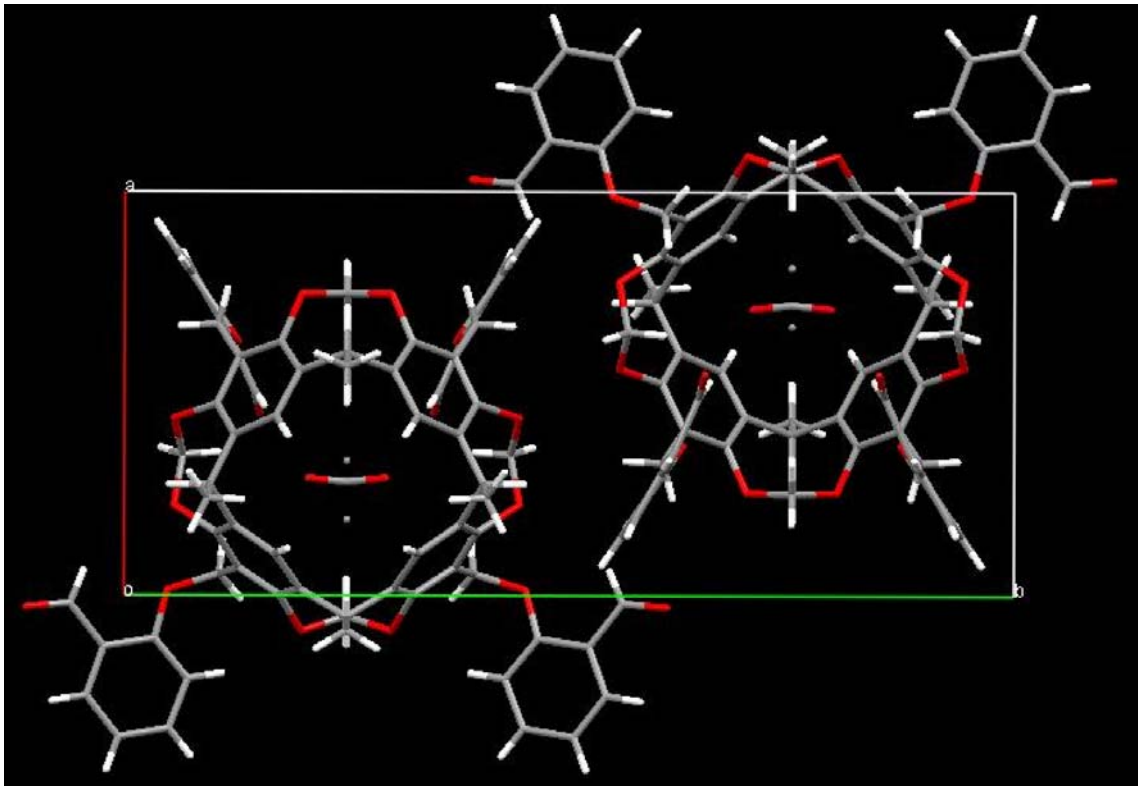

Figure 6.21: Unit cell of **6**.

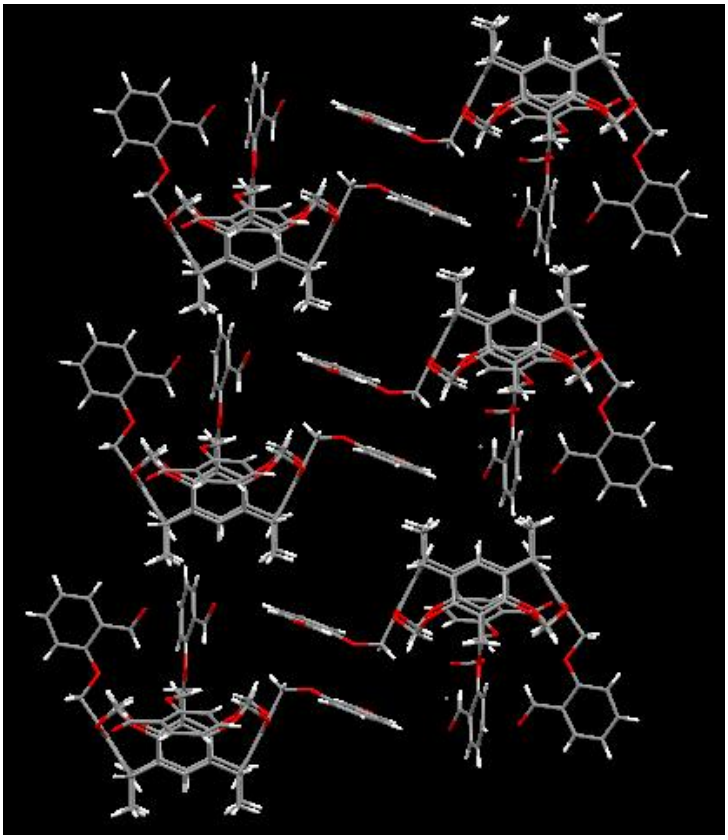

Figure 6.22: Representative layer showing nature of the packing in the crystal structure of **6**.

Interestingly, the layers pack such that they face the same direction. This is in contrast to the layering seen in both **19** and **5**, and similar to **22**. The layering can be seen in Figure 6.23, where the respective layers are coloured differently as done previously. For purposes of clarity, a side view of the layering is presented.

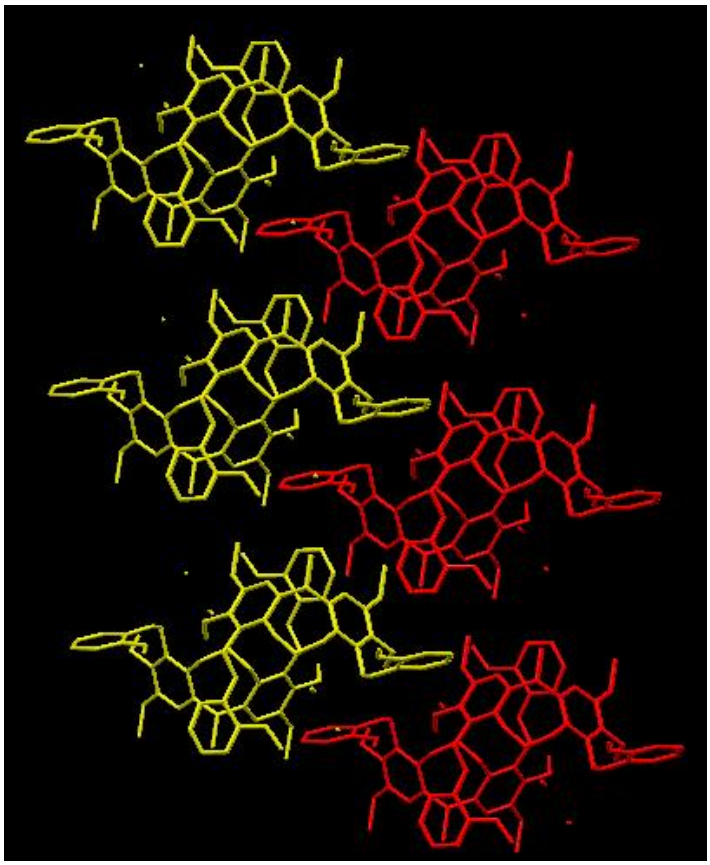

Figure 6.23: Layering orientation present in the crystal structure of **6**.

6.2 Synthetic Intermediates From Ligands Bearing Longer Bridges

The synthesis undertaken in Chapter 5 yielded fewer crystal structures than in Chapter 3; only two structures were obtained from the synthetic work, both of which were previously reported. However, a short discussion of the data obtained will be presented, with comparison to the reported structures. Both sets of data were collected at WITS as per the instrument details and refinement methods set out at the beginning of this chapter. Graphics were again rendered using Mercury. Table 6.2 shows selected crystal data for compounds **31** and **33** appearing with the corresponding data from the respective previously reported structural data.[1, 9, 10]

Table 6.2: Selected refinement data for compounds **31** and **33**, together with the respective corresponding data for the equivalent, previously reported structures.

	31	***Reported equivalent of 31***	**33**	***Reported equivalent of 33***
Acquisition temperature (K)	173	295	173	296
Crystal system	orthorhombic	orthorhombic	monoclinic	monoclinic
Space group	*Pnma*	*Pnma*	$P2_{1/c}$	$P2_{1/c}$
a (Å)	20.436	20.200	7.671	7.745
b (Å)	11.935	12.011	16.120	16.233
c (Å)	24.712	24.675	7.252	7.367
α (º)	90.000	90.000	90.000	90.000
β (º)	90.000	90.000	99.374	98.908
γ (º)	90.000	90.000	90.000	90.000
V (Å^3)	6027.2	5986.70	884.88	915.01
Z	4	4	4	4
D_c (g cm^{-3})	0.695	1.418	1.719	1.663
R_{int}	0.084	-	0.049	0.028
$R1$ [$F^2 > 2\sigma(F^2)$]	0.067	0.074	0.027	0.038

*6.2.1 Bromocavitand, **31***

Cavitand **31**, as discussed in Chapter 5, serves as the synthetic precursor for the lithiation reaction which produces the versatile tetrol cavitand **32**. As in the case of **20**, **31** is the product of the alkylation of the hydroxyl groups of the preceding resorcin[4]arene. The crystal structure of **31** has been reported previously by Sherman *et al.* [9] over 17 years ago. Table 6.2 indicates that **31** and the reported data are similar in many aspects, in particular with regards to the parameters of the unit cell, which is expected due to both structures belonging to identical space groups and crystal systems. The agreement value (*R*1) of 6.7 % in the case of **31**, however, is better relative to that reported by Sherman et al. (7.4 %), conceivably due to the lower data acquisition temperature.

The molecular structure of **31** again shows the presence of residual solvent molecules from the recrystalisation process, as seen in a number of molecular structures above. As shown in Figure 6.24, acetone is present between the 2-phenylethyl feet of **31**, while a disordered chloroform molecule partially occupies the molecular cavity.

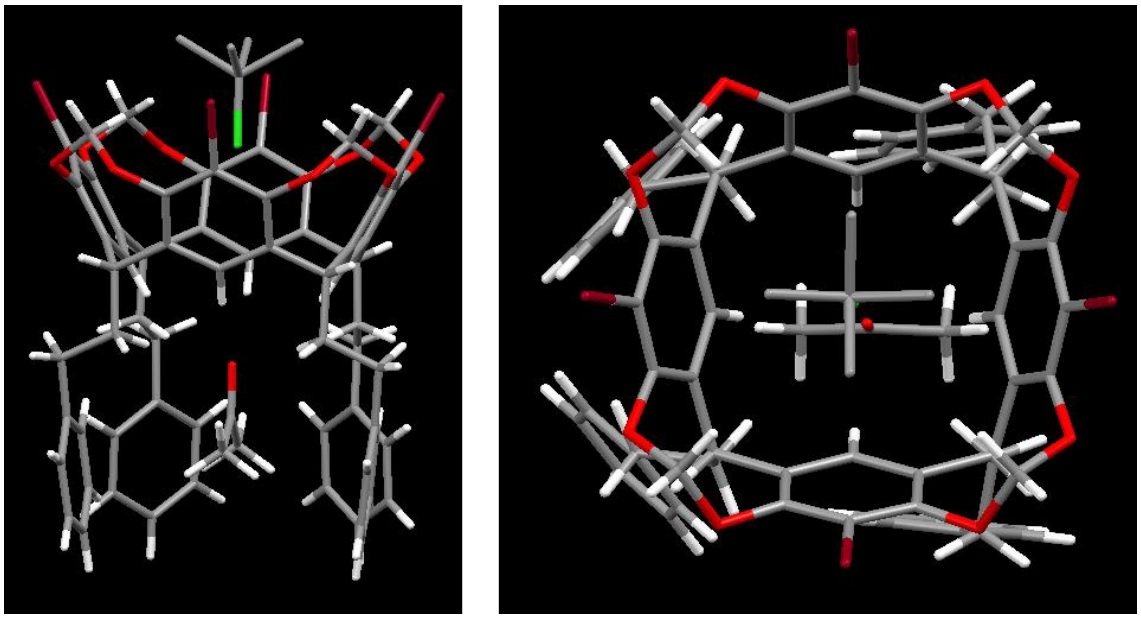

Figure 6.24: Molecular structure of **31** from side on (left), and above (right).

The presence of the residual acetone disrupts any aromatic interactions as seen above in the case of **17**, and as such the orientation of the aromatic moieties present in the feet of **31** largely resembles the orientation seen in **20**. This phenomenon is further illustrated in Figure 6.25.

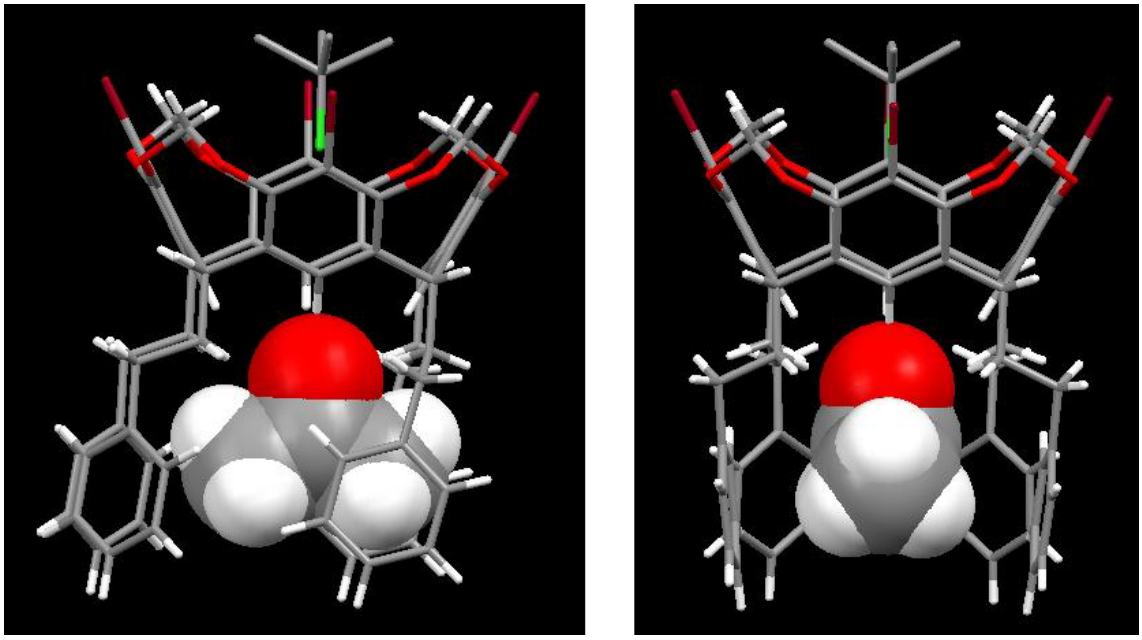

Figure 6.25 The orientation of the acetone in **31**, disrupting the phenyl rings of the feet.

With regards to the packing of the individual cavitand molecules, the orientation of these is such that the molecular cavities face in the same direction relative to their neighbours, tilted at an angle of approximately 20° to form rows of equivalently orientated cavitand molecules. The row above or below has molecular cavities facing in the same direction, however, this now appears slanted in the opposite direction to the first row. The degree of tilt appears to be the same, and yields a 'zigzag' appearance to a layer of molecules which is very similar to that seen in the case of **20** and **5**, as discussed above. Figure 6.26 shows the packing present in a representative layer of **31**.

The next layer possesses the same arrangement of individual molecules, but is rotated by 180°. The orientation of this next layer, relative to the first can be seen in Figure 6.27, where the cavitand molecules have been coloured differently to clarify packing orientation. Red illustrates the layer in front, as it appears in Figure 6.26, with the second layer appearing behind in yellow. In addition, the lack of any significant hydrogen bond donors and acceptors in **31** results in the absence of any hydrogen bonding interactions in the packing of **31**.

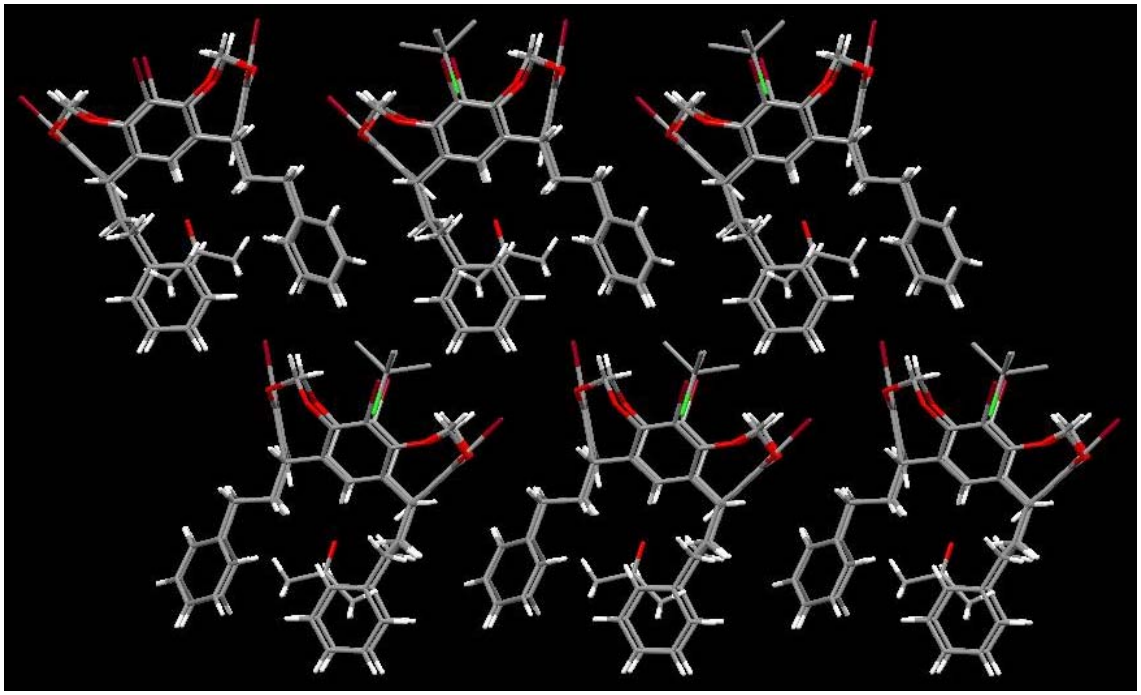

Figure 6.26: Representative layer showing nature of the packing in the crystal structure of **31**.

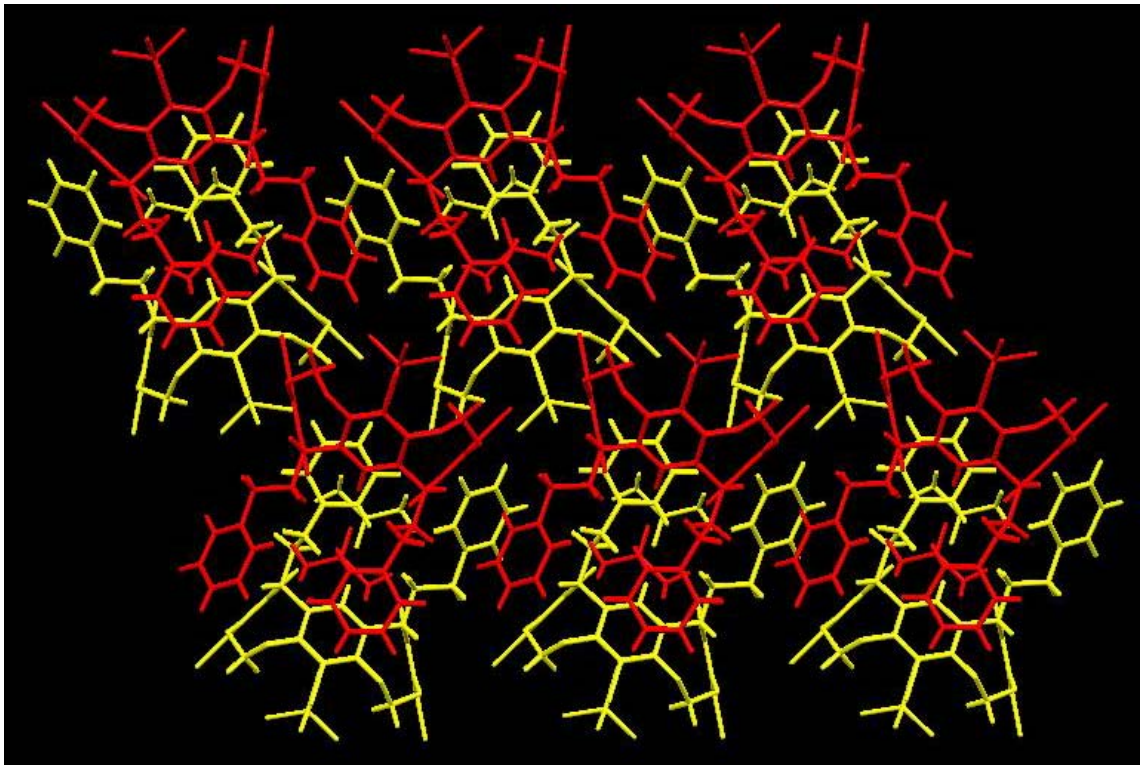

Figure 6.27: Orientation of the layering present in the crystal structure of **31**.

*6.2.2 o-(2-Bromoethoxy)benzaldehyde, **33***

Compound **33** is a fundamental building block towards the formation of the synthetic precursor to the *in situ* cyclisation and preparation of target ligand **37** in this study. The crystals for single crystal X-ray analysis were obtained by heating **33** to beyond its melting point (51-52 °C) and thereafter letting it cool to room temperature. The molecular structure of **33** can be seen in Figure 6.28. It is evident from the side view (right) that both the aldehyde group and the ether oxygen atom are found almost in the same plane as the benzene ring, with the bromine atom appearing perpendicular to this plane. This is in keeping with observations made by Wang *et al.* who have reported this structure previously.[10]

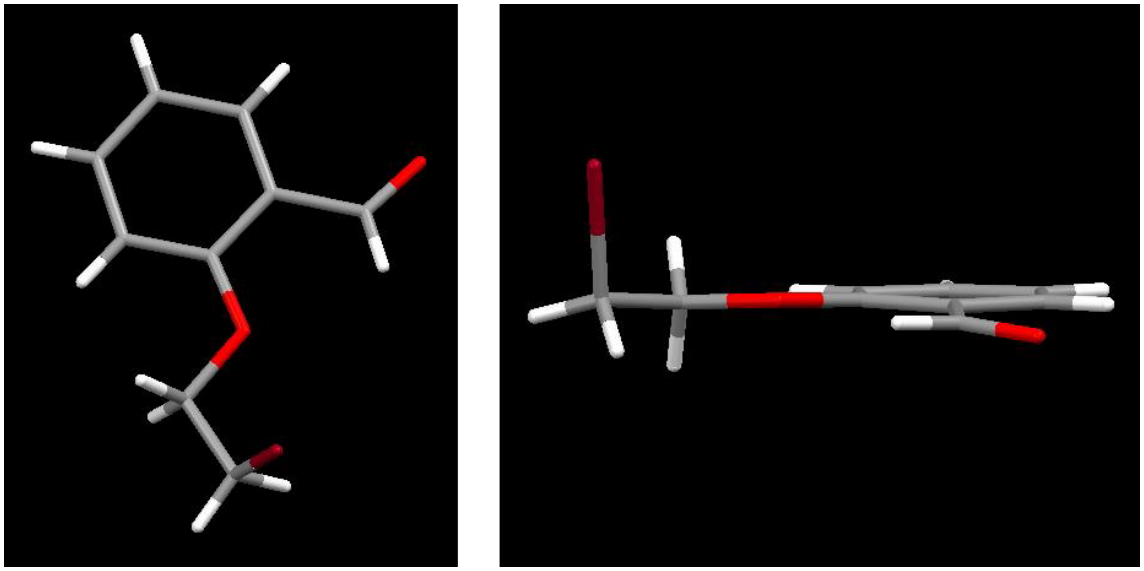

Figure 6.28: Molecular structure of **33** from above (left), and side on (right).

The functional groups present in **33** give rise to both intra- and intermolecular hydrogen bonding. An intramolecular hydrogen bond is present between the proton associated with the aldehyde functional group, and the ether oxygen atom; while an intermolecular hydrogen bond appears between a proton belonging to the $-CH_2Br$ functionality and the aldehyde oxygen atom from a neighbouring residue. These interactions are illustrated in Figure 6.29, which shows the intramolecular interaction on the left, and the intermolecular interaction on the right. The distance over which the hydrogen bonds act in the crystal structure of **33** correspond closely too the equivalent interactions reported by Wang *et al.* Thus for the intramolecular hydrogen bond, the interaction is in the order of 2.43 Å (exactly matching the reported distance), while that for the intermolecular interaction is 2.52 Å (closely matching the reported distance of 2.59 Å).

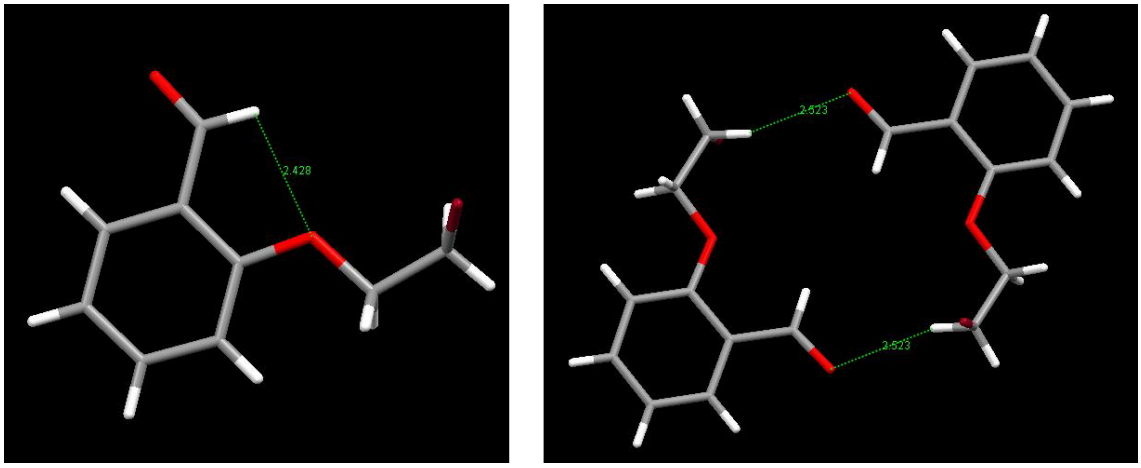

Figure 6.29: Illustration of the intramolecular (left) and intermolecular (right) hydrogen bonding interactions present in **33**.

In terms of packing within the crystal structure, extensive π-π interactions result in the individual molecules of **33** stacking. The packing is such that columns of molecules are observed where the individual moieties (within a single column) are arranged parallel relative to the neighbouring units above and below. The molecules are further found to lie slightly offset from the horizontal. The neighbouring column is arranged in a similar fashion, but the slight offset from the horizontal occurs in the opposite direction. The packing arrangement is illustrated in Figure 6.30 below.

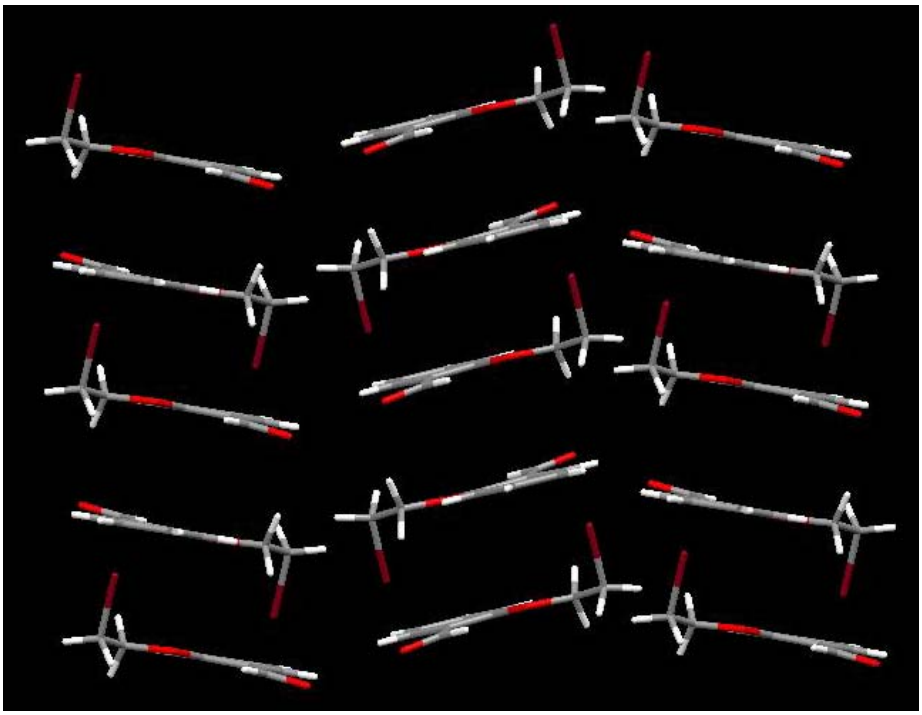

Figure 6.30: Layering orientation present in the crystal structure of **33**.

In terms of further comparison to the reported structure, the data presented in Table 6.2 indicates that the two data sets share very similar unit cell parameters. However, as in the case of **31**, the lower data acquisition temperature in the case of **33** conceivably results in a better agreement value ($R1$) of 2.7 % relative to the reported value of 3.8 % by Wang *et al*.

6.3 Conclusion

The crystal structures of the synthetic intermediates above clearly illustrate the ability of resorcin[4]arene-based molecules to act as hosts, as discussed in Chapter 1. In addition, the inherent rigidity of cavitands can be seen in the structures of **20**, **5**, **22**, **6** and **31**. The structure of **17** is an excellent illustration of the host capabilities of resorcin[4]arenes, and demonstrates the hydrogen bonding which is characteristic of resorcin[4]arenes. Although the structures of the cavitands discussed are slightly different in terms of functional groups at the extra-annular position, and feet in particular, there are close similarities regarding the nature of the packing and layering seen. This is especially true of the simpler cavitands, **5**, **20** and **31**. Additionally, **33** represents a much simpler organic molecule but still exhibits notable properties in the solid state, in particular intra- and intermolecular hydrogen bonding.

REFERENCES

1. All crystallographic data pertaining to all of the structures appears in its entirety in Appendix 3, on the CD accompanying this work.
2. ***a)*** *CrysAlis CCD* and *CrysAlis RED*. Version 1.170, Oxford Diffraction Ltd. (2003), Oxford Diffraction Ltd., Abingdon, Oxford; ***b)*** R.H. Blessing, *Acta Cryst.*, **1995**, *A51*, 33-38; ***c)*** *SHELXTL*. Version 5.1 (includes XS, XL, XP, XSHELL). Bruker AXS, Inc., Madison, Wisconsin, USA.
3. ***a)*** *APEX2*. Version 2.0-1. Bruker AXS, Inc., Madison, Wisconsin, USA.; ***b)*** *SAINT-NT*. Version 6.0 (includes XPREP and SADABS). Bruker AXS, Inc., Madison, Wisconsin, USA.
4. Mercury Version 1.4.2. I.J. Bruno, J.C. Cole, P.R. Edington, M.K. Kessler, C.F. Macrae, P. Mc Cabe, J. Pearson, R. Taylor, *Acta Cryst.*, **2002**, *B58*, 389-397.
5. The full data sets pertaining to the five crystal structures can be found in Appendix 3, on the CD accompanying this thesis. All five have further been deposited on the crystallographic database of the Cambridge Crystallographic Data Centre (CCDC), and are available free of charge *via* www.ccdc.cam.ac.uk/data_request/cif. The structures bear the following CCDC numbers: **5**: 662519, **6**: 634046, **17**: 662145, **20**: 662298, **22**: 662146.
6. For reviews on aromatic interactions in structures, see ***a)*** C.A. Hunter, K.R. Lawson, J. Perkins, C.J. Urch, *J. Chem. Soc. Perkin Trans. 2*, **2001**, 651-669; ***b)*** M. Nishio, *CrystEng. Comm.*, **2004**, *6*, 130-158.
7. ***a)*** K. Kobayashi, T. Shirasaka, E. Horn, N. Furukawa, *Tetrahedron Lett.*, **1999**, *40*, 8883-8886; ***b)*** K.N. Rose, L.J. Barbour, G.W. Orr, J.L. Atwood, *J. Chem. Soc. Chem. Comm*., **1998**, 407-408.
8. ***a)*** D. Eisler, W. Hong, M.C. Jennings, R.J. Puddephatt, *Organometallics*, **2002**, *21*, 3955-3960; ***b)*** L. Sebo, F. Diederich, V. Gamlich, *Helv. Chim. Acta*, **2000**, *83*, 93-113.
9. J.C. Sherman, C.B. Knobler, D.J. Cram, *J. Am. Chem. Soc.*, **1991**, *113*, 2194-2204.
10. The data for **33** has been reported and discussed by B-T. Zhao, J-G. Wang, P-Z. Hu, L-F. Ma, L-Y. Wang, *Acta Cryst.*, **2005**, *E61*, o2398-o2400.

CHAPTER 7

CONCLUSION

The initial synthetic procedures used in this study towards the synthesis of the proposed cavitand-capped porphyrin target ligands were unable to afford the product. Both the *in situ* synthetic approach and the direct capping approach indicated that the short -CH_2O- ether bridges used to link the cavitand to the porphyrin were the primary reason for the failed synthesis; the bridges proving to be too short to allow capping of the porphyrin. The synthetic observations, together with the literature on cavitand-capped porphyrin synthesis, support the notion that the success of *both* synthetic approaches is subject to bridge length, and shows that there exists a *minimum* requirement of bridge length which allows for a successful synthesis; the -CH_2O- ether bridges falling short of this minimum.

Subsequent computational studies on the target ligand indicated that access to the ligand cavity could only be achieved *via* the ligand apertures. Therefore, the viability of using the investigated apertures to obtain selectivity based on size was confirmed. In terms of the initial synthetic target, the investigation indicated (*via* minimisation and molecular dynamics) that the chosen -CH_2O- bridges were too short in length to afford an aperture size which was able to allow the size selective entry of a paraffin terminus into the ligand cavity. Thus, even if synthesis was achieved, the ligand could not provide adequate apertures to perform regioselective oxidation.

However, the use of longer bridges in simulations, in particular those comprising four or five atoms, did afford more accommodating apertures. Given these results, therefore, the synthetic target was adjusted towards ligands bearing -$O(CH_2)_2O$- (four atom) and -$O(CH_2)_3O$- (five atom) bridges. The subsequent synthesis employed the *in situ* approach, which was found to be successful in affording these new target molecules, with complete characterisation using UV-Vis and NMR spectroscopic methods, as well as mass spectrometry. The ligands were only obtained on the implementation of the Adler conditions for the final *in situ* cyclisation step in synthesis; this confirmed previously reported observations for analogous ligands. Additionally, this step made use of microwave heating. The new and hitherto unreported means of heating was found to increase yields appreciably, as well as aid in simplifying the isolation of the five-atom bridged ligand.

Bearing in mind the suggestion of the existence of a minimum bridge length requirement for a successful synthesis of such ligands, further investigation revealed that synthesis involving bridges consisting of three atoms failed to afford a capped porphyrin. The minimum requirement was thus identified as four atoms.

A viable and effective synthetic protocol for the preparation of two new cavitand-capped porphyrins for use in regioselective oxidative catalysis has thus been identified. Indeed, the protocol has yielded a ligand bearing the shortest bridges hitherto reported for cavitand-capped porphyrins bearing four interconnecting bridges. It therefore also possesses the smallest molecular cavity hitherto reported for such capped porphyrin host molecules.

In order to evaluate the efficacy of these ligands in the proposed catalysis, metallation of the porphyrin moiety is required. Additionally, computational methods can be used in preliminary investigations of the complexation and decomplexation behaviour of host-guest systems based on the synthesised host molecules. These threads therefore represent scope for further investigation.

CHAPTER 8

EXPERIMENTAL

General

All solvents and reagents were obtained from Acros, Aldrich, Fluka, Merck or Alfa-Aesar. Unless otherwise stated, these were used without further purification. Microwave synthesis was completed using a CEM Liberty microwave peptide synthesiser, using sealed borosilicate tubes. Thin-layer chromatography (TLC) was conducted on aluminium-backed, precoated silica gel plates (Merck, silica gel 60, 20 cm X 20 cm). Column chromatography was performed with silica gel 60 (Merck, particle size 0.040-0.063 mm). Proton NMR spectra were recorded at 298 K at 300 MHz on a Varian Unity Inova spectrometer; carbon NMR spectra were recorded at 75 MHz with the same instrument under the same conditions. Instances where proton and carbon NMR spectra were recorded at 400 MHz (100 MHz for ^{13}C experiments) a Varian Oxford spectrometer or a Bruker Avance spectrometer were used, at an operating temperature of 298 K. Proton and carbon NMR spectra recorded at 600 MHz (150 MHz for ^{13}C experiments) were done using a Bruker Ultrashield spectrometer. Chemical shifts are reported in parts per million (ppm). Ultraviolet-Visible (UV-Vis) spectra were recorded at 298 K on a Varian Cary 50 CONC single beam UV-Vis spectrophotometer, using a quartz cell of 1 cm path length. A scan speed of 150 nm per minute was used. Infrared (IR) spectra were recorded on a Nicolet Impact 400 spectrophotometer at 293 K, as KBr discs. Wavenumbers are reported in units of cm^{-1}, where *sh* refers to a shoulder, *br* refers to a broad signal, and *w* to a weak signal. Elemental microanalyses were obtained using a Leco CHNS-932 micro-elemental analyzer, and are reported for novel compounds. All melting points are uncorrected. Mass spectrometric data was obtained using a Bruker micrOTOF-Q II instrument operating at ambient temperatures, using 1 mg of analyte per litre of solvent.

*2,5,8,11,14,17,20,23-Octamethylpentacyclo[19.3.1.1^{3,7}.1^{9,13}.1^{15,19}]octacosa-1(25),3,5,7(28),9,11,13(27),15,17,19(26),21,23-dodecaene-4,6,10,12,16,18,22,24-octol Stereoisomer **(3)*** **[1]**

To a stirring solution of water (150 mL), ethanol (150 mL) and 32% aqueous HCl (75 mL), 2-methylresorcinol, **1**, (15.04 g, 0.121 mol) was added. The reaction solution was cooled to 0 °C in an ice-salt bath, before acetaldehyde, **2**, (5.32 g, 0.121 mol) was added slowly over 30 minutes. Once addition was complete, the solution was allowed to slowly attain room temperature, after which time it was refluxed at 80 °C for 24 hours. The solution was cooled to room temperature, and the orange needles that separated were filtered from the solution. The material was washed with cold 1:1 ethanol:water until the washings were light yellow, before being collected and stirred in hexane overnight. The solid was filtered from hexane and dried, to yield the title compound as an orange powder. The material was suitable for use in subsequent reactions without further purification. (16.29 g, 90 %), mp 226-228 °C. ^{1}H NMR [d_6-DMSO, 300 MHz]: δ = 1.69 (d, 12 H, C*H*$_3$), 1.94 (s, 12 H, Ar C*H*$_3$), 4.44 (q, 4 H, C*H*CH$_3$), 7.40 (s, 4 H, Ar *H*), 8.68 (s, 8 H, O*H*). ^{13}C NMR [$CDCl_3$, 75 MHz]: δ = 149.23, 126.27, 121.74, 120.48, 111.89, 28.84, 20.67, 10.51. IR (KBr): 3440*br*, 3245*sh*, 2950, 2910, 2860*w*, 1605, 1475, 1445*sh*, 1360*w*, 1330*w*, 1315*w*, 1255*w*, 1210, 1170*w*, 1110, 1060, 915, 880, 820, 760*w*, 715*w*, 660*sh*, 610*sh*, 555, 505.

*1,7,11,15,21,23,25,28-Octamethyl-2,20:3,19-dimetheno-1H,21H,23H,25H-bis[1,3]dioxocino[5,4-i:5',4'-i']benzo[1,2-d:5,4-d']-bis[1,3]benzodioxocin Stereoisomer **(4)*** **[2]**

Dry **3** (1.00 g, 1.66 mmol) and Cs_2CO_3 (3.00 g, 9.21 mmol) was added to stirring, dry DMSO (10 mL) in a pressure tube (ACE pressure tube, Aldrich). To the resulting pink solution, CH_2BrCl (3.00 mL, 46.0 mmol) was added before further DMSO (10 mL). The tube was sealed and heated at 88 °C for 16 hours. After cooling to room temperature, the tube contents were poured into 2% HCl (200 mL) and the voluminous solid formed was filtered and washed with water. The cream coloured solid was chromatographed on silica gel using a mobile phase of 7:3 hexane-ethyl acetate. The fractions collected were concentrated on a rotary evaporator to yield a cream coloured solid. The solid was stirred in methanol overnight, and filtered off to yield the product as a white powder. (0.95 g, 88 %), mp >300 °C. ^{1}H NMR [$CDCl_3$, 300 MHz]: δ = 1.73 (d, 12 H, C*H*$_3$), 2.00 (s, 12 H, Ar C*H*$_3$), 4.26 (d, 4 H, inner of OC*H*$_2$O), 4.97 (q, 4 H, C*H*CH$_3$),

5.91 (d, 4 H, outer of OCH_2O), 7.10 (s, 4 H, Ar *H*). ^{13}C NMR [$CDCl_3$, 75 MHz]: δ = 152.86, 138.86, 123.57, 117.00, 98.47, 31.24, 16.11, 10.32. IR (KBr): 2960, 2930*w*, 2880*sh*, 1725, 1665*sh*, 1580*w*, 1460, 1425*w*, 1400*w*, 1375*w*, 1335, 1295, 1230, 1205*sh*, 1150, 1100, 1020*sh*, 975, 915*w*, 880*w*, 785, 740, 680, 645, 590, 495, 450*w*.

*7,11,15,28-Tetrakis(bromomethyl)-1,21,23,25-tetramethyl-2,20:3,19-dimetheno-1H,21H,23H,25H-bis[1,3]dioxocino[5,4-i:5',4'-i']benzo[1,2-d:5,4-d']-bis[1,3]benzodioxocin Stereoisomer **(5)*** [3]

Vacuum dried methyl cavitand **4** (1.00 g, 1.54 mmol) and *N*-bromosuccinimide (1.10 g, 6.31 mmol) were added to CCl_4 (100 mL). A catalytic amount of benzoyl peroxide was added to the solution, and the solution allowed to reflux overnight. The light orange solution was then allowed to cool to room temperature, during which time a succinimide precipitate formed. The precipitate was filtered off, and the yellow filtrate concentrated on a rotary evaporator. The resulting solid was chromatographed on silica gel using a mobile phase of 3:1 hexane-ethyl acetate. The fractions that were collected were concentrated on a rotary evaporator, and the yellow solid product that resulted stirred in methanol overnight. The solution was then filtered to yield the title compound as an off-white powder. (0.96 g, 69 %), mp >300 °C. ^{1}H NMR [$CDCl_3$, 300 MHz]: δ = 1.74 (d, 12 H, CH_3), 4.43 (s, 8 H, CH_2Br), 4.56 (d, 4 H, inner of OCH_2O), 5.01 (q, 4 H, C*H*CH_3), 6.02 (d, 4 H, outer of OCH_2O), 7.26 (s, 4 H, Ar *H*). ^{13}C NMR [$CDCl_3$, 75 MHz]: δ = 153.12, 138.99, 124.44, 120.48, 99.04, 31.18, 22.95, 16.05. IR (KBr): 2980*w*, 2940*w*, 2875*w*, 1595, 1415, 1440*w*, 1400, 1345, 1305, 1250, 1205, 1145, 1100, 1095, 1050*w*, 1010*w*, 980, 935*w*, 895*sh*, 805, 750, 695, 600, 560, 490*w*, 480.

*Tetrasalicylaldehyde **6***

To a stirring solution of salicylaldehyde (1.01 g, 8.30 mmol) in dry THF (70 mL) under a nitrogen atmosphere, NaH (60% suspension in mineral oil, 0.33 g, 8.30 mmol) was added. To the resulting bright yellow solution, bromomethyl cavitand **5** (1.00 g, 1.04 mmol) was added as a solution in dry THF (10 mL), dropwise over 30 minutes. The solution was refluxed for 4 days; TLC using a mobile phase of 3:2 hexane-ethyl acetate showed mono-, di-, tri- and tetra-substituted products. Over this time, the solution became grey in colour. Once cooled to room temperature, the solution was concentrated on a rotary evaporator. The products were

chromatographed on silica gel using a mobile phase of 3:2 hexane-ethyl acetate. Fractions of 12 mL were collected, and TLC performed on them in the same mobile phase, such that all fractions containing the desired tetra-substituted product (R_f = 0.37) were combined, and the undesired products discarded. Once all the fractions containing the desired product were collected, they were concentrated on a rotary evaporator to yield an off-white solid. The material was then stirred in methanol, followed by hexane, before being filtered and collected to yield the title compound as a white solid. (0.35 g, 28 %), mp 127-130 °C. ^{1}H NMR [$CDCl_3$, 300 MHz]: δ = 1.88 (d, *J* = 7.6 Hz, 12 H, C*H*$_3$), 4.57 (d, *J* = 6.9 Hz, 4 H, inner of OC*H*$_2$O), 4.96 (s, 8 H, ArOC*H*$_2$Ar), 5.05 (q, *J* = 7.1 Hz, 4 H, C*H*CH$_3$), 5.82 (d, *J* = 6.8 Hz, 4 H, outer of OC*H*$_2$O), 7.04 (t, *J* = 7.1 Hz, 4 H, Ar *H*), 7.14 (d, *J* = 8.5 Hz, 4 H, Ar *H*), 7.40 (s, 4 H, cavitand Ar *H*), 7.53 (t, *J* = 7.0 Hz, 4 H, Ar *H*), 7.73 (d, *J* = 7.6 Hz, 4 H, Ar *H*), 10.18 (s, 4 H, Ar C*H*O). ^{13}C NMR [$CDCl_3$, 75 MHz]: δ = 189.83, 160.93, 154.04, 139.09, 135.88, 129.70, 125.56, 121.77, 121.43, 114.18, 100.00, 62.07, 31.22, 16.14. IR (KBr): 2985*w*, 2940*w*, 2870*w*, 1735, 1690, 1600, 1585*w*, 1480*w*, 1465, 1400*w*, 1385*w*, 1340*sh*, 1300*w*, 1290, 1240*w*, 1220*w*, 1195*w*, 1165, 1100, 1075*w*, 1020*w*, 975, 940*w*, 850, 835*w*, 755, 670*w*, 645*w*, 585*w*, 500*w*, 445*w*. Anal Calcd for $C_{68}H_{56}O_{16}$ (1129.17): C 72.33, H 4.99. Found: C 72.58, H 5.08.

5,10,15,20-Tetrakis(2-methoxyphenyl)-21H,23H-porphyrin ***(11)*** *(Lindsey conditions)* **[4]**

To dry, freshly distilled $CHCl_3$ (1.5 L), 2-methoxybenzaldehyde **8** (2.04 g, 0.015 mol) and freshly distilled pyrrole **9** (1.00 g, 0.015 mol) was added under a nitrogen atmosphere with vigorous stirring. The reaction vessel was shielded from light, and BF_3 (as the diethyl ethearate complex, 0.16 mL) was added *via* syringe. The solution was allowed to stir for 1.5 hours, at which time 2,3-dichloro-5,6-dicyano-*p*-benzoquinone (DDQ, 2.55 g, 0.011 mol) was added as a powder and the solution heated to 60 °C. After 1.5 hours of heating, the solution was allowed to attain room temperature, and triethylamine (10 mL) was added to neutralize excess acid. After 20 minutes of stirring, 40 g of silica was added directly to the reaction vessel for preadsorption of the crude material. Chromatography was performed (in some instances, up to three times) on silica gel using a mobile phase of 95:5 $CHCl_3$-methanol to give the title compound as a dark purple microcrystalline solid, consisting of a mixture of four isomers. (0.96 g, 35 %), mp >300 °C. ^{1}H NMR [$CDCl_3$, 300 MHz]: δ = 3.56, 3.58, 3.60 (3 s, rel. int. 1:2:1, 12 H, 4 OC*H*$_3$), 7.28-7.36 (m, 8 H, 4 *H*C(3'), 4 *H*C(5')), 7.76 (t, 4 H, *H*C(4')), 7.93, 7.99, 8.03 (3 d, rel. int. 1:2:1, 4 H, *H*C(6')), 8.69, 8.80 (2 s, rel. int. 2:1, 8 H, *H*C(β) of pyrrole). ^{13}C NMR [$CDCl_3$, 75 MHz]: δ = 159.48, 159.45, 135.73, 135.66, 135.58, 131.41, 131.24, 129.67, 119.35, 115.48, 110.91,

55.86. IR (KBr): 3445*w*, 3320*w*, 3000*w*, 2935*w*, 2720*w*, 1700*w*, 1595*w*, 1585, 1560*w*, 1490, 1465, 1434, 1405*w*, 1375*w*, 1350, 1295*w*, 1250, 1215*w*, 1185, 1160*w*, 1110, 1050, 1030, 995*w*, 985*w*, 965, 860*w*, 800, 795*w*, 755, 725, 670*w*, 650, 570, 490. UV-Vis ($CHCl_3$): 644.05, 589.72, 550.57, 513.93, 443.32, 419.47 (Soret), 400.32*sh*, 365*sh*, 350*sh*.

5,10,15,20-Tetrakis(2-hydroxyphenyl)-21H,23H-porphyrin ***(12)*** **[4, 5]**

To dry, freshly distilled CH_2Cl_2 (50 mL), tetramethoxyporphyrin **11** (2.00 g, 2.72 mmol) was added as a solid under a nitrogen atmosphere to give a purple solution. To this, BBr_3 (8.7 mL, 0.093 mol) was added to the solution via syringe, and the reaction vessel shielded from light. After stirring for 5 hours, water (30 mL) was carefully added to the bright green solution to neutralise excess acid, and the product precipitated from solution. The contents of the reaction vessel were transferred to a 500 mL beaker, and the solution treated carefully with a saturated solution of $NaHCO_3$, so turning the solution purple. Once effervescence subsided, the solution was subjected to extraction using ethyl acetate. The organic layers were collected and dried over anhydrous Na_2SO_4 before gravity filtration. The solution was concentrated on a rotary evaporator, suspended in a small amount of hexane and filtered. The retained dark purple material was washed further with hexane to give the title compound as a purple solid. (1.68 g, 91 %), mp >300 $^{\circ}$C. TLC (SiO_2, 9:1 $CHCl_3$-Et_2O): R_f 0.19 ($\alpha\alpha\alpha\alpha$ isomer), 0.33 ($\alpha\alpha\alpha\beta$), 0.46 ($\alpha\alpha\beta\beta$), 0.59 ($\alpha\beta\alpha\beta$). ^{1}H NMR [$CDCl_3$, 300 MHz]: δ = 4.93 (br. s, 4 H, O*H*), 7.32-7.39 (m, 8 H, 4 *H*C(3'), 4 *H*C(5')), 7.68-7.76 (t, 4 H, *H*C(4')), 7.95 (m, 4 H, *H*C(6')), 8.91 (s, 8 H, *H*C(β) of pyrrole). ^{13}C NMR [$CDCl_3$, 75 MHz]: δ = 155.54, 135.02, 130.67, 127.37, 119.64, 115.63. IR (KBr): 3630-3220v. *br*, 3120*w*, 3100*w*, 2925*w*, 2850*w*, 1690*w*, 1650*w*, 1640*w*, 1625*w*, 1610*w*, 1585*w*, 1560, 1470*w*, 1455, 1380*w*, 1350, 1290, 1250*w*, 1220, 1185*w*, 1160, 1100, 965, 885*w*, 815, 800*w*, 755, 730*w*, 650, 475*w*, 460*w*. UV-Vis ($CHCl_3$): 642.55, 586.99, 547.05, 512.95, 418.46 (Soret), 398.53, 350*sh*, 310*sh*.

2,8,14,20-Tetrapentyl-5,11,17,23-tetramethylpentacyclo[19.3.1.1^{3,7}.1^{9,13}.1^{15,19}]octacosa-1(25),3,5,7(28),9,11,13(27),15,17,19(26),21,23-dodecaene-4,6,10,12,16,18,22,24-octol Stereoisomer ***(16)*** **[6]**

To a stirring solution of water (100 mL), ethanol (100 mL) and 32% aqueous HCl (50 mL), 2-methylresorcinol, **1**, (10.28 g, 0.08 mol) was added. The reaction vessel was immersed in an ice-salt bath and the solution cooled to temperatures within a range of 0-5 °C, before hexanal, **13**, (8.30 g, 0.08 mol) was added slowly over 60 minutes. Once addition was complete, the solution was allowed to slowly attain room temperature, after which time it was refluxed at 80 °C for 24 hours. The solution was cooled to room temperature, and water added in order to precipitate out the crude product. The orange-brown material that separated was filtered from the solution. The material was washed with cold 1:1 ethanol:water until the washings were light yellow, before being collected, redissolved in warm methanol and recrystallized overnight. The resulting off white material was then filtered from the methanol solution and thereafter stirred in hexane to remove residual aldehyde. The solid was filtered from hexane and dried, to yield the title compound as an off-white powder. (10.93 g, 64 %), mp >300 °C. ^{1}H NMR [d_6-DMSO, 300 MHz]: δ = 0.86 (t, 12 H, C*H*$_3$), 1.33 (m, 24 H, (C*H*$_2$)$_3$), 1.94 (s, 12 H, Ar C*H*$_3$), 2.20 (m, 8 H, C*H*$_2$), 4.18 (t, 4 H, C*H*(CH$_2$)$_4$CH$_3$), 7.25 (s, 4 H, Ar *H*), 8.67 (s, 8 H, O*H*). ^{13}C NMR [$CDCl_3$, 75 MHz]: δ = 149.16, 125.00, 121.30, 111.76, 34.50, 33.20, 31.67, 27.884, 22.51, 14.20, 10.24. IR (KBr): 3425*br*, 2940*sh*, 2930, 2845, 1600, 1470, 1445*sh*, 1360*sh*, 1325, 1300*w*, 1260, 1185*w*, 1160*w*, 1080, 1010*w*, 915*w*, 880*w*, 765*w*, 710*w*, 660*w*, 555*w*, 500.

2,8,14,20-Tetrakis(2-phenylethyl)-5,11,17,23-tetramethylpentacyclo[19.3.1.1^{3,7}.1^{9,13}.1^{15,19}]octacosa-1(25),3,5,7(28),9,11,13(27),15,17,19(26),21,23-dodecaen-4,6,10,12,16,18,22,24-octol Stereoisomer ***(17)***

To a stirring solution of water (100 mL), ethanol (200 mL) and 32% aqueous HCl (50 mL), 2-methylresorcinol, **1**, (12.41 g, 0.10 mol) was added. The reaction vessel was immersed in an ice-salt bath and the solution cooled to temperatures within a range of 0-5 °C, before 3-phenylpropionaldehyde, **14**, (13.42 g, 0.10 mol) was added slowly over 30 minutes. Once addition was complete, the solution was allowed to slowly attain room temperature, after which time it was refluxed at 80 °C for 48 hours. The solution was cooled to room temperature, and water added in order to precipitate the crude product. The brown material that separated was filtered off. The material was washed with cold 1:1 ethanol:water until the washings were light

yellow, before being collected, redissolved in warm methanol and recrystallized overnight. The resulting peach-coloured material was then filtered from the methanol solution and thereafter stirred in hexane to remove residual aldehyde. The solid was filtered off and dried, to yield the title compound as a peach-coloured microcrystalline solid. (13.93 g, 58 %), mp 282-284 °C. ^{1}H NMR [d_6-DMSO, 300 MHz]: δ = 1.97 (s, 12 H, Ar C*H*$_3$), 2.49-2.50 (m, 28 H, C*H*$_2$CH$_2$Ar, and DMSO as solvent signal), 4.26-4.30 (t, *J* = 7.0 Hz, 4 H, C*H*CH$_2$CH$_2$Ar), 7.13-7.29 (m, 20 H, C$_6$*H*$_5$), 7.39 (s, 4 H, Ar *H*), 8.73 (s, 8 H, O*H*). ^{13}C NMR [$CDCl_3$, 75 MHz]: δ = 149.34, 142.40, 128.70, 128.38, 125.81, 125.00, 111.88, 40.53, 40.25, 39.13, 38.86, 10.26. IR (KBr): 3395*br*, 3005*w*, 2925, 2845*w*, 1600, 1470, 1450*sh*, 1380*w*, 1340*w*, 1300, 1255*sh*, 1190, 1098, 1035*w*, 925*w*, 895, 845*sh*, 795*sh*, 750, 705, 560*w*, 500. Anal Calcd for $C_{64}H_{64}O_8$ (961.195): C 79.97, H 6.71. Found: C 80.42, H 6.79.

2,8,14,20-Tetra-undecyl-5,11,17,23-tetramethylpentacyclo[19.3.1.1^{3,7}.1^{9,13}.1^{15,19}]octacosa-1(25),3,5,7(28),9,11,13(27),15,17,19(26),21,23-dodecaen-4,6,10,12,16,18,22,24-octol Stereoisomer ***(18)*** **[6, 7]**

To a cooled (0 °C), stirring solution of 2-methylresorcinol, **1**, (5.01 g, 0.04 mol) in ethanol (75 mL) and 32% aqueous HCl (25 mL), dodecanal, **15**, (7.44 g, 0.04 mol) was added as a solution in ethanol (50 mL) over half an hour. Once addition was complete, the solution was allowed to slowly attain room temperature, after which time it was refluxed at 75 °C for 24 hours. The solution was cooled to room temperature and the crude product precipitated out as an orange solid. The orange material was filtered from the solution and repeatedly washed with methanol. Thereafter, the solid was collected and stirred in methanol for 4 hours, before being filtered and dried under vacuum, to yield a peach coloured powder. (8.56 g, 73 %), mp 286-287 °C. ^{1}H NMR [d_6-acetone, 300 MHz]: δ = 0.91 (t, 12 H, C$_{10}$H$_{20}$C*H*$_3$), 1.32 (m, 72 H, C$_9$*H*$_{18}$), 2.08 (s, 15 H, Ar C*H*$_3$ and acetone as solvent signal), 2.30 (m, 8 H, C*H*$_2$C*H*$_2$C$_9$H$_{19}$), 4.34 (t, 4 H, C*H*CH$_2$C$_{10}$H$_{21}$), 7.43 (s, 4 H, Ar *H*), 7.98 (s, 8 H, O*H*). ^{13}C NMR [$CDCl_3$, 75 MHz]: δ = 149.34, 126.82, 124.48, 121.02, 110.90, 34.28, 33.65, 31.57, 29.47, 29.41, 29.35, 29.22, 28.192, 27.94, 22.24, 13.27, 8.69. IR (KBr): 3370*br*, 2925, 2850, 1612, 1467, 1441, 1377*w*, 1335*w*, 1269, 1198, 1163, 1116*w*, 1096, 926, 894, 873*sh*, 783, 720, 561.

*7,11,15,28-Tetramethyl-1,21,23,25-tetrapentyl-2,20:3,19-dimetheno-1H,21H,23H,25H-bis[1,3]dioxocino[5,4-i:5',4'-i']benzo[1,2-d:5,4-d']-bis[1,3]benzodioxocin Stereoisomer **(19)*** [8, 9]

To a solution of CH_2BrCl (7.1 mL, 0.113 mol) and K_2CO_3 (43.5 g, 0.335 mol) in dry, degassed DMF (700 mL), octol **16** (20.0 g, 0.024 mol) in DMF (100 mL) was added over 1.5 hours. After stirring for 24 hours at room temperature under a nitrogen atmosphere, CH_2BrCl (7.1 mL, 0.113 mol) was added and the solution heated to 45 °C. After a further 24 hours, a further aliquot of CH_2BrCl (7.1 mL, 0.113 mol) was added, and the solution heated to 65 °C. After 48 hours at 65 °C, the pink solution was cooled to room temperature, before being neutralized by a 2M HCl solution. After filtering off the resulting solid, the solvent was removed via rotary evaporation before any remaining carbonate salts were neutralized with 2M HCl. The resulting solid was filtered off, and all solid materials combined before being washed with methanol. The crude product was obtained as a light brown solid. Chromatography on silica gel using a mobile phase of 75:25 hexane-ethyl acetate, followed by stirring in methanol, gave the title compound as an off-white solid. (2.53 g, 12 %), mp 136-137 °C. ^{1}H NMR [$CDCl_3$, 300 MHz]: δ = 0.89 (t, 12 H, C*H*$_3$), 1.15-1.35 (m, 24 H, (C*H*$_2$)$_3$), 1.95 (s, 12 H, Ar C*H*$_3$), 2.10-2.20 (m, 8 H, C*H*$_2$), 4.25 (d, 4 H, inner of OC*H*$_2$O), 4.73 (t, 4 H, C*H*$(CH_2)_4CH_3$), 5.85 (d, 4 H, outer of OC*H*$_2$O), 6.95 (s, 4 H, Ar *H*). ^{13}C NMR [$CDCl_3$, 75 MHz]: δ = 153.22, 137.96, 123.62, 117.56, 98.51, 37.01, 32.09, 31.72, 29.94, 27.68, 22.72, 14.14, 10.36. IR (KBr): 2927, 2859, 1594*w*, 1465, 1398*w* , 1377*w* , 1303, 1236, 1152, 1092, 974, 790*w* , 726*w* , 678*w* , 587, 494.

*7,11,15,28-Tetramethyl-1,21,23,25-tetrakis(2-phenylethyl)-2,20:3,19-dimetheno-1H,21H,23H,25H-bis[1,3]dioxocino[5,4-i:5',4'-i']benzo[1,2-d:5,4-d']-bis[1,3]benzodioxocin Stereoisomer **(20)***

Dry **17** (1.00 g, 1.66 mmol) and Cs_2CO_3 (3.00 g, 9.21 mmol) were added to stirring, dry DMSO (10 mL) in a pressure tube (ACE pressure tube, Aldrich). To the resulting pink solution, CH_2BrCl (3.00 mL, 46.0 mmol) was added before further DMSO (10 mL). The tube was sealed and heated at 88 °C for 16 hours. After cooling to room temperature, the tube contents were poured into 2% HCl (200 mL) and the voluminous solid formed was filtered and washed with water. The cream coloured solid was chromatographed on silica gel using a mobile phase of 70:30 hexane-ethyl acetate (R_f = 0.59). The fractions collected were concentrated on a rotary evaporator to yield a cream coloured solid. The solid was stirred in methanol overnight, and filtered to yield the product as a white powder. (0.97 g, 92 %), mp 145-147 °C. ^{1}H NMR

[$CDCl_3$, 300 MHz]: δ = 2.00 (s, 12 H, Ar C*H*$_3$), 2.44-2.52 (m, 8 H, C*H*$_2$$CH_2$Ar), 2.62-2.67 (m, 8 H, CH_2C*H*$_2$Ar), 4.26 (d, *J* = 7.0 Hz, 4 H, inner of OC*H*$_2$O), 4.83 (t, *J* = 8.0 Hz, 4 H, C*H*CH_2CH_2Ar), 5.88 (d, *J* = 7.0 Hz, 4 H, outer of OC*H*$_2$O), 7.00 (s, 4 H, Ar *H*), 7.11-7.23 (m, 20 H, C_6*H*$_5$). ^{13}C NMR [$CDCl_3$, 75 MHz]: δ = 153.48, 141.91, 137.79, 128.55, 125.96, 117.35, 98.51, 37.16, 34.53, 32.64, 10.38. IR (KBr): 2920, 2850*w*, 1755, 1625*w*, 1590, 1455, 1430*sh*, 1400*w*, 1360*w*, 1340*w*, 1295, 1230, 1145, 1080, 1005*w*, 975, 915*sh*, 800*sh*, 790*w*, 750, 695, 675*sh*, 615*sh*, 595, 500*w*. Anal Calcd for $C_{68}H_{64}O_8$ (1009.24): C 80.92, H 6.39. Found: C 81.25, H 6.49.

7,11,15,28-Tetramethyl-1,21,23,25-tetraundecyl-2,20:3,19-dimetheno-1H,21H,23H,25H-bis[1,3]dioxocino[5,4-i:5',4'-i']benzo[1,2-d:5,4-d']-bis[1,3]benzodioxocin Stereoisomer ***(21)*** **[2, 6]**

Dry **18** (1.00 g, 0.086 mmol) and Cs_2CO_3 (3.00 g, 9.21 mmol) were added to stirring, dry DMSO (10 mL) in a pressure tube (ACE pressure tube, Aldrich). To the resulting solution, CH_2BrCl (3.00 mL, 46.0 mmol) was added before further DMSO (10 mL). The tube was sealed and heated at 88 °C for 16 hours. After cooling to room temperature, the tube contents were poured into 2% HCl (200 mL) and left overnight. The resulting sticky orange residue was extracted into $CHCl_3$. The organic layer was then dried over $MgSO_4$, before being directly adsorbed onto silica. The crude product was chromatographed on silica gel using a mobile phase of chloroform. The fractions collected were concentrated on a rotary evaporator to yield a light orange coloured solid. The solid was stirred in methanol overnight, filtered and dried under vacuum overnight to yield the purified product. (0.67 g, 64 %), mp 168-170 °C. ^{1}H NMR [$CDCl_3$, 300 MHz]: δ = 0.88 (t, 12 H, $C_{10}H_{20}$C*H*$_3$), 1.24 (m, 72 H, C_9*H*$_{18}$), 1.95 (s, 12 H, Ar C*H*$_3$), 2.16 (m, 8 H, C*H*$_2$$CH_2C_9H_{19}$), 4.25 (d, 4 H, inner of OC*H*$_2$O), 4.73 (t, 4 H, C*H* $CH_2C_{10}H_{21}$), 5.85 (d, 4 H, outer of OC*H*$_2$O), 6.94 (s, 4 H, Ar *H*). ^{13}C NMR [$CDCl_3$, 75 MHz]: δ = 153.22, 137.95, 123.60, 117.58, 98.508, 36.958, 31.966, 52.86, 138.86, 123.57, 117.00, 98.47, 36.96, 31.97, 29.90, 29.75, 29.43, 27.98, 22.72, 14.15, 10.36. IR (KBr): 2918, 2850, 1728, 1466, 1428*w*, 1397*w*, 1371*w*, 1302, 1232, 1152, 1090, 1020, 974, 794, 719, 677, 637*w*, 587.

*7,11,15,28-Tetrakis(bromomethyl)-1,21,23,25-tetrapentyl-2,20:3,19-dimetheno-1H,21H,23H,25H-bis[1,3]dioxocino[5,4-i:5',4'-i']benzo[1,2-d:5,4-d']-bis[1,3]benzodioxocin Stereoisomer **(22)*** **[3, 9]**

Vacuum dried methyl cavitand **19** (1.00 g, 1.15 mmol) and *N*-bromosuccinimide (0.90 g, 5.04 mmol) were added to CCl_4 (100 mL). A catalytic amount of benzoyl peroxide was added to the solution, and the solution allowed to reflux overnight under irradiation of white light. The orange solution accompanied by a succinimide precipitate was then allowed to cool to room temperature. The precipitate was filtered off, and the orange filtrate concentrated on a rotary evaporator. The resulting solid was chromatographed on silica gel using a chloroform mobile phase. The collected fractions were concentrated on a rotary evaporator, and the orange solid product stirred in methanol overnight. The solution was then filtered, and the product dried overnight to yield the title compound as a dark orange powder. (1.03 g, 76 %), mp 280-282 $^{\circ}$C. ^{1}H NMR [$CDCl_3$, 300 MHz]: δ = 0.89 (t, 12 H, C*H*$_3$), 1.28-1.50 (m, 24 H, (C*H*$_2$)$_3$), 2.15-2.22 (m, 8 H, C*H*$_2$), 4.40 (s, 8 H, C*H*$_2$Br), 4.55 (d, 4 H, inner of OC*H*$_2$O), 4.76 (t, 4 H, C*H*(CH$_2$)$_4$CH$_3$), 6.02 (d, 4 H, outer of OC*H*$_2$O), 7.11 (s, 4 H, Ar *H*). ^{13}C NMR [$CDCl_3$, 75 MHz]: δ = 153.55, 138.13, 124.55, 121.18, 98.17, 36.87, 32.68, 31.98, 30.08, 27.55, 22.67, 14.10. IR (KBr): 2926, 2858, 1589*w*, 1470, 1453, 1398, 1241, 1147, 1056*w*, 1013, 970, 936, 784*w*, 683*w*, 607, 583, 559, 474.

*7,11,15,28-Tetrakis(bromomethyl)-1,21,23,25-tetraundecyl-2,20:3,19-dimetheno-1H,21H,23H,25H-bis[1,3]dioxocino[5,4-i:5',4'-i']benzo[1,2-d:5,4-d']-bis[1,3]benzodioxocin Stereoisomer **(24)*** **[7]**

Vacuum dried methyl cavitand **21** (1.00 g, 0.83 mmol) and *N*-bromosuccinimide (1.10 g, 6.31 mmol) were added to C_6H_5Cl (100 mL). A catalytic amount of benzoyl peroxide was added to the solution, and the solution allowed to reflux overnight under irradiation of white light. The orange solution, accompanied by a succinimide precipitate, was then allowed to cool to room temperature. The precipitate was filtered off, and the orange filtrate concentrated on a rotary evaporator. The resulting solid was chromatographed on silica gel using a chloroform mobile phase. The collected fractions were concentrated on a rotary evaporator, and the orange solid product stirred in methanol overnight. The solution was then filtered, and the purified product dried overnight to yield the title compound as a dark orange powder. (0.86 g, 68 %), mp >300 $^{\circ}$C. ^{1}H NMR [$CDCl_3$, 300 MHz]: δ = 0.85 (t, 12 H, $C_{10}H_{20}CH_3$), 1.13 (m, 72 H, C_9H_{18}), 2.16 (m,

8 H, C*H*$_2$CH$_2$C$_9$H$_{19}$), 4.38 (s, 8 H, C*H*$_2$Br), 4.53 (d, 4 H, inner of OC*H*$_2$O), 4.72 (t, 4 H, C*H* CH$_2$CH$_2$C$_9$H$_{19}$), 6.05 (d, 4 H, outer of OC*H*$_2$O), 7.14 (s, 4 H, Ar *H*). ^{13}C NMR [CDCl$_3$, 75 MHz]: δ = 153.54, 138.11, 124.53, 121.00, 98.89, 36.82, 31.96, 30.09, 29.82, 29.72, 29.43, 27.88, 22.72, 14.16. IR (KBr): 2921, 2851, 1589*w*, 1470, 1454, 1432*w*, 1398*w*, 1349*w*, 1303*w*, 1241, 1148, 1057, 1014, 968, 940, 815*w*, 720*w*, 683, 584, 560. UV-Vis (CHCl$_3$): 290.00, 250.50.

General procedure for direct capping of porphyrin **[10]**

Porphyrin **12** (0.31 g, 0.46 mmol) was added as a purple powder to a 2-necked round bottom flask (fitted with a double layer condenser) which had been flushed with nitrogen. Dry THF (100 mL) was then added, and the porphyrin solution degassed with nitrogen for ten minutes. Thereafter, oven-dried (110 $^{\circ}$C) K_2CO_3 (2.00 g, 0.020 mol) was added to the solution, which was then heated to 110 $^{\circ}$C under a nitrogen atmosphere. During the heating period, bromomethyl cavitand (**5**, **22** and **24**) (0.59 mmol) was added as a THF solution (100 mL) dropwise over 30 minutes. Once the addition was completed, the solution was kept under nitrogen and allowed to reflux at 110 $^{\circ}$C for five days. After this period, TLC was performed on the reaction solution using a benzene mobile phase. Once reaction was complete, the solution was cooled to room temperature, and the THF removed *in vacuo*. The resulting purple solid was dissolved in chloroform, and the solution washed with 1 M HCl, water (repeated three times) and brine (repeated twice). The organic layer was subsequently dried over Na_2SO_4. The material was adsorbed onto silica, and chromatographed using a benzene mobile phase. The violet band which eluted was collected, the benzene removed and the resultant purple solid stirred in methanol overnight. Filtration from the methanol yielded the reaction product.

*Tetrasalicylaldehyde **27***

To a stirring solution of salicylaldehyde (0.36 g, 2.69 mmol) in dry THF (50 mL) under a nitrogen atmosphere, NaH (60% suspension in mineral oil, 0.065 g, 2.69 mmol) was added. To the resulting bright yellow solution, bromomethyl cavitand **22** (0.400 g, 0.34 mmol) was added as a solution in dry THF (20 mL) dropwise over 30 minutes. The solution was refluxed for 3 days; TLC, using a mobile phase of 1:1 hexane-ethyl acetate, showed tri- and tetra-substituted products. Over this time, the solution became grey in colour. Once cooled to room

temperature, the solution was concentrated on a rotary evaporator. The products were chromatographed on silica gel using a mobile phase of 1:1 hexane-ethyl acetate. Fractions of 12 mL were collected and TLC performed on them in the same mobile phase, such that all fractions containing the desired tetra-substituted product (R_f = 0.56) were combined, and the undesired products discarded. Once all the fractions containing the desired product were collected, they were concentrated on a rotary evaporator to yield a white solid. The material was then stirred in methanol, before being filtered and collected to yield the title compound as a white solid. (0.33 g, 80 %), mp 136-138 °C. ^{1}H NMR [$CDCl_3$, 400 MHz]: δ = 0.91 (t, *J* = 7.1 Hz, 12 H, C*H*$_3$), 1.36 (m, 24 H, (C*H*$_2$)$_3$), 2.26 (m, 8 H, C*H*$_2$), 4.54 (d, *J* = 7.1 Hz, 4 H, inner of OC*H*$_2$O), 4.83 (t, *J* = 8.1 Hz, 4 H, C*H*(CH$_2$)$_4$CH$_3$), 4.95 (s, 8 H, ArOC*H*$_2$Ar), 5.77 (d, *J* = 7.0 Hz, 4 H, outer of OC*H*$_2$O), 7.03 (t, *J* = 7.5 Hz, 4 H, Ar *H*), 7.14 (d, *J* = 8.4 Hz, 4 H, Ar *H*), 7.27 (s, 4 H, cavitand Ar *H*), 7.53 (td, *J* = 8.9 Hz, 4 H, Ar *H*), 7.73 (dd, *J* = 7.5 Hz, 4 H, Ar *H*), 10.17 (s, 4 H, Ar C*H*O). ^{13}C NMR [$CDCl_3$, 75 MHz]: δ = 189.93, 160.95, 154.44, 138.19, 135.87, 129.70, 125.55, 121.93, 121.41, 114.17, 100.07, 62.11, 36.94, 32.02, 30.12, 27.58, 22.70, 14.13. IR (KBr): 2929, 2859, 1686, 1597, 1476, 1454, 1378, 1283, 1240, 1189*w*, 1151, 1088, 1019*w*, 964, 853, 755, 654, 585, 487*w*, 441*w*. Anal Calcd for $C_{84}H_{88}O_{16}$ (1353.59): C 74.54, H 6.55. Found: C 74.89, H 6.68.

2,8,14,20-Tetrakis(2-phenylethyl)-pentacyclo-[19.3.1.1^{3,7}.1^{9,13}.1^{15,19}]octacosa-1(25),3,5,7(28),9,11,13(27),15,17,19(26),21,23-dodecaene-4,6,10,12,16,18,22,24-octol Stereoisomer ***(29)*** **[6]**

To a stirring solution of ethanol (400 mL) and 32% aqueous HCl (100 mL), resorcinol, **28**, (20.0 g, 0.182 mol) was added. The reaction solution was cooled to -4 °C in an ice-salt bath, before 3-phenylpropionaldehyde, **14**, (24.15 g, 0.180 mol) was added slowly over 30 minutes. Once addition was complete, the solution was allowed to slowly attain room temperature over a period of 24 hours, after which time it was refluxed at 80 °C. After approximately 6 hours of reflux, the solution went from a clear, orange solution to a cloudy solution containing a red suspension. After 3 days of reflux, the reaction mixture was cooled to room temperature before further cooling to 0 °C in an ice bath. The solution was filtered and the retained product washed with cold 1:1 ethanol:water before being collected and stirred in hexane overnight. The solid was filtered from hexane and dried, to yield the title compound as an orange powder. The material was suitable for use in subsequent reactions without further purification. (30.82 g, 75 %), mp >300 °C dec. ^{1}H NMR [d_6-acetone, 400 MHz]: δ = 2.52-2.61 (m, 16 H, C*H*$_2$C*H*$_2$Ar),

4.38 (m, 4 H, C*H*CH_2CH_2Ar), 6.25 (s, 4 H, Ar *H*), 7.14-7.26 (m, 20 H, $CH_2CH_2C_6H_5$), 7.74 (s, 4 H, Ar *H*), 8.53 (s, 8 H, O*H*). ^{13}C NMR [d_6-acetone, 100 MHz]: δ = 152.86, 143.46, 129.45, 129.17, 126.46, 125.65, 125.24, 103.79, 37.00, 35.59, 34.64. IR (KBr): 3222*br*, 2936*w*, 2863*w*, 1606, 1495, 1442, 1359*w*, 1325*sh*, 1290, 1210, 1163, 1089, 1078*sh*, 1029*w*, 846, 743, 703, 502.

*5,11,17,23-Tetrabromo-2,8,14,20-tetrakis(2-phenylethyl)pentacyclo [19.3.1.1^{3,7}.1^{9,13}.1^{15,19}]octacosa-1(25),3,5,7(28),9,11,13(27),15,17,19(26),21,23-dodecaen-4,6,10,12,16,18,22,24-octol Stereoisomer **(30)*** **[8, 11]**

Dry **29** (25.0 g, 0.027 mol) was suspended in glacial acetic acid (500 mL) in an open round-bottomed flask with vigorous stirring in a well ventilated fume cupboard. The resulting orange suspension was treated with a solution of elemental bromine (11.1 mL, 0.221 mol) in glacial acetic acid (50 mL), which was added over 30 seconds. After a further 30 seconds, the solution turned a light brown colour, and a small amount of HBr gas was liberated. The reaction mixture was subsequently heated to 30 °C which was maintained overnight. Once cooled to room temperature, the solution was filtered and the retained solid collected before being stirred in deionised water for 8 hours. The product was obtained as a white solid by filtration of this aqueous suspension to give the title compound which was pure enough for use in subsequent reactions. (29.33 g, 87 %), mp 259-261 °C dec. ^{1}H NMR [d_6-acetone, 400 MHz]: δ = 2.59-2.81 (m, 16 H, CH_2CH_2Ar), 4.50-4.53 (m, 4 H, C*H*CH_2CH_2Ar), 7.13-7.24 (m, 20 H, $CH_2CH_2C_6H_5$), 7.77 (s, 4 H, Ar *H*), 8.38 (s, 8 H, O*H*). ^{13}C NMR [d_6-acetone, 100 MHz]: δ = 149.03, 143.02, 129.42, 129.29, 126.68, 125.02, 125.57, 100.83, 37.15, 36.68, 35.33. IR (KBr): 3388*br*, 29345*w*, 1611, 14955*w*, 1468, 1454*sh*, 1342*w*, 1302, 1250*w*, 1204*w*, 1178*w*, 1152, 1087, 1028*w*, 933, 746, 696.

*7,11,15,28-Tetrabromo-1,21,23,25-tetrakis(2-phenylethyl)-2,20:3,19-dimetheno-1H,21H,23H,25H-bis[1,3]dioxocino[5,4-i:5',4'-i']benzo[1,2-d:5,4-d']-bis[1,3]benzodioxocin Stereoisomer **(31)*** **[8, 12]**

To a solution of CH_2BrCl (16.3 mL, 0.243 mol) and oven-dried (110 °C) K_2CO_3 (99.25 g, 0.718 mol) in dry, degassed DMF (700 mL), octol **30** (25.0 g, 0.0205 mol) in DMF (100 mL) was added over 1.5 hours. After stirring for 24 hours at room temperature under a nitrogen

atmosphere, CH_2BrCl (16.3 mL, 0.243 mol) was added and the solution heated to 45 °C. After a further 24 hours, a further aliquot of CH_2BrCl (16.3 mL, 0.243 mol) was added, and the solution heated to 63 °C. After 48 hours at 65 °C, the light brown solution was cooled to room temperature, and the K_2CO_3 neutralised by the addition of a 6 % HCl solution. The crude product simultaneously precipitated from solution, and was collected on filtration of the neutralized reaction mixture. The cream-coloured solid was suspended in methanol and stirred for 24 hours, before being filtered from the methanol and dried. The material was chromatographed on silica gel using a chloroform mobile phase, before being stirred once again in methanol, filtered and dried to give the title compound as an off-white solid. (25.90 g, 70 %), mp 285-290 °C dec. ^{1}H NMR [$CDCl_3$, 400 MHz]: δ = 2.47-2.49 (m, 8 H, C*H*$_2$CH$_2$Ar), 2.62-2.64 (m, 8 H, CH$_2$C*H*$_2$Ar), 4.41 (d, 4 H, inner of OC*H*$_2$O), 4.94 (t, 4 H, C*H*CH$_2$CH$_2$Ar), 5.95 (d, 4 H, outer of OC*H*$_2$O), 7.09-7.24 (m, 24 H, Ar *H* and CH$_2$CH$_2$C$_6$*H*$_5$). ^{13}C NMR [$CDCl_3$, 100 MHz]: δ = 152.84, 141.74, 139.69, 129.25, 128.92, 126.81, 119.52, 114.41, 99.03, 38.33, 34.79, 32.89. IR (KBr): 2939*w*, 1729*w*, 1602*w*, 1469*sh*, 1452, 1415, 1299, 1234, 1091, 1057*w*, 1017, 984*sh*, 957, 790*w*, 745, 699, 586.

1,21,23,25-Tetrakis(2-phenylethyl)-2,20:3,19-dimetheno-1H,21H,23H,25H-bis[1,3]dioxocino[5,4-i:5',4'-i']benzo[1,2-d:5,4-d']-bis[1,3]benzodioxocin-7,11,15,28-tetrol Stereoisomer ***(32)*** **[13]**

A solution of vacuum-dried **31** (5.0 g, 3.94 mmol) in dry THF (800 mL) was set to stir in an oven-dried round-bottomed flask under a nitrogen atmosphere, sealed with a septum. The solution was cooled to -80 °C, and treated with *n*-butyllithium (~ 1.6 M solution in hexane, 40.0 mL, 64 mmol), which was rapidly added *via* the septum using a syringe. After 1 minute, trimethyl borate (12 mL, 105 mmol) was added, so turning the solution into a dark yellow emulsion. The flask and its contents were removed from the cooling bath, and allowed to attain room temperature slowly, during which time the emulsion disappeared to yield a yellow solution. After stirring at room temperature for 1 hour, the solution was again cooled to -80 °C, and treated with 1:1 15 % H_2O_2:1.5 M NaOH (100 mL) to give a viscous, white reaction mixture. The solution was allowed to warm to ambient temperature and stirred overnight, over which time it cleared to give a clear, slightly yellow solution. Thereafter, $Na_2S_2O_5$ (20 g, 0.105 mol) was carefully added to the stirring solution, which resulted in the formation of two layers. The THF was subsequently removed *in vacuo* to yield a white solid in the residual water, which was filtered. The mixture of alcohols was preadsorbed onto silica before being subjected to

chromatography on silica gel. The gravity column (30 cm in length X 5.5 cm in diameter) was gradient eluted, starting with 100 % chloroform, accompanied by the slow addition of methanol towards a final chloroform-methanol ratio of 85:15. The tetrol title compound was exclusively isolated as the most polar fraction (R_f = 0.16, by TLC in 85 :15 chloroform:methanol) and found to be pure. (1.80 g, 45 %), mp >300 °C dec. TLC (SiO_2, 3:1 EtOAc-Hexane): R_f 0.14 (tetrol), 0.34 (triol), 0.56 (diol), 0.70 (mono-ol). ^{1}H NMR [d_6-acetone, 400 MHz]: δ = 2.55-2.2.61 (m, 8 H, C*H*$_2$CH$_2$Ar), 2.63-2.68 (m, 8 H, CH$_2$C*H*$_2$Ar), 4.42 (d, 4 H, inner of OC*H*$_2$O), 4.79 (t, 4 H, C*H*CH$_2$CH$_2$Ar), 5.83 (d, 4 H, outer of OC*H*$_2$O), 7.18-7.25 (m, 24 H, Ar *H* and CH$_2$CH$_2$C$_6$*H*$_5$), 7.96 (s, 4 H, Ar O*H*). ^{13}C NMR [d_6-acetone, 100 MHz]: δ = 143.54, 143.48, 143.33, 139.44, 129.34, 129.25, 126, 61, 111.30, 100.74, 38.17, 35.21, 33.04. IR (KBr): 3368*br*, 2938*w*, 1587, 1492, 1468, 1446*sh*, 1320, 1150, 1106, 1066, 1018, 983*sh*, 969*sh*, 735*w*, 697*sh*, 692*sh*, 591, 511.

2-(2-bromoethoxy)benzaldehyde ***(33)*** **[14]**

To a stirring solution of oven-dried (110 °C) K_2CO_3 (13.0 g, 0.0941 mol) in dry DMF (80 mL), salicylaldehyde (10.0 g, 0.0819 mol) was added so turning the solution bright yellow. After 10 minutes of stirring at room temperature, 1,2-dibromoethane (123.07 g, 0.655 mol) was added and the reaction mixture left to stir further for 3 days. Thereafter, the mixture was poured into water, and the liberated oil extracted from the aqueous emulsion with diethyl ether. The organic layer was treated with 10 % NaOH (3 times) followed by extraction with water (twice) before being dried over Na_2SO_4. The diethyl ether was evaporated, and the excess 1,2-dibromoethane reagent removed *via* high vacuum distillation. The yellow oil obtained was cooled to room temperature to yield the title compound as a yellow, crystalline solid. (13.11 g, 70 %), mp 50-52 °C. ^{1}H NMR [$CDCl_3$, 400 MHz]: δ = 3.69 (t, 2 H, OCH$_2$C*H*$_2$Br), 4.40 (t, 2 H, OC*H*$_2$CH$_2$Br), 6.94 (d, 1 H, Ar *H*), 7.04 (t, 1 H, Ar *H*), 7.52 (td, 1 H, Ar *H*), 7.81 (dd, 1 H, Ar *H*), 10.41 (s, 1 H, Ar C*H*O). ^{13}C NMR [$CDCl_3$, 100 MHz]: δ = 189.60, 160.40, 135.93, 128.48, 125.22, 121.52, 112.70, 68.23, 28.81. IR (KBr): 2863*w*, 1676, 1596, 1581*sh*, 1482, 1452, 1396, 1382, 1289, 1240*sh*, 1230*sh*, 1188, 1163, 1104, 1011, 944, 878, 827, 763, 754*sh*, 653, 567, 497, 448, 407.

*2-(2-bromopropoxy)benzaldehyde **(34)*** [14]

Application of the above procedure for **33**, using salicylaldehyde (10.0 g, 0.0819 mol) and 1,3-dibromopropane (132.26 g, 0.655 mol), yielded the title compound as a yellow oil. (19.29 g, 97 %). ^{1}H NMR [$CDCl_3$, 400 MHz]: δ = 2.37 (m, 2 H, CH_2CH_2 CH_2), 3.60 (t, 2 H, OCH_2CH_2Br), 4.21 (t, 2 H, OCH_2CH_2Br), 6.97-7.03 (m, 2 H, Ar *H*), 7.52 (td, 1 H, Ar *H*), 7.81 (dd, 1 H, Ar *H*), 10.45 (s, 1 H, Ar C*H*O). ^{13}C NMR [$CDCl_3$, 100 MHz]: δ = 189.57, 161.01, 136.11, 128.63, 124.95, 121.06, 112.58, 65.92, 32.10, 29.74. IR (KBr): 2870*w*, 1726*sh*, 1683, 1597, 1583*sh*, 1485, 1456, 1386, 1283, 1237, 1189, 1160, 1102, 1041*sh*, 1021, 928, 836, 808*w*, 753, 647, 599, 563, 501, 439.

*Tetrasalicylaldehyde **35***

To a stirring solution of oven-dried (110 °C) K_2CO_3 (0.69 g, 5.00 mmol) in dry DMF (40 mL), dry **32** (0.50 g, 0.490 mmol) was added and stirred until completely dissolved. To the resulting light yellow solution, **33** (0.90 g, 3.93 mmol) was added and the reaction mixture gently heated at 55 °C for three days. During this period, the solution became yellow and cloudy, with a white precipitate deposited on the sides of the reaction vessel. The mixture was cooled to room temperature, at which time the unreacted K_2CO_3 and the white precipitate gravity-filtered from the solution. The filtrate was collected, and the DMF removed *in vacuo*, yielding a dark yellow, oily residue. Methanol was added to the residue to remove excess **33** and precipitate out the title compound. The resultant white suspension was stirred overnight, and the title compound was obtained by filtration from the methanol as a pure, white powder. (0.74 g, 93 %), mp 106-108 °C dec. ^{1}H NMR [$CDCl_3$, 400 MHz]: δ = 2.39-2.46 (m, 8 H, CH_2CH_2Ar), 2.59-2.63 (m, 8 H, CH_2CH_2Ar), 4.33 (m, 20 H, inner of OCH_2O and OCH_2CH_2O), 4.72 (t, *J* = 7.8 Hz, 4 H, $CHCH_2CH_2Ar$), 5.64 (d, *J* = 7.1 Hz, 4 H, outer of OCH_2O), 6.80 (s, 4 H, cavitand Ar *H*), 6.99 (m, 4 H, Ar *H*), 7.16 (m, 4 H, Ar *H*), 7.18-7.24 (m, 20 H, $CH_2CH_2C_6H_5$), 7.52 (td, *J* = 7.8 Hz, *J* = 1.8 Hz, 4 H, Ar *H*), 7.80 (dd, *J* = 7.9 Hz, *J* = 1.7 Hz, 4 H, Ar *H*), 10.31 (s, 4 H, Ar C*H*O). ^{13}C NMR [$CDCl_3$, 100 MHz]: δ = 189.97, 161.36, 148.42, 144.38, 141.93, 138.95, 136.04, 128.26, 128.04, 126.12, 125.19, 121.05, 114.49, 112.91, 99.43, 71.58, 68.32, 37.19, 34.52, 32.36. IR (KBr): 2939*w*, 2870*w*, 1683, 1599, 1480, 1455*sh*, 1438, 1315, 1286, 1188*w*, 1155, 1103, 1018, 980, 938*sh*, 831, 752, 697, 654*w*, 587. Anal Calcd for $C_{100}H_{88}O_{20}$ (1609.77): C 74.61, H 5.51. Found: C 74.73, H 5.57.

*Tetrasalicylaldehyde **36***

Application of the above procedure for **35**, using dry **32** (0.50 g, 0.490 mmol) and **34** (0.95 g, 3.93 mmol), yielded the title compound as a pure, white powder. (0.66 g, 81 %), mp 96-100 °C dec. ^{1}H NMR [$CDCl_3$, 400 MHz]: δ = 2.13-2.16 (mt, *J* = 6.0 Hz, 8 H, $CH_2CH_2CH_2$), 2.41-2.45 (m, 8 H, CH_2CH_2Ar), 2.60-2.64 (m, 8 H, CH_2CH_2Ar), 4.14 (t, *J* = 5.8 Hz, 8 H, CH_2CH_2O), 4.25 (t, *J* = 6.0 Hz, 8 H, CH_2CH_2O), 4.33 (d, *J* = 7.1 Hz, 4 H, inner of OCH_2O), 4.74 (t, *J* = 7.9 Hz, 4 H, $CHCH_2CH_2Ar$), 5.63 (d, *J* = 7.1 Hz, 4 H, outer of OCH_2O), 6.79 (s, 4 H, cavitand Ar *H*), 6.98 (m, 4 H, Ar *H*), 7.13 (m, 4 H, Ar *H*), 7.18-7.24 (m, 20 H, $CH_2CH_2C_6H_5$), 7.50 (td, *J* = 7.8 Hz, *J* = 1.8 Hz, 4 H, Ar *H*), 7.81 (dd, *J* = 7.9 Hz, *J* = 1.9 Hz, 4 H, Ar *H*), 10.48 (s, 4 H, Ar C*H*O). ^{13}C NMR [$CDCl_3$, 100 MHz]: δ = 189.88, 161.48, 148.49, 144.44, 141.89, 138.90, 136.11, 128.72, 128.56, 126.17, 125.10, 120.85, 114.23, 112.61, 99.51, 70.00, 65.29, 37.21, 34.60, 32.52, 30.00. IR (KBr): 2944*w*, 1684, 1598, 1456*sh*, 1438*sh*, 1387*w*, 1285, 1240, 1188*w*, 1152, 1103, 1047, 1018, 976, 841*w*, 754, 698, 588. Anal Calcd for $C_{104}H_{96}O_{20}$ (1665.87): C 74.98, H 5.81. Found: C 75.19, H 5.90.

*Cavitand-capped porphyrin **37** (reflux, Adler conditions)*

Propionic acid (200 mL) was stirred in a 250 mL round-bottomed flask, and heated to reflux in air. Once gently refluxing, **35** (0.20 g, 0.12 mmol) was added to the reaction vessel and left to dissolve. On dissolution, the reaction vessel was shielded from light, and freshly distilled pyrrole **9** (0.0330 g, 0.49 mmol) added to the solution. Over a period of approximately 10 minutes, the reaction mixture went black. Reflux continued for a further 20 minutes, at which time the heating ceased, and the reaction was left to stir while slowly attaining room temperature. Stirring continued overnight, and the vessel contents poured into a separating funnel. Water, saturated with $NaHCO_3$, and CH_2Cl_2 (100 mL) was added to the separating funnel, and the reaction mixture subsequently extracted *carefully*. The extraction of the organic layer was repeated once more with aqueous $NaHCO_3$, and after effervescence subsided completely, the organic layer was dried over Na_2SO_4, filtered and preadsorbed onto silica (3 g). Silica gel chromatography using a benzene eluant afforded a purified purple material. Once the benzene was removed, the purple residue was dissolved in a small amount of $CHCl_3$, and methanol allowed to slowly diffuse into the solution in order to recrystallise the title compound. After 2 days, **37** was isolated as a dark purple, microcrystalline solid. (0.023 g, 11 %), mp >300 °C. ^{1}H NMR [$CDCl_3$, 400 MHz]: δ = -2.88 (s, 2 H, N*H*), 2.12-2.18 (m, 8 H, CH_2CH_2Ar), 2.38-

2.43 (m, 8 H, CH_2CH_2Ar), 3.14 (d, *J* = 7.3 Hz, 4 H, inner of OCH_2O), 3.48 (t, *J* = 5.6 Hz, OCH_2CH_2O), 4.35 (t, *J* = 5.5 Hz, OCH_2CH_2O), 4.42 (t, *J* = 7.9 Hz, 4 H, $CHCH_2CH_2Ar$), 5.12 (d, *J* = 7.3 Hz, 4 H, outer of OCH_2O), 6.36 (s, 4 H, cavitand Ar *H*), 6.95-6.99 (m, 8 H, $CH_2CH_2C_6H_5$), 7.09-7.12 (m, 12 H, $CH_2CH_2C_6H_5$), 7.31-7.36 (m, 4 H, Ar *H*), 7.42 (d, *J* = 8.4 Hz, 4 H, Ar *H*), 7.77 (td, *J* = 7.3 Hz, *J* = 1.8 Hz, 4 H, Ar *H*), 7.85 (dd, *J* = 7.4 Hz, *J* = 1.7 Hz, 4 H, Ar *H*), 8.71, 8.82 (both s, 8 H, *H*C(β) of pyrrole). ^{13}C NMR [$CDCl_3$, 100 MHz]: δ = 158.10, 158.03, 149.99, 146.76, 143.41, 141.58, 138.15, 138.07, 136.52, 131.49, 129.76, 128.44, 128.27, 125.89, 119.93, 115.49, 112.90, 112.13, 99.24, 71.29, 67.87, 36.58, 34.20, 32.22. IR (KBr): 2923*w*, 1598*w*, 1578*w*, 1468, 1437, 1313, 1245, 1209, 1151, 1112, 1048, 1021, 978, 874*w*, 797, 748, 697, 650*w*, 586, 481. UV-Vis ($CHCl_3$): 647, 588, 547, 513, 419 (Soret), 398.53, 399*sh*. MS (ESI-TOF) Calcd for $C_{116}H_{94}O_{16}N_4$: 1800.6771. Found: 1800.5112.

*Cavitand-capped porphyrin **37** (microwave heating, Adler conditions)*

Propionic acid (4 mL) was added to a borosilicate microwave reaction tube containing **35** (0.076 g, 0.05 mmol). Once the material dissolved, freshly distilled pyrrole **9** (0.0138 g, 0.20 mmol) was added, together with a small stirrer bar, and the tube sealed with a Teflon-lined cap. The tube was inserted into the microwave heating unit, and heated rapidly whilst stirring to 160 °C. Once the temperature had been attained, it was maintained for five minutes, after which time the tube was allowed to cool to room temperature. The vessel was removed from the microwave, shielded from light and its cap removed, before being allowed to stir overnight in air. The vessel contents were then poured into a separating funnel. Water, saturated with $NaHCO_3$, and CH_2Cl_2 (100 mL) were added, and the reaction mixture extracted *carefully*. The extraction of the organic layer was repeated once more with aqueous $NaHCO_3$, and after effervescence subsided completely, the organic layer was dried over Na_2SO_4, filtered and preadsorbed onto silica (2 g). Silica gel chromatography using a benzene eluant afforded a purified purple material. Once the benzene was removed, the purple residue was dissolved in a small amount of $CHCl_3$, and methanol allowed to slowly diffuse into the solution in order to recrystallise the title compound. After a day, **37** was isolated as a dark purple, microcrystalline solid. (0.020 g, 23 %)

*Cavitand-capped porphyrin **38** (microwave heating, Adler conditions)*

Propionic acid (4 mL) was added to a borosilicate microwave reaction tube containing **36** (0.077 g, 0.05 mmol). Once the material dissolved, freshly distilled pyrrole **9** (0.0138 g, 0.20 mmol) was added, together with a small stirrer bar, and the tube sealed with a Teflon-lined cap. The tube was inserted into the microwave heating unit, and heated rapidly whilst stirring to 160 °C. Once the temperature had been obtained, it was maintained for five minutes, after which time the tube was allowed to cool to room temperature. The vessel was removed from the microwave, shielded from light and its cap removed, before being allowed to stir overnight in air. The vessel contents were then poured into a separating funnel. Water, saturated with $NaHCO_3$, and CH_2Cl_2 (100 mL) was added, and the reaction mixture extracted *carefully*. The extraction of the organic layer was repeated once more with aqueous $NaHCO_3$, and after effervescence subsided completely, the organic layer was dried over Na_2SO_4, filtered and preadsorbed onto silica (2 g). Silica gel chromatography using a 95:5 chloroform:ethyl acetate eluant afforded a purified purple material. This material was preadsorbed once more onto silica, before being subjected to column chromatography using a benzene eluant. This yielded a purple, oily residue upon removal of the benzene. Methanol was added to precipitate out the purified capped porphyrin, which was filtered from the methanol and carefully collected. The material was dissolved in a small amount of $CHCl_3$, and methanol allowed to slowly diffuse into the solution in order to recrystallise the title compound. Recrystallisation was repeated, and after three days, **38** was isolated as a dark purple, microcrystalline solid. (0.014 g, 15 %), mp >300 °C. ^{1}H NMR [$CDCl_3$, 400 MHz]: δ = -2.82 (s, 2 H, N*H*), 1.87 (m, 8, $OCH_2CH_2CH_2O$), 2.14-2.19 (m, 8 H, CH_2CH_2Ar), 2.40-2.43 (m, 8 H, CH_2CH_2Ar), 3.29 (d, *J* = 7.4 Hz, 4 H, inner of OCH_2O), 3.44 (t, *J* = 5.6 Hz, $OCH_2CH_2CH_2O$), 4.19 (t, *J* = 5.7 Hz, $OCH_2CH_2CH_2O$), 4.44 (t, *J* = 8.2 Hz, 4 H, $CHCH_2CH_2Ar$), 5.16 (d, *J* = 7.4 Hz, 4 H, outer of OCH_2O), 6.39 (s, 4 H, cavitand Ar *H*), 6.95-6.97 (m, 8 H, $CH_2CH_2C_6H_5$), 7.09-7.10 (m, 12 H, $CH_2CH_2C_6H_5$), 7.30 (t, *J* = 7.4 Hz, 4 H, Ar *H*), 7.38 (d, *J* = 8.5 Hz, 4 H, Ar *H*), 7.72 (t, *J* = 7.5 Hz, 4 H, Ar *H*), 7.85 (dd, *J* = 7.3 Hz, *J* = 1.0 Hz, 4 H, Ar *H*), 8.73 (s, 8 H, *H*C(β) of pyrrole). ^{13}C NMR [$CDCl_3$, 100 MHz]: δ = 158.40, 147.16, 143.79, 141.67, 138.15, 136.89, 132.03, 130.87, 129.66, 128.81, 128.44, 128.28, 125.87, 119.88, 115.80, 113.28, 112.86, 99.15, 69.30, 68.17, 65.80, 38.75, 36.66, 34.29, 32.15, 30.74. IR (KBr): 2922, 2852*w*, 1598*w*, 1578*w*, 1469, 1438, 1316, 1255, 1209*w*, 1153, 1106, 1049, 1020*w*, 966, 800, 750, 697, 648*w*, 587, 484. UV-Vis ($CHCl_3$): 647, 591, 549, 515, 420 (Soret), 400*sh*. MS (ESI-TOF) Calcd for $C_{120}H_{102}O_{16}N_4$: 1856.7397. Found: 1856.5912.

*2-chloromethoxybenzaldehyde **(39)*** [15]

To a stirring solution of oven-dried (110 °C) K_2CO_3 (6.50 g, 0.0471 mol) in dry DMF (80 mL), salicylaldehyde (5.0 g, 0.0410 mol) was added so turning the solution bright yellow. After 10 minutes of stirring at room temperature, bromochloromethane (42.44 g, 0.328 mol) was added and the reaction mixture left to stir further for 3 days. Thereafter, the mixture was poured into water, and the liberated oil extracted from the aqueous emulsion with diethyl ether. The organic layer was treated with 10 % NaOH (3 times) followed by extraction with water (twice) before being dried over Na_2SO_4. The diethyl ether was evaporated, and the excess bromochloromethane reagent removed under reduced pressure to give a white, crystalline solid. (4.68 g, 67 %), mp 118-120 °C. ^{1}H NMR [$CDCl_3$, 400 MHz]: δ = 6.02 (s, 2 H, C*H*$_2$), 7.14-7.20 (m, 1 H, Ar *H*), 7.34-7.43 (m, 1 H, Ar *H*), 7.58-7.66 (m, 1 H, Ar *H*), 7.85-7.94 (m, 1 H, Ar *H*), 10.47 (s, 1 H, Ar C*H*O). ^{13}C NMR [$CDCl_3$, 100 MHz]: δ = 189.58, 157.36, 136.35, 128.95, 126.47, 123.02, 115.70, 91.57. IR (KBr): 2863, 1687, 1597, 1582*sh*, 1479, 1459, 1414, 1388, 1284, 1215, 1194, 1159, 1101, 1004, 829, 753, 643, 580, 41414, 1388, 1284, 1215, 1194, 1159, 1101, 1004, 829, 753, 643, 580, 479, 438.

*Tetrasalicylaldehyde **40***

To a stirring solution of **32** (0.50 g, 0.490 mmol) in dry THF (50 mL) under a nitrogen atmosphere, NaH (60% suspension in mineral oil, 0.16 g, 6.53 mmol) was added. To the resulting cream-coloured solution, **39** (0.68 g, 4.0 mmol) was added and the solution gently heated to reflux. The reaction continued for 3 days, during which time the solution assumed a grey colour. TLC, using a mobile phase of 1:1 hexane-ethyl acetate, showed the desired product (R_f = 0.40) in addition to excess **39** (R_f = 0.60). After 3 days, the reaction mixture was cooled to room temperature, and concentrated on a rotary evaporator. The products were chromatographed on silica gel using a mobile phase of 1:1 hexane-ethyl acetate. The eluant was concentrated on a rotary evaporator to give a yellow residue. Trituration of this residue with hexane yielded a white solid, which was subsequently stirred in methanol to remove residual **39**. Filtration of this solution yielded the title compound as a white solid. (0.26 g, 34 %), mp 113-115 °C dec. ^{1}H NMR [$CDCl_3$, 400 MHz]: δ = 2.43-2.49 (m, 8 H, C*H*$_2$CH$_2$Ar), 2.64-2.68 (m, 8 H, CH$_2$C*H*$_2$Ar), 4.44 (d, *J* = 6.8 Hz, 4 H, inner of cavitand OC*H*$_2$O), 4.79 (t, *J* = 7.9 Hz, 4 H, C*H*CH$_2$CH$_2$Ar), 5.39 (s, 4 H, OC*H*$_2$O), 5.96-5.99 (m, 8 H, outer of cavitand OC*H*$_2$O and extra-annular OC*H*$_2$O), 6.66 (s, 4 H, cavitand Ar *H*), 7.12-7.22 (m, 24 H, CH$_2$CH$_2$C$_6$*H*$_5$ and Ar *H*),

7.35 (d, *J* = 8.4 Hz, 4 H, Ar *H*), 7.59 (t, *J* = 7.8 Hz, 4 H, Ar *H*), 7.84 (d, *J* = 7.7 Hz, 4 H, Ar *H*), 10.44 (s, 4 H, Ar C*H*O). ^{13}C NMR [d_6-acetone, 100 MHz]: δ = 189.27, 143.57, 143.50, 143.39, 143.34, 143.28, 139.46, 136.92, 129.36, 129.26, 128.76, 126.62, 123.62, 116.45, 111.33, 100.76, 91.60, 38.19, 35.24, 33.05. IR (KBr): 2933, 1690, 1599, 1492*w*, 1461, 1444, 1319*w*, 1244, 1209, 1149, 1102, 1067, 977, 832*w*, 752, 697, 645*w*, 590, 512*w*. Anal Calcd for $C_{96}H_{80}O_{20}$ (1553.66): C 74.22, H 5.19. Found: C 74.57, H 5.26.

7,11,15,28-Tetra(3-bromopropoxy)-1,21,23,25-tetrakis(2-phenylethyl)-2,20:3,19-dimetheno-1H,21H,23H,25H-bis[1,3]dioxocino[5,4-i:5',4'-i']benzo[1,2-d:5,4-d']-bis[1,3]benzodioxocin Stereoisomer ***(42)***

To a stirring solution of oven-dried (110 °C) K_2CO_3 (0.69 g, 5.00 mmol) in dry DMF (40 mL), dry **32** (0.50 g, 0.490 mmol) was added and stirred until completely dissolved. To the resulting light yellow solution, 1,3-dibromopropane (0.79 g, 3.93 mmol) was added and the reaction mixture gently heated at 50 °C for three days. During this period, the solution became yellow and cloudy, with a white precipitate deposited on the sides of the reaction vessel. The mixture was cooled to room temperature, at which time the unreacted K_2CO_3 and the white precipitate gravity-filtered from the solution. The filtrate was collected, and the DMF removed *in vacuo*, yielding a dark yellow, oily residue. Methanol was added to the residue to remove excess 1,3-dibromopropane and precipitate out the title compound. The resultant white suspension was stirred overnight, and the title compound was obtained by filtration from the methanol as a pure, white powder. (0.46 g, 63 %), mp 110-113 °C dec. ^{1}H NMR [$CDCl_3$, 400 MHz]: δ = 2.11-2.19 (m, 8 H, $CH_2CH_2CH_2$), 2.42-2.48 (m, 8 H, CH_2CH_2Ar), 2.64-2.68 (m, 8 H, CH_2CH_2Ar), 3.59 (t, *J* = 6.5 Hz, 8 H, $OCH_2CH_2CH_2Br$), 4.07(t, *J* = 5.5 Hz, 8 H, $OCH_2CH_2CH_2Br$), 4.38 (d, *J* = 7.0 Hz, 4 H, inner of OCH_2O), 7.11-7.20 (m, 20 H, $CH_2CH_2C_6H_5$). ^{13}C NMR [$CDCl_3$, 100 MHz]: δ = 148.46, 144.20, 141.73, 138.75, 128.59, 128.43, 126.04, 114.12, 99.43, 70.87, 37.04, 34.48, 33.31, 32.37, 30.25. IR (KBr): 2937*w*, 1470, 1438, 1316, 1150, 1104*w*, 1018, 979, 749*w*, 698, 587, 485. Anal Calcd for $C_{76}H_{76}O_{12}Br_4$ (1501.03): C 60.81, H 5.10 Br 21.29. Found: C 61.02, H 5.25 Br 21.35.

REFERENCES

1. D.J. Cram, S. Karbach, H-E Kim, C.B. Knobler, E.F. Maverick, J.L. Ericson, R.C. Helgeson, *J. Am. Chem. Soc.*, **1988**, *110*, 2229-2237.
2. E. Roman, C. Peinador, S. Mendoza, A.E. Kaifer, *J. Org. Chem.*, **1999**, *64*, 2577-2578.
3. T.N. Sorrell, F.C. Pigge, *J. Org. Chem.*, **1993**, *58*, 784-785.
4. L. Huang, Y. Chen, G-Y. Gao, X.P. Zhang, *J. Org. Chem.*, **2003**, *68*, 8179-8184.
5. B. Staubli, H. Fretz, U. Piantini, W-D Woggon, *Helv. Chim. Acta*, **1987**, *70*, 1173-1193.
6. L. M. Tunstad, J.A. Tucker, E. Dalcanale, J. Weiser, J.A. Bryant, J.C. Sherman, R.C. Helgeson, C.B. Knobler, D.J. Cram, *J. Org. Chem.*, **1989**, *54*, 1305-1312.
7. J.S. Gardner, Q.P. Peterson, J.O. Walker, B.D. Jensen, B. Adhikary, R.G. Harrison, J.D. Lamb, *J. Membr. Sci.*, **2006**, 165-176.
8. J.A. Bryant, M.T. Blanda, M. Vincenti, D.J. Cram, *J. Am. Chem. Soc.*, **1991**, *113*, 2167-2172.
9. H. Boeriggter, W. Verboom, D.N. Reinhoudt, *J. Org. Chem.*, **1997**, *62*, 7148-7155.
10. ***a)*** J. Nakazawa, J. Hagiwara, M. Mizuki, Y. Shimazaki, F. Tani, Y. Naruta, *Angew. Chem. Int. Ed. Engl*., **2005**, *44*, 3744-3746; ***b)*** J. Nakazawa, J. Hagiwara, M. Mizuki, Y. Shimazaki, F. Tani, Y. Naruta, *Bull. Chem. Soc. Jpn.*, **2006**, *79*, 1431-1443.
11. B. Noll, F. Weinhelt, H. Weinhelt, S. Hauptmann, G. Mann, D. Herhardt, W. Mertens, VEB Chemiekombinat Bitterfield, Germany, Ger (East), **1991**, Patent no. DD 287481.
12. A.R. Mezo, J.C. Sherman, *J. Org. Chem.*, **1998**, *63*, 6824-6829.
13. J.C. Sherman, C.B. Knobler, D.J. Cram, *J. Am. Chem. Soc.*, **1991**, *113*, 2194-2204.
14. H. Nate, K. Matsuki, A. Tsunashima, H. Ohtsuka, Y. Sekine, K. Oda, Y. Honma, A. Ishida, H. Nakai, H. Wada, M. Takeda, H. Yabana, Y. Hino, T. Nagao, *Chem. Pharm. Bull.*, **1987**, *35*, 2394-2411.
15. R. Ringom, T. Benneche, *Acta Chim. Scand.*, **1999**, *53*, 41-47.

APPENDICES

APPENDIX 1

Spectroscopic Data

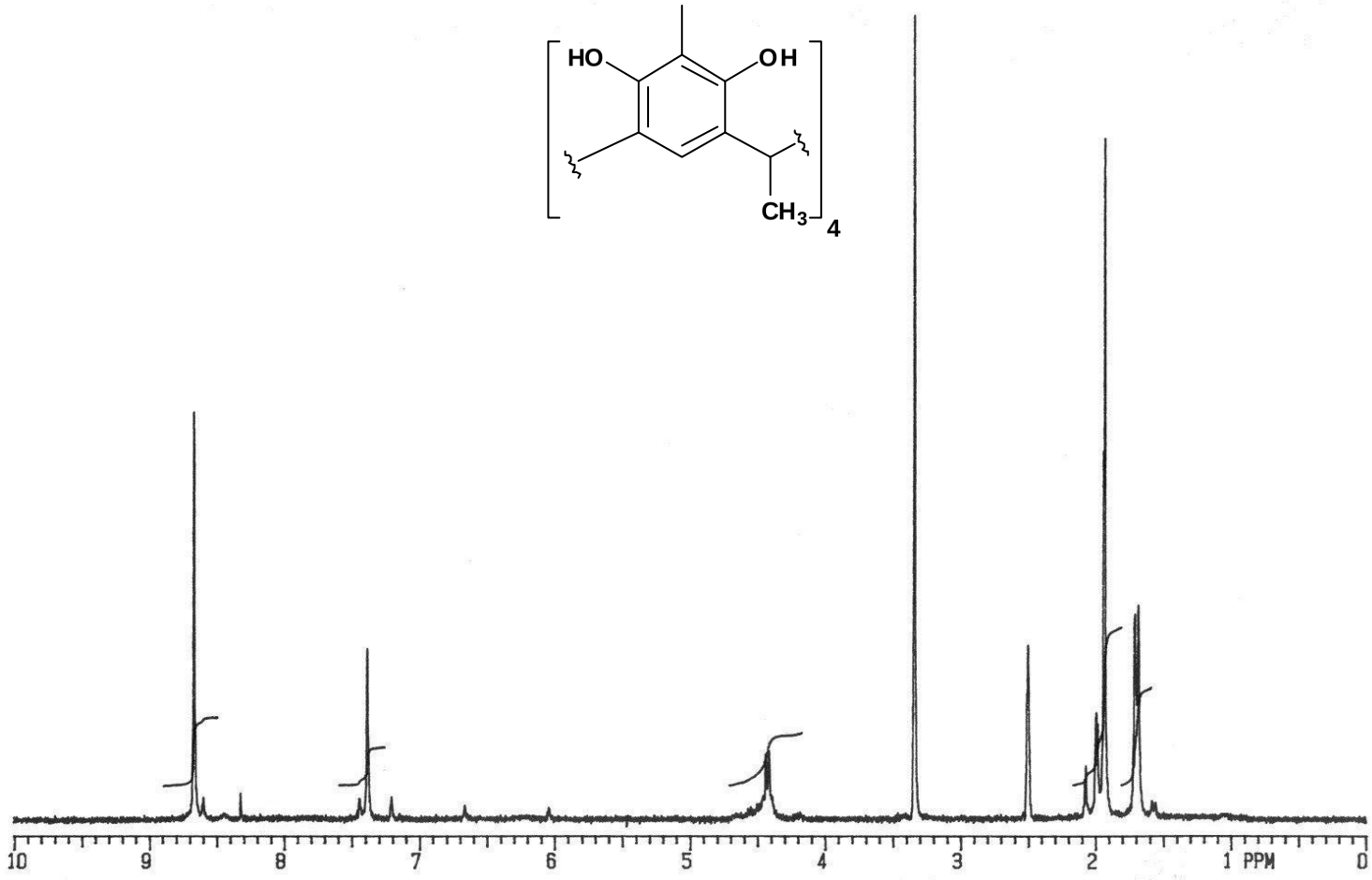

Spectrum 1.1: ^{1}H NMR spectrum of 3 in d_6-DMSO (300 MHz)

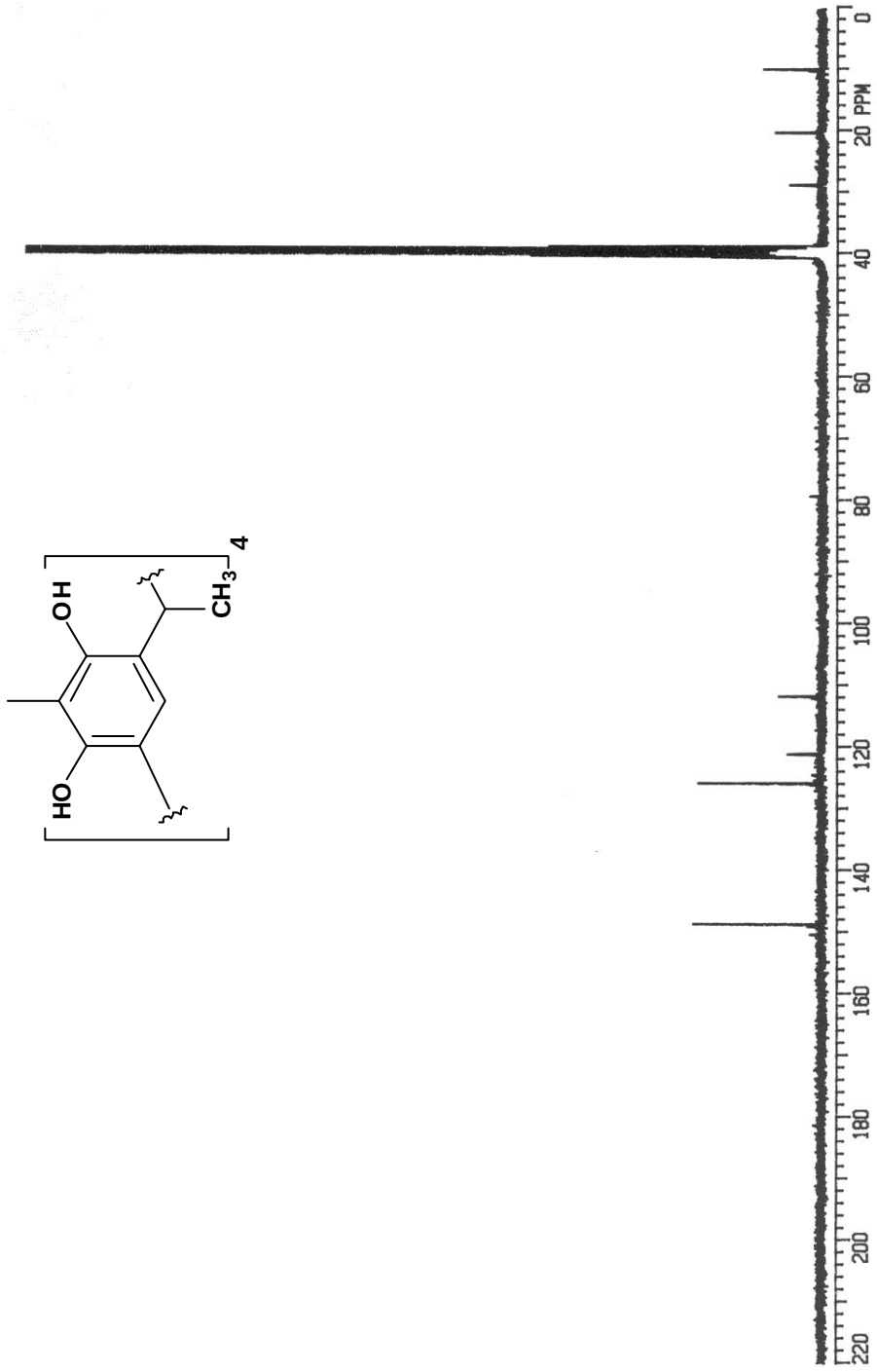

Spectrum 1.2: ^{13}C NMR spectrum of 3 in d_6-DMSO (75 MHz)

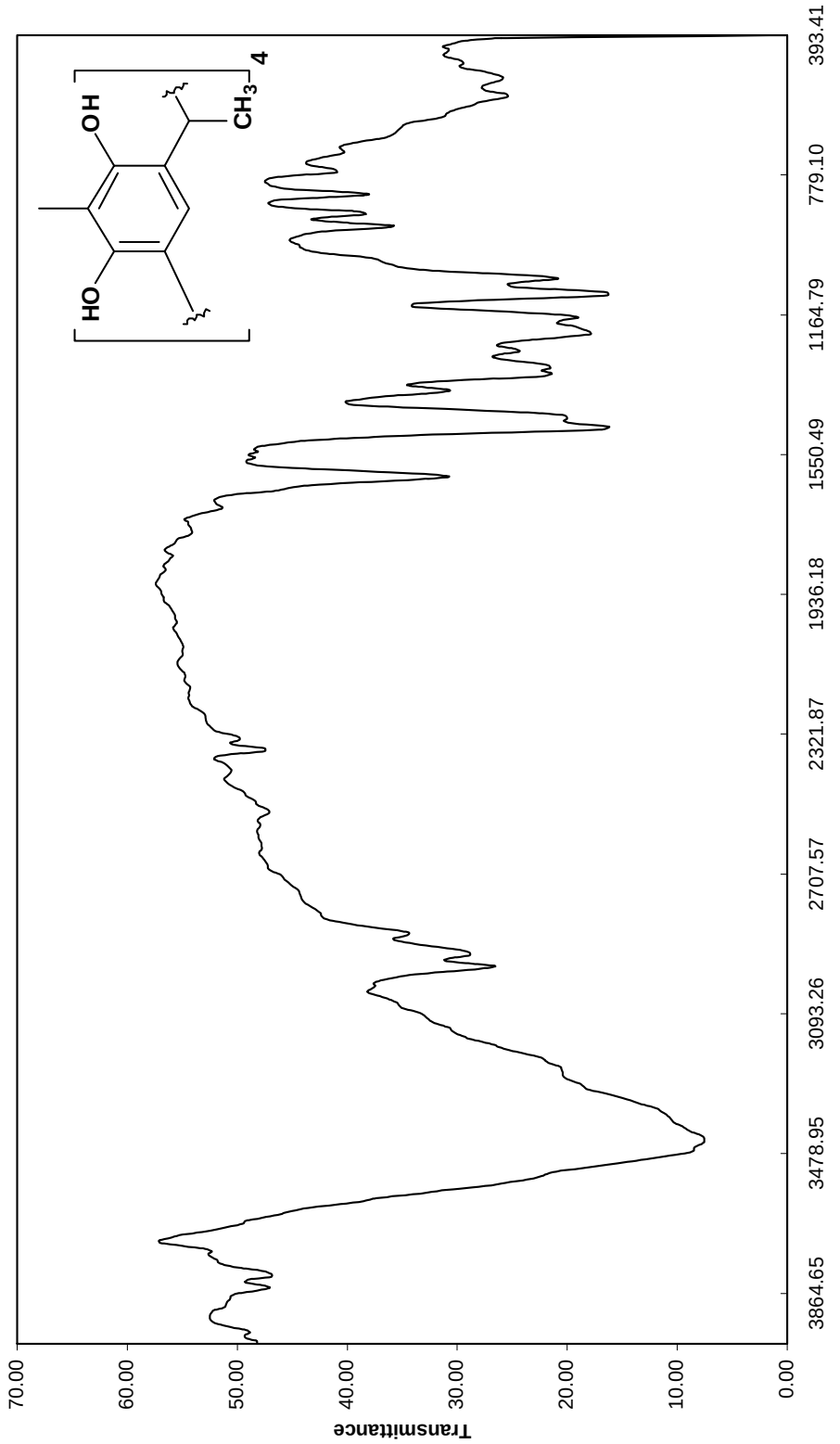

Spectrum 1.3: Infrared spectrum of 3 (KBr)

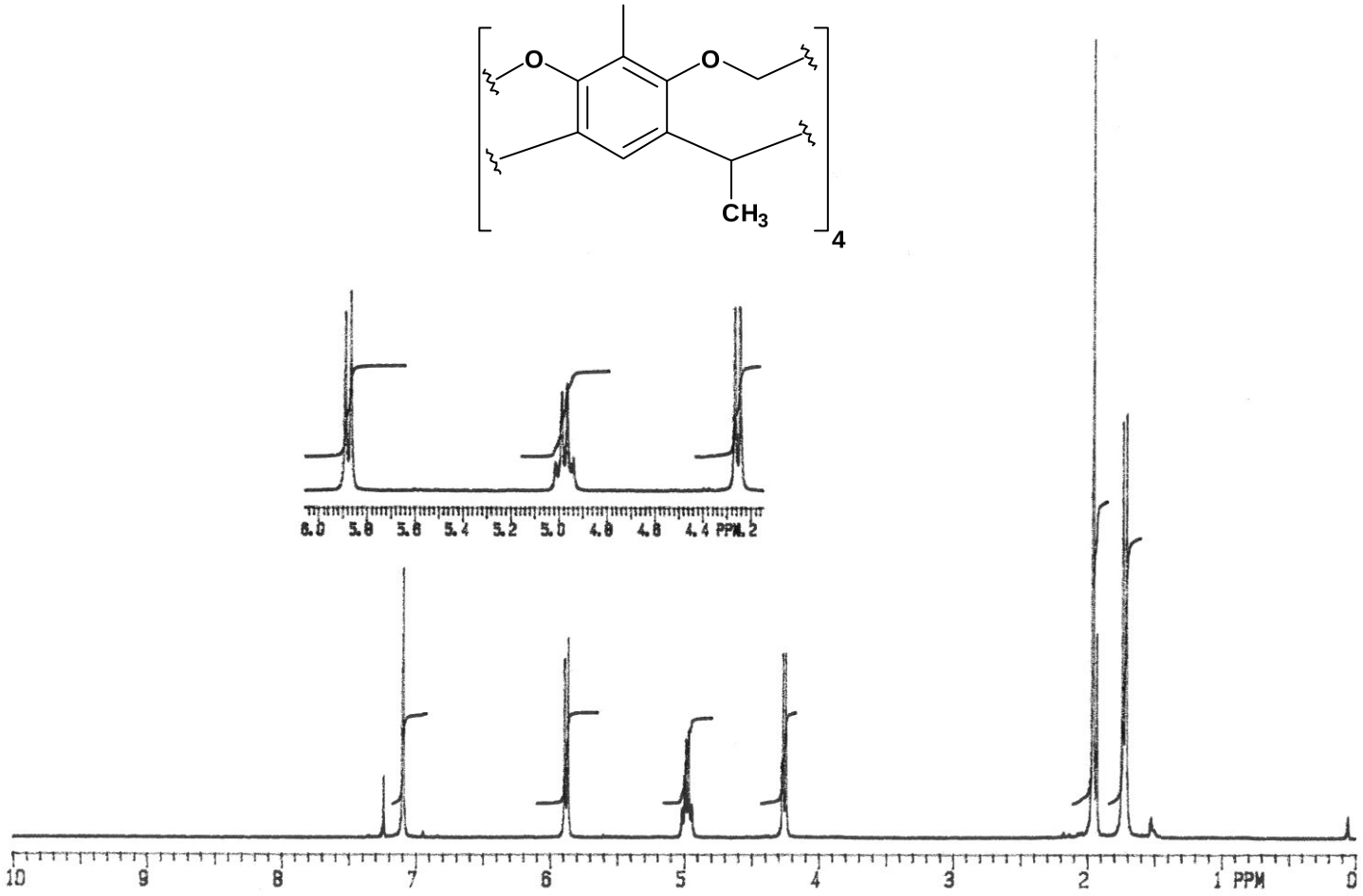

Spectrum 1.4: ^{1}H NMR spectrum of 4 in $CDCl_3$ (300 MHz)

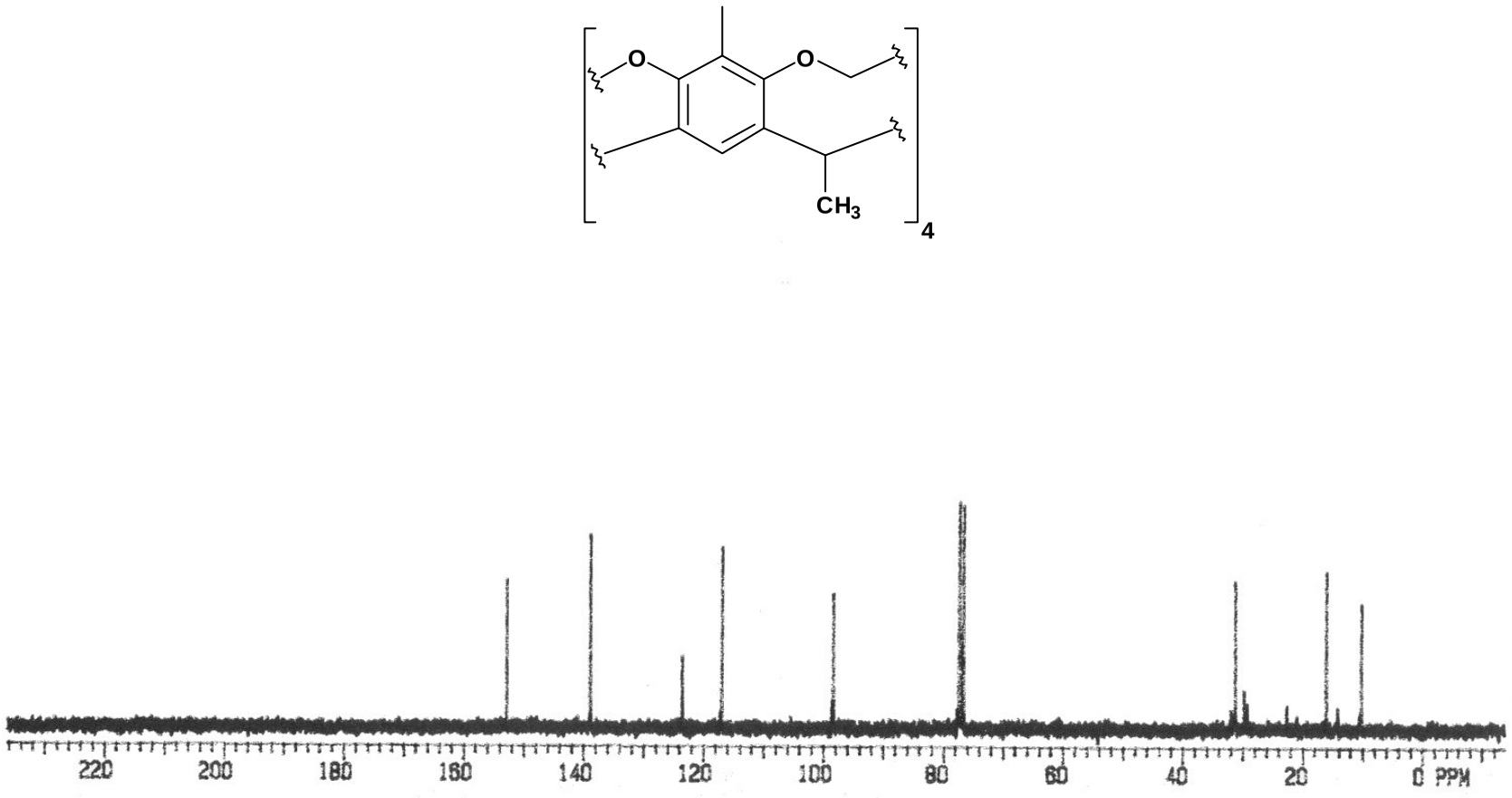

Spectrum 1.5: ^{13}C NMR spectrum of 4 in $CDCl_3$ (75 MHz)

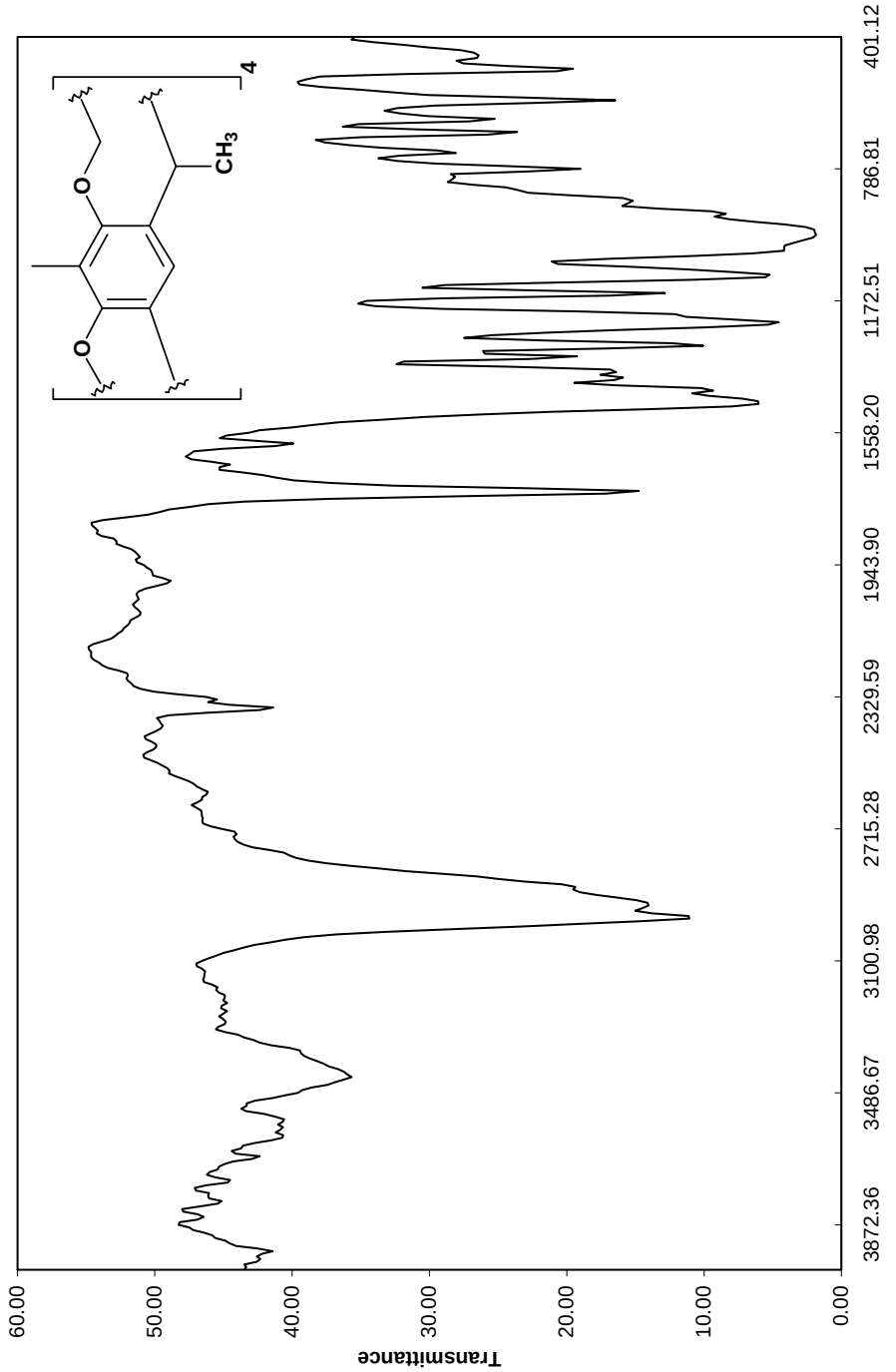

Spectrum 1.6: Infrared spectrum of 4 (KBr)

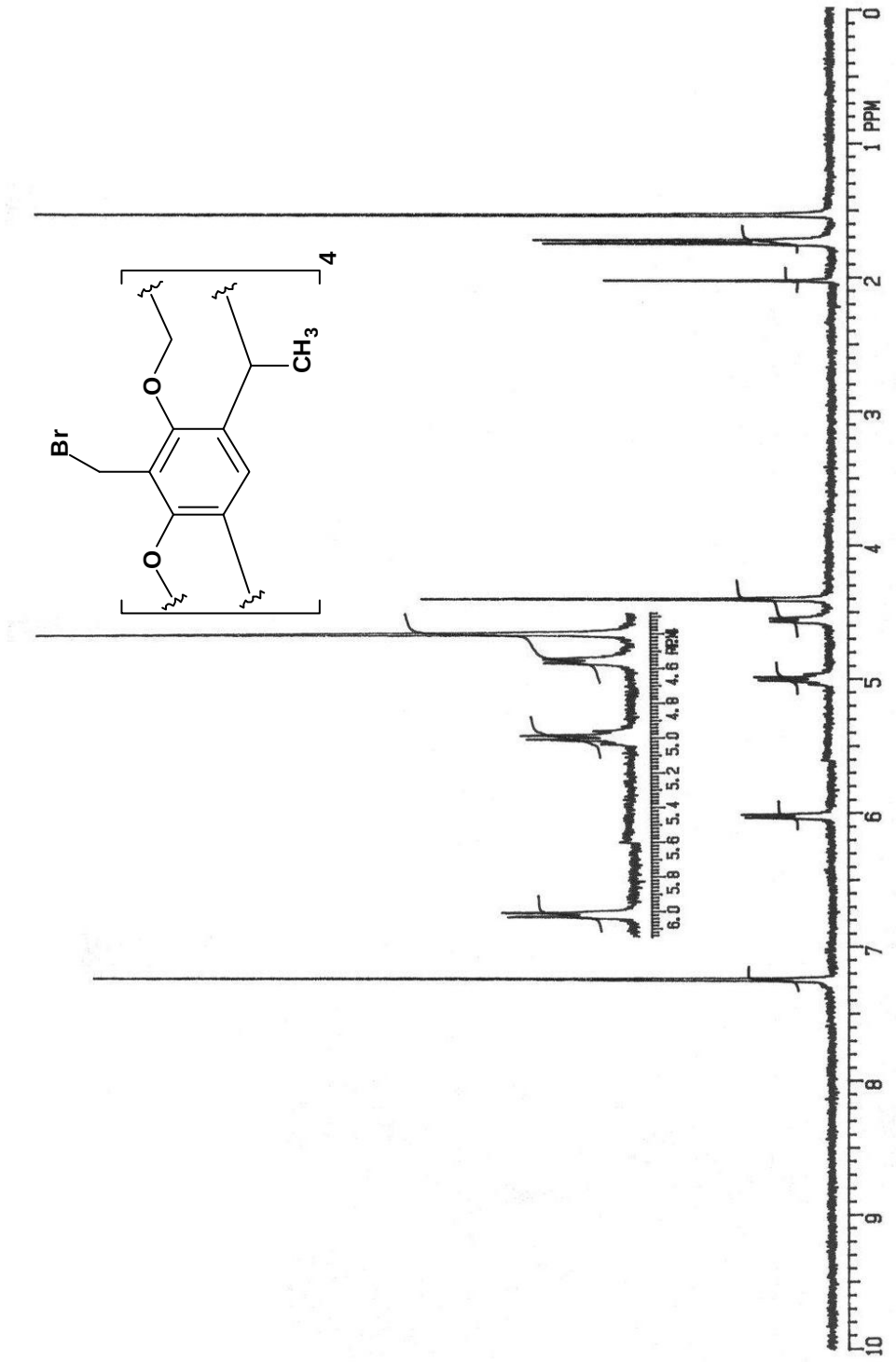

Spectrum 1.7: ^{1}H NMR spectrum of 5 in $CDCl_3$ (300 MHz)

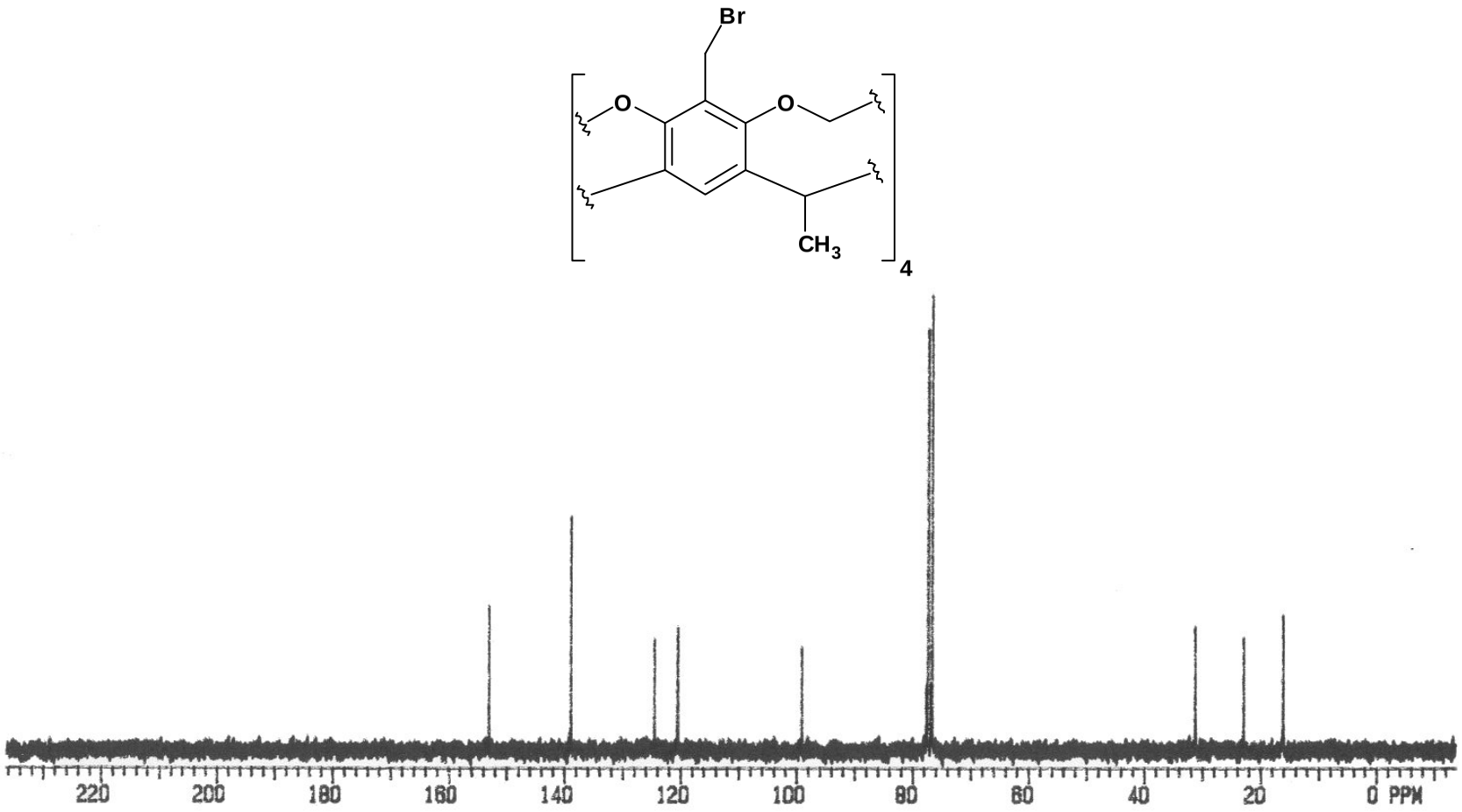

Spectrum 1.8: ^{13}C NMR spectrum of 5 in $CDCl_3$ (75 MHz)

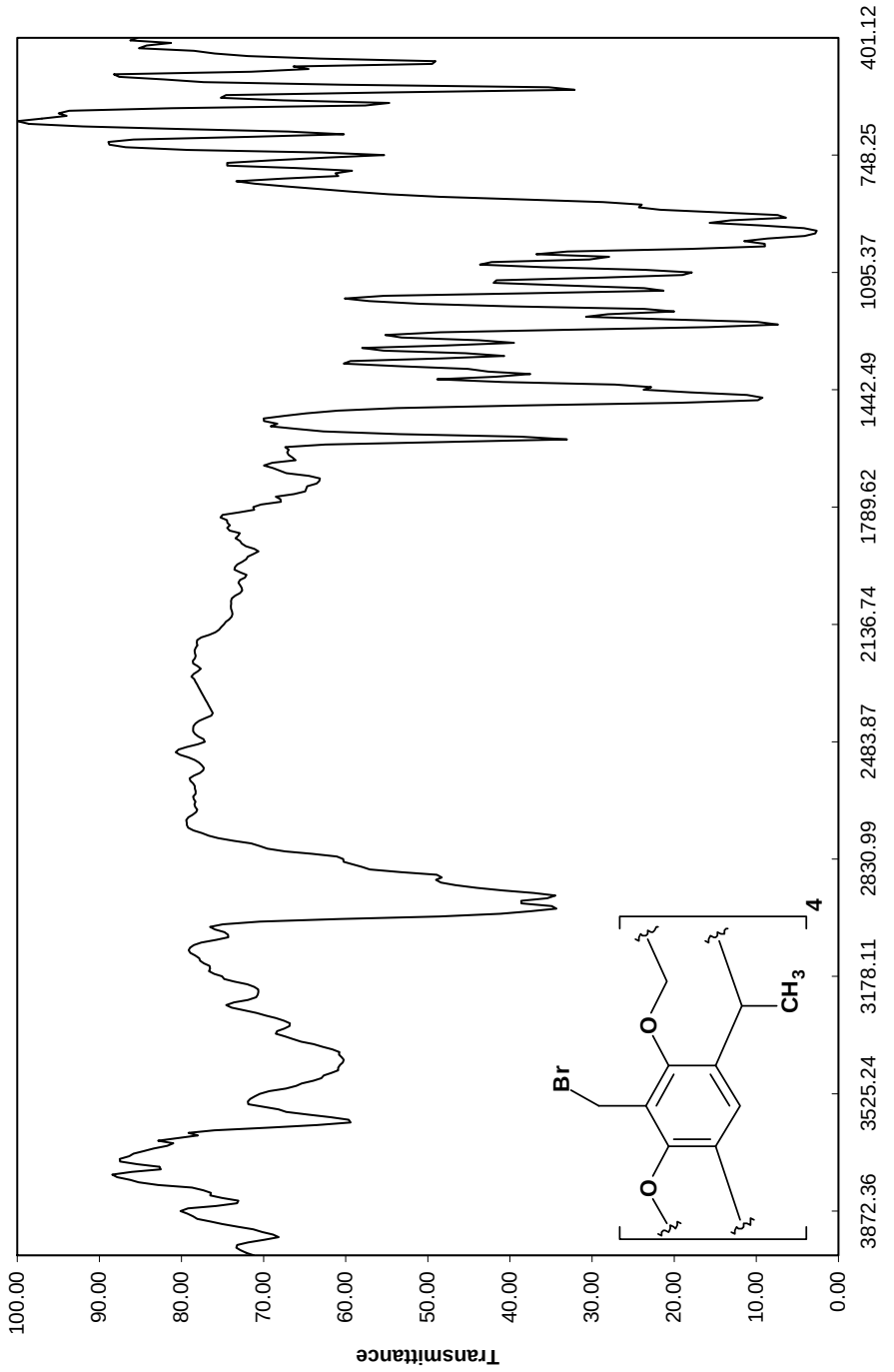

Spectrum 1.9: Infrared spectrum of 5 (KBr)

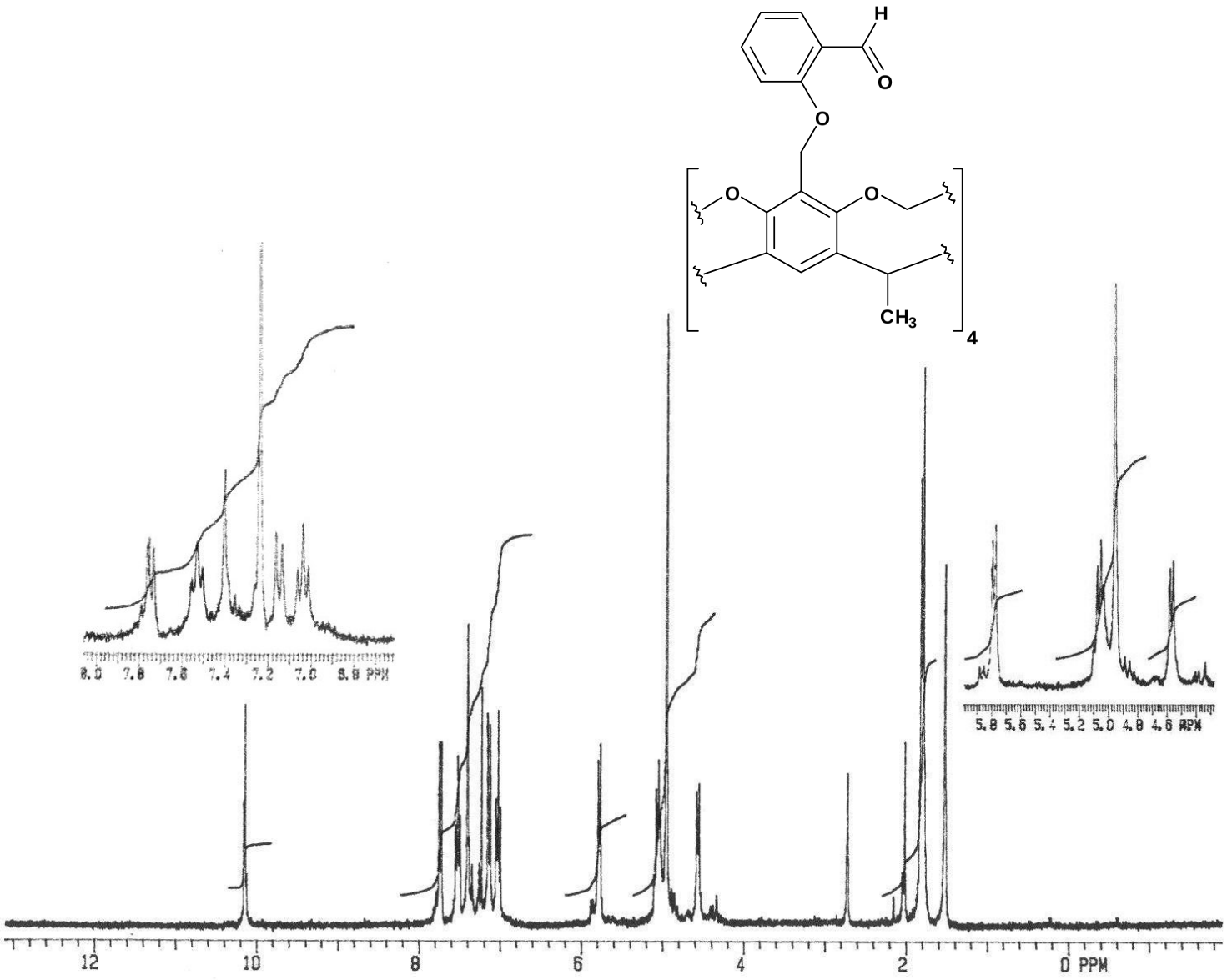

Spectrum 1.10: ^{1}H NMR spectrum of 6 in $CDCl_3$ (300 MHz)

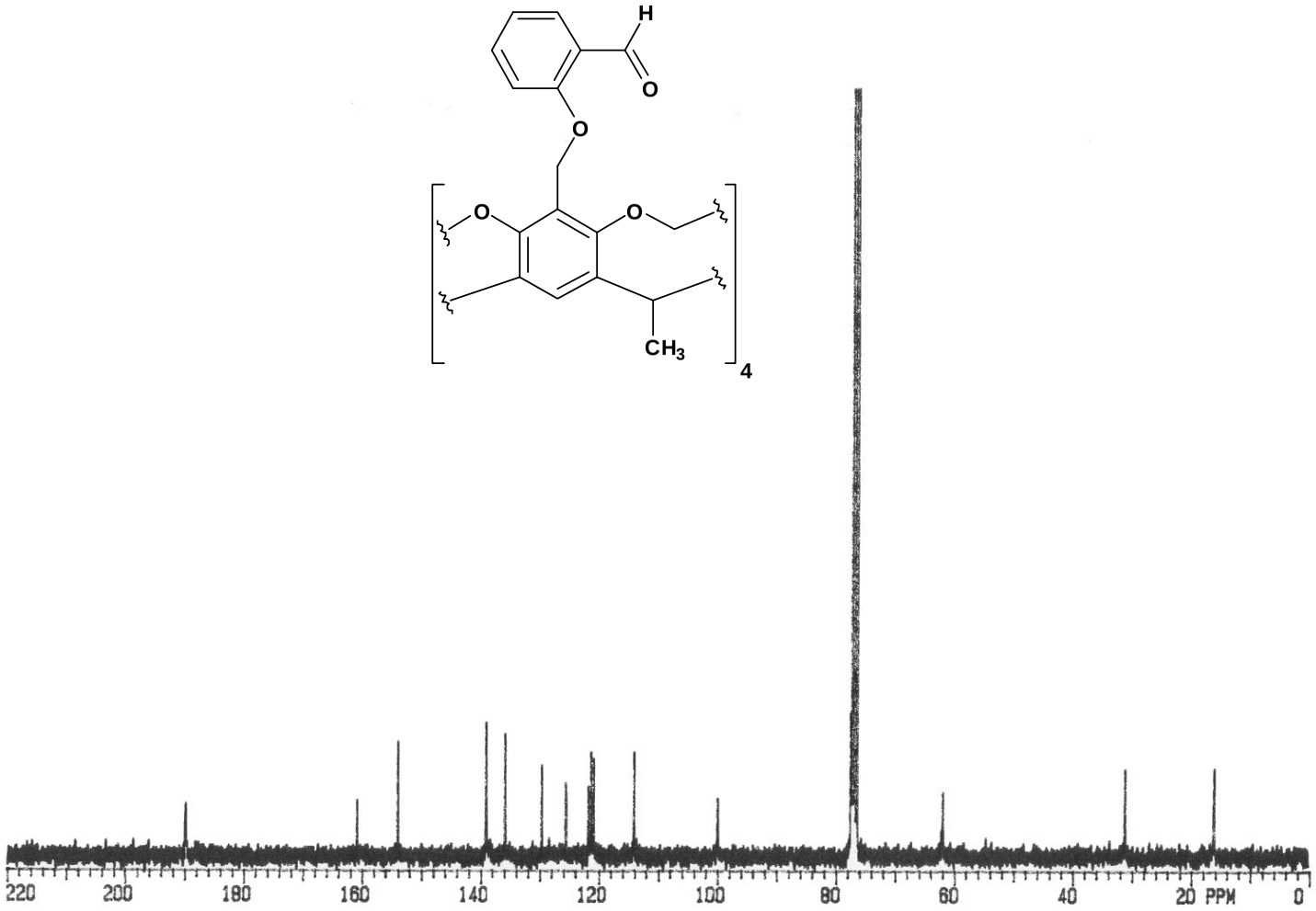

Spectrum 1.11: ^{13}C NMR spectrum of 6 in $CDCl_3$ (75 MHz)

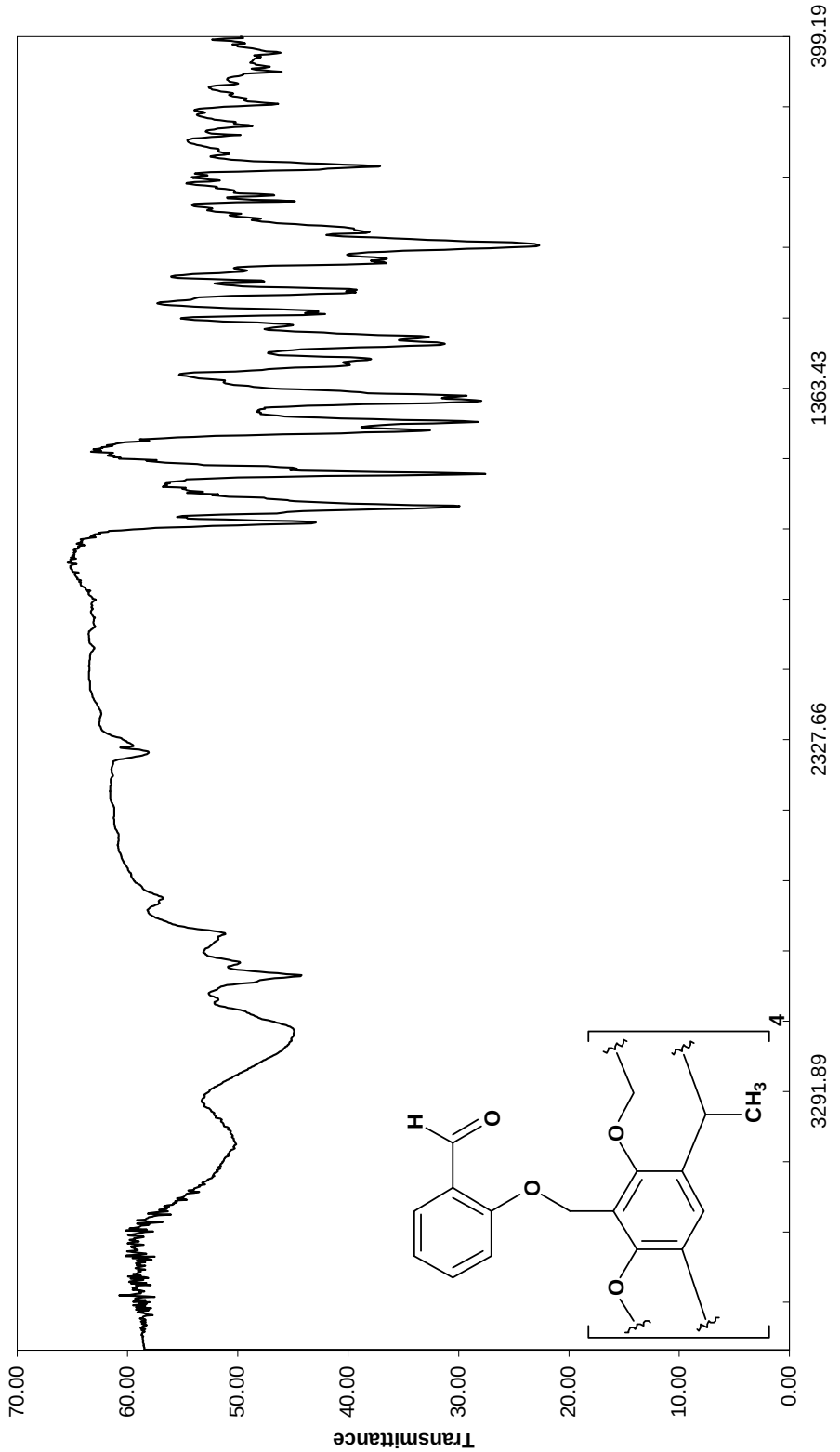

Spectrum 1.12: Infrared spectrum of 6 (KBr)

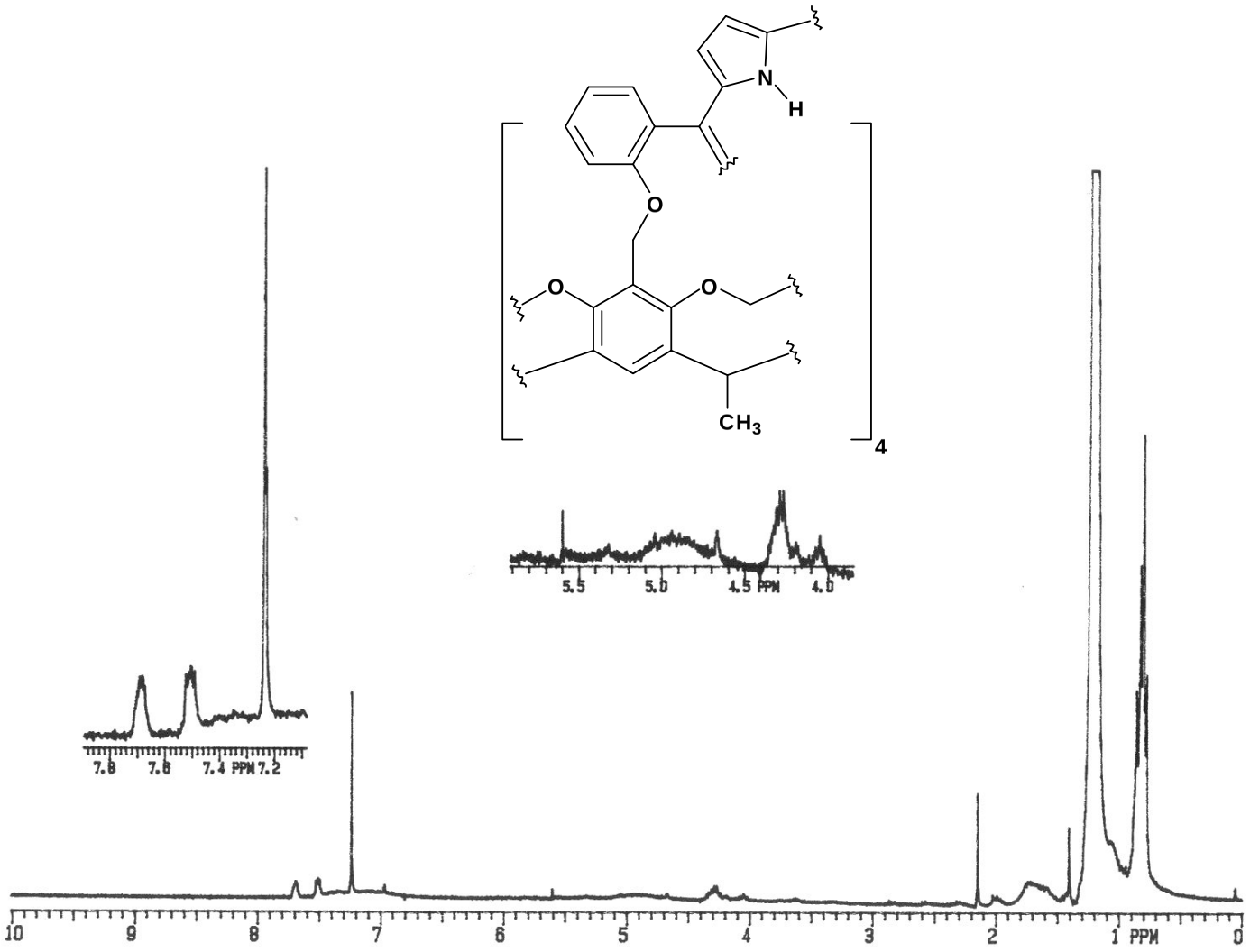

Spectrum 1.13: ^{1}H NMR spectrum of material from attempted synthesis of 7 in $CDCl_3$ via the *in situ* approach (300 MHz)

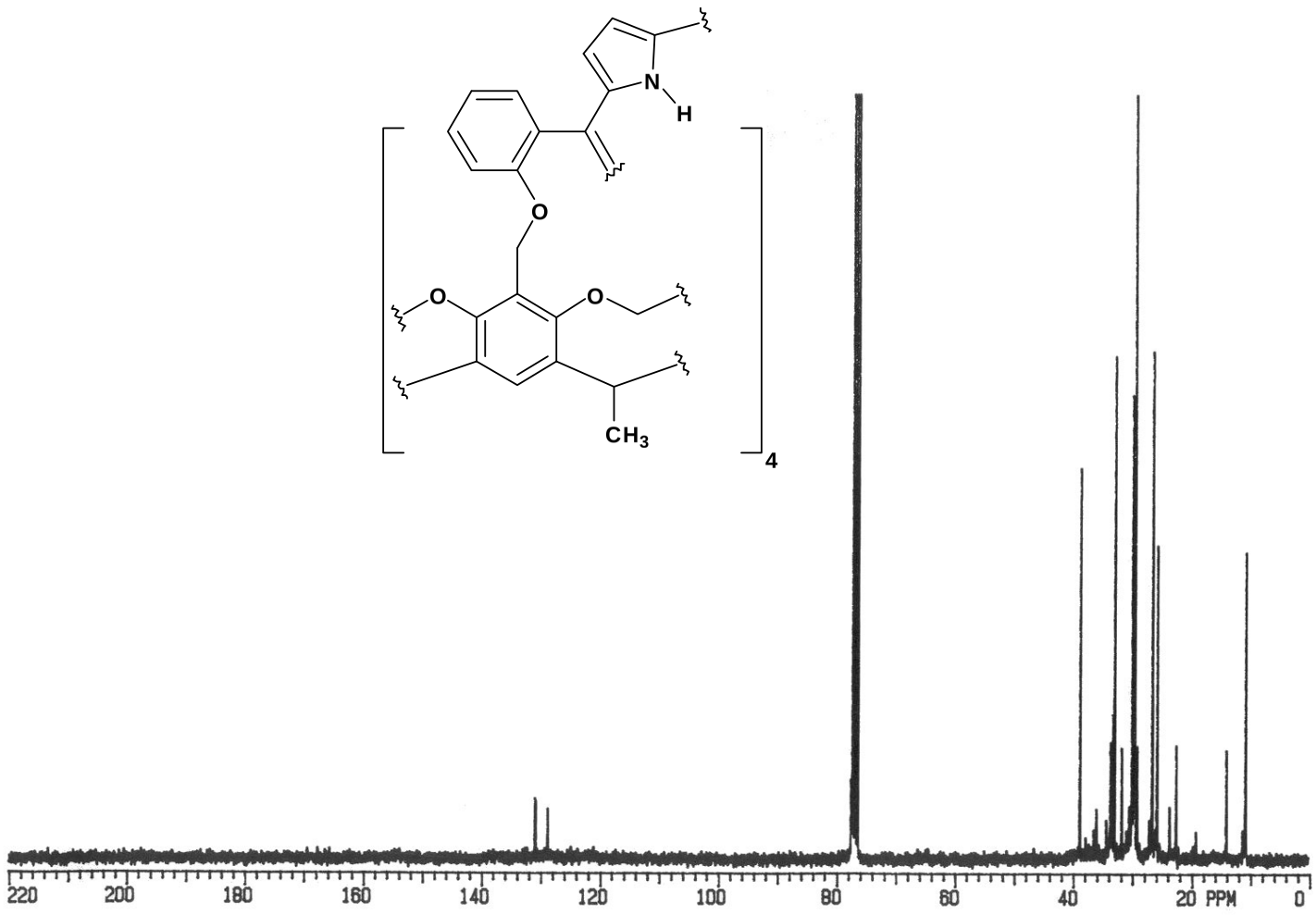

Spectrum 1.14: ^{13}C NMR spectrum of material from attempted synthesis of 7 in $CDCl_3$ via the *in situ* approach (75 MHz)

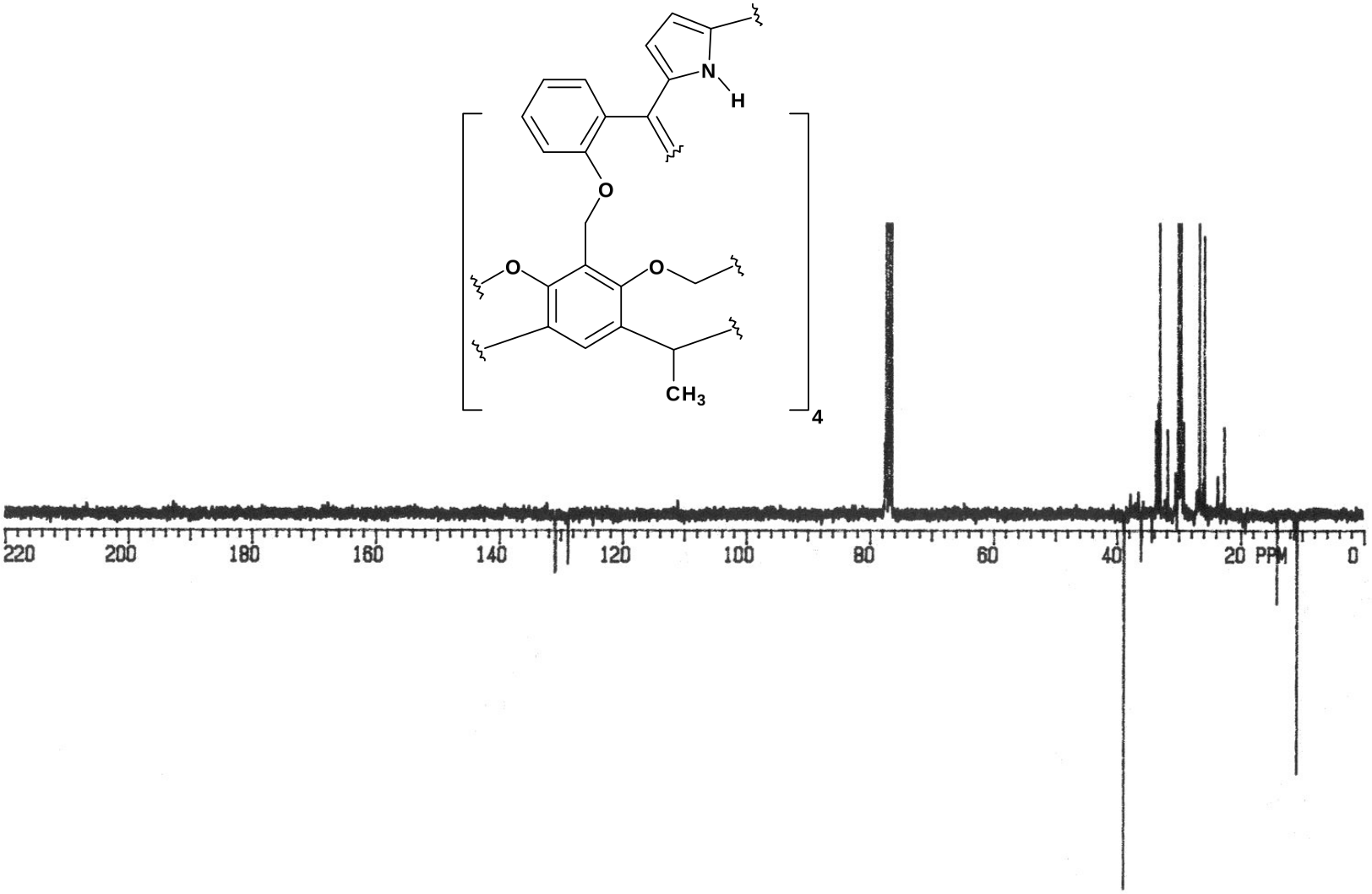

Spectrum 1.15: APT ^{13}C NMR spectrum of material from attempted synthesis of 7 in $CDCl_3$ via *in situ* approach (75 MHz)

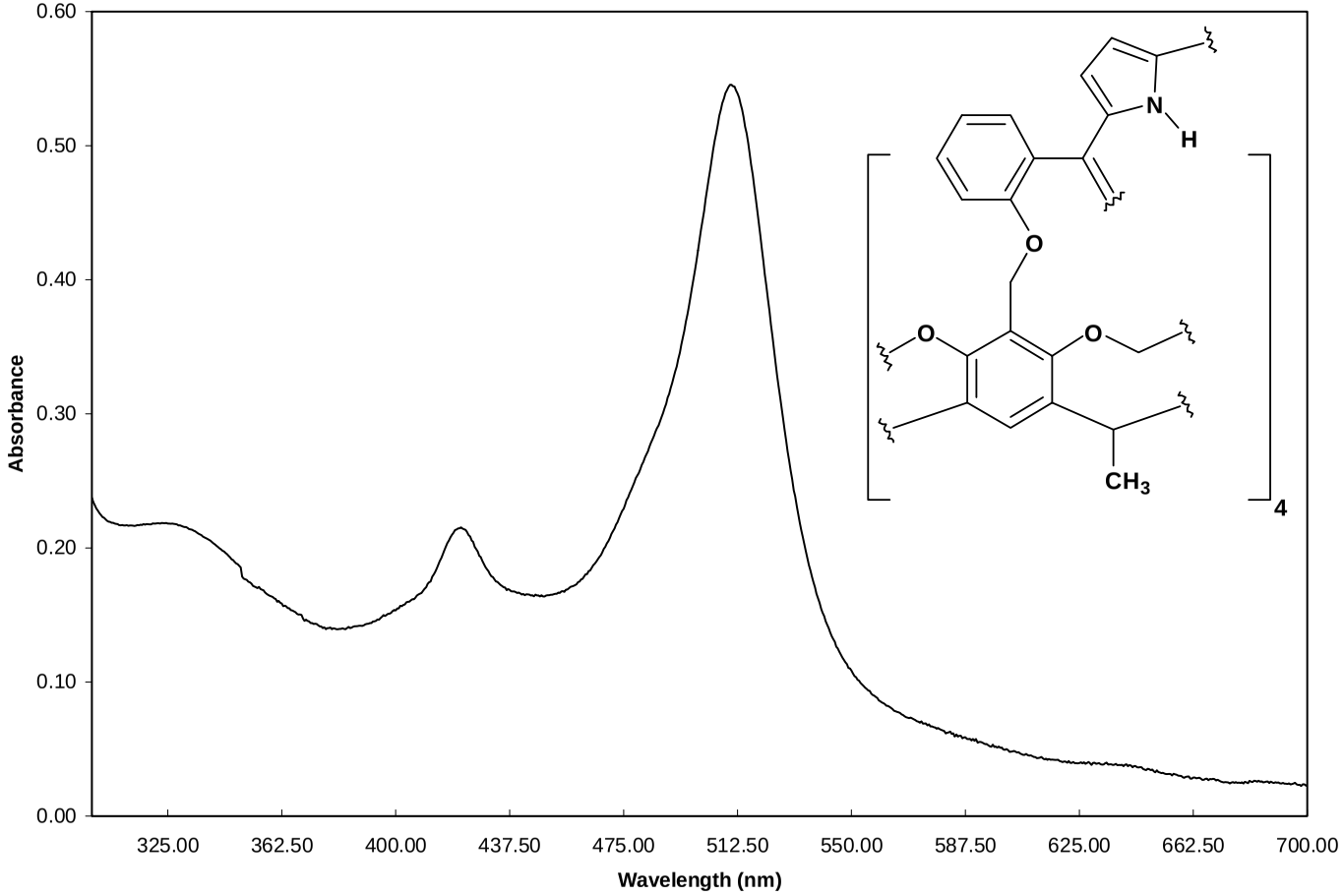

Spectrum 1.16: UV-Visible spectrum of material from attempted synthesis of 7 via *in situ* approach from 300-700 nm ($CHCl_3$)

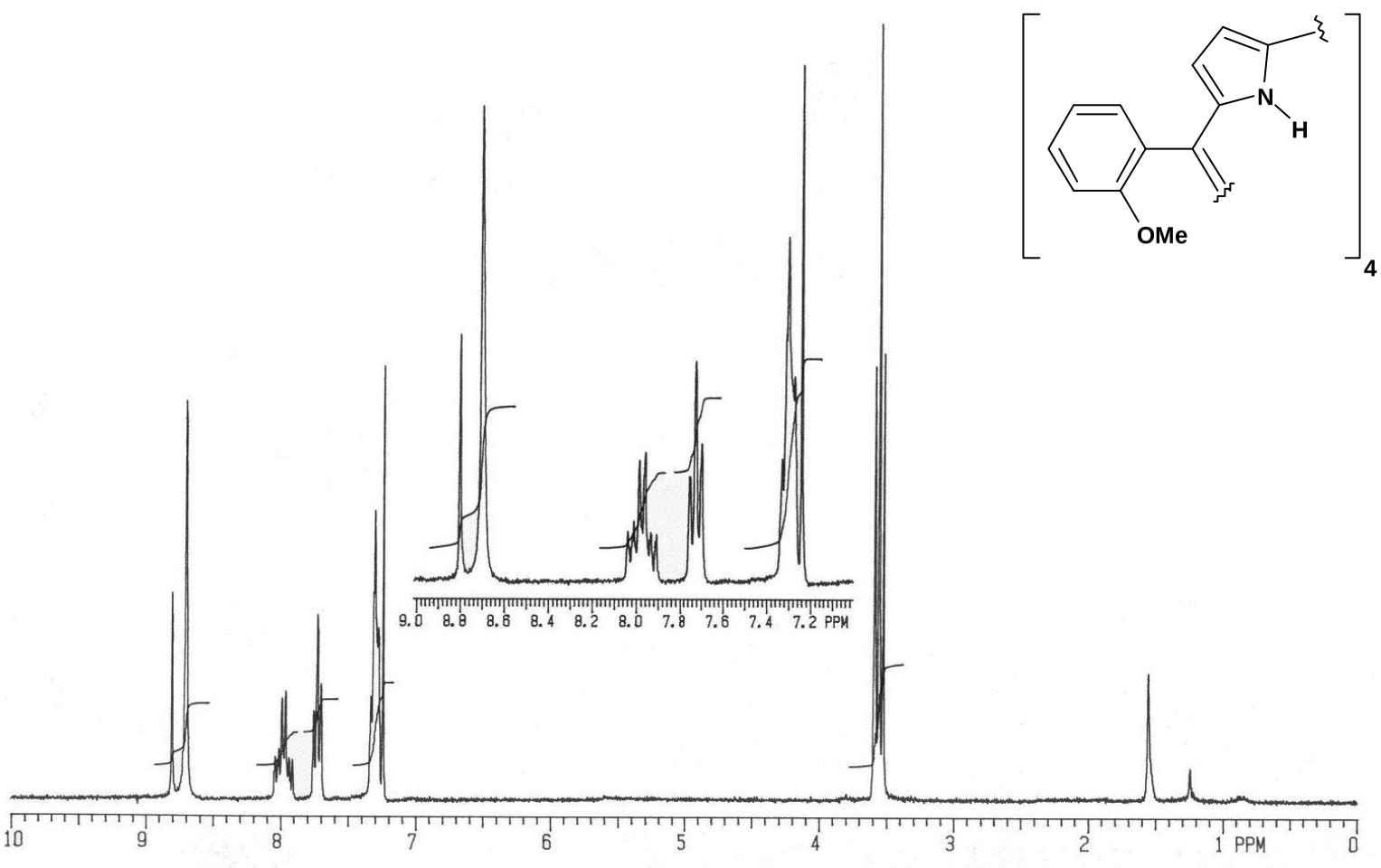

Spectrum 1.17: ^{1}H NMR spectrum of 11 in $CDCl_3$ (300 MHz)

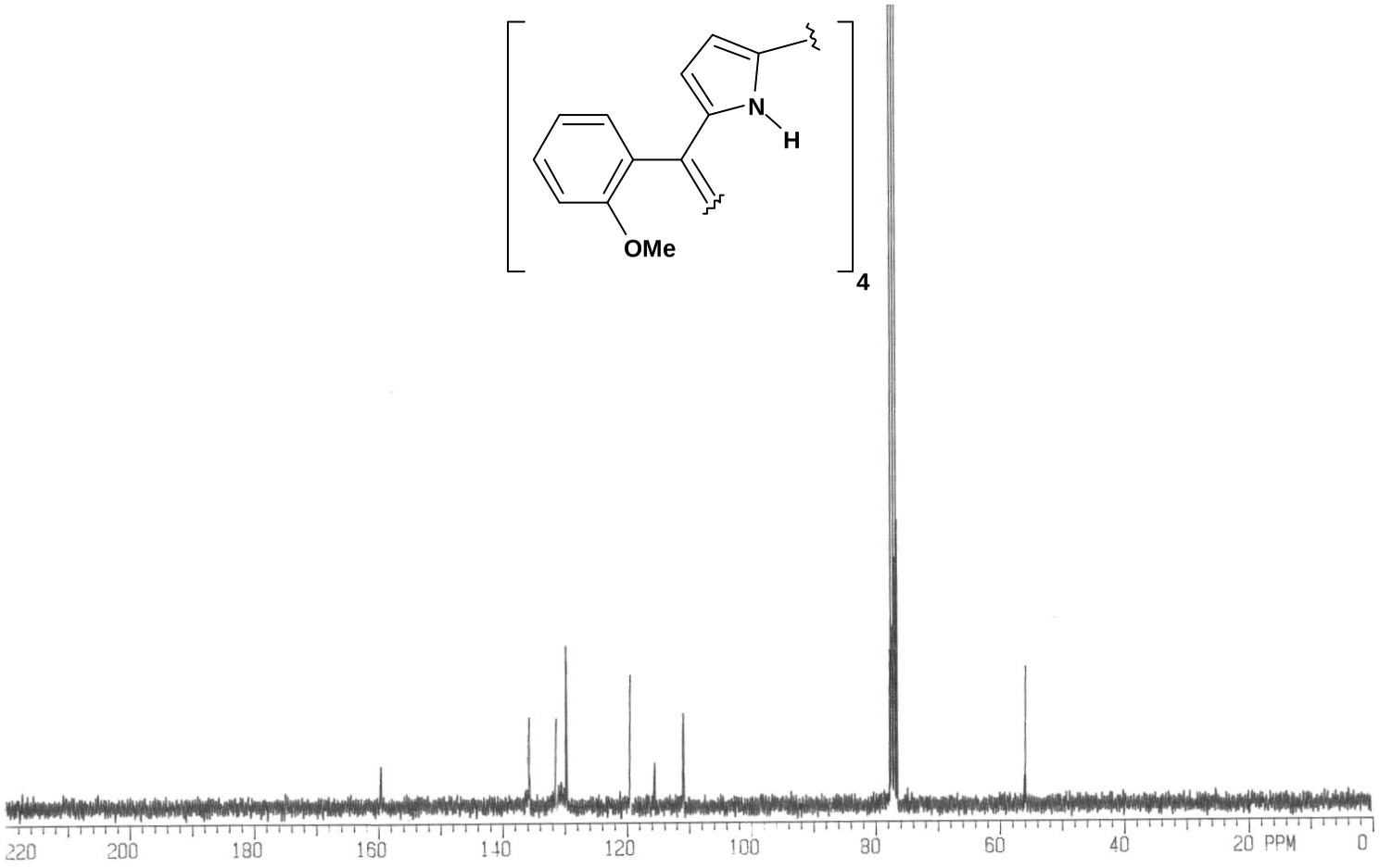

Spectrum 1.18: ^{13}C NMR spectrum of 11 in $CDCl_3$ (75 MHz)

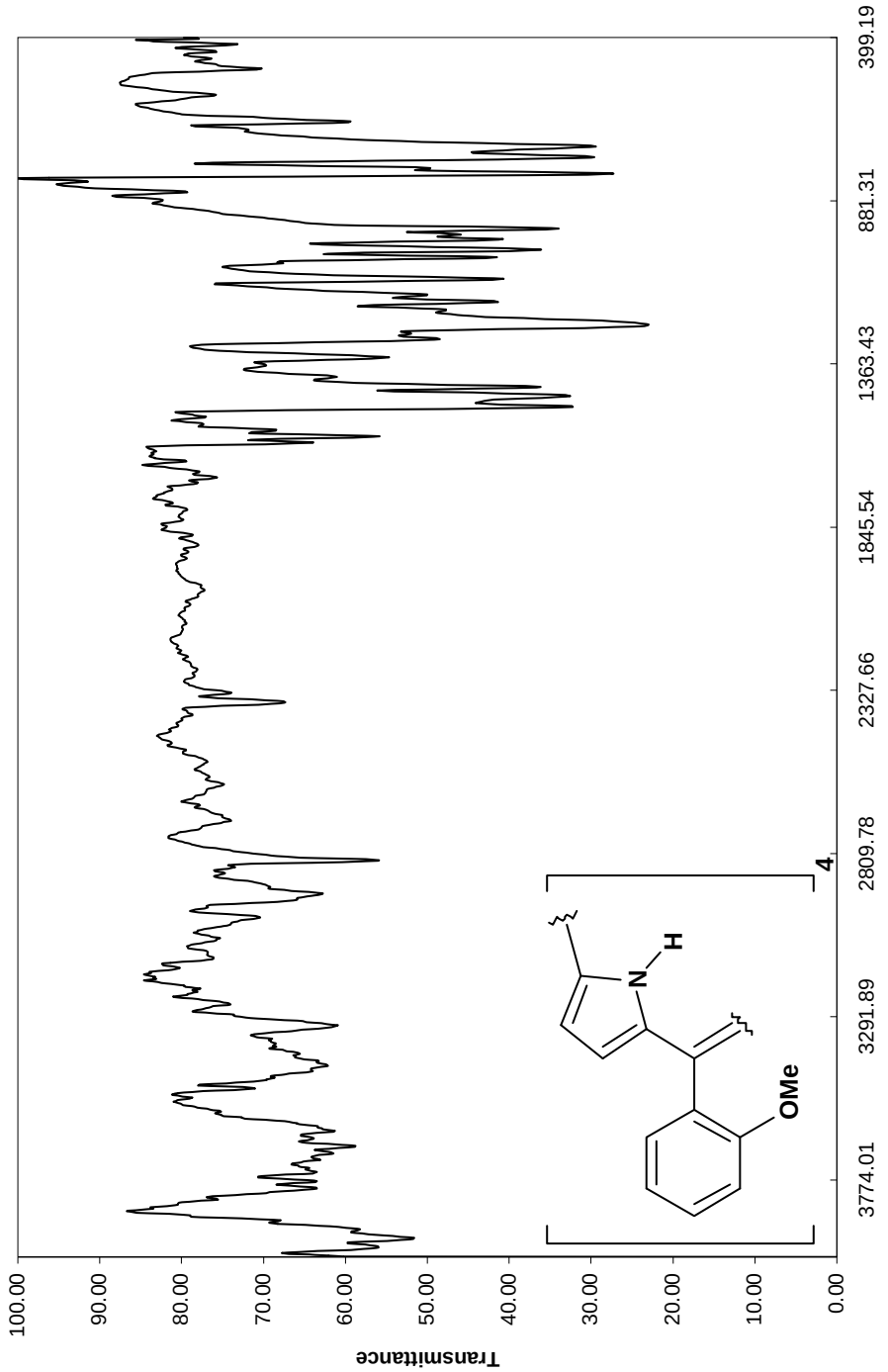

Spectrum 1.19: Infrared spectrum of 11 (KBr)

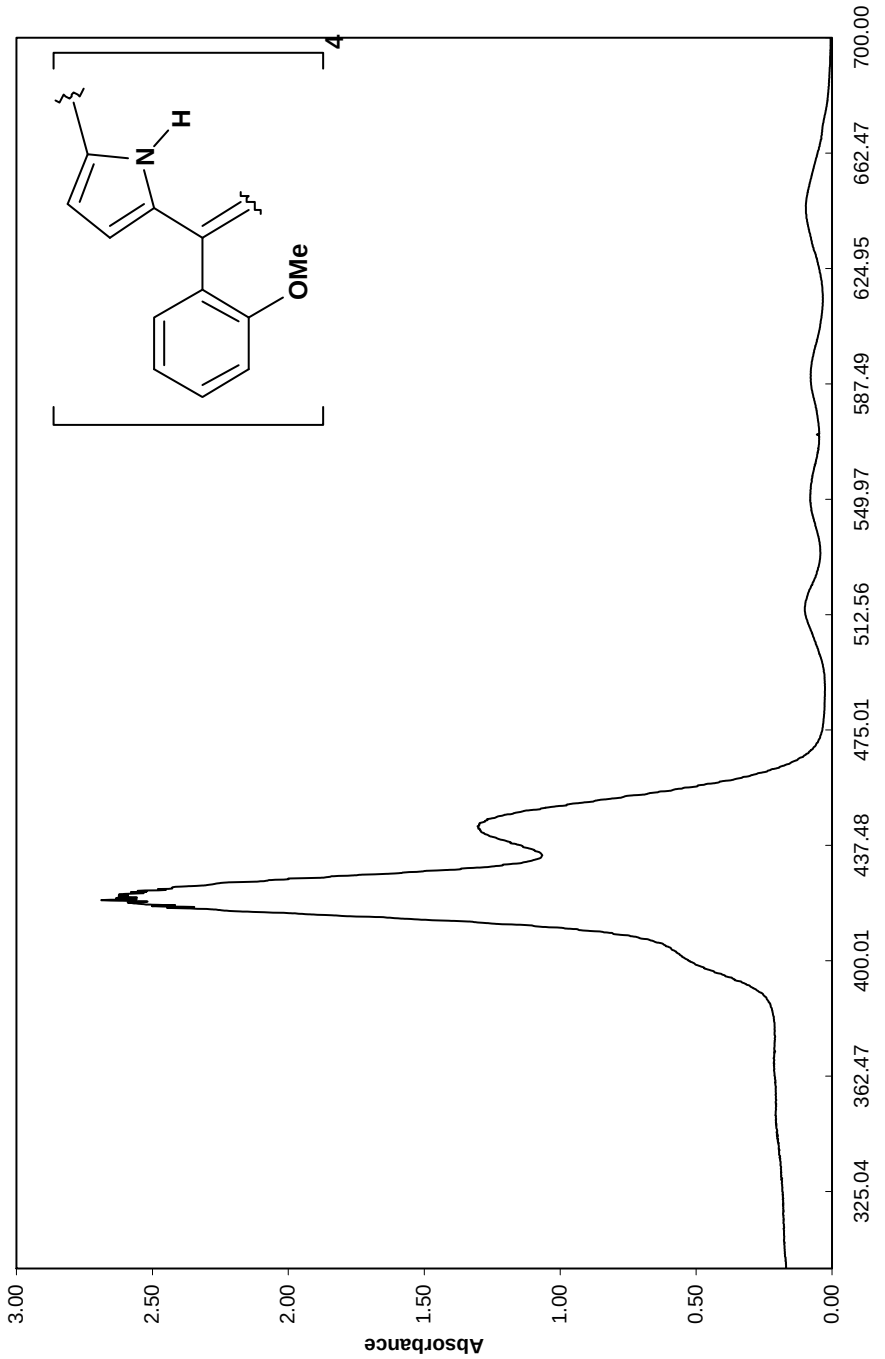

Spectrum 1.20: UV-Visible spectrum of 11 from 300-700 nm ($CHCl_3$)

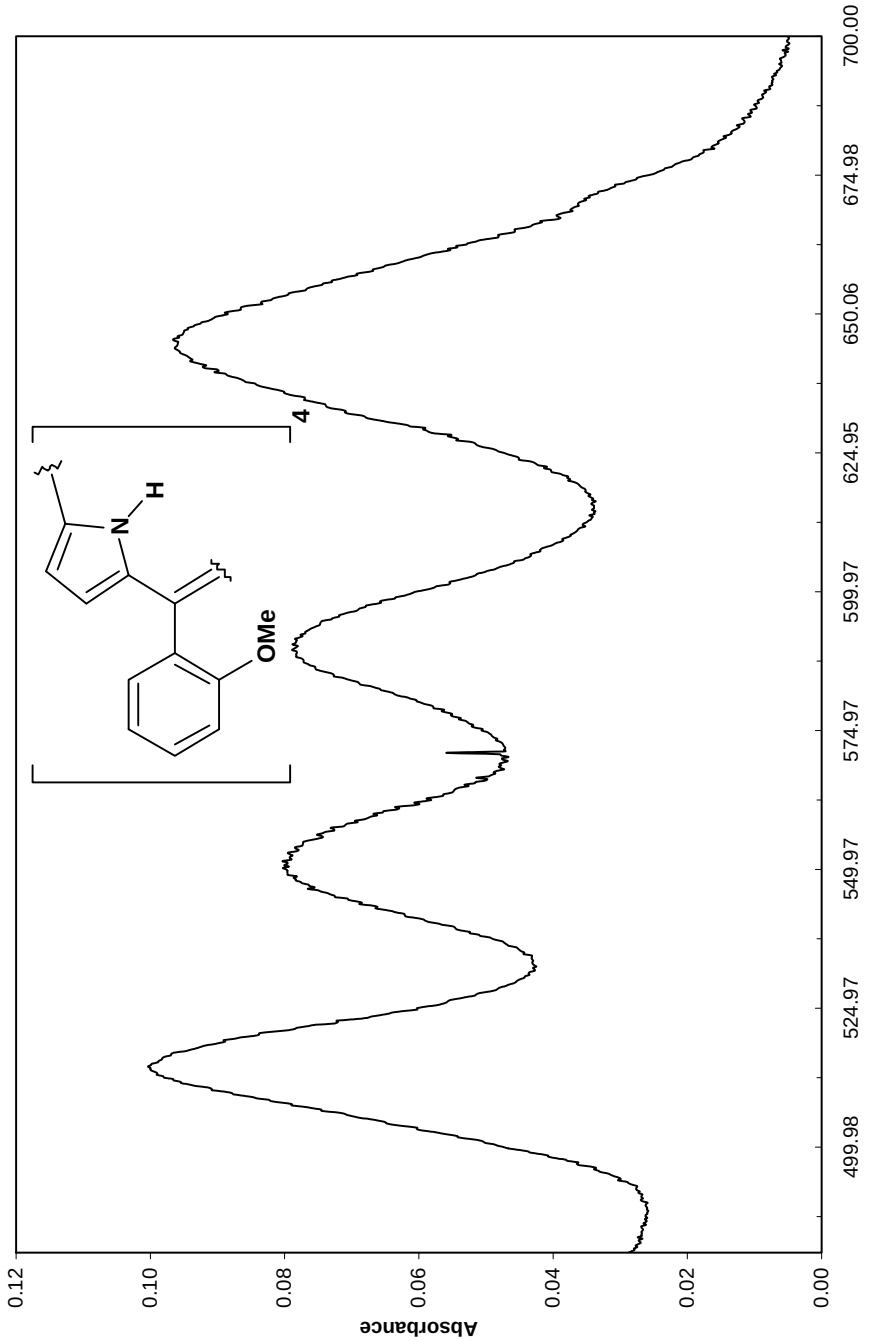

Spectrum 1.21: UV-Visible spectrum of 11 from 480-700 nm ($CHCl_3$)

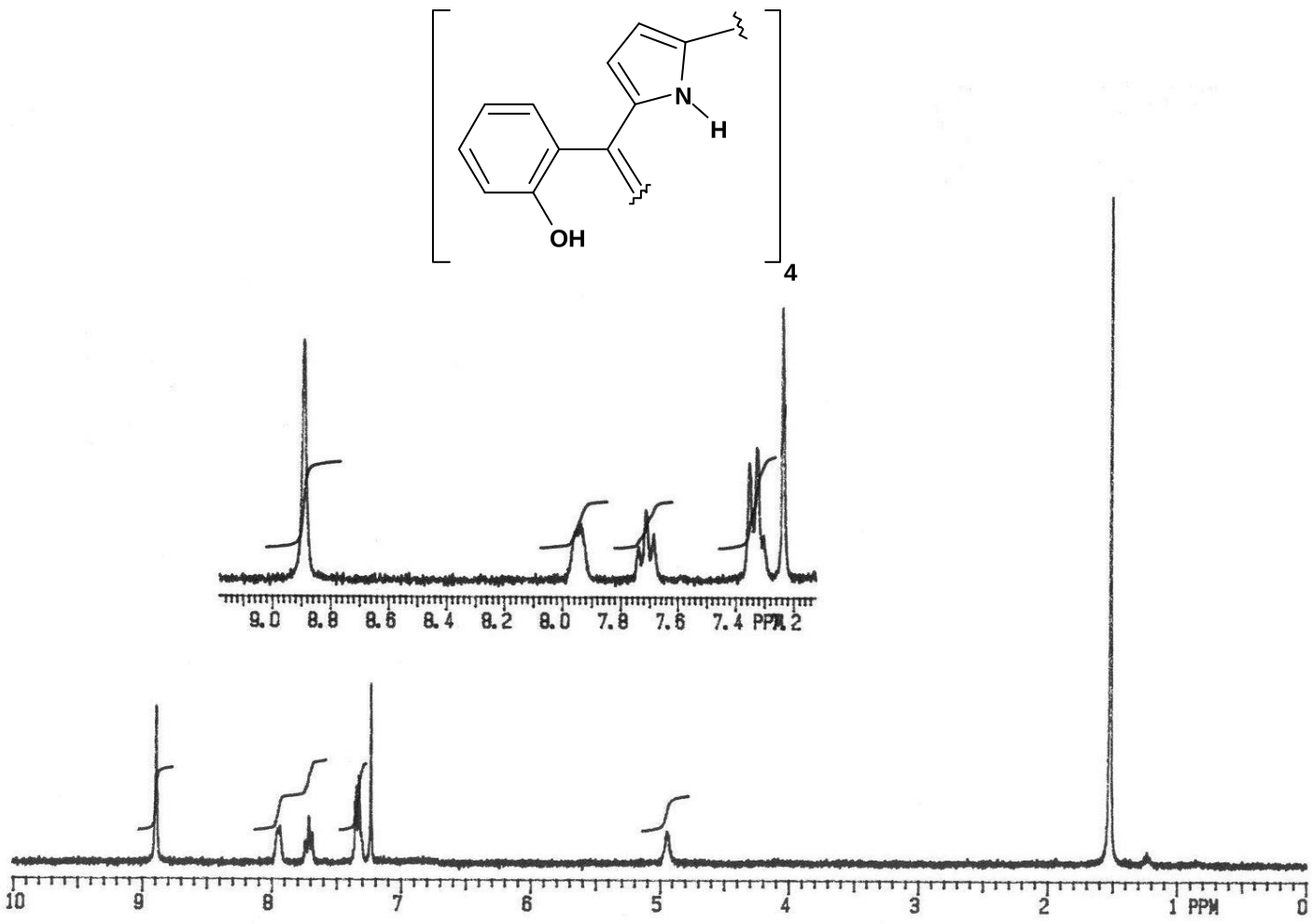

Spectrum 1.22: ^{1}H NMR spectrum of 12 in $CDCl_3$ (300 MHz)

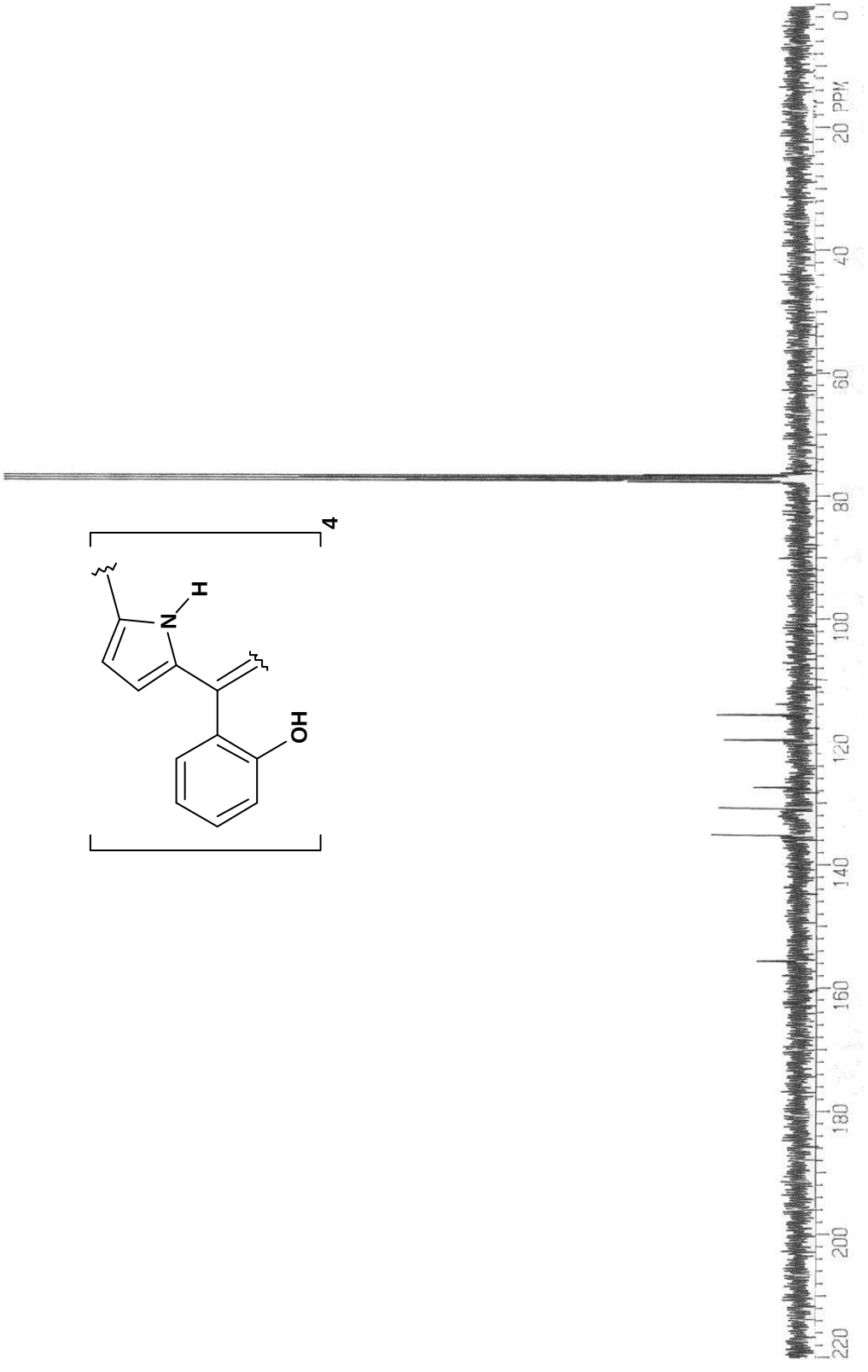

Spectrum 1.23: ^{13}C NMR spectrum of 12 in $CDCl_3$ (75 MHz)

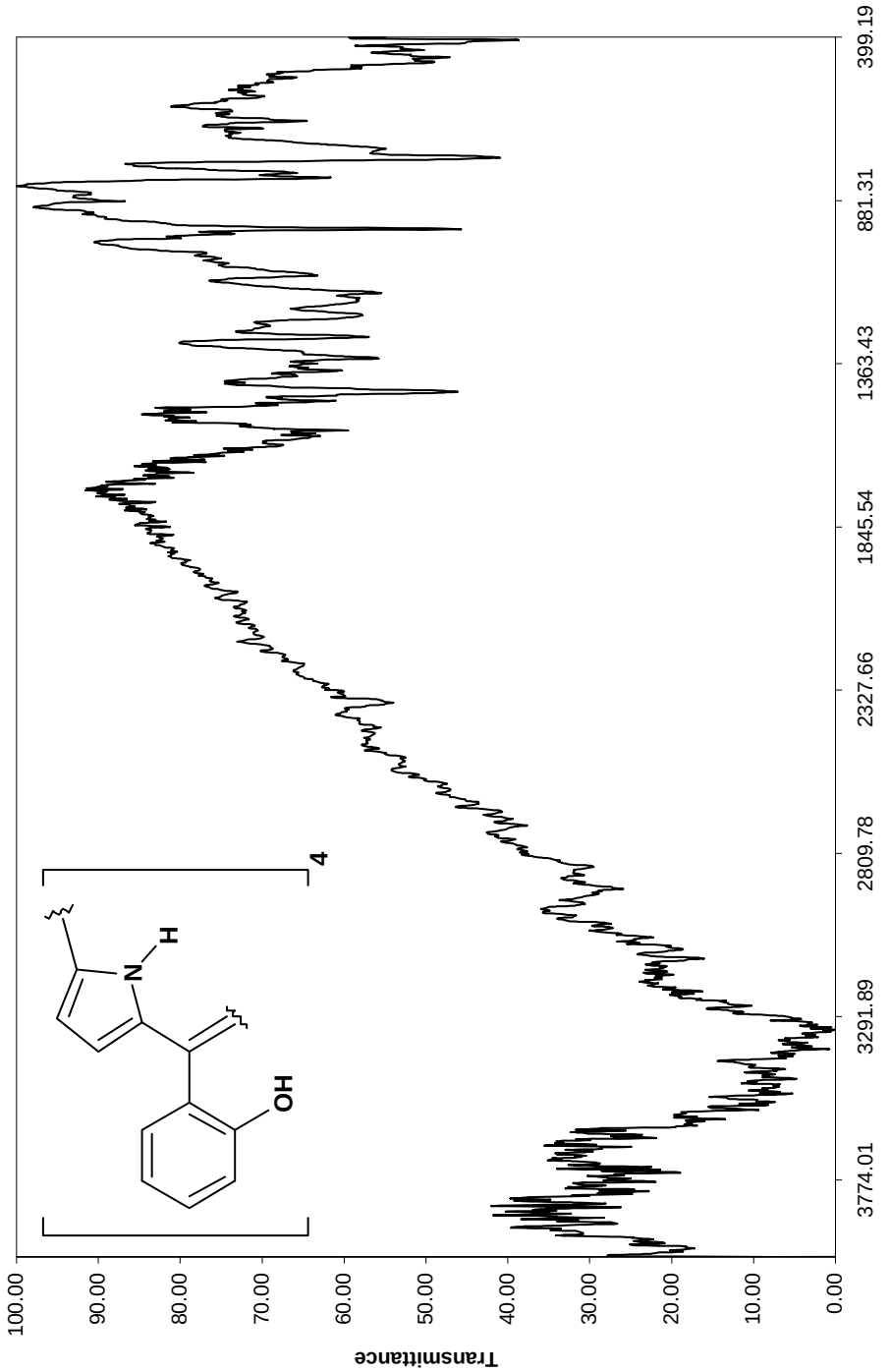

Spectrum 1.24: Infrared spectrum of 12 (KBr)

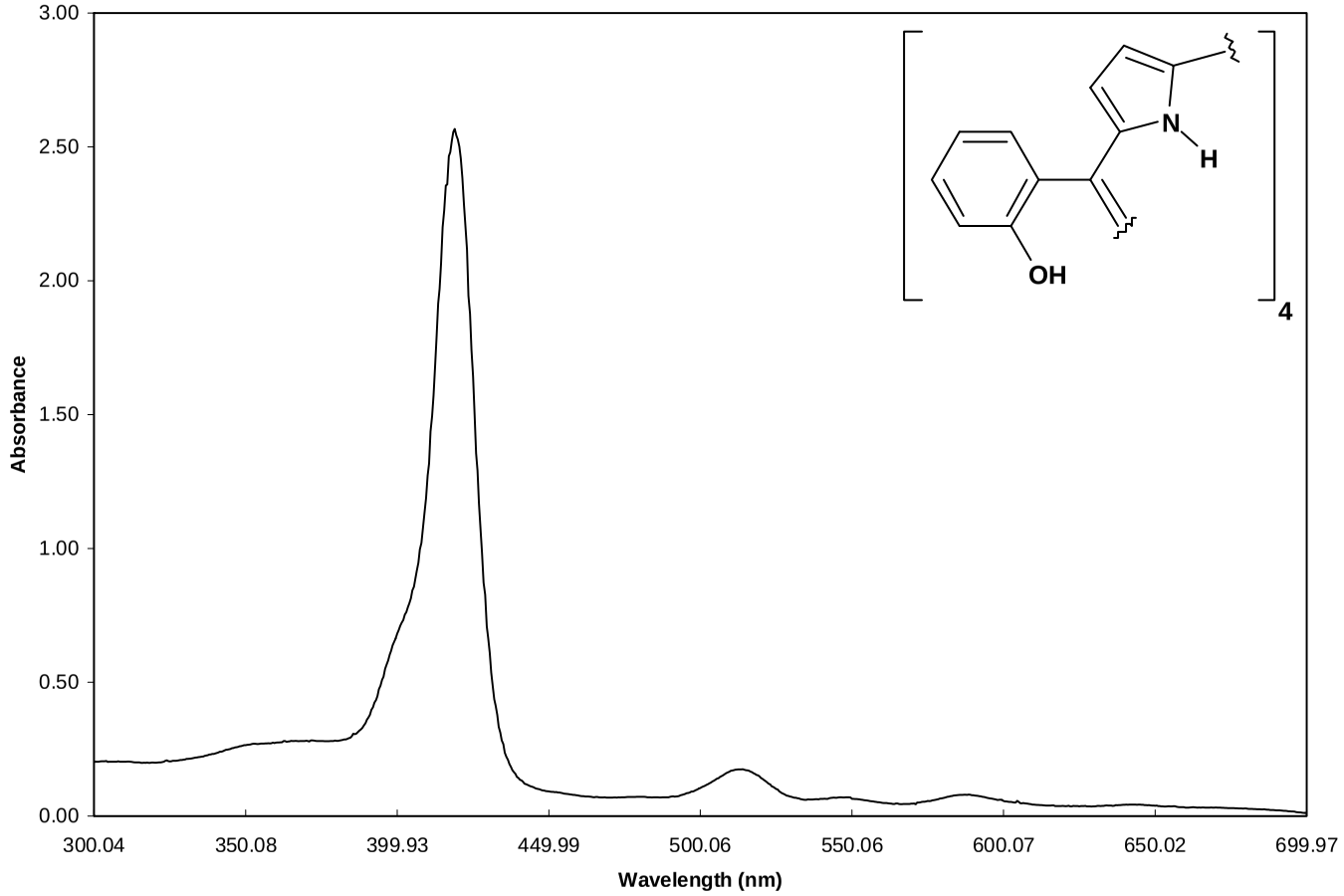

Spectrum 1.25: UV-Visible spectrum of 12 from 300-700 nm ($CHCl_3$)

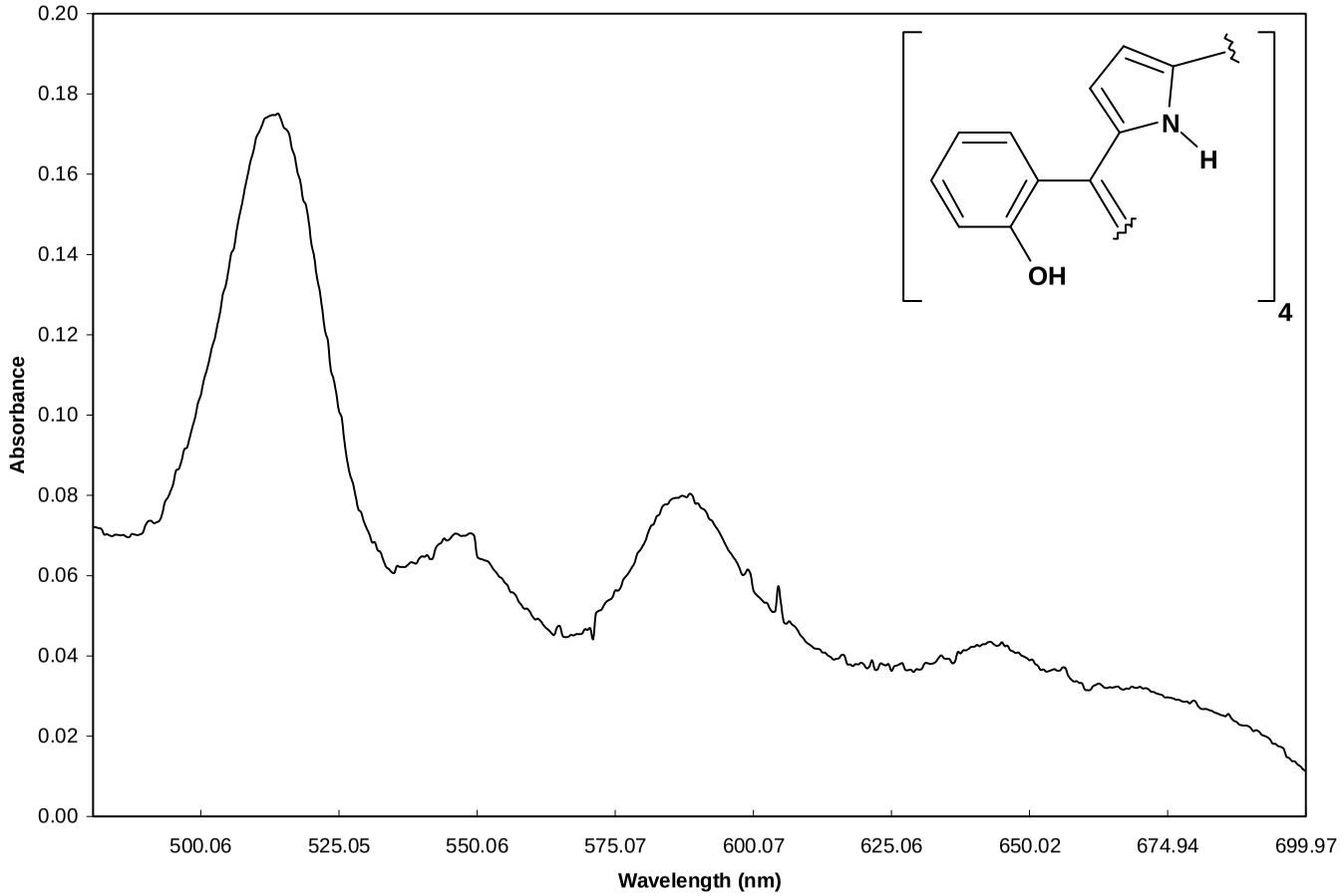

Spectrum 1.26: UV-Visible spectrum of 12 from 300-700 nm ($CHCl_3$)

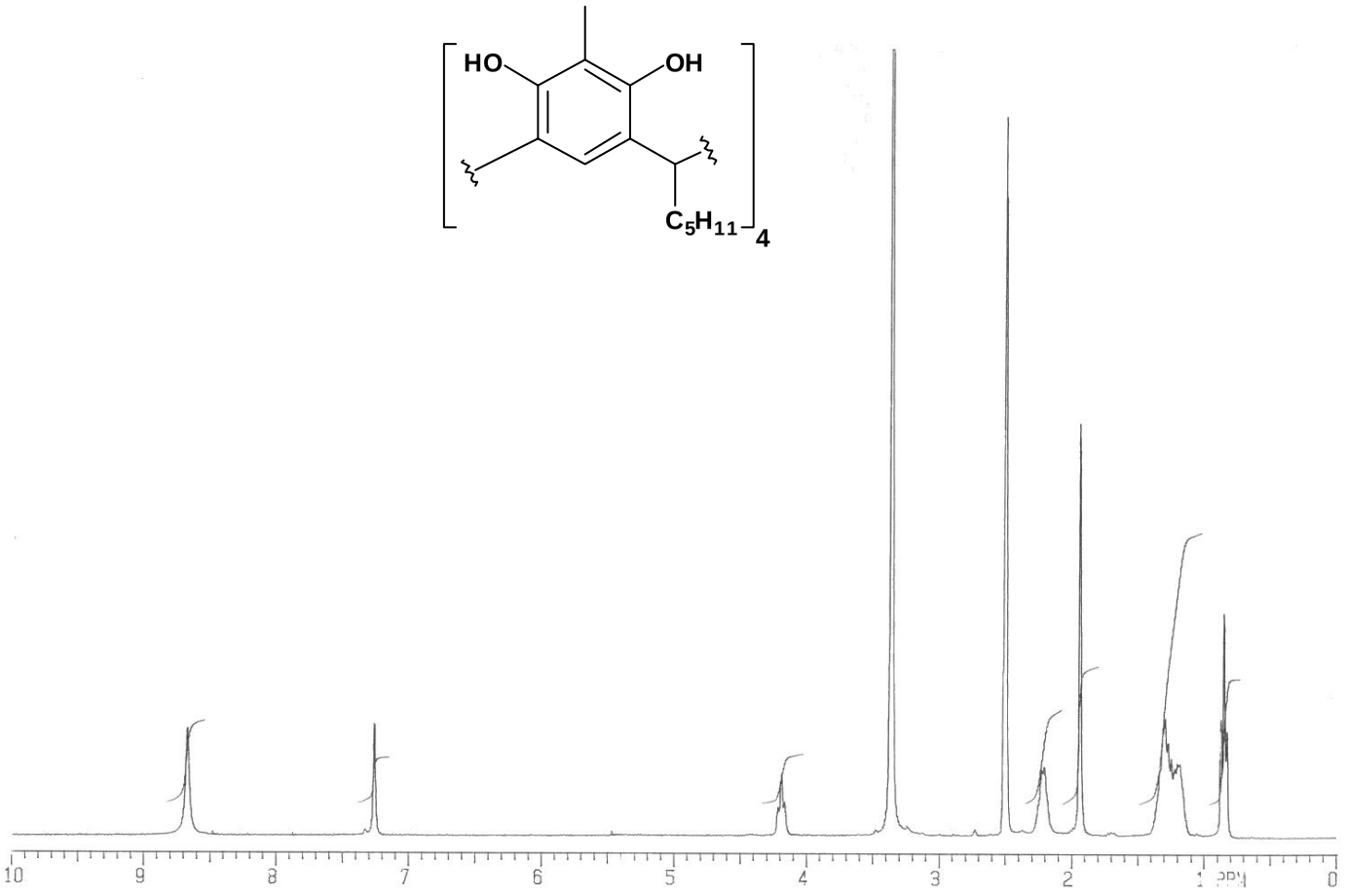

Spectrum 1.27: ^{1}H NMR spectrum of 16 in d_6-DMSO (300 MHz)

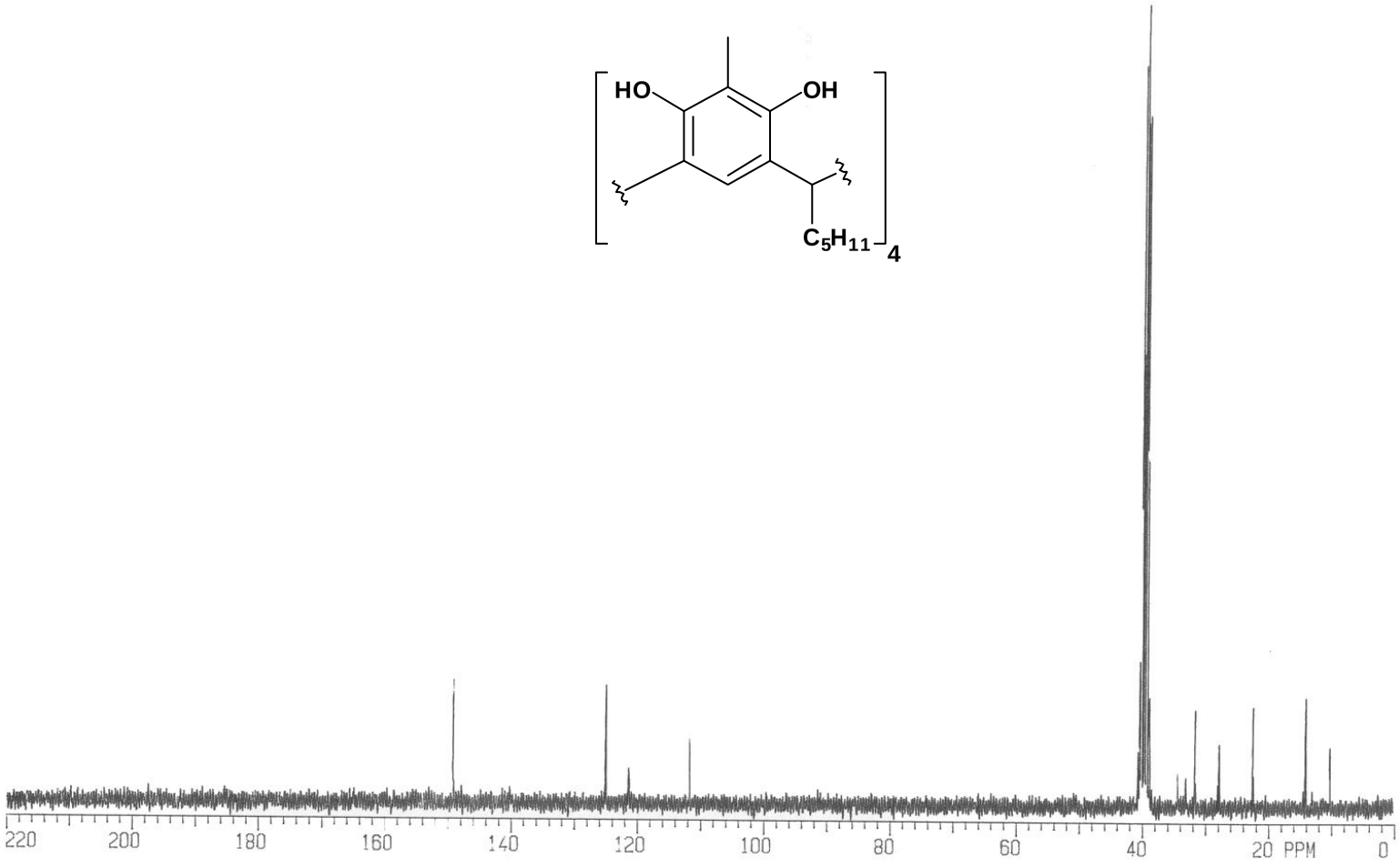

Spectrum 1.28: ^{13}C NMR spectrum of 16 in d_6-DMSO (75 MHz)

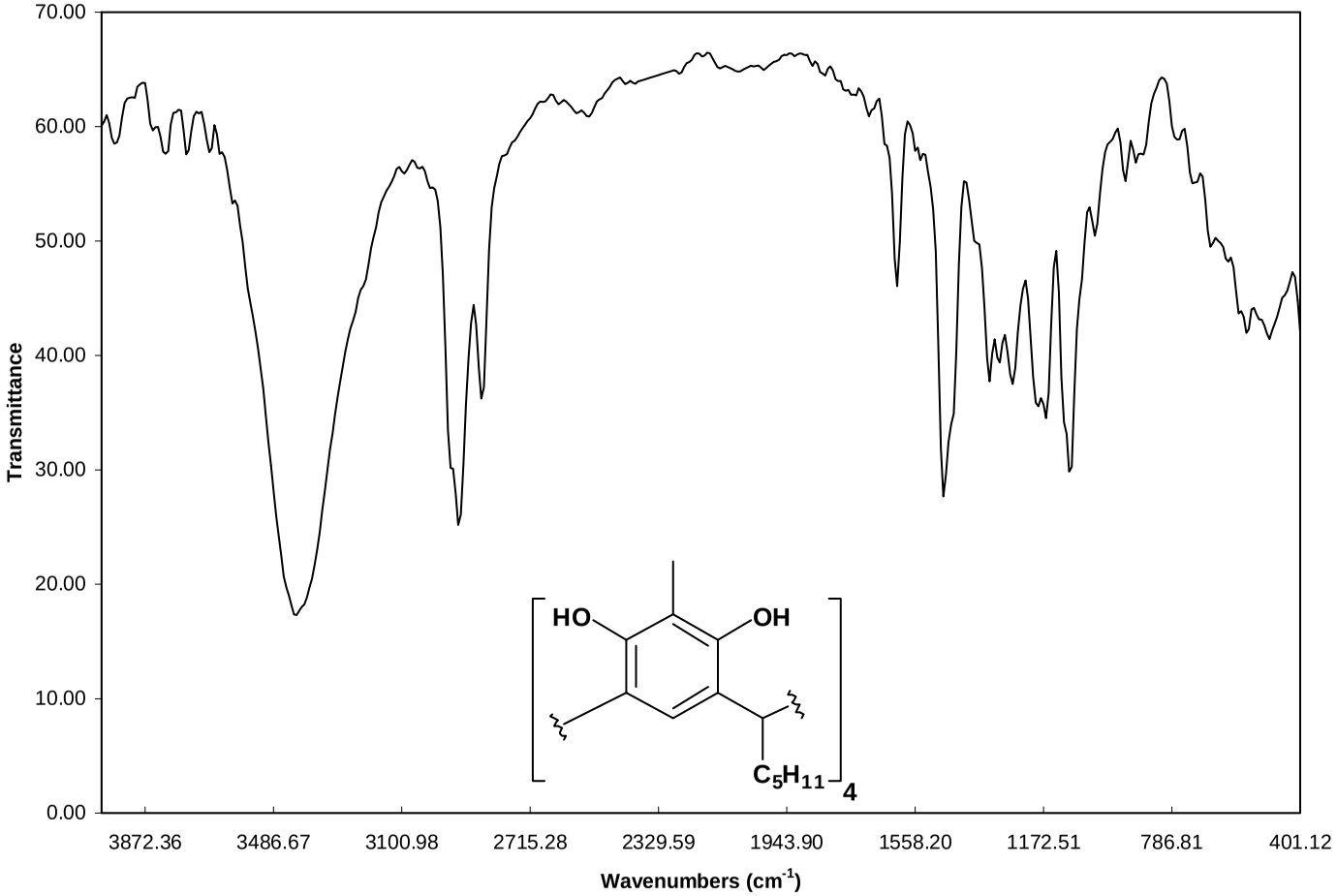

Spectrum 1.29: Infrared spectrum of 16 (KBr)

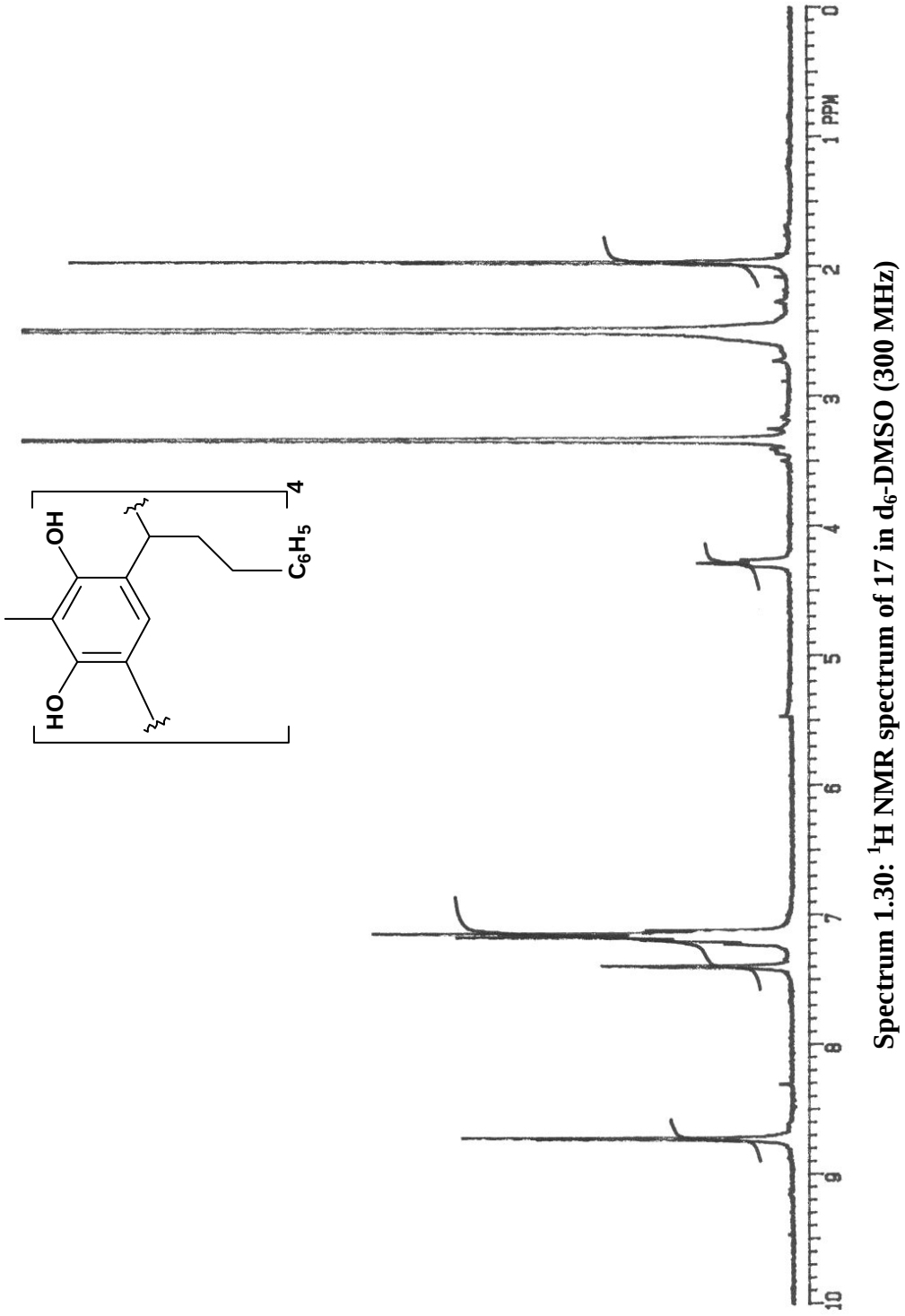

Spectrum 1.30: ^{1}H NMR spectrum of 17 in d_6-DMSO (300 MHz)

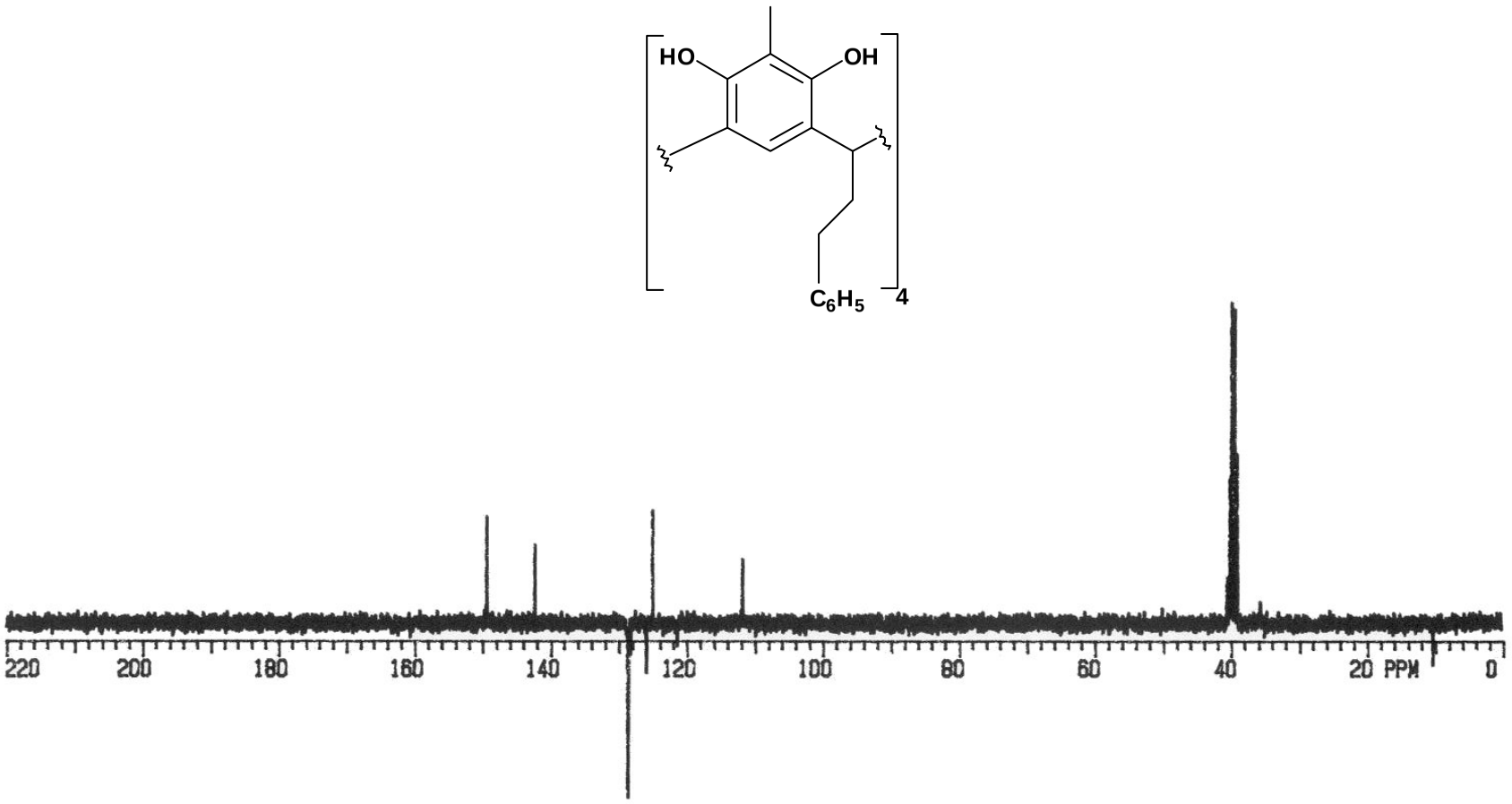

Spectrum 1.31: ^{13}C NMR spectrum of 17 in d_6-DMSO (75 MHz)

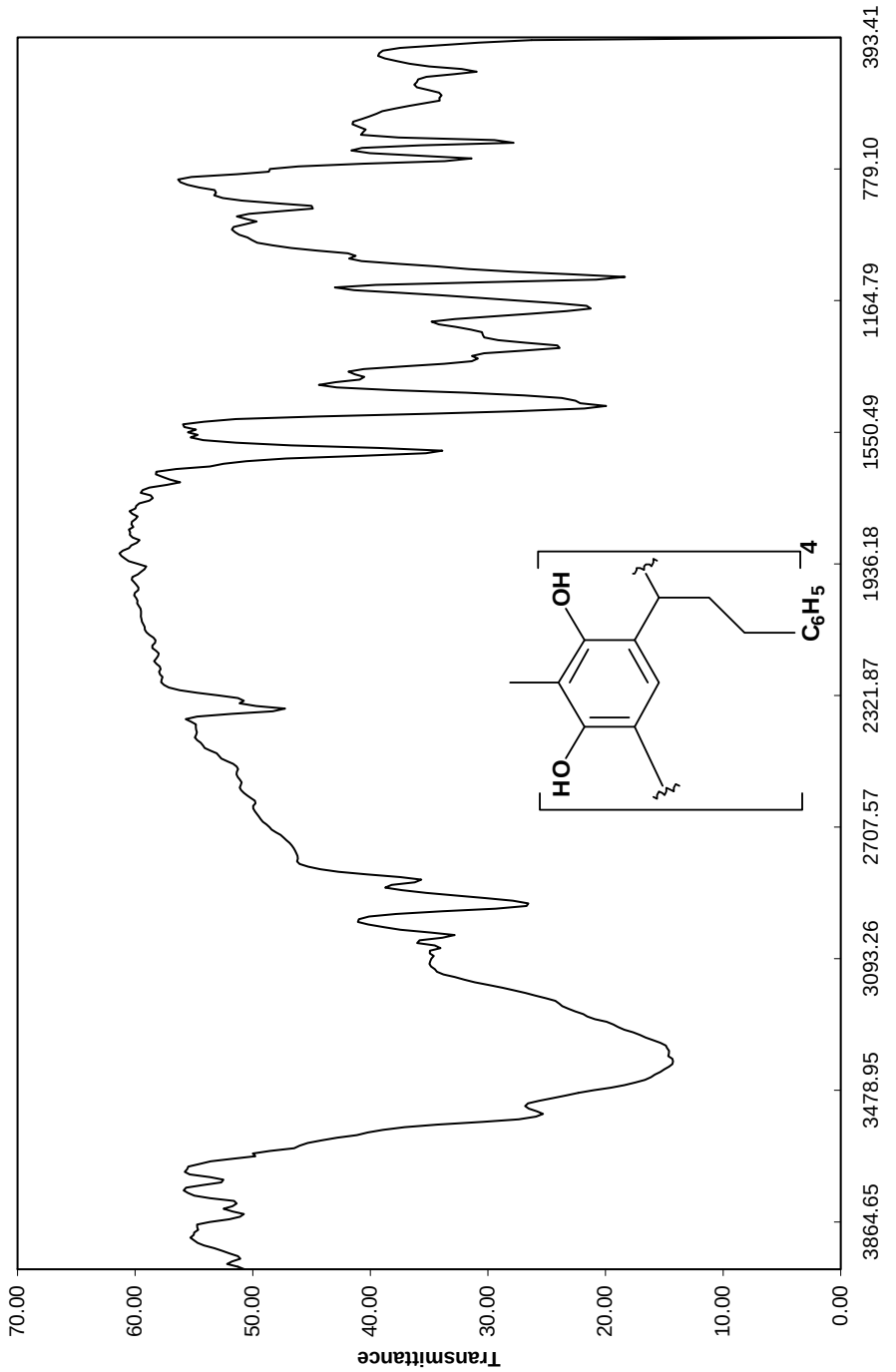

Spectrum 1.32: Infrared spectrum of 17 (KBr)

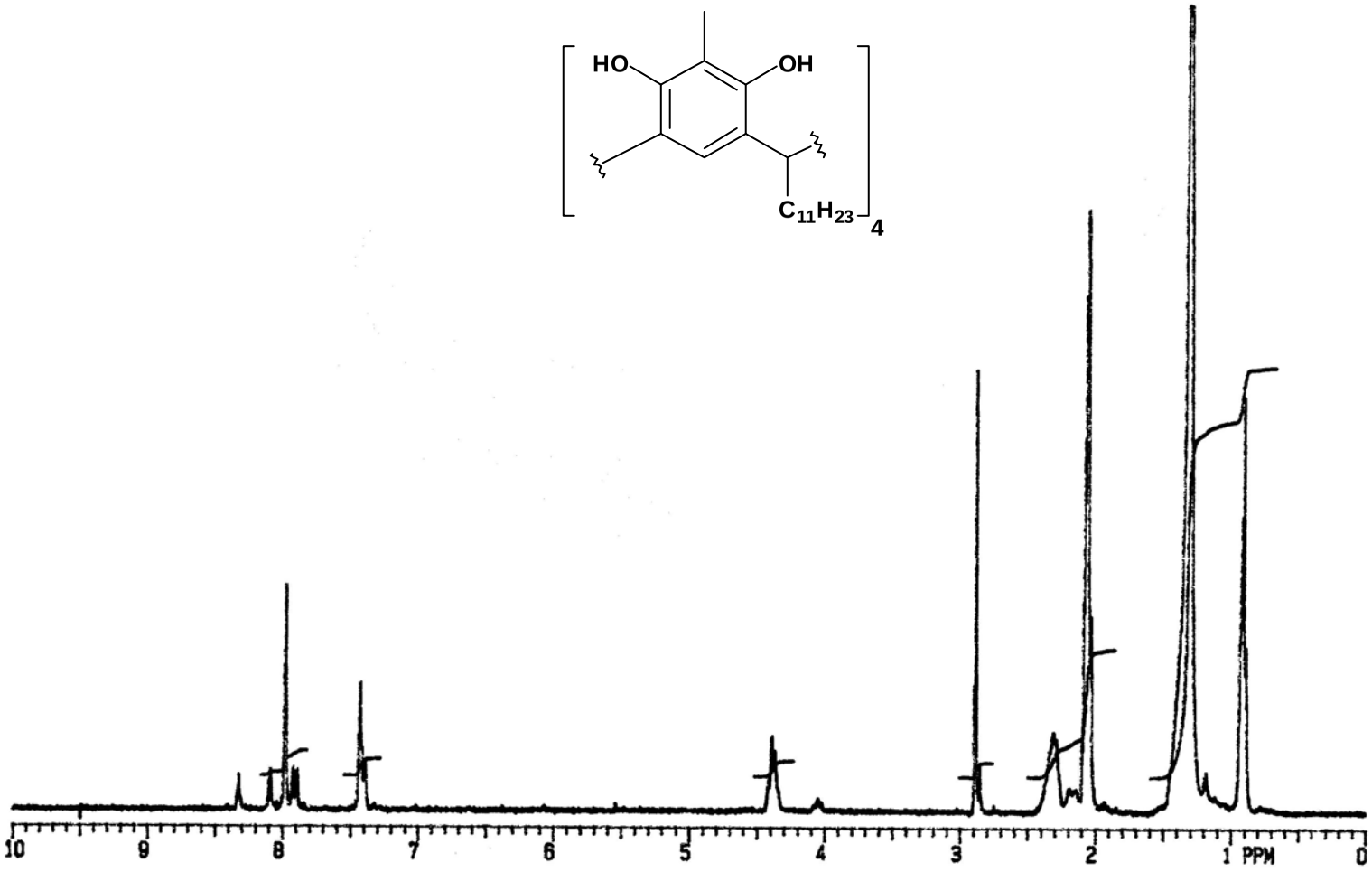

Spectrum 1.33: ^{1}H NMR spectrum of 18 in d_6-acetone (300 MHz)

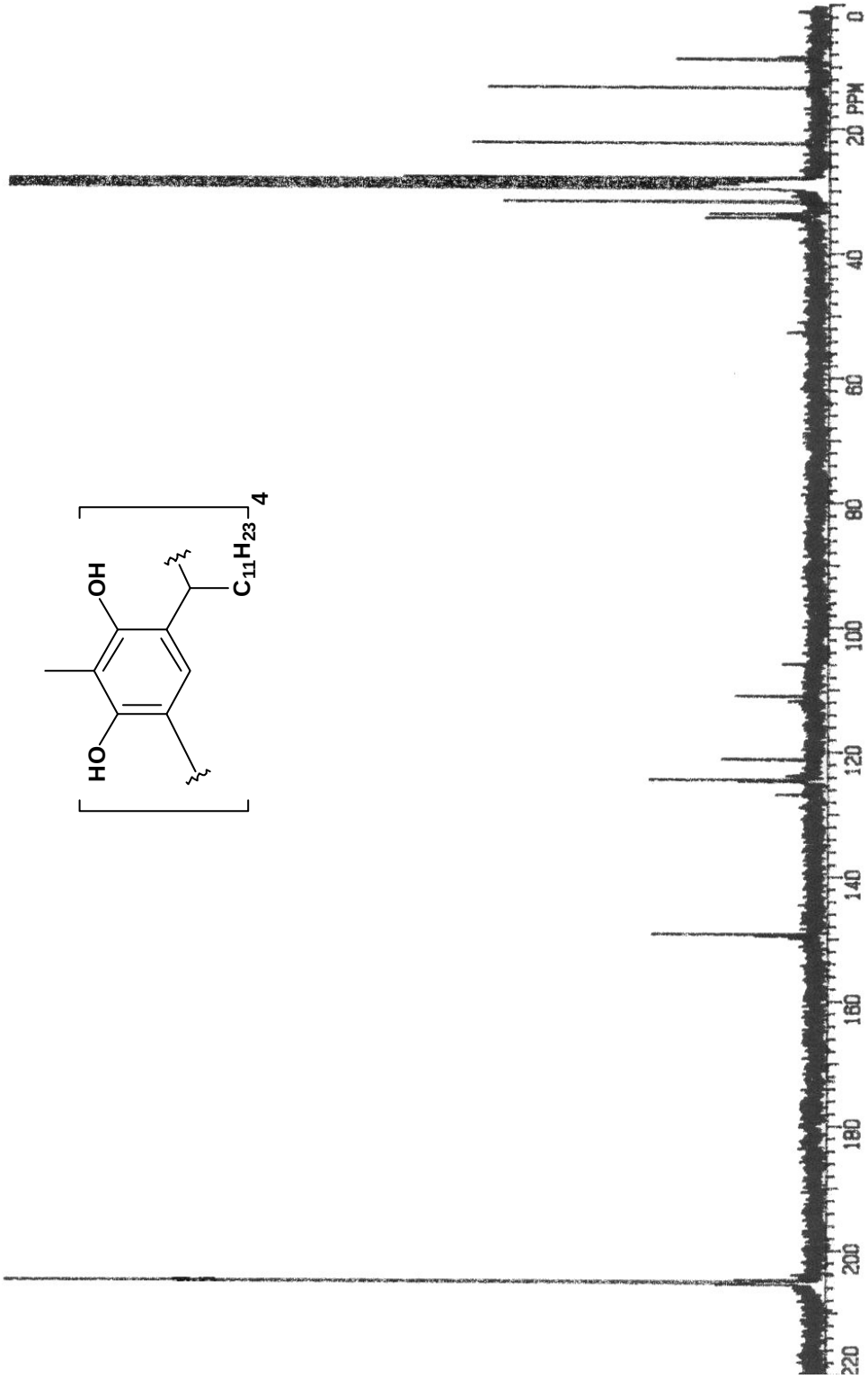

Spectrum 1.34: ^{13}C NMR spectrum of 18 in d_6-acetone (75 MHz)

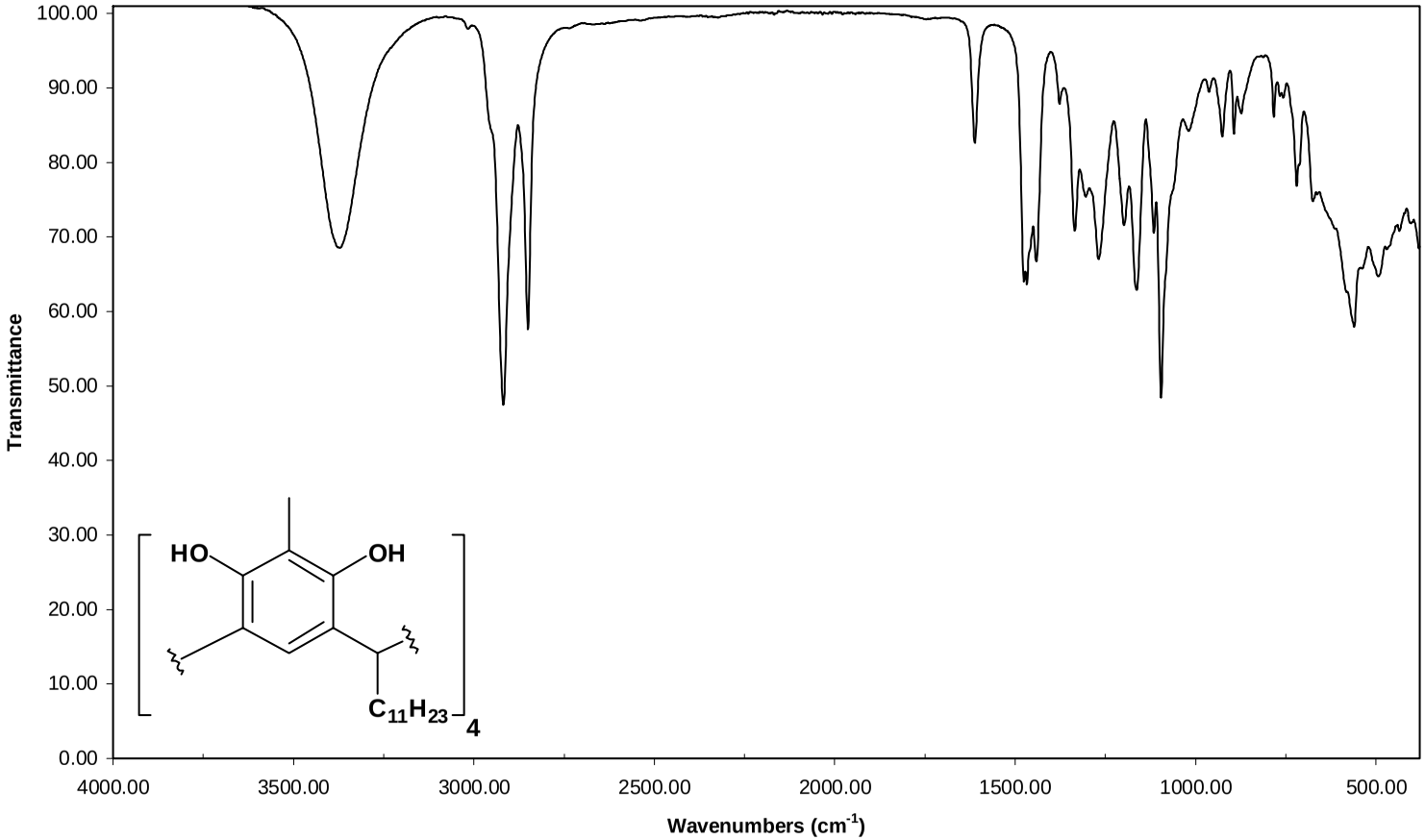

Spectrum 1.35: Infrared spectrum of 18 (KBr)

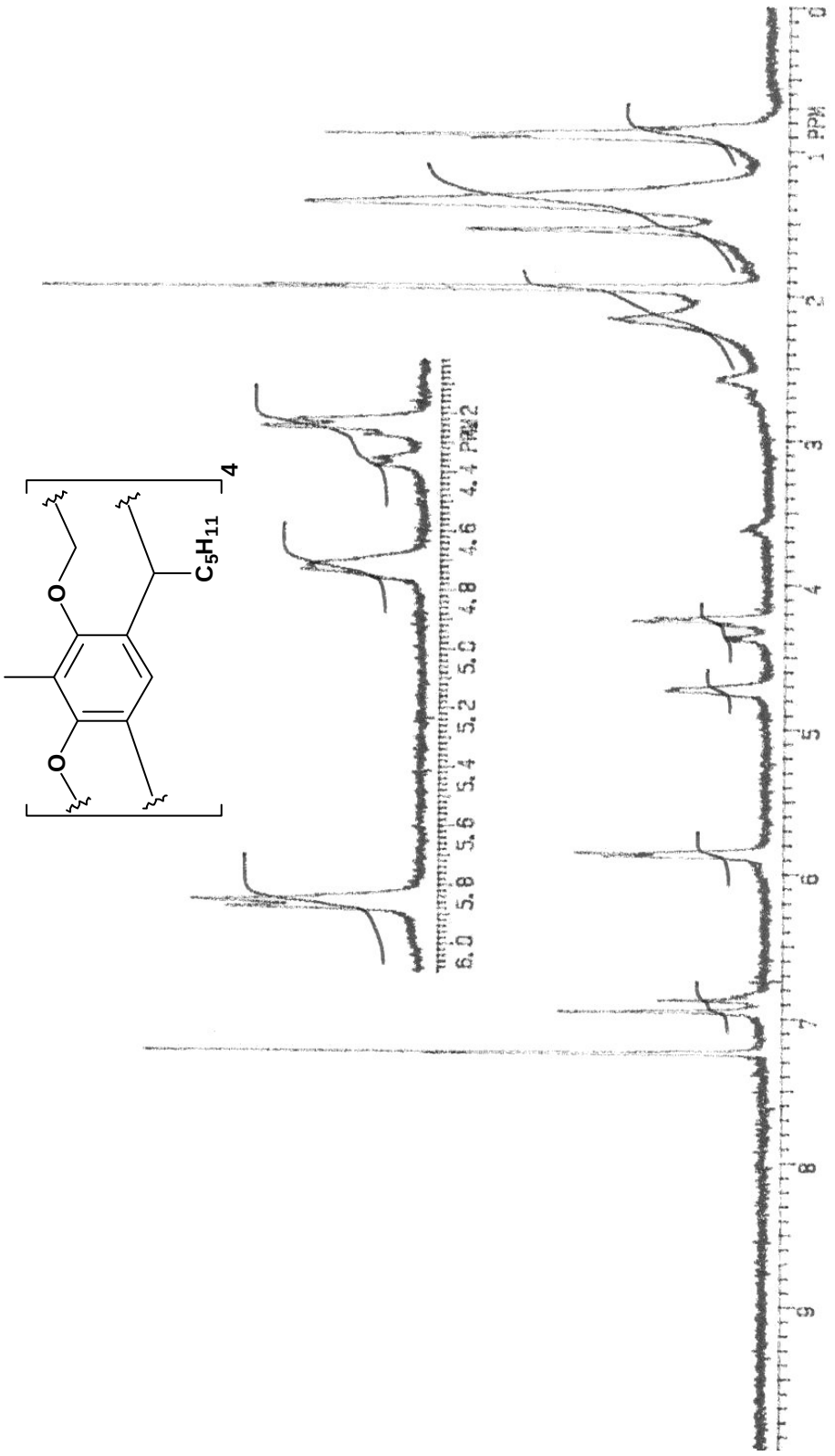

Spectrum 1.36: ^{1}H NMR spectrum of 19 in $CDCl_3$ (300 MHz)

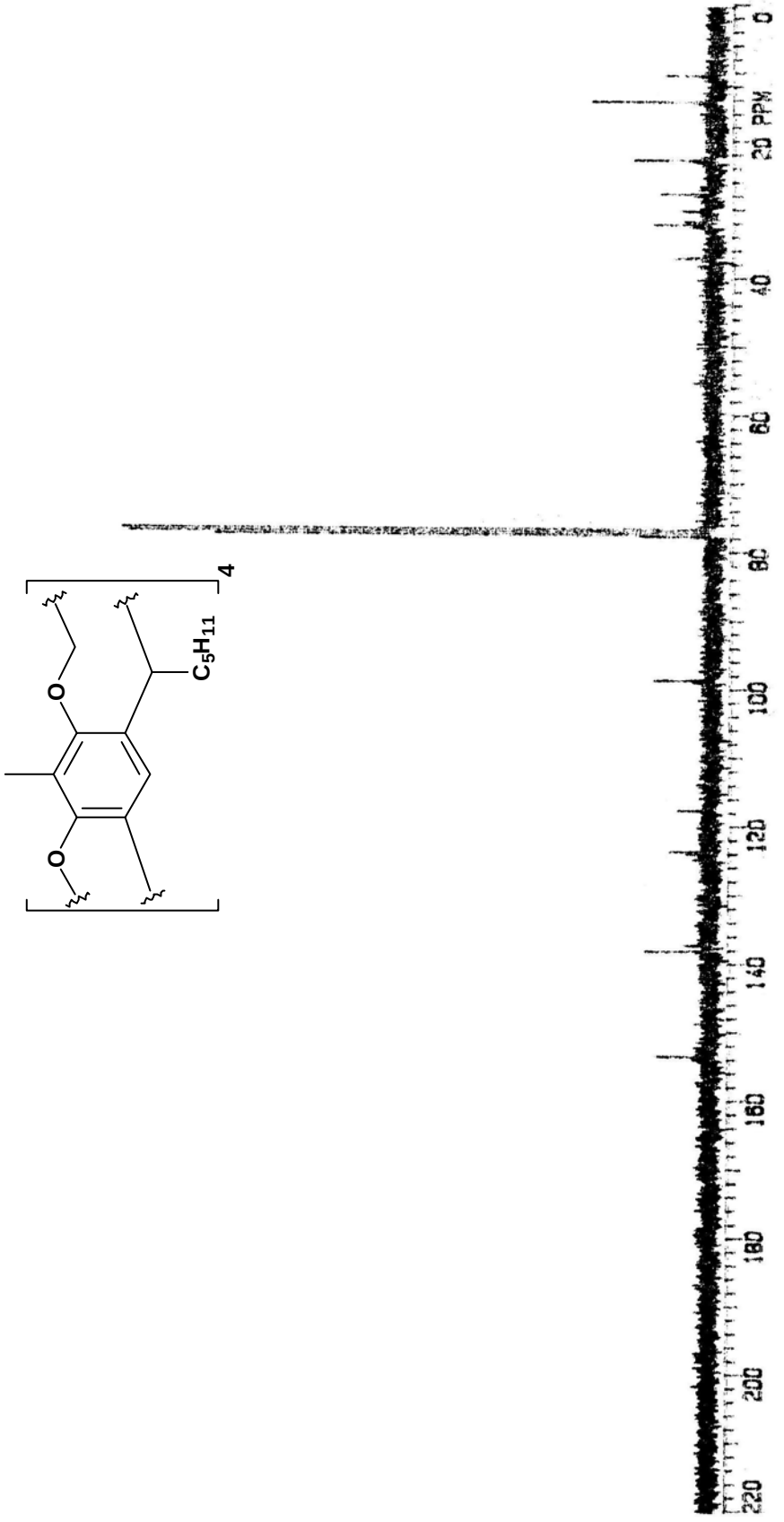

Spectrum 1.37: ^{13}C NMR spectrum of 19 in $CDCl_3$ (75 MHz)

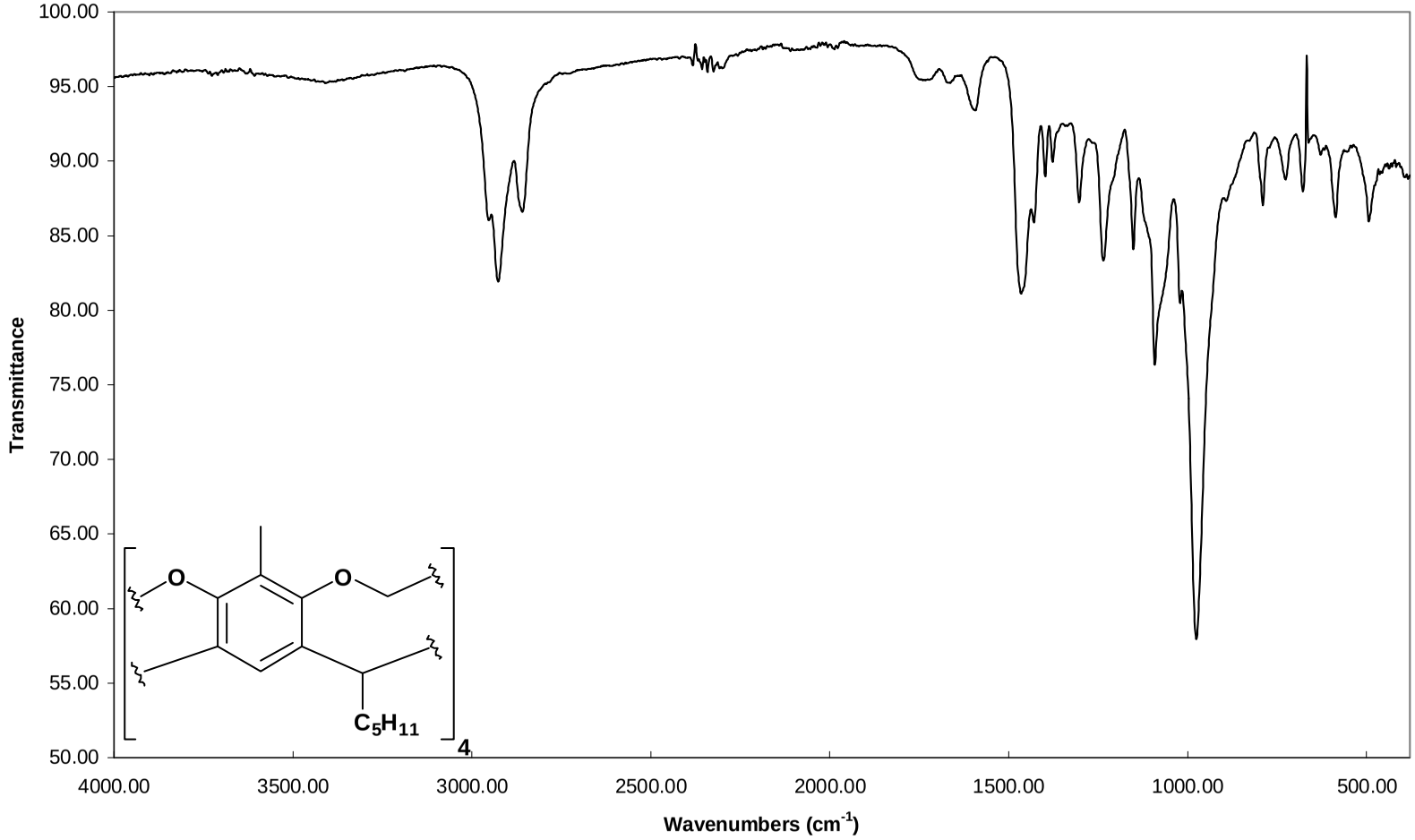

Spectrum 1.38: Infrared spectrum of 19 (KBr)

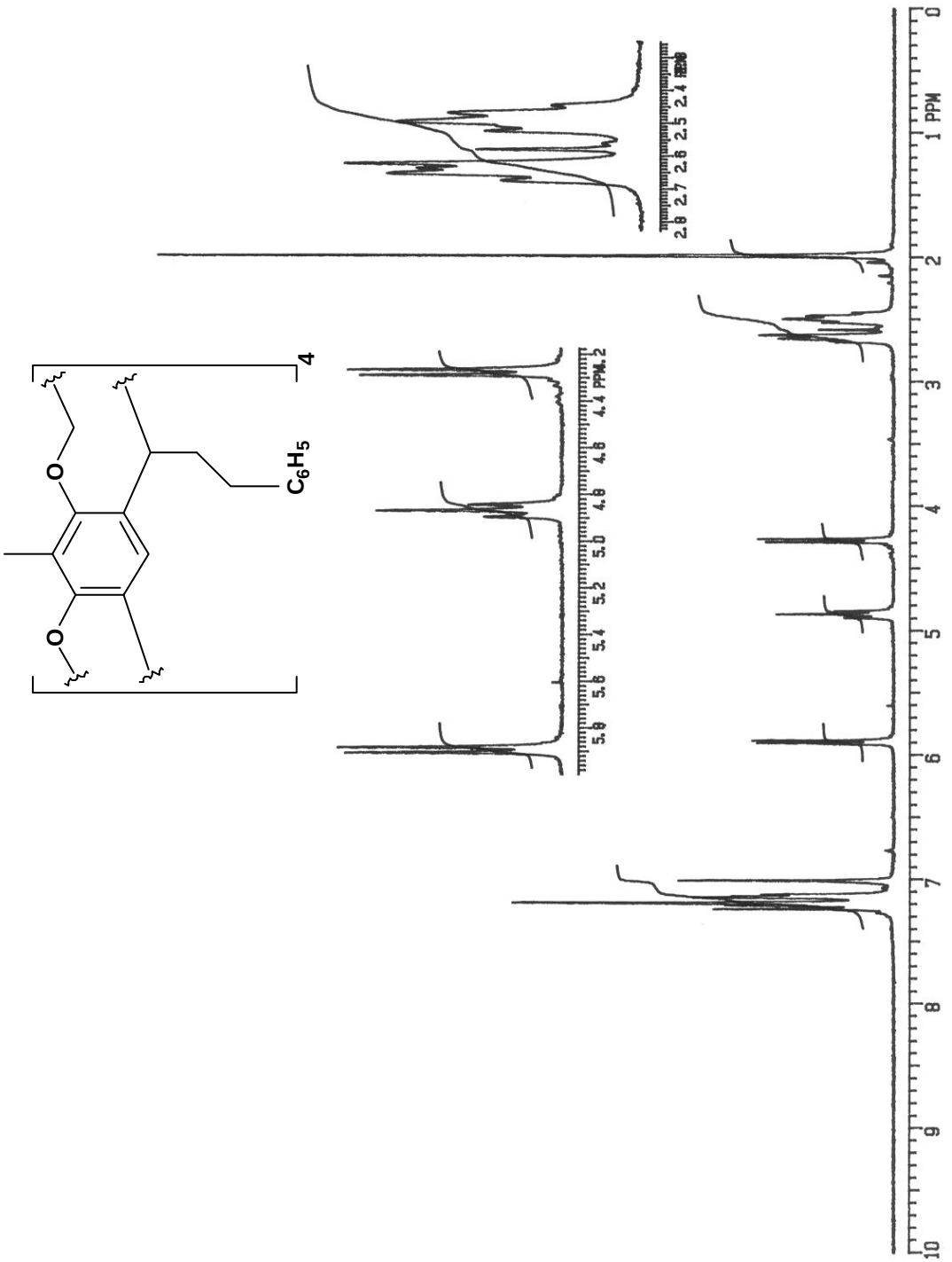

Spectrum 1.39: ^{1}H NMR spectrum of 20 in $CDCl_3$ (300 MHz)

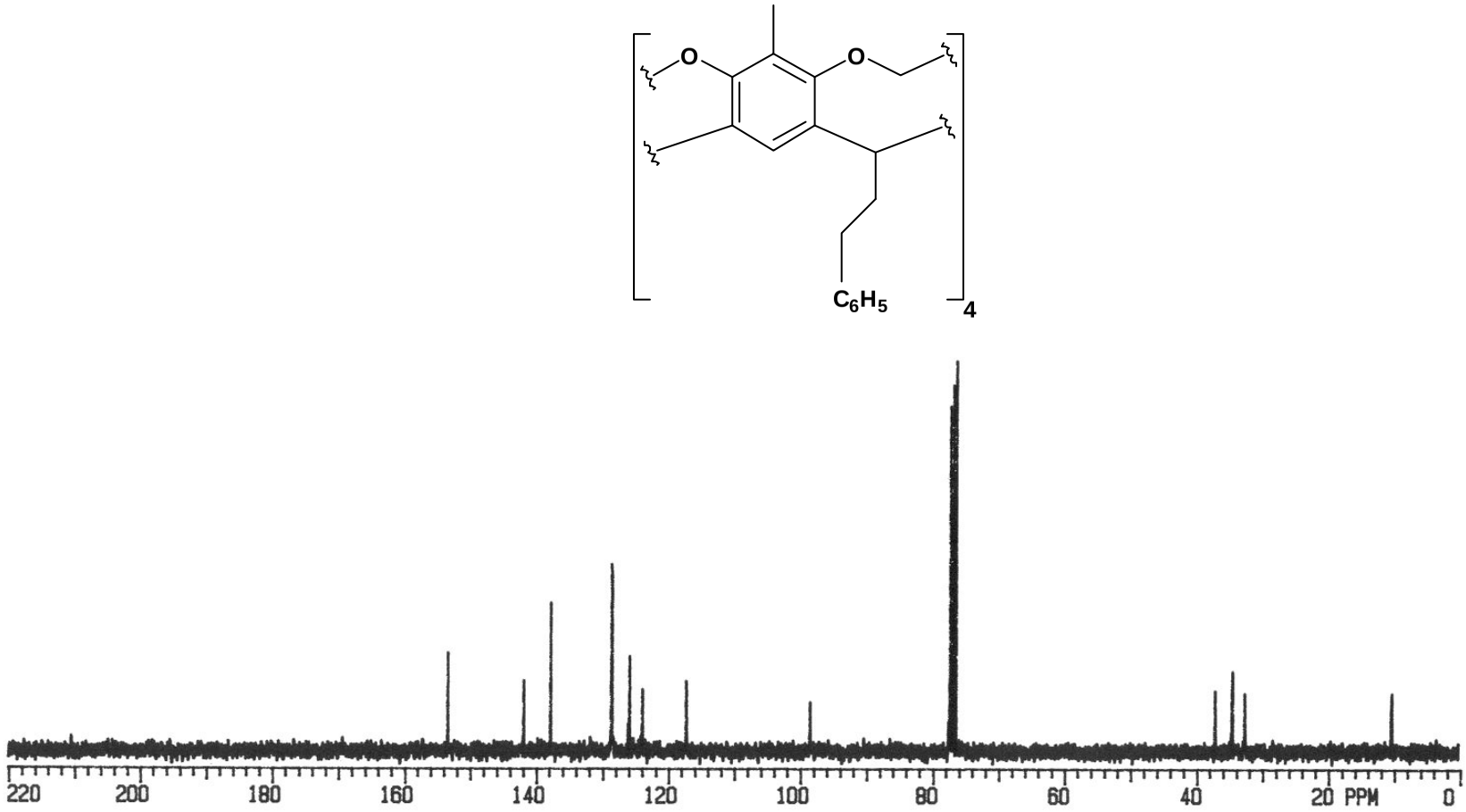

Spectrum 1.40: ^{13}C NMR spectrum of 20 in $CDCl_3$ (75 MHz)

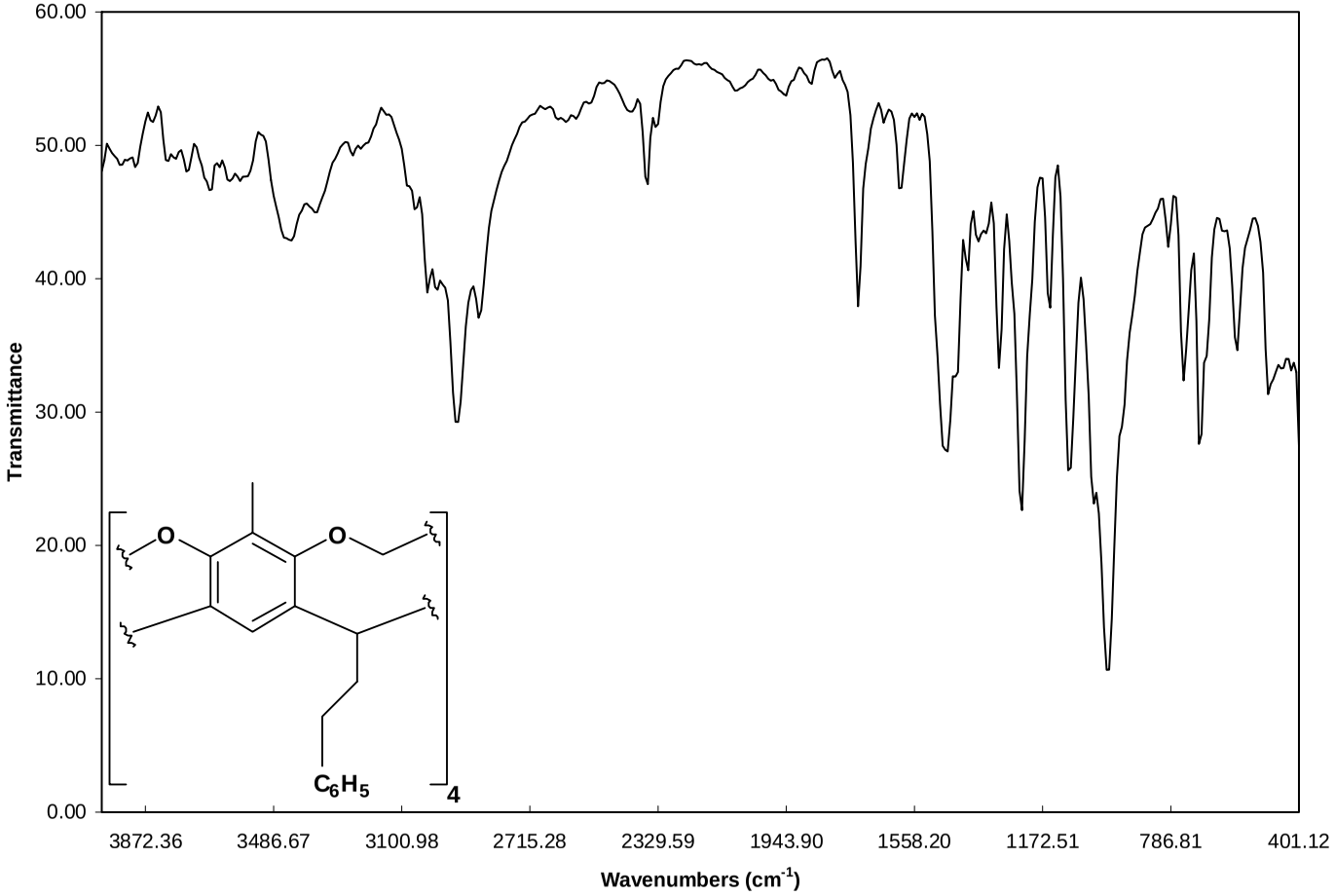

Spectrum 1.41: Infrared spectrum of 20 (KBr)

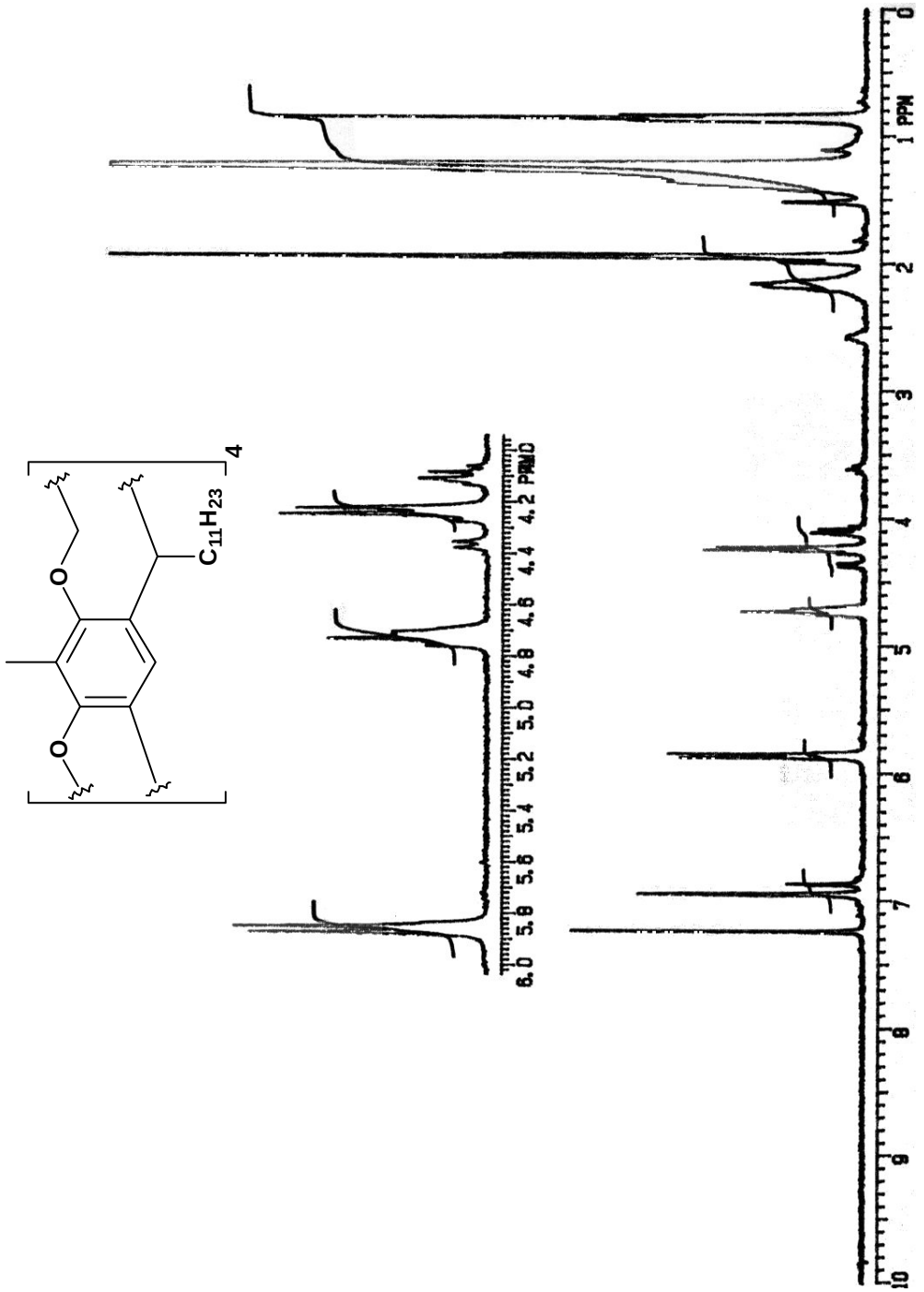

Spectrum 1.42: ^{1}H NMR spectrum of 21 in $CDCl_3$ (300 MHz)

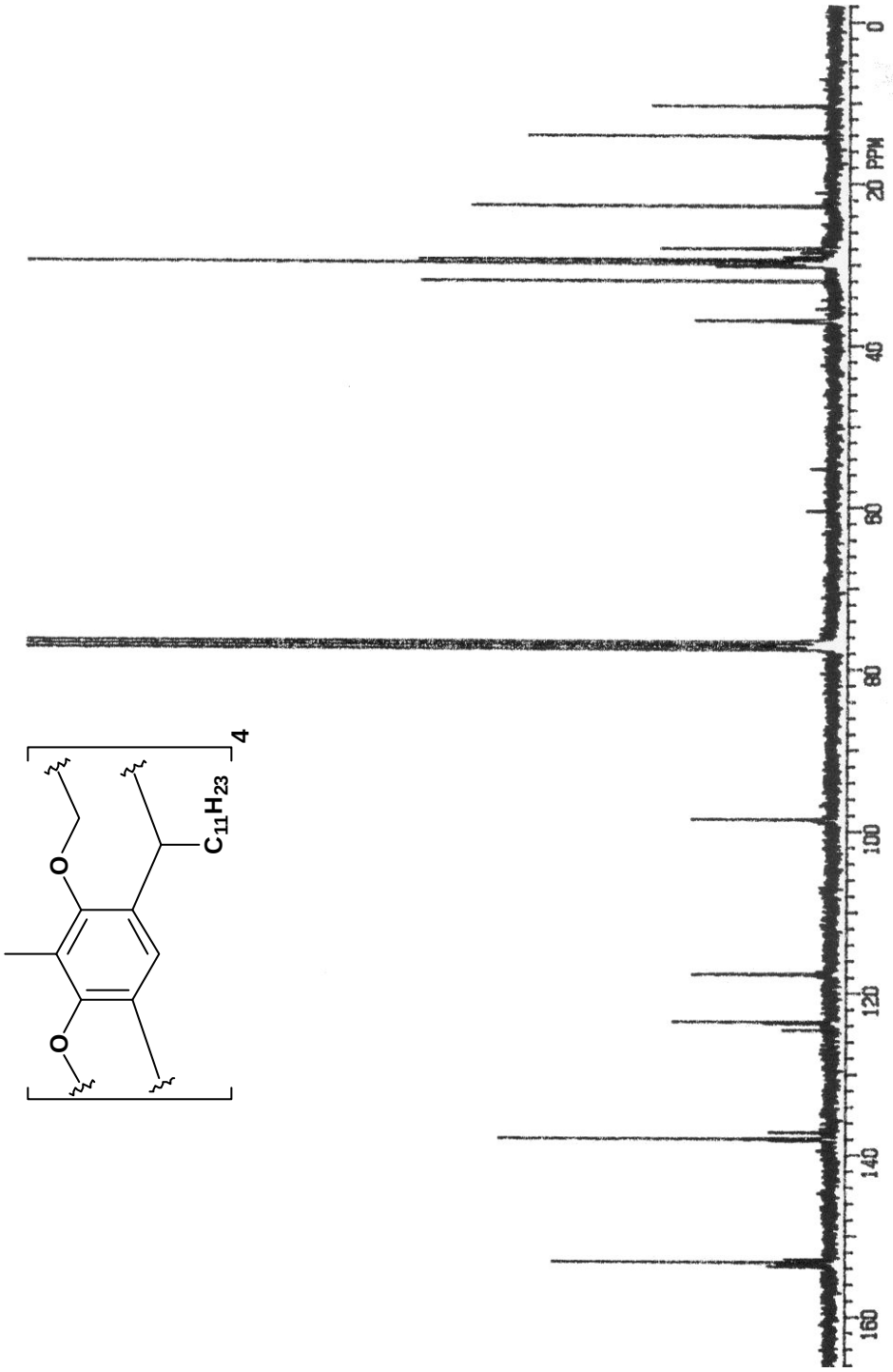

Spectrum 1.43: ^{1}H NMR spectrum of 21 in $CDCl_3$ (75 MHz)

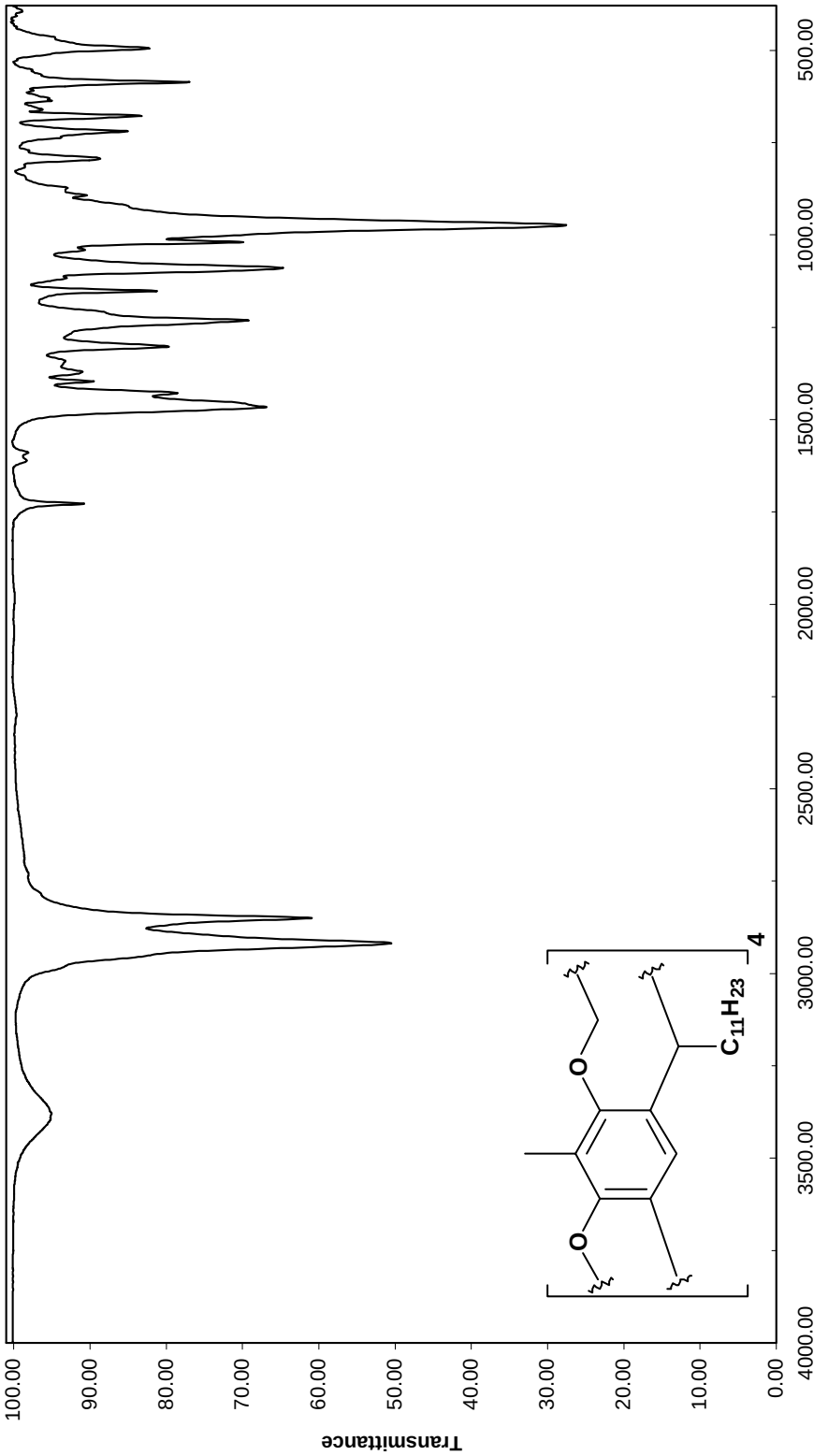

Spectrum 1.44: Infrared spectrum of 21 (KBr)

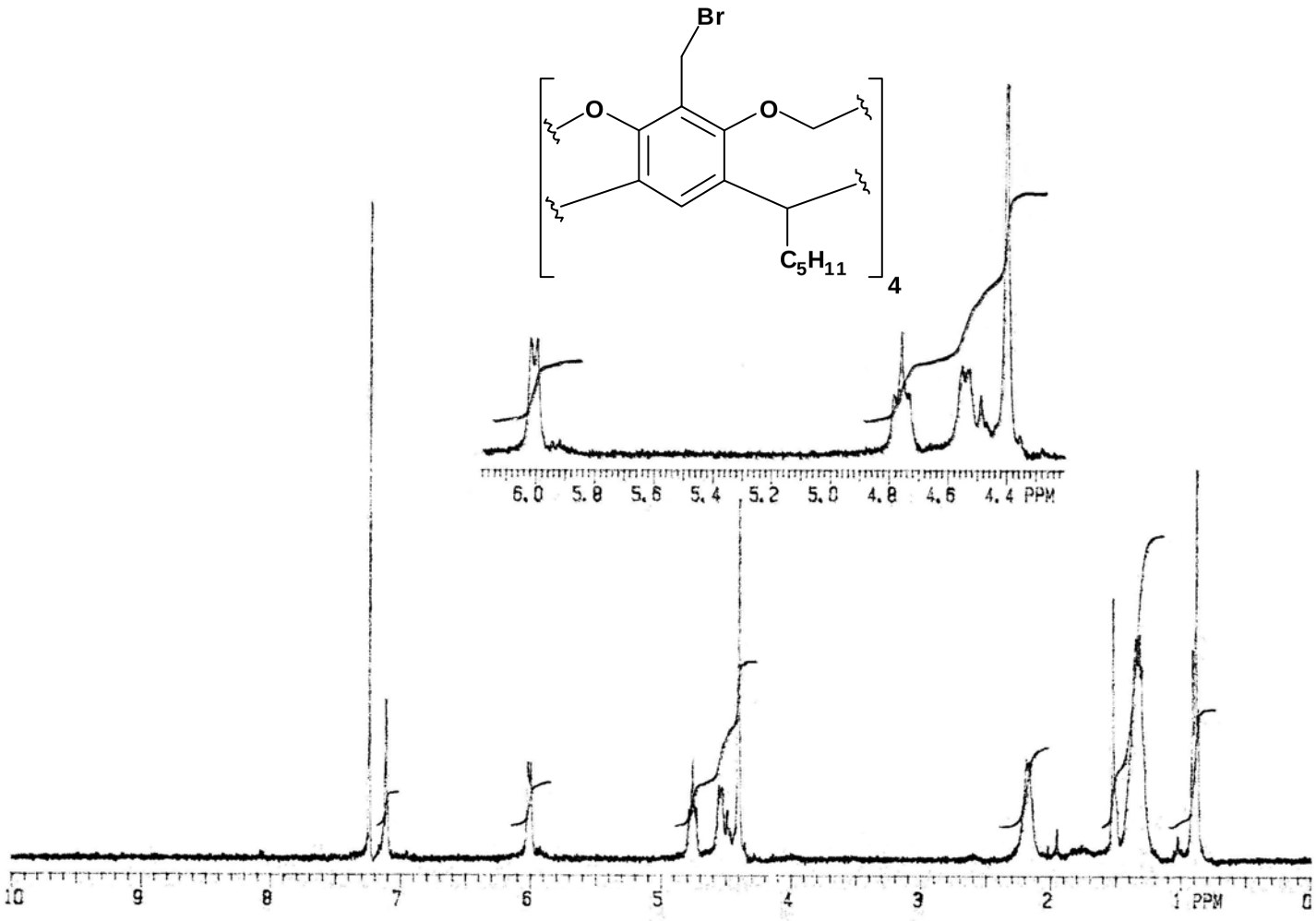

Spectrum 1.45: ^{1}H NMR spectrum of 22 in $CDCl_3$ (300 MHz)

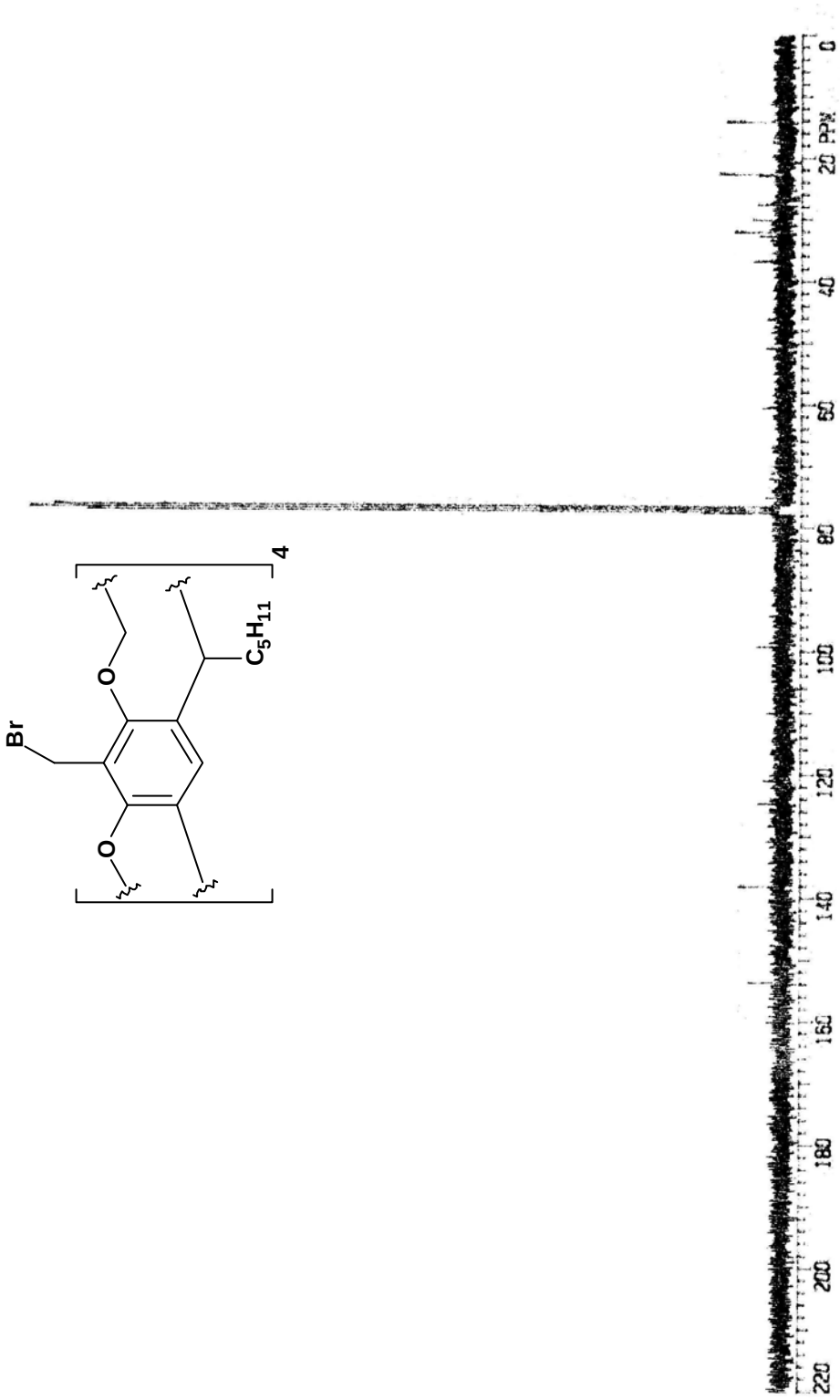

Spectrum 1.46: ^{13}C NMR spectrum of 22 in $CDCl_3$ (75 MHz)

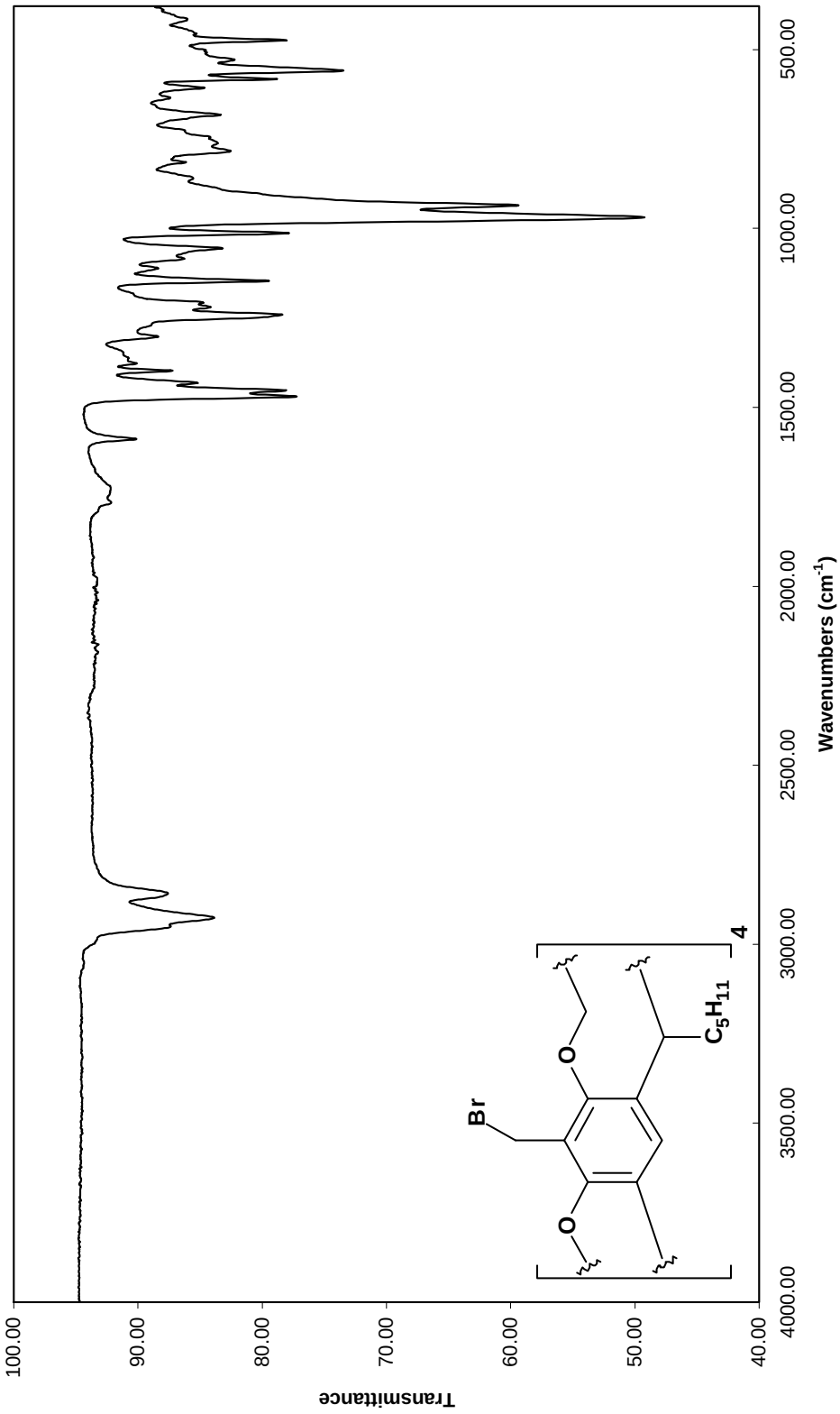

Spectrum 1.47: Infrared spectrum of 22 (KBr)

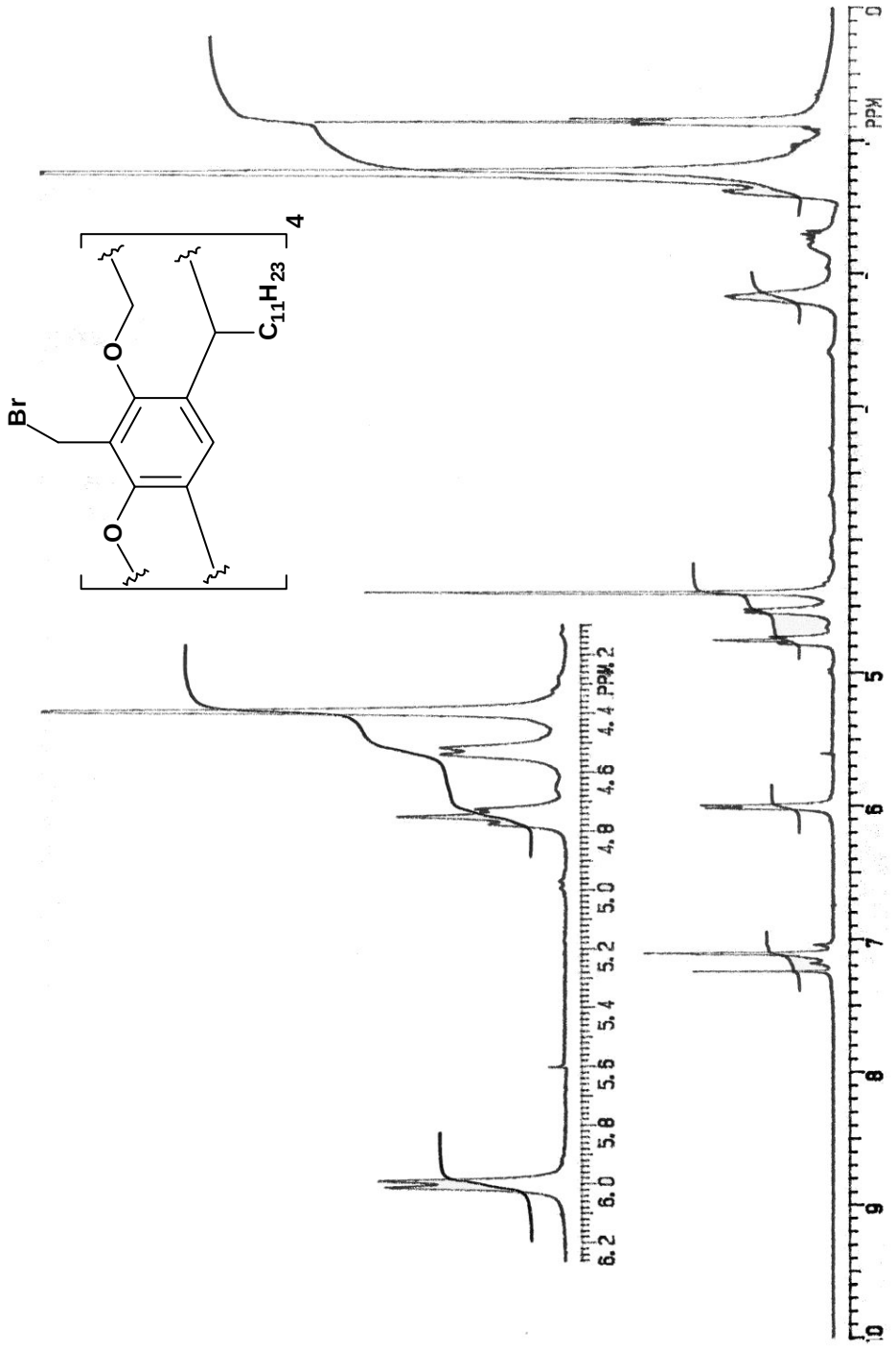

Spectrum 1.48: ^{1}H NMR spectrum of 24 in $CDCl_3$ (300 MHz)

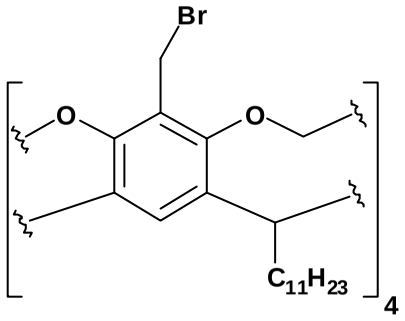

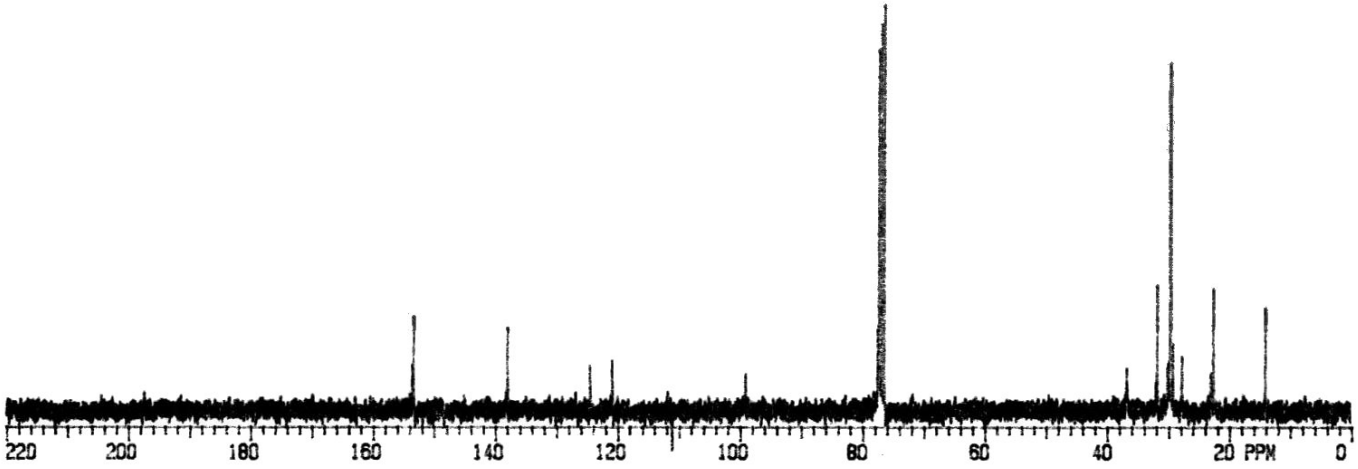

Spectrum 1.49: ^{13}C NMR spectrum of 24 in $CDCl_3$ (75 MHz)

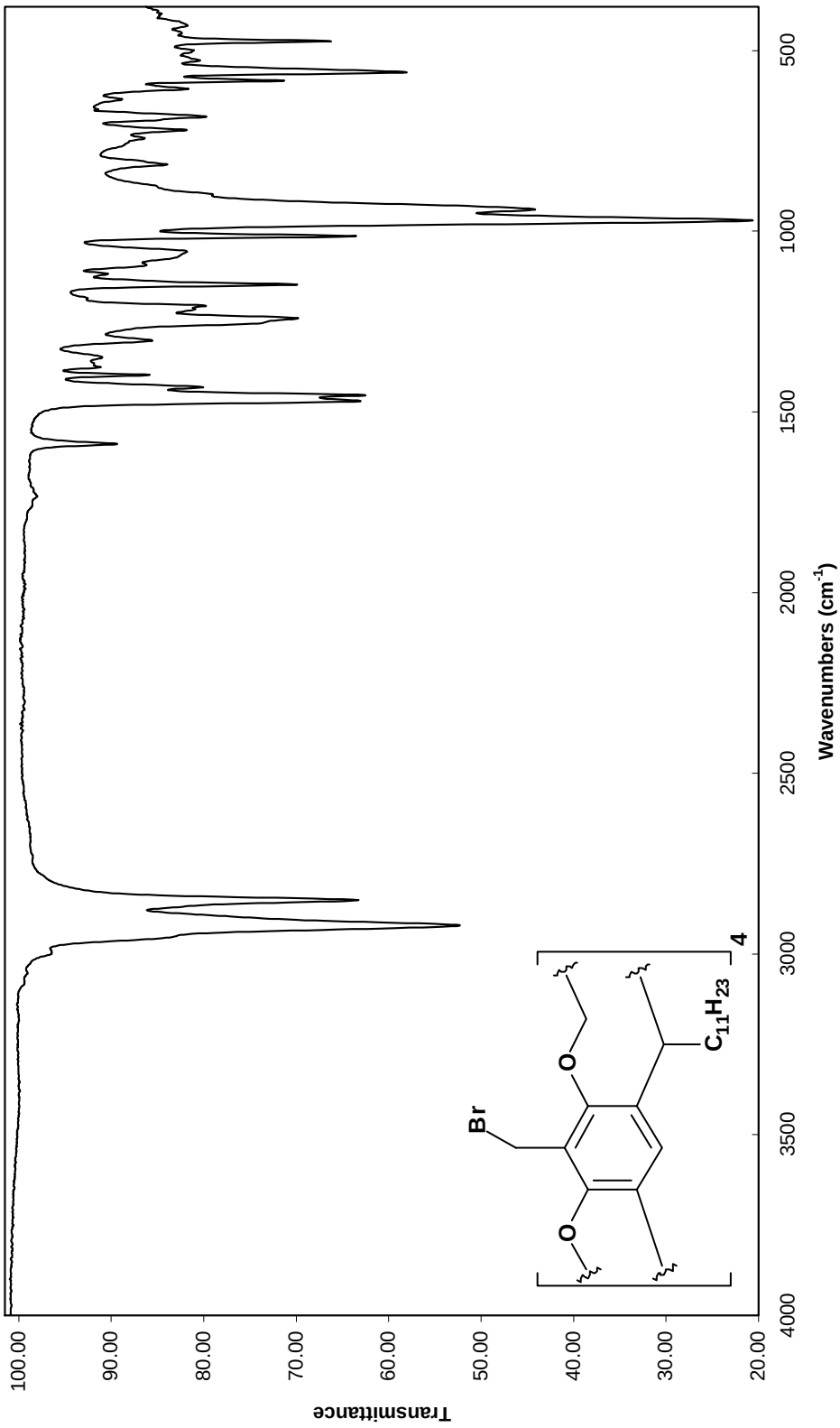

Spectrum 1.50: Infrared spectrum of 24 (KBr)

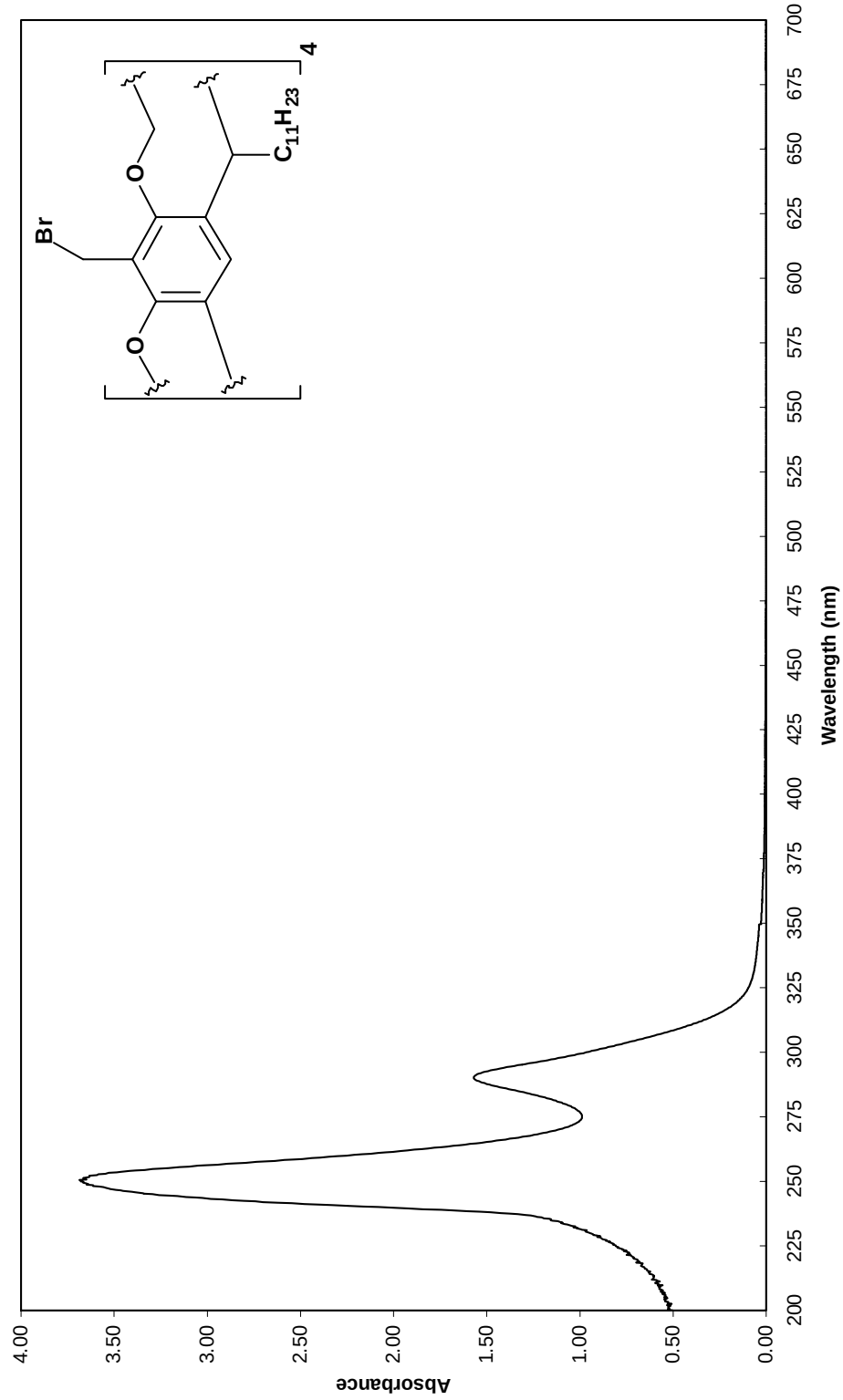

Spectrum 1.51: UV-Visible spectrum of 24 from 200-700 nm ($CHCl_3$)

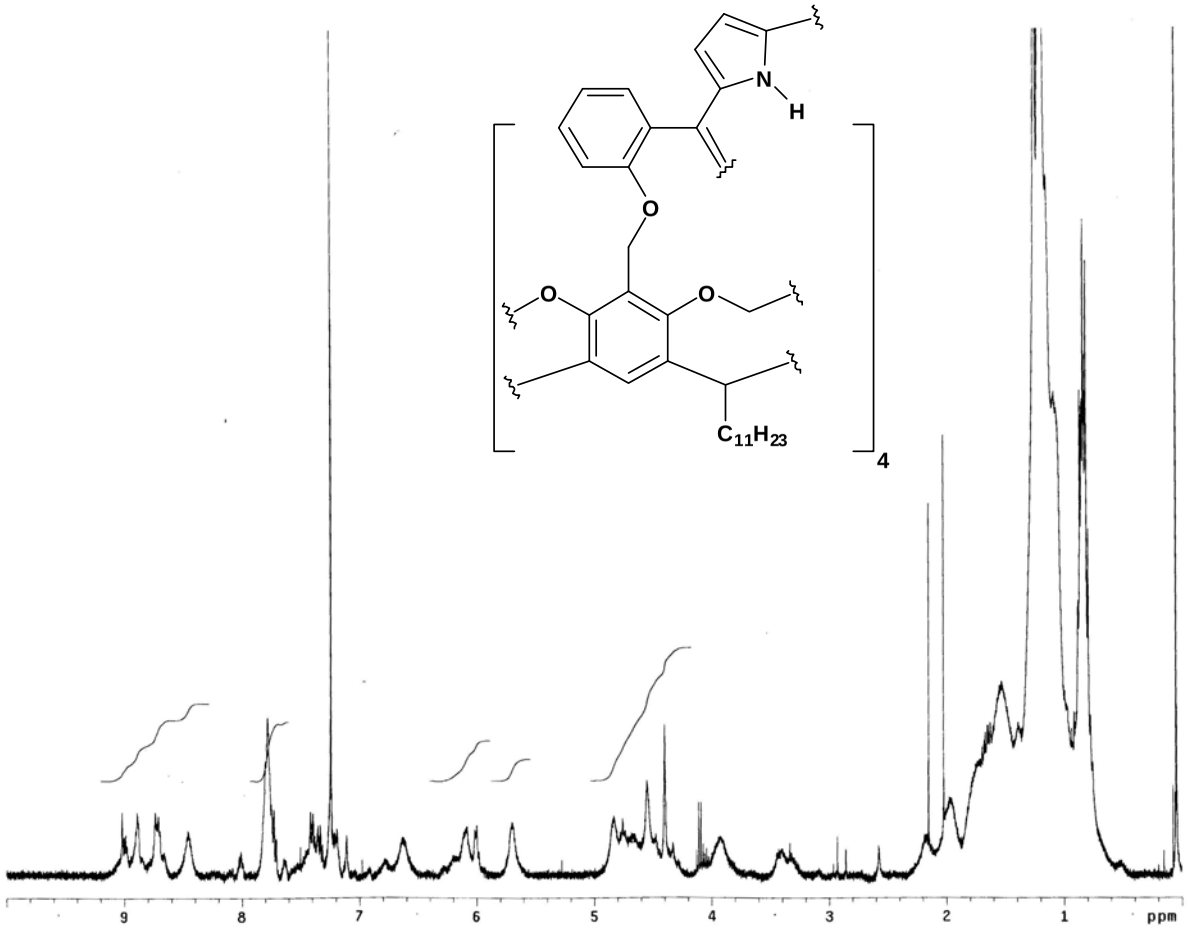

Spectrum 1.52: ^{1}H NMR spectrum of 26 in $CDCl_3$ (400 MHz)

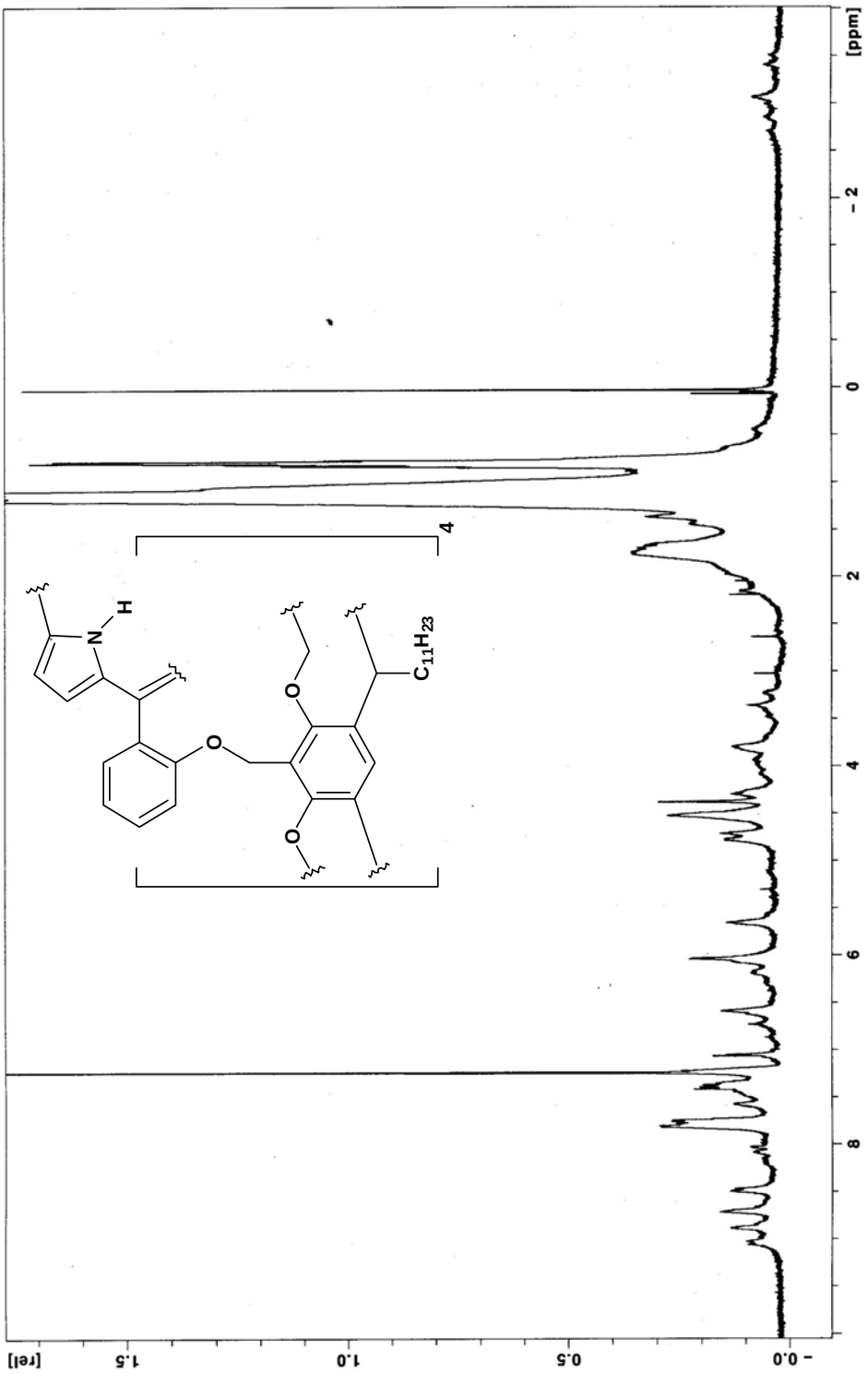

Spectrum 1.53: Low temperature ^{1}H NMR spectrum of 26 in $CDCl_3$ (600 MHz)

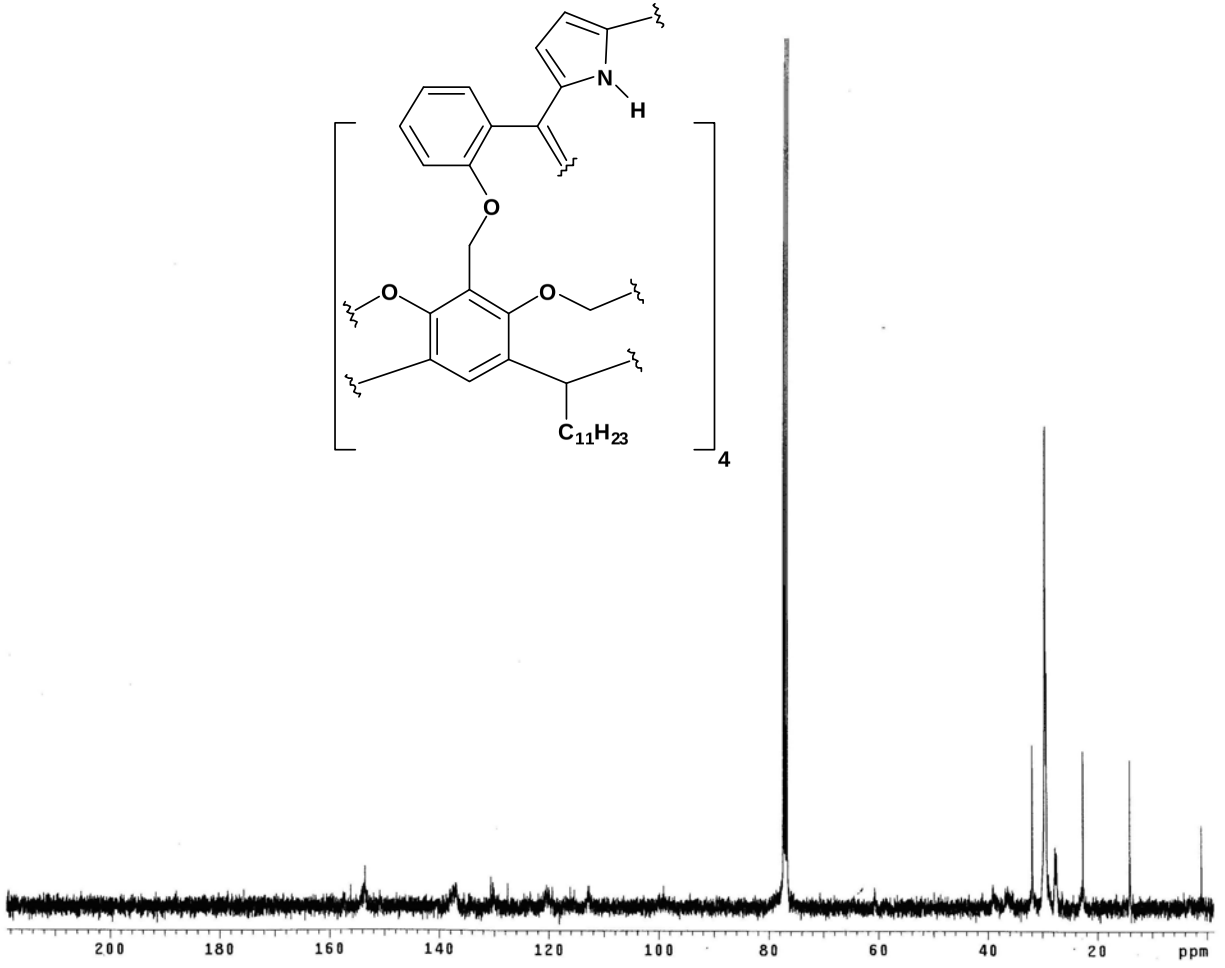

Spectrum 1.54: ^{13}C NMR spectrum of 26 in $CDCl_3$ (100 MHz)

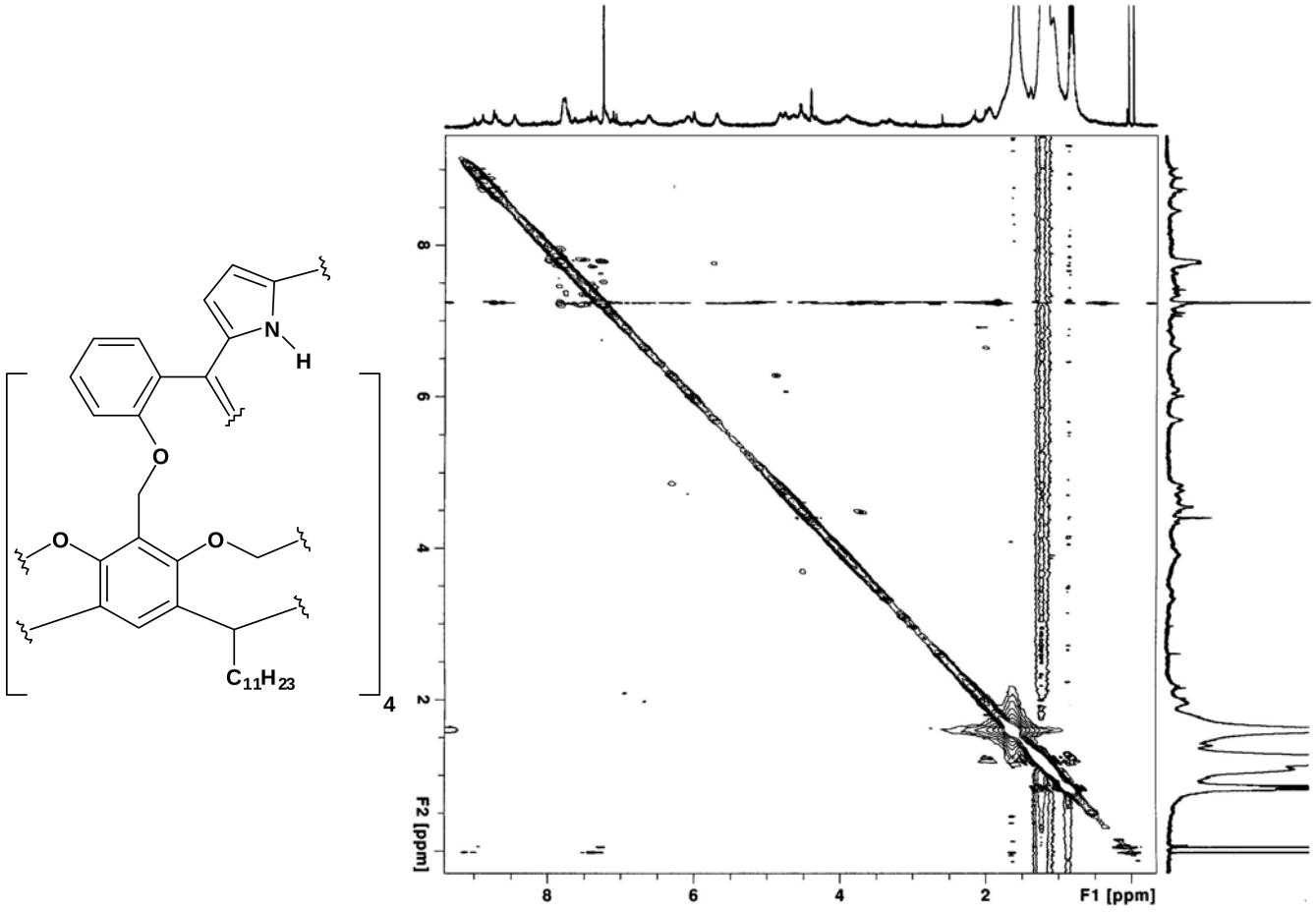

Spectrum 1.55: NOESY spectrum of 26 in $CDCl_3$ at room temperature

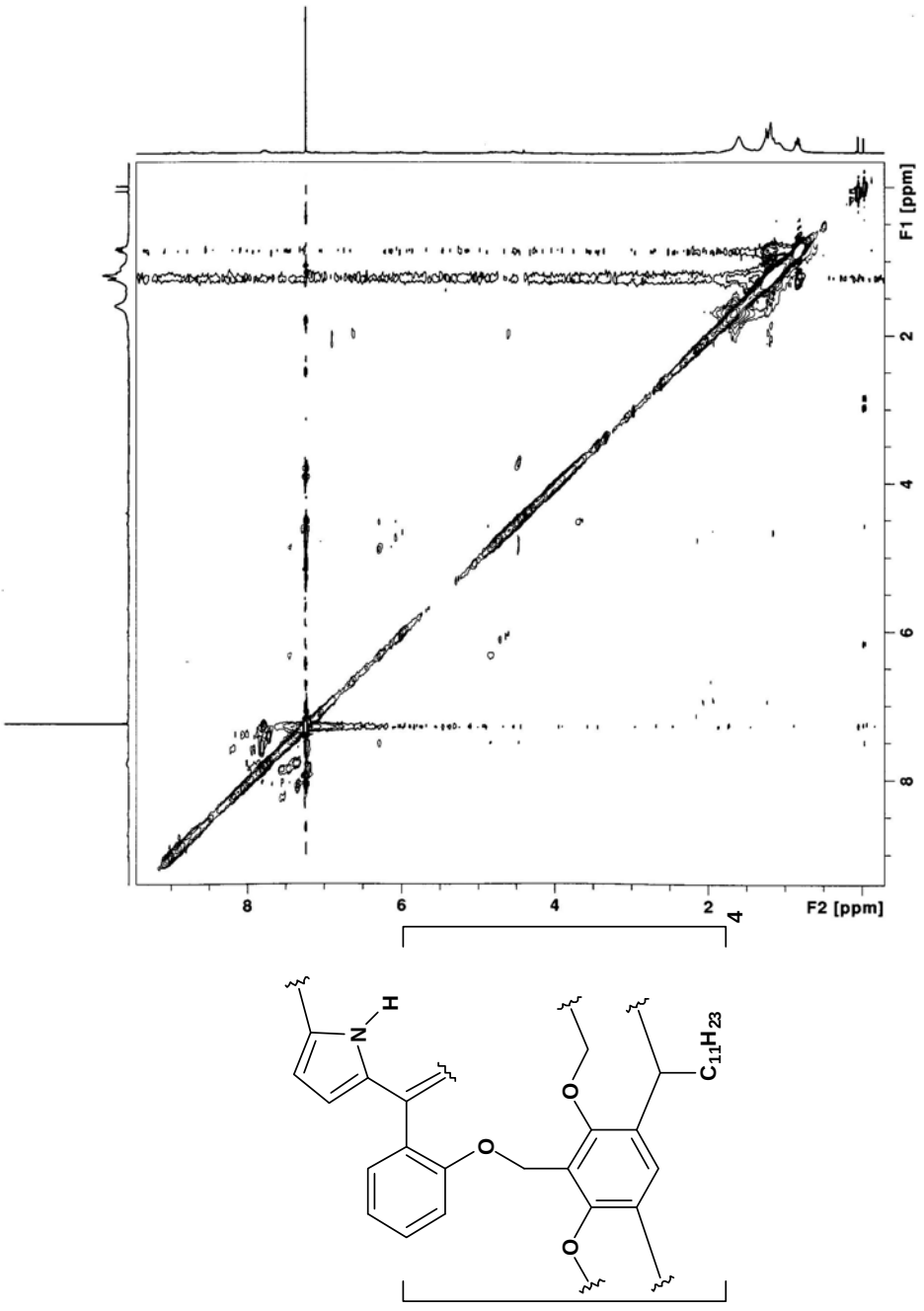

Spectrum 1.56: NOESY spectrum of 26 in $CDCl_3$ at low temperature

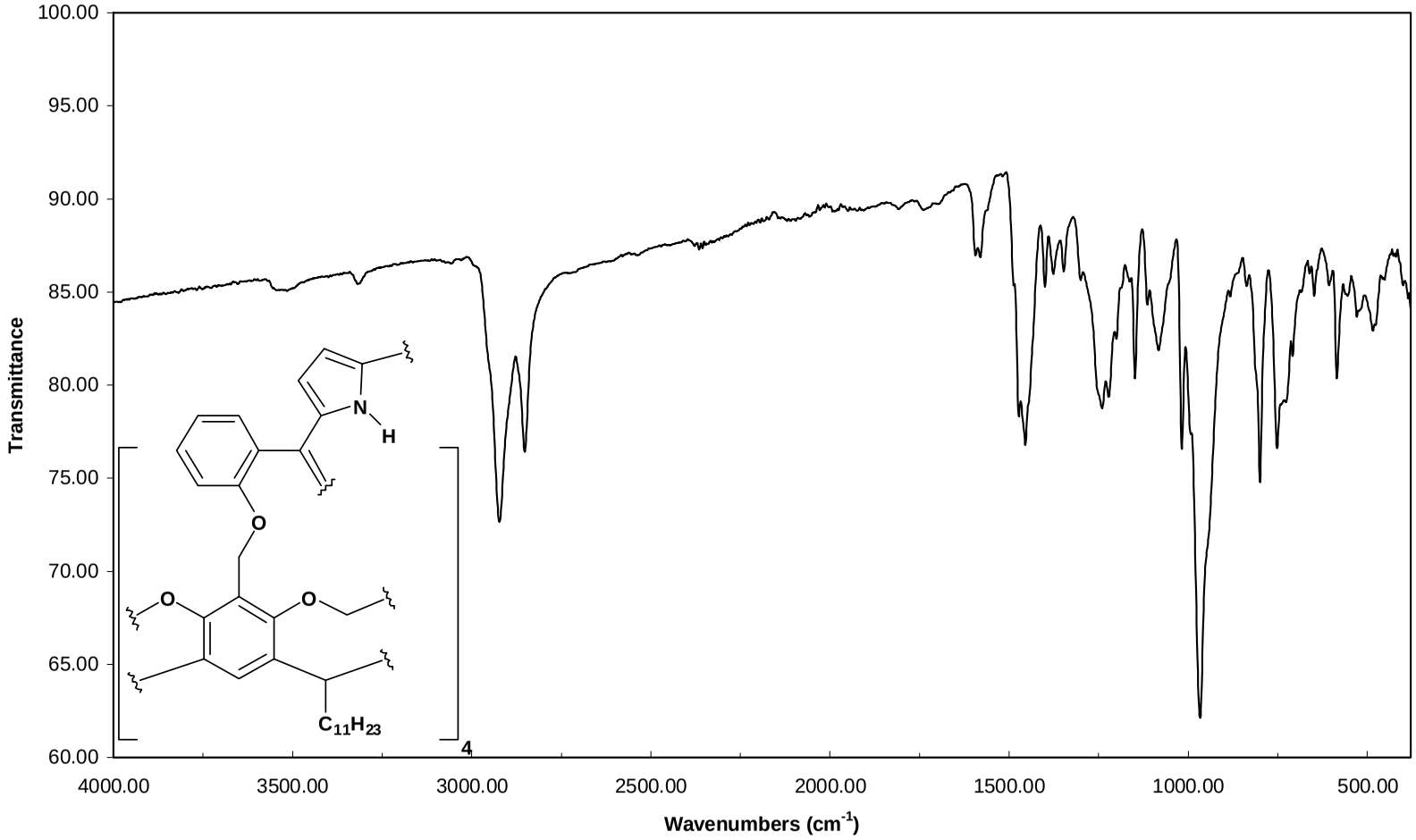

Spectrum 1.57: Infrared spectrum of 26 (KBr)

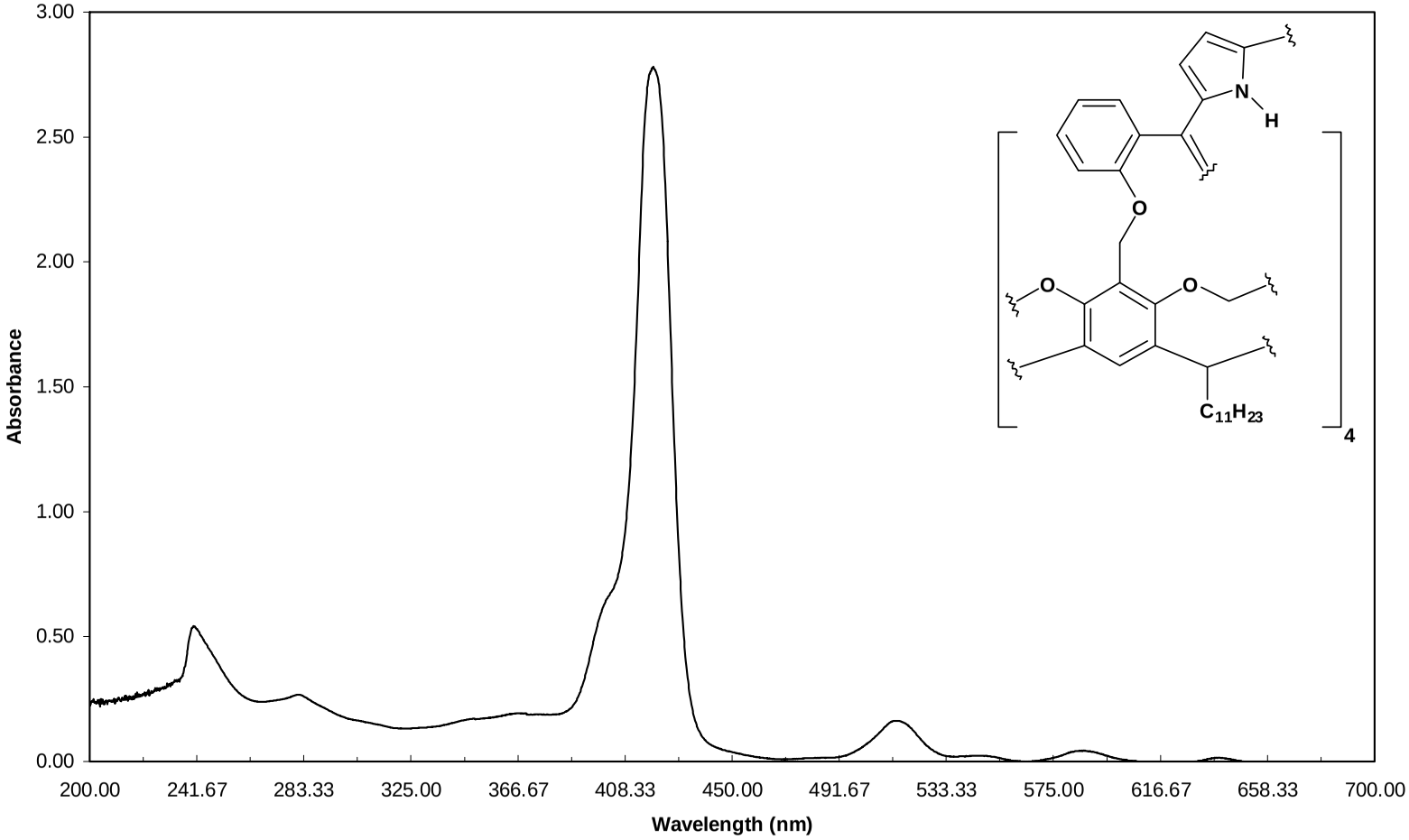

Spectrum 1.58: UV-Visible spectrum of 26 from 200-700 nm ($CHCl_3$)

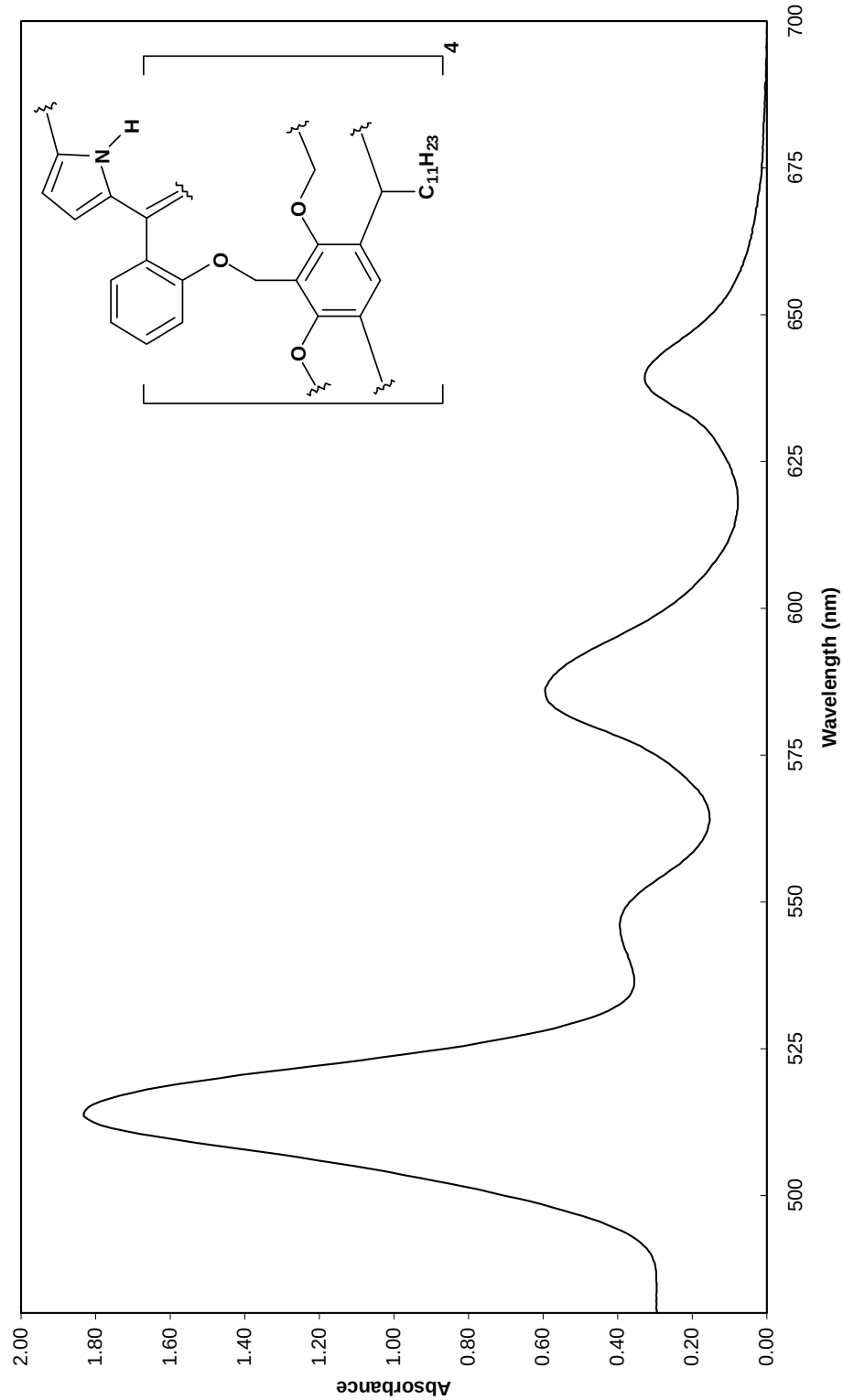

Spectrum 1.59: UV-Visible spectrum of 26 from 480-700 nm ($CHCl_3$)

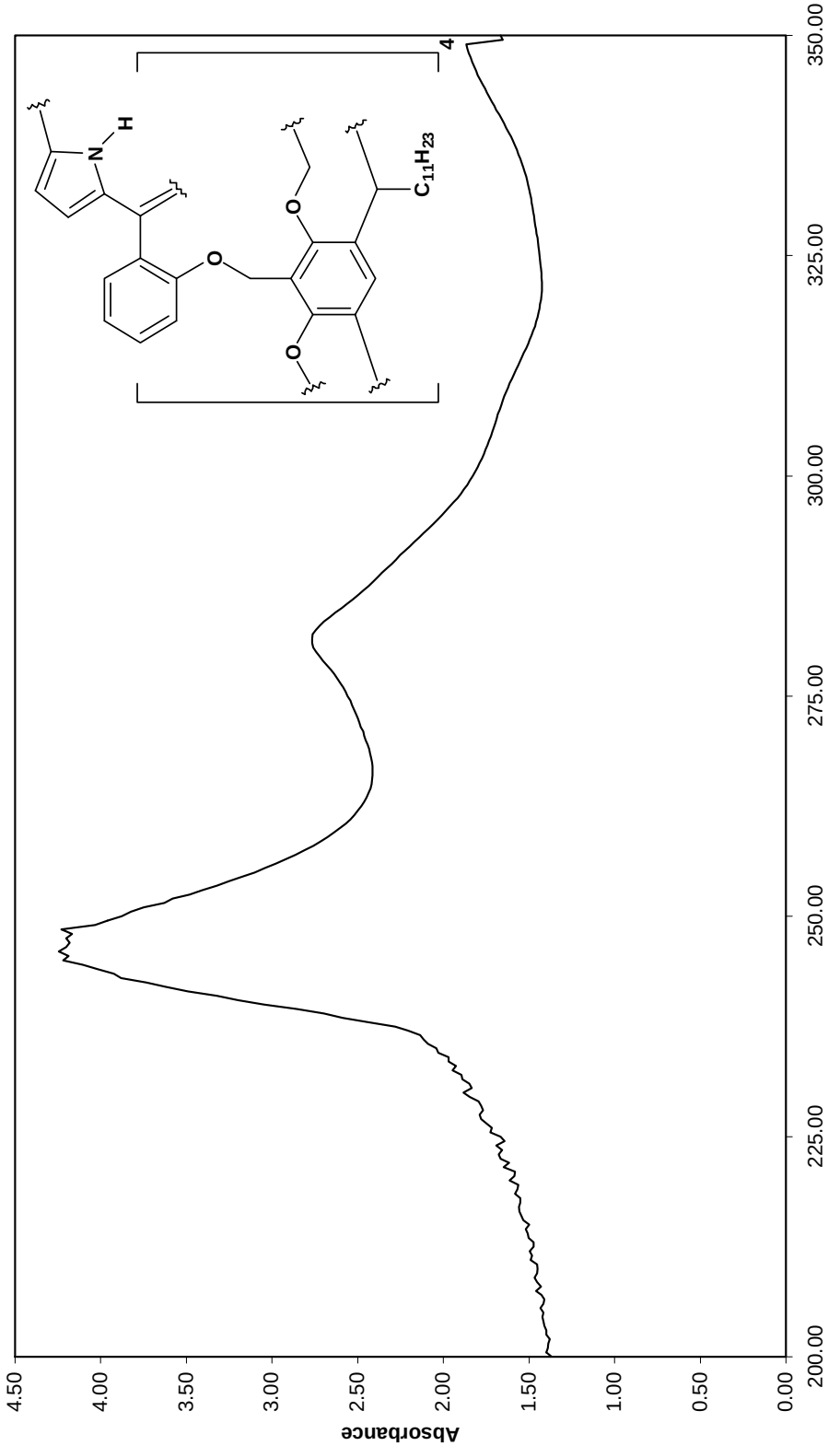

Spectrum 1.60: UV-Visible spectrum of 26 from 200-350 nm ($CHCl_3$)

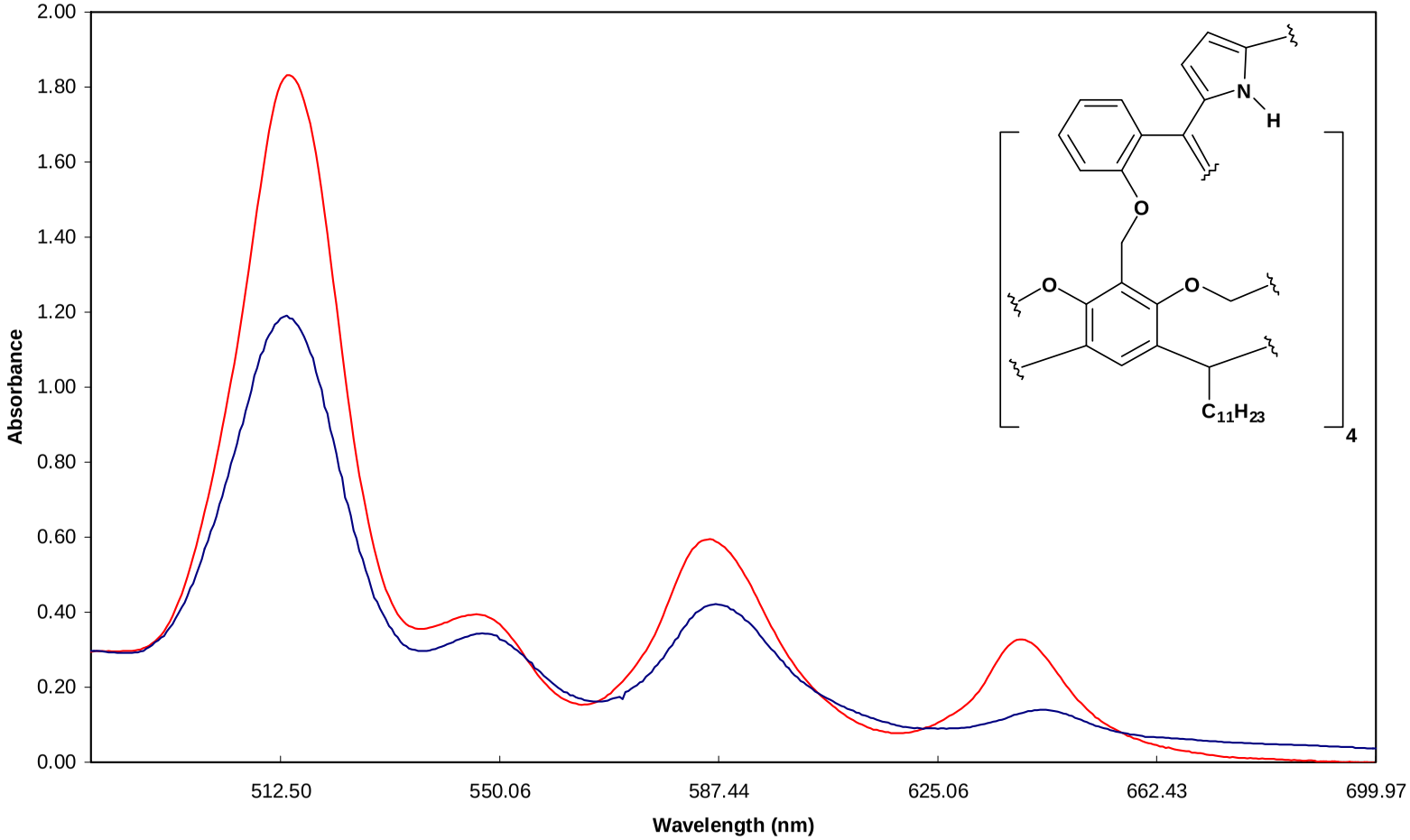

Spectrum 1.61: Comparison of UV-Visible spectra of 26 (red) and 12 (blue) from 480-700 nm ($CHCl_3$)

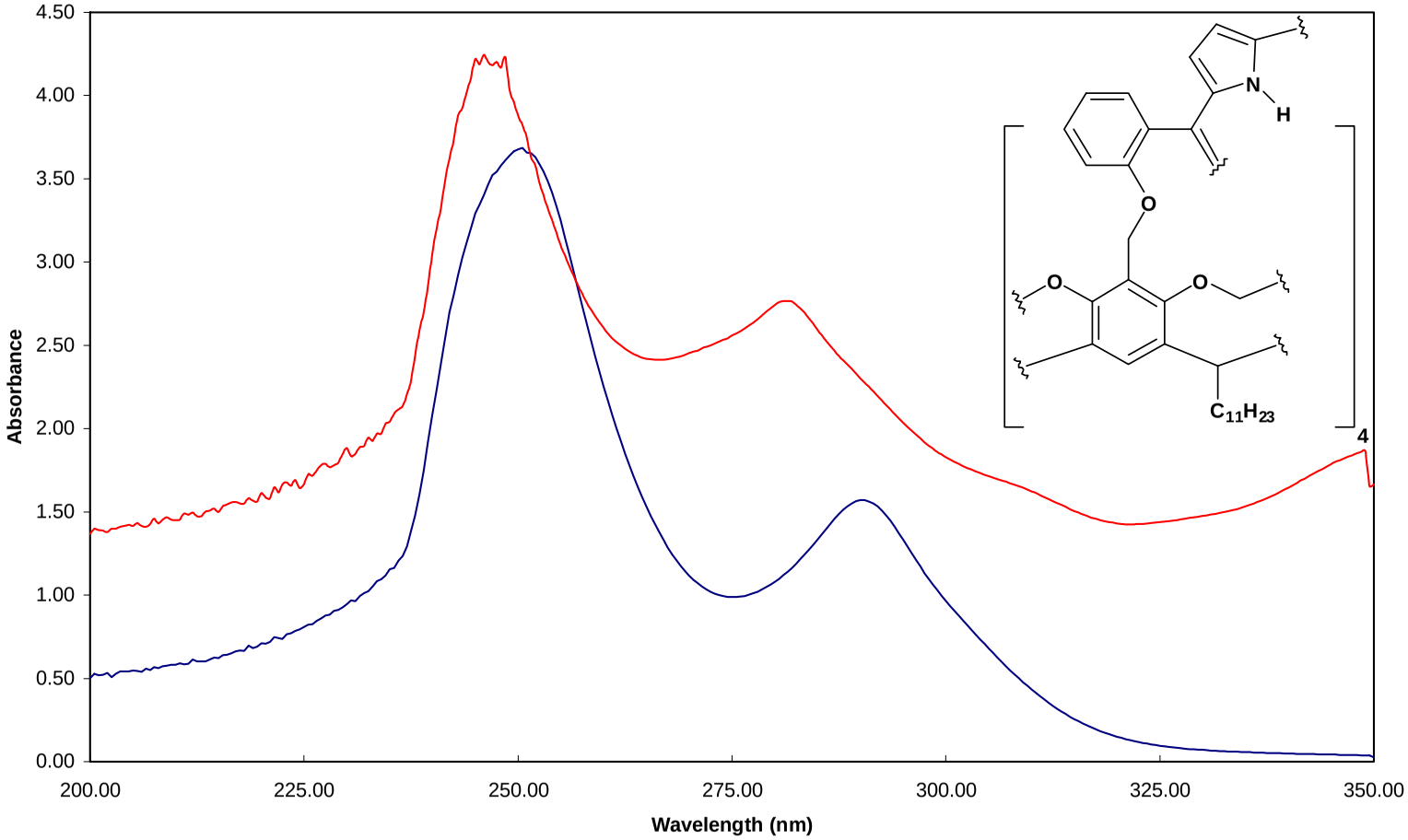

Spectrum 1.62: Comparison of UV-Visible spectra of 26 (red) and 24 (blue) from 200-350 nm ($CHCl_3$)

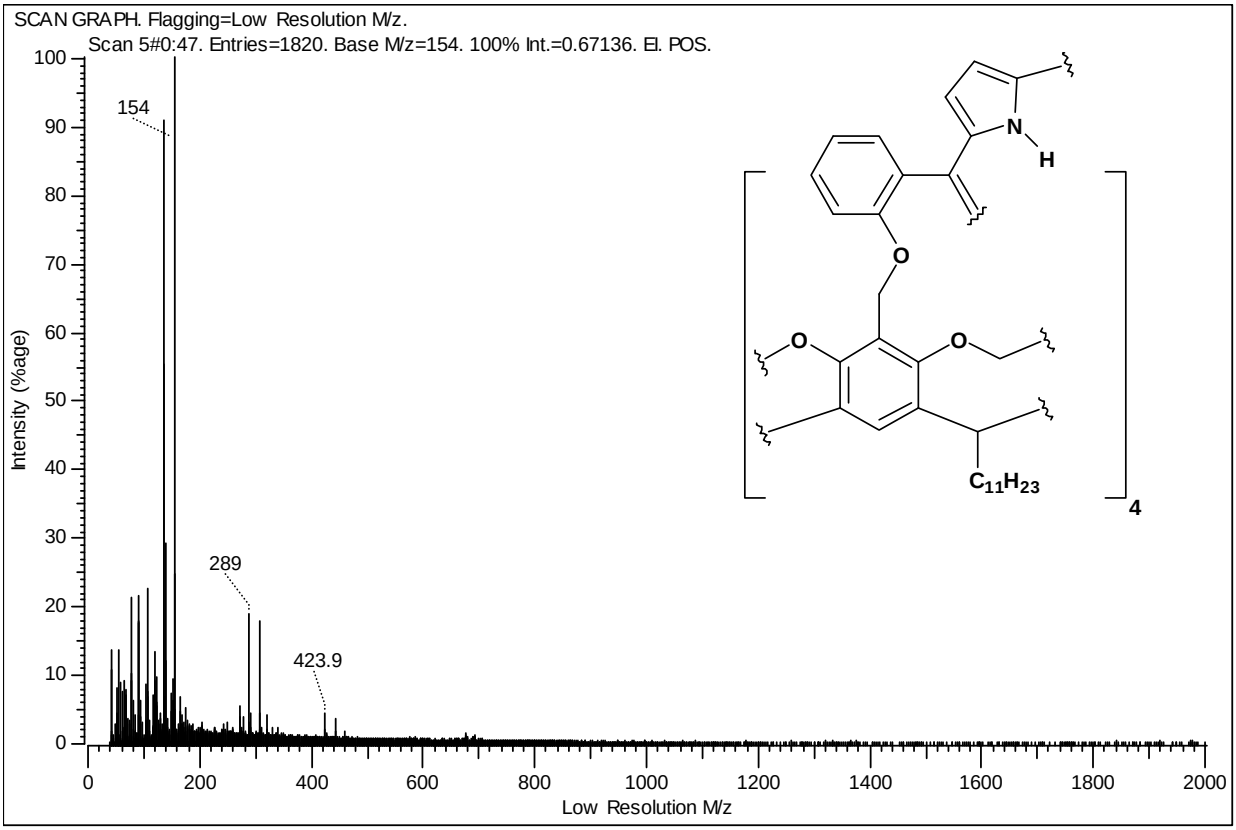

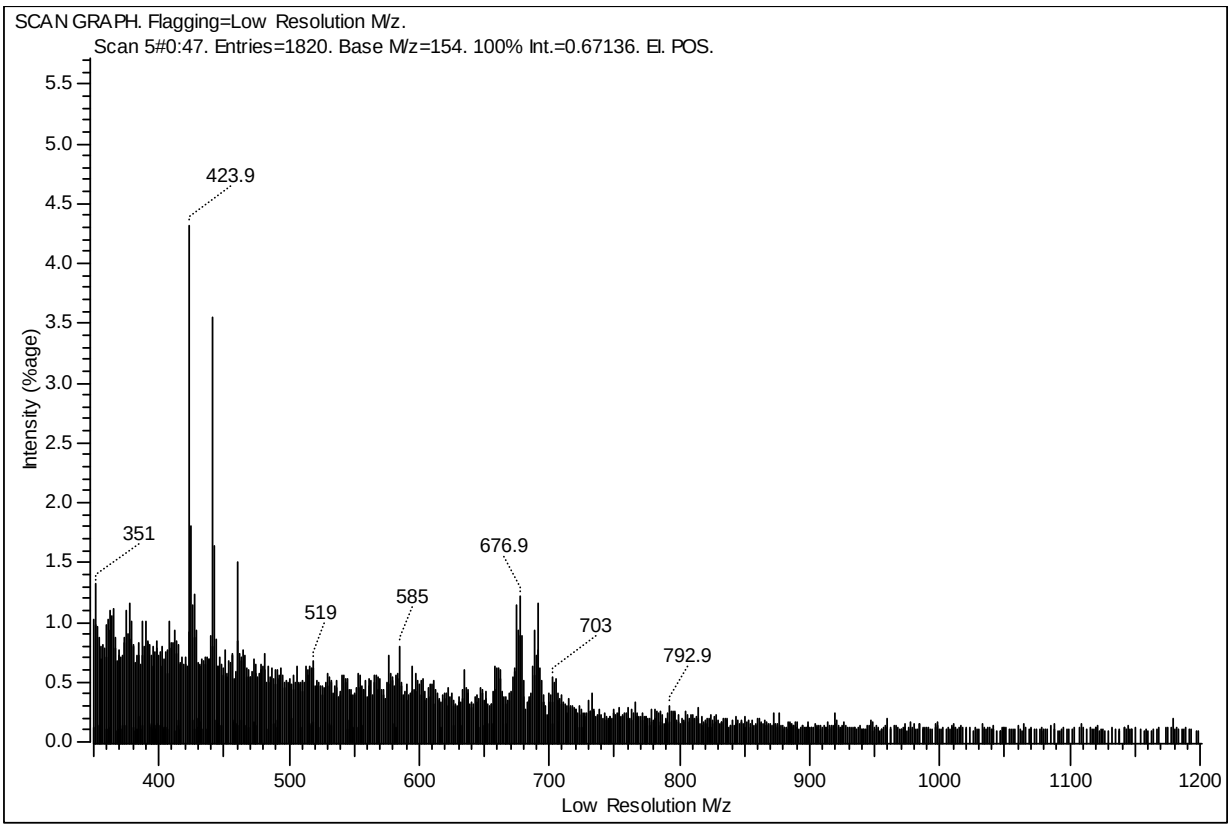

Spectrum 1.63: FAB mass spectrum of 26

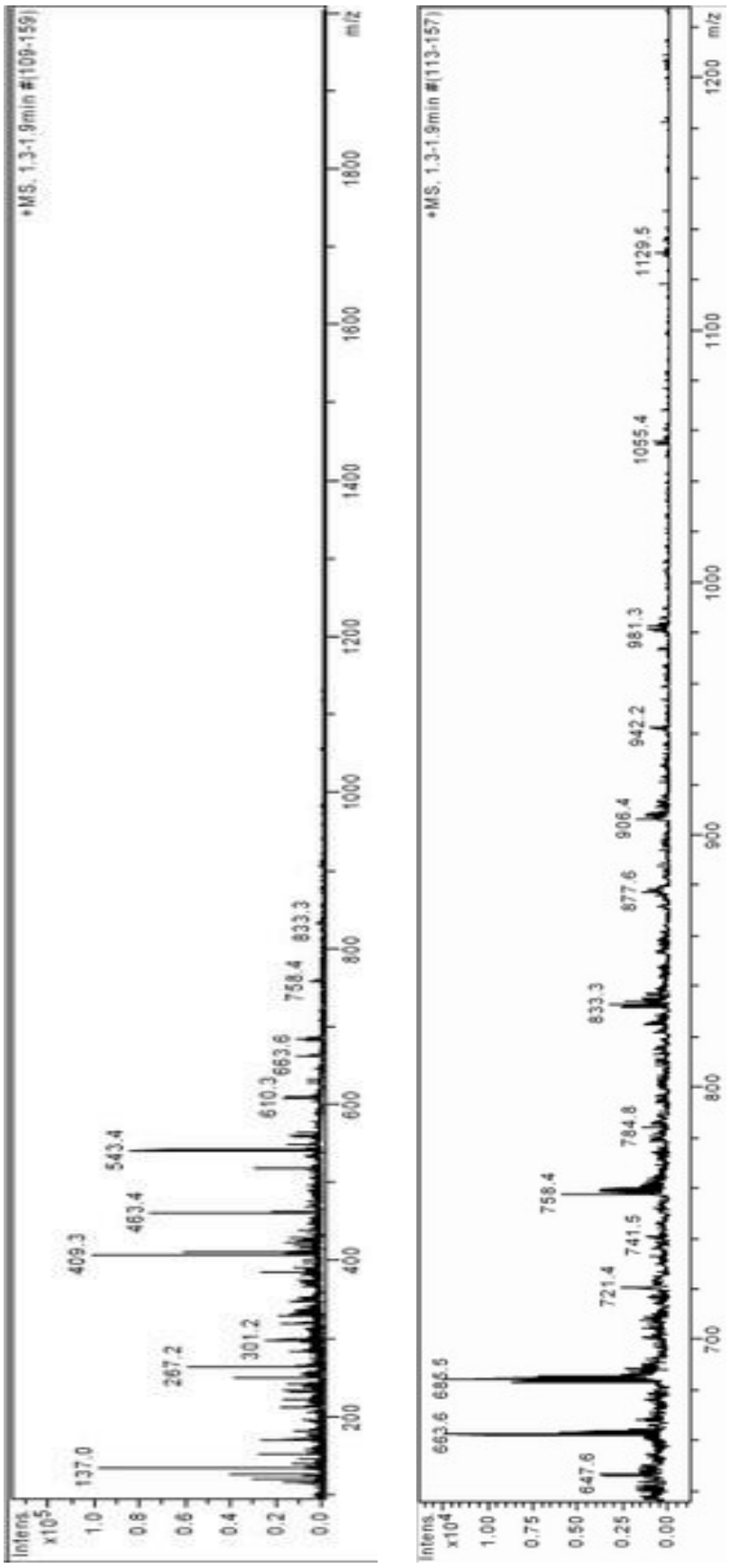

Spectrum 1.64: ESI mass spectrum of 26

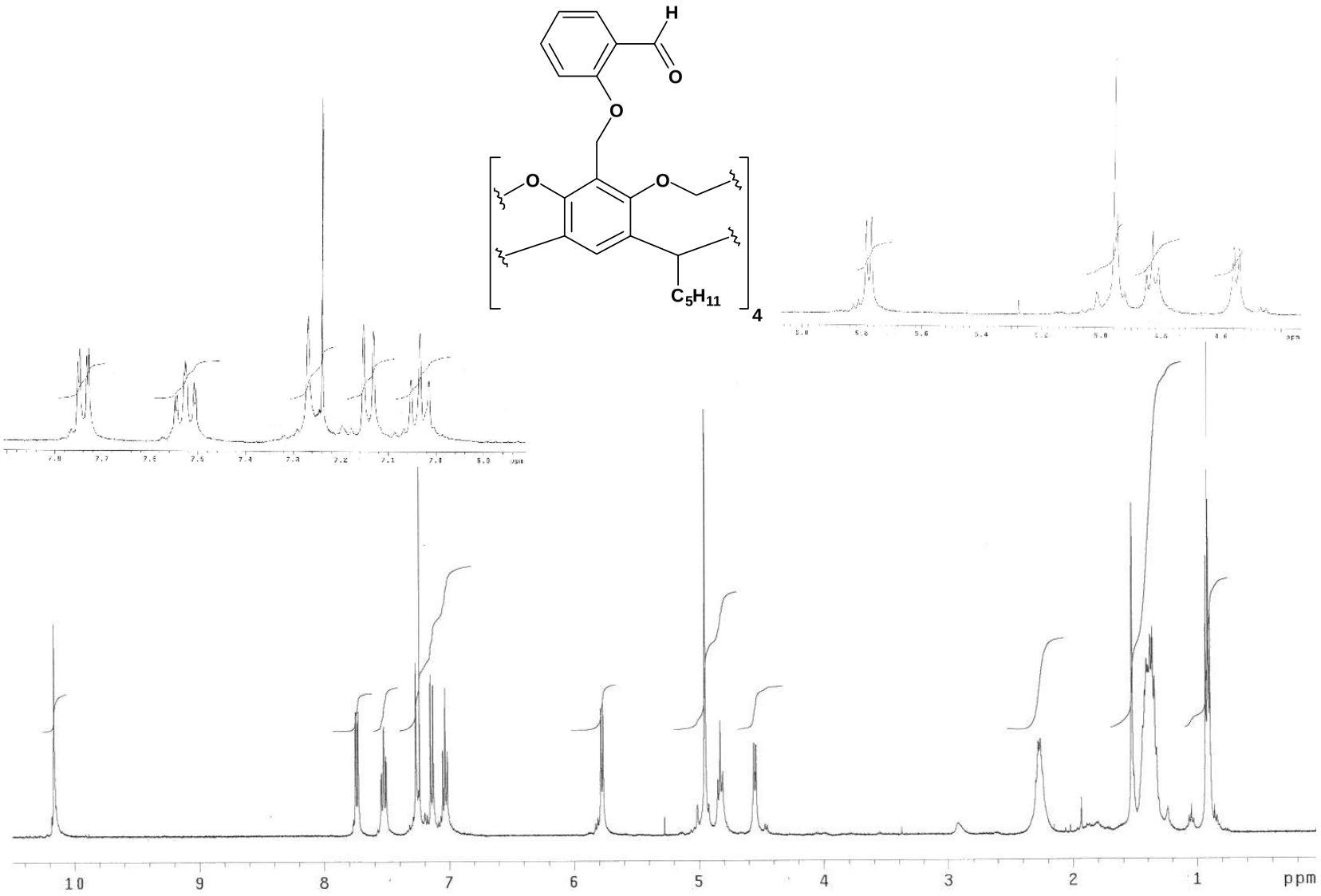

Spectrum 1.65: ^{1}H NMR spectrum of 27 in $CDCl_3$ (400 MHz)

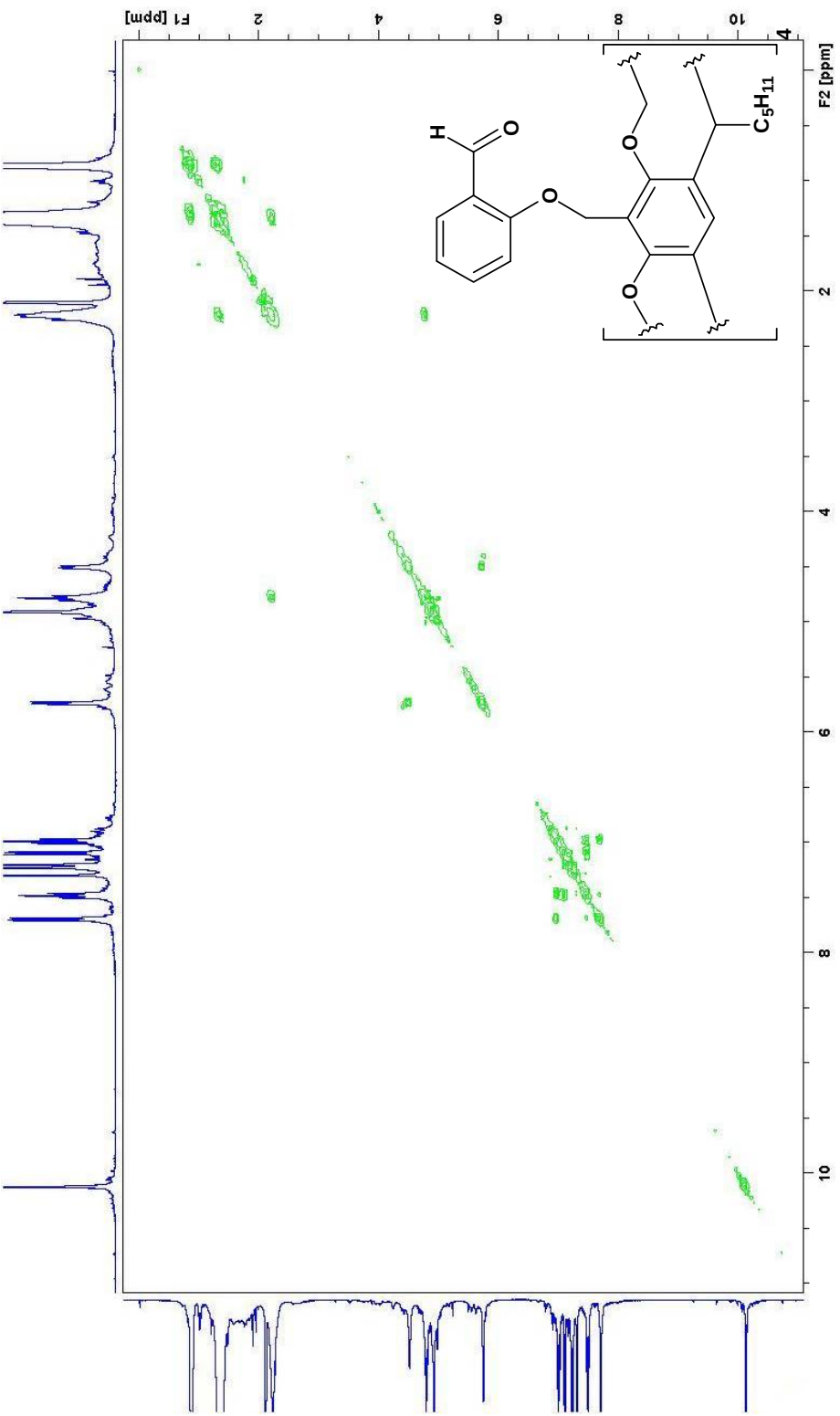

Spectrum 1.66: COSY NMR spectrum of 27 in $CDCl_3$ (400 MHz)

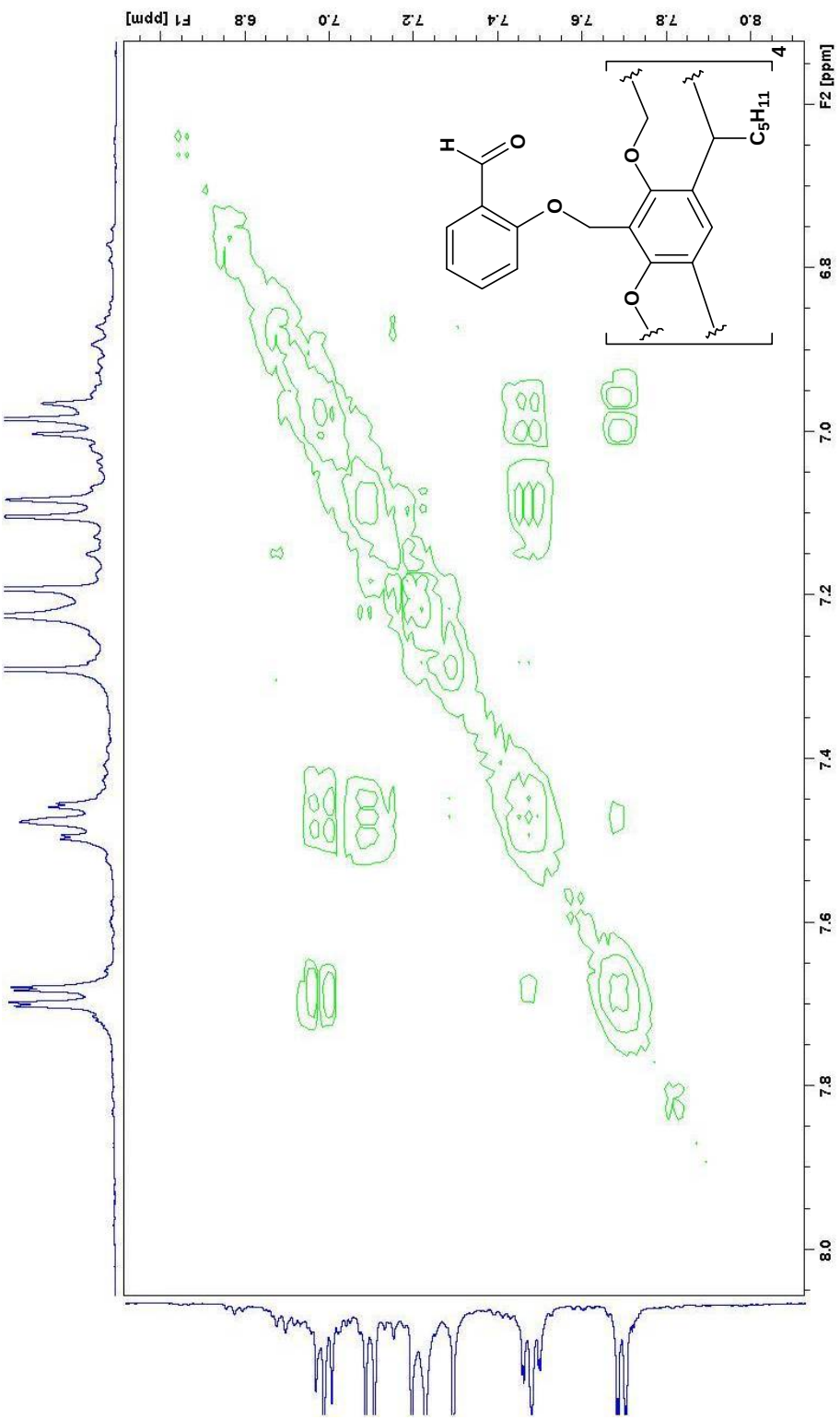

Spectrum 1.67: ^{1}H NMR spectrum of 27 in $CDCl_3$ (400 MHz)

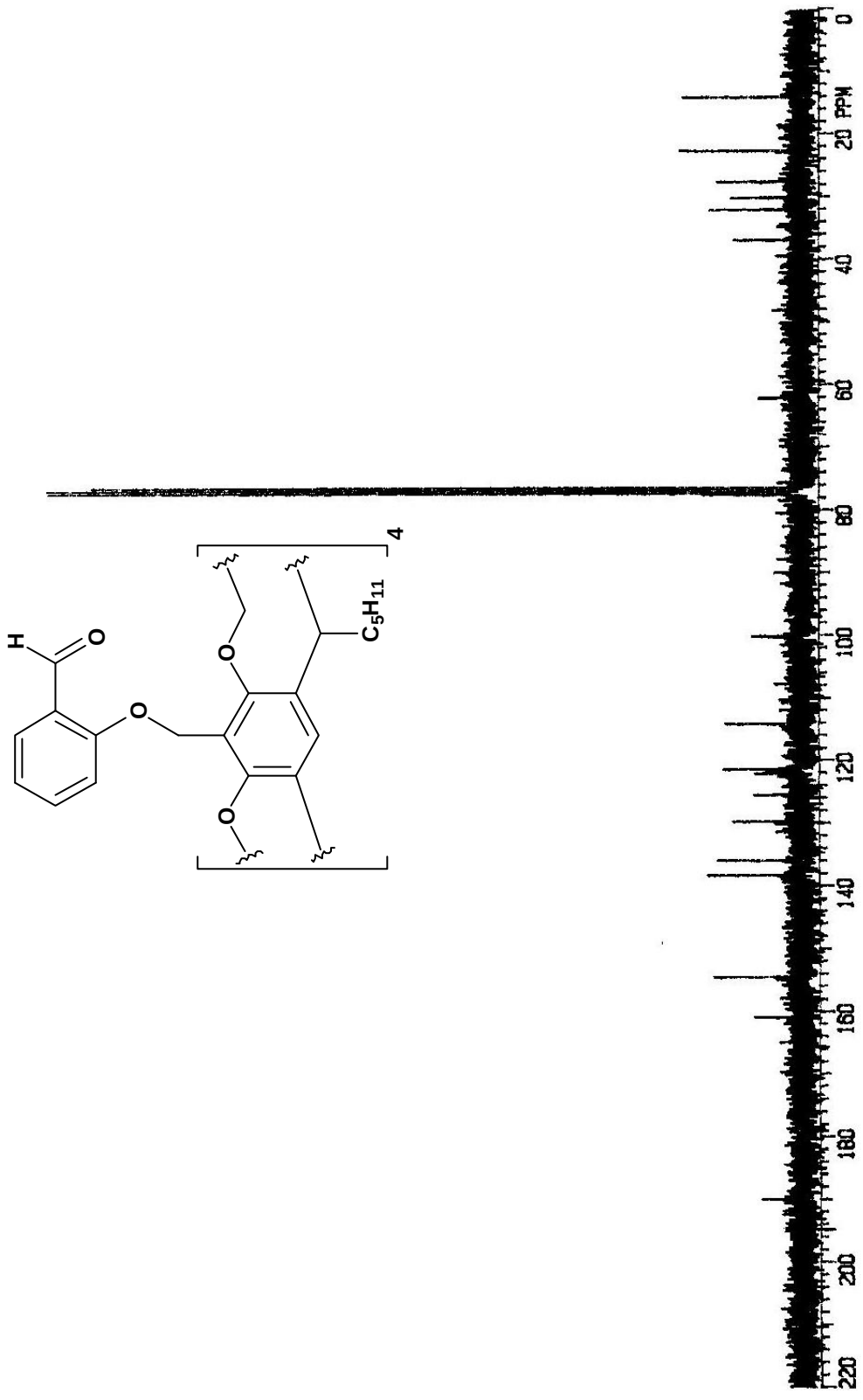

Spectrum 1.68: ^{13}C NMR spectrum of 27 in $CDCl_3$ (75 MHz)

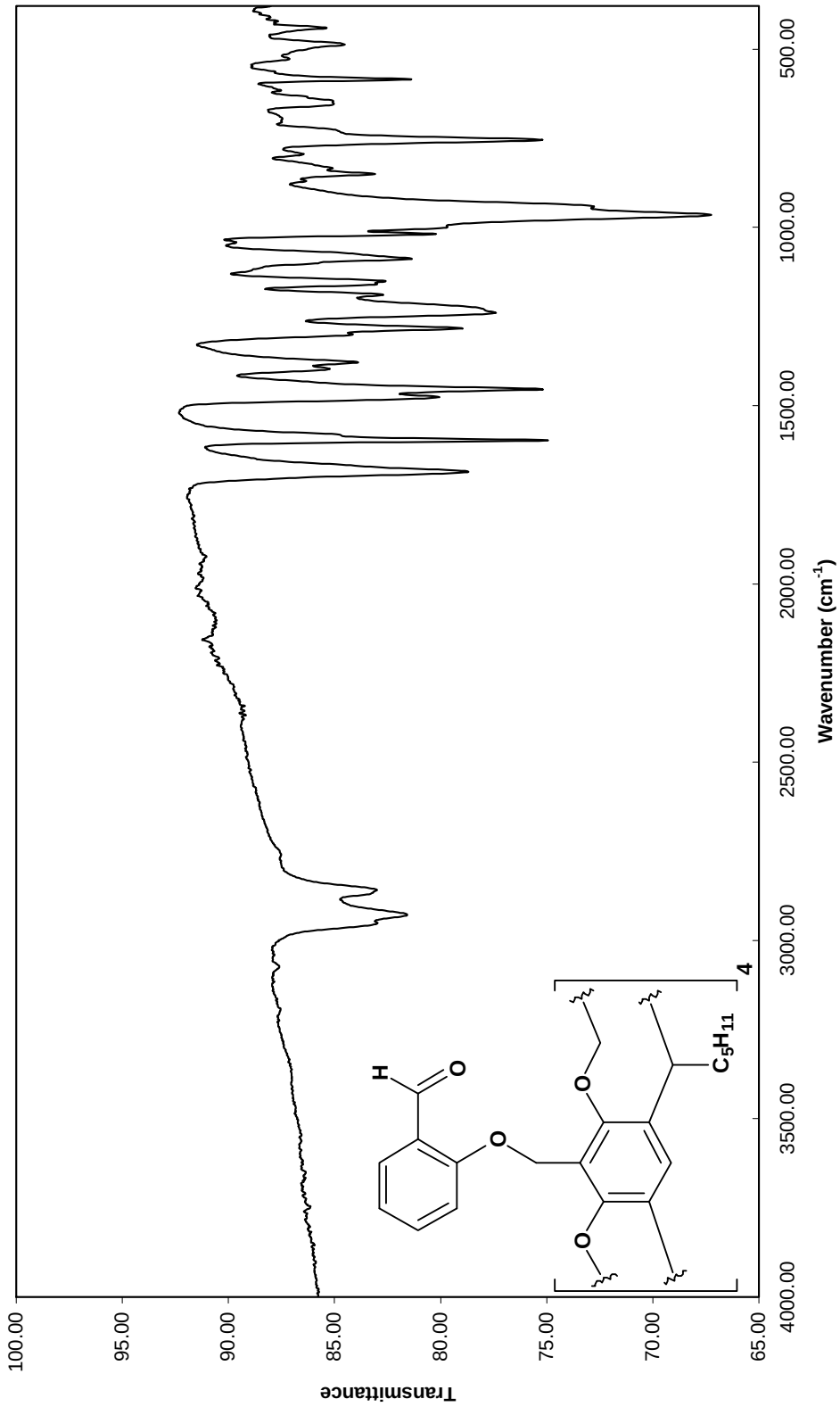

Spectrum 1.69: Infrared spectrum of 27 (KBr)

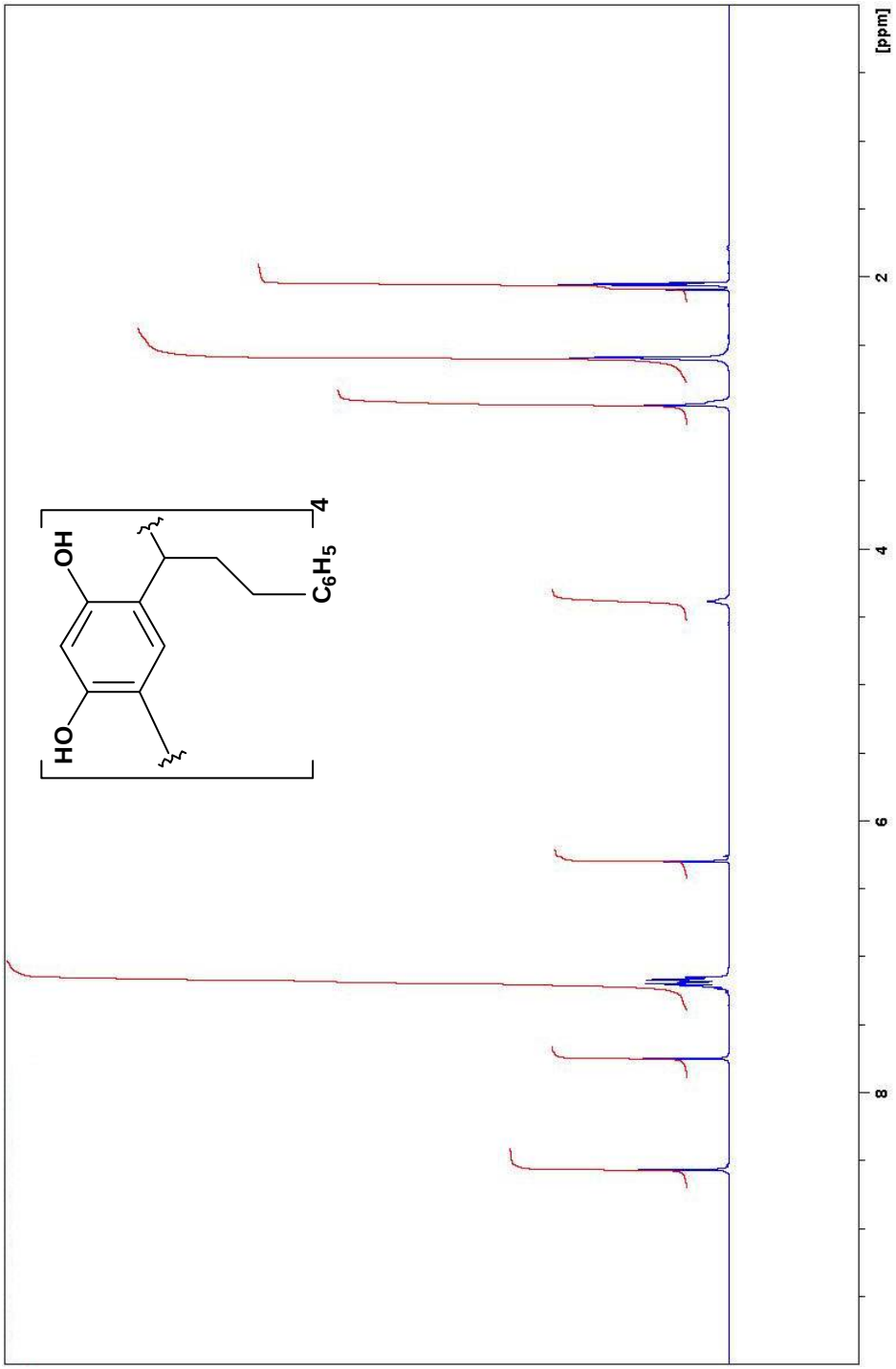

Spectrum 1.70: ^{1}H NMR spectrum of 29 in d_6-acetone (400 MHz)

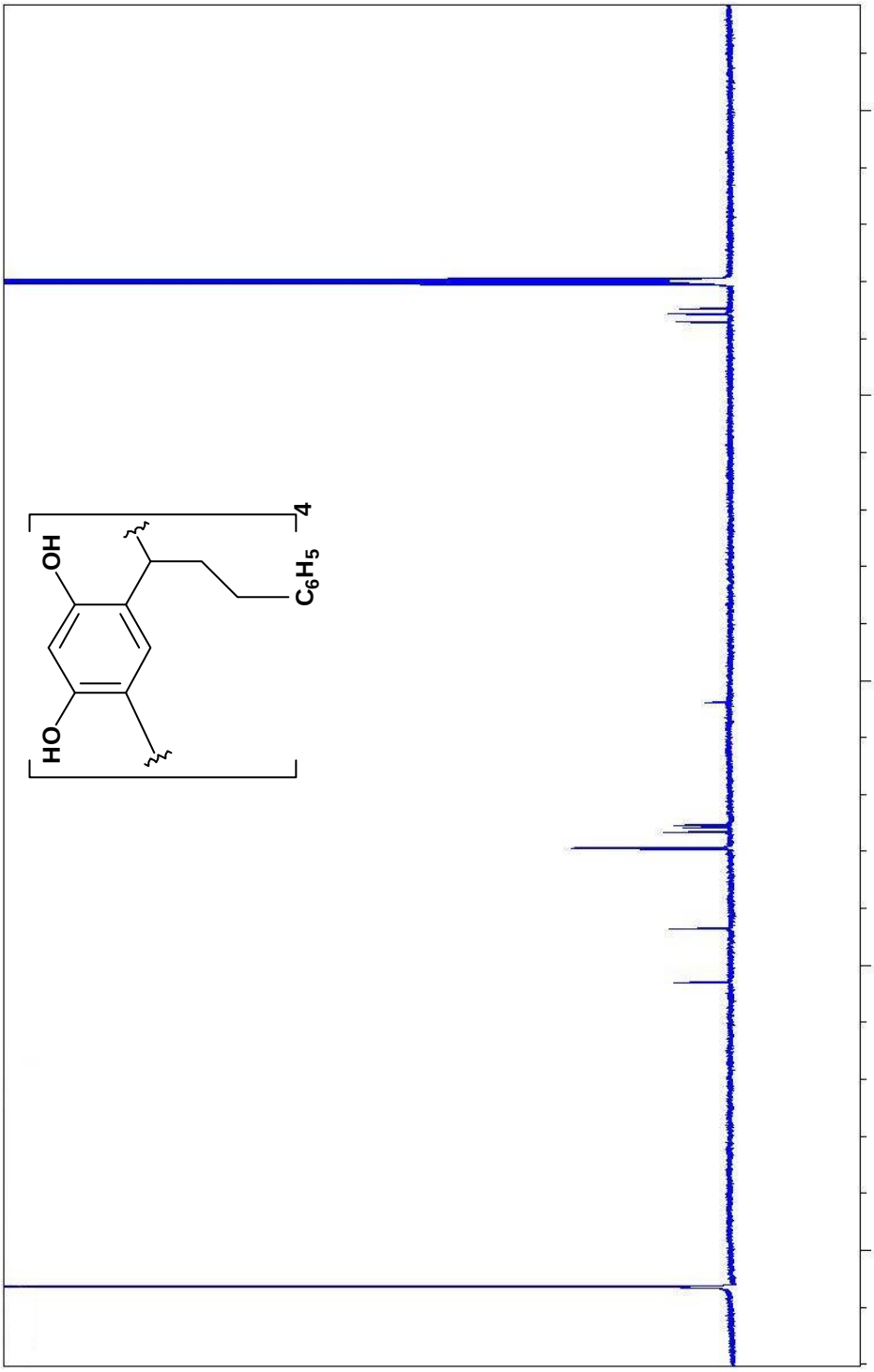

Spectrum 1.71: ^{13}C NMR spectrum of 29 in d_6-acetone (100 MHz)

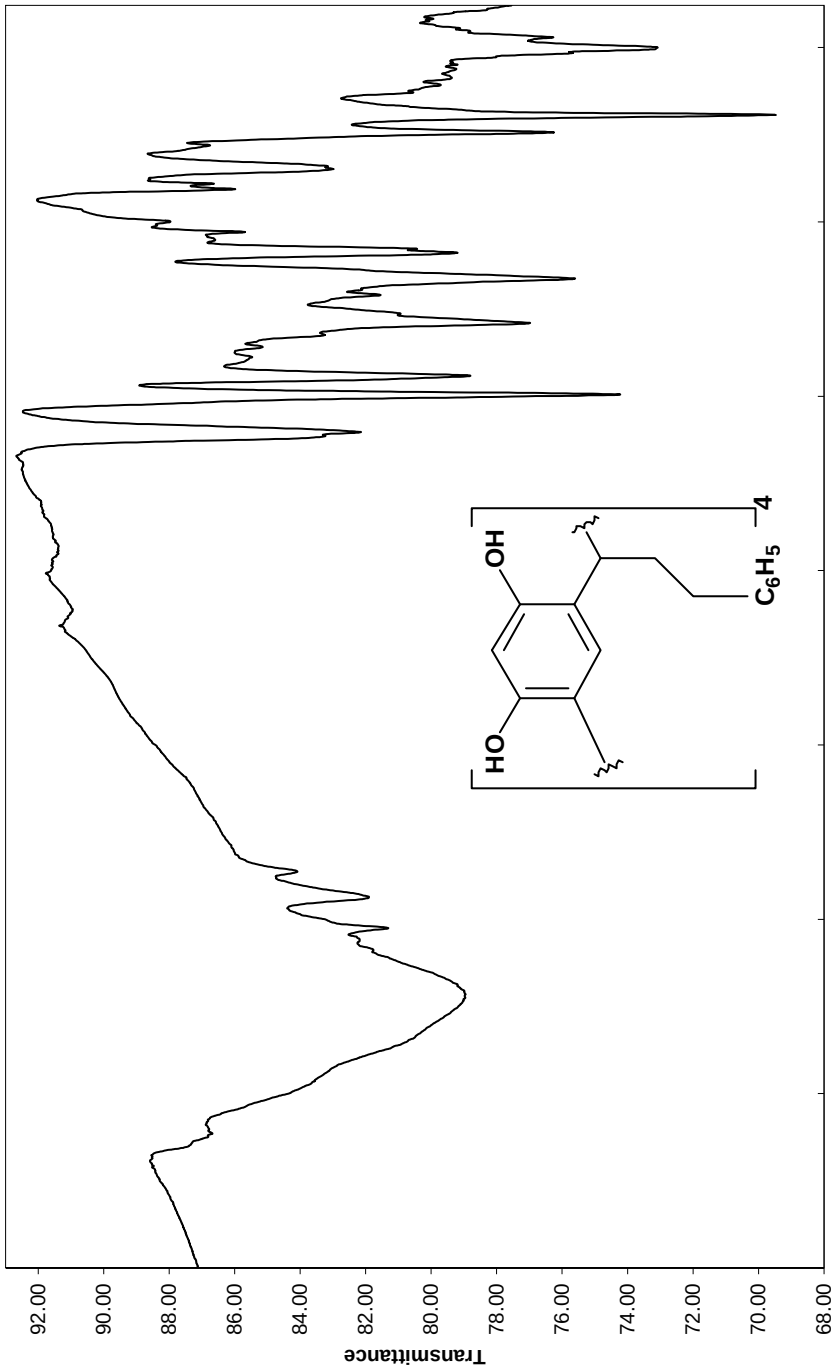

Spectrum 1.72: Infrared spectrum of 29 (KBr)

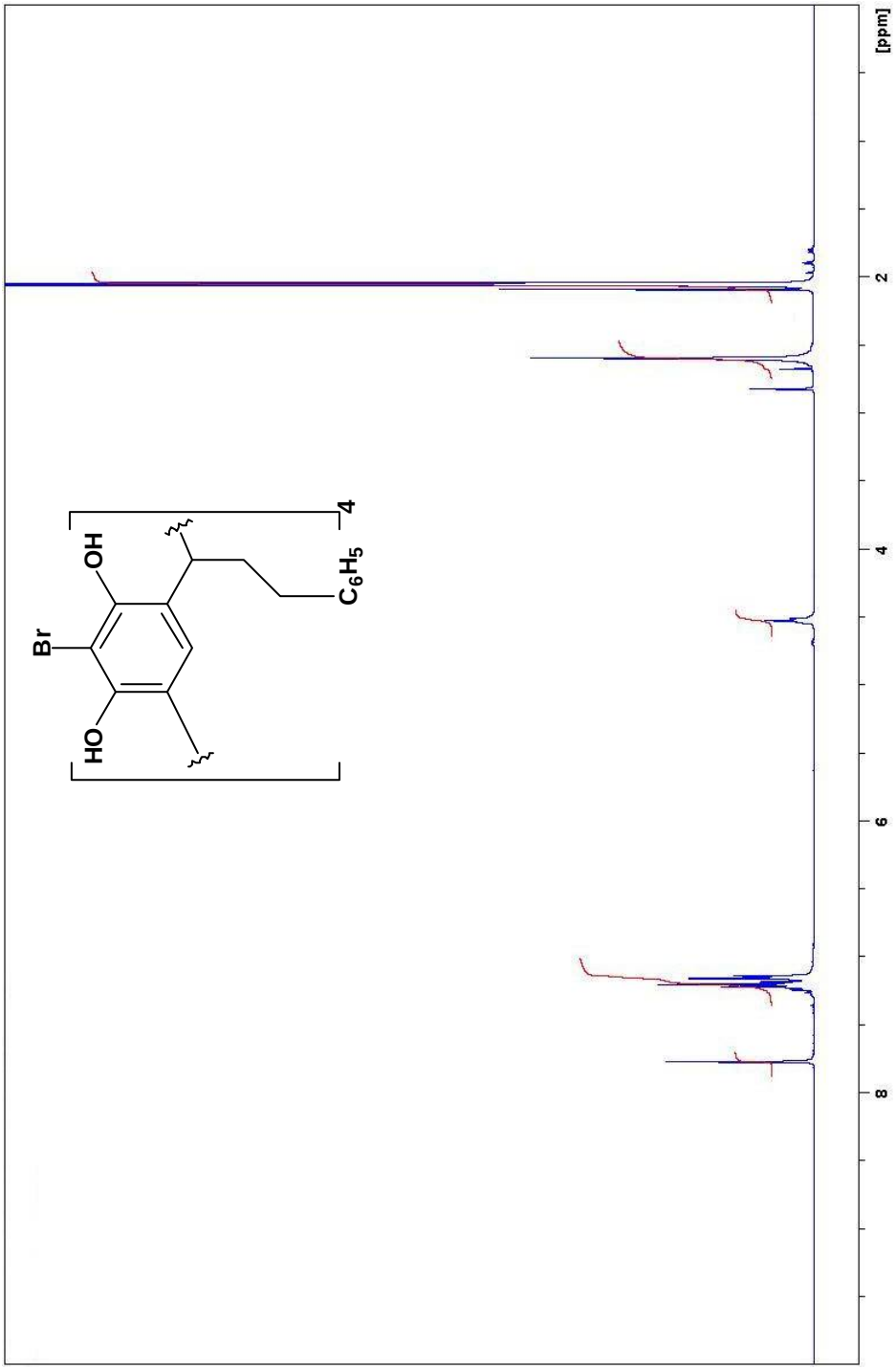

Spectrum 1.73: ^{1}H NMR spectrum of 30 in d_6-acetone (400 MHz)

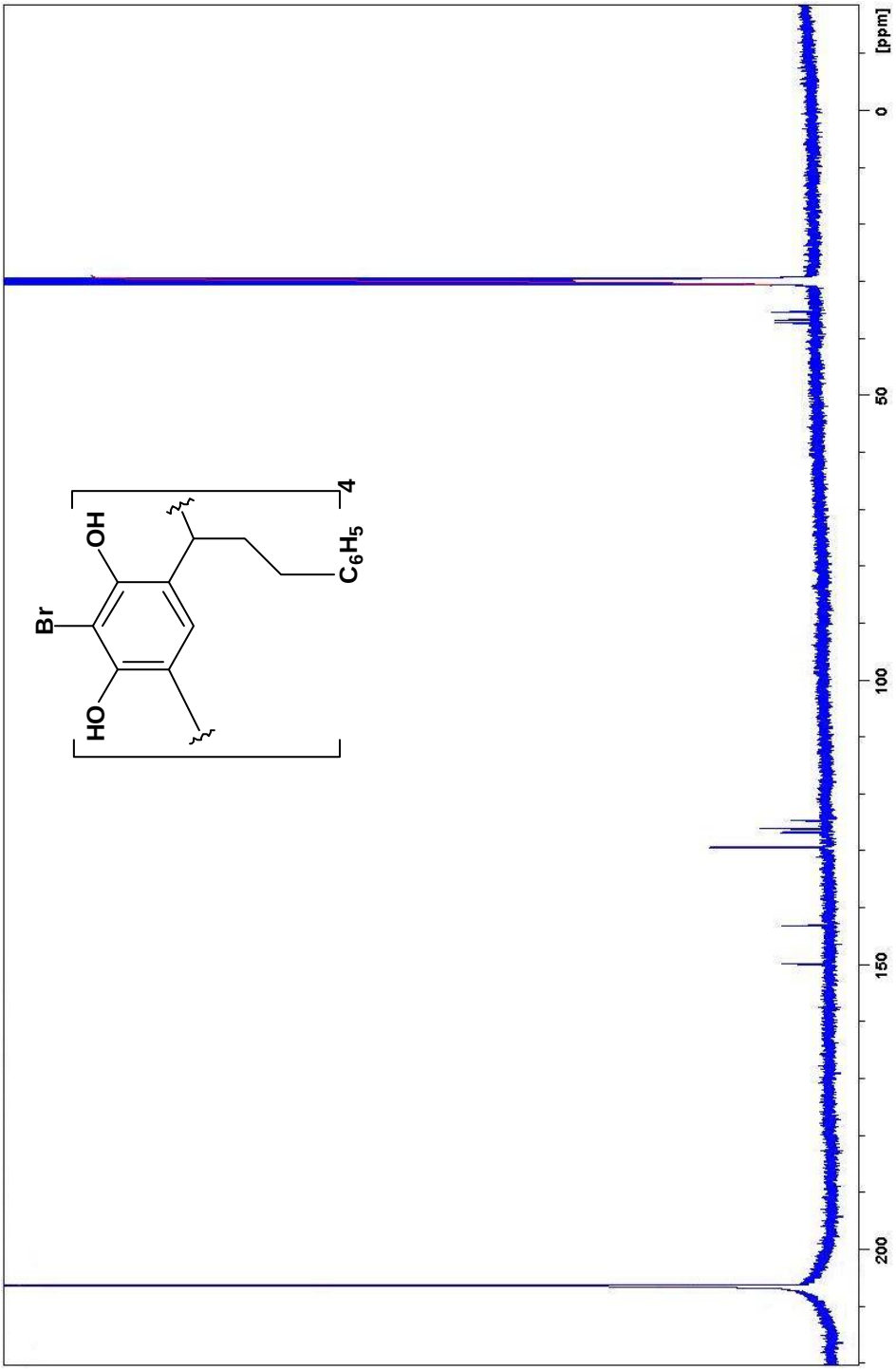

Spectrum 1.74: ^{13}C NMR spectrum of 30 in d_6-acetone (100 MHz)

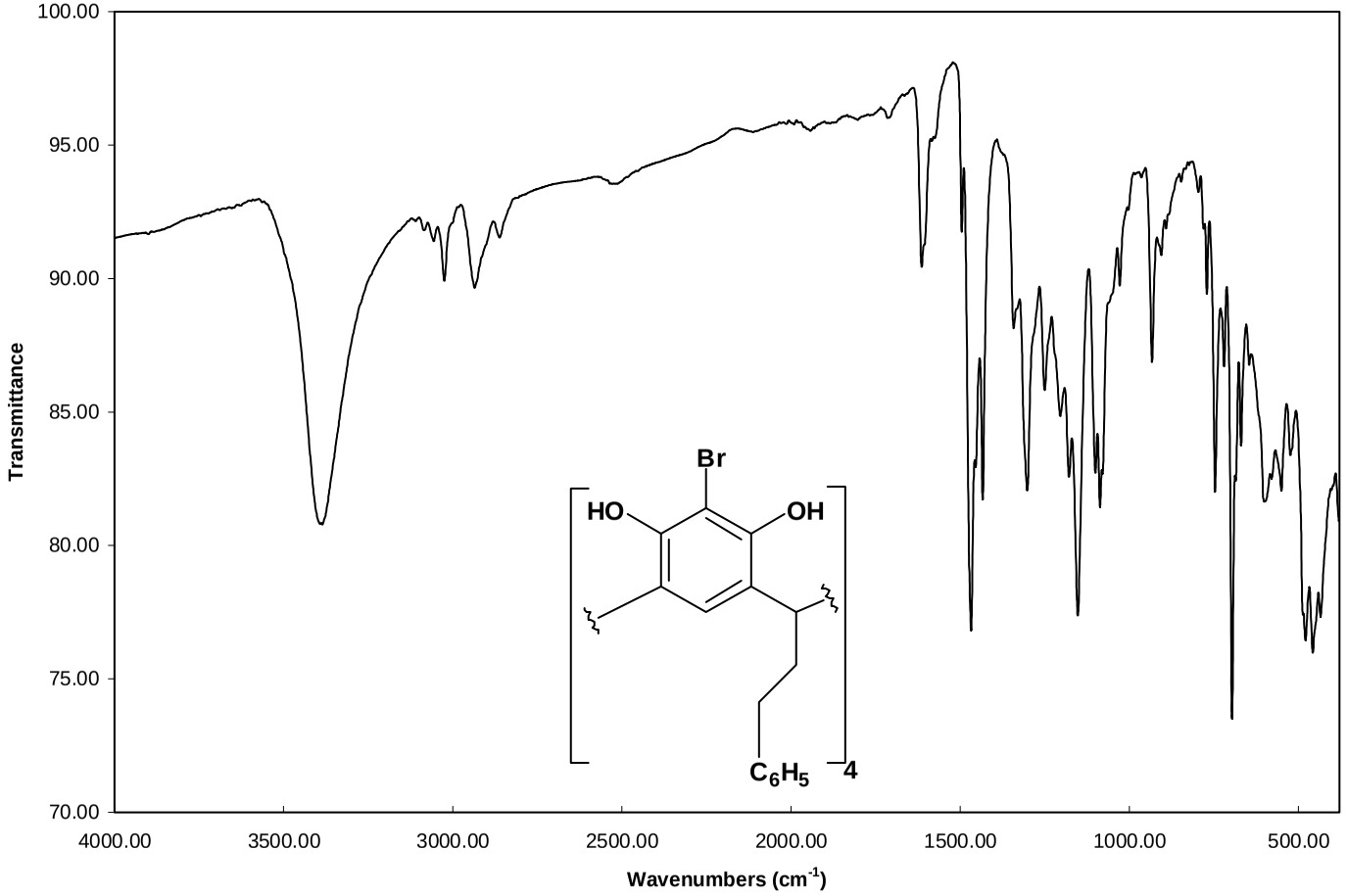

Spectrum 1.75: Infrared spectrum of 30 (KBr)

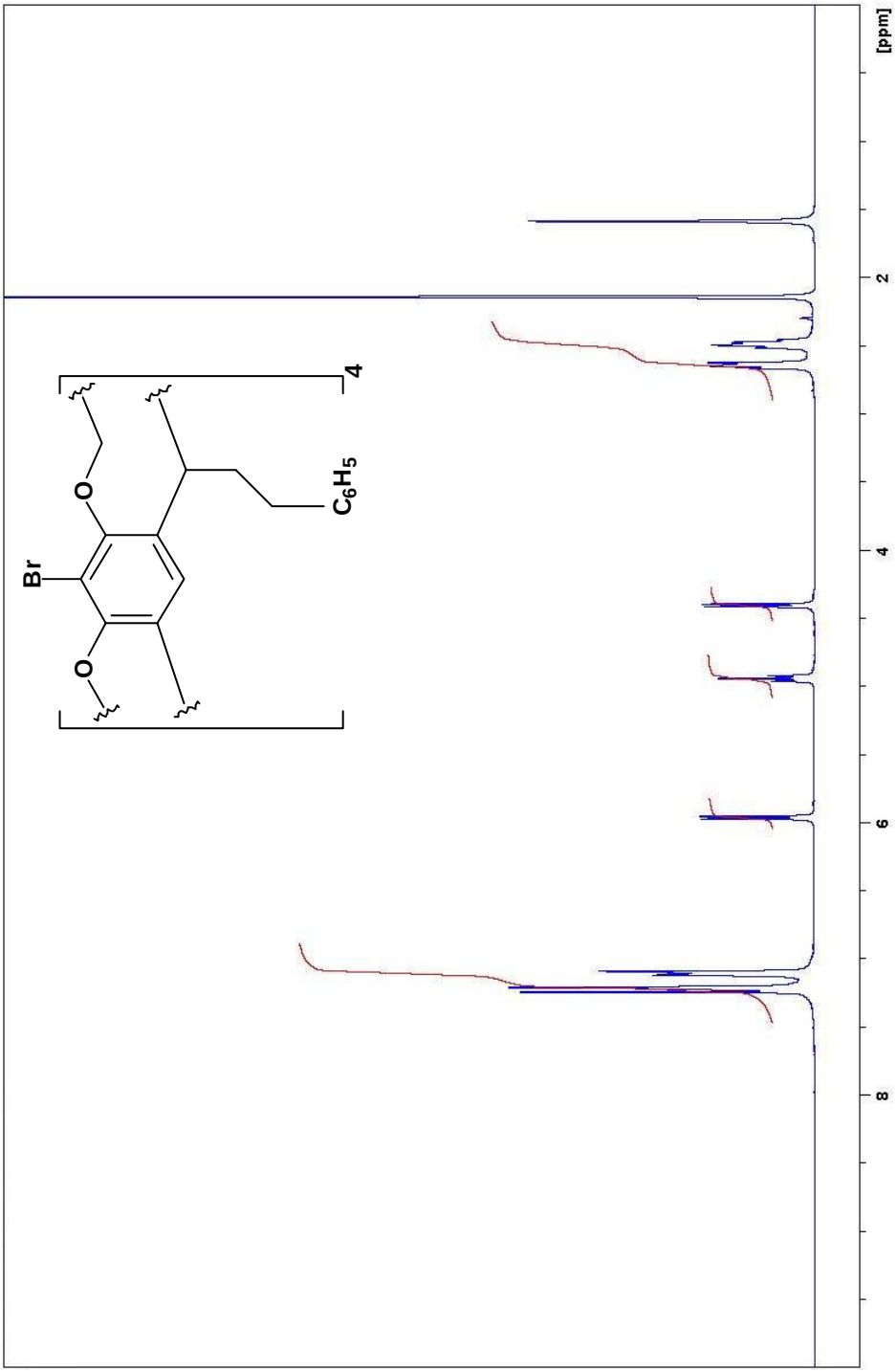

Spectrum 1.76: ^{1}H NMR spectrum of 32 in $CDCl_3$ (400 MHz)

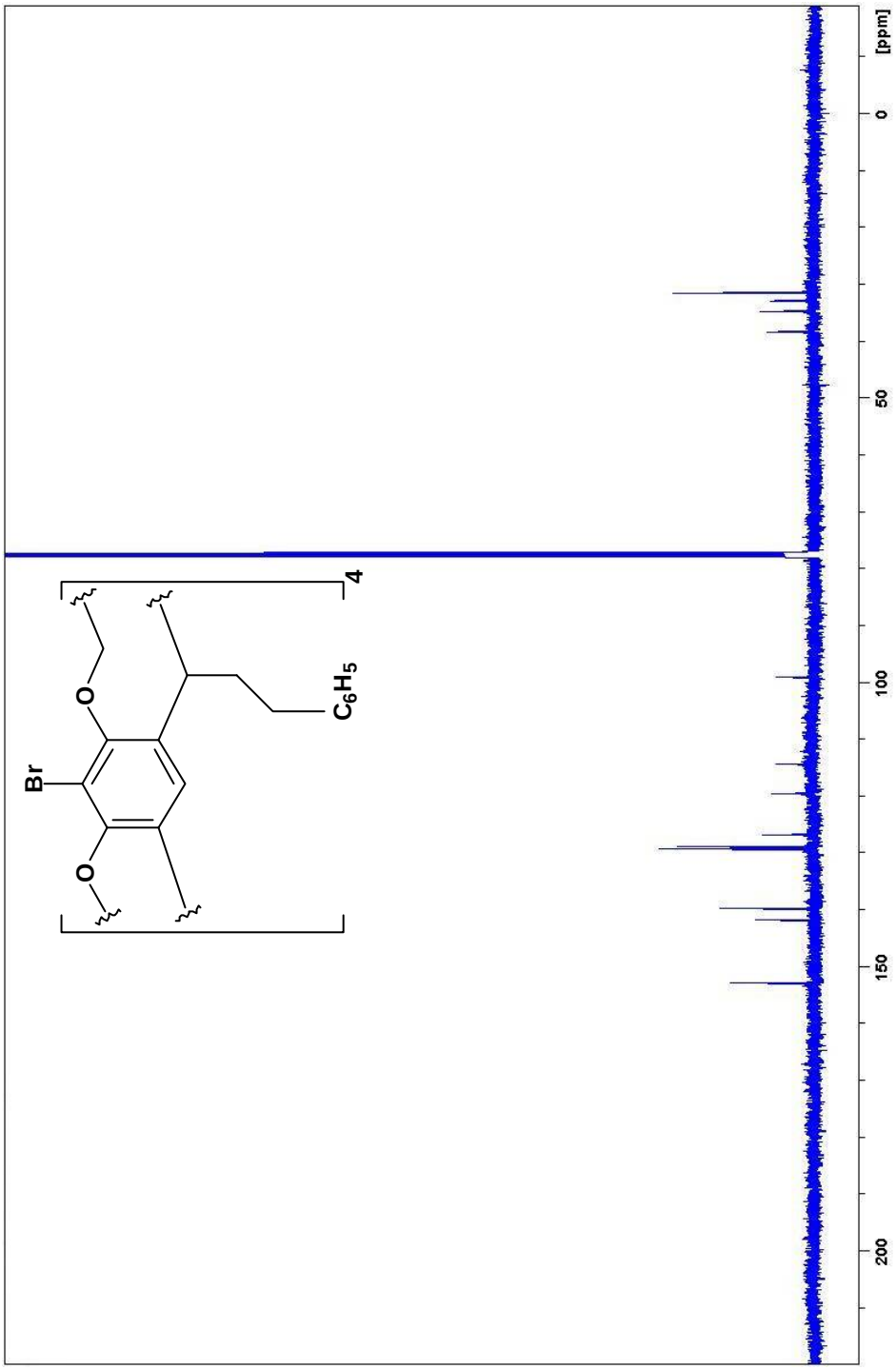

Spectrum 1.77: ^{13}C NMR spectrum of 31 in $CDCl_3$ (100 MHz)

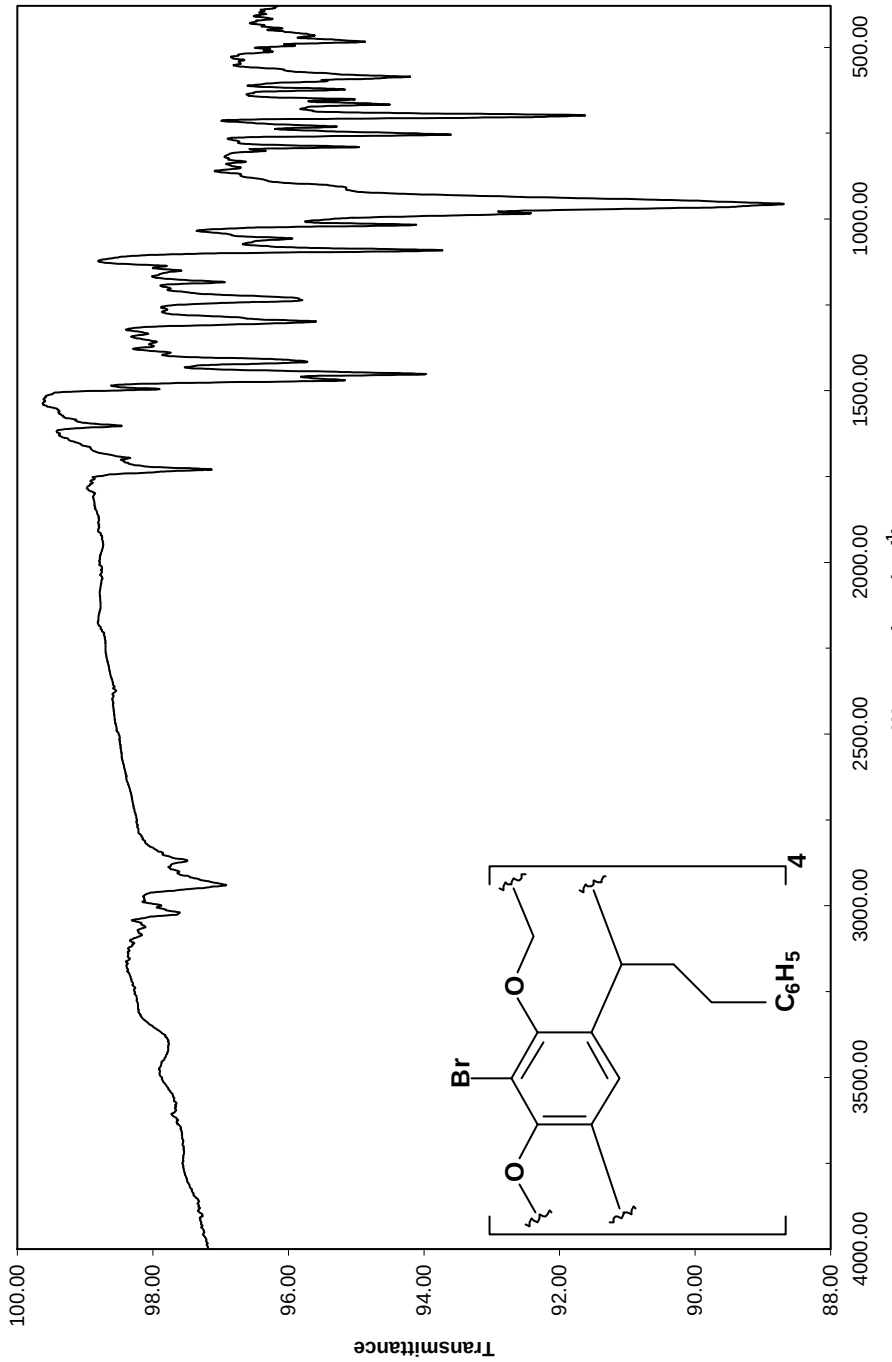

Spectrum 1.78: Infrared spectrum of 31 (KBr)

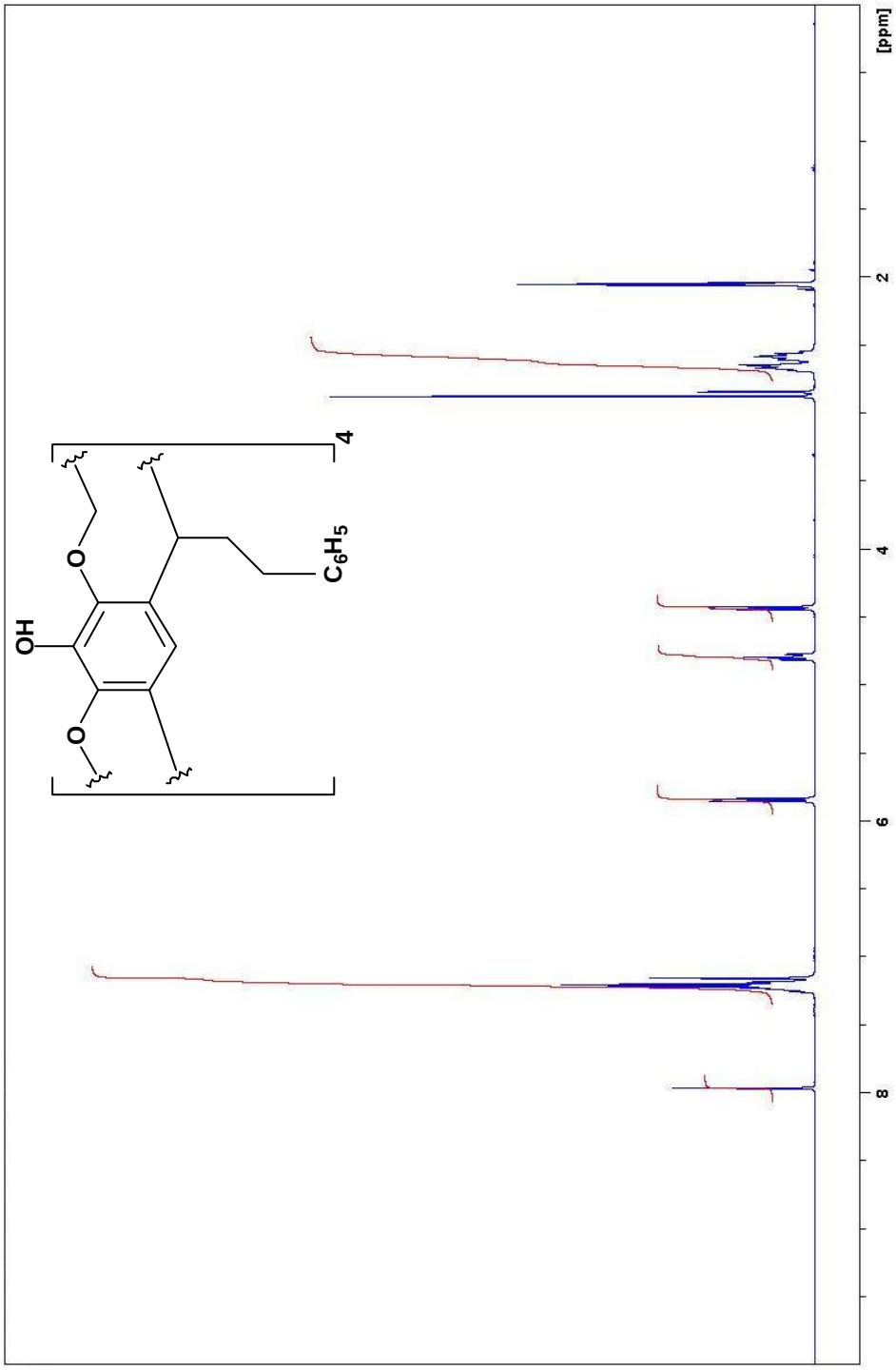

Spectrum 1.79: ^{1}H NMR spectrum of 32 in d_6-acetone (400MHz)

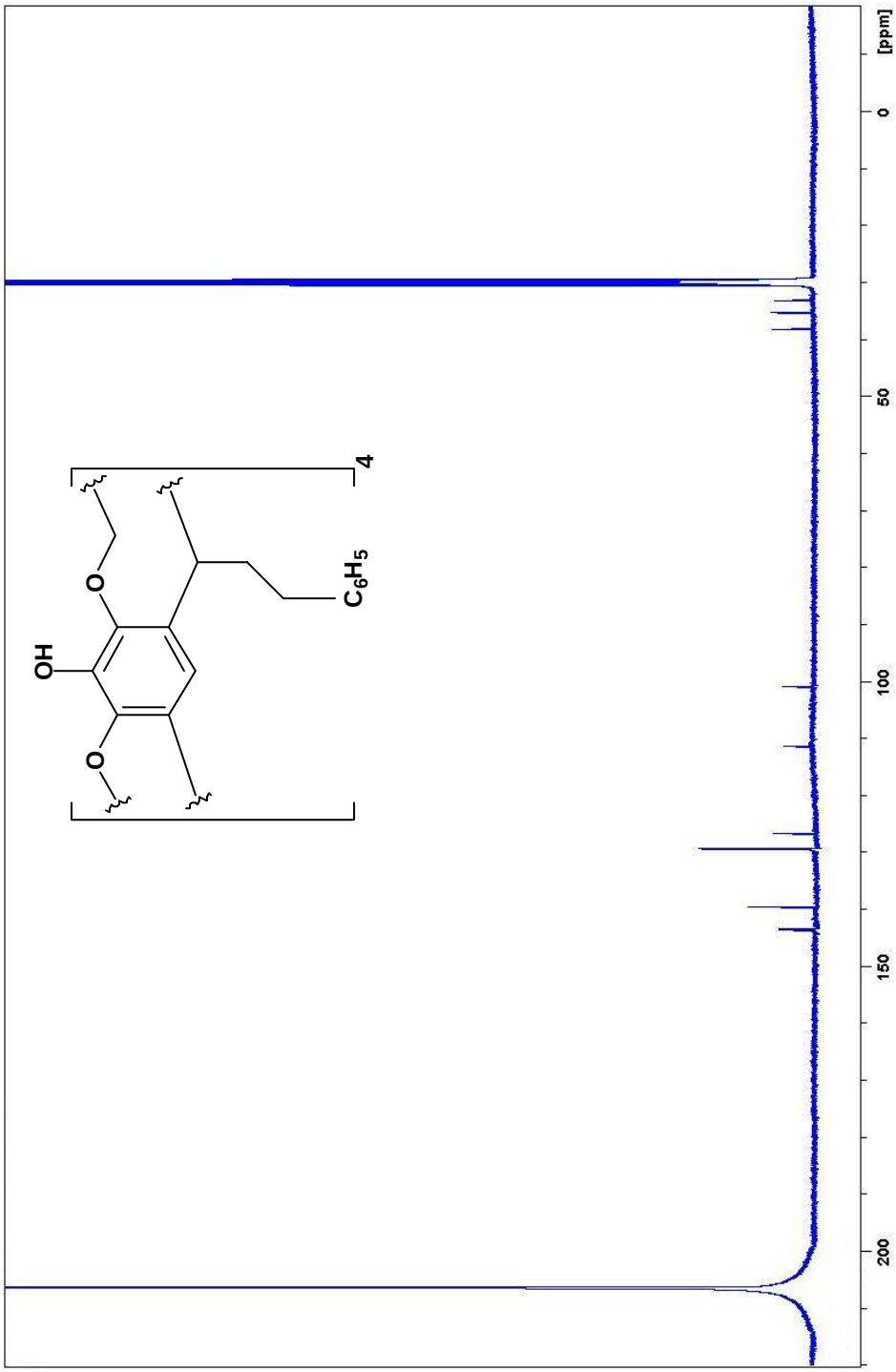

Spectrum 1.80: ^{1}H NMR spectrum of 32 in d_6-acetone (100 MHz)

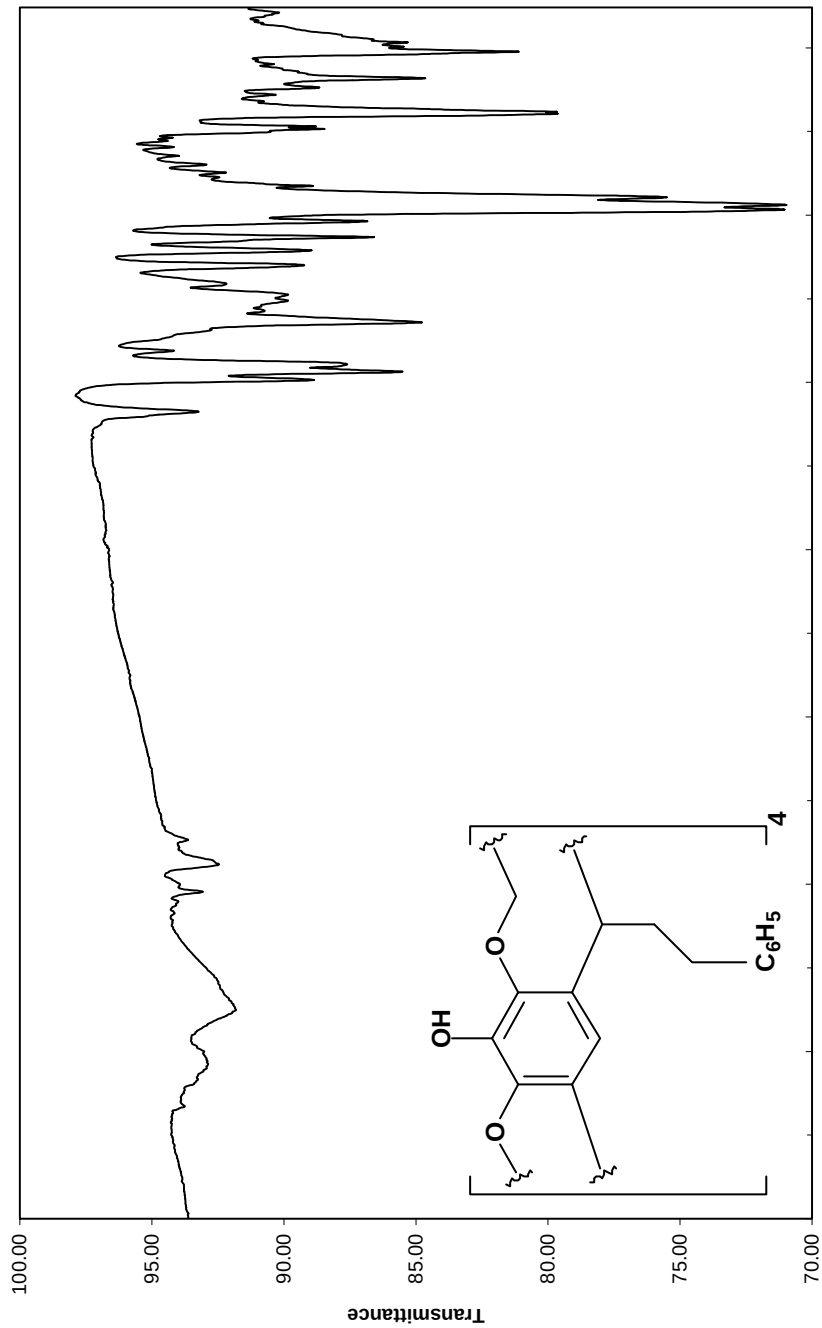

Spectrum 1.81: Infrared spectrum of 32 (KBr)

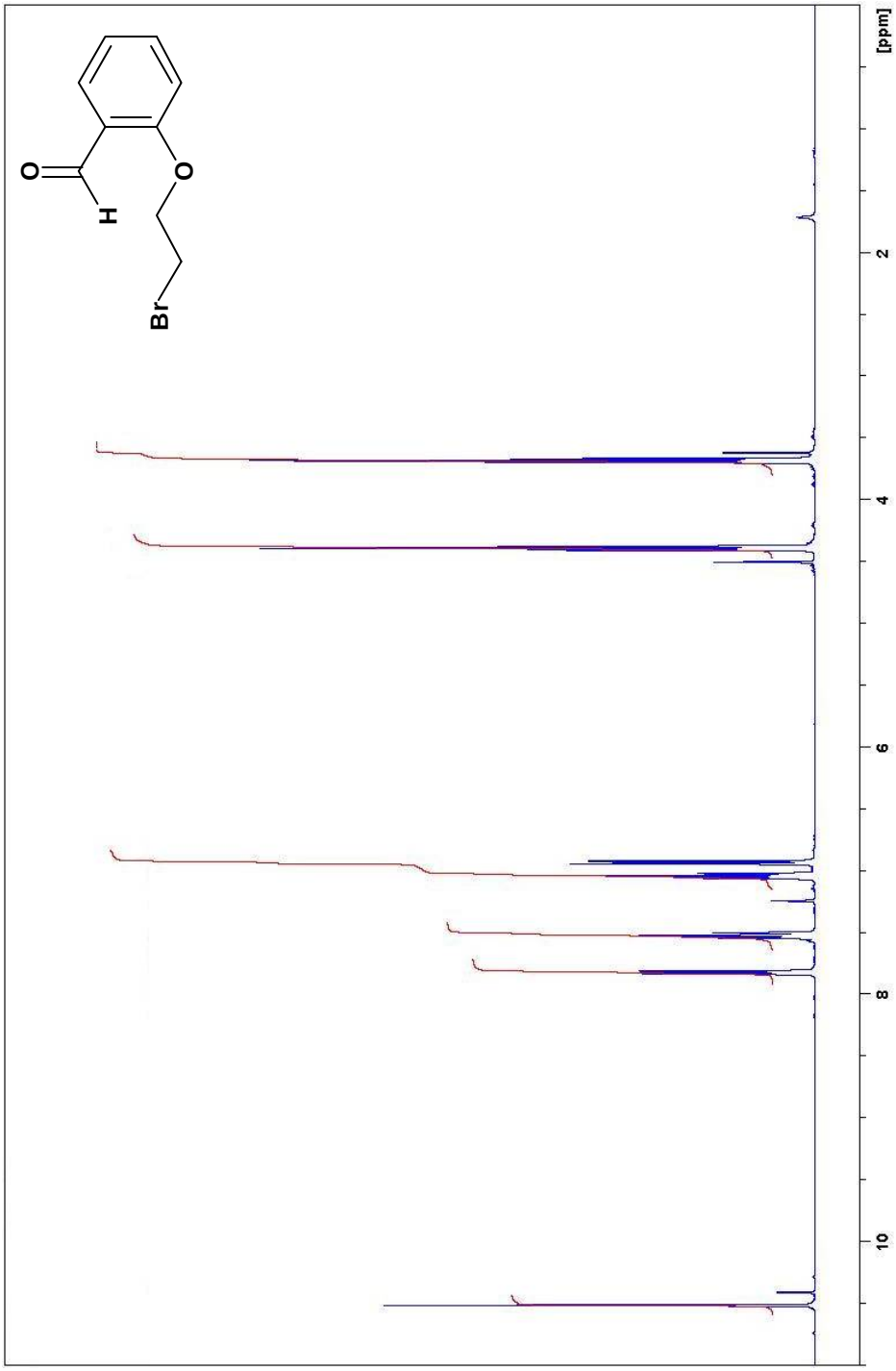

Spectrum 1.82: ^{1}H NMR spectrum of 33 in $CDCl_3$ (400 MHz)

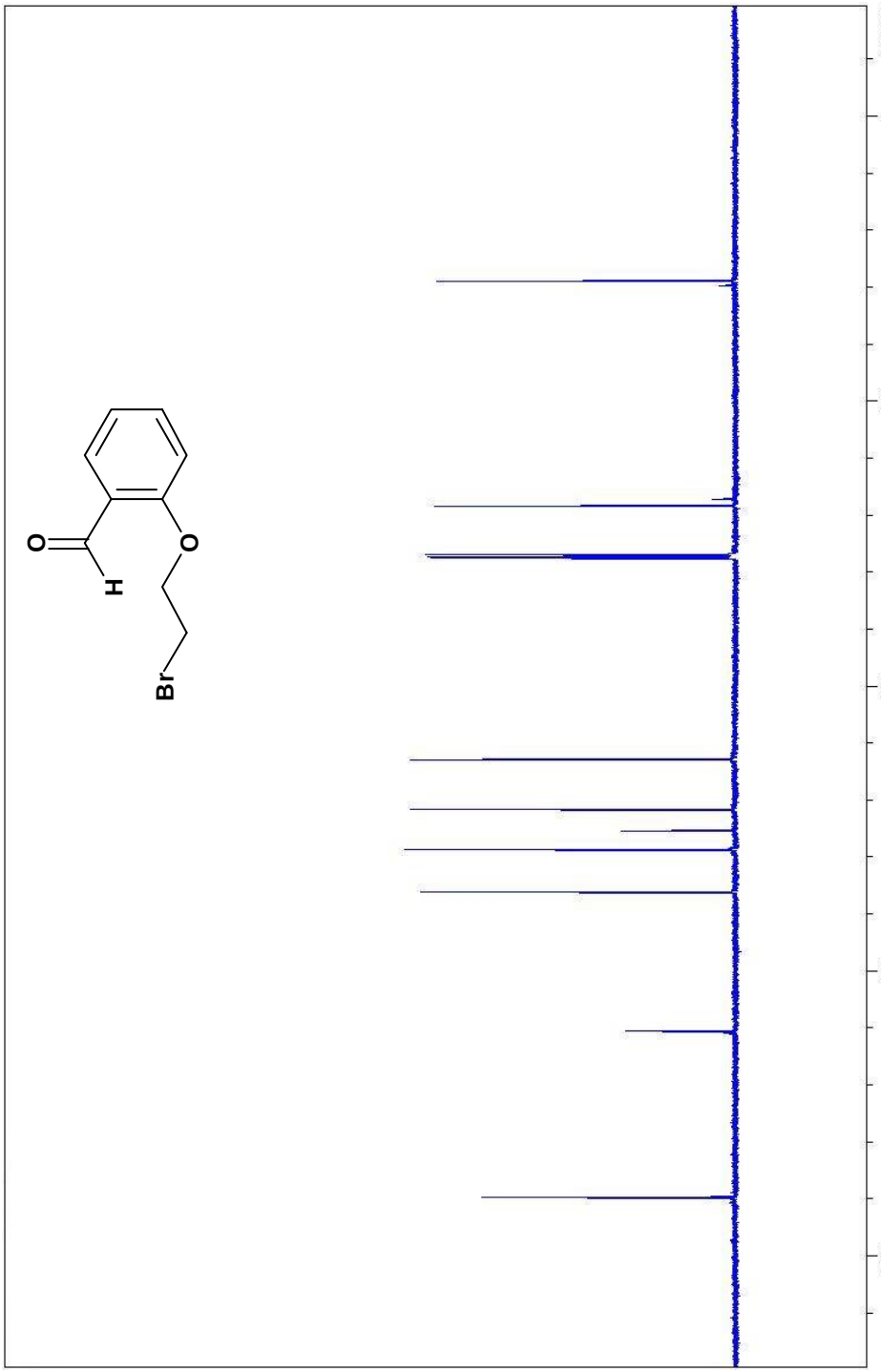

Spectrum 1.83: ^{13}C NMR spectrum of 33 in $CDCl_3$ (100 MHz)

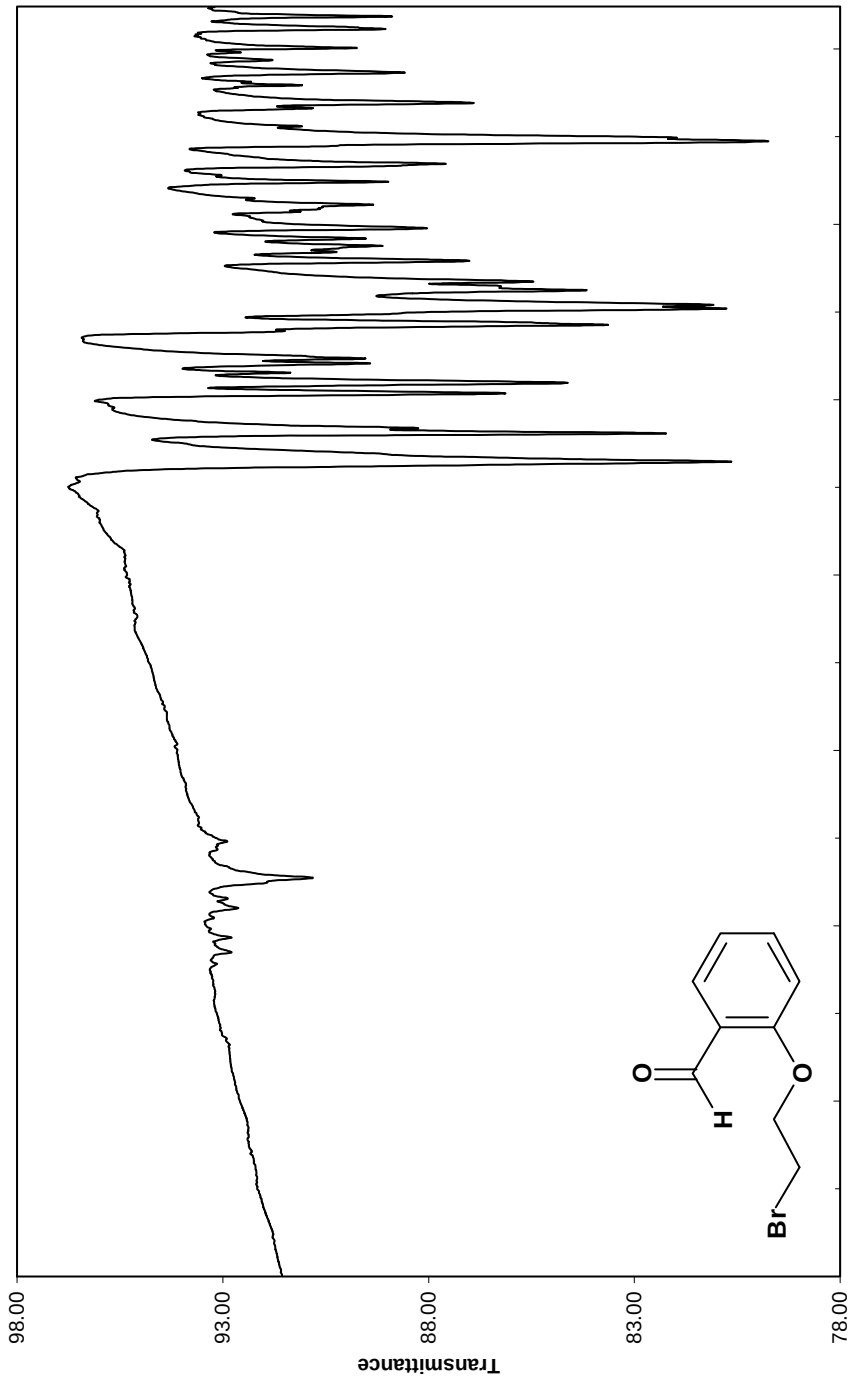

Spectrum 1.84: Infrared spectrum of 33 (KBr)

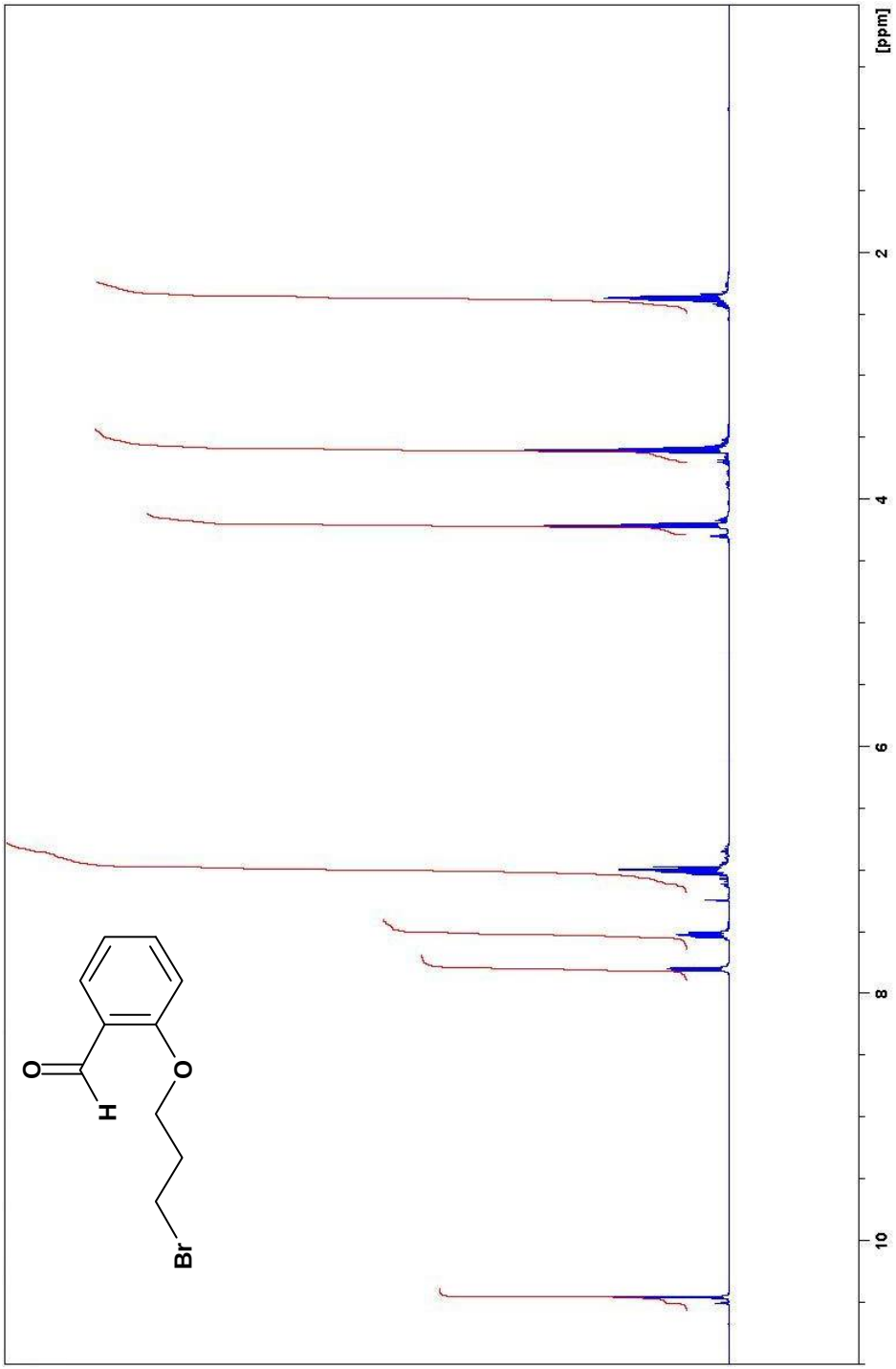

Spectrum 1.85: ^{1}H NMR spectrum of 34 in $CDCl_3$ (400 MHz)

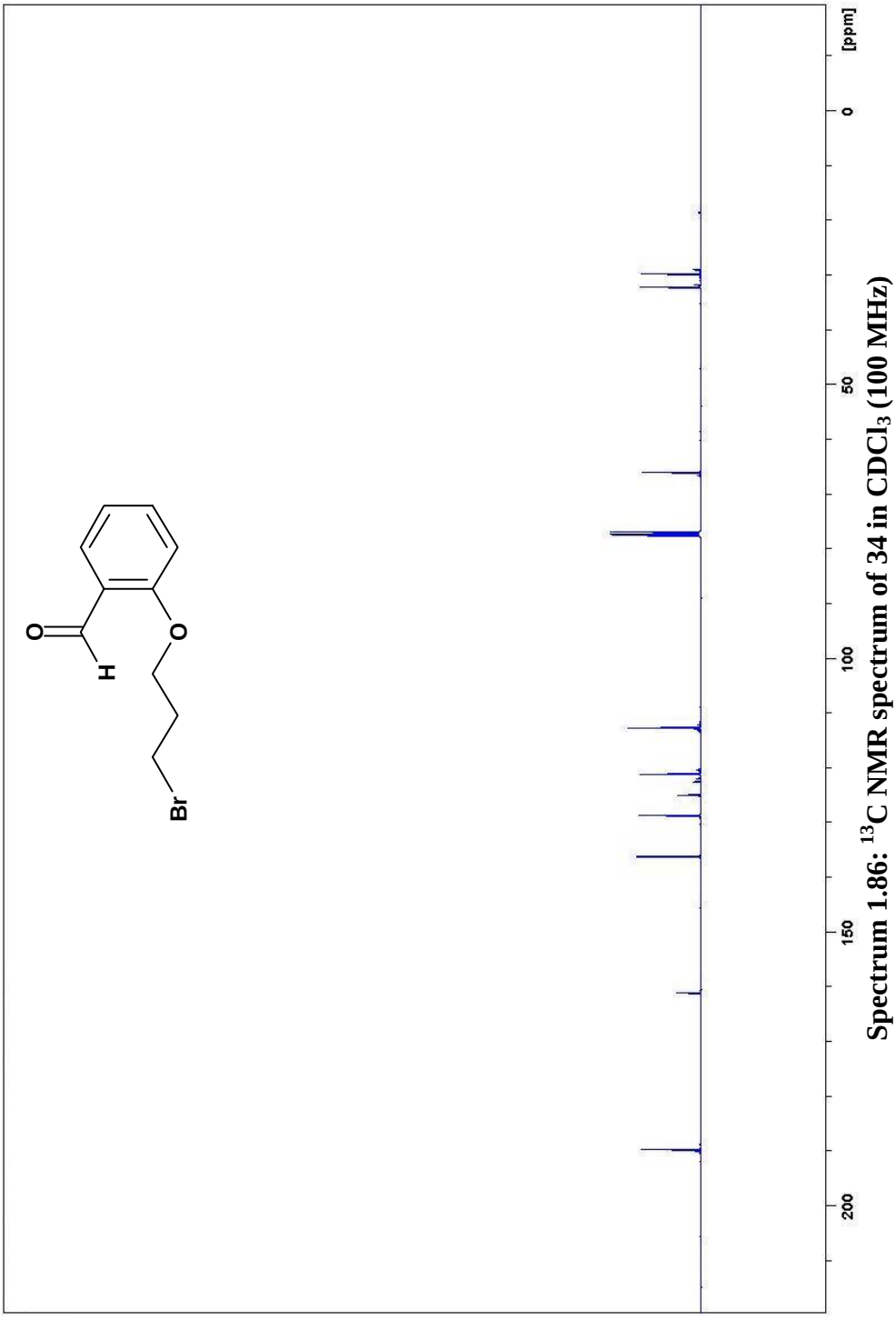

Spectrum 1.86: ^{13}C NMR spectrum of 34 in $CDCl_3$ (100 MHz)

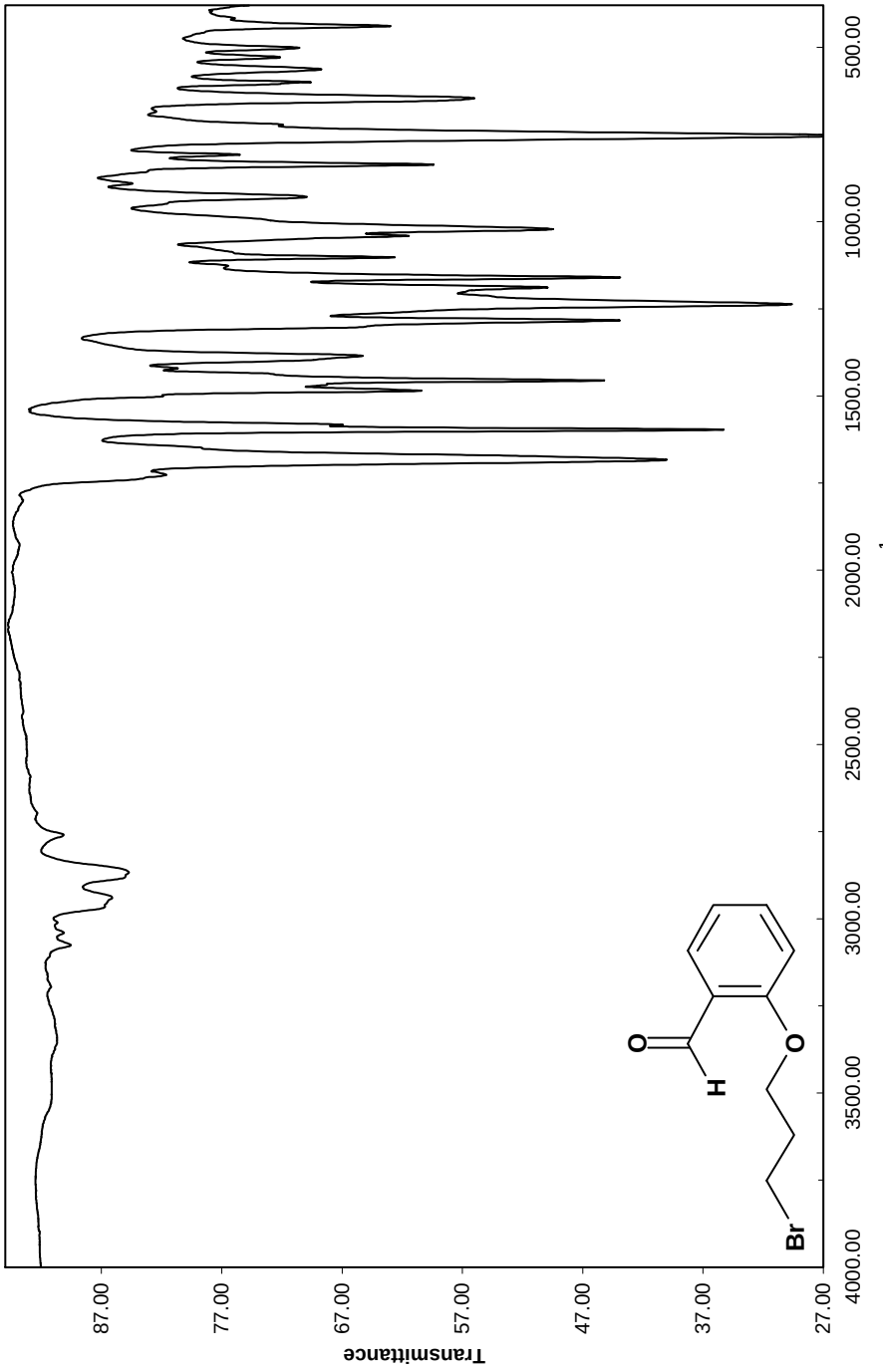

Spectrum 1.87: Infrared spectrum of 34 (KBr)

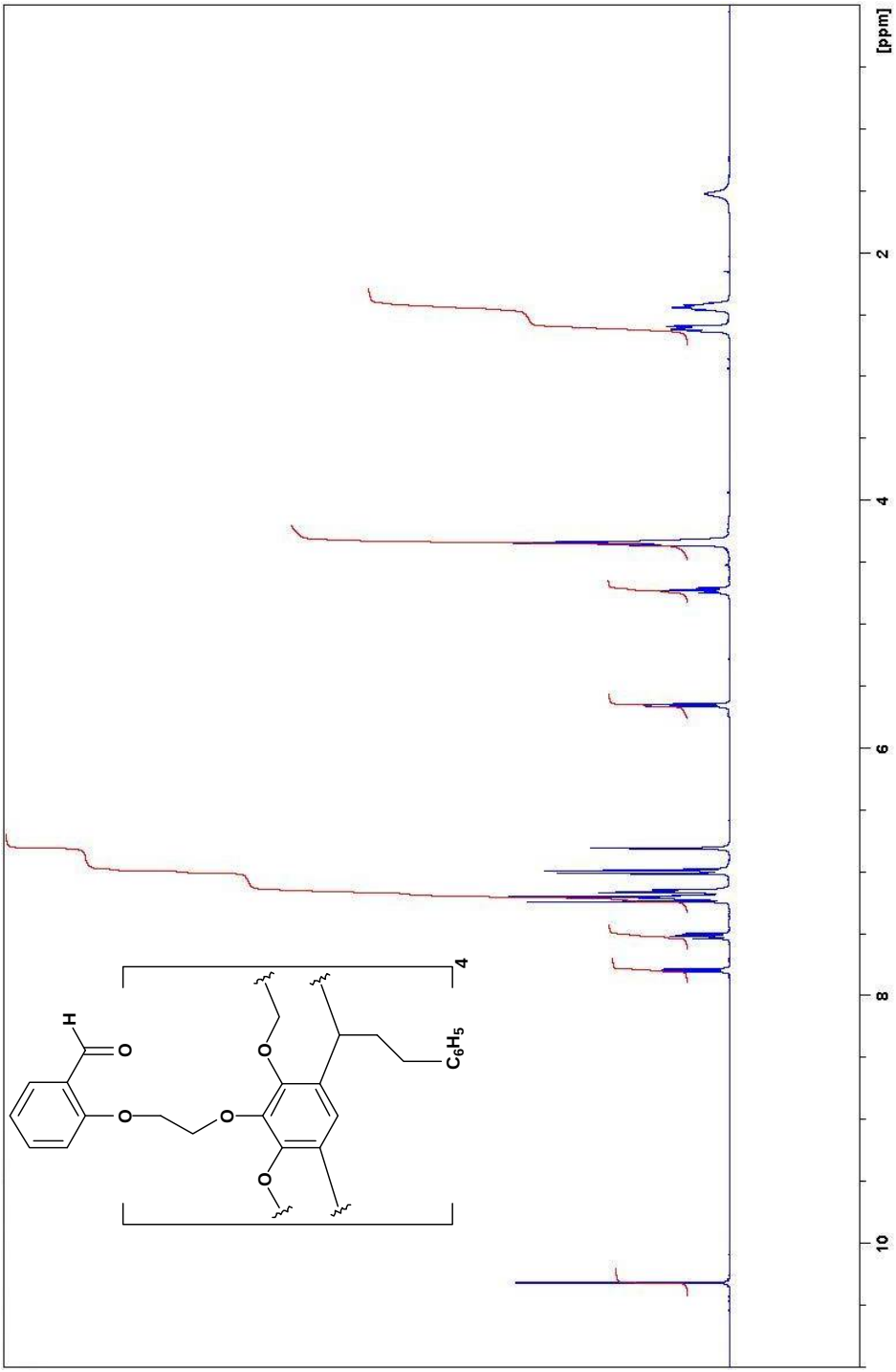

Spectrum 1.88: ^{1}H NMR spectrum of 35 in $CDCl_3$ (400 MHz)

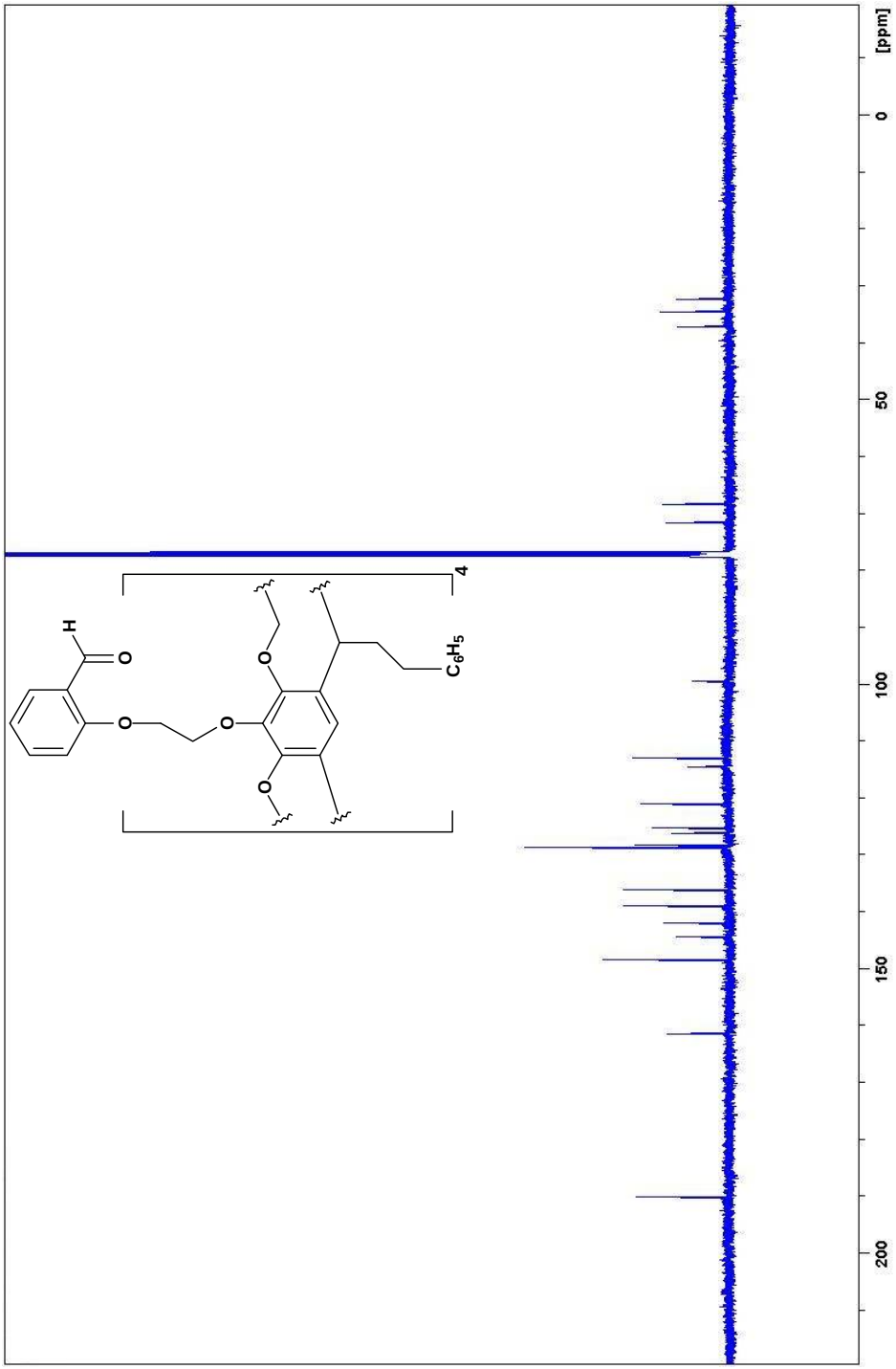

Spectrum 1.89: ^{13}C NMR spectrum of 35 in $CDCl_3$ (100 MHz)

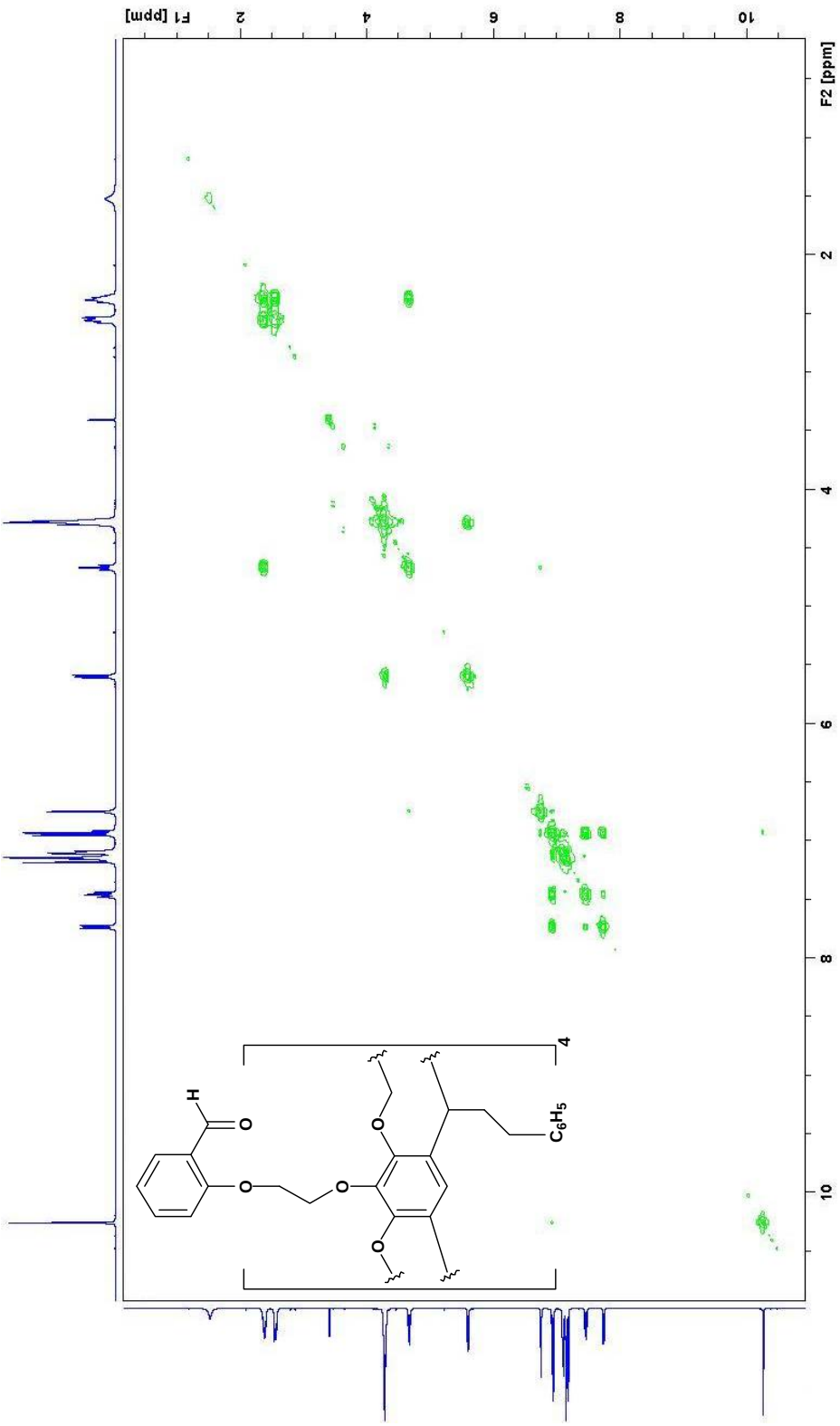

Spectrum 1.90: COSY spectrum of 35 in $CDCl_3$ (400 MHz)

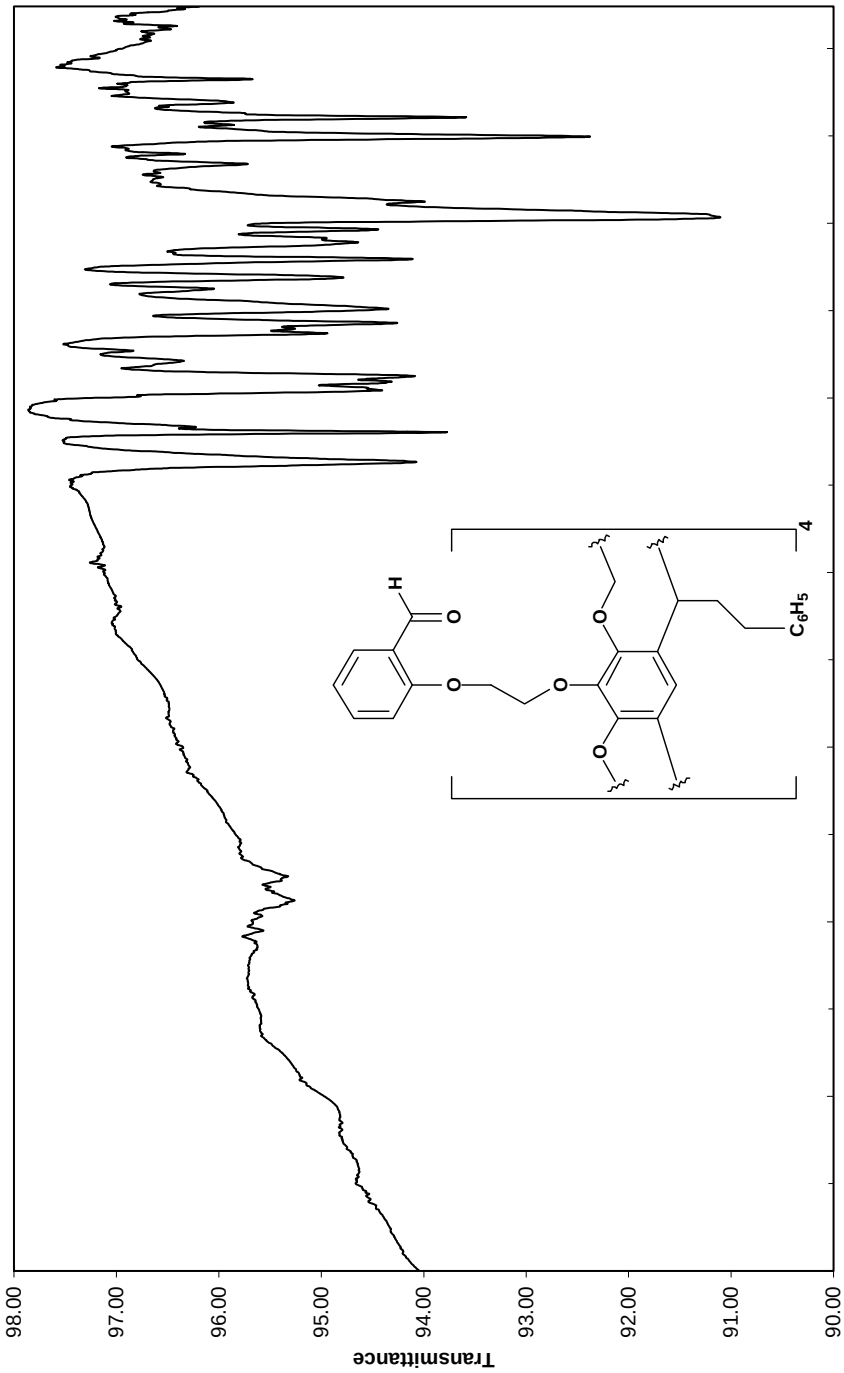

Spectrum 1.91: Infrared spectrum of 35 (KBr)

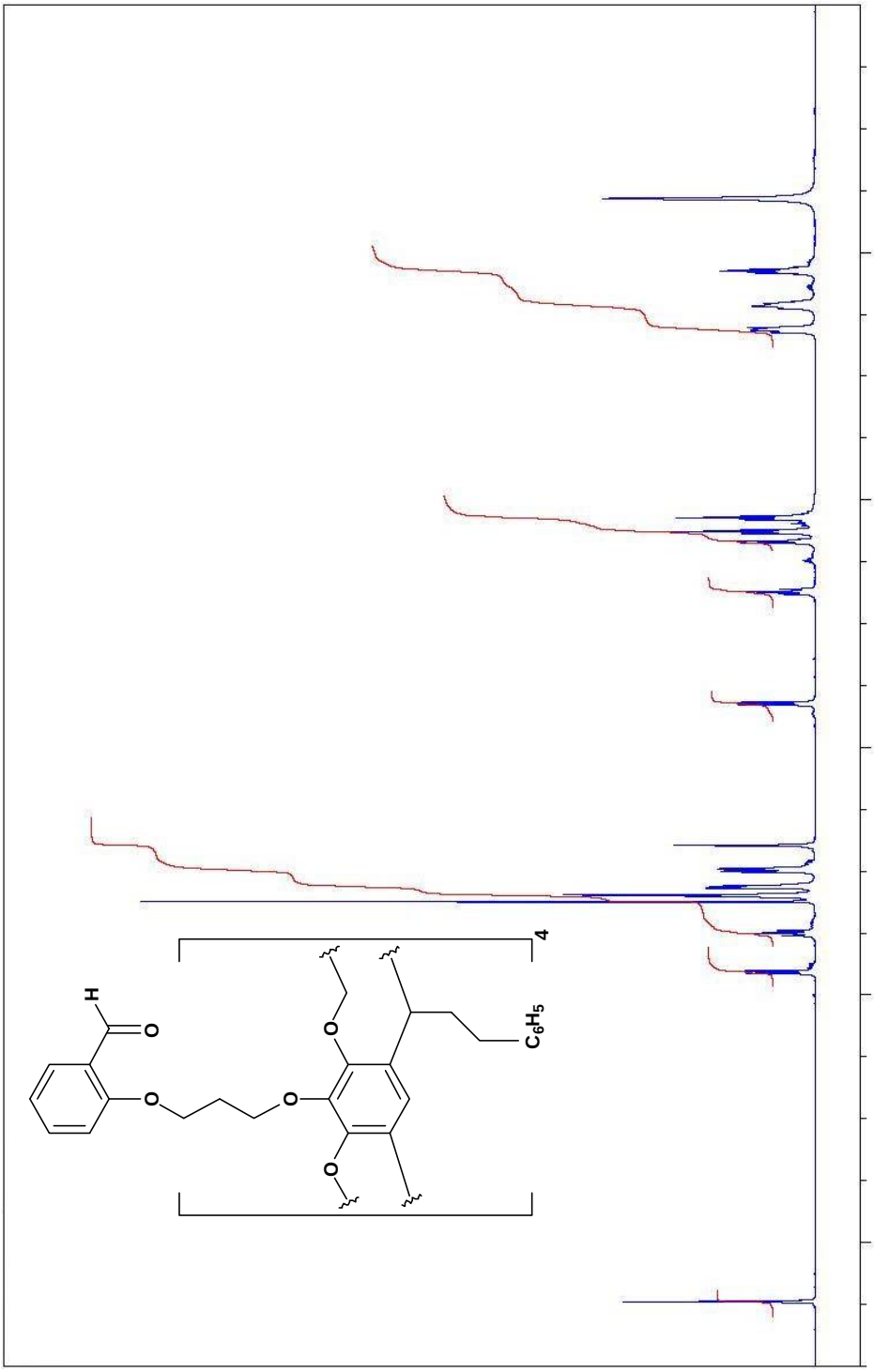

Spectrum 1.92: ^{1}H NMR spectrum of 36 in $CDCl_3$ (400 MHz)

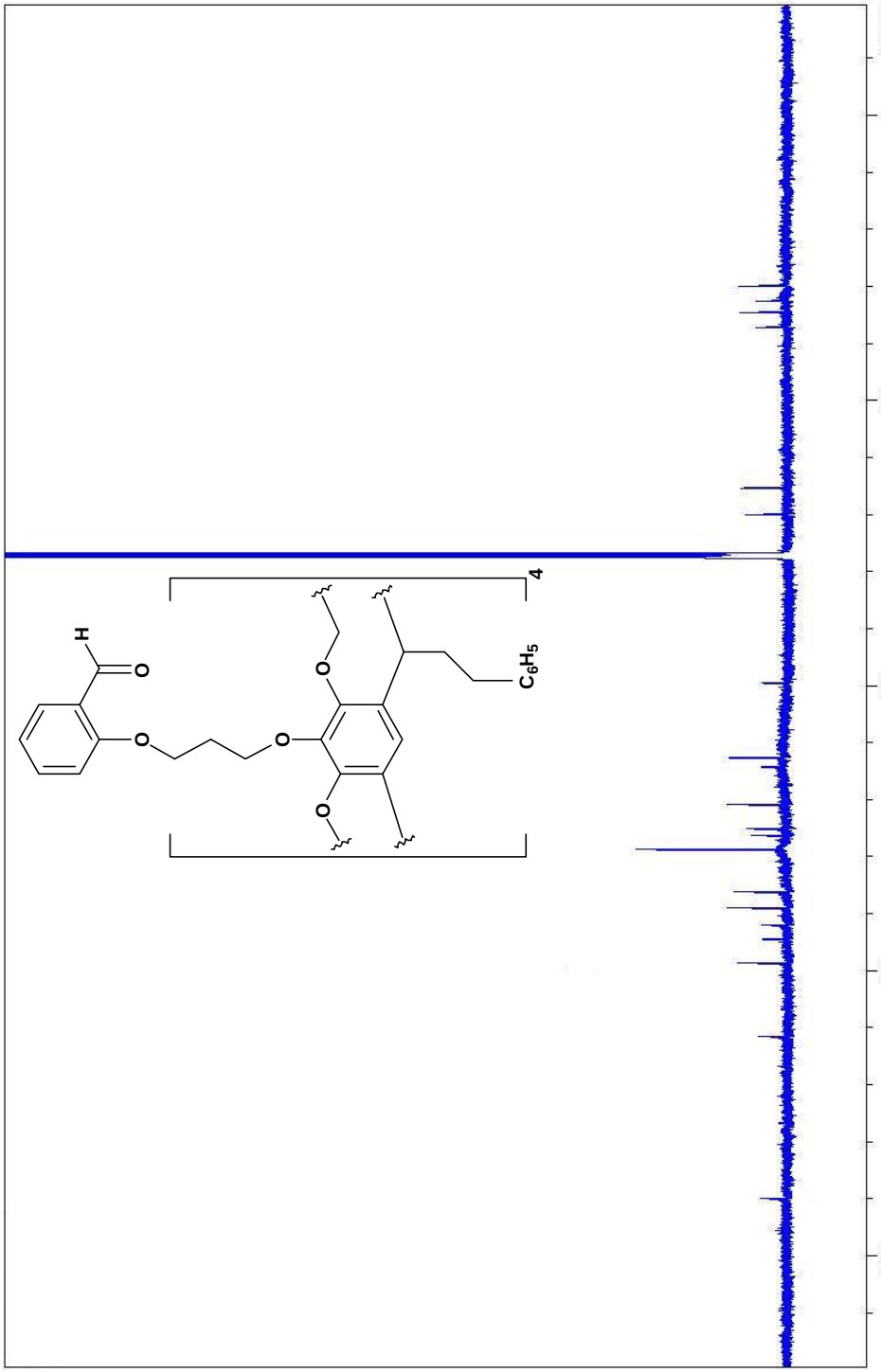

Spectrum 1.93: ^{13}C NMR spectrum of 36 in $CDCl_3$ (100 MHz)

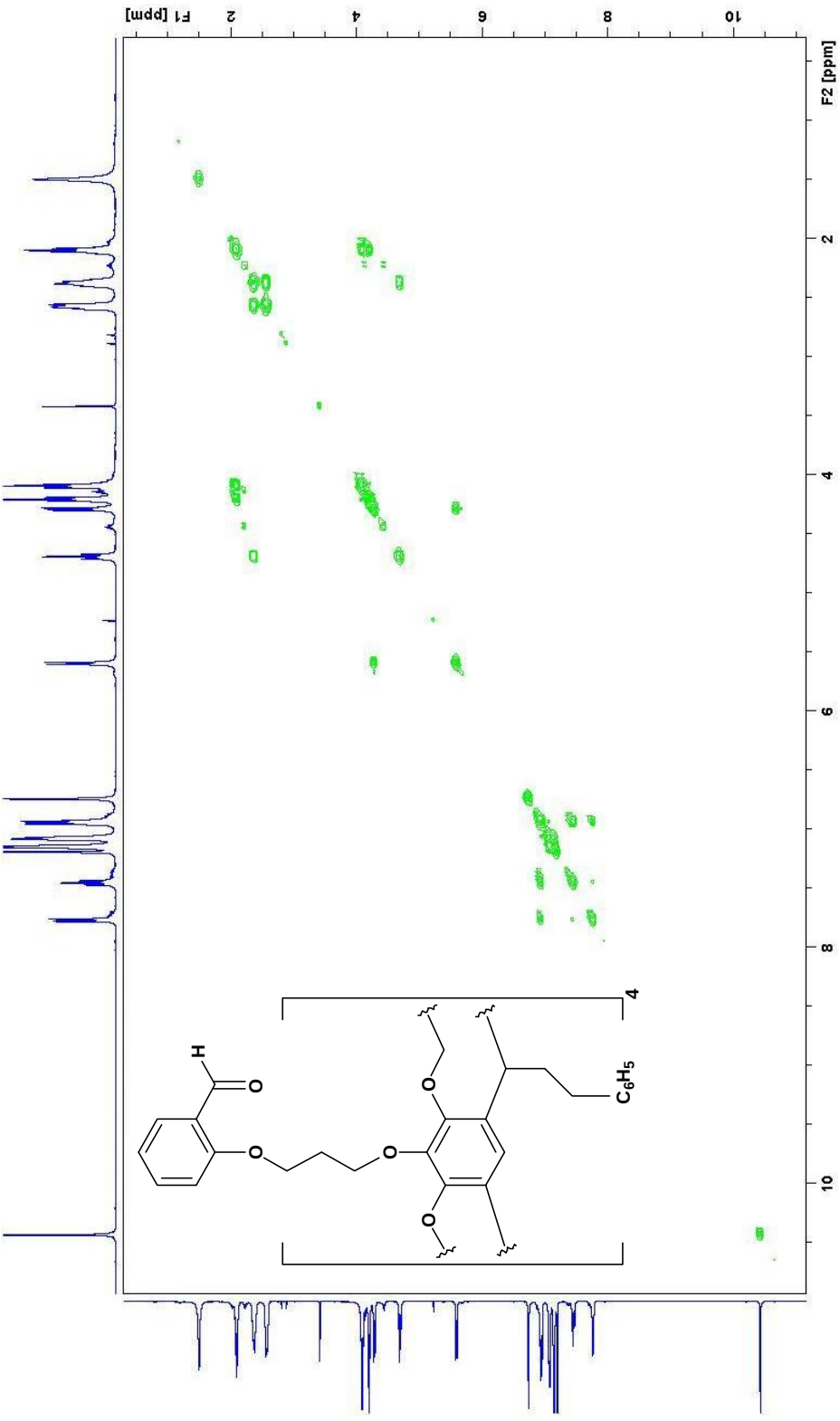

Spectrum 1.94: COSY spectrum of 36 in $CDCl_3$ (100 MHz)

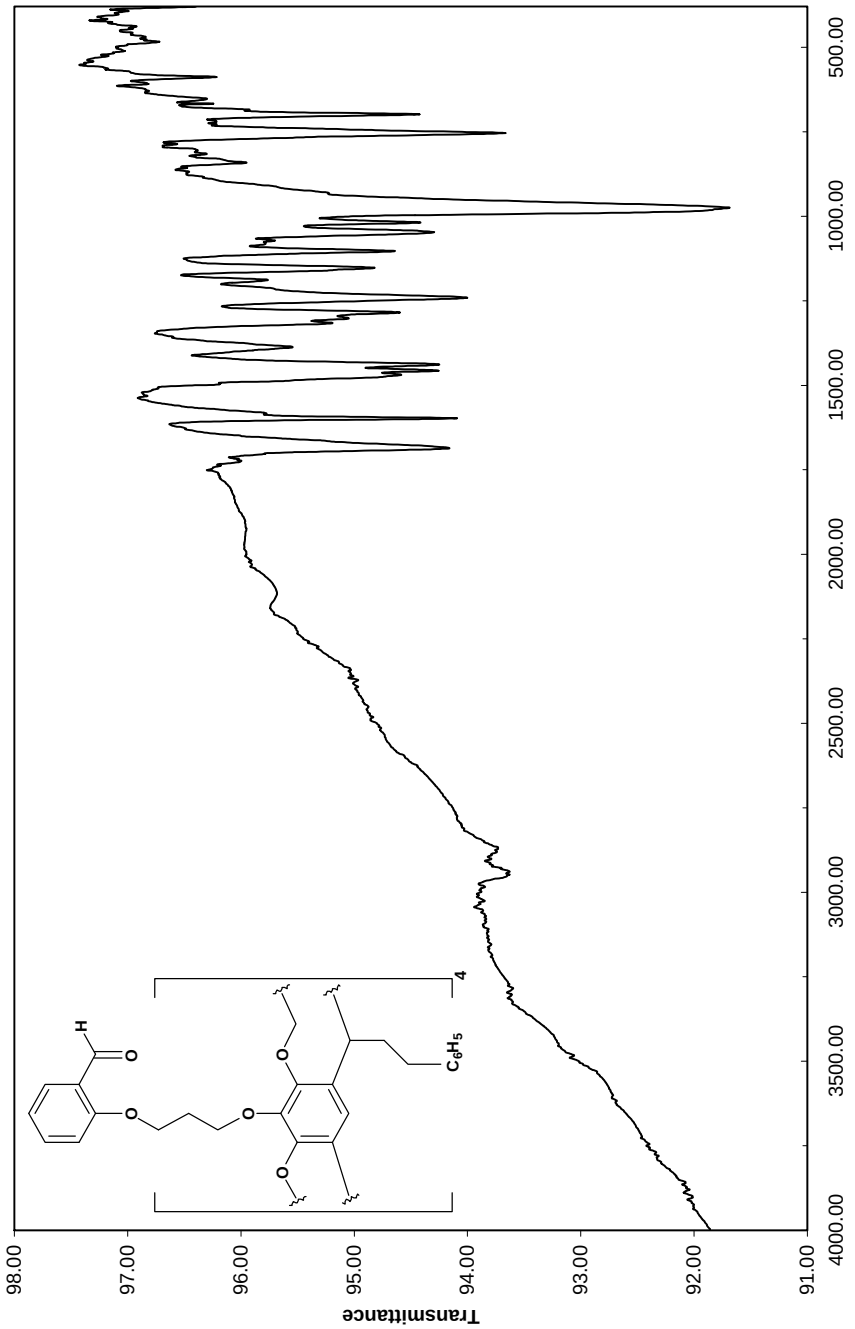

Spectrum 1.95: Infrared spectrum of 36 (KBr)

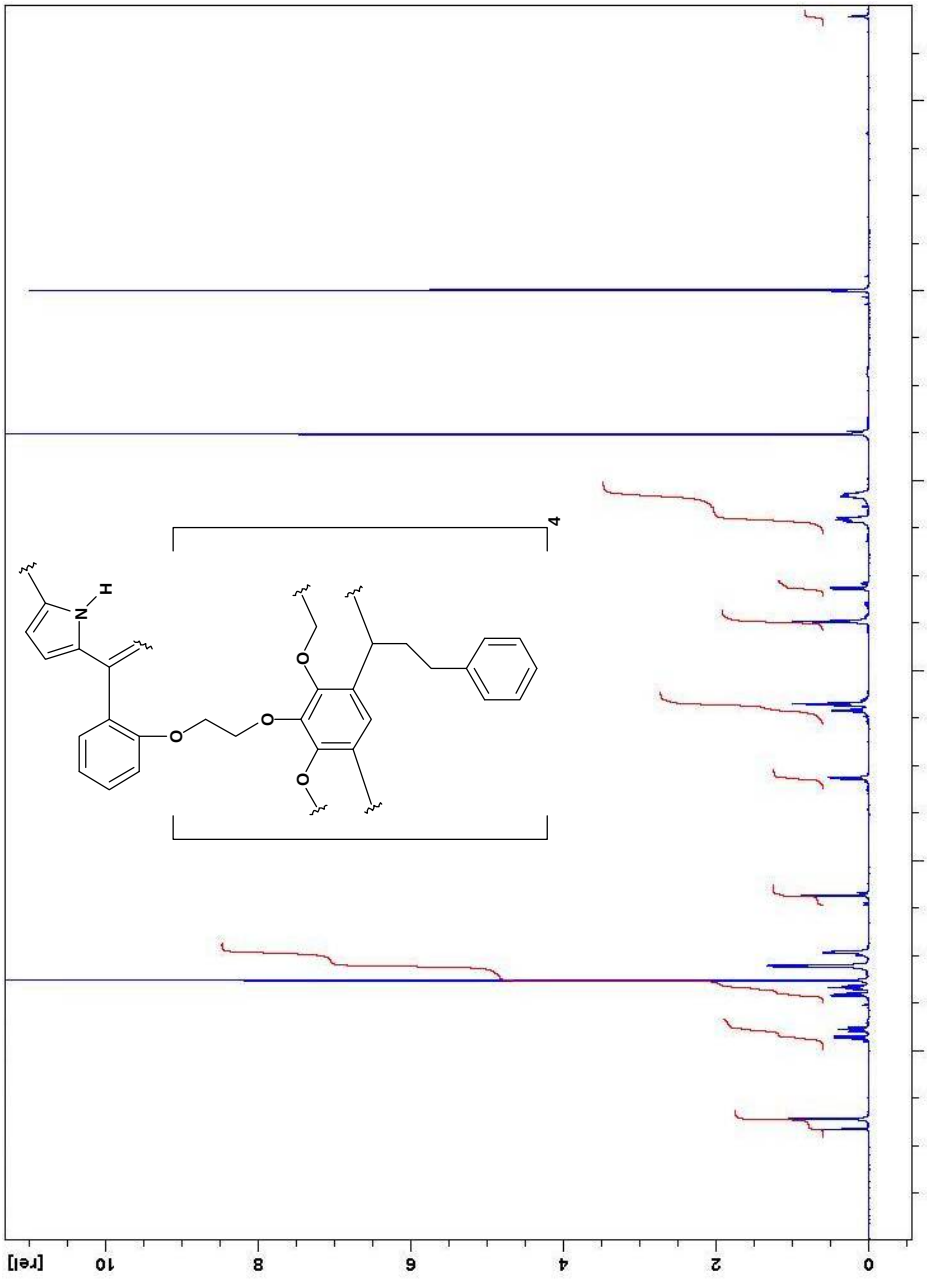

Spectrum 1.96: ^{1}H NMR spectrum of 37 in $CDCl_3$ (400 MHz)

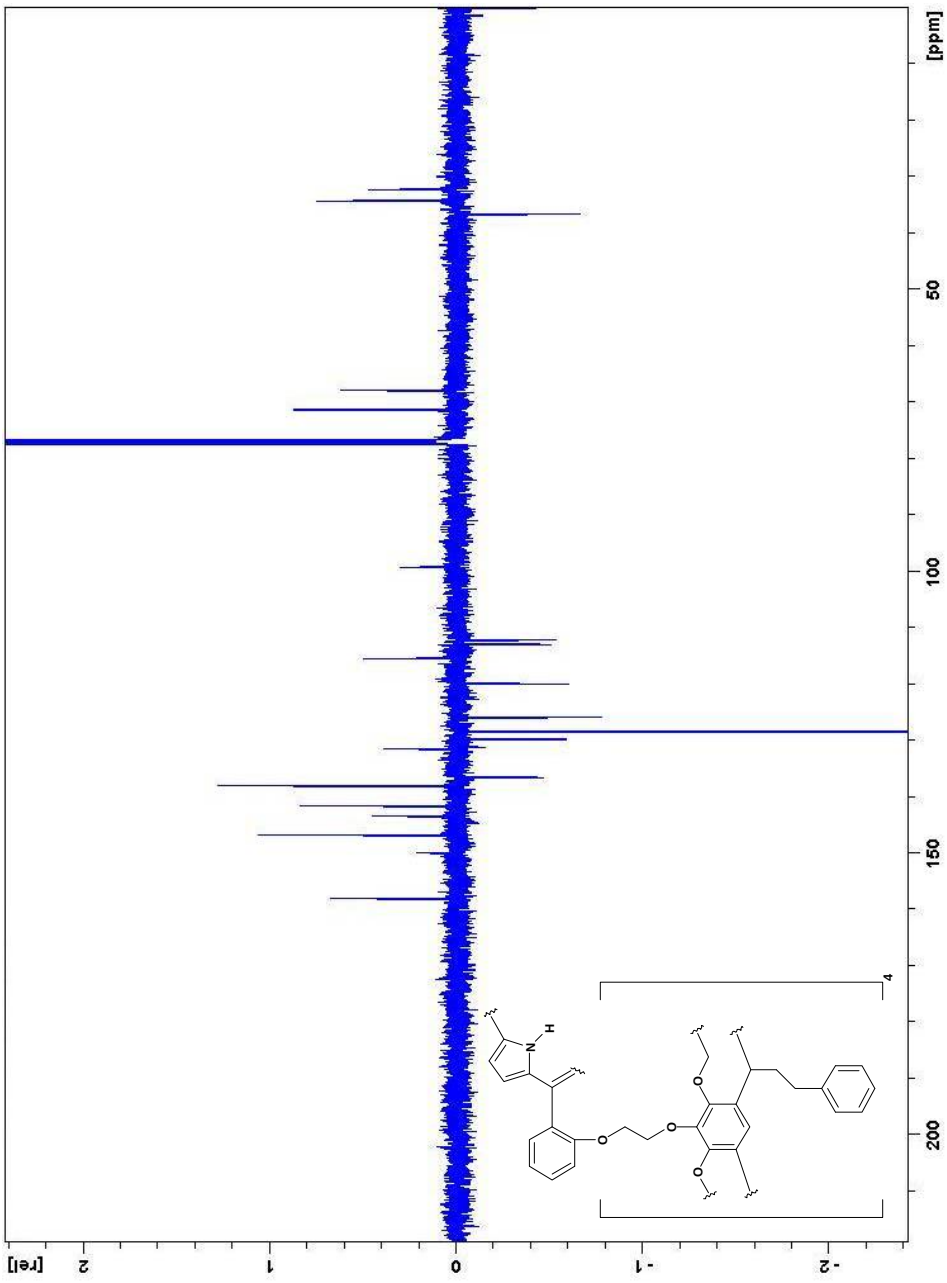

Spectrum 1.97: ^{13}C APT NMR spectrum of 37 in $CDCl_3$ (100 MHz)

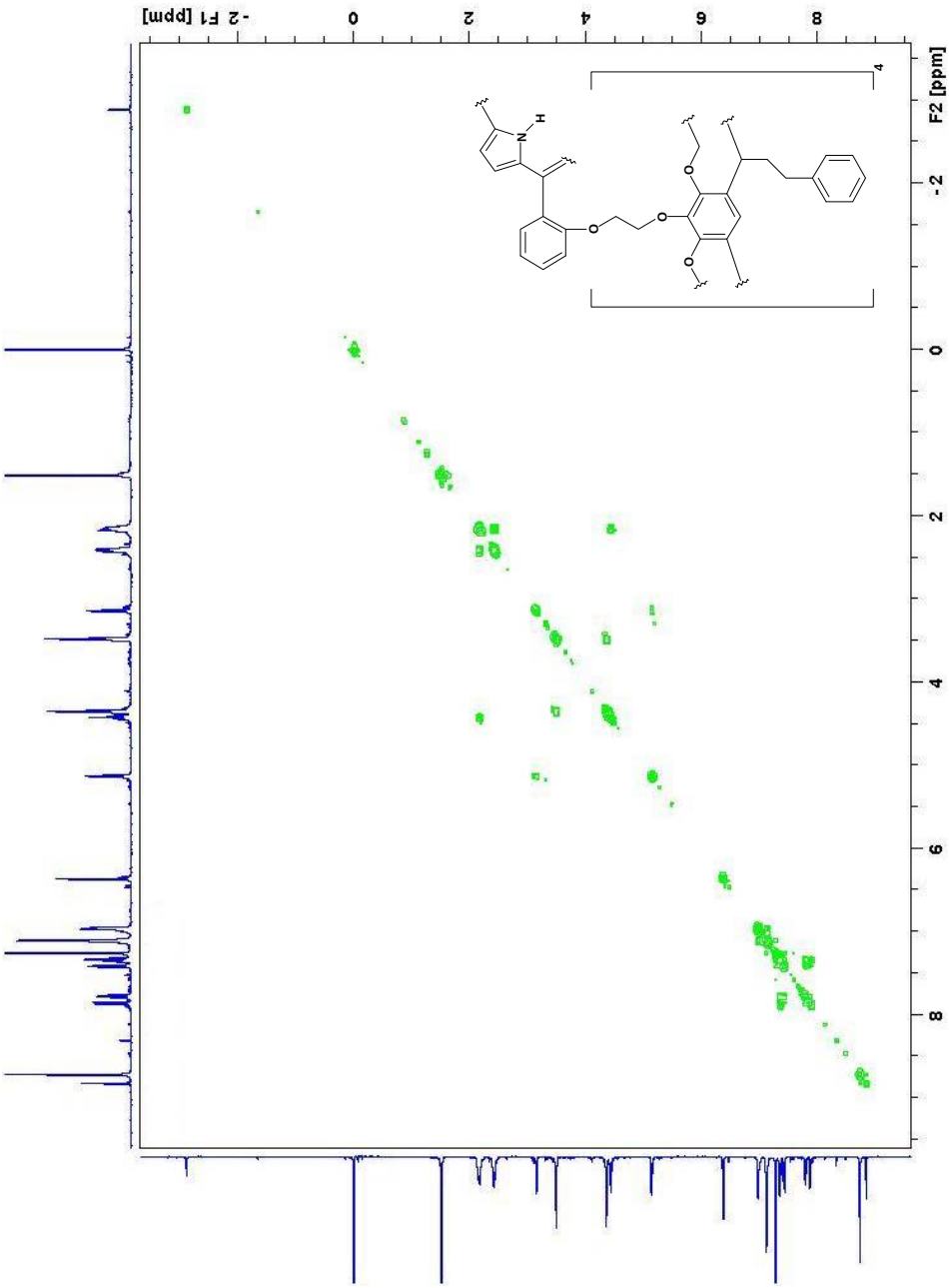

Spectrum 1.98: COSY spectrum of 37 in $CDCl_3$ (100 MHz)

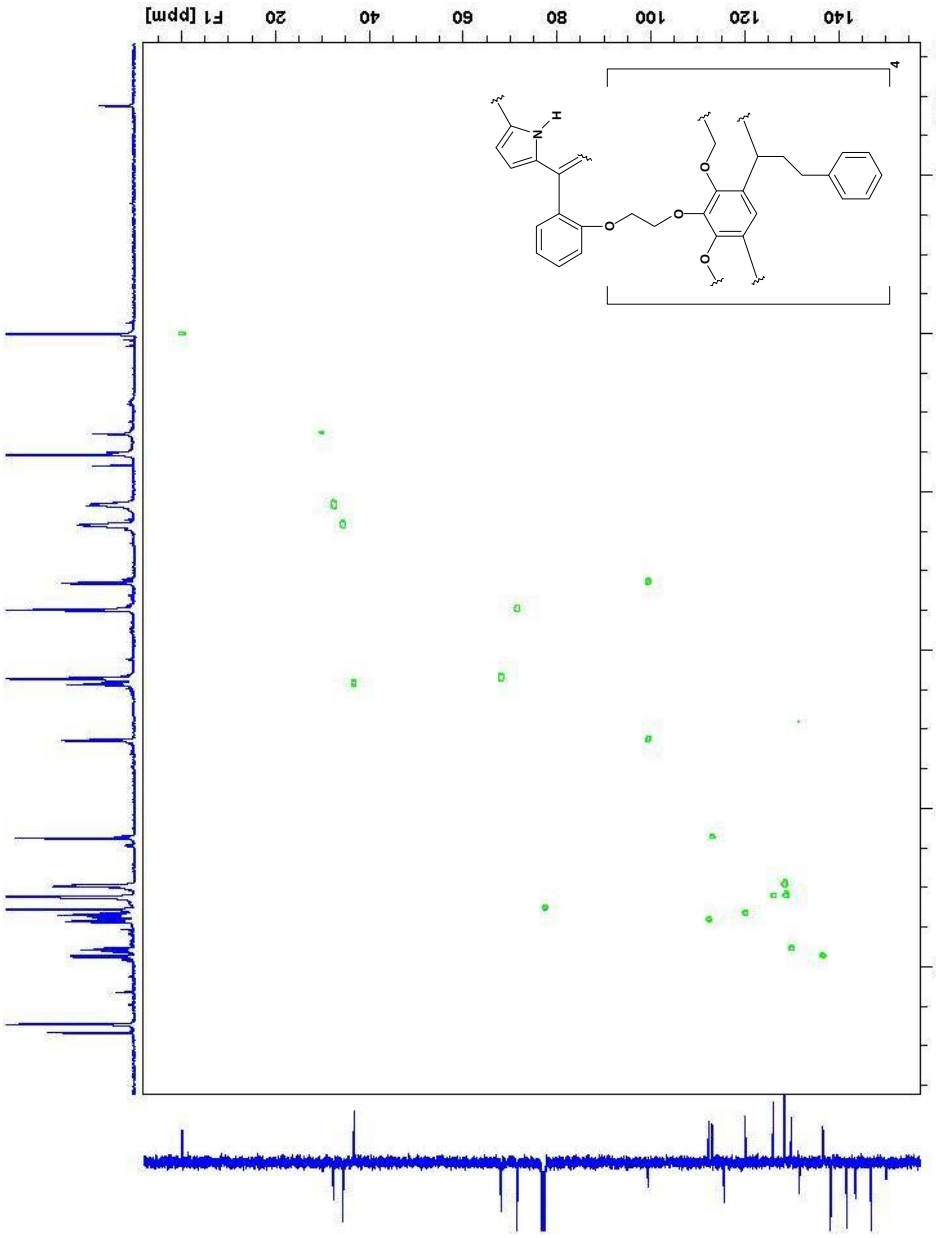

Spectrum 1.99: HSQC spectrum of 37 in $CDCl_3$ (100 MHz)

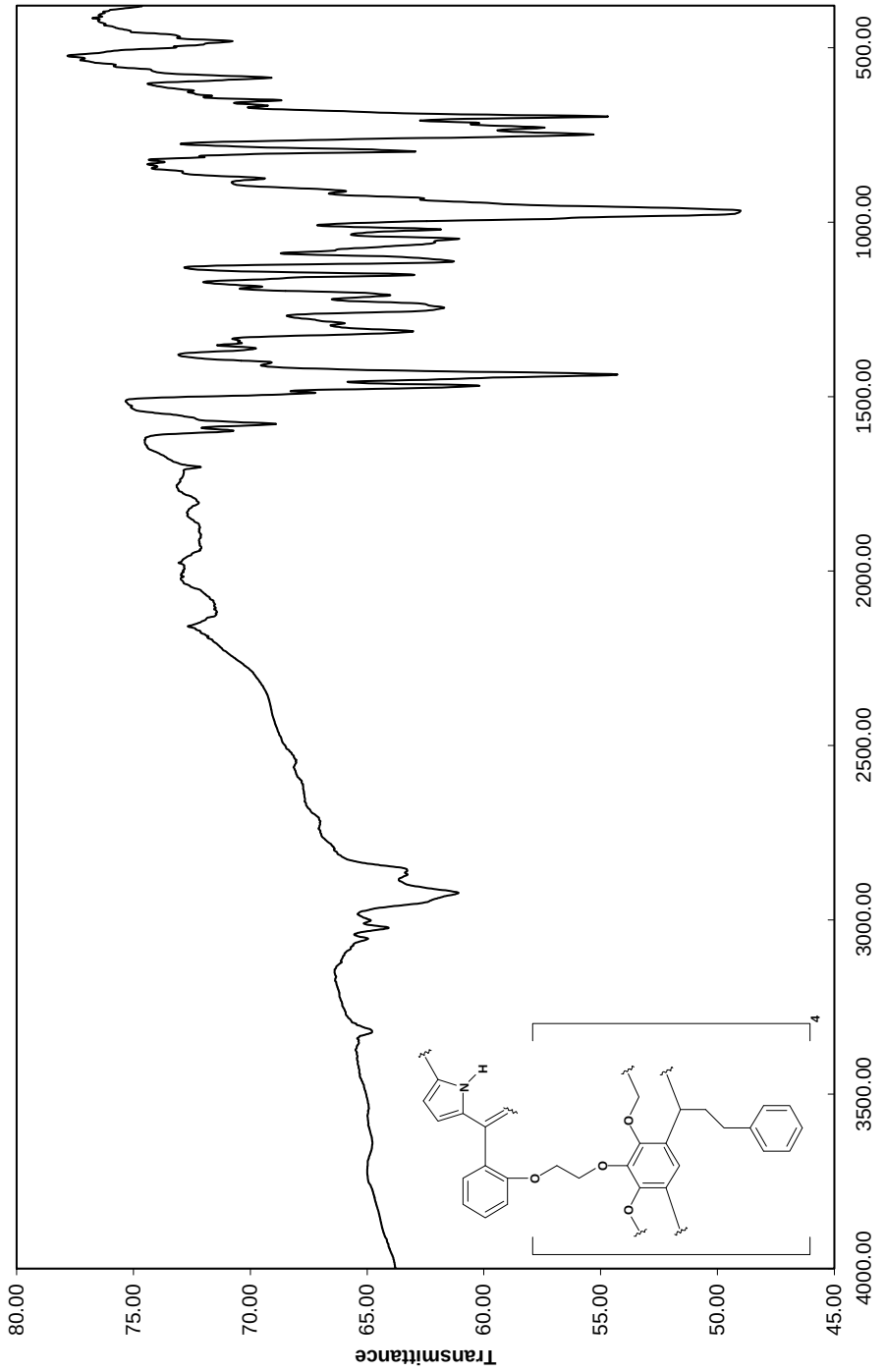

Spectrum 1.100: Infrared spectrum of 37 (KBr)

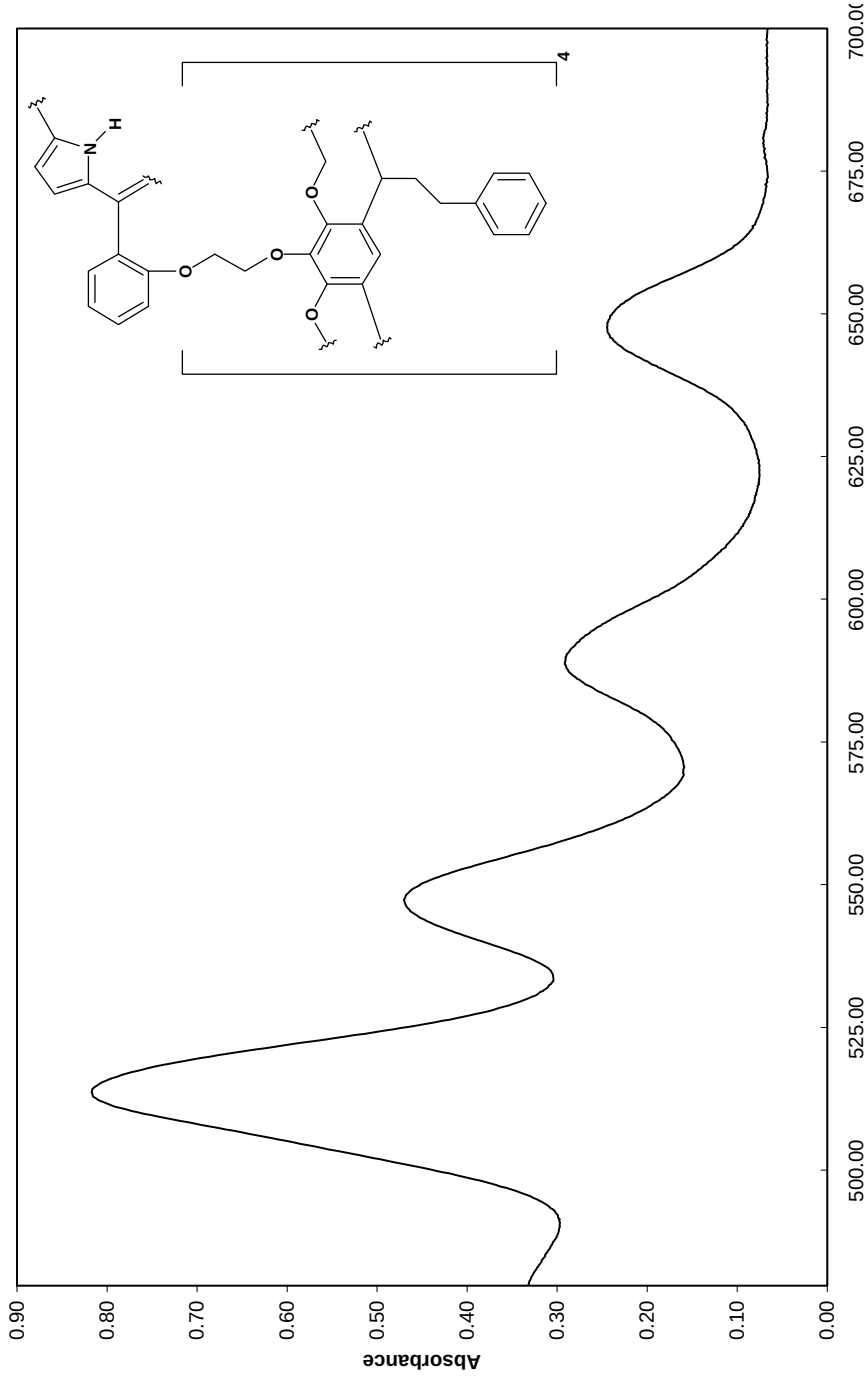

Spectrum 1.101: UV-Visible spectrum of 37 from 480-700 nm ($CHCl_3$)

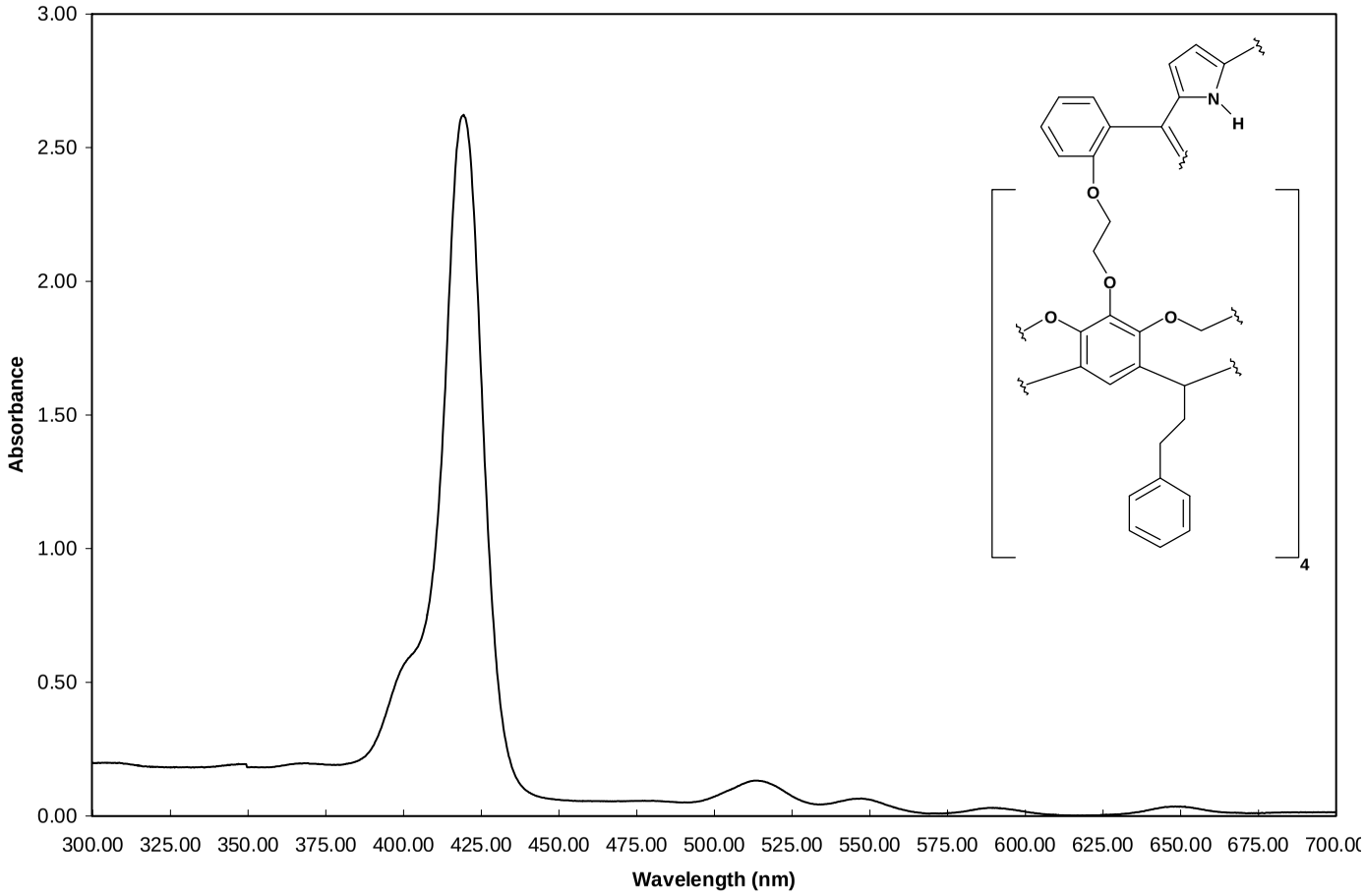

Spectrum 1.102: UV-Visible spectrum of 37 from 300-700 nm ($CHCl_3$)

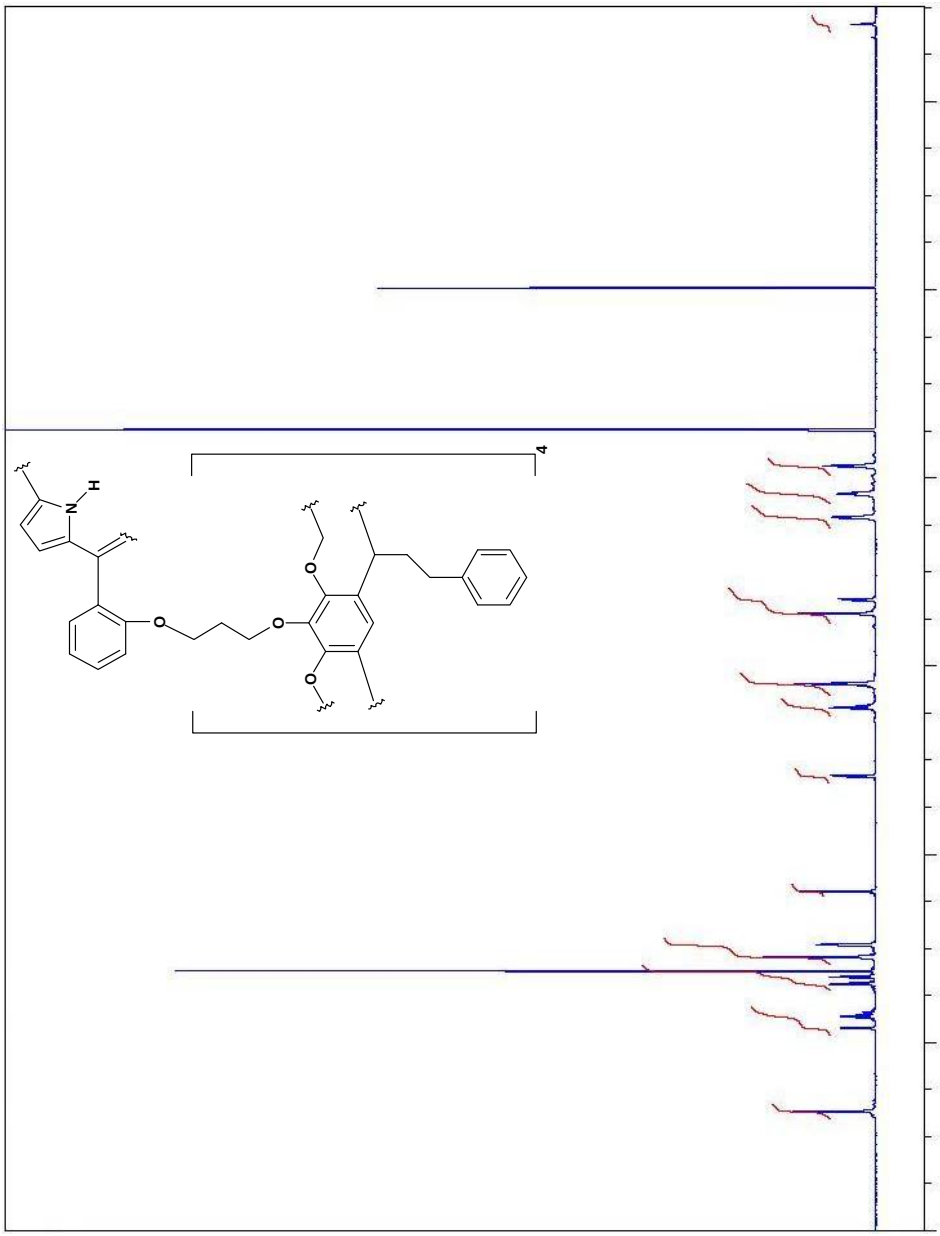

Spectrum 1.103: ^{1}H NMR spectrum of 38 in $CDCl_3$ (400 MHz)

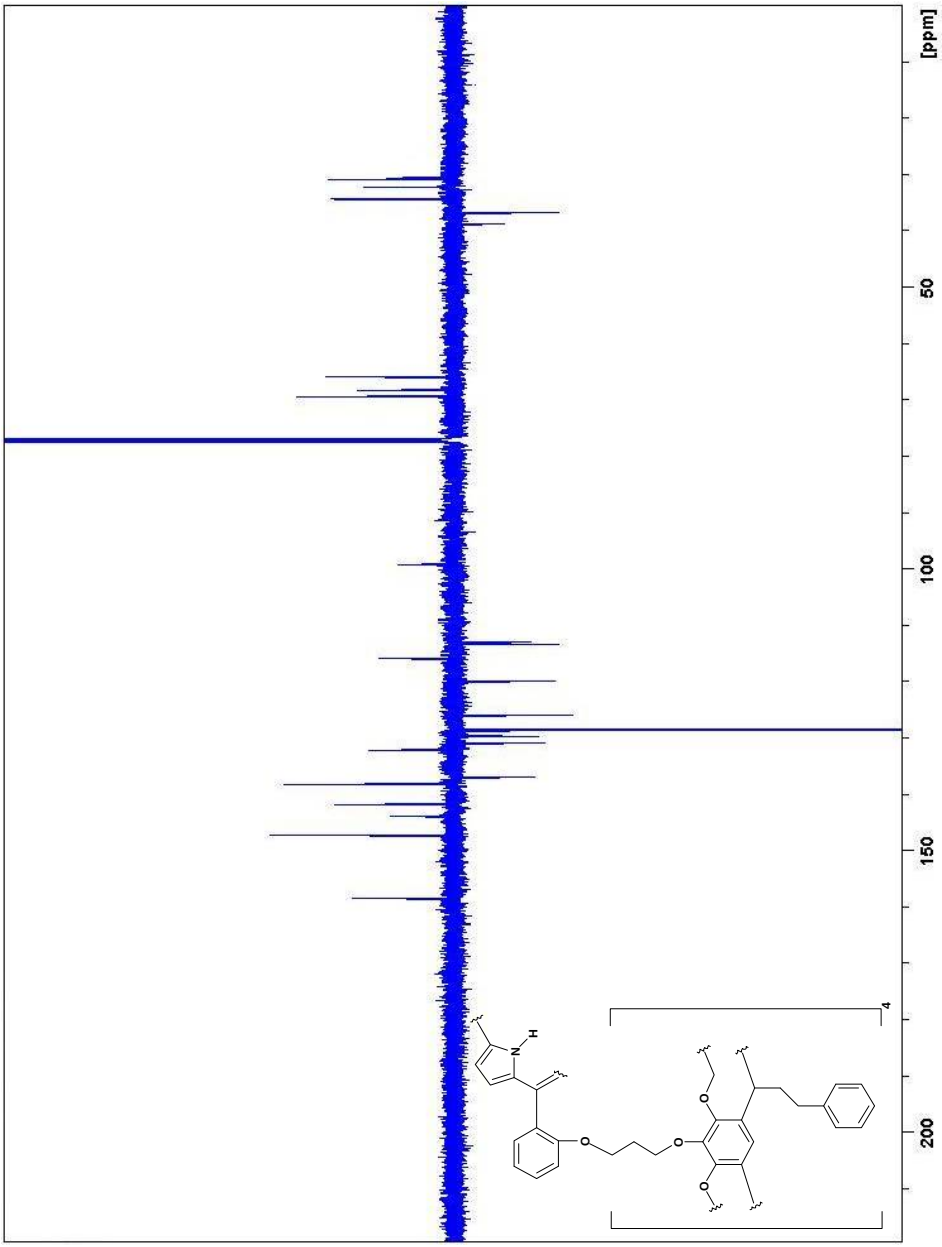

Spectrum 1.104: ^{13}C APT NMR spectrum of 38 in $CDCl_3$ (100 MHz)

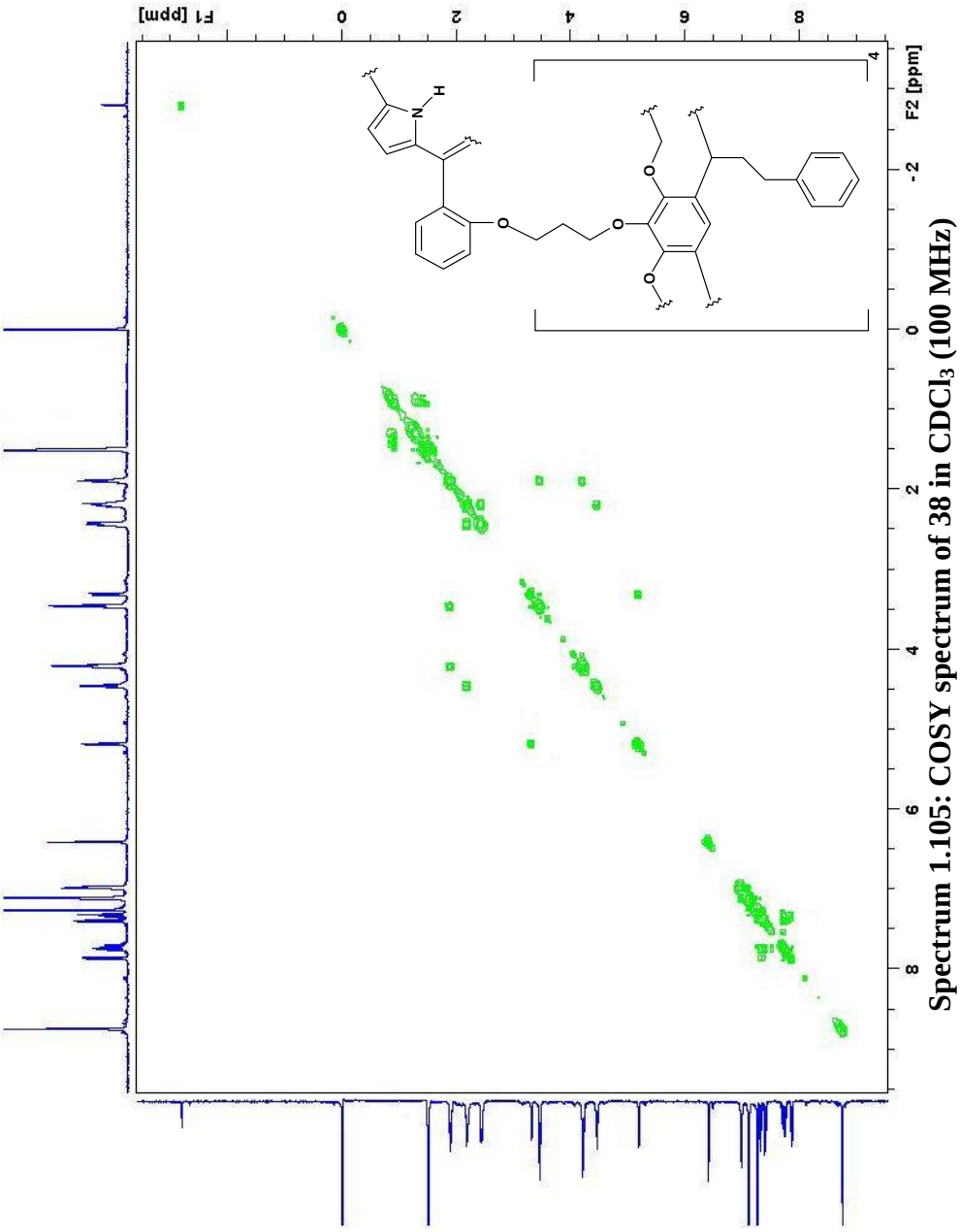

Spectrum 1.105: COSY spectrum of 38 in $CDCl_3$ (100 MHz)

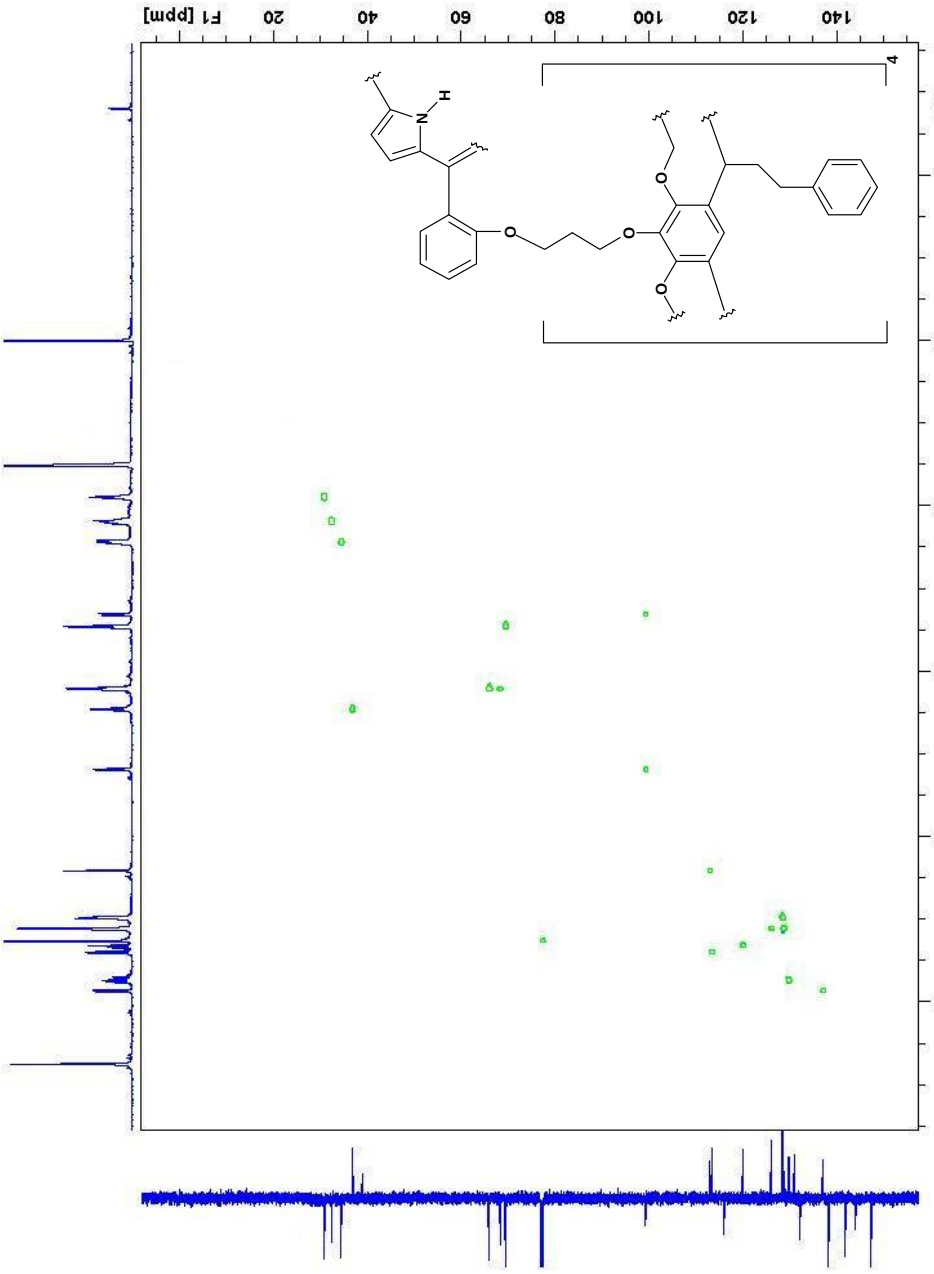

Spectrum 1.106: HSQC spectrum of 38 in $CDCl_3$ (100 MHz)

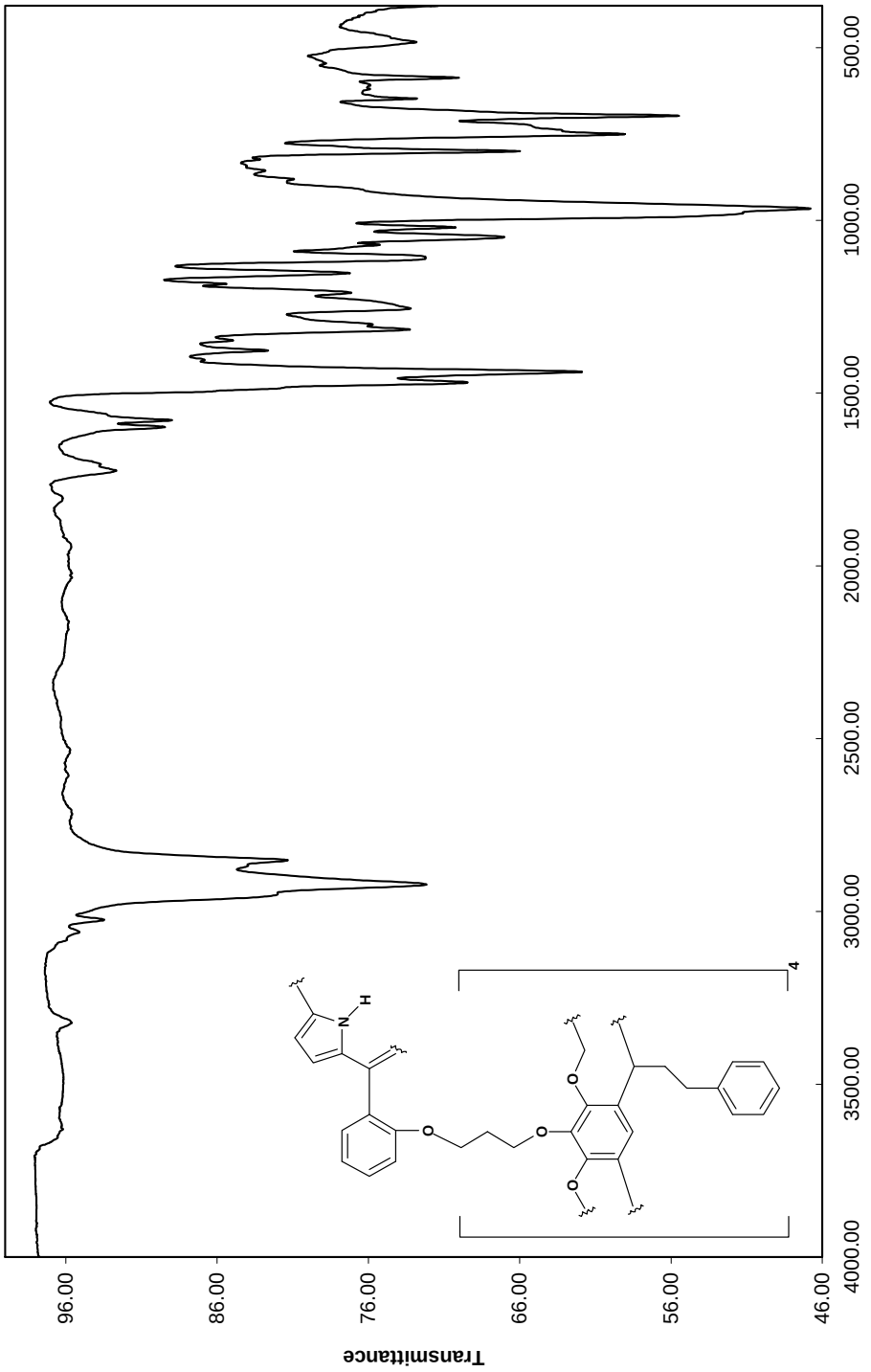

Spectrum 1.107: Infrared spectrum of 38 (KBr)

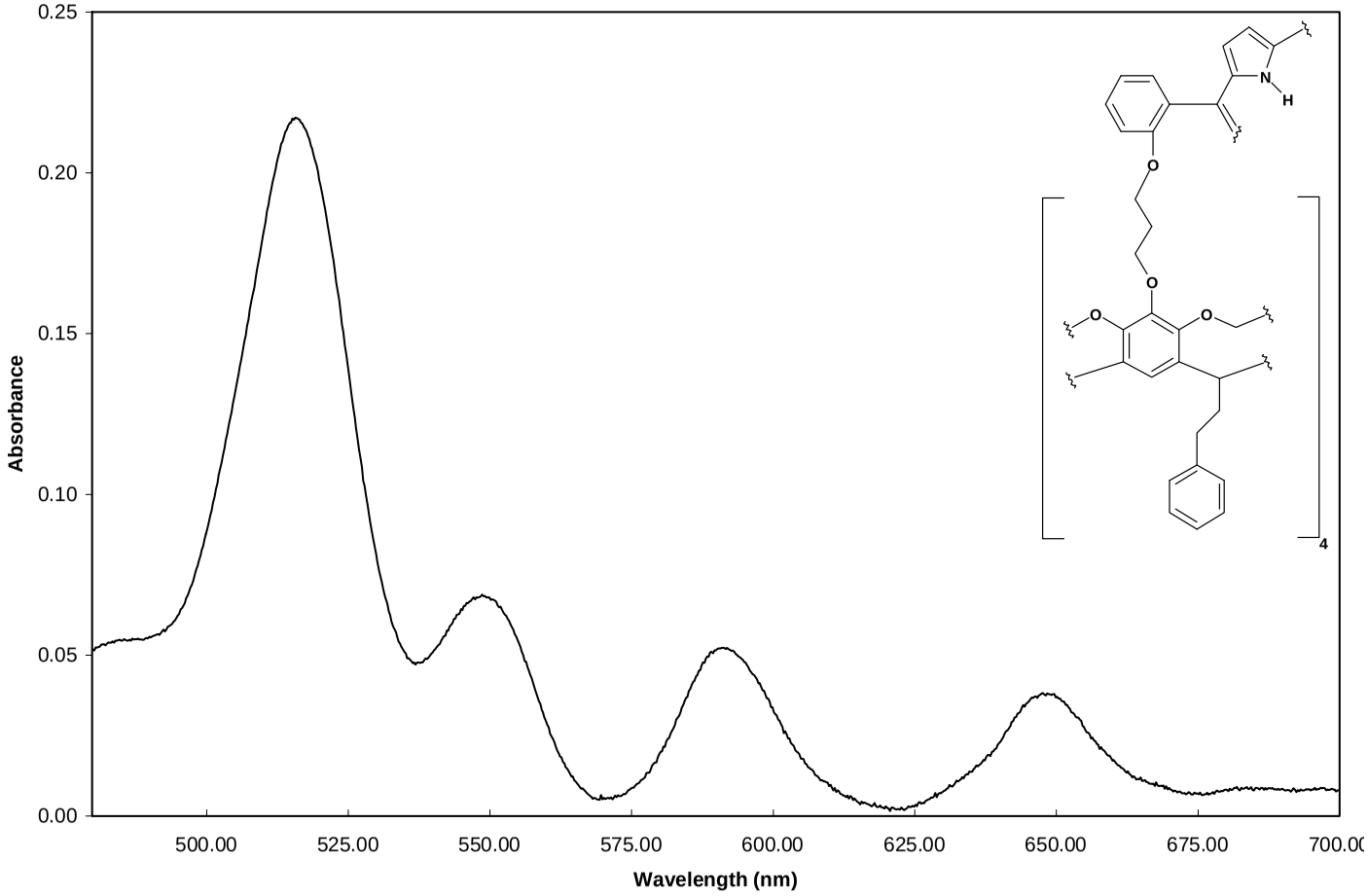

Spectrum 1.108: UV-Visible spectrum of 38 from 480-700 nm ($CHCl_3$)

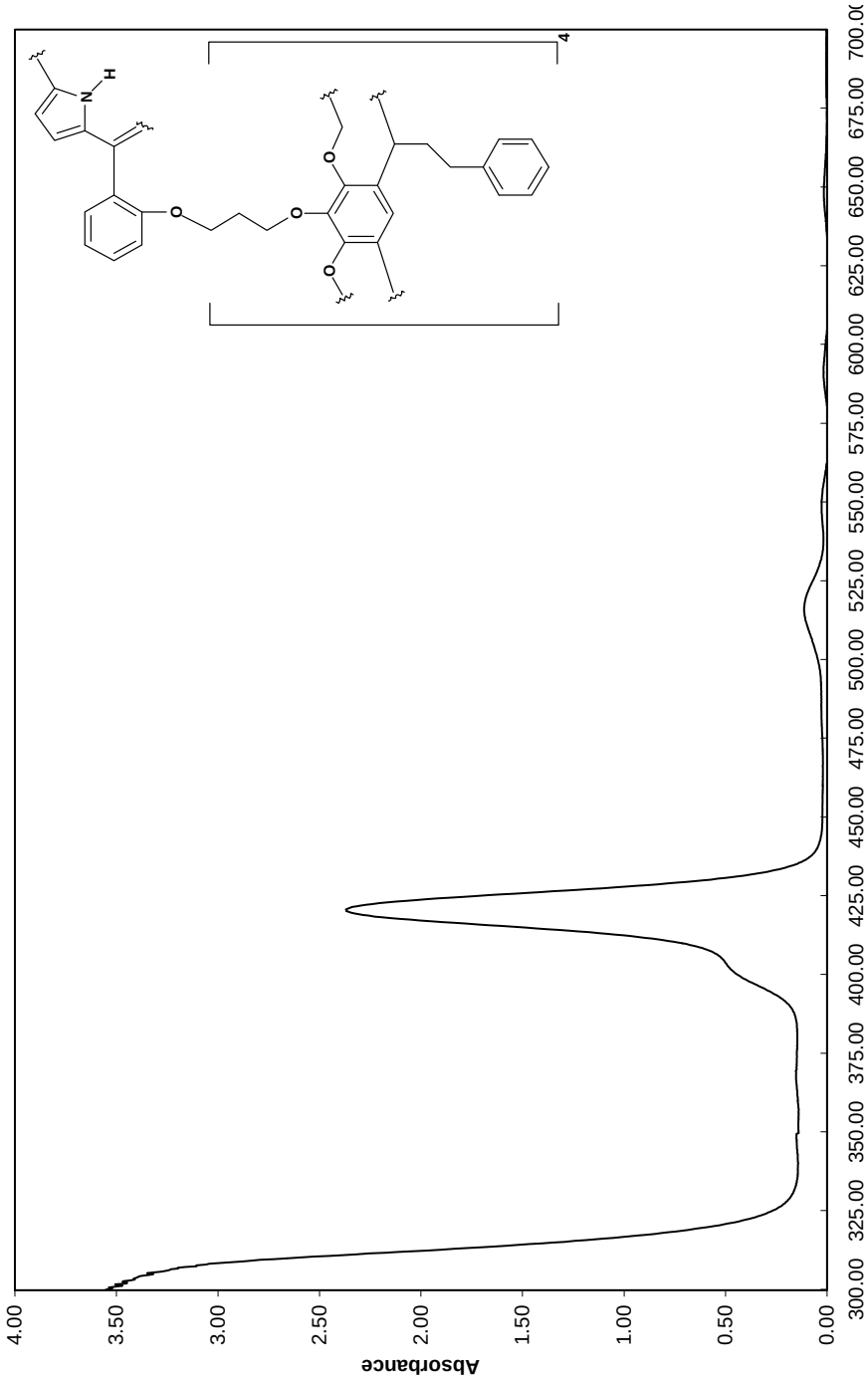

Spectrum 1.109: UV-Visible spectrum of 38 from 300-700 nm ($CHCl_3$)

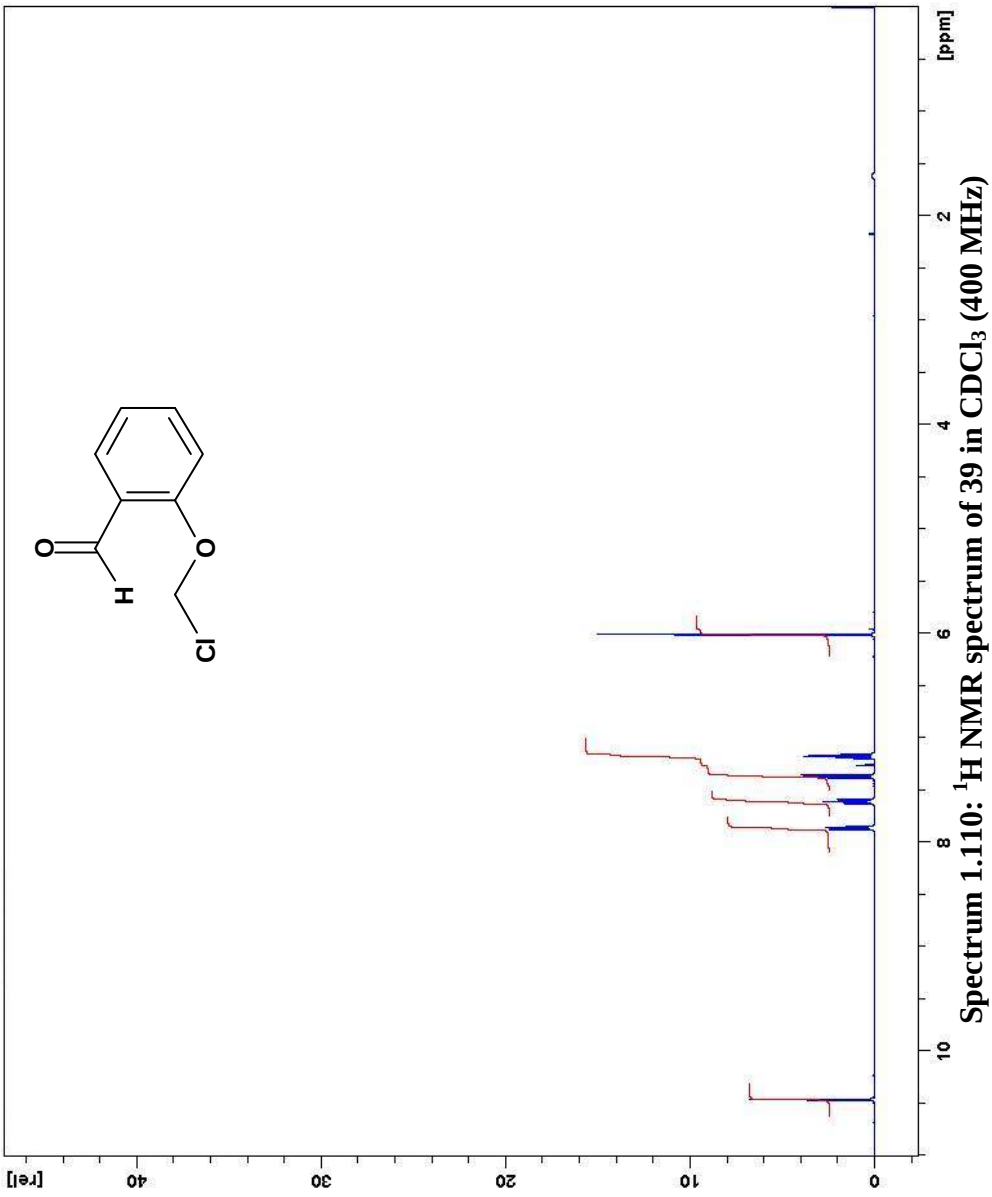

Spectrum 1.110: ^{1}H NMR spectrum of 39 in $CDCl_3$ (400 MHz)

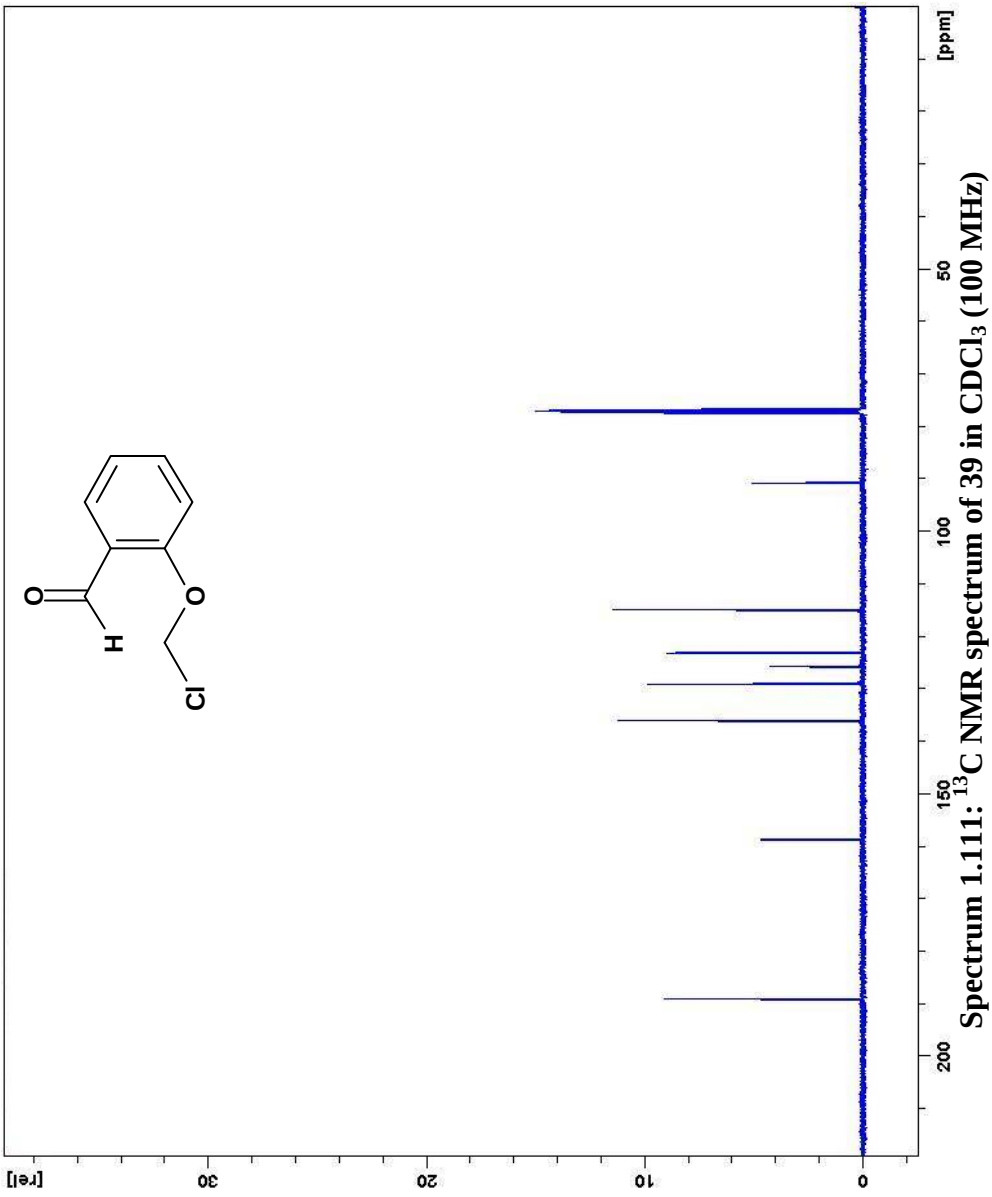

Spectrum 1.111: ^{13}C NMR spectrum of 39 in $CDCl_3$ (100 MHz)

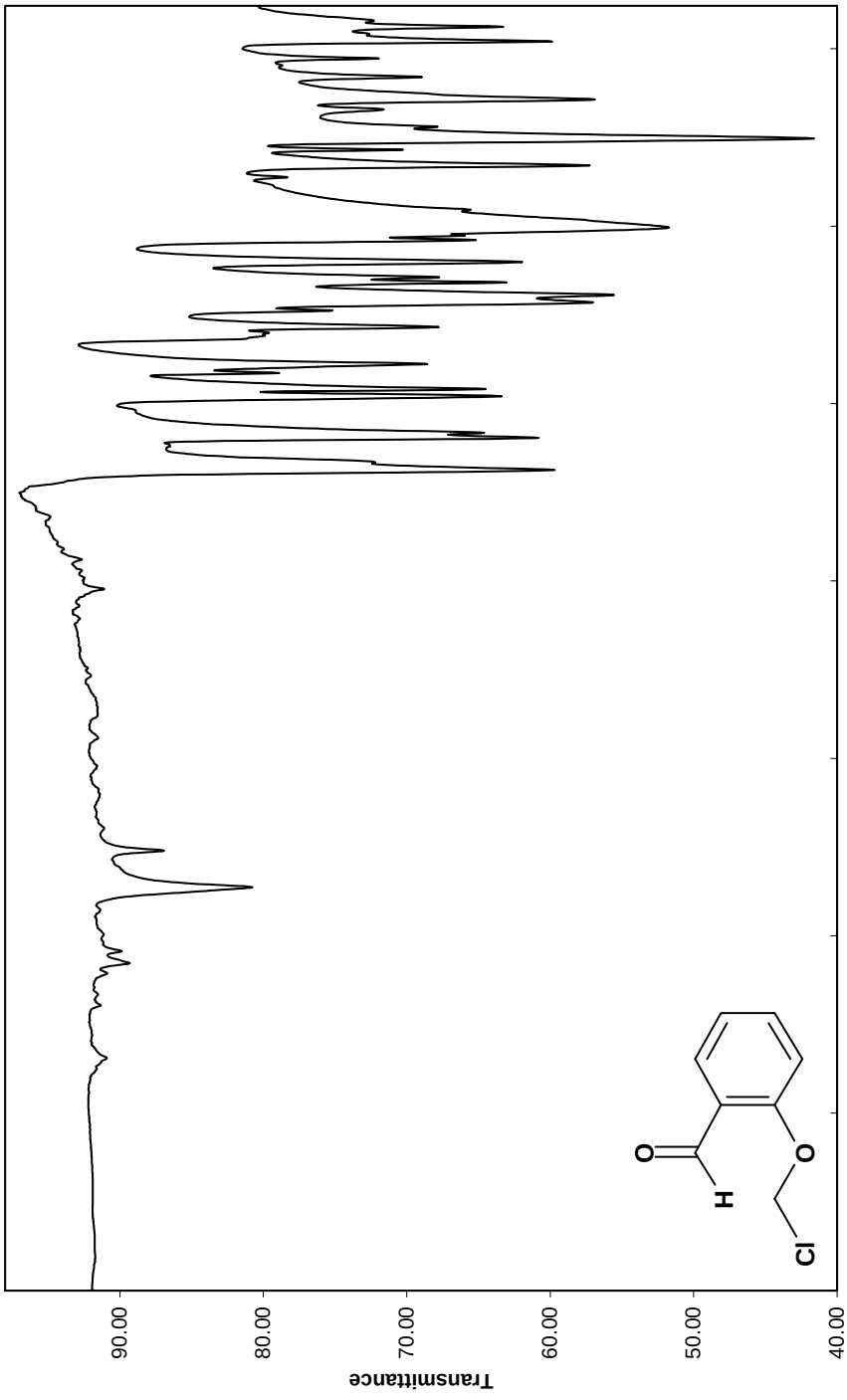

Spectrum 1.112: Infrared spectrum of 39 (KBr)

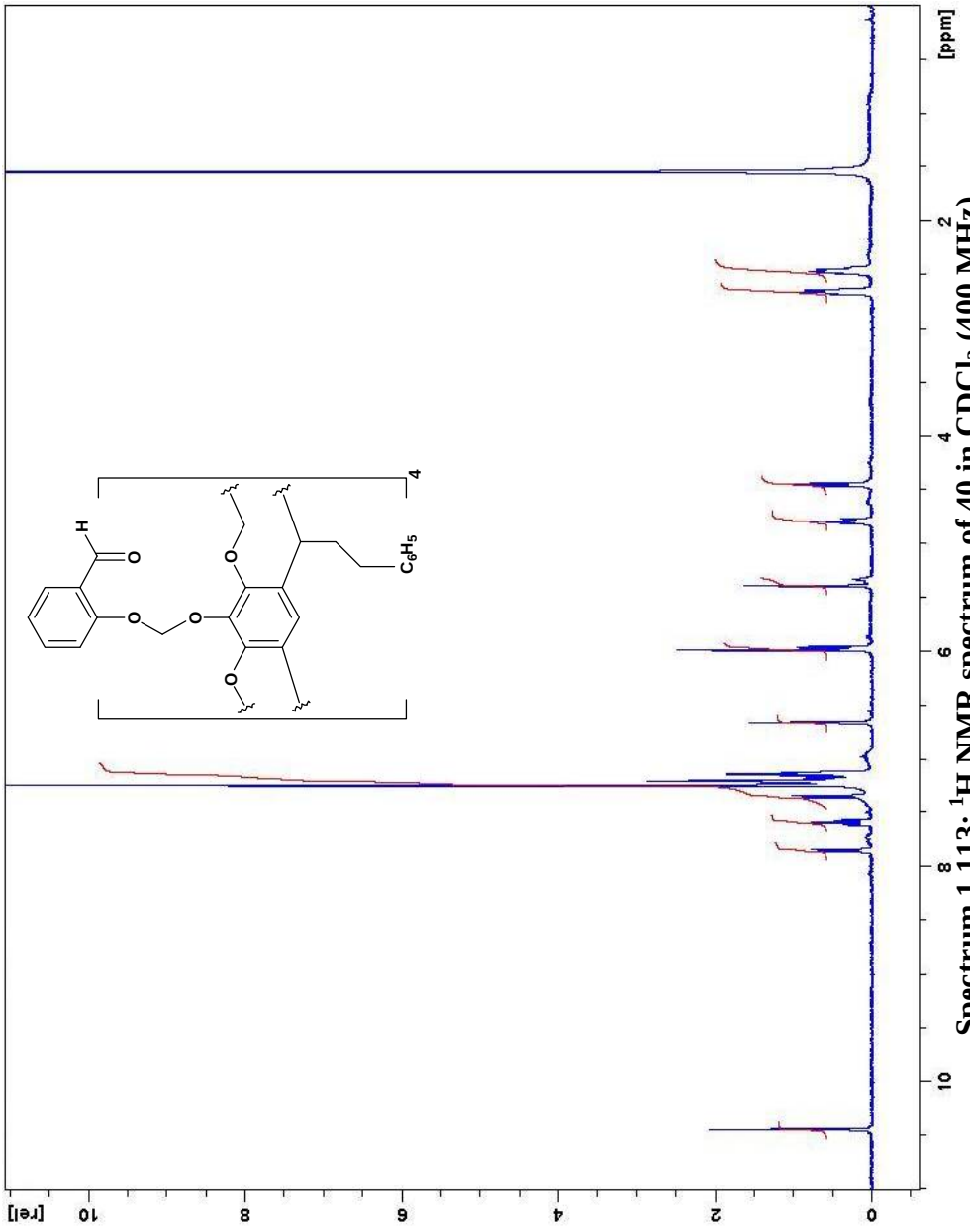

Spectrum 1.113: ^{1}H NMR spectrum of 40 in $CDCl_3$ (400 MHz)

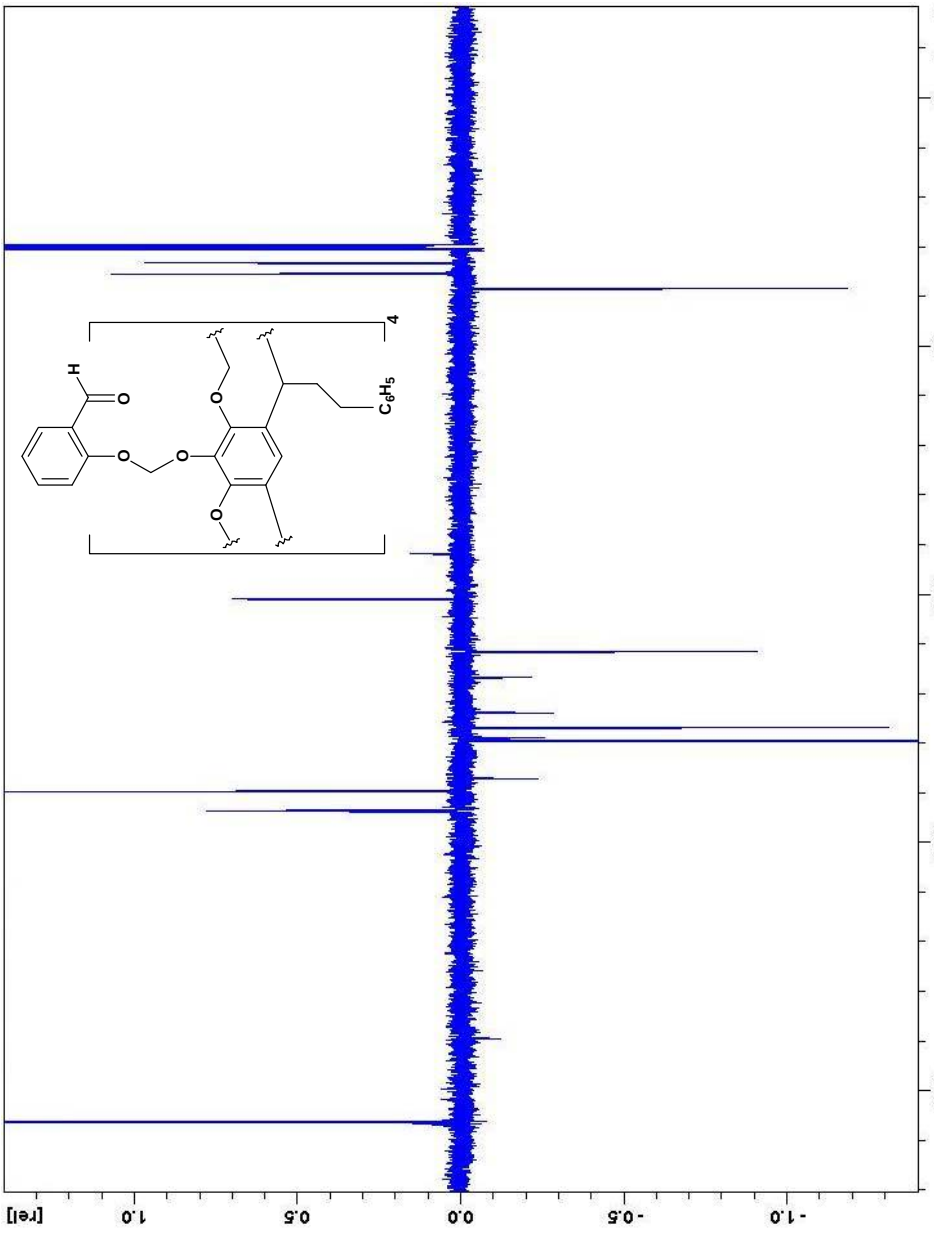

Spectrum 1.114: ^{13}C APT NMR spectrum of 40 in $CDCl_3$ (100 MHz)

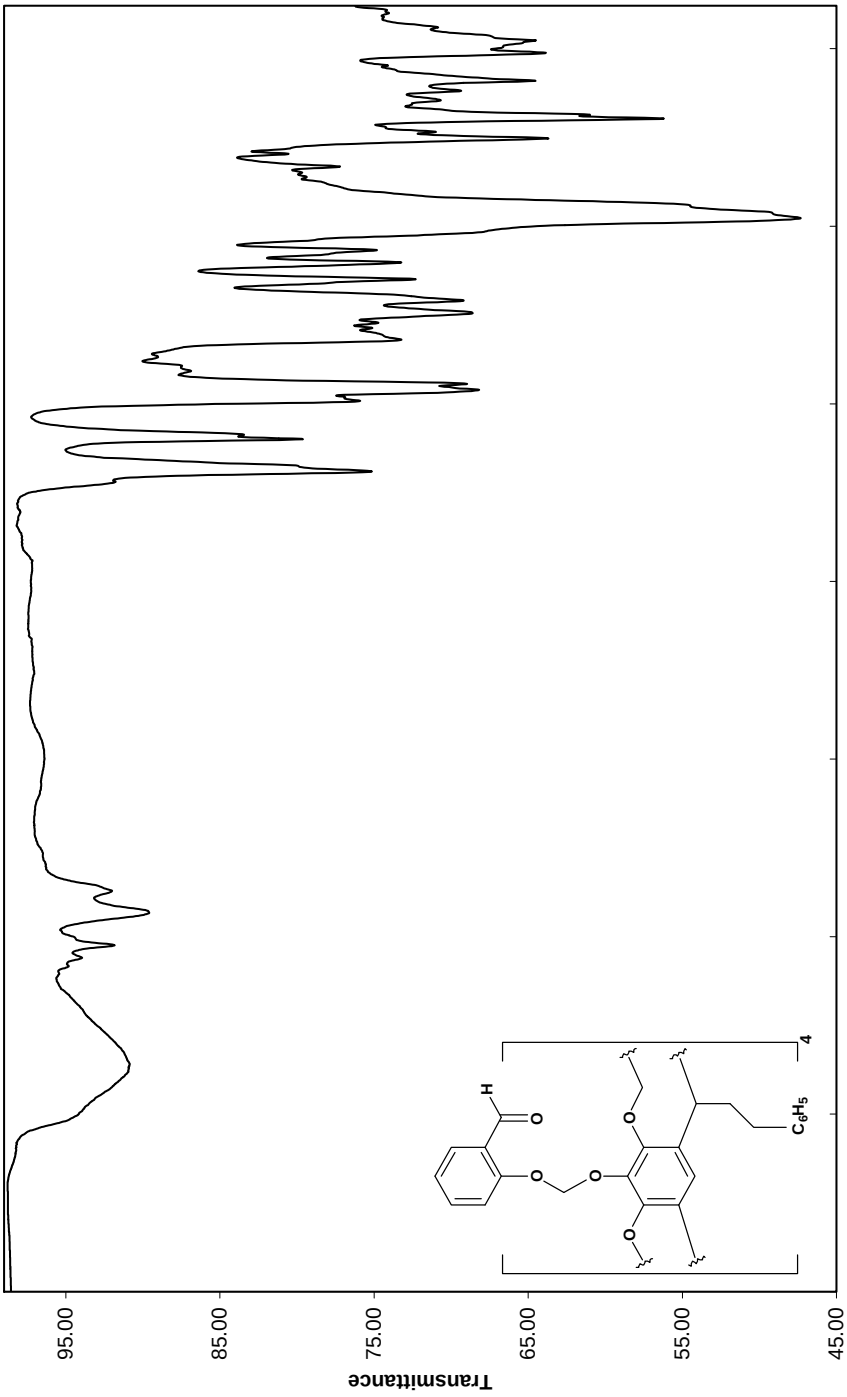

Spectrum 1.115: Infrared spectrum of 40 (KBr)

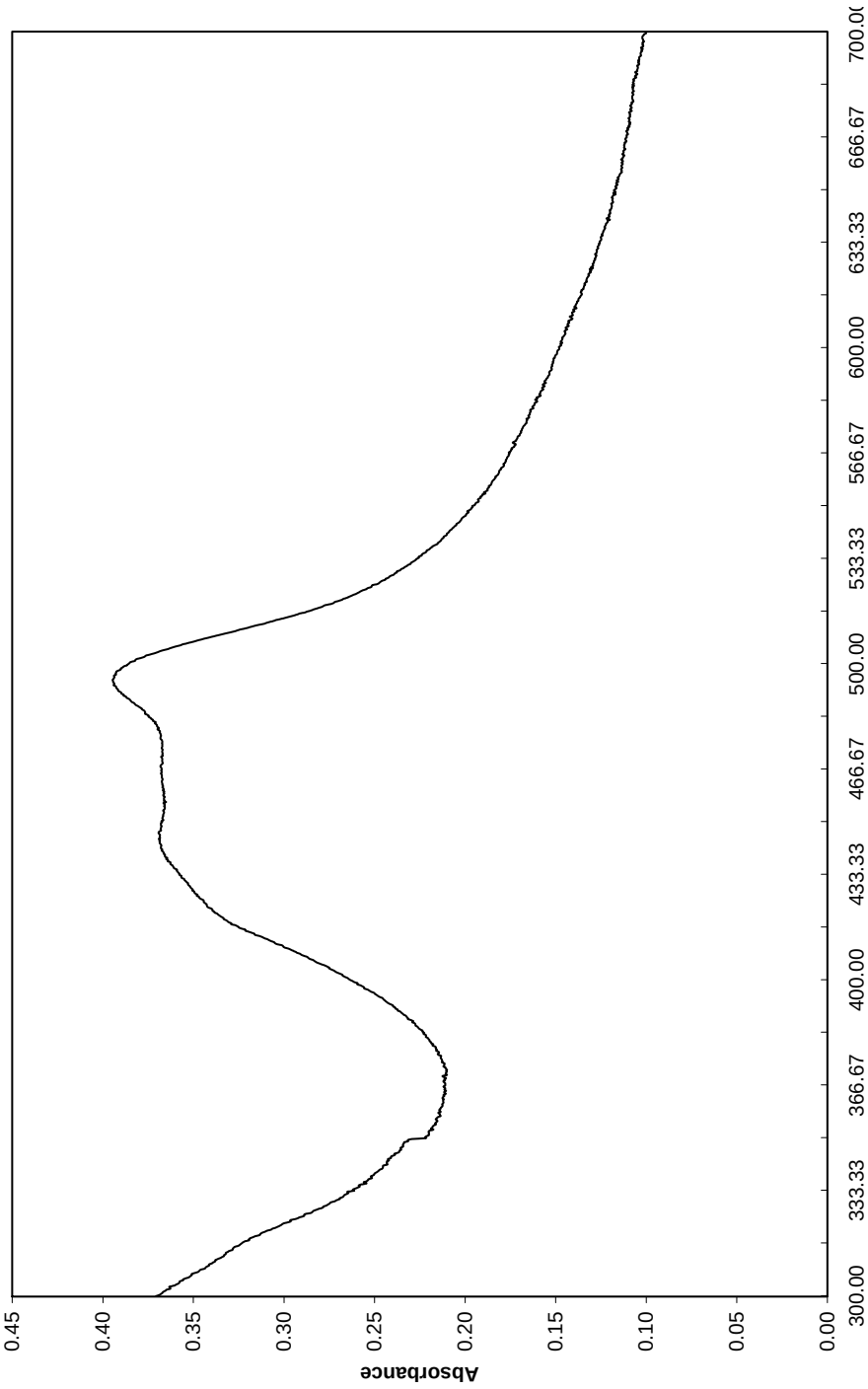

Spectrum 1.116: UV-Visible spectrum of material from attempted synthesis of 41 ($CHCl_3$)

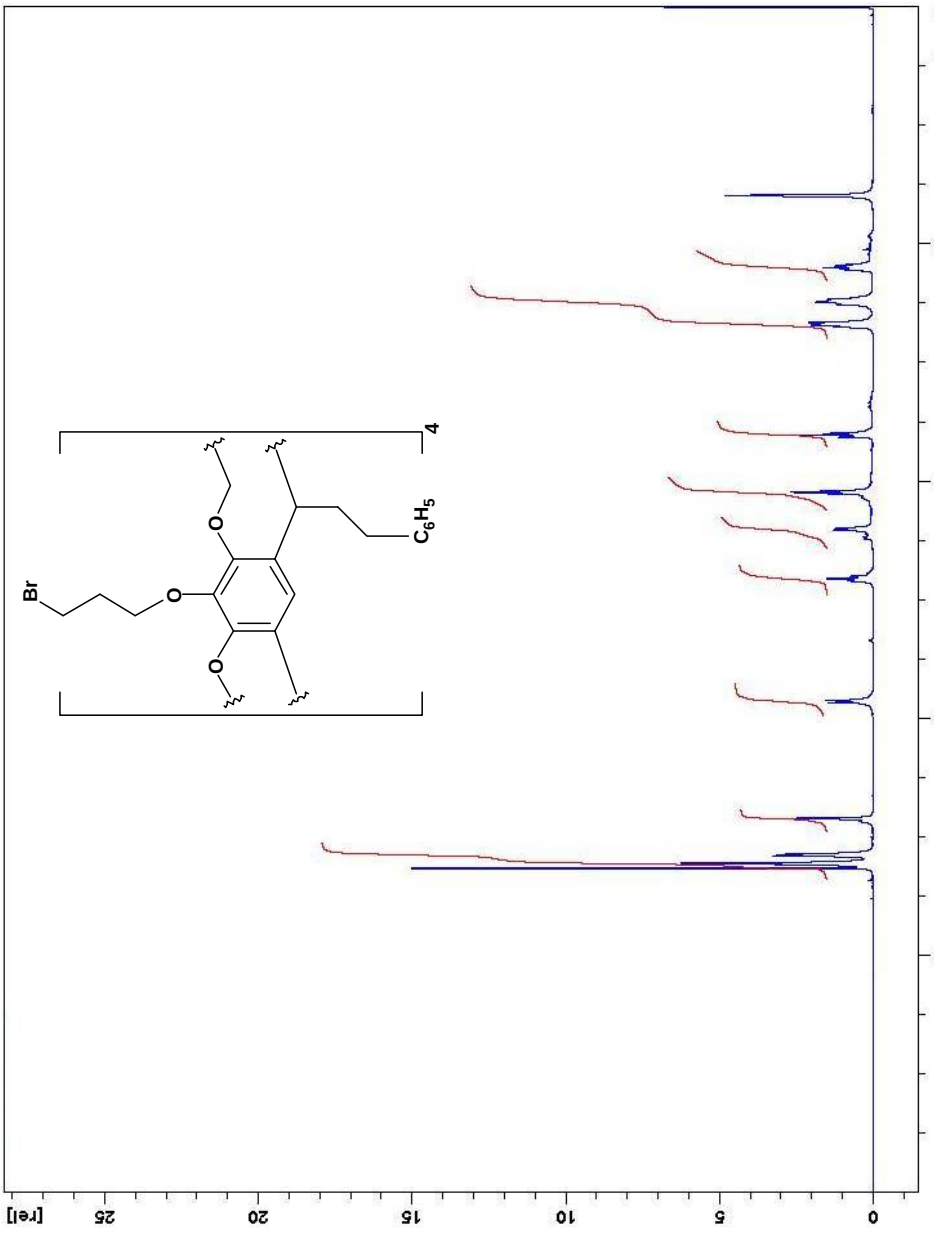

Spectrum 1.117: ^{1}H NMR spectrum of 42 in $CDCl_3$ (400 MHz)

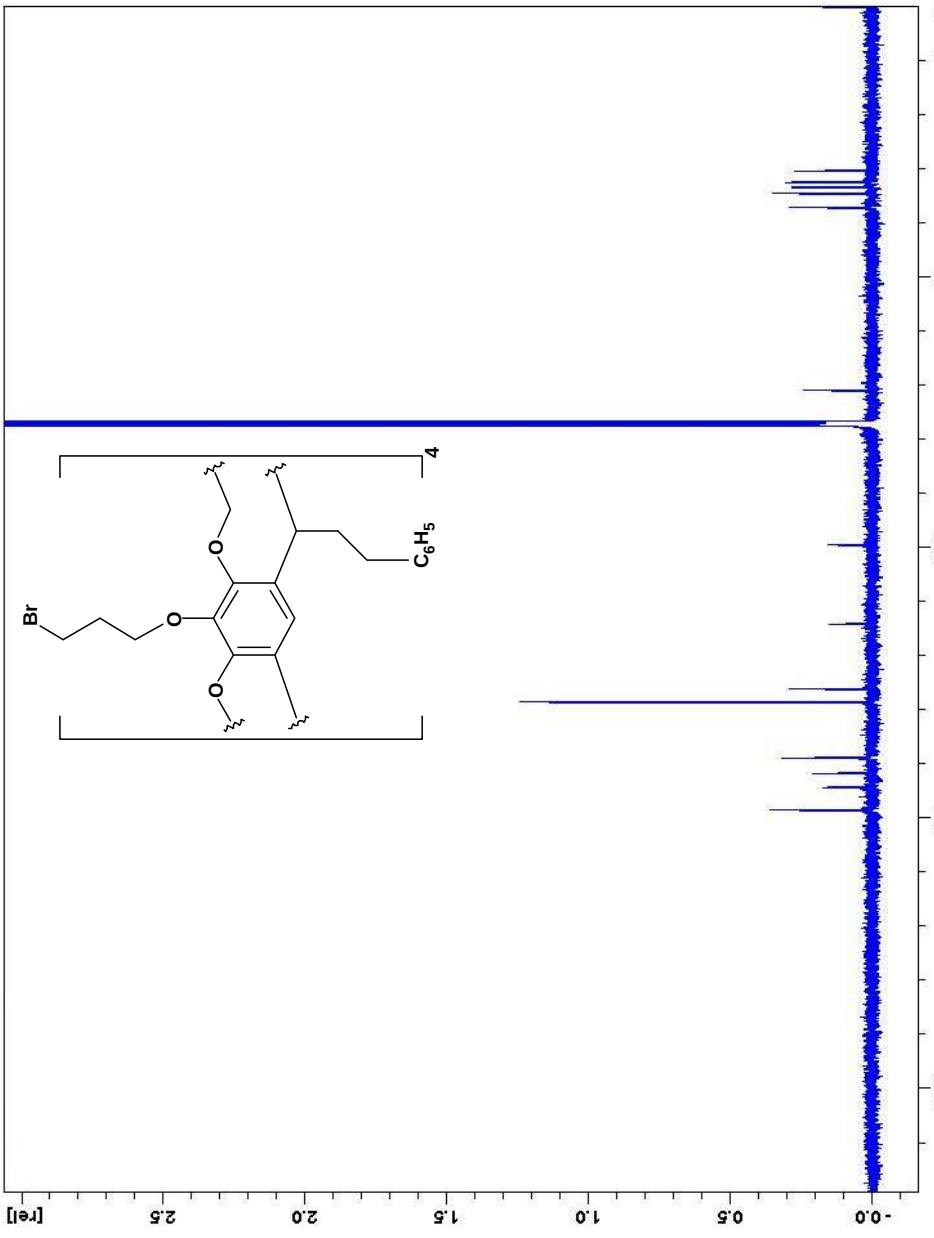

Spectrum 1.118: ^{13}C APT NMR spectrum of 42 in $CDCl_3$ (100 MHz)

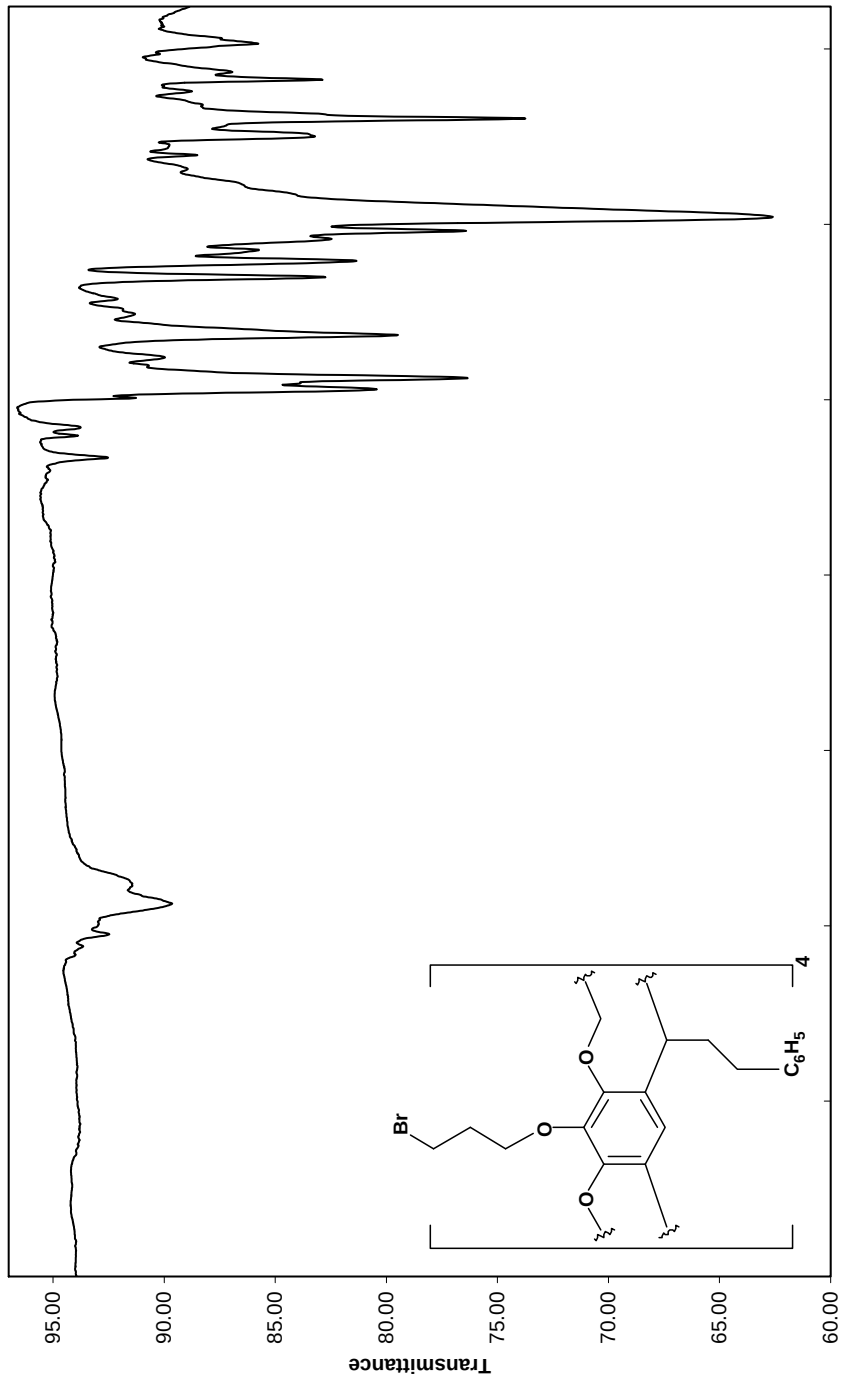

Spectrum 1.119: Infrared spectrum of 42 (KBr)